Determination of the Scale of Fluctuation of Cone Penetration Test Data Obtained from an Alluvial Site in Missouri

A Thesis presented to
the Faculty of the Graduate School
at the University of Missouri-Columbia

In Partial Fulfillment
of the Requirements for the Degree
Master of Science

by
LAURA SUTTON

Dr. John J. Bowders, P.E. Thesis Supervisor

May 2018

The undersigned, appointed by the dean of the Graduate School, have examined the thesis entitled

DETERMINATION OF THE SCALE OF FLUCTUATION OF CONE PENETRATION TEST DATA OBTAINED FROM AN ALLUVIAL SITE IN MISSOURI

Presented by Laura A. Sutton

A candidate for the degree of Master of Science

And hereby certify that in their opinion it is worthy of acceptance

Dr. John J. Bowders, P.E., Chair

Dr. Erik Loehr, P.E.

Dr. Allen Thompson, P.E.

DEDICATION

First and foremost, I wish to express my deepest gratitude to God, the creator of all things geotechnical; to Jesus, who reveals the sacred value of the people we civil engineers faithfully serve; and to the Spirit, who supplies wisdom, inspiration and love that makes such work possible.

I dedicate this work to many loving friends and family because with their support all things are possible. Also, all my best efforts are always given to my children, Ellie, Abby, Katie and Toby Kinnear, who have journeyed with me as I've pursued my degree and career. I could not have done it without their loving patience, encouragement and fortitude. I'm so proud! Also, thanks Dad and Mom, Ed & Carol Sutton, for your amazing support now and always; all my best qualities I believe I inherited from you. I appreciate the loving encouragement from my siblings, Donna Cann and Jeff Hindes, Eddie and Christine Sutton, and their families when hope was nearly lost. Thanks too to my dear friends, the Overstreet, Murphy, and Gillman families, Dave Riazi and all the saints at Summitview, Woodlandville United Methodist, Harrisburg Christian and Element churches, who not only supported me but also loved my entire family for many years.

ACKNOWLEDGEMENTS

My journey has been a long and meandering process with many helpful hands contributing along the way. I owe the University of Missouri, specifically the Civil & Environmental Engineering department, a most sincere thanks for being the final stop toward completing my Master's degree. An enormous debt of gratitude is owed to the world's greatest adviser, Dr. John J. Bowders, Jr., who believed in me from day one. He invests an incredible amount of time and energy not only to my education but to all his students; I would not have made it without him. I am most thankful to Dr. Erik Loehr and Dr. Allen Thompson for their contributions to my thesis and my education as professors and committee members. I am also thankful to Dr. Brent Rosenblad and Dr. Ahmed Abu El-Ela for their patience and skill as instructors both to learn from and to work with as their teaching assistant. I also thank my professors and the staff at Missouri University of Science and Technology and Colorado State University, including Dr. Charles D. Shackelford, for a firm educational foundation that has stood the test of time.

Without the many hours of field work and analysis at the Labadie site and the cooperation of those at Ameren Missouri, Reitz and Jens, Inc. and Gredell Engineering Resources, Inc., this thesis would have been impossible. I am especially thankful to Paul Reitz for his generous support of my education. Also, Jeffrey Fouse, Chris Cook and Joe Gilliam at Reitz & Jens were invaluable at obtaining and deciphering the mountain of data to make this analysis feasible.

TABLE OF CONTENTS

DEDICATION i
ACKNOWLEDGEMENTS ii
LIST OF TABLES v
LIST OF FIGURES v
ABSTRACT vii
1.0 INTRODUCTION 1
1.1 Background 1
1.2 Objective 2
1.3 Scope 5
1.4 Layout of Thesis 7
2.0 LITERATURE REVIEW 8
2.1 Introduction 8
2.2 Ding 8
2.3 Robertson 11
2.4 Kulhawy et al. 14
2.5 DeGroot & Baecher 17
2.6 Firouzianbandpey, Griffiths, Ibsen & Andersen 19
2.7 Uzielli, Vannucchi & Phoon (2005a, 2005b) 20
2.8 Lloret-Cabot, Fenton & Hicks 22
2.9 Bouayad 22
2.10 Uzielli, Lacasse, Nadim & Phoon 23
2.11 Griffiths & Fenton 26
2.12 Luo & Juang 31
2.13 Summary 34
3.0 MATERIALS AND METHODS 37
3.1 Introduction 37
3.2 Site Description 39
3.3 Site Investigation 41
3.4 Site Geology and Soils 41
3.5 Soil Identification and Classification 49

3.6 Normalizing Data for Statistical Analysis 52
3.7 Random Fields 55
3.8 Basic Definitions 56
3.9 Autocorrelation Function 59
3.10 Scale of Fluctuation/Autocorrelation Length 63
3.11 Summary 66
4.0 RESULTS AND DISCUSSION 68
4.1 Introduction 68
4.2 Cone Tip Resistance and Friction Ratio Contrast 69
4.3 Trend Analysis 75
4.3 Summary 81
5.0 CONCLUSIONS 82
5.1 Summary 82
5.2 Conclusions 83
5.3 Recommendations 84
5.3.1 Practical Implications 84
5.3.2 Suggested Further Research 86
REFERENCES 89

APPENDIX A A-1
APPENDIX B B-1

LIST OF TABLES

Table 4-1 Summary of Average Vertical Scale of Fluctuation Results for All HSU at the Labadie UWL Site 71
Table 4-2 Summary of Average Vertical Scale of Fluctuation Results for HSU with Fit to Autocorrelation Model ($R^2 \geq 0.9$) for the Labadie UWL Site.....72

LIST OF FIGURES

Figure 1-1: Illustration of scale of fluctuation, SoF δ or θ. (Nie et al., 2015) 4
Figure 2-1 Schematic of Typical Cone Penetration Rod (Robertson & Cabal 2015).....11
Figure 2-2: Types of Uncertainties (Kulhawy et al. 1995) 15
Figure 2-3: Illustration of the importance of including correlation in geotechnical analysis. Generic parameters, ξ, has similar statistical parameters but not correlation within the site. The top figures are weakly correlated, and the bottom figures are strongly correlated (Uzielli et al. 2006). 24
Figure 2-4: As the average normalized tip resistance, q_{c1N}, increases the soil becomes coarser. The plot demonstrates that the scale of fluctuation for the normalized tip resistance, $\delta(q_{c1N})$ slightly increases as the material becomes more cohesionless. The different shape data sets represent results from different sites (Uzielli et al. 2006). 25
Figure 2-5: Typical simulations shown the effect of the normalized scale of fluctuation, Θ_c. The upper slope is weakly correlated with a smaller scale of fluctuation and the lower slope is strongly correlated with a larger scale of fluctuation. (Griffiths and Fenton 2004) 27
Figure 2-6: Random field realization and finite element mesh for differently correlated slopes. The normalized scale of fluctuation is 0.5, which is weakly correlated, and 2, which is strongly correlated, for the upper and lower figures respectively. (Griffiths and Fenton 2004) 28
Figure 2-7: Assuming an infinite scale of fluctuation, θ_c, the probability of failure, p_f, will be overestimated in this example if the coefficient of variation, V_c, is below 0.65. Conversely, the probability of failure will be underestimated in a case with a coefficient of variation above 0.65 if a homogeneous soil mass (infinite θ_c) is assumed. 30
Figure 2-8: Probability of failure for the Ultimate Limit State versus the Scale of Fluctuation for drilled shafts in sand. (from Luo and Juang, 2012) 33
Figure 3-1 The site for the proposed utility waste landfill shows its close proximity to the Missouri River, which indicates alluvial composition (Gredell and Reitz & Jens 2011)..40
Figure 3-2 Boring and sounding locations and cross-sections (Gredell and Reitz & Jens 2011) 44
Figure 3-3 Site Stratigraphy: Cross-Section E-E' (Gredell and Reitz & Jens 2011) 45
Figure 3-4 Site Stratigraphy: Cross-Section F-F' (Gredell and Reitz & Jens 2011).....46
Figure 3-5: Legend for Figure 3-3 and Figure 3-4 (Gredell and Reitz & Jens 2011).....47
Figure 3-6 Typical Cone Penetration Test (CPT) Sounding (Gredell and Reitz & Jens 2011) 48
Figure 3-7 Robertson Classification 1990 Chart from Robertson and Cabal (2015). 51

Figure 3-8 Variation in Soil Properties from Phoon and Kulhawy (1999).....54
Figure 3-9 Relationship of Correlated Data from Baecher & DeGroot (1993).....58
Figure 3-10 Typical Results - Cone tip resistance with Scale of Fluctuation Equal to 1.1 feet.....61
Figure 3-11 Typical Results - Friction Ratio with Scale of Fluctuation Equal to 0.3 feet 61
Figure 4-1: Sutton's results are within typical literature values for the cone tip resistance. 69
Figure 4-2: Sutton's results are within typical literature values for the friction ratio. 70
Figure 4-3 Deformations measured from CPT: The cone measures a larger volume of soil than the sleeve (Melnikov and Boldyrev 2014). The colored zones and numbers represent areas of different deformations. Shear is represented on the right. Compression is represented on the left with negative and positive values representing areas of compression and expansion respectively. 74
Figure 4-4 Scale of Fluctuation vs Number of Samples. No bias is apparent at any layer thickness for both cone tip resistance and friction ratio. 75
Figure 4-5 Cone Tip Resistance Results – Scale of Fluctuation vs Number of Samples ..76
Figure 4-6: Friction Ratio Results – Scale of Fluctuation vs Number of Samples.....76
Figure 4-7: Scale of Fluctuation vs the COV. The site at Labadie, Missouri is comprised of a few homogeneous fine-grained soil layers. 77
Figure 4-8 Scale of fluctuation vs the COV of the cone tip resistance for cohesionless soils 78
Figure 4-9 Scale of fluctuation vs the COV of the friction ratio for cohesionless soils....79
Figure 4-10: Scale of fluctuation vs Average Overburden-Normalized Cone Tip Resistance for all soil types.....80
Figure 4-11: Scale of Fluctuation vs the Average Overburden-Normalized Friction Ratio for all soil types.....81

ABSTRACT

To account for uncertainty in geotechnical projects, knowledge of the uncertainties should be understood. Many sources of uncertainties can be reduced with increased sampling and good practices, but due to the nature of geomaterials, inherent uncertainties cannot be eliminated. Inherent uncertainties can be quantified by a statistical analysis. While some statistical descriptors, such as mean and standard deviation are common, the scale of fluctuation is less studied as it requires a large amount of data. The scale of fluctuation indicates the thickness of a soil layer which has correlated properties.

Large quantities of data can be obtained from the cone penetration test (CPT). The CPT was used for a site investigation for a coal combustion residual landfill, providing ideal measurements to investigate the variability of the alluvial site on the Missouri River.

The goal of Sutton's thesis is to determine if side resistance measurements, reported as the friction ratio, of cone penetration testing are less correlated than cone tip resistance measurements as previous research indicates. The results of this analysis agree with earlier analyses that the variability of the cone tip resistance is less than the skin friction. The average vertical scale of fluctuation for the cone tip resistance was 1.3 feet and 1.5 feet for sand and gravelly sand, respectively. The average vertical scale of fluctuation for the friction ratio was 0.7 feet and 0.8 feet for the sand and gravelly sand, respectively.

As increased computing power allows more complex modelling to become readily available, the shift to probabilistic analyses of such models allows for a more realistic assessment of the variability and correlation of subsurface properties. Several examples are discussed with show the effect of correlation and illustrate the need for both typical and site specific probabilistic parameters.

1.0 INTRODUCTION

1.1 Background

The field of engineering requires logical judgement and decision making. Experimental results and empirical relationships often inform decisions and designs as a standard of practice for many types of problems. Geotechnical engineering problems include natural materials which have variable properties. Often the sampling protocol only allows limited material to be evaluated. Lack of sufficient data is often remedied with the application of engineering judgement (Christian 2004). The judgement required to correctly assess these values can be obtained by experience, personal and case studies, as well as by statistical analyses. Christian stated that experts are usually too confident in their estimates and tend to underestimate the uncertainty in their estimates (2004). Christian plainly states a solution including that "the first step is to recognize the extent of our ignorance and to understand when it arises" (2004). While engineers can apply factors of safety to projects to deal with the uncertainties in projects, there are problems with this method (Baecher 1986). If factors of safety are assigned to design and loading parameters, the overall final factor of safety of the design may not be known (Baecher 1986). Engineers should have a grasp of the variability and distribution of the measured values to correctly evaluate these properties and to decide if these properties can be applied to materials at nearby unmeasured locations. Reliability of a design depends on four factors according to Christian (2004): the input uncertainties, the reliability analysis, the geotechnical models and the final interpretation. The first item, input uncertainties, is the focus of this thesis.

1.2 Objective

The goal of this analysis is to determine if side resistance measurements, reported as the friction ratio, of cone penetration testing are less correlated than cone tip resistance measurements as previous research indicates. Obtaining statistical information from case studies can add to the body of knowledge about in-situ testing techniques. As this body of knowledge grows, it can be used to help engineers more accurately assess the variability of geotechnical properties. While site specific data are always recommended, a range of typical values can help designers predict values and help correctly assign factors of safety or resistance factors to design inputs. Kulhawy, Phoon and Grigoriu (1995) performed an "extensive literature review" to find typical values for the uncertainties of common soil properties (Kulhawy et al. 1995). Understanding typical values can help pinpoint unusual data and provide guidance if site specific data are lacking. Geotechnical data are used to identify soil types and design parameters in variable, natural materials. These soil properties are correlated and do not vary randomly, and this inherent variability is due to depositional processes (Elkateb et al. 2003a, Fenton 1999). Geotechnical variability can be represented by the mean, the standard deviation, and the scale of fluctuation. (Jaska et al. 1994).

The objective of this study is to determine the scale of fluctuation of both the friction ratio and cone tip resistance of CPT soundings to help engineers become aware of the variability of these measurements. As shown in Figure 1-1, the scale of fluctuation indicates the thickness of a soil layer with similar or correlated properties, so data points within the vertical scale of fluctuation length can be expected to be similar (Nie et al. 2015, Phoon & Kulhawy 1999). According to Lloret-Cabot et al. (2014), the scale of

fluctuation “describes the spatial variability of a property in a random field.” Conversely, data points farther apart than the length of scale of fluctuation will not be correlated. As the scale of fluctuation approaches zero the expected values of nearby measurements will be uncorrelated or random. As the scale of fluctuation increases and approaches infinity, all measurements would be expected to be uniform. Previous studies indicate that, for an assumed homogeneous soil layer, the vertical scale of fluctuation of the friction ratio is less than the vertical scale of fluctuation of the tip resistance.

If the vertical scale of fluctuation is established for a site, then a reliability analysis could be performed to thoroughly evaluate the performance of a geotechnical design. Studies are discussed, which demonstrate practical application and the importance of evaluating the scale of fluctuation.

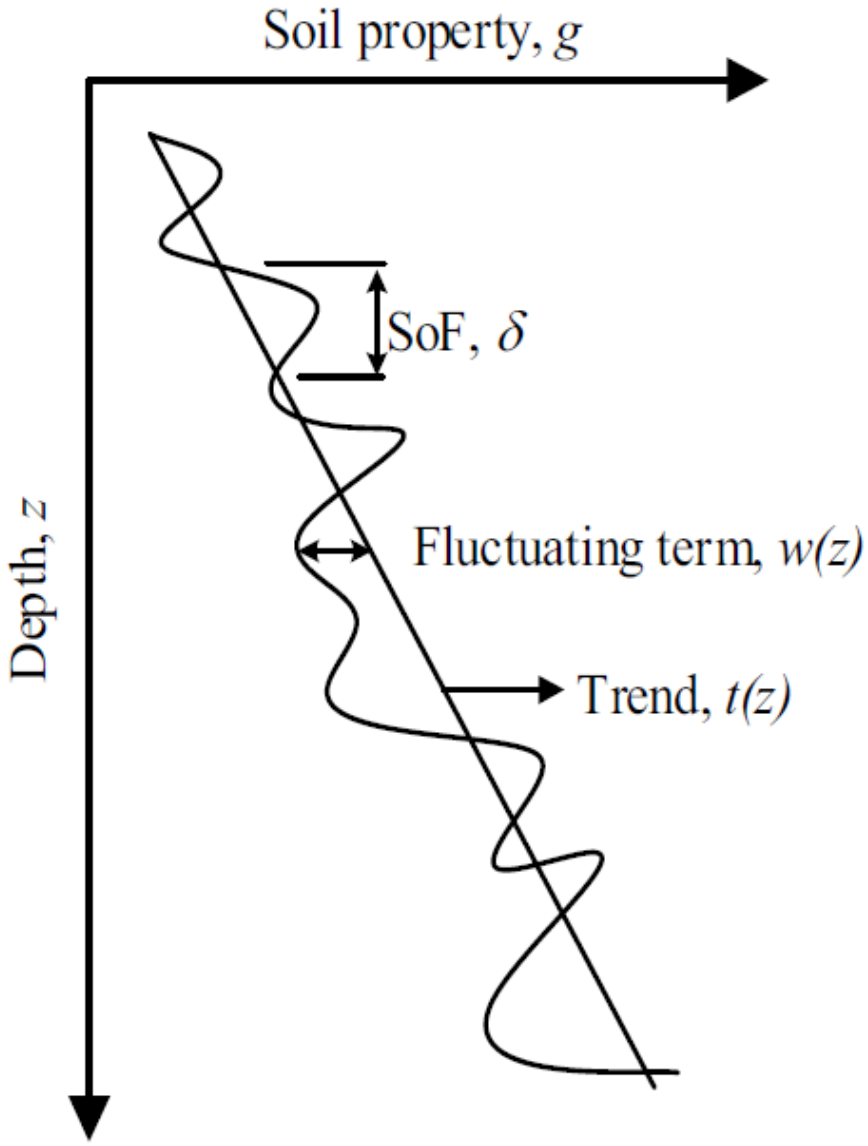

Figure 1-1: Illustration of scale of fluctuation, SoF δ or θ. (Nie et al., 2015)

1.3 Scope

The scope of this thesis encompasses two goals: comparing two measurements from cone penetration testing (CPT) and adding to the limited typical values for the scale of fluctuation.

Two main measurements determined by cone penetration testing are the cone tip resistance and the sleeve friction measurement. Since these measurements occur on the same probe, it could be assumed that the same distribution of variability would occur in both measurements and that both measurements evaluate the same soil volumes. This thesis attempts to verify or refute previous research which indicates that the correlations differ when evaluated by the scale of fluctuation. The scale of fluctuation indicates the thickness of a soil layer that can be expected to have similar properties. Data located closer than the scale of fluctuation is expected to have related or correlated values, while data located farther than the scale of fluctuation is expected to be unrelated or uncorrelated.

Sutton's thesis attempts to discern differences in the uncertainties of measurement from the cone penetration tests. Since the measurements of the probe's sleeve friction and cone tip resistance are obtained simultaneously, it could be assumed that the correlations of both measurements are identical. Research indicates that the soil volumes affected by these measurements differ; therefore, the correlation lengths differ as well. This difference is quantifiable by contrasting the scales of fluctuation of both measurements.

By determining the project specific scales of fluctuation, more data could be added to the body of knowledge to help determine typical values. Kulhawy, Phoon and Grigoriu (1995) suggest that typical values of the scale of fluctuation are important for properly

assessing specific site parameters. While much data exists for the mean, standard deviation and coefficient of variation for CPT data, the scale of fluctuation is not as prevalent. Sutton's thesis attempts to add to the body of knowledge about typical values for alluvial sites comprised mainly of cohesionless soils.

1.4 Layout of Thesis

This thesis is organized into five chapters to present the previous and current research and to suggest future research. Chapter 2 focuses on a review of the research pertaining to soil property uncertainties, in-situ CPT testing, and the scale of fluctuation as found in the literature. Chapter 3 details the site in Missouri and outlines the procedure followed for the probabilistic computations. A brief overview of statistics as it applies to geotechnical soil variability is included in Chapter 3. Chapter 4 reveals the results of the analysis and discusses observed trends in the results. Finally, the conclusions are presented in Chapter 5 as well as suggestions for further research.

2.0 LITERATURE REVIEW

2.1 Introduction

Some may argue that statistical analysis may be preferred over engineering judgement, but the most robust analysis would include both probabilistic computations and personal, experienced judgement of local geology along with Terzaghi's observational method. Terzaghi argued the importance of considering how geotechnical properties differ from the average values and insisted that engineers consider "the most unfavorable possibilities" which eventually led to the observational method still practiced today (Christian 2004). The observational method requires an iterative design approach where the project assumptions are confirmed and re-analyzed, if needed, based on the actual site conditions observed during construction. Quantifying uncertainty is an added step to help make the "observational method" more robust (Christian 2004). Statistical analysis allows designs to be more "reliable and economical," and the conclusions from investigations can be backed by more thorough analysis rather than strictly intuition or engineering judgement (DeGroot and Baecher 1993).

2.2 Ding

The difference in design properties from the actual properties or uncertainties due to limited measurements can be dealt with in many ways. Factors of safety in allowable stress design include all sources of variability and uncertainty (Ding 2014). Traditional conservative factors of safety applied to each design parameter cause the actual overall factor of safety to be unknown, to be not repeatable, and to vary from project to project due to differences in data available (Baecher 1986). Some sites may be more uniform, with more field data and known loading situations, while other sites may be highly

variable with a large range of possible loading conditions; therefore, a universal factor of safety may be unreasonable. Baecher (1986) states that the causes of failures are "unanticipated loads, gross errors, inadequate maintenance, and failure to account for some factors in design." Failure to "honor the detailed ground heterogeneity" of the site by simply using average values could result in an analysis "on the unsafe side" (Elkateb et al. 2003a). The factor of safety is often chosen based on engineering judgement rather than quantitative analysis which could result in under- or overdesigned projects with unknown probabilities of failure (Ding 2014).

Reliability based designs account for uncertainties in design. Uncertainties of soil properties are required to properly access the reliability-based design (Kulhawy et al. 1995, Uzielli et al. 2005a, Bouayad 2017). Load and resistance factor design (LRFD) accounts for specific uncertainties and variabilities in loads and resistances (Ding 2014). LRFD assigns factors to each load or resistance based, in part, by uncertainty of the load or resistance to loading as well as limit state and target reliability which is considered more precise (Ding 2014). Missouri Department of Transportation (MODOT) Engineering Policy Guide indicates the use of factors modified by the coefficient of variation (COV) of the data, which applies penalties for larger variability. This method accounts for the uncertainties, where applicable, but does not uniformly cause an overly conservative approach if the design parameters are more certain. The partial factor design method from Europe and Canada further specifies portions of the factors of safety to design properties separately (Ding 2014). Finally, reliability-based design can directly use probability distributions to determine the probability of failure of a design where soil and load properties are modeled as random variables (Ding

2014). These methods can be used together; Ding describes using the probabilistically determined factors in an LRFD design (2014). The Probabilistic Model Code of the Joint Committee on Structural Safety suggests the use "instead of one uncertainty factor for the computational model as a whole, one may consider the use of partial uncertainty factors related to the components of the computational model" to account for soil uncertainties (JCSS 2006).

Ding analyzed the effect of the number of samples on the final design of a shallow foundation (2014). She found that there is an increase in the reliability of a design with 30 or more data points and decreasing returns on obtaining more data. Often, traditional geotechnical investigations do not include even 30 data points per boring. While the state of practice is moving toward the use of partial uncertainty factors in building codes, this effort must be supported by knowledge of expected statistical properties of various geotechnical measurements to allow estimates during preliminary planning or if there are limited data. In order to obtain sufficient data for statistical analysis, the testing method must record many measurements. The cone penetration test (CPT) is gaining popularity as a useful in-situ testing method to identify soil types and estimate soil properties which supply large numbers of measurements.

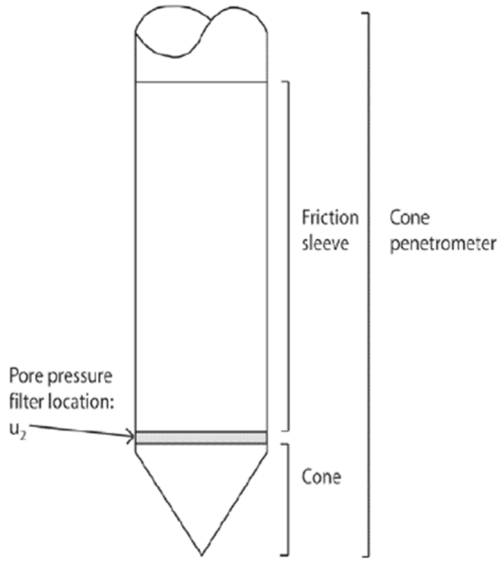

Figure 2-1 Schematic of Typical Cone Penetration Rod (Robertson & Cabal 2015)

2.3 Robertson

Cone Penetration Testing (CPT) involves near continuous measurements from a 1.5-inch diameter probe with a cone, as represented in Figure 2-1, that is pushed into the soil according to ASTM D 5778-07 "Standard Test Method for Performing Electronic Friction Cone and Piezocone Penetration Testing of Soils," shown in Figure 2-1. The measurements recorded include cone tip resistance and the sleeve resistance as well as the pore pressure behind the cone. The force on the cone is divided by the projected cone area to calculate the cone tip resistance, q_c. The force on the friction sleeve is divided by the sleeve area to calculate the sleeve resistance, f_s. The cone tip resistance is corrected for area and pore pressure: $q_t = q_c + (1 - a)u$ where q_t is the total cone tip resistance, a is the net area ratio and u is the measured pore pressure. The net area ratio is defined as: $a = \frac{d^2}{D^2}$ where d is the diameter of the load cell support and D is the diameter of the cone and the net area ratio commonly equals 0.85.

CPT results are used to identify soil behavior or response and not its composition (Uzielli et al., 2005b, Robertson 1990, Robertson 2016 and Fenton 1999). Robertson indicates that the CPT data can be affected by many factors including: "stress history, in situ stresses, sensitivity, stiffness, microfabric and void ratio" (1990). It has been suggested

that CPT data are “sensitive to deposition conditions, loading history, and variations in fines content” (Elkateb et al. 2005).

CPT method is fast, continuous, repeatable, reliable and widely used (Firouzianbandpey 2014, Jaska et al. 1994, Robertson 2016, Uzielli et al. 2005a, Bouayad 2017). In-situ testing reduces the errors due to sample disturbance of traditional soil sampling and laboratory testing which can lead to measurement bias and a flawed design as long as the effect of the probe is limited (Jaska et al. 1994). The electric CPT is less dependent on user or procedural errors and is only affected by the rate of penetration (Kulhawy & Trautmann 1996). In clays, an increase in penetration rate has been shown to increase the cone tip resistance by up to 10% (Kulhawy & Trautmann 1996) as such Kulhawy and Trautmann suggest adherence to the ASTM D3441 (ASTM D5778 for electric systems) standard rate of 2 cm/sec. Also, depth readings can be affected by a lack of verticality. Tests with “well-defined specifications, accepted practices, and standardized equipment have relatively small test variability” (Kulhawy & Trautmann 1996). The testing uncertainty of in-situ measurements are due to equipment, procedural and random variances. The CPT electric equipment has been shown to have a coefficient of variation (COV) of approximately 3 percent and random error COV of 5 percent for q_c and 10 percent for f_s. The total COV for CPT measurements is 8 percent for q_c and 12 percent for f_s (Kulhawy & Trautmann 1996) with a typical expected range of COV of 5 to 15 percent. Total COV for standard penetration test was 15 to 45 percent, the COV for the Vane Shear test was 10 to 20 percent; the COV of the CPT was the smallest except for dilatometer test which was 5 to 15 percent as well (Kulhawy & Trautmann 1996, Jaska et al. 1994).

In order to classify the soil based on CPT charts, the data must be normalized to account for the effects of overburden pressure. Without normalizing the data, the soil's apparent type would appear to change as the probe gets deeper as the cone tip resistance increases with depth (Robertson 1990). Ideally the cone tip resistance could be corrected for changes in in-situ horizontal stress, but determining horizontal stresses is difficult. Therefore, the normalization includes the vertical stress input only as determined by unit weights and ground water levels. In order to compensate for this trend, normalized tip resistance, Q_t, is calculated using Equation 1 and is used to classify the soil type (Robertson 1990):

$$Q_t = \frac{q_t - \sigma_{v0}}{\sigma'_{v0}} \qquad \text{Eqn. 1}$$

Where q_t is the measured tip resistance, σ'_{v0} is the effective vertical stress, σ_{v0} is the total vertical stress. The measured force on the sleeve is also divided by its area, to determine the side friction, $f_s = F_s/A_f$. These values can be normalized to account for overburden pressure as shown below.

Normalized friction ratio, F_R, is calculated using Equation 2 (Robertson, 1990):

$$F_R = \frac{f_s}{q_t - \sigma_{vo}} \qquad \text{Eqn. 2}$$

where q_t is the measured tip resistance, f_s is the sleeve friction, σ_{vo} is the total vertical stress.

2.4 Kulhawy et al.

According to Kulhawy and Trautmann, uncertainties are often dealt with in geotechnical engineering using an engineer's judgment and experience rather than quantitatively addressed (Kulhawy et al. 1996). In order to use more rigorous design methods, such as load resistance factor design (LRFD) and reliability analyses, numerical values must be used to quantify the uncertainties. The resistance factors used in design should vary depending on the variability of the load or resistance being assessed. The variability can be quantified by the coefficient of variation and scale of fluctuation of the soil property at the specific site (Kulhawy et al. 1995). There are less data available to judge a typical CPT cone tip resistance's scale of fluctuation (7-10 studies) as compared to other typical soil properties, such as CPT cone tip resistance's COV (12-57 studies) (Kulhawy et al. 1995); therefore, more available site analyses could be useful to add to the body of knowledge for typical values. Kulhawy indicated that, in general, the inherent variability for sand is greater than that for fine grained soil (1995), which alone could be useful in assigning design parameters once the soil type has been identified. Also, typical values may not be truly representative of "typical" if the data are limited, Phoon and Kulhawy advises caution with such limited data (1995). Many geotechnical site investigations contain small amounts of soil property measurements, which could bias the reported values. While typical values are useful for preliminary studies or as a check for measured properties, ideally site-specific statistics should be determined for each project (Kulhawy et al. 1995). According to a summary of about 10 studies by Kulhawy (1995) the scale of fluctuation in the vertical direction for the cone tip resistance reported as both sand and clay was 0.3-7.2 feet (0.1-2.2 meters) and corrected cone tip resistance for strictly clay ranged from 0.6-1.6 feet

(0.2-0.5 meters). In the horizontal direction, the scale of fluctuation for soil reported as both sand and clay was much greater, 10-260 feet (3-80 meters). According to Phoon & Kulhawy (1995), the scale of fluctuation for the corrected cone tip resistance for clays was smaller (less than 0.5 m) than the scale of fluctuation for the uncorrected cone tip resistance (which was less than 2.2 m for sands or clays). The scale of fluctuation can be dependent on the sampling interval (Phoon & Kulhawy 1999) as well as soil type.

Design values can be affected by different sources of uncertainties as categorized in Figure 2-2.

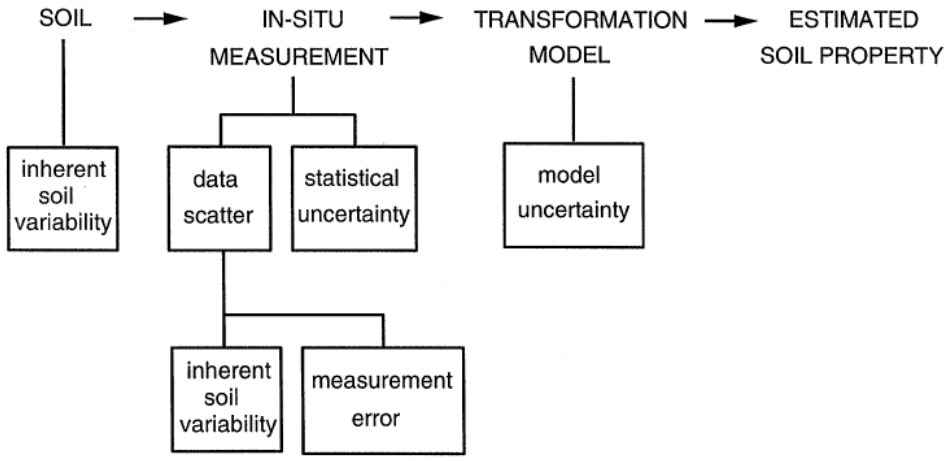

Figure 2-2: Types of Uncertainties (Kulhawy et al. 1995)

Uncertainty or variability in soil properties due to the depositional process is termed inherent variability or aleatory uncertainty (Ding 2014, Christian 2004). Soil variability is due to its "formation which include: sedimentation, parent material, weathering (mechanical and chemical), topography, organisms, structural defects, layering and time" (Jaska et al. 1994). Additional testing does not help us predict aleatory or

inherent uncertainty (Christian 2004), and it appears as random error (Baecher 1986, Baecher & DeGroot 1993). Christian (2004) calls variability about a trend line 'data scatter.' Once a measurement has been taken, the data scatter can be due to actual spatial or temporal variations or random testing errors (Christian 2004). Two main causes of soil heterogeneity are differences due to layering of dissimilar materials and inherent spatial variability of properties due to deposition and loading differences (Elkateb et al. 2005b). Measurement error can be due to many factors, including "equipment, procedure, human errors, and random testing effects." Kulhawy indicates that there can be errors, from equipment and procedures, introduced into the data which are typically not documented and cannot be later parsed out from the data (1995).

Kulhawy and Trautmann (1996) investigated the measurement error for field tests, including the CPT. They measured controlled laboratory tests to assess the variability of soil parameters. Inherent variability was limited by creating uniform soil deposits in the laboratory. The coefficient of variation of measurement errors for electric CPTs was 5 to 15 percent (Phoon & Kulhawy 1999). Measurement errors can cause uniform bias throughout a site (Baecher 1986).

Epistemic uncertainties due to the lack of knowledge, which can be improved with more data (Christian 2004), is also called knowledge uncertainty (Ding 2014). Also, statistical errors, which appear as systemic errors (Baecher 1986) from limited data, can be improved by getting more data. Christian (2004) states that systemic errors can be divided into errors in the trend and bias in measurements. Biases in the data can come from small data sets, as is often the case in geotechnical investigations (Christian 2004).

The mean and standard deviations of a few samples may not correctly describe the entire site (Christian 2004).

Transformation uncertainty occurs when transforming field or lab measurements to design parameters by using empirical or theoretical correlations which also appears as systemic error (Baecher 1986).

Some additional sources of uncertainty include using properties from more than one soil type, trends which are not removed, and soil data obtained at different times (Kulhawy et al. 1995). Including additional types of error would make the soil layer seem more varied than if only the inherent variability due to geological changes were considered (Kulhawy et al. 1995). Kulhawy indicated that soil layers properly classified into homogeneous units are "sufficiently homogeneous for the evaluation of inherent variability" (1995). Since soil is an ever-changing natural material, soil properties can also vary in time as well as location. Studies should indicate the sampling time frame for proper analysis and comparison.

The magnitude of each of the many sources of uncertainty depends on many factors including: the site, the testing protocol, and the models used. Therefore, comparison of typical values which include errors from many sources is difficult and, in effect, fraught with possible errors (Kulhawy et al. 1995).

2.5 DeGroot & Baecher

Statistical analysis often ignores the fact that soil properties are correlated, which can help assess properties at untested locations (DeGroot & Baecher 1993). Correlation means that the value of a soil property at one location is likely to be similar to the soil

nearby, which creates a “waviness” about the trend line if the property is plotted with depth (DeGroot & Baecher 1993). Three methods can be used to determine correlation length: moment estimators, inverse estimation from stochastic interpolations and using probabilities to find the maximum likelihood parameters

(DeGroot & Baecher 1993). DeGroot & Baecher concede that the optimum method to determine correlation is the maximum likelihood method. This technique involves determining the values of properties that have the greatest probability of producing the observed soil properties measured in the field (DeGroot & Baecher 1993) which requires complex statistical inputs and computations. Moment estimators are relatively simple calculations of the statistical descriptors of a set of data, such as the mean, variance, standard deviation, autocovariance, and autocorrelation (DeGroot & Baecher 1993). Inverse estimation is used in mining engineering to estimate the values at an untested location based on measured values at another location. This method requires data from “an extensive exploration program” (DeGroot & Baecher 1993). Inverse estimation involves minimizing the error between predicted and actual values of variance by removing one actual value of a soil property and using the remaining values to estimate the removed value. Parameters of the autocovariance function are varied until the error between the actual and predicted value is minimized. According to DeGroot & Baecher (1993), evaluation of the statistical properties obtained using this method have not been performed.

Moment estimators are computationally straightforward and have, therefore, been commonly used including the mean and coefficient of variation, but less commonly calculated is the scale of fluctuation (Kulhawy et al. 1995). Some typical values for the

scale of fluctuation were compiled by Kulhawy et al. (1995) as presented in Section 2.4. Several researchers have investigated the scale of fluctuation of CPT measurements to help engineers determine the expected variability of both cone tip resistance and sleeve friction, which is represented as the friction ratio.

2.6 Firouzianbandpey, Griffiths, Ibsen & Andersen

Firouzianbandpey et al. (2014) investigated the scales of fluctuation, both vertically and horizontally, from CPT data at two sites in northern Denmark to characterize the uncertainty. Limited data can cause more uncertainty which could cause designs to be overly conservative (Firouzianbandpey 2014). The sites were mainly comprised of sand and silty sand with some gravel near the Limfjord river basin deposit and in the harbor of Frederikshaun. The soil profiles were classified using Robertson's 1990 method, and CPT data were sampled every 2 cm.

After classification, the layers composed of one soil type were analyzed further by Firouzianbandpey et al. (2014). The layers' means, standard deviations and COVs were calculated as well as the correlation length, also known as the scale of fluctuation. The largest COVs were reported for gravel layers for both the normalized cone tip resistance, q_{c1N}, and the friction ratio, F_R. Silt mixtures and cohesive layers had the lowest COV, which indicates the least variability. The average vertical scale of fluctuation of the cone tip resistance for both sites was 0.45-0.5 meters (1.5-1.6 feet). The average vertical scale of fluctuation of the friction ratio for both sites was 0.2 meters (0.7 ft).

Firouzianbandpey et al. indicate that the friction ratio measures a smaller volume of soil adjacent to the sleeve, than the cone tip resistance which measures a larger volume of

soil beneath the advancing cone. Therefore, several closely space cone tip resistance measurements will include the same soil volume with similar measurements.

2.7 Uzielli, Vannucchi & Phoon (2005a, 2005b)

Uzielli et al. (2005a, 2005b) characterized the data from normalized CPT as random fields in order to account for the overburden stress and stress history. The authors state that the data should not "violate weak stationarity in resulting residuals." Stationarity is defined by Baecher and Christian (2003) as data which is statistically homogeneous, which indicates that the data's basic statistical values are independent of location. Therefore, the mean and standard deviation do not vary greatly throughout the deposit and the autocorrelation function is only a function of the separation distance and not the actual depth in the deposit. Stationarity was achieved by only considering data that initially by passed the Bartlett limit and further checking with a modified Bartlett test. The Bartlett test is a statistical test used to determine if the variances of the data are equal and the data are uniform. The modified Bartlett test was created by Phoon, Quek and An (2003) to account for the fact that soil data are naturally correlated. Using these tests, they identified homogeneous soil units (HSU). Of the 304 soundings studied, only 40 were sufficiently homogeneous to be analyzed for cone tip resistance, q_{c1N}, and only 24 data sets could be used to analyze side resistance expressed as friction ratio, F_R.

The soil layer had to conform to certain requirements in order to be considered homogeneous. Data points separated by larger distances were not used due to "the well-accepted fact that the estimated autocorrelation coefficients become less reliable with increasing lags and are deemed not significantly different from zero inside the range +/- r_b, Bartlett limit" (Uzielli et al. 2005a). To classify the soil type, the authors

calculated the soil behavior class index, I_c. The soil behavior class index is a single parameter that combines both the cone tip resistance and the friction ratio of CPT to simplify soil classification. In order to identify the soil layer as homogeneous, the COV had to be less than 0.1 over at least 4.5 m. The COV was larger for cohesionless soils, which indicates a greater variability (Uzielli et al. 2005a, Uzielli et al. 2005b).

After the initial analysis, stationarity was further tested with the modified Bartlett test. The classical Bartlett test can exclude similar materials if the data are correlated, which is often the case with closely sampled CPT data (Phoon et al. 2003). Therefore, the modified Bartlett test was created for correlated data. Additionally, the HSU was accepted if the autocorrelation model fits the initial part of a curve with coefficient of determination, R^2, greater than 0.9. In their study, the most likely soil types to meet the study criteria for homogeneity were sandy soils. Additional requirements of data sets for their study were a measurement interval less than 5 cm (2 inches) to allow "sufficient resolution," the groundwater levels reliably reported to calculate q_{c1N} and F_R, and a length of the sounding greater than or equal to 10 m (33 ft) to allow "stationarity assessment and be large enough for useful statistical analysis."

Uzielli found that q_{c1N} is more strongly correlated than F_R. Their study indicated that the standard deviation for q_{c1N} and F_R increased from cohesive to cohesionless soils; therefore, CPT data are more variable in sand than in clay. As mentioned above, the authors indicate that the volume affected by the cone tip is a larger volume than the volume affected by the sleeve friction, so several data points in a row repeat in several readings at the cone tip location. These repeated readings make the cone tip resistance data appear more correlated. Also, they stated that normalizing the data makes it more

correlated because it “minimized systemic in situ effects” (Uzielli et al. 2005a, Uzielli et al. 2005b).

2.8 Lloret-Cabot, Fenton & Hicks

Lloret-Cabot et al. (2014) compared the traditional approach of determining the vertical and horizontal scales of fluctuation (or correlation length) with a new approach and applied both methods to a case study at a sandy site located on an artificial island created in the Canadian Beaufort Sea. The traditional approach fits a model to the CPT data. When data are limited the model typically does not fit the field data well. Lloret-Cabot et al. used a more complex method which simulates a random field of normalized de-trended tip resistance and calculated the scale of fluctuation for many simulations restricting the statistical properties of the simulations to that of the actual CPT data. The results by Lloret-Cabot et al. indicate that the stimulation method was superior when the data points were limited as in the horizontal direction (with only a few data points within the scale of fluctuation length), but the results were very similar in the vertical direction when the data points were very close together, such as 2 cm intervals.

2.9 Bouayad

Bouayad (2017) assessed the scale of fluctuation of the cone tip resistance at a sandy site in northern Algeria as part of a larger study of liquefaction potential. Ten CPT soundings were conducted from 10 m (33 ft) to 13 m (43 ft) in dense fine sand and silty sand overlain by loose to medium dense sand. The cone tip resistance data, taken at 2 cm (0.066 ft) intervals, were de-trended by removing a linear trend with depth and then were statistically analyzed by fitting the autocorrelation function to the autocorrelation theoretical model. Bouayad found the best-fit model for that data was the cosine

exponential model. The vertical scale of fluctuation for the cone tip resistance at this sandy site was 0.32 m (1.0 ft) to 1.31 m (4.3 ft), with an average of 0.78 m (2.6 ft) and COV of 40%.

2.10 Uzielli, Lacasse, Nadim & Phoon

A thorough overview of the state of practice of analyzing soil variability was discussed by Uzielli et al. (2006). Often basic statistical analyses include the mean and standard deviation of a set of measurements, but preferably spatial correlation would be included as well. As shown in Figure 2-3, two data sets showing a generic parameter, ξ, can have similar statistical parameters but very different correlations. The properties in the top plan view shows a weak correlation and would have a small value for the scale of fluctuation, but the bottom plan view shows a strong correlation. Structures would respond differently in these two scenarios. The authors explain that random field theory can be used to describe the spatial variability of a site and reliability models can then be analyzed.

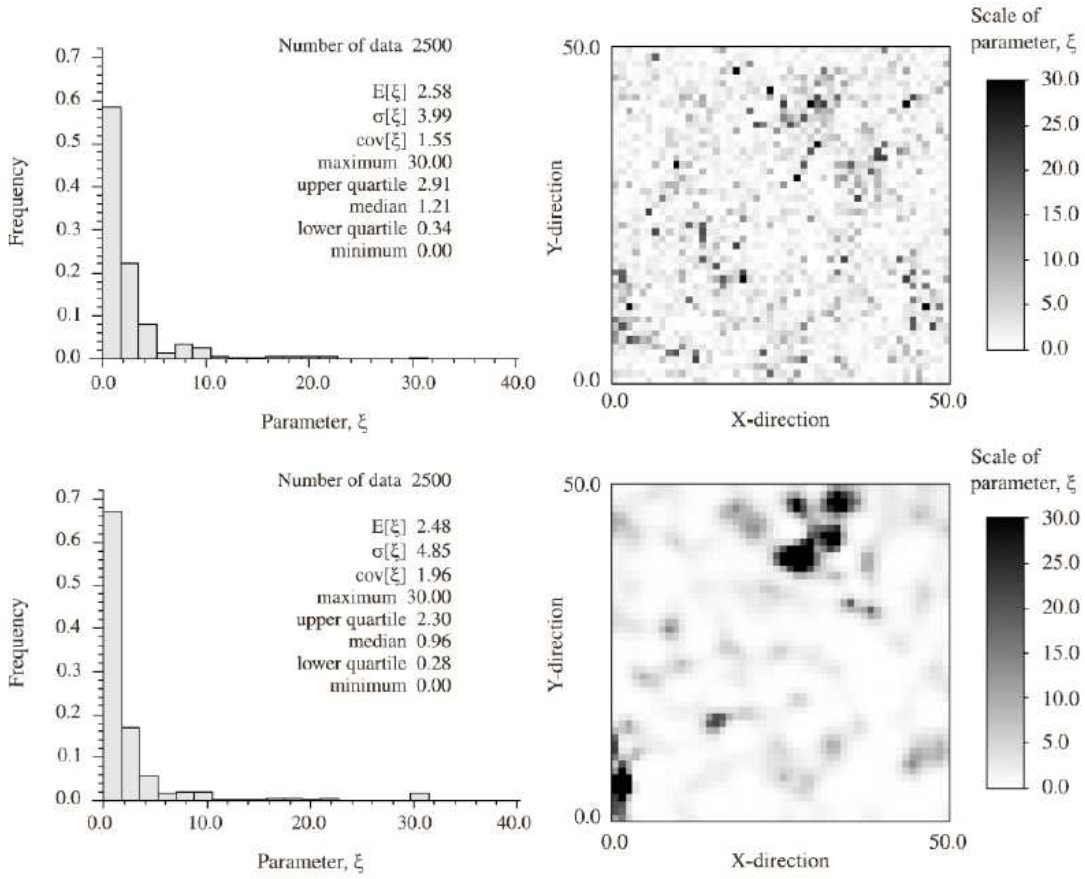

Figure 2-3: Illustration of the importance of including correlation in geotechnical analysis. Generic parameters, ξ, has similar statistical parameters but not correlation within the site. The top figures are weakly correlated, and the bottom figures are strongly correlated (Uzielli et al. 2006).

The random field can be described by the mean, standard deviation, and the scale of fluctuation and its corresponding autocorrelation model. The scale of fluctuation can be affected by several factors: the direction, the trend which was removed to create the random field as described in Section 3.6, and the method of estimating and fitting the models. Therefore, these choices need to be described in the analysis. Generally, due to the soil formation process, the scale of fluctuation in the vertical direction is much less than in the horizontal direction. The scale of fluctuation increases as the sampling interval increases according to research. Also, trend removal decreases the scale of fluctuation. Additionally, research indicates that the scale of fluctuation is dependent on soil type if all other factors remain constant. According to Uzielli, the vertical scale of fluctuation for cohesionless soils is generally slightly larger than cohesive soils as demonstrated in Figure 2-4, although the plot reveals a large degree of data scatter.

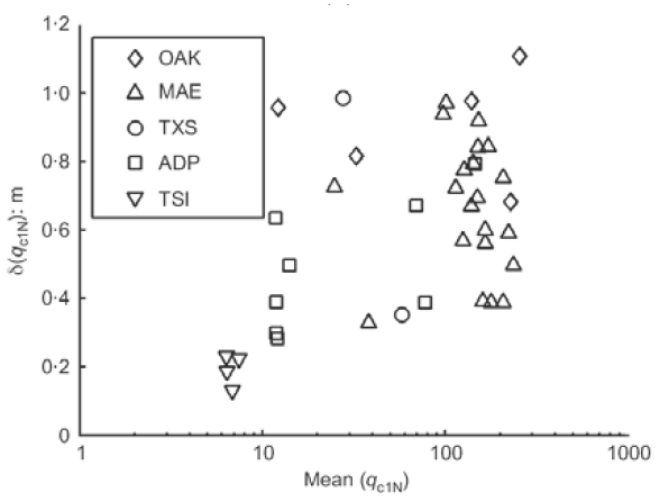

Figure 2-4: As the average normalized tip resistance, q_{c1N}, increases the soil becomes coarser. The plot demonstrates that the scale of fluctuation for the normalized tip resistance, $\delta(q_{c1N})$ slightly increases as the material becomes more cohesionless. The different shape data sets represent results from different sites (Uzielli et al. 2006).

Uzielli et al. reported that the CPT failure zone is affected by the soil stiffness. Stiffer materials exhibit larger failure zones; therefore, the failure zone in dense sand would be larger than in soft cohesive soils. Closely spaced CPT measurements within a larger failure zone would be strongly correlated. The volume of soil measured by the sleeve friction is not as soil type dependent and is smaller than the tip resistance; therefore, the sleeve friction is weakly correlated as the research by Uzielli et al. summarizes in Section 2.7.

Using the scale of fluctuation, in addition to the mean and standard deviation, is useful for a thorough reliability-based analysis. The authors indicate that random field modeling allows finite element techniques to assess the reliability of geotechnical designs. Including variability allows a more complex and more realistic representation of the actual site conditions. They suggest that a footing resting on a variable site will fail to one side or the other rather than the ideally symmetrical failure. The authors do concede that while more accurate and realistic, random field simulation and finite element type analyses are more complex and not commonplace yet.

2.11 Griffiths & Fenton

A probabilistic approach was applied to several different geotechnical problems by Griffiths and Fentin, including slope stability in 2004. For the slope stability analysis, they used a random field finite-element method to include spatial correlation and statistical parameters in the site description with simulations, such as the simulations shown in Figure 2-5. The upper slope shown is weakly correlated and has a normalized scale of fluctuation for shear strength equal to 0.2. The normalized scale of fluctuation is the scale of fluctuation divided by the slope height, H. A homogeneous slope would have

a scale of fluctuation equal to infinity. The lower soil mass in Figure 2-5 is strongly correlated with a normalized scale of fluctuation for shear strength equal to 2.0. The magnitude of the soil properties assigned randomly are indicated by the shading, with weaker soil elements shaded darker.

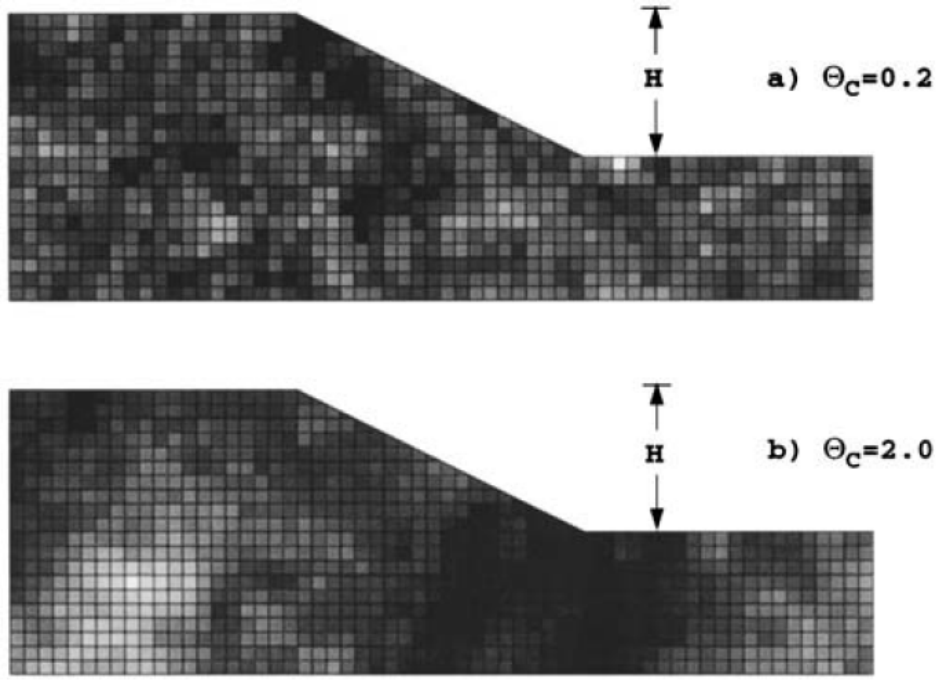

Figure 2-5: Typical simulations shown the effect of the normalized scale of fluctuation, Θ_c. The upper slope is weakly correlated with a smaller scale of fluctuation and the lower slope is strongly correlated with a larger scale of fluctuation. (Griffiths and Fenton 2004)

One-thousand Monte Carlo simulations were run for each case in the study with the same statistical properties of a log-normally distributed shear strength, a set mean and standard deviation, but varying correlation, which was assumed isotropic. The simulated properties were randomly located and resulted in varying areas of weak and strong materials used to calculate the probability of failure. Figure 2-6 illustrates the effect of

including correlation on the slope's performance. The upper image in Figure 2-6 is weakly correlated with a normalized scale of fluctuation of 0.5 and the lower image is strongly correlated with a normalized scale of fluctuation of 2. The finite-element model allowed the failure surface to fail through a unique failure path along weaker material rather than a fixed failure plane, such as circular as traditional slope stability often assumes. The strongly correlated slope has a path of failure through a larger correlated weak zone, whereas the weakly correlated slope has many smaller failure zones throughout as the shown in Figure 2-6.

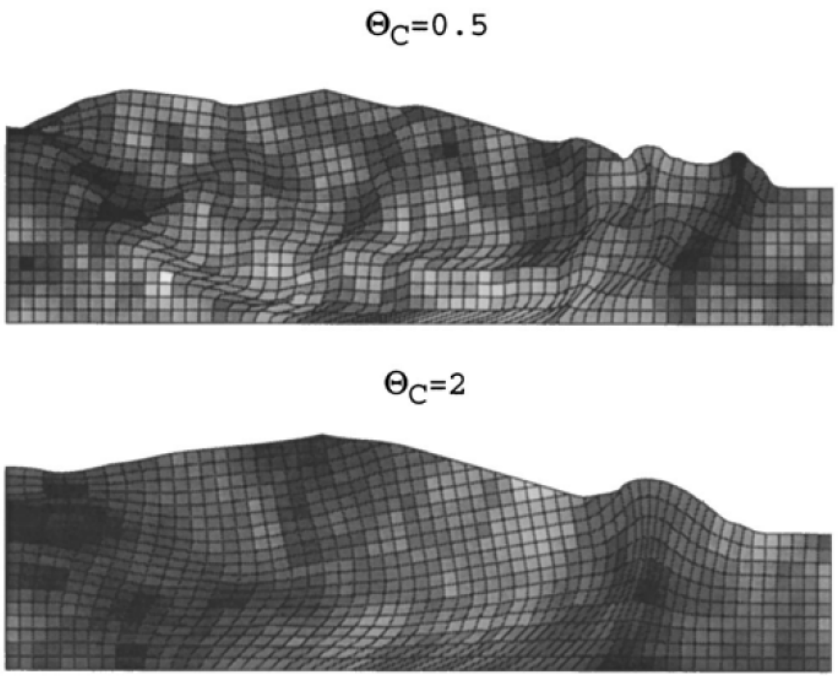

Figure 2-6: Random field realization and finite element mesh for differently correlated slopes. The normalized scale of fluctuation is 0.5, which is weakly correlated, and 2, which is strongly correlated, for the upper and lower figures respectively. (Griffiths and Fenton 2004)

A parametric study of the probability of failure was performed by Griffiths and Fenton. They found that the scale of fluctuation can either increase or decrease the probability of failure depending on the coefficient of variation of the soil as shown in Figure 2-7. For their study, failure was defined as a factor safety less than one in a homogeneous slope, which occurred for the given slope geometry at a normalized mean shear strength of 0.17. Therefore, in the reliability study, failure was defined as any realization that created a probability that the mean normalized shear strength would be less than 0.17. The coefficient of variation that caused the mean normalized shear strength to be 0.17 in the random finite-element method was determined to be 0.65 and that would cause a probability of failure equal to 0.38. As can be seen in Figure 2-7, increasing the variability in the soil mass by increasing the coefficient of variations, V_c, increases the probability of failure at all scales of fluctuation. A uniform soil mass is represented by a large scale of fluctuation, θ_c, with an upper limit of infinity. For this example, less variable cases, with V_c less than 0.65, creates a greater probability of failure in soil masses that are strongly correlated than lesser correlated soil masses. This is because weakly correlated structures do not readily allow weak elements to connect to cause a weaker failure surface; therefore, such a case would be less likely to fail than a more uniform case. Conversely, cases with greater variation, such that the V_c is greater than 0.65, the uniform case of θ_c equal to infinity underestimates the probability of failure. With greater variation in the soil parameters, the authors suggest that the much weaker elements in poorly correlated soil masses dominate the strength and cause failure more often.

.

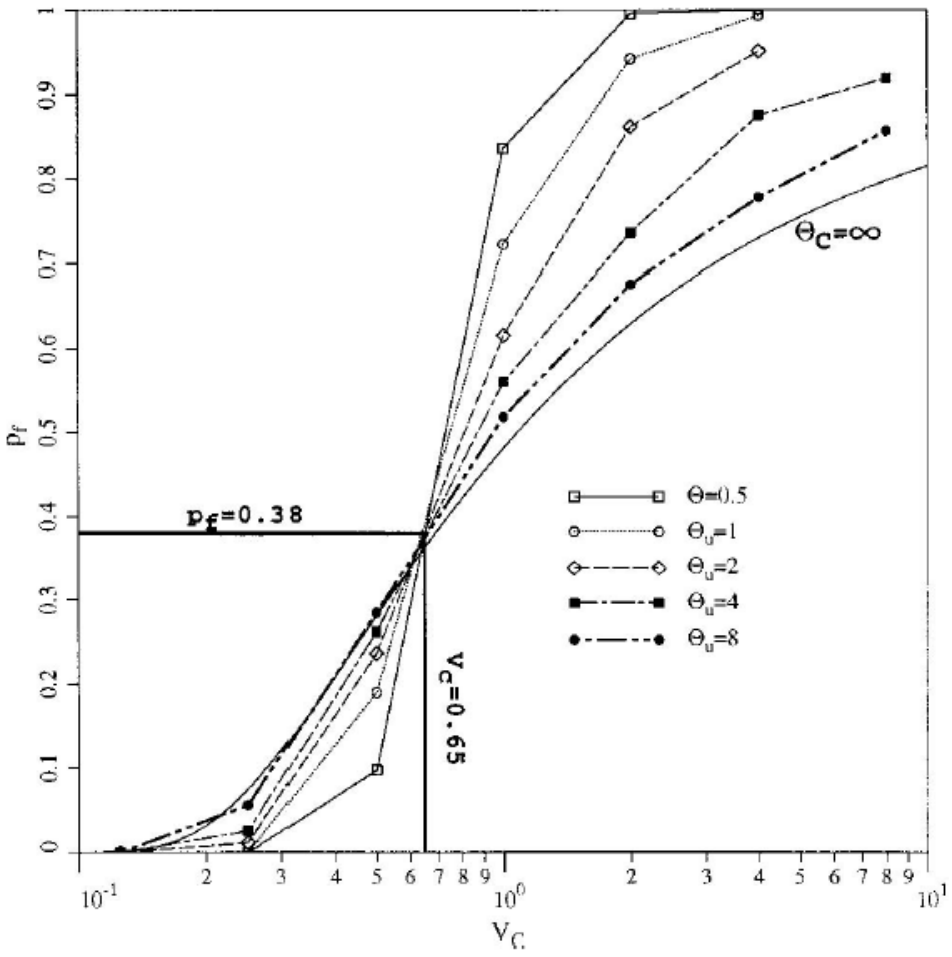

Figure 2-7: Assuming an infinite scale of fluctuation, θ_c, the probability of failure, p_f, will be overestimated in this example if the coefficient of variation, V_c, is below 0.65. Conversely, the probability of failure will be underestimated in a case with a coefficient of variation above 0.65 if a homogeneous soil mass (infinite θ_c) is assumed.

While the parametric study is useful for evaluating the effects of various properties, practicing engineers must evaluate the site materials using actual laboratory or in-situ measurements. Slope stability analysis requires the input of the shear strength of the material. Undrained shear strength can be estimated indirectly using the measurements obtained from CPT soundings using Equation 3 (Robertson 2013).

$$s_u = (q_t - \sigma_{vo})/N_{kt} \quad \text{Eqn. 3}$$

where s_u is the undrained shear strength, q_t it the corrected cone tip resistance, σ_{vo} is the total vertical stress, and N_{kt} is the cone factor chosen based on soil stiffness, OCR and soil sensitivity. The cone factor can be estimated by Equation 4:

$$N_{kt} = 10.5 + 7\log(F_r) \quad \text{Eqn. 4}$$

where F_r is the normalized friction ratio.

Since the shear strength is a function of both the cone tip resistance and the friction ratio, consideration of the correlation of both measurements would need to be considered when analyzing the reliability of a slope. Also, consideration that a transformation uncertainty is introduced into the analysis when using an indirect measurement from the CPT data is important as it adds an additional source of uncertainty.

2.12 Luo & Juang

While Griffiths and Fenton's study clearly illustrates the effect of the scale of fluctuation as a measure of soil correlation in slope stability; these concepts could also be applied to other geotechnical projects, such as drilled shafts and piles.

Luo and Juang (2012) reported a new approach to incorporate spatial variability into the design of drilled shafts in loose sand. The variability in the friction angle for the side and tip resistance was estimated using the first-order reliability method using spatial averages and a spreadsheet instead of the more complex random field modeling. Spatial averages use a variance reduction factor, which is a function of the scale of fluctuation and the depth interval, to adjust the variance of the soil measurement to account for correlation.

A parametric analysis was performed to determine the effect of the scale of fluctuation and coefficient of variation of the angle of internal friction; therefore, all other parameters were constant. As shown in Figure 2-8, the coefficient of variation, was set at 0.10, 0.15 and 0.20 and the scale of fluctuation, θ, ranged from 0.5 m (1.6 ft) to 100 m (328 ft). The authors indicate that typical range for the vertical scale of fluctuation in soil is 0.5 to 3 m (1.6 to 9.8 ft). The largest values of scale of fluctuation represent a very strongly correlated or uniform field. If variability and correlation is ignored, a homogenous, uniform field of properties is usually assumed. Therefore, the largest values of the scale of fluctuation shown in Figure 2-8 can be considered to be equivalent to the results of a uniform soil profile. The plot shows an increase in the probability of failure for drilled shafts as the scale of fluctuation increases or the soil profile becomes more correlated. Therefore, the actual probability of failure may be far less than would be calculated in a reliability analysis ignoring the scale of fluctuation. This would likely result in an overly conservative and more expensive design. The authors also examined minimal depths of embedment to achieve a given probability of failure and found that as the scale of fluctuation was increased, which moves the soil mass closer to uniformity, the required depth increased. For example, to achieve the same probability of failure, at a set diameter of 0.9 m, the required depths for scales of fluctuation of 0.5 m, 3 m, and infinity were 4.8 m, 5.8 m and 6.2 m, respectively. Therefore, unless the soil profile is strictly uniform, the depth could be overdesigned by nearly 30%.

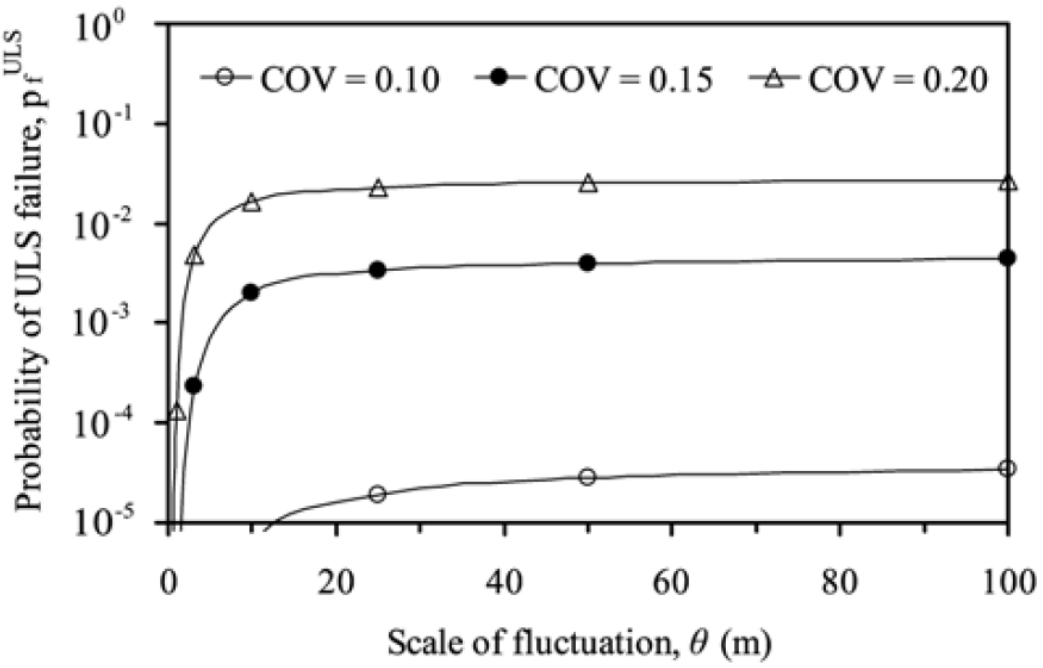

Figure 2-8: Probability of failure for the Ultimate Limit State versus the Scale of Fluctuation for drilled shafts in sand. (from Luo and Juang, 2012)

While Luo and Juang's study examined the correlation of the angle of internal friction, similar reliability studies could be performed using the correlation results from Sutton's thesis to similarly determine deep foundation capacities as correlations have been established using CPT measurements as direct methods for estimating pile resistance (Eslami and Fellinius 1997). The Schmertmann and Nottingham method uses the sleeve friction and cone resistance to estimate the unit shaft resistance and unit toe resistance using the Equations 5 and 6 (Eslami and Fellinius 1997).

$$r_s = Kf_s \quad \text{Eqn. 5}$$

where r_s is the unit shaft resistance, K is a dimensionless coefficient, and f_s is the sleeve friction.

$$r_t = N_c S_u \quad \text{Eqn. 6}$$

$$S_u = \frac{q_c}{N_k} \quad \text{Eqn. 7}$$

where r_t is the unit toe resistance, N_c is the bearing capacity factor, S_u is the undrained shear strength, q_c is the cone resistance, and N_k is a dimensionless coefficient.

2.13 Summary

Uncertainties in soil properties are inevitable in geotechnical engineering, but tools are available to systematically and logically deal with these unknowns. A great deal of study has previously been performed to attempt to specify and categorize potential errors in geotechnical measurements as summarized by Ding and Baecher & DeGroot. While good testing protocols, ample measurements, and an understanding of physical trends affecting these measurements are essential, inherent variability will always exist as a source of uncertainty. The objective of this study was to determine the scale of fluctuation of both the friction ratio and cone tip resistance of CPT soundings to help engineers become aware of the existence of the correlation in these measurements. The scale of fluctuation indicates the thickness of a soil layer with similar or correlated properties.

To better quantify this uncertainty, researchers have attempted to collect typical values of these inherent variabilities as reported by statistical parameters, such as mean, standard deviation, coefficient of variation, and correlation length as in Kulhawy et al. (1995). Limited data exist for the scale of fluctuation, also known as the correlation length. Typical values are useful for planning site investigations, estimating preliminary designs or designs based on limited data.

Large quantities of data are obtained by measuring the cone tip resistance and sleeve friction from a cone penetration test (CPT). CPT is gaining popularity and is a reliable in-situ test as described by Robertson. Lloret-Cabot created a method for estimating the scale of fluctuation with many or few soil property measurements. With large number of data points, there was no difference in their new method and simply fitting the autocorrelation model to the data as explained in Section 3.9.

Some studies have determined that the cone tip resistance is more correlated, as shown by a larger scale of fluctuation values, than the friction ratio for CPT. Firouzianbandpey et al. and Uzielli et al. explain that the volume of soil impacted by the cone tip is greater than that impacted by the sleeve friction; therefore, several measurements would include some of the same soil volume for closely spaced measurements.

Reliability studies, such as Griffiths and Fenton's, performed using random-field finite element procedures highlight the effect that correlation of soil properties have on the behavior and ultimately the performance of geotechnical projects. Ignoring the correlations of a given soil measurement or property could potentially be unconservative. Conversely, the reliability study by Luo and Juang show that ignoring

the correlation of soil properties would cause drilled shaft design to be overconservative.

The issue of soil variability and correlation is complex and requires further study. Sutton's thesis attempts to provide a set of typical values for the vertical scale of fluctuation at a sandy site for CPT measurements since few values have been provided in the literature. Also, as reliability analyses become more commonplace, there is a need for greater understanding of the complex nature of soil properties and their variation. This variation can be described using statistical parameters, including the scale of fluctuation. The scale of fluctuation is not a common property among practicing geotechnical engineers, and its importance is not widely recognized. Therefore, Sutton's thesis also seeks to analyze the difference in the scale of fluctuation for two different CPT measurements and introduce why the correlation of such parameters is important to successful and economical projects.

3.0 MATERIALS AND METHODS

3.1 Introduction

Quantifying the inherent variability for geotechnical properties requires an understanding of statistical properties such as the mean, standard deviation and scale of fluctuation. Less study has been reported on the scale of fluctuation as large quantities of data are required. Sutton's thesis performed the necessary computations to determine the vertical scale of fluctuation for an alluvial site. This information is useful to help engineers become aware of the variability of these measurements. The scale of fluctuation indicates the thickness of a soil layer with similar or correlated properties when measurements are modeled as a random field to identify the spatial variability. Data points can be expected to be similar within the vertical scale of fluctuation length. Conversely, data points farther apart than the length of scale of fluctuation will not be correlated. As the scale of fluctuation approaches zero the expected values of measurements will be uncorrelated or random. As the scale of fluctuation increases and approaches infinity, all measurements would be expected to be uniform. Previous studies indicate that, for an assumed homogeneous soil layer, the friction ratio has a smaller scale of fluctuation than the cone tip resistance.

As mentioned above, relatively large quantities of data are required for meaningful statistical analysis. Traditional geotechnical site investigations often employ infrequent sampling, such as every 2 to 5 feet depth. Such data are not close enough to assess the scale of fluctuation, since typical values of the scale of fluctuation are less than 5 feet; therefore, the number of data points is insufficient to estimate the scale of fluctuation statistically. The increased popularity of cone penetration testing (CPT) allows for the

measurement of many more data points. Measurements can be recorded every couple inches, which is likely close enough to capture the scale of fluctuation.

The detailed site investigation of a coal combustion residuals landfill in central Missouri, contained not only closely measured cone penetration data, but also many soundings to allow for a thorough analysis of the large 400-acre site. This large quantity of data is ideal for statistical analysis to compare to previous research. The quantity of data allowed for relatively computationally straight forward analysis as detailed below. The scale of fluctuation value was selected that best fit the field data to the exponential model.

3.2 Site Description

The current study evaluates the variability of a primarily sandy site located in central Missouri in Franklin County in Labadie, Missouri, which is approximately 40 miles southwest of Saint Louis, Missouri. The 400-acre site is the location of the Labadie Power Plant Utility Waste Landfill for Ameren UE (Figure 3-1). The data were obtained in 2009 as part of a detailed site investigation (DSI) performed according to the Missouri Department of Natural Resources (Gredell and Reitz & Jens 2011)

Building the coal combustion residuals landfill required a thorough hydrological assessment of the alluvial deposits, which included cone penetration tests. The site is located south of the Missouri River. The detailed site investigation (DSI) indicated that the site is within "an area of Holocene-age alluvial deposits largely derived from the Missouri River which lies within 1,400 feet of the northwest corner of the site" (Gredell and Reitz & Jens 2011). The site was relatively flat crop land and is comprised primarily of sand and gravel with some silt and clay. These alluvial deposits are generally about 100 feet thick overlying bedrock comprised of sandstone and dolomite. The bedrock formation is Joachim Dolomite, St. Peter Sandstone, Cotter-Jefferson City Dolomite or Powell Dolomite. Groundwater at the site is generally less than 20 feet below the surface and flows through the permeable sand and gravel as an unconfined aquifer. The depositional process was determined as fluvial due to its proximity to the Missouri river, both past and present positions. Fluvial deposits consist of "channel-filled sands and gravel bars, natural levees, crevasse splays, channel lag, floodplain, flood basin and cut-off meanders" (Gredell and Reitz & Jens 2011). The DSI indicates that historic

documents suggest a northward movement of the Missouri river which left filled-in channels and cut-off meanders.

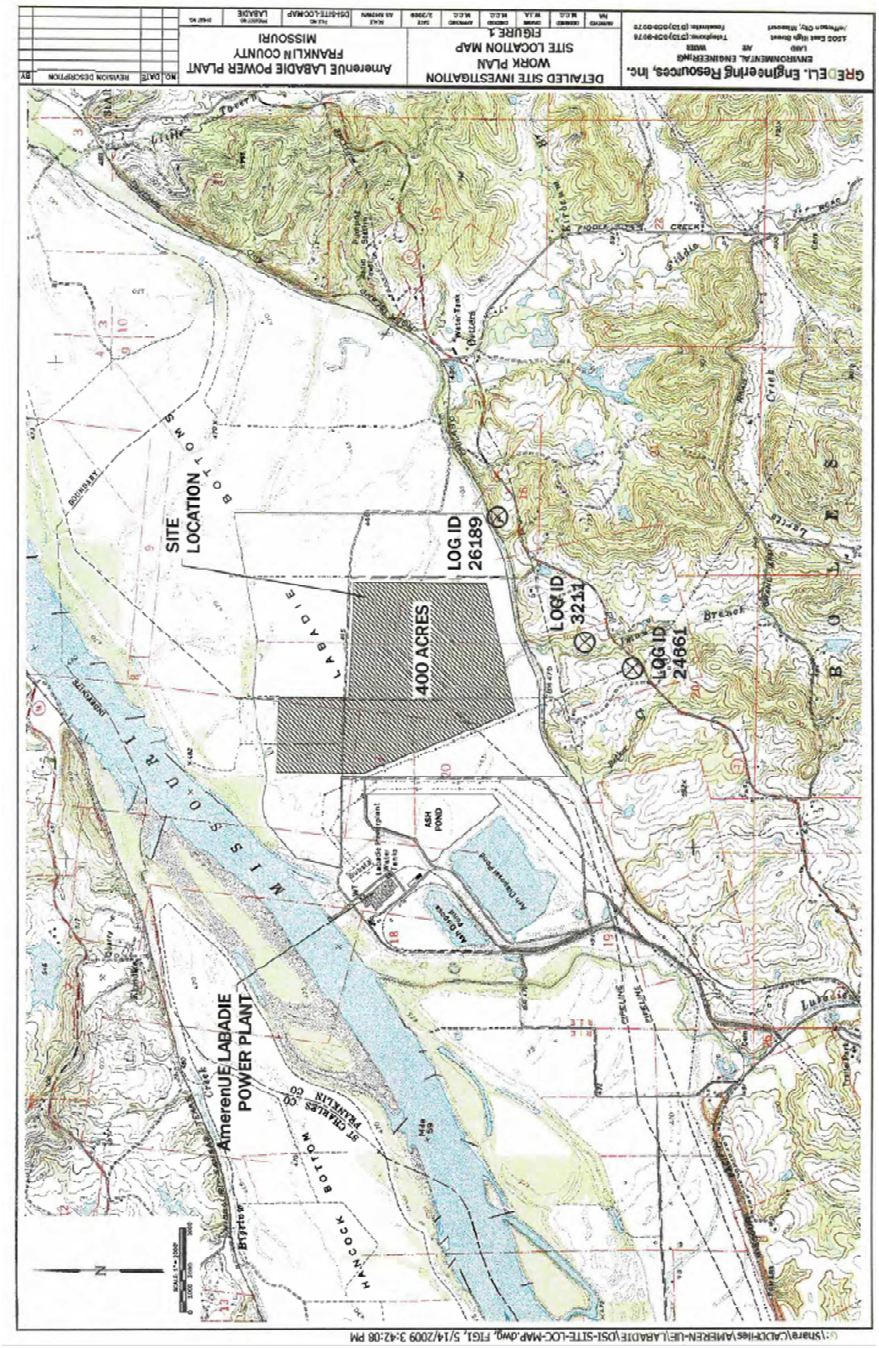

Figure 3-1 The site for the proposed utility waste landfill shows its close proximity to the Missouri River, which indicates alluvial composition (Gredell and Reitz & Jens 2011)

3.3 Site Investigation

The detailed site investigation included 97 piezometers, 22 geotechnical borings, and 93 CPT soundings completed in 2009 as part of a preliminary investigation. The locations were evenly spaced throughout the site as shown in Figure 3-2 using a global positioning system device. The borings and soundings were used to determine soil characteristics and depositional trends (Gredell and Reitz & Jens 2011) and the piezometers were used to assess the ground water characteristics.

3.4 Site Geology and Soils

The large number of borings provided a detailed assessment of the soils at the site. The soil is mostly sand, then gravel and silt and the smallest soil component is clay. The sand is "very fine- to very coarse-grained sequences spanning almost the entire depth of investigation to intervals of thin, discontinuous, relatively fine-grained material marked by a high degree of interbedding with silt and clay" (Gredell and Reitz & Jens 2011). Generally, the gravel layers were sandy gravel, as pure gravel was only found in a few locations. Overlaying the sand layers are 7-10 feet of silt and clay at the ground surface. These fine-grained soils varied from homogeneous layers to finely interbedded silt and clay layers. Also, interbedded with sand on the site at deeper depths are high plastic clay layers which were described as "gley"-colored, which is greyish blue. The DSI indicates that these "gley"colors were the results of anaerobic conditions where iron was chemically altered in "backswamp areas or within isolated, cut-off meander loops of a river" (Gredell and Reitz & Jens 2011).

These soil layers varied throughout the site as shown in cross-sections from the DSI presented as Figures 3-3 to 3-5. The results from a typical CPT sounding is shown in

Figure 3-6 and all CPT logs are provided in Appendix A. Generally, the soils became less fine grained with increasing depth. "This vertical sequencing is typical of fluvially derived sediments deposited during the ebb and flow of flood events or during shifts of the main channel and associated tributaries and reflects the fact that the investigative area resides within a portion of the pre-channelized drainage pattern of the Missouri river alluvial plain" (Gredell and Reitz & Jens 2011).

The geology was described in the DSI (Gredell and Reitz & Jens 2011).

> "Regionally, the Labadie area is located along the northeastern limits of the Ozark Plateau Physiographic Province. This province typically marks the extent of the CambroOrdovician age outcrops constituting the "Ozark Hills" and transitions to the north into geologically younger rock formations assigned to the Mississippian and Pennsylvanian Systems, regionally known as the Glaciated Plains. The Missouri River marks the approximate boundary between these two provinces and is, in essence, an ice-marginal stream delineating the approximate southernmost extent of glaciation during the most recent glacial epochs. The site is located within the alluvial plain of the Missouri river. This area essentially has the configuration of a large river-marginal or point bar deposit that has accreted along the south side of the river valley as the main channel of the Missouri River progressively migrated northward away from the site."

Cross-sections from the DSI (Gredell and Reitz & Jens 2011) divide the stratigraphy into five categories: channel deposits, channel margin/splay deposits, flood plain/levee

deposits, flood basin deposits and backswamp/cut-off deposits as shown in Figures 3-3 to 3-5. Channel deposits generally are comprised of well-graded, coarse to very coarse sands with trace to abundant gravel created as bar deposits. Channel margin/splay deposits are similar to channel deposits but with smaller, medium grain size sand that is poorly graded with less gravel. Channel margin/splay deposits were created along the edge of channels where the current was slower or deposited during a flood. Flood plain/levee deposits are categorized as poorly-graded fine-grained sand that is relatively thick and homogeneous and is the most common type of deposit encountered at the site. CPT soundings describe this deposit as sand, sand to silty sand, or silty sand to sandy silt. The layers were deposited during river flooding. Results of a typical sounding is shown in Figure 3-7. Flood basin deposits consist of silt and clay with thin sand layers at the ground surface. They were deposited during "low-energy/high sediment loading seen in the backwaters of major flood events" (Gredell and Reitz & Jens 2011). Finally, backswamp/cut-off deposits consist of highly variable thin, interbedded layers of sand, silt, and high plasticity clay that is "gley" colored, which indicated an anaerobic condition.

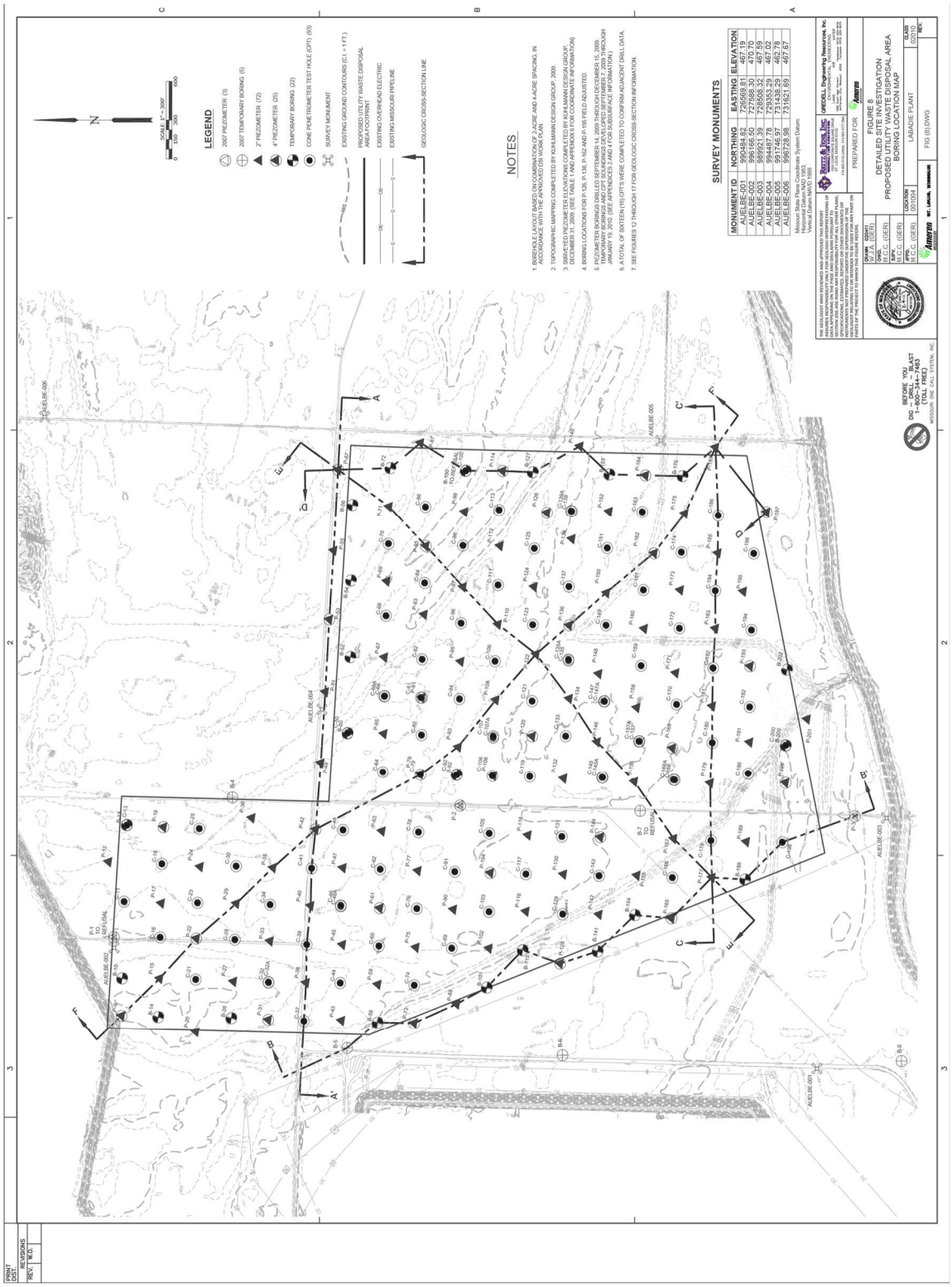

Figure 3-2 Boring and sounding locations and cross-sections (Gredell and Reitz & Jens 2011)

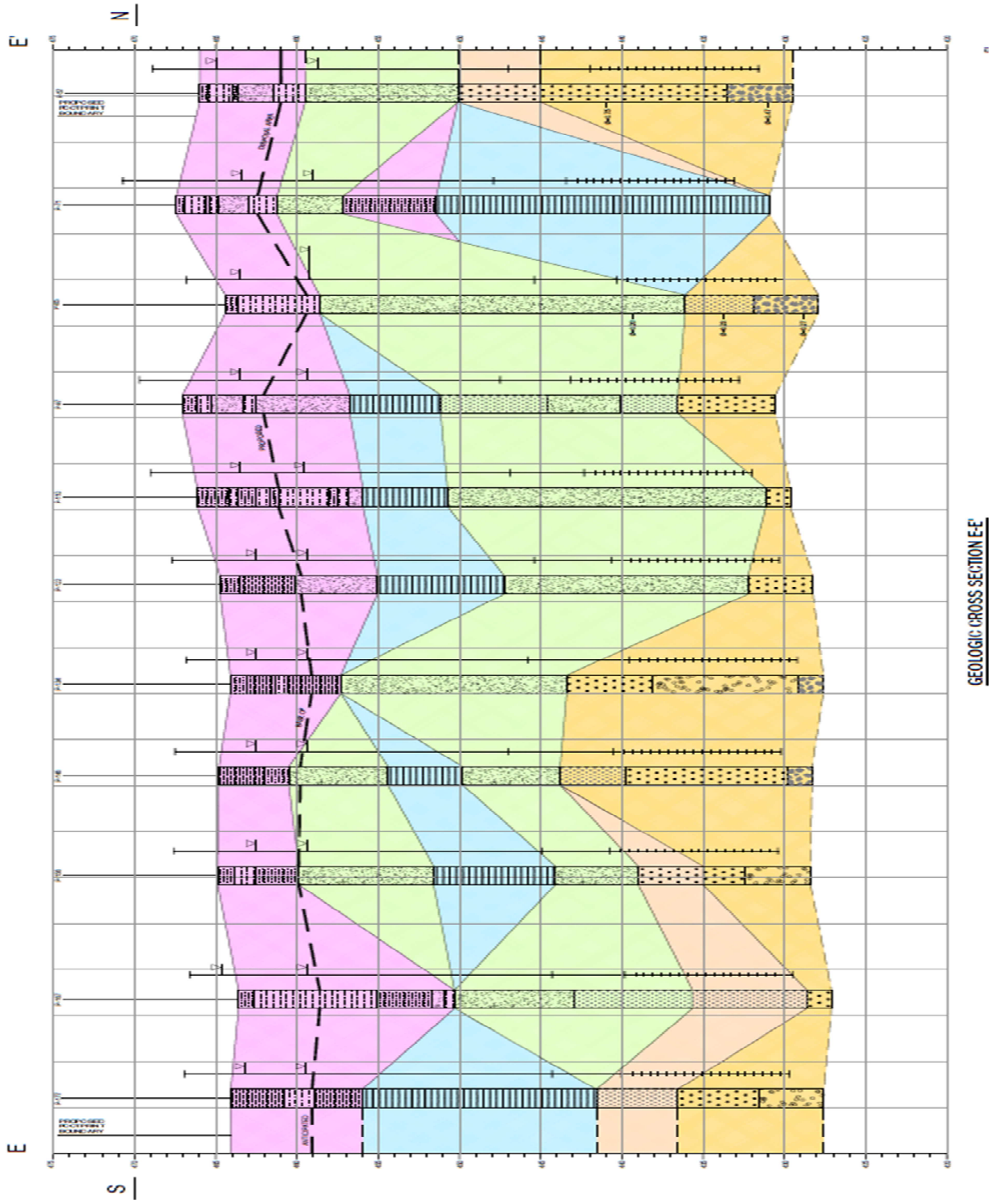

Figure 3-3 Site Stratigraphy: Cross-Section E-E' (Gredell and Reitz & Jens 2011)

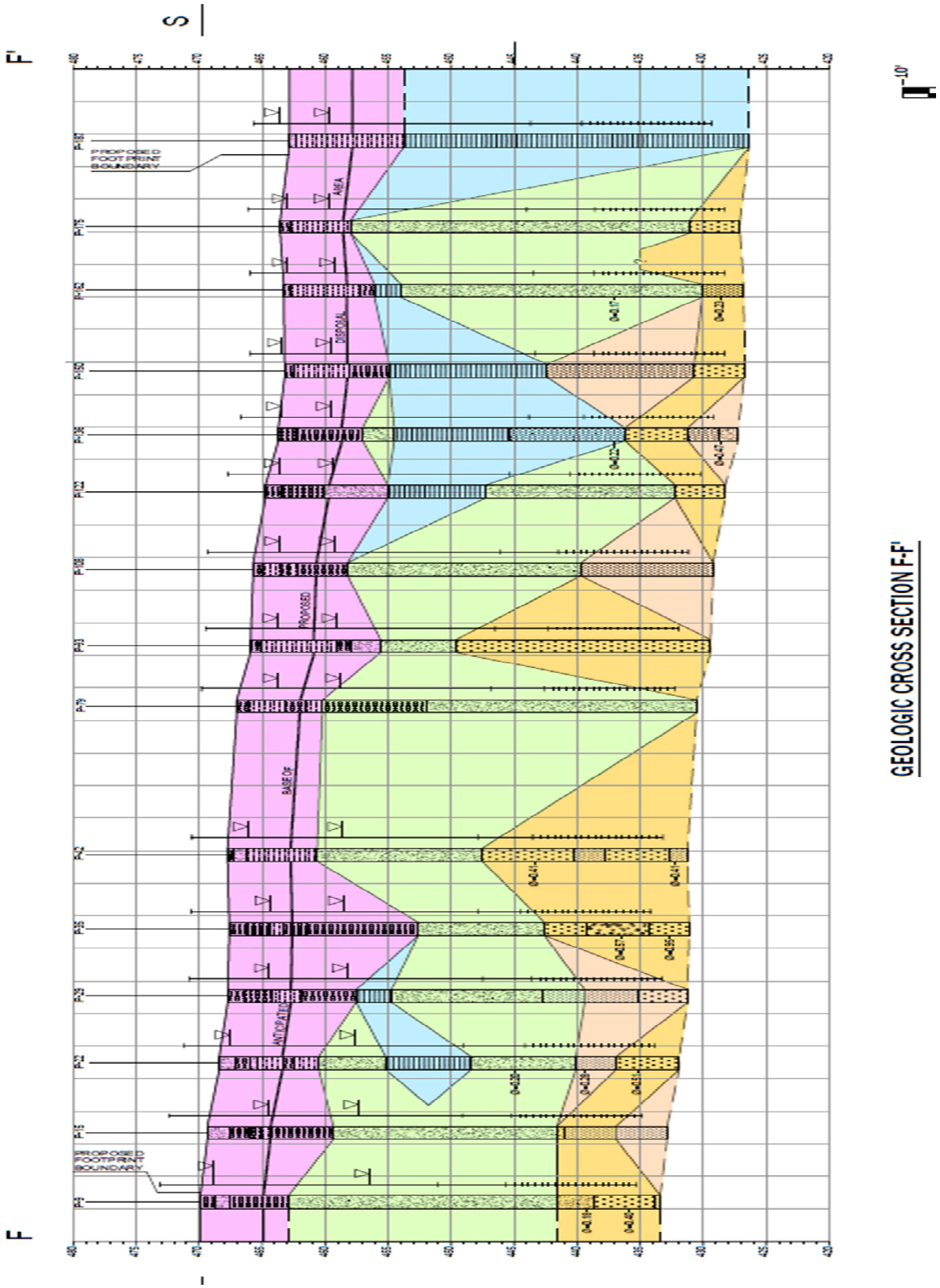

Figure 3-4 Site Stratigraphy: Cross-Section F-F' (Gredell and Reitz & Jens 2011)

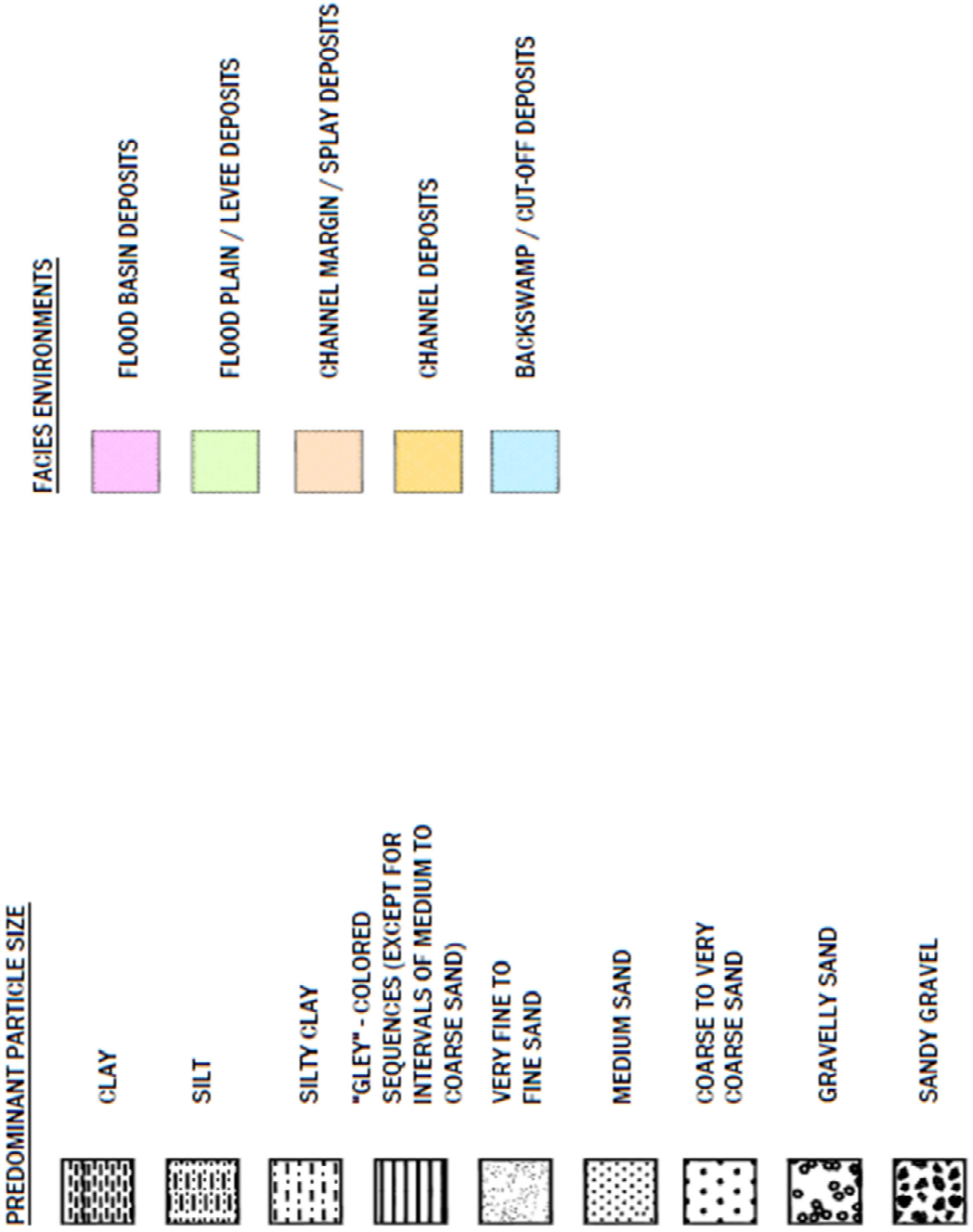

Figure 3-5: Legend for Figure 3-3 and Figure 3-4 (Gredell and Reitz & Jens 2011)

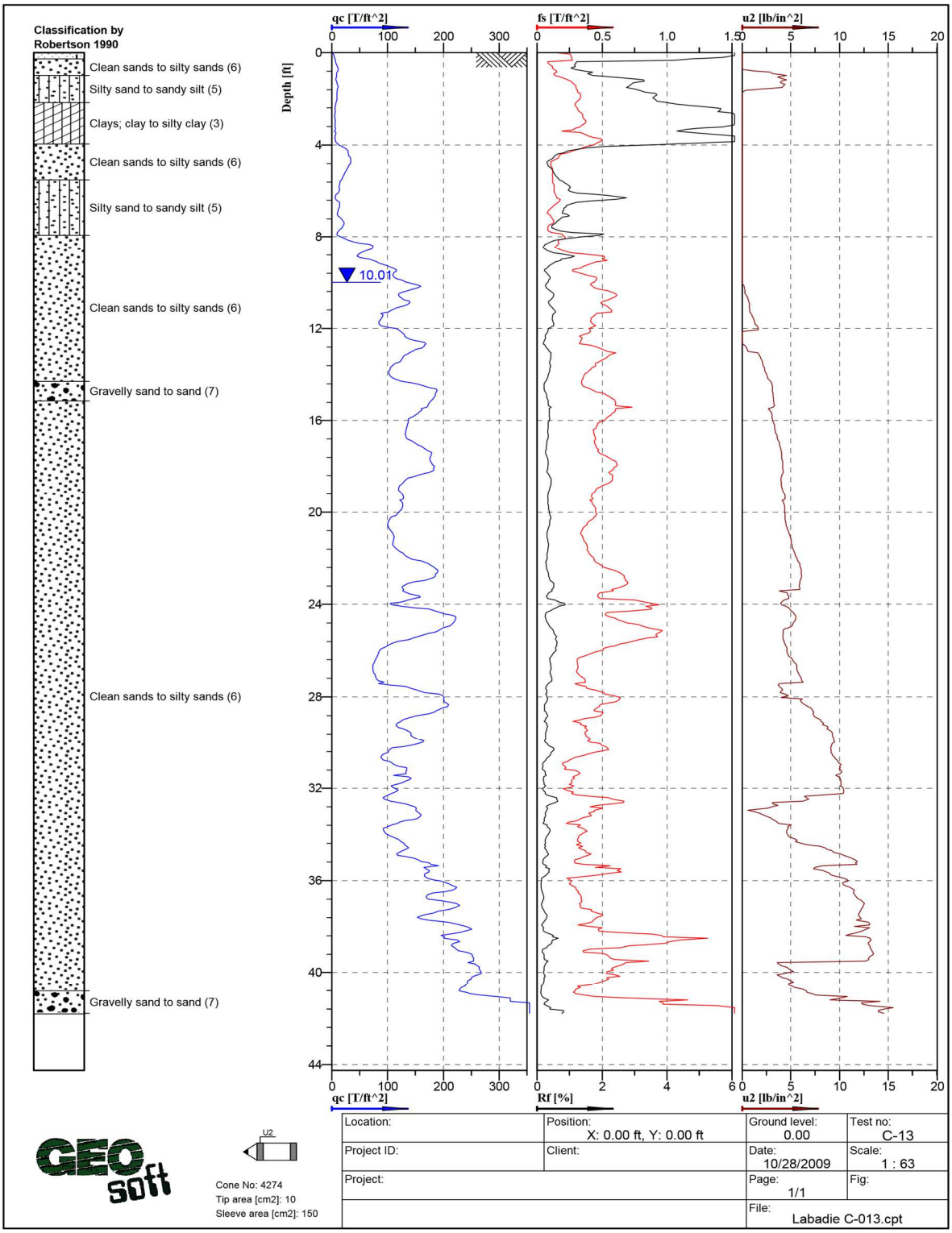

Figure 3-6 Typical Cone Penetration Test (CPT) Sounding (Gredell and Reitz & Jens 2011)

3.5 Soil Identification and Classification

Cone Penetration Tests were performed throughout the site according to standard ASTM D 577807, and measurements were recorded every 2 cm. *CPT Pro* software was used to classify layers greater than 0.5 feet as one of nine soil behavior types according to the normalized cone tip resistance and friction ratio as shown in Figure 3-7 (Robertson and Cabal 2015, Robertson 1990, Robertson 2016).

According to Robertson (1990), the CPT classification charts cannot classify soils based on the composition, as in the Unified Soil Classification System which includes grain size and plasticity. The Robertson classification charts classify soil based on behavior, such as "strength, stiffness, compressibility and drainage" of soils near the advancing probe (Robertson 1990, 2016). While the 1990 Robertson method maintains composition-based labels, such as sand and clay, Robertson suggests a transition to more behavior-based labels, such as clay-like – contractive, transitional and sand-like – dilative (2016). Additionally, Robertson (2016) recommends using classification charts with the normalized cone tip resistance and friction ratio instead of classifying with B_q and normalized cone tip resistance as measurements of u_2, which is the pore water pressure behind the cone tip, are sometimes not as reliable due to a lack of saturation. Therefore, in this thesis, the homogeneous soil layers were determined with the normalized cone tip resistance and friction ratio as shown in Figure 3-7. The Robertson 1990 classification system is more reliable than the previous Robertson 1986 classification system as it accounts for the stresses by normalizing the data as discussed below. In order to compare past research and the original detailed site investigation, this paper will use traditional soil classifications: gravel, sand, silt and clay.

After obtaining homogeneous soil units, as classified by Robertson 1990, layers thicker than approximately 4 feet were further analyzed as zero-mean random fields to find the correlation length as discussed in Sections 3.6 through 3.9.

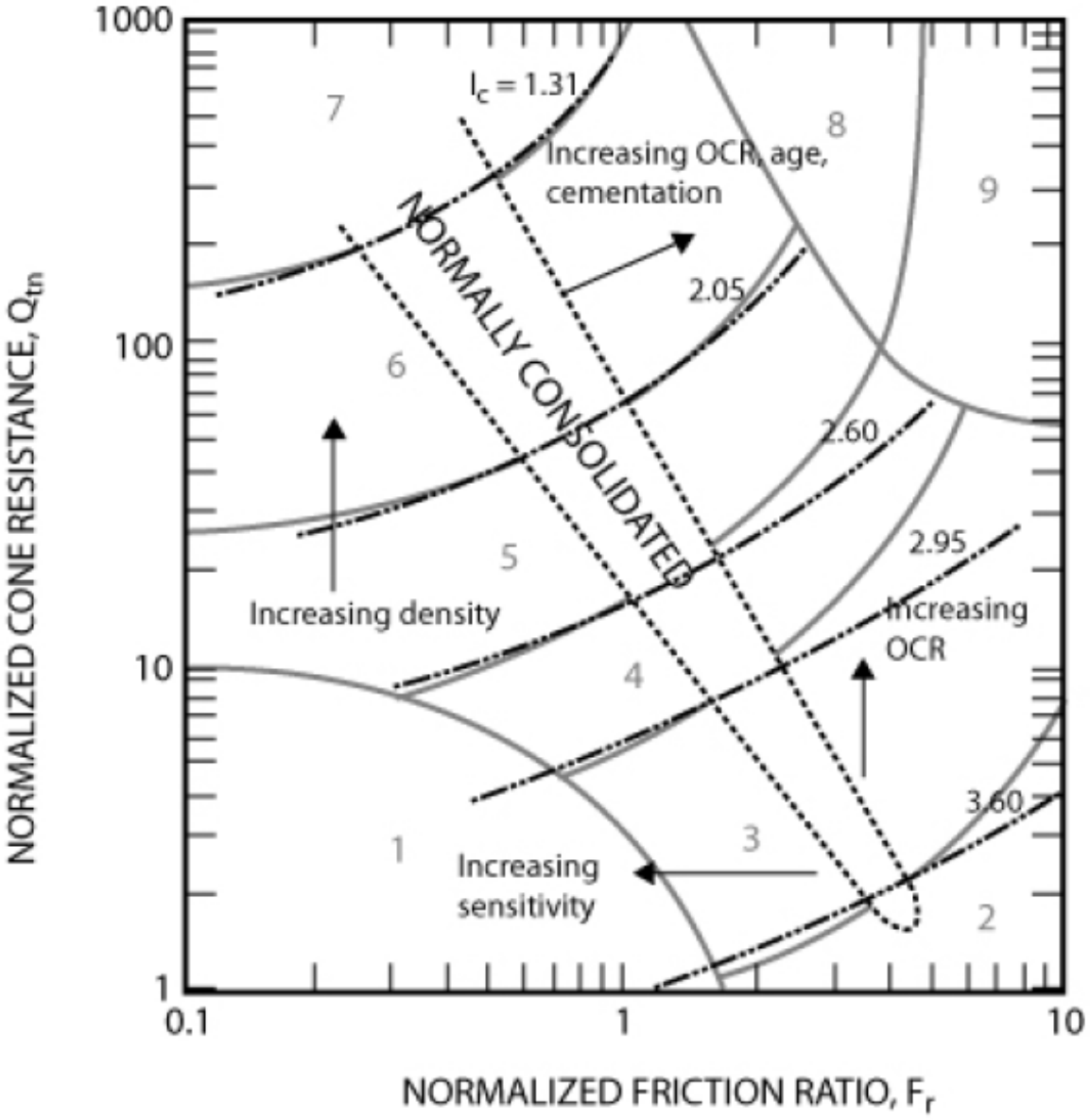

Figure 3-7 Robertson Classification 1990 Chart from Robertson and Cabal (2015).

1. Sensitive Fine Grained
2. Organic Soils -Peats
3. Clays – Clays to Silty Clay
4. Silt Mixture – Clayey Silt to Silty Clay
5. Sand Mixtures – Silty Sand to Sandy Silt
6. Sands – Clean Sand to Silty Sand
7. Gravelly Sand to Sand
8. Very Stiff Sand to Clayey Sand
9. Very Stiff, fined grained

3.6 Normalizing Data for Statistical Analysis

CPT data have a non-linear relationship with overburden stress (Moss et al. 2006, Uzielli 2005a), and this trend should be removed before statistical analysis can be performed. Cohesive soils are affected by the overconsolidation ratio and cohesionless soils are affected by the relative density, lateral earth pressure, angularity, compressibility and crushing strength (Moss et al. 2006). The data can be considered as the sum of the assumed trend and a random component combined to create the actual data shown by CPT as shown in Figure 3-8 (Phoon & Kulhawy 1999, Jaska 2007). Removal of the trend will transform data into a random field, and failure to remove the trend can affect the statistical analysis. The final data set is a function of the removed trend; therefore, the assumed trend should be clearly defined and preferably have some justification in the physical realm as opposed to a mathematical manipulation. If the depth of the analysis is small, the difference in soil properties with depth may be negligible (Kulhawy et al. 1995).

Investigating the study of the effects of overburden on field testing data began with research by Olsen, who used databases of sand chamber tests and clay field tests to discern a relationship (Moss et al. 2006). Later Robertson and Wride made further refinement and the relationship is shown in Equation 8. Sutton's thesis maintained the exponents assigned to soil types as in Robertson & Wride's 1998 publication, "Evaluating Cyclic Liquefaction Potential Using the Cone Penetration Test." Firouzianbandpey corrected their measurements according to Equation 8 and suggests this method is used in most studies (2014).

To apply this overburden correction the soil layer must be homogeneous because the exponent, n, varies by soil type (Moss et al. 2006).

$$q_{c1N} = \left(\frac{q_c}{P_a}\right) C_{Q,} \qquad C_Q = \left(\frac{P_a}{\sigma'_{v0}}\right)^n \qquad \text{Eqn. 8}$$

where q_{c1N} is the normalized cone tip resistance, q_c is the measured cone tip resistance, C_Q is the correction for overburden stress, n is 0.5, 1.0, and 0.7 for cohesionless, cohesive and intermediate soils, respectively, σ'_{v0} is the effective vertical stress and P_a is the atmospheric pressure.

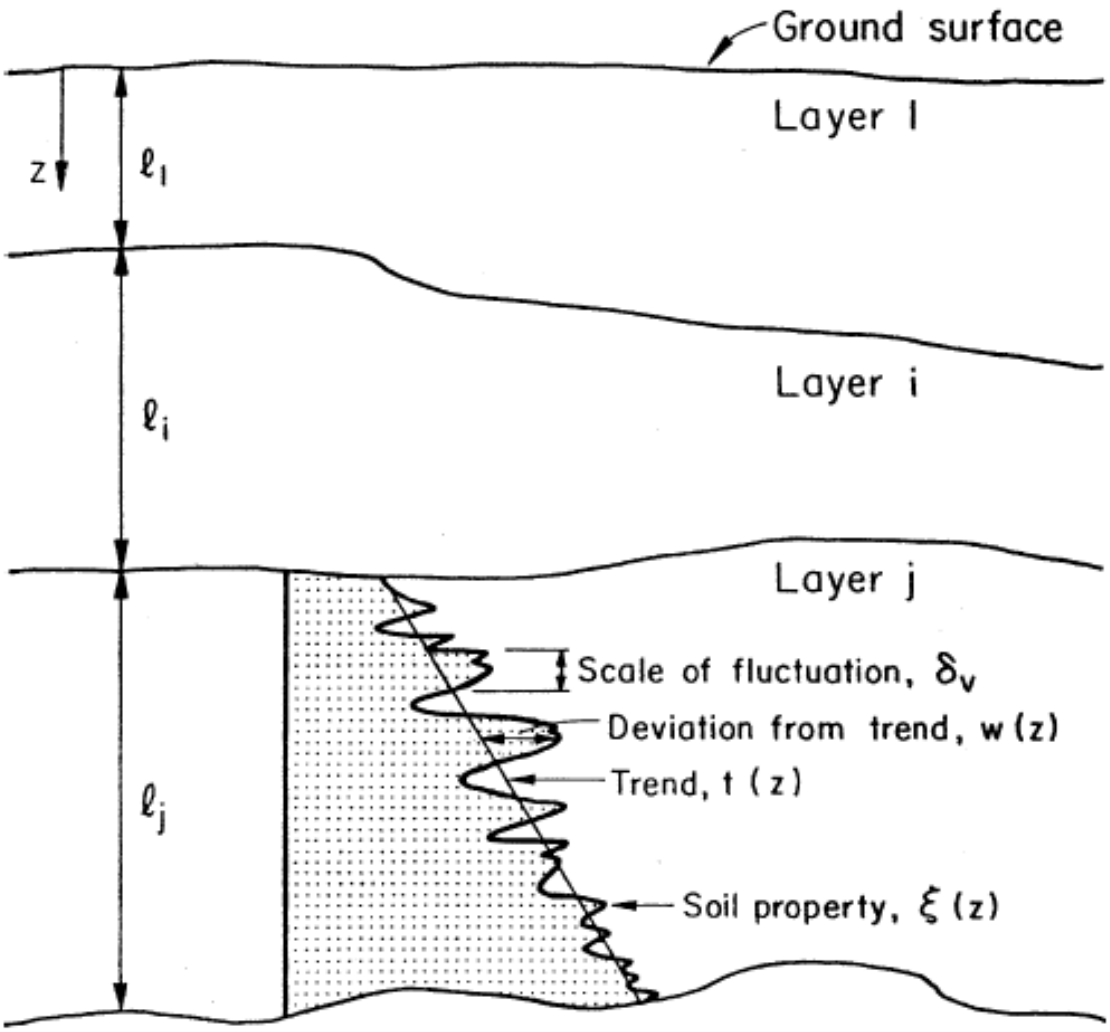

Figure 3-8 Variation in Soil Properties from Phoon and Kulhawy (1999)

At shallow depths the effective stress is low, and the value of C_Q increases unreasonably. Originally, according to Robertson and Wride, the upper limit for C_Q was 2 at low effective stresses (1998). According to Youd and Idriss (2001), the upper bound for C_Q was amended to 1.7 by National Center for Earthquake Engineering Research workshop consensus as a more reasonable limit, which was followed in this thesis. Firouzianbandpey states that limited research has been done on stress normalized CPT data (2014).

Also, the friction ratio was normalized for overburden stress using Equation 9:

Normalized friction ratio (Robertson, 1990):

$$F_R = \frac{f_s}{q_t - \sigma_{vo}} \qquad \text{Eqn. 9}$$

where f_s is the pore water pressure corrected friction measurement, q_t is the pore water pressure corrected cone tip resistance, and σ_{vo} is the total overburden stress.

Individual CPT soundings from this study were "time-invariant" as defined by Kulhawy et al. (1995) and each sounding wa completed within one day. All CPT soundings were completed from October 22, 2009, to December 28, 2009.

3.7 Random Fields

After the data were normalized for physical trends, it was converted to a random field with stationary mean and variance. The data were normalized to have a mean equal to zero and a standard deviation equal to 1 using Equation 10 (Firouzianbandpey et al. 2014):

$$x_i' = \frac{x_i - m_x}{\sigma_x} \quad \text{Eqn. 10}$$

where x_i' is the normalized data point, x_i is the original data point, m_x is the average or mean value, and σ_x is the standard deviation.

A random field is described by the COV and scale of fluctuation (Phoon & Kulhawy 1999). Phoon et al. (2003) state that the "fluctuating component is typically assumed to be statistically homogeneous or stationary without rigorous statistical verification" but if the soil layer is not truly statistically uniform then a bias can be introduced into the profile. Phoon et al. 2003 created a modified Bartlett test using Monte Carlo simulation to check the uniformity of a soil layer. Using statistical analysis could provide a logical method for dividing soil into homogeneous layers (Phoon et al. 2003).

3.8 Basic Definitions

After homogeneous soil layers were normalized, the following calculations were performed to determine the statistical properties.

Average or mean, m_x, represents the best estimate of a soil property (Baecher and Christian 2003). In Equation 11, x_i represents the data collected and n is the number of data points.

$$m_x = \left(\frac{1}{n}\right) \sum x_i \quad \text{Eqn. 11}$$

Standard deviation, σ_x, represents the uncertainty of a soil property (Baecher and Christian 2003).

$$\sigma_x = \sqrt{\frac{\sum (x_i - m_x)^2}{n}} \quad \text{Eqn. 12}$$

Coefficient of variation, COV, which estimates the relative dispersion (Baecher and Christian 2003).

$$COV = \frac{\sigma_x}{m_x} \quad \text{Eqn. 13}$$

Variance, Var(X), which represents the average scattering from the mean

$$Var(X) = \frac{1}{n}\sum_{i=1}^{n}(x_i - m_x)^2 = \sigma_x^2 \quad \text{Eqn. 14}$$

Scatter among data points can be described with the above basic statistical parameters, but variability can be further described with the correlation coefficients and scale of fluctuation. Correlated data tends to be all above or below the trend line (Nie et al. 2015). According to Lloret-Cabot et al. (2014), the scale of fluctuation "describes the spatial variability of a soil property in a random field." Data points can be expected to be similar within the length of the scale of fluctuation. Conversely, data points farther apart than the length of scale of fluctuation will not be correlated. As the scale of fluctuation approaches zero all points are uncorrelated. As the scale of fluctuation increases and approaches infinity, all data points in the field are uniform. Knowing typical values for the scale of fluctuation could help engineers estimate soil properties at nearby locations that were not sampled or tested during a site investigation.

Together the variance and correlation can help engineers better understand data from in-situ testing. Figure 3-9 (Baecher & DeGroot 1993) shows the relationship between variance, denoted σ^2 in Figure 3-9, and correlation length, which is labeled r_o. High variance from the trendline shows a greater range of values and low variance indicates that the data fall with a range of values more closely following the trendline. A large

scale of fluctuation (high autocovariance distance) shows that values are similar to values at nearby locations, and a soil layer with small scale of fluctuation (low autocovariance length) are not similar to nearby locations (Baecher & DeGroot 1993, Phoon et al. 2003). Soils deposited at similar times in similar ways are likely to be correlated with nearby measurement points.

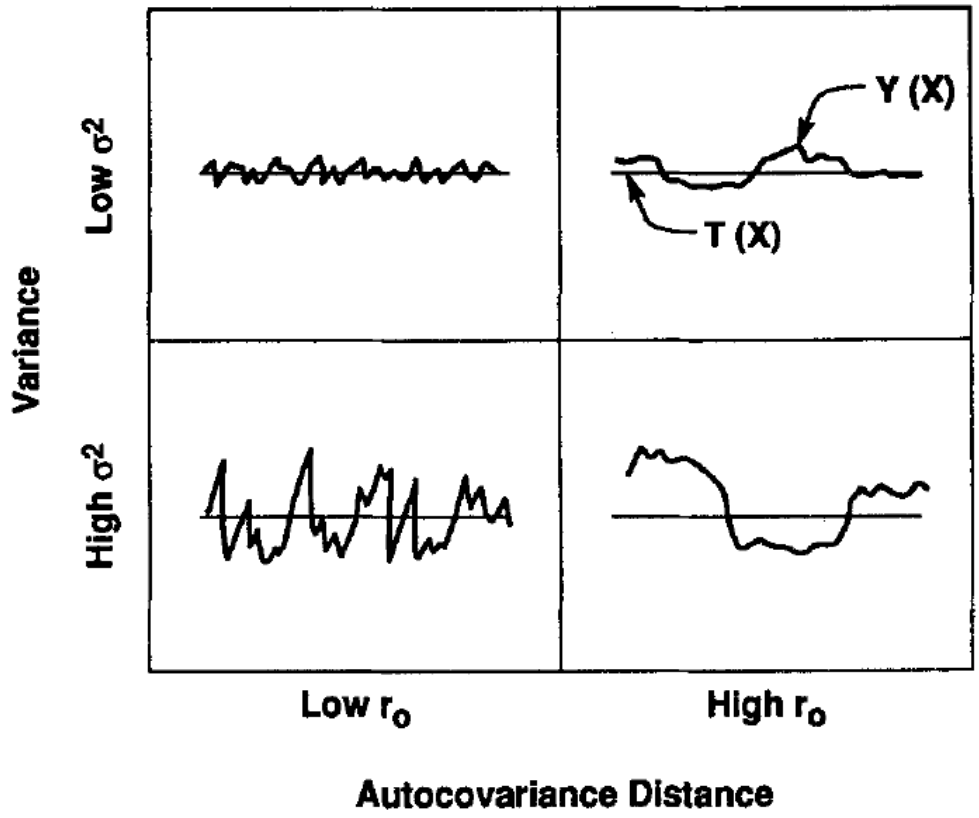

Figure 3-9 Relationship of Correlated Data from Baecher & DeGroot (1993)

3.9 Autocorrelation Function

While the variance can describe the behavior of one set of data, the covariance describes the relationship between two sets of data. Due to the relative ease of computations, moment estimators were used for this study. Basic statistical descriptors are used to estimate the covariance of two sets of data, X_1 and X_2. Since the current research contains large numbers of data points closely sampled, the traditional method of simply fitting a model to the data is deemed appropriate and the method suggested by Lloret-Cabot (2014) need not be used.

As shown in Equation 15, dividing the covariance by the standard deviations make the covariance into the dimensionless coefficient of correlation, ρ_{x1x2}, between X_1 and X_2.

$$\rho_{x_1,x_2} \equiv \frac{Cov[X_1,X_2]}{\sigma_1\sigma_2} \qquad \text{Eqn. 15}$$

where σ is the standard deviation of the data set.

Since the standard deviation of the data set is defined by:

$$\sigma = \sqrt{\frac{\sum(X-m)^2}{n}} \qquad \text{Eqn. 16}$$

Where X is the data point, n is the number of data points in the layer, and m is the mean.

Since the data are assumed to be stationary with a constant mean and standard deviation, the equation simplified to assume that σ_1 equals σ_2, so:

$$\sigma_1\sigma_2 = \frac{\sum(X_1-m)^2}{n} \qquad \text{Eqn. 17}$$

The covariance can be written as:

$$Cov[X_1, X_2] = \frac{\sum(X_1 - m)(X_2 - m)}{n} \quad \text{Eqn. 18}$$

Therefore, the correlation coefficient is

$$\rho_{x_1,x_2} \equiv \frac{\sum(X_1 - m)(X_2 - m)}{\sum(X_1 - m)^2} \quad \text{Eqn. 19}$$

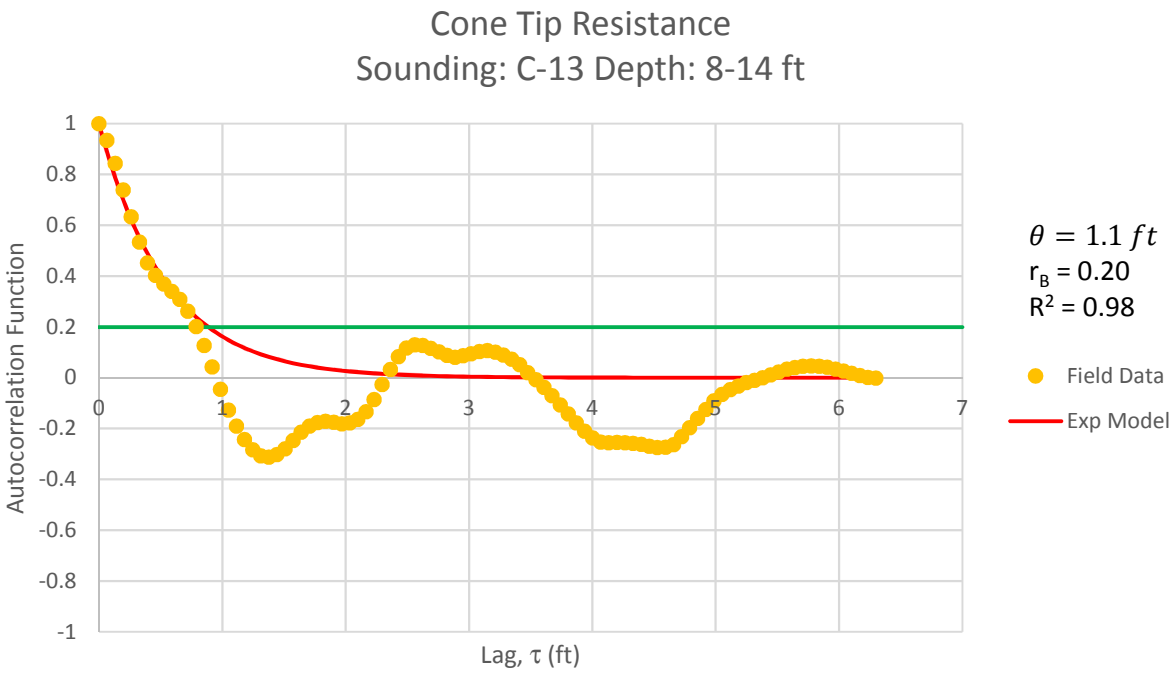

Figure 3-10 Typical Results - Cone tip resistance with Scale of Fluctuation Equal to 1.1 feet

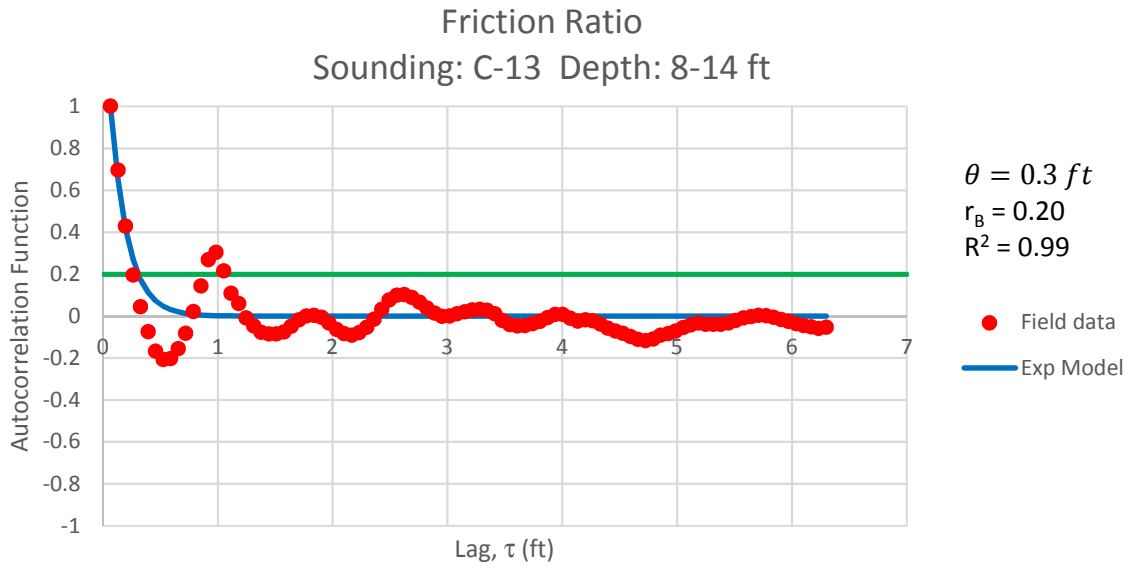

Figure 3-11 Typical Results - Friction Ratio with Scale of Fluctuation Equal to 0.3 feet

Since the data being compared were the same type of data, the correlation coefficient is termed the autocorrelation coefficient or function, as shown along the y-axis in Figures 3-10 and 3-11.

The autocorrelation coefficient will be a number between -1 and +1. The closer to either extreme indicates a more strongly linearly correlated relationship, negatively correlated if -1 and directly correlated if +1 (Kulhawy et al. 1995, Baecher 1986). As the correlation coefficient approaches zero there is no relationship between two data sets. One would expect that data from a homogeneous soil unit would be more uniform for a given soil property (Kulhawy et al. 1995). The following categories were suggested by Jaska et al. (2007).

- Absolute value of correlation is greater than or equal to 0.8 – Strong correlation
- Absolute value of correlation is between 0.2 and 0.8 – Correlation exists
- Absolute value of correlation is less than or equal to 0.2 – Weak correlation and independent points

For geomaterials, a large value for the scale of fluctuation indicates a soil which slowly fluctuates about the trend which is a more "continuous deposit" (Jaska et al. 2007). A small scale of fluctuation value indicates a geomaterial that varies more sporadically about the trend (Jaska et al. 2007).

For the data at Labadie, each data point was sampled at intervals of 0.066 feet. The distance is termed lags of 0.066-foot increments and the coefficient of correlation was determined at increasing lags, such as 0.066 ft, 0.132 ft, 0.198 ft, 0.264 ft….H, where H is the layer thickness.

3.10 Scale of Fluctuation/Autocorrelation Length

After the data are transformed to a de-trended, zero-mean random field and the autocorrelation coefficient is calculated, the data can be fit to a variety of models to determine the autocorrelation length, also known as the scale of fluctuation. Several models have been used in the literature, including exponential, exponential oscillatory, quadratic exponential oscillatory, bilinear (Firouzianbandpey et al. 2014, Nie et al. 2015). Phoon et al. (2003) and Fenton (1999a) state that the single exponential autocorrelation model is most widely used and is shown in Equation 20.

$$\text{correlation coefficient, } \rho(\tau) = e^{\left(-\left(\frac{2|\tau|}{\theta}\right)\right)} \qquad \text{Eqn. 20}$$

where θ = scale of fluctuation (autocorrelation length) and τ = difference between two sequences of depth, or lag.

The model is a "finite scale model" because the correlation falls to zero very quickly after a separation distance, τ, larger than θ is reached (Fenton 1999). This can be seen an example of typical results in Figures 3-10 and 3-11. All results used for estimating the scale of fluctuation are provided in Appendix B.

The autocorrelation length can be calculated for all separation distances; but as the distance increases, autocorrelation length estimates worsen (Jaska et al. 1994, Jaska 2007). Some estimate that the autocorrelation equation is only valid up to maximum lag of less than ¼ of the total sampling length (Phoon et al. 2003, Nie et al. 2015). As in the research by Uzielli et al. (2005a, 2005b), this thesis only used data to estimate the

autocorrelation lengths where an estimated Barlett limit was exceeded as described below.

Typical plots used to determine the scale of fluctuation for the CPT sounding are shown in Figures 3-10 and 3-11. The coefficient of determination, R^2, was calculated only for the initial part of the curves where the Bartlett limit, r_B, was exceeded (Uzielli et al. 2005, Jaska et al. 1994, Jaska 2007):

$$r_B = \frac{1.96}{\sqrt{n_d}} \approx \frac{2}{\sqrt{N}} \quad \text{Eqn. 21}$$

where n_d is the number of data points in the homogeneous layer. Uzielli et al. (2005a) indicate that this equation is well-accepted as the limit where the correlation coefficient becomes unreliable and "are deemed not significantly different from zero inside the range +/- r_b." Also, Sutton's research followed Uzielli et al. (2005a) requirement that there must be at least four data points where the autocorrelation coefficient was greater than r_b to deem that soil layer uniform.

The sampling distance must be smaller than the correlation length or scale of fluctuation to calculate the scale of fluctuation correctly (Lloret-Cabot et al. 2014). If the true scale of fluctuation is 0.1 m and the data readings are 1 m apart, then estimating the scale of fluctuation accurately will not be possible. Also, if there is a small number of data points, then the estimated scale of fluctuation will be less reliable than if it were calculated with a larger number of data points according to Lloret-Cabot et al. (2014).

Uzielli et al. (2005a) stated that their study models inherent variability as "zero-mean weakly stationary random field with finite-scale correlation structure". Bouayad (2017)

concurs that statistical analysis requires stationary data by removing the trend from the field data. Stationarity indicates that the statistical properties such as autocovariance is the same at all locations (Baecher & DeGroot 1993, Elkateb et al. 2005a). Jaska (2007) referenced Baecher & Christian (2003) who indicate that generally soils may not truly be stationary as statistical analysis assumes.

According to Lloret-Cabot et. al (2014) random fields are used "to model soil heterogeneity (inherent variability) in advanced stochastic analyses." Once trend is removed, the data can often be considered a random field (Kulhawy et al. 1995) if several requirements can be met. Elkateb et al. (2005a) state that the trend need not be linear. The data are a homogeneous random variable that is statistically homogeneous if two things are true (Kulhawy et al. 1995, Jaska 2007, Phoon et al. 2003):

1. "the mean and variance do not change with depth"
2. "the correlation between the deviations at two different depths is a function only of their separation distance and not their absolute positions."

Kulhawy states that if the data are detrended the first point should be met. Also, the fluctuations should be nearly uniform (Kulhawy et al. 1995). Note that the detrended, homogeneous data are a result of the detrending model used which, in turn, could conceivable introduce further error or changes to the final results. Kulhawy states that the soil property is likely uniform if the data were used from a soil layer identified as homogeneous. For the purposes of this research, this assumption was considered true as that is the standard procedure in engineering practice. The data were classified according to the Robertson 1990 classification CPT method and then detrended within each homogeneous soil unit.

3.11 Summary

The site investigation of a 400-acre site for a coal combustion residual landfill in central Missouri provided a large quantity of cone penetration testing (CPT) data for a statistical variability analysis.

Nearly 100 CPT soundings were evenly spaced throughout the alluvial site near the Missouri River. The site consisted primarily of fine to coarse sand with some gravel layers underlying up to 10 feet of surface clays and silts deposited through the channel and along the flood plain as the rivers path has shifted. The data from the CPT soundings, the cone resistance and friction ratio, were analyzed using the CPT Pro software and classified according to the Robertson 1990 system. The Robertson 1990 classification system required that the data are normalized to account for the effects of overburden pressure.

One hundred ninety-six (196) uniform layers were initially identified, and the data from each layer were transformed into random fields and analyzed statistically. The mean, standard variance and coefficient of variation (COV) were calculated for each layer's data set. The random field of data was created by converting the data to a zero-mean, single standard deviation data sets.

While the mean, standard deviation and COV describe the overall properties of the data and its variability, the variability within the data can better be described by including the autocorrelation coefficient and correlation length. The relationship between different data points within the data set is described by the autocorrelation coefficient, which ranges from -1 to 1. The autocorrelation length, or scale of fluctuation, indicates the length that a data point is related to adjacent points. Points farther apart than the scale of

fluctuation will likely be unrelated or random, while points closer than the scale of fluctuation will likely be associated to nearby points. Therefore, the designer can estimate the variability of a given deposit or soil type.

4.0 RESULTS AND DISCUSSION

4.1 Introduction

The objective of this study is to determine the scale of fluctuation of both the friction ratio and cone tip resistance of CPT soundings to help engineers become aware of the variability of these measurements. Previous studies indicate that, for an assumed homogeneous soil layer, the friction ratio has a smaller vertical scale of fluctuation than the cone tip resistance. The scale of fluctuation is an indicator of the correlation of nearby soil parameters. Data points within the vertical scale of fluctuation are likely related to nearby locations, but data points farther apart than the length of scale of fluctuation will not be correlated and are considered randomly assigned.

The large volume of data from the detailed site investigation at a utility waste landfill in Missouri was synthesized into a statistical comparison between the variability in the measurements of the sleeve friction, presented as the friction ratio, and the cone tip resistance. The variability was represented by estimating the vertical scale of fluctuation for the cone tip resistance and friction ratio for homogeneous soil units (HSU). Nearly 200 soil layers were initially analyzed to fit the exponential model for the autocorrelation function. As described in Section 3.10, homogenous soil units with less than four points greater than the Bartlett limit or with a coefficient of determination less than 0.9 were eliminated due to the poor match to the model. Sixty-three layers were eliminated, but 133 soil layers were found to be a good fit with the model.

The final results of the analysis are shown below. The discussion of the differences between the scales of fluctuation for the cone tip resistance and the friction ratio is in Section 4.2. Several plots were analyzed in Section 4.3 to reveal trends in the data and to provide insight into the measurements.

4.2 Cone Tip Resistance and Friction Ratio Contrast

As can be seen in Tables 4-1 and 4-2, analyses of the CPT data from the Labadie site confirms previous research which states that the average vertical scale of fluctuation is less for the friction ratio (0.5 to 0.8 ft) than for the cone tip resistance (0.5 to 1.5 ft), except for the few clay samples where the scale of fluctuations were equivalent. This conclusion agrees with the findings of Firouzianbandpey et al. (2014) and Uzielli et al. (2005a, 2005b).

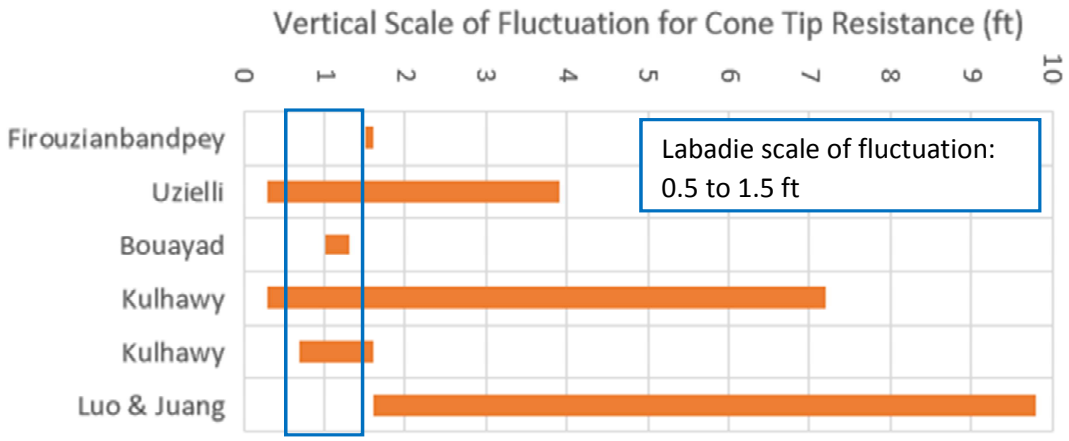

Figure 4-1: Sutton's results are within typical literature values for the cone tip resistance.

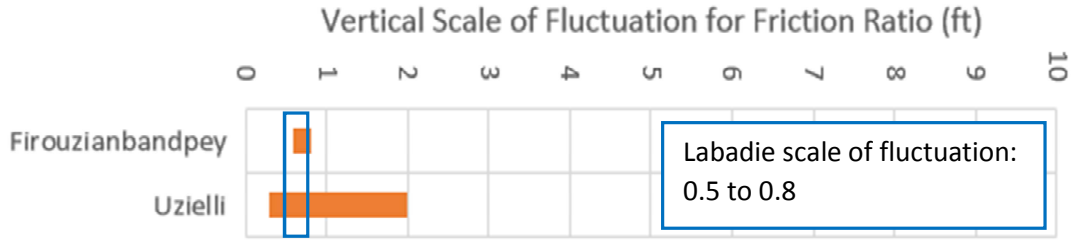

Figure 4-2: Sutton's results are within typical literature values for the friction ratio.

Also, these values for the scale of fluctuation for the cone tip resistance are within the 'typical' values listed by Kulhawy et al. discussed in Section 2.4. As shown in Figures 4-1 and 4-2, the results from the Labadie landfill are reasonable based on reported values in the literature. Kulhawy et al. (1995) did not provide data for estimated scale of fluctuation for the friction ratio. Uzielli et al. (2005a, 2005b) concluded that the normalized cone tip resistance (q_{c1N}) was more correlated than the friction ratio (F_R) with scales of fluctuations equal to 0.3 to 3.9 ft and 0.3 to 2.0 ft, respectively, for their study of over 300 soundings. The study by Firouzianbandpey et al. (2014) in Denmark also stated the same conclusion with average scales of fluctuation for normalized cone tip resistance (q_{c1N}) and friction ratio (F_R) of 1.6 ft and 0.7 ft, respectively. The amount of data for all soil types, except "Clean Sands to Silty Sands (6)" and "Gravelly Sand to Sand (7)" was too small to be conclusive. As described above, the site primarily consists of sands and gravels.

Table 4-1 Summary of Average Vertical Scale of Fluctuation Results for All HSU at the Labadie UWL Site

Soil Type	No. of HSU	Layer Thickness (ft)		Scale of Fluctuation (ft)					
				Normalized Cone Resistance			Normalized Friction Ratio		
		Min	Max	Min	Max	Avg	Min	Max	Avg
Clays; clay to silty clay (3)	8	4.1	8.5	0.3	1.9	0.7	0.04	0.6	0.3
Clayey silt to silty clay (4)	1	4.1		0.9		--	0.5		--
Silty sand to sandy silt (5)	2	4.1	5.0	0.5	1.6	1.1	0.5	1.5	1.0
Clean sands to silty sands (6)	157	4.1	30.0	0.3	5.0	1.3	0.02	2.0	0.7
Gravelly sand to sand (7)	28	3.9	12.0	0.6	3.5	1.6	0.1	3.5	0.8
Total	196								

Table 1 includes all data from the 196 initial homogeneous soil units as classified by the Robertson 1990 method. Removing homogeneous soil units (HSU) that did not conform to the required fit of the exponential model (R^2 equal to at least 0.9 for at least four points) eliminated 63 soil layers. With the poor fit layers removed, the overall result is still the same; the friction ratio is consistently less correlated than the cone tip resistance.

Table 4-2 Summary of Average Vertical Scale of Fluctuation Results for HSU with Fit to Autocorrelation Model ($R^2 \geq 0.9$) for the Labadie UWL Site

Soil Type	No. of HSU	Layer Thickness (ft)		Scale of Fluctuation (ft)					
				Normalized Cone Resistance			Normalized Friction Ratio		
		Min	Max	Min	Max	Avg	Min	Max	Avg
Clays; clay to silty clay (3)	2	5.2	6.0	0.4	0.5	0.5	0.5	0.5	0.5
Clayey silt to silty clay (4)	1	4.1		0.9		--	0.5		--
Silty sand to sandy silt (5)	2	4.1	5.0	0.5	1.6	1.1	0.5	1.5	1.0
Clean sands to silty sands (6)	108	4.1	30.0	0.3	3.6	1.3	0.1	2.0	0.7
Gravelly sand to sand (7)	20	3.9	11.9	0.6	3.5	1.5	0.3	1.5	0.8
Total	133								

Firouzianbandpey et al. (2014) and Uzielli et al. (2005a, 2005b) explain that the cone tip resistance is affected by failing a larger volume of soil than the side friction, which only measures the resistance of the soil adjacent to the sleeve as seen in Figure 4-1. Since the cone tip fails a larger volume of soil as compared to the sampling interval, several readings can have similar measurements and are, therefore, correlated.

The different soil volumes affected by the CPT probe can be shown by the diagram in Figure 4-3 which displays isolines of compression and the shear deformations of a CPT probe pushed into air-dried fine sand. Melnikov and Boldyrev measured the deformations shown by the particle image velocimetry technique. The research involved driving a CPT probe into a laboratory specimen of sand while obtaining photos every 3

seconds during the cone penetration and measuring the locations of markers attached to the inside of the observation glass measured to the nearest 0.01 mm. Figure 4-1 shows the areas of compression deformations on the left half of the image and areas of shear deformation on the right half of the image. The image also shows that the volume affected by the cone is approximately a cylinder with a radius of 4.3 times the diameter of the probe. As can be seen, the soil volume being displaced and, therefore, stressed is much smaller adjacent to the sleeve as contrasted to the soil volume being displaced and measured by the cone tip resistance.

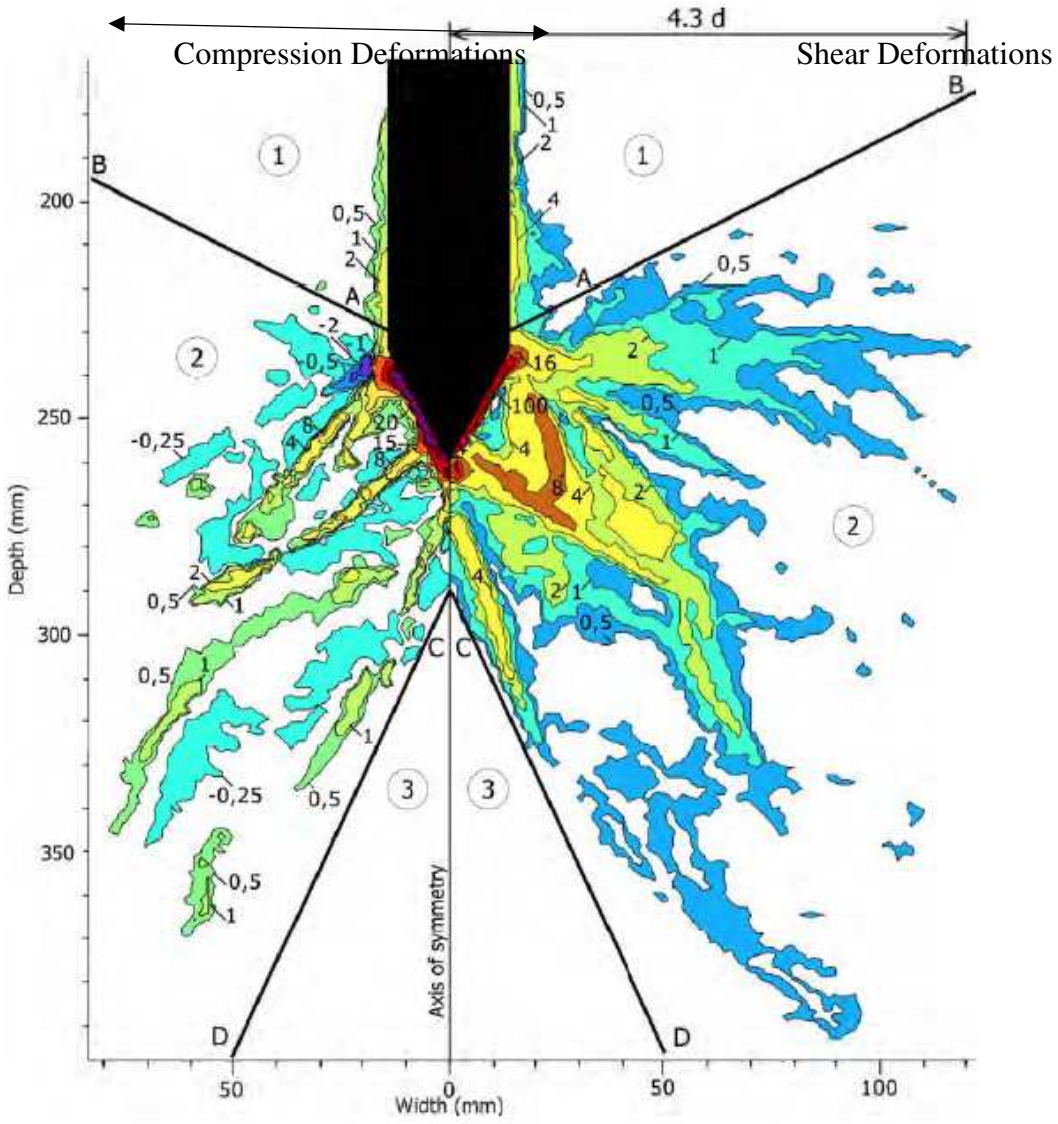

Figure 4-3 Deformations measured from CPT: The cone measures a larger volume of soil than the sleeve (Melnikov and Boldyrev 2014). The colored zones and numbers represent areas of different deformations. Shear is represented on the right. Compression is represented on the left with negative and positive values representing areas of compression and expansion respectively.

4.3 Trend Analysis

Data trends were analyzed to determine if trends would be revealed. Although the measurement spacing throughout all the soundings remained constant, 0.02 m, the number of samples varied from 61 to 468 since the total length of the assumed homogeneous layers varied. The results for all soil types with the required best fit are shown in Figure 4-2. No apparent trend, based on the number of samples for the cone tip resistance or friction ratio, was revealed. Therefore, the data appear unbiased in terms of sample length for the sampling rate employed in the investigation.

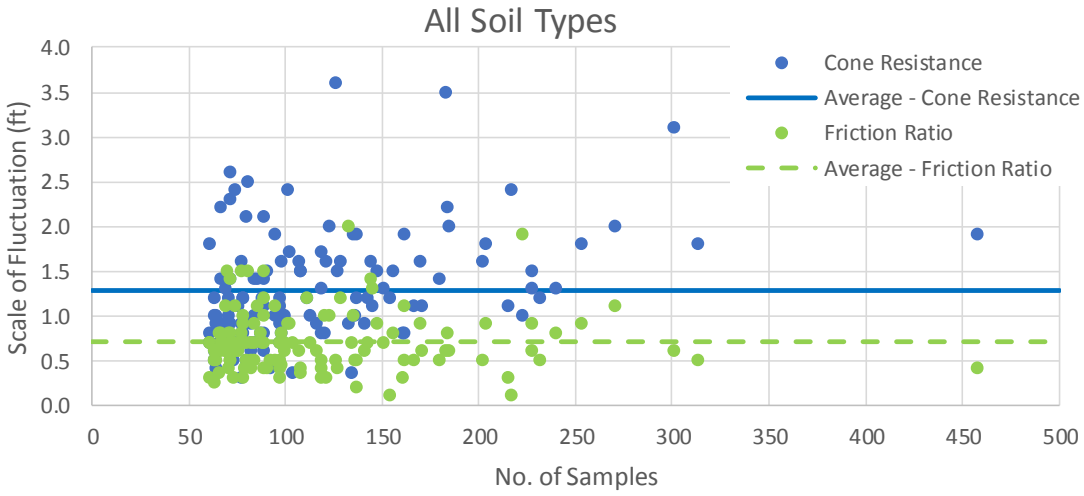

Figure 4-4 Scale of Fluctuation vs Number of Samples. No bias is apparent at any layer thickness for both cone tip resistance and friction ratio.

While the data appear stationary when considering the sample size, broad trends can be recognized for the CPT data at the Labadie, Missouri site when the soil types are examined. Figures 4-3, 4-4 and Table 4-2 demonstrate that generally as the particle size increases the average scale of fluctuation for both the cone tip resistance and the friction

type (except soil type #5) increases. The limited data for fine-grained soils makes this observation untenable.

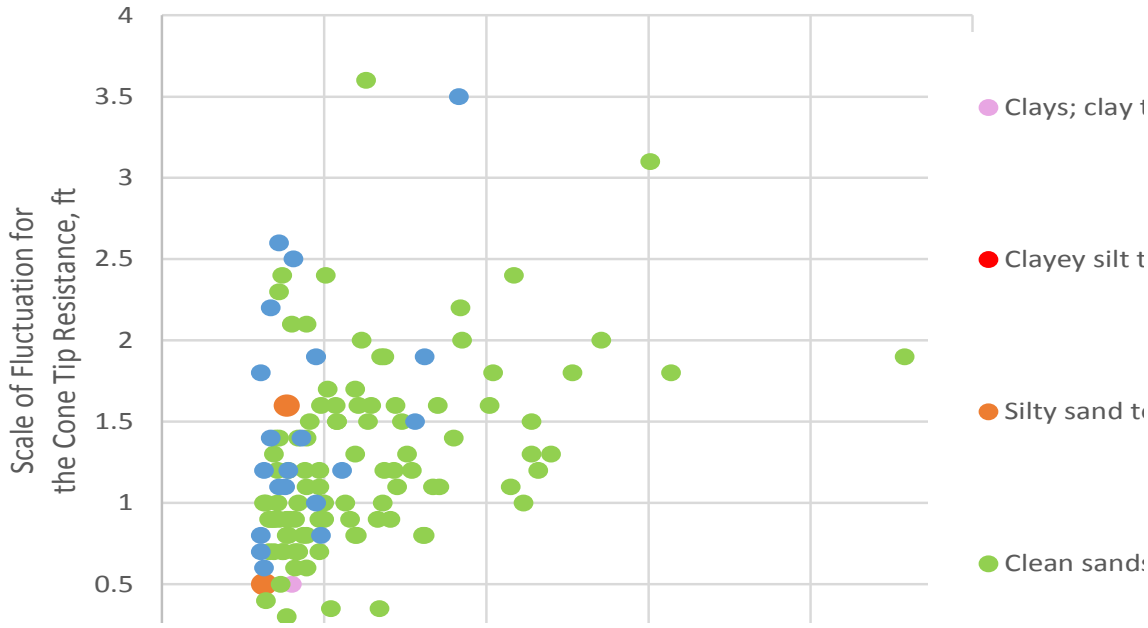

Figure 4-5 Cone Tip Resistance Results – Scale of Fluctuation vs Number of Samples

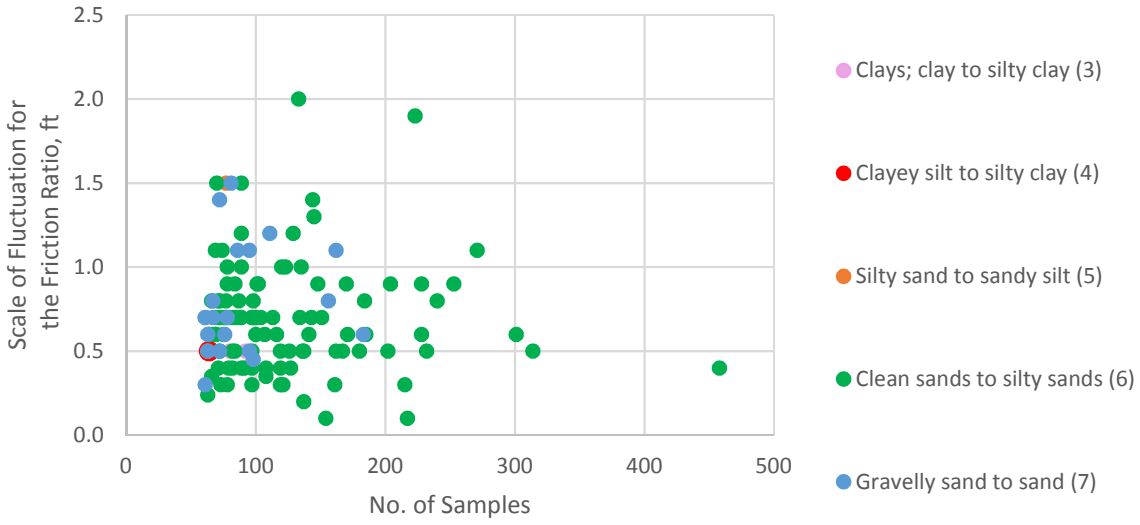

Figure 4-6: Friction Ratio Results – Scale of Fluctuation vs Number of Samples

Since both the coefficient of variation (COV) and the scale of fluctuation are indicators of variability, it would be expected that data sets with larger COVs would also have longer scales of fluctuation. Figures 4-5, 4-6, and 4-7 show the results of the data analyses. Both cone tip resistance and friction ratio are shown in Figure 4-5 for cohesive soils as the quantity of fine-grained soils is very limited. Plotting any relationship between the scale of fluctuations and COV demonstrates that there are too few data points for cohesive soils at this site to draw useful conclusions.

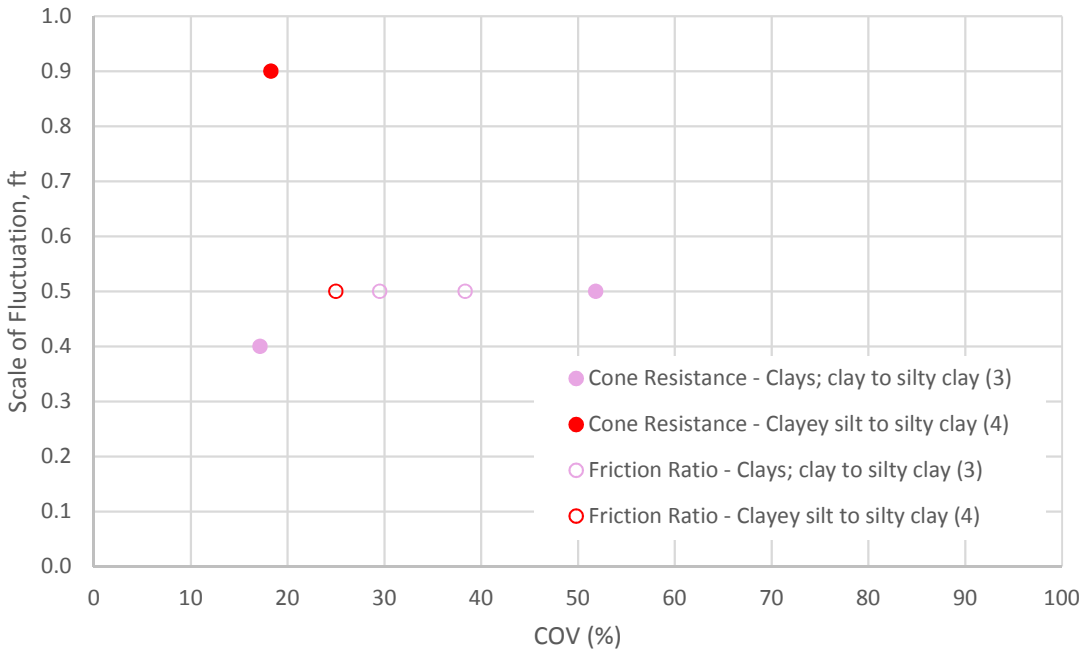

Figure 4-7: Scale of Fluctuation vs the COV. The site at Labadie, Missouri is comprised of a few homogeneous fine-grained soil layers.

The results for cone tip resistance and friction ratio are shown for the cohesionless soils in Figures 4-6 and 4-7, respectively. The data are too limited for 'Silty Sand to Sandy Silt (soil type #5) layers to draw any valid conclusions. Results from soil

type #6, 'Clean Sand to Silty Sand', and soil type #7, 'Gravelly Sand to Sand', exhibit an upward trend in the data for cone tip resistance in Figure 4-6. The range of the scales of fluctuation of the cone tip resistance increases as the COV increases for 'Clean Sand to Silty Sand' layers, which would indicate that as the variability of the data increase there are some poorly correlated layers as well as some closely correlated layers. For 'Clean Sands to Silty Sands', at a COV of about 45%, the scale of fluctuation ranges from 0.4 to 3.6 ft, whereas at a COV of about 15%, the scale of fluctuation ranges from 0.4 to 0.9 ft. For 'Gravelly Sand to Sand' layers, as the variability increases, as represented by an increasing COV, the data become more correlated and have a larger scale of fluctuation for the cone tip resistance as shown by the best fit line in Figure 4-6. Similar trends do not appear in the data for the scale of fluctuation for the friction ratio as shown in Figure 4-7 indicating that the correlation of sleeve friction measurements is not affected by change in the variability of the soil layer.

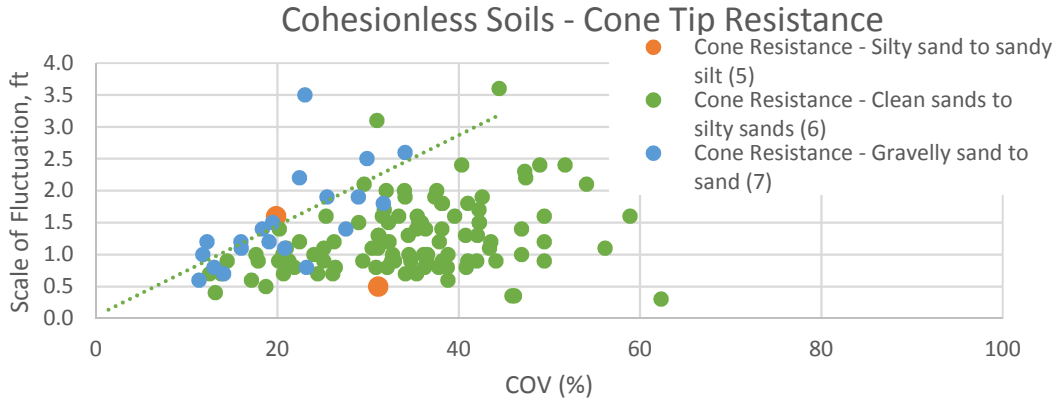

Figure 4-8 Scale of fluctuation vs the COV of the cone tip resistance for cohesionless soils

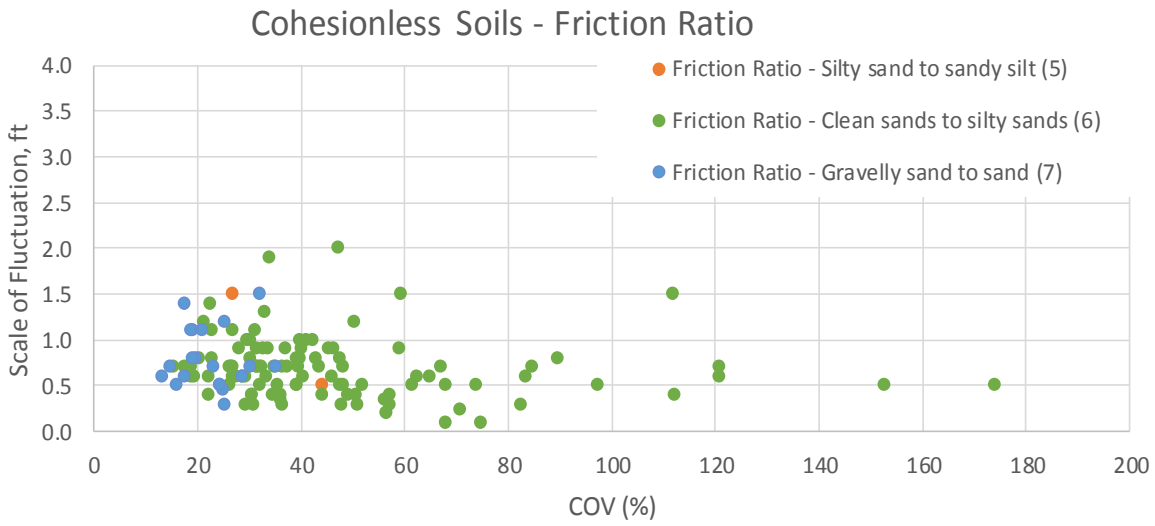

Figure 4-9 Scale of fluctuation vs the COV of the friction ratio for cohesionless soils

As the mean normalized cone tip resistance increases, the soil type generally becomes coarser whereas as the mean friction ratio increases, the soil type generally becomes finer as shown in

Figures 4-8 and 4-9. The data were normalized to remove the effect of overburden pressure. As mentioned above, there is insufficient data to assess the trends at this site for cohesive soils. Results for cohesionless soils reveal no obvious trends except for soil type #7, 'Gravelly Sand to Sand' and the mean cone tip resistance. For 'Gravelly Sand to Sand' layers, as the mean cone tip resistance increases, the scale of fluctuation increases. This trend would indicate increased correlation in the data as the soil layers become denser. This trend confirms observations made in the literature. As mentioned in Section 2.10, Uzielli et al. (2006) indicate that stiffer materials cause a greater volume of soil to fail by the advancing CPT probe. The larger volume would appear more correlated with

closely space measurements evaluating some of the same material in consecutive readings.

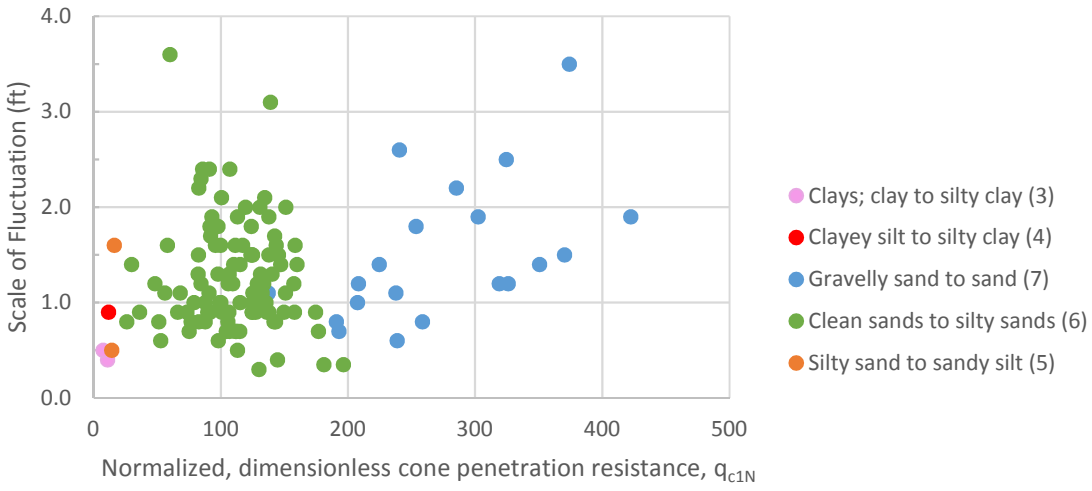

Figure 4-10: Scale of fluctuation vs Average Overburden-Normalized Cone Tip Resistance for all soil types

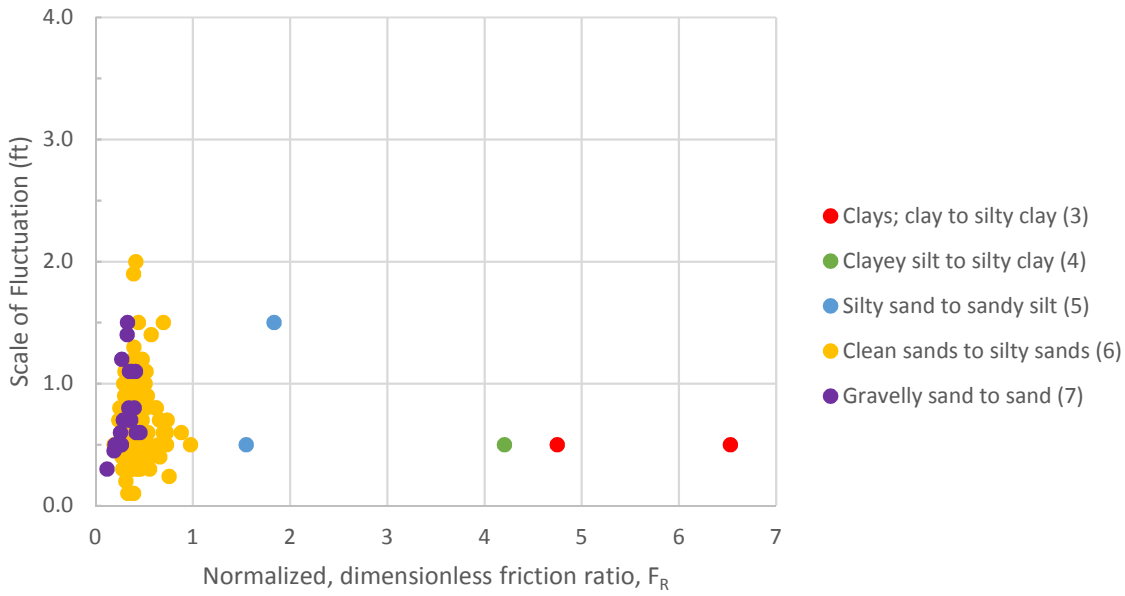

Figure 4-11: Scale of Fluctuation vs the Average Overburden-Normalized Friction Ratio for all soil types.

4.3 Summary

The results of the statistical analysis from the CPT data at the coal combustion residual landfill site confirms the results of previous research. The number of statistically uniform cohesive soils on the site were too few to make any conclusions. For the cohesionless soil types that were on site, the scale of fluctuation of the friction ratio is less than the scale of fluctuation for the cone tip resistance. This indicates that the cone tip resistance is more correlated and less variable than the friction ratio. Also, this indicates that the volume of soil measured is different for each measurement despite the fact that a single probe measures both simultaneously. The small measurement interval for cone tip resistance measures some of the same soil in consecutive cone tip resistance measurements, which would make the adjacent measurements similar or correlated. Since a smaller volume of

soil is affected by the sleeve friction measurement, the friction ratio would be less affected by consecutive readings and appears less correlated.

No biases were observed relating to the number of samples which represents the data set length.

Also, a few trends were noticed relating the COV and scale of fluctuation. Only the 'Clean Sands to Silty Sand' layers and 'Gravelly Sand to Sand' layers revealed a direct correlation. Similarly, the 'Gravelly Sand to Sand' soil was the only soil type to show increasing correlation, as expressed by a larger scale of fluctuation, as the cone tip resistance increased.

5.0 CONCLUSIONS

5.1 Summary

The cone penetration test (CPT) has gained popularity as a reliable and fast in-situ testing method. The CPT was used for a detailed site investigation for a coal combustion residual landfill in Missouri. Ninety-three soundings provided an ideal set of measurements to investigate the inherent variability of the alluvial site adjacent to the Missouri River.

The data were normalized for overburden and classified according to the 1990 Robertson classification system and then analyzed statistically. Basic statistical parameters, such as mean, standard deviation and coefficient of variation were calculated for homogeneous layers greater than about 4 feet. Then, the data were converted into a zero-mean random field, and the vertical autocorrelation function was calculated and plotted for each homogeneous soil unit. The exponential model

was chosen to fit the field data and the vertical scale of fluctuation was estimated. Data that poorly fit the model were eliminated to obtain the final set of results as presented in Section 4.

5.2 Conclusions

The resulting statistical analysis of the measurements from the site agree with previous research that the correlation of the cone tip resistance measurement is less than the sleeve friction measurement as the average vertical scale of fluctuation for the cone tip resistance was larger than the average vertical scale of fluctuation for the friction ratio. The average scale of fluctuation for the cone tip resistance was 1.3 feet and 1.5 feet for the 'Clean Sand to Silty Sand (#6)' and 'Gravelly Sand to Sand (#7)' soil types respectively. The average scale of fluctuation for the friction ratio was 0.7 feet and 0.8 feet for the 'Clean Sand to Silty Sand (#6)' and 'Gravelly Sand to Sand (#7)' soil types respectively.

Also, possible trends were observed in the results. The data for 'Silty Sand to Sandy Silt' were too limited to note any trends. The 'Clean Sand to Silty Sand (#6)' exhibit an increasing range of scale of fluctuation as the COV for cone tip resistance increases but such trend was not observed in the scale of fluctuation of the friction ratio. For 'Clean Sands to Silty Sands (#6)', at a COV of about 45%, the scale of fluctuation of the cone tip resistance ranges from 0.4 to 3.6 ft, whereas at a COV of about 15%, the scale of fluctuation of the cone tip resistance only ranges from 0.4 to 0.9 ft. For 'Gravelly Sand to Sand (#7)' layers, as the variability increases, as represented by an increasing COV, it appears to be directly correlated to the scale of fluctuation for the cone tip resistance as shown by the best fit line in Figure 4-6.

As shown in Figure 4-3, the volume of soil affected by the testing is the volume surrounding the probe with a diameter 8.6 times the diameter of the probe. The sleeve resistance is affected by a smaller volume and is a more precise point measurement. The larger volume affected by the cone tip resistance makes it an average measurement. With closely spaced measurements of less than one inch, several readings of the cone tip resistance are testing portions of the same soil volume within the area of cone tip failure mass. The smaller scale of fluctuation of the friction ratio indicates a weaker correlation for that measurement than that of the cone tip resistance.

5.3 Recommendations

5.3.1 Practical Implications

Geotechnical engineers, using the CPT for determination of site parameters, should fully understand the effect of the advancing probe and the volume of soil that is affected by each measurement. Different failure mechanisms are being employed and different soil volumes are being tested; therefore, the variability and correlation of the measurements should ideally be considered independently. Therefore, greater factors of safety or penalties could be assigned to designs making use of the friction ratio than the factors of safety for designs dependent on the cone tip resistance values. If designers attempt to create more economical designs, the correlation becomes more important. As discussed in Sections 2.11 and 2.12, the combination of variability, as represented by the coefficient of variation, and correlation, as represented by the scale of fluctuation, can greatly affect the outcome of a geotechnical design. Conditions with high probability of failure, such as slopes with high COV and small scale of fluctuation, should be given higher factors of safety or lower resistance factors.

Often both measurements, the sleeve friction and cone tip resistance, are combined and transformed into a design parameter. As mentioned in Section 2.11, the CPT measurements were used to estimate the undrained shear strength to analyze a slope. No consideration was mentioned that the correlation for each measurement were different even in a study strictly analyzing the importance of including correlation in a reliability study. Also, the correlation in both the vertical and horizontal direction was assumed equivalent even though Griffiths and Fenton conceded that was incorrect. Even researchers using complex finite element models must simplify the problem in order to solve the problem or better illustrate the project goal, which was showing the effect of correlation on the probability of failure for a simple slope. Ideally, the models and assumptions would closely approximate the field conditions and would address the difference in correlation for sleeve friction and cone tip resistance.

While probabilistic analyses are not commonplace among geotechnical engineers, the value of such techniques is obvious and relevant as code requirements move toward probabilistic or risk-based analyses. Uzielli et al. (2006) state that geotechnical analyses are still primarily deterministic in practice, but modern computers provides the power to model more complex and realistic soil profiles.

> "The gap between geotechnical research and practice needs to be narrowed. It is perhaps illusory that such gap may ever be eliminated. However, a greater acceptance of variability as a major actor in geotechnical practice would help reduce such gap. Reduction of the gap should occur from both sides; research should merge the mathematical techniques and geotechnical data into a more

> readily usable format; practice should increasingly recognize the importance of addressing data in the light of uncertainty, and accept the necessity to acquire additional competence regarding the statistical treatment of data. There is little doubt that a shift to an uncertainty-based perspective is taking place. The joint effort of researchers and practitioners should aim towards a full recognition of the benefits of such development" (Uzielli et al. 2006).

As Christian was quoted in the introduction, a good first step in understanding is recognizing what knowledge we do not have and addressing the deficiency. Since in-depth variability analyses are not standard practice for geotechnical engineers, the importance of addressing the correlation of soil properties may not be recognized.

5.3.2 Suggested Further Research

While this thesis confirms previous research concerning the apparent differences in the nature of the correlations of CPT measurements, additional research would be beneficial. As mentioned above, data concerning the scale of fluctuation is limited. Therefore, additional site investigations should be studied in order to assess the typical values for the scale of fluctuation to help engineers estimate typical values in preliminary investigations or as confirmation of site specific results. Once typical values are understood, reliability analysis could include the effects of possible correlation or preferably site specific correlation conditions. Discussion of variability as reported by the statistical parameters, including the scale of fluctuation, reminds designers of the variability of soils as naturally deposited materials and informs their decisions when choosing design parameters.

While more well-documented and detailed statistical analyses are needed from any site, additional data are especially needed for cohesive homogenous soil units to better ascertain the variability of fine-grained deposits. The site in Labadie, Missouri did not contain sufficient homogeneous clay or silt deposits to make any useful observations.

While the soil volumes affected by the sleeve friction and the cone tip penetration are different, the two terms used to report the measurements are inter-related. The friction ratio contains the cone tip resistance as shown in Eqn. 2. This definition of the friction ratio and Robertson's classification system requires plotting a variable against itself on the same graph, which is erroneous (Fellinius and Eslami 2000). Therefore, the contrast between the variability of the sleeve friction and cone tip may not be best represented by the comparison of the friction ratio and the cone tip resistance. While the classification of the soil type may be reliably estimated by plotting the friction ratio and the cone tip resistance, another procedure may be preferred to compare correlation. To more properly assess the variability and the correlation of the soil adjacent to the sleeve, a statistical analysis should be made directly of the sleeve friction.

Finally, the challenge of researchers to close the gap between theory and practice remains. As the use of CPT is more commonplace, large amounts of data are easily obtained, which allows site specific probabilistic analysis. Researchers' advanced mathematical and computing skills should continue to create and present probabilistic analysis techniques for practitioners to easily apply to real world projects that either have abundant CPT data or limited data typical or traditional geotechnical site investigations.

Similarly, the practicing geotechnical engineer should seek to understand and assess the variability of soil parameters, to move toward probabilistic methods and to design projects that account for such uncertainties. The future of geotechnical engineering has an increased probability of success if the gap between practice and research continues to narrow as Uzielli et al. (2006) challenged over 10 years ago.

REFERENCES

Baecher, G.B. and J.T. Christian (2003). *Reliability and Statistics in Geotechnical Engineering*, Wiley India Pvt. Ltd, New Delhi.

Baecher, G.B. (1986). "Geotechnical Error Analysis" Transportation Research Record 1105, <http://onlinepubs.trb.org/Onlinepubs/trr/1986/1105/1105-003.pdf> (Oct. 1, 2017).

Bouayad, D. (2017). "Assessment of Sandy Soil Variability Based on CPT Data," *Procedia Engineering*, 175, 310-315.

Christian, J.T. (2004). "Geotechnical Engineering: How Well Do We Know What We Are Doing?" *Journal of Geotechnical and Geoenvironmental Engineering*, ASCE, 130(10), 985-1003.

DeGroot, D.J. and G.B. Baecher (1993). "Estimating Autocovariance of In-Situ Soil Properties," *Journal of Geotechnical Engineering*, 119 (1), 147-166.

Ding, D. (2014). "Reliability of Shallow Foundations Designed Using LRFD Considering Uncertainty from Different Numbers of Strength Measurements," PhD Dissertation, Department of Civil and Environmental Engineering, University of Missouri-Columbia.

Elkateb T., R. Chalaturnyk, and P.K. Robertson (2003a). "An overview of soil heterogeneity: quantification and implications on geotechnical field problems," *Canadian Geotechnical Journal*, 40, 1-15.

Elkateb T., R. Chalaturnyk, and P.K. Robertson (2003b). "Simplified Geostatistical Analysis of Earthquake-Induced Ground Response at the Wildlife Site, California, U.S.A," *Canadian Geotechnical Journal*, 40, 16-35.

Eslami, A and B.H. Fellenius (1997). "Pile Capacity Estimated from CPT Data," International Society for Soil Mechanics and Geotechnical Engineering < https://www.issmge.org/uploads/publications/1/31/1997_01_0023.pdf > (January 20, 2018).

Gredell Engineering Resources, Inc. and Reitz & Jens, Inc. (2011) "Detailed Site Investigation (DSI) for Ameren Missouri Labadie Power Plant Proposed Utility Waste Disposal Area," <https://www.efis.psc.mo.gov/mpsc/common components/appeal_item_no.asp?attach_id=2014016359&caseno=EA-2012-0281&Dr_no= > (April 28, 2016).

Griffiths, D.V. and G.A. Fenton (2004). "Probabilistic Slope Stability Analysis by Finite Elements," *Journal of Geotechnical and Geoenvironmental Engineering*, ASCE, 130(5). 507-518.

Fellinius, B.H. and A. Eslami (2000). "Soil Profile Interpreted from CPTu Data," Year 2000 Geotechnics, Geotechnical Engineering Conference, Bangkok, Thailand, 1-18.

Fenton, G. (1999). "Estimation for Stochastic Soil Models," Journal of Geotechnical and Geoenvironmental Engineering, ASCE. 125 (6), 470-485.

Firouzianbandpey, S., D.V. Griffiths, L.B. Ibsen & L.V. Andersen (2014). "Spatial Correlation Length of Normalized Cone Data in Sand: Case Study in the North of Denmark," *Canadian Geotechnical Journal*, 844-857.

Jaska, M.B. (2007). "Modeling the Natural Variability of Over-Consolidated Clay in Adelaide, South Australia," *Characterisation and Engineering Properties of Natural Soils*, Tan, Phoon, Hight & Leroueil (eds), Taylor & Francis Group, London.

Jaksa, M.B., P.I. Brooker, W.S. Kaggwa, P.D.A. van Holst Pellekaan, and J.L. Cathro (1994). "Modelling the Lateral Spatial Variation of the Undrained Shear Strength of a Stiff, Overconsolidated Clay Using a Horizontal Cone Penetration Test," University of Adelaide, Department of Civil and Environmental Engineering, Research Report R117.

Joint Committee on Structural Safety, JCSS (2006). "JCSS Probabilistic Model Code, Part III – Resistance Models – 3.07 Soil Properties," <http://www.jcss.byg.dtu.dk/Publications/Probabilistic_Model_Code> (July 10, 2017).

Kulhawy, F.H., K. Phoon, M.D. Grigoriu (1995). "Reliability-Based Design of Foundations for Transmission Line Structures" Electric Power Research Institute, Research Project 1493-04, TR-105000, 4-1 to 4-54.

Kulhawy, F.H. and C. H. Trautmann, (1996). "Estimation of In-Situ Test Uncertainty" in *Uncertainty in the Geologic Environment: From Theory to Practice* (eds C. D. Shackleford, P. P. Nelson, and M. J. S. Roth), ASCE Geotechnical Special Publication No. 58, 269-286

Lloret-Cabot, N., G.A Fenton, M.A. Hicks (2014). "On the Estimation of Scale of Fluctuation in Geostatistics," *Georisk: Assessment and Management of Risk for Engineered Systems and Geohazards,* 8 (2), 129-140.

Luo, Z. and C.H. Juang (2012). "Efficient Reliability-Based Design of Drilled Shafts in Sand Considering Spatial Variability," *Journal of GeoEngineering*, 7 (2), 59-68.

Melnikov, A.V. and G.G. Boldyrev (2014). "Experimental Study of Sand Deformations During a CPT," 3rd International Symposium of Cone Penetration Testing, Nevada.

Moss R.E.S., R.B. Seed and R.S. Olsen (2006). "Normalizing the CPT for Overburden Stress," *Journal of Geotechnical and Geoenvironmental Engineering*, 132 (3), 378-387.

Nie, X., J. Zhang, H. Huang, Z. Liu and S. Lacasse (2015). "Scale of Fluctuation for Geotechnical Probabilistic Analysis," *Geotechnical Safety and Risk V*, T. Schweckendiek et al. (eds).

Phoon, K.K. and Kulhawy, F.H. (1999). "Characterization of Geotechnical Variability," *Canadian Geotechnical Journal*, 36, 612-624.

Phoon, K.K., S.T. Quek and P. An (2003). "Identification of Statistically Homogeneous Soil Layers Using Modified Bartlett Statistics," *Journal of Geotechnical and Geoenvironmental Engineering*, ASCE, 129(7), 649-659.

Robertson, P.K. (1990). "Soil Classification Using the Cone Penetration Test." *Canadian Geotechnical Journal*, 27, 151-158.

Robertson, P.K. (2013). "The James K. Mitchell Lecture: Interpretation of in-situ tests – some insights," Geotechnical and Geophysical Site Characterization 4, Coutinho and Mayen (eds), Taylor and Francis Group, London

Robertson, P.K. (2016). "Cone Penetration Test (CPT)-based Soil Behaviour Type (SBT) Classification System – An Update," *Canadian Geotechnical Journal*, 53, 1910-1927.

Robertson, P.K. and K.L. Cabal (2015). "Guide to Cone Penetration Testing for Geotechnical Engineering." 6th Ed., Gregg Drilling & Testing, Inc.

Robertson & Wride (1998). "Evaluating Cyclic Liquefaction Potential Using the Cone Penetration Test." Canadian Geotech Journal 35, 442-459.

Uzielli M., G. Vannucchi and K.K. Phoon (2005a) "Random Field Characterization of Stress Normalised Cone Penetration Testing Parameters," *Geotechnique*, 55(1), 3-20.

Uzielli, M., G. Vannucchi and K.K. Phoon (2005b). "Investigation of Correlation Structures and Weak Stationarity Using the CPT Soil Behavior Classification Index," *International Association for Structural Safety and Reliability (ICOSSAR)*, Augusti, Schueller, Ciampoli (eds), Millpresss, Rotterdam.

Uzielli, M.G., S. Lacasse, F. Nadim, and K.K. Phoon (2006). "Soil Varibility Analysis for Geotechnical Practice," < https://www.researchgate.net/profile/Marco_Uzielli /publication/266136333_Soil_Variability_Analysis_for_Geotechnical_Practice/links /57062beb08aef745f717a52d/Soil-Variability-Analysis-for-Geotechnical-Practice.pdf > (January 5, 2018).

Youd, T. L. and Idriss, I. M. (2001). "Liquefaction Resistance of Soils: Summary Report from the 1996 NCEER and 1998 NCEER/NCF Workshops on Evaluation of Liquefaction Resistance of Soils," *Journal of Geotechnical and Geoenvironmental Engineering*, 127(4), 297-313.

APPENDIX A

CPT Sounding Logs

Figure A - 1: Cone Penetration Test Sounding Log, C-11 1
Figure A - 2: Cone Penetration Test Sounding Log, C-13 2
Figure A - 3: Cone Penetration Test Sounding Log, C-16 3
Figure A - 4: Cone Penetration Test Sounding Log, C-18 4
Figure A - 5: Cone Penetration Test Sounding Log, C-21 5
Figure A - 6: Cone Penetration Test Sounding Log, C-23 6
Figure A - 7: Cone Penetration Test Sounding Log, C-25 7
Figure A - 8: Cone Penetration Test Sounding Log, C-28 8
Figure A - 9: Cone Penetration Test Sounding Log, C-30 9
Figure A - 10: Cone Penetration Test Sounding Log, C-32A 11
Figure A - 11: Cone Penetration Test Sounding Log, C-34 11
Figure A - 12: Cone Penetration Test Sounding Log, C-37 12
Figure A - 13: Cone Penetration Test Sounding Log, C-39 13
Figure A - 14: Cone Penetration Test Sounding Log, C-41 14
Figure A - 15: Cone Penetration Test Sounding Log, C-44 15
Figure A - 16: Cone Penetration Test Sounding Log, C-46 16
Figure A - 17: Cone Penetration Test Sounding Log, C-49A 17
Figure A - 18: Cone Penetration Test Sounding Log, C-48 18
Figure A - 19: Cone Penetration Test Sounding Log, C-50 19
Figure A - 20: Cone Penetration Test Sounding Log, C-60 20
Figure A - 21: Cone Penetration Test Sounding Log, C-62 21
Figure A - 22: Cone Penetration Test Sounding Log, C-64 22
Figure A - 23: Cone Penetration Test Sounding Log, C-66 23
Figure A - 24: Cone Penetration Test Sounding Log, C-66A 24
Figure A - 25: Cone Penetration Test Sounding Log, C-68 25
Figure A - 26: Cone Penetration Test Sounding Log, C-70 26
Figure A - 27: Cone Penetration Test Sounding Log, C-74 27
Figure A - 28: Cone Penetration Test Sounding Log, C-76 28
Figure A - 29: Cone Penetration Test Sounding Log, C-78 29
Figure A - 30: Cone Penetration Test Sounding Log, C-79 30
Figure A - 31: Cone Penetration Test Sounding Log, C-80 31
Figure A - 32: Cone Penetration Test Sounding Log, C-81 32
Figure A - 33: Cone Penetration Test Sounding Log, C-82 33
Figure A - 34: Cone Penetration Test Sounding Log, C-84 34
Figure A - 35: Cone Penetration Test Sounding Log, C-86 35
Figure A - 36: Cone Penetration Test Sounding Log, C-89 36
Figure A - 37: Cone Penetration Test Sounding Log, C-91 37
Figure A - 38: Cone Penetration Test Sounding Log, C-92 38
Figure A - 39: Cone Penetration Test Sounding Log, C-94 39
Figure A - 40: Cone Penetration Test Sounding Log, C-96 40
Figure A - 41: Cone Penetration Test Sounding Log, C-98 41
Figure A - 42: Cone Penetration Test Sounding Log, C-100 42
Figure A - 43: Cone Penetration Test Sounding Log, C-103 43
Figure A - 44: Cone Penetration Test Sounding Log, C-105 44
Figure A - 45: Cone Penetration Test Sounding Log, C-106 45
Figure A - 46: Cone Penetration Test Sounding Log, C-107 46
Figure A - 47: Cone Penetration Test Sounding Log, C-107A 47
Figure A - 48: Cone Penetration Test Sounding Log, C-109 48
Figure A - 49: Cone Penetration Test Sounding Log, C-111 49
Figure A - 50: Cone Penetration Test Sounding Log, C-113 50

Figure A - 51: Cone Penetration Test Sounding Log, C-117 51
Figure A - 52: Cone Penetration Test Sounding Log, C-119 52
Figure A - 53: Cone Penetration Test Sounding Log, C-121 53
Figure A - 54: Cone Penetration Test Sounding Log, C-123 54
Figure A - 55: Cone Penetration Test Sounding Log, C-125 55
Figure A - 56: Cone Penetration Test Sounding Log, C-129 56
Figure A - 57: Cone Penetration Test Sounding Log, C-131 57
Figure A - 58: Cone Penetration Test Sounding Log, C-133 58
Figure A - 59: Cone Penetration Test Sounding Log, C-135A 59
Figure A - 60: Cone Penetration Test Sounding Log, C-137 60
Figure A - 61: Cone Penetration Test Sounding Log, C-139 61
Figure A - 62: Cone Penetration Test Sounding Log, C-139A 62
Figure A - 63: Cone Penetration Test Sounding Log, C-143 63
Figure A - 64: Cone Penetration Test Sounding Log, C-145 64
Figure A - 65: Cone Penetration Test Sounding Log, C-145A 65
Figure A - 66: Cone Penetration Test Sounding Log, C-147 66
Figure A - 67: Cone Penetration Test Sounding Log, C-147A 67
Figure A - 68: Cone Penetration Test Sounding Log, C-149 68
Figure A - 69: Cone Penetration Test Sounding Log, C-151 69
Figure A - 70: Cone Penetration Test Sounding Log, C-157 70
Figure A - 71: Cone Penetration Test Sounding Log, C-157A 71
Figure A - 72: Cone Penetration Test Sounding Log, C-159 72
Figure A - 73: Cone Penetration Test Sounding Log, C-161 73
Figure A - 74: Cone Penetration Test Sounding Log, C-163 74
Figure A - 75: Cone Penetration Test Sounding Log, C-166 75
Figure A - 76: Cone Penetration Test Sounding Log, C-168 76
Figure A - 77: Cone Penetration Test Sounding Log, C-170 77
Figure A - 78: Cone Penetration Test Sounding Log, C-172 78
Figure A - 79: Cone Penetration Test Sounding Log, C-174 79
Figure A - 80: Cone Penetration Test Sounding Log, C-180 80
Figure A - 81: Cone Penetration Test Sounding Log, C-182 81
Figure A - 82: Cone Penetration Test Sounding Log, C-184 82
Figure A - 83: Cone Penetration Test Sounding Log, C-186 83
Figure A - 84: Cone Penetration Test Sounding Log, C-190 84
Figure A - 85: Cone Penetration Test Sounding Log, C-192 85
Figure A - 86: Cone Penetration Test Sounding Log, C-194 86
Figure A - 87: Cone Penetration Test Sounding Log, C-196 87
Figure A - 88: Cone Penetration Test Sounding Log, C-198 88
Figure A - 89: Cone Penetration Test Sounding Log, C-200 89

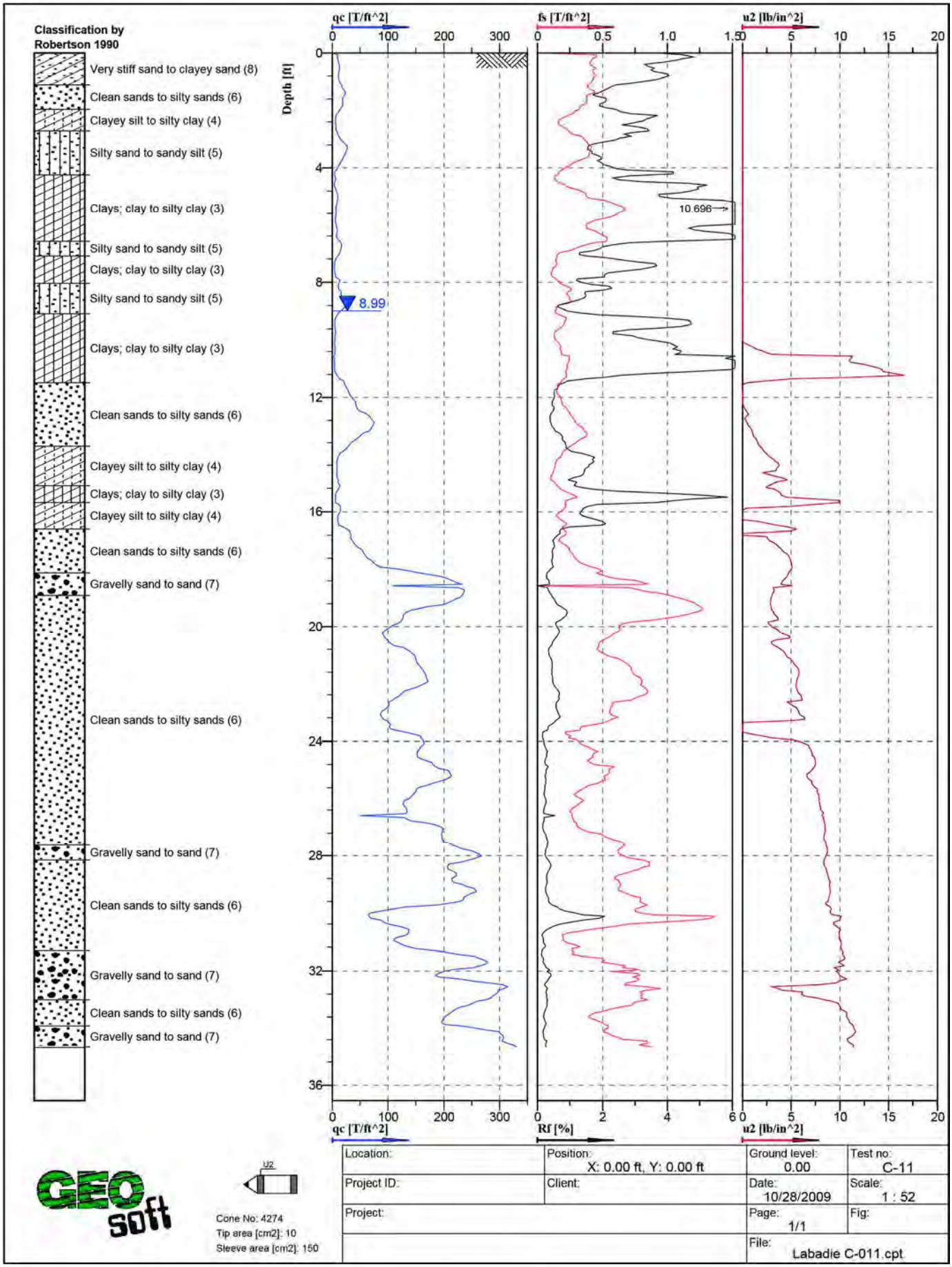

Figure A - 1: Cone Penetration Test Sounding Log, C-11

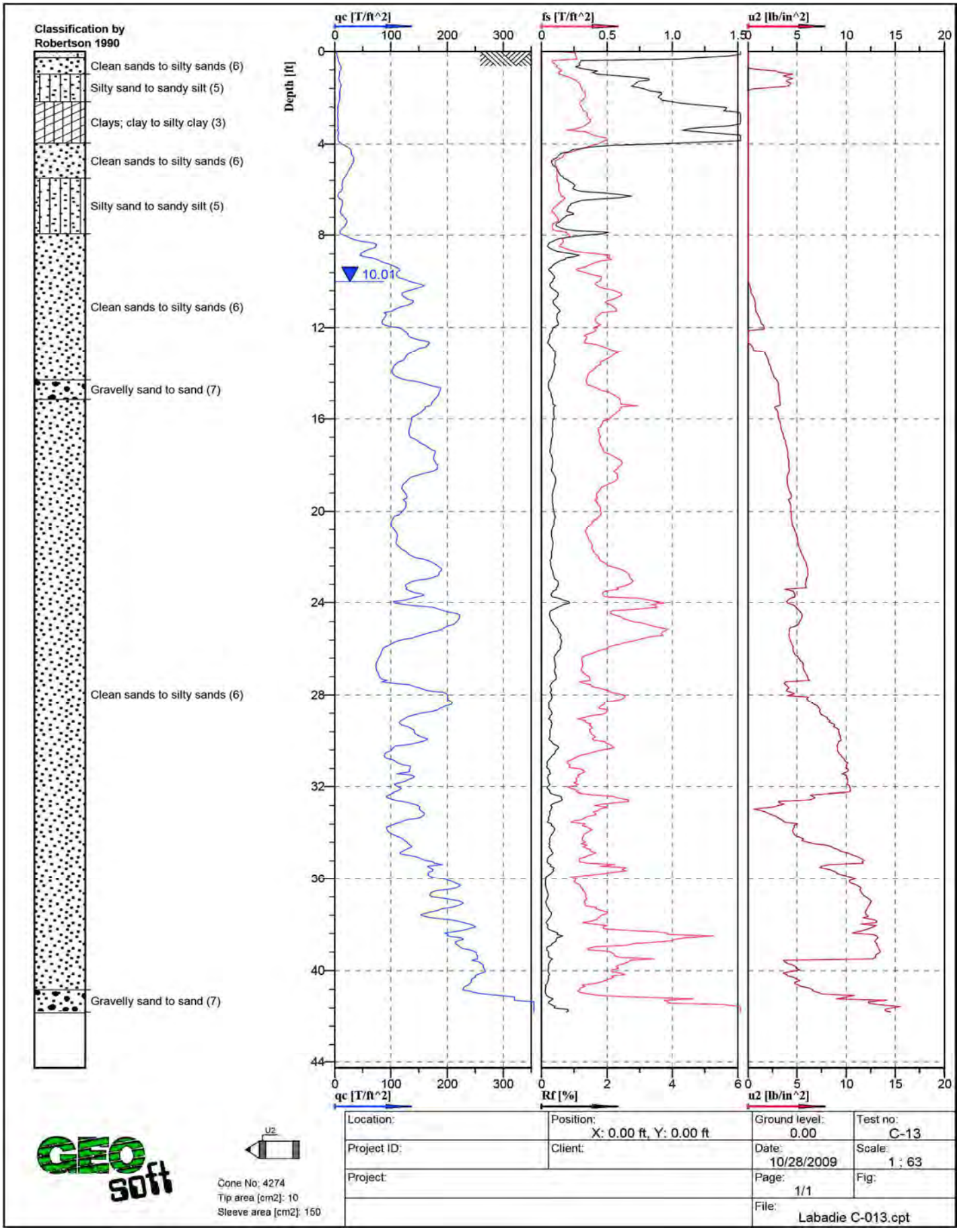

Figure A - 2: Cone Penetration Test Sounding Log, C-13

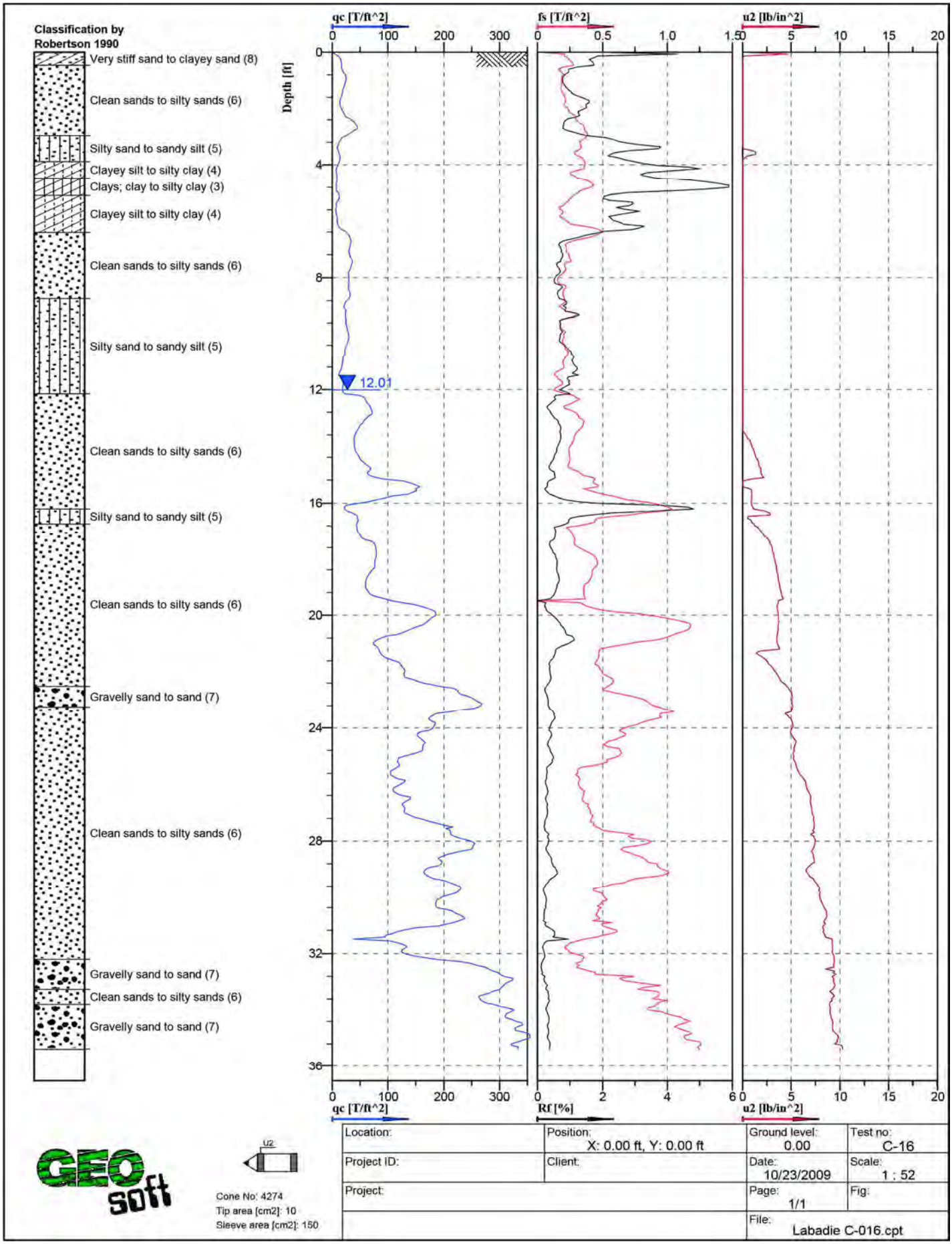

Figure A - 3: Cone Penetration Test Sounding Log, C-16

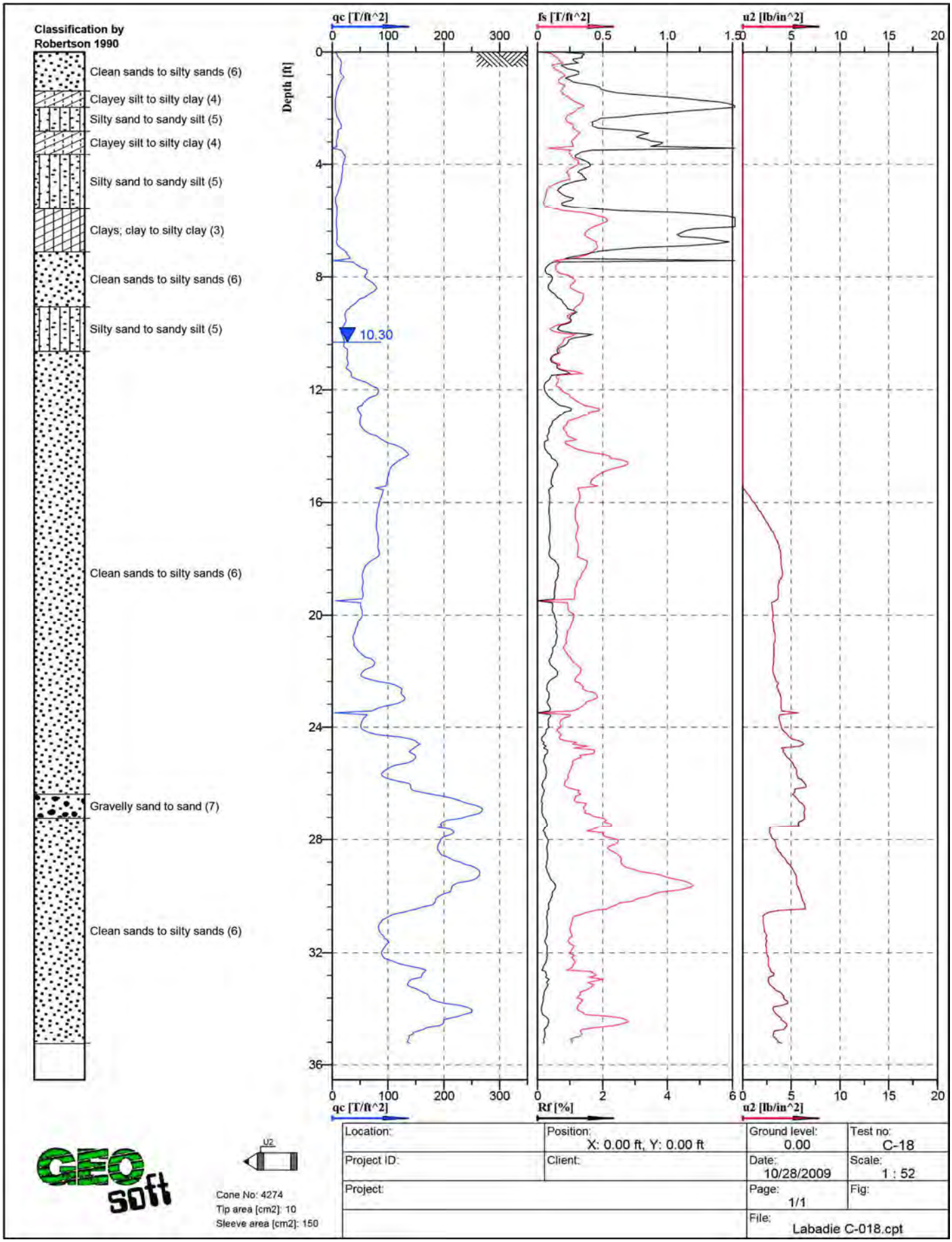

Figure A - 4: Cone Penetration Test Sounding Log, C-18

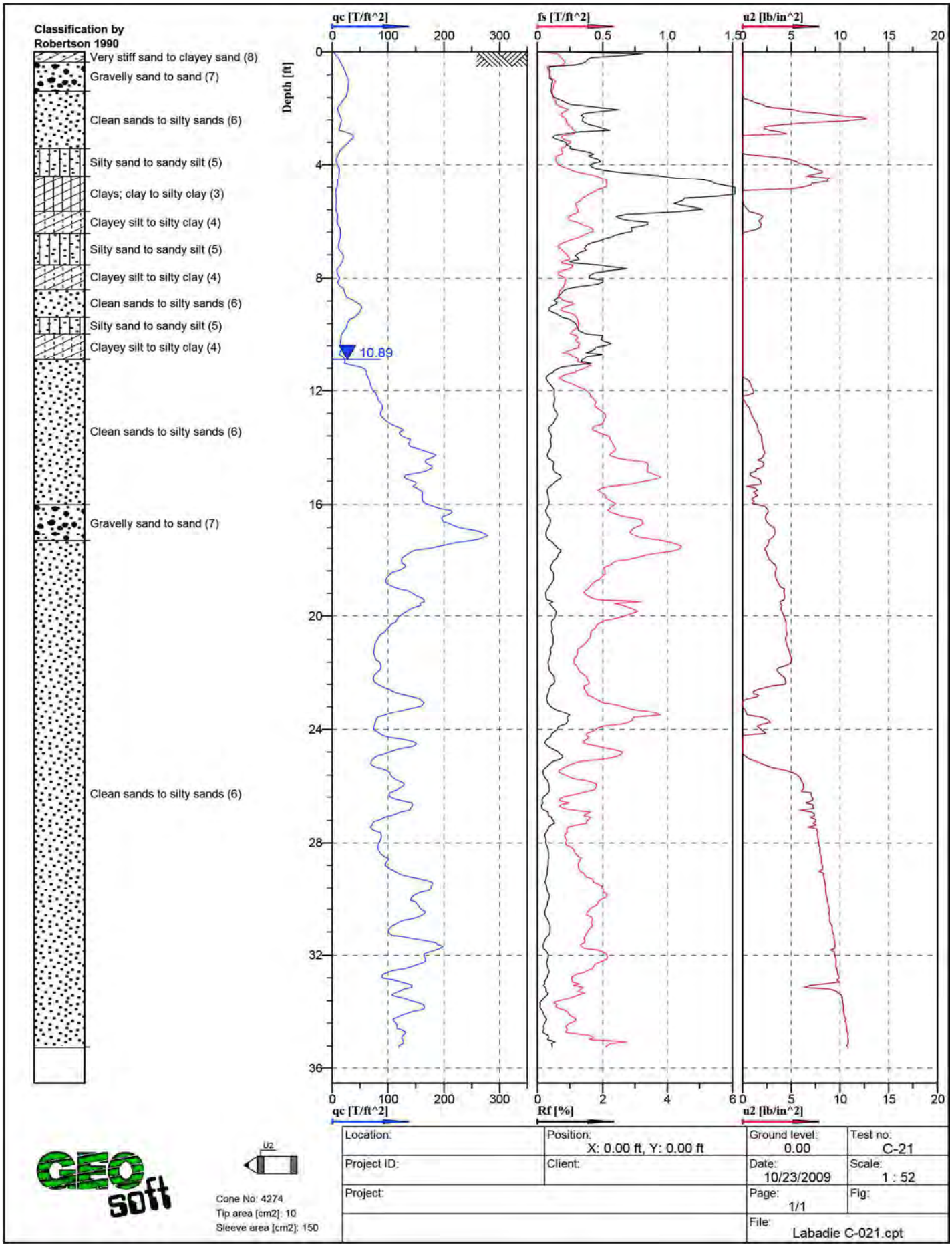

Figure A - 5: Cone Penetration Test Sounding Log, C-21

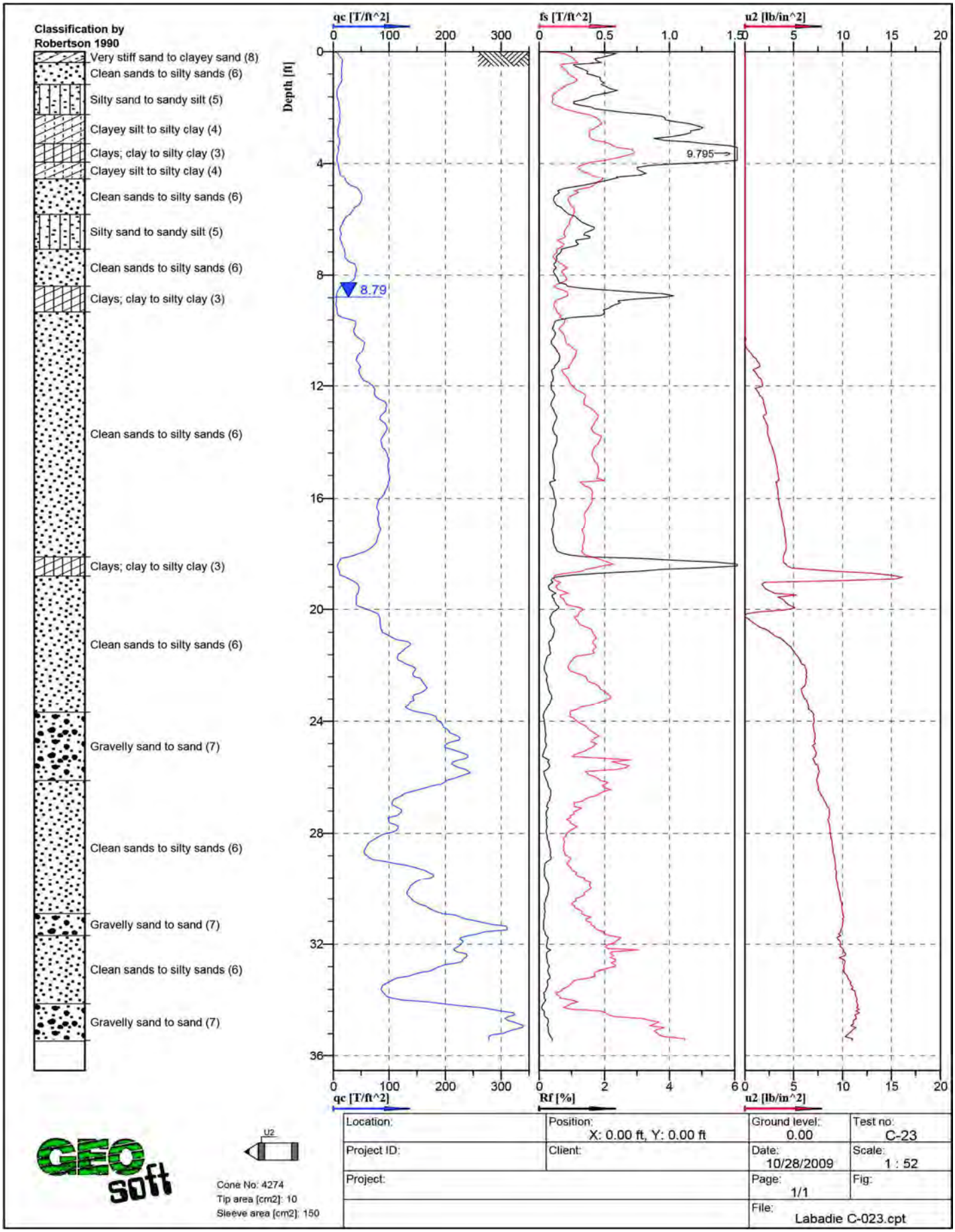

Figure A - 6: Cone Penetration Test Sounding Log, C-23

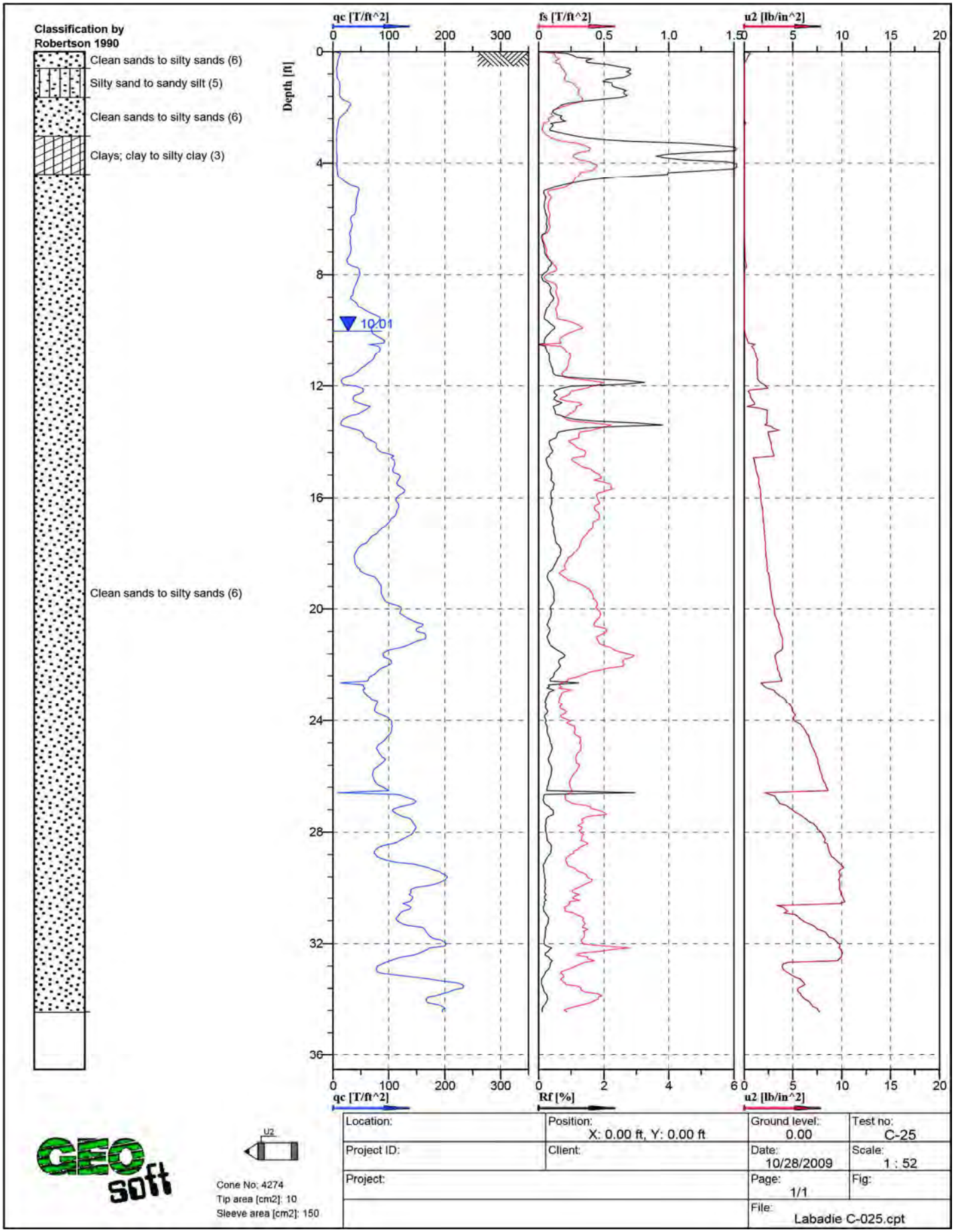

Figure A - 7: Cone Penetration Test Sounding Log, C-25

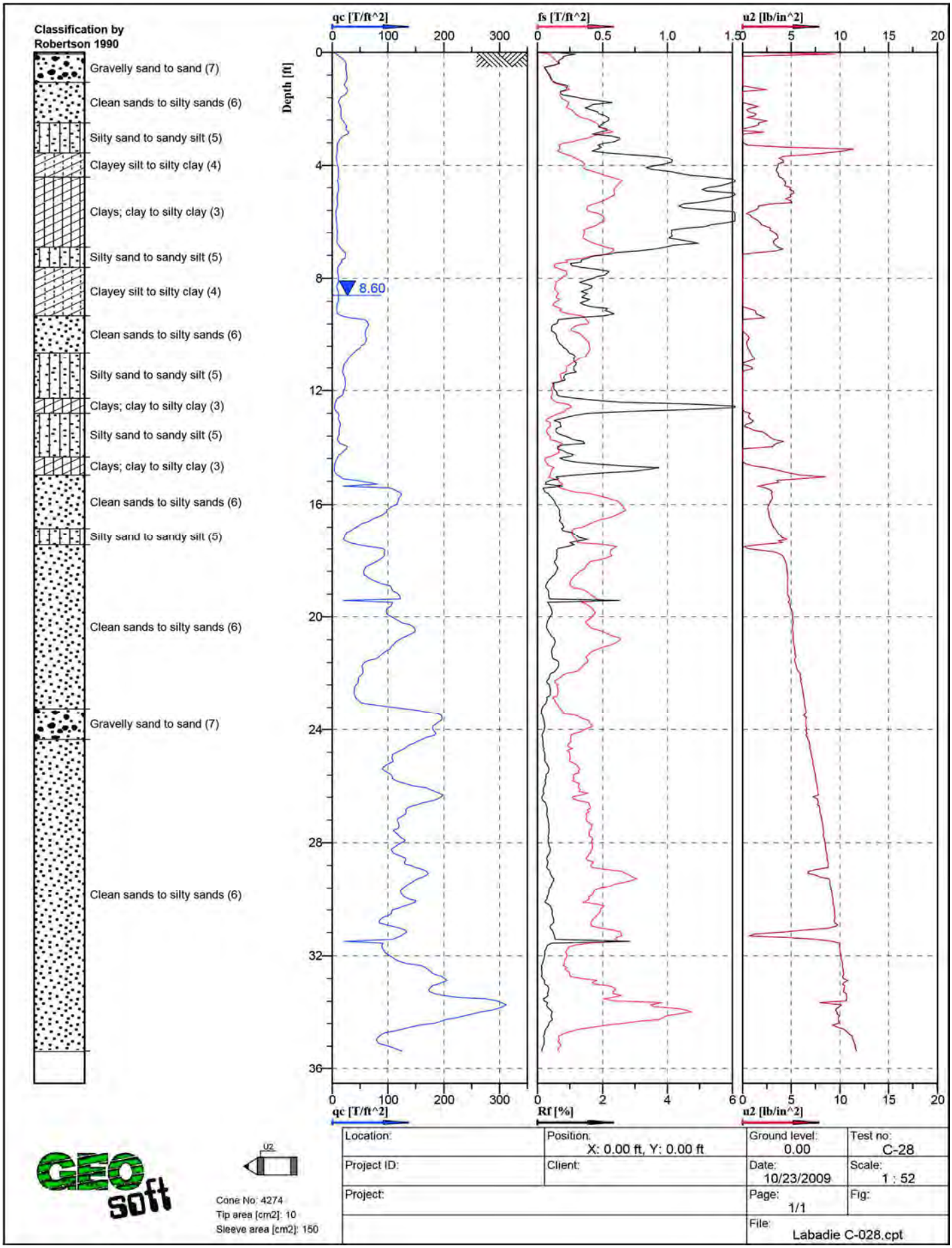

Figure A - 8: Cone Penetration Test Sounding Log, C-28

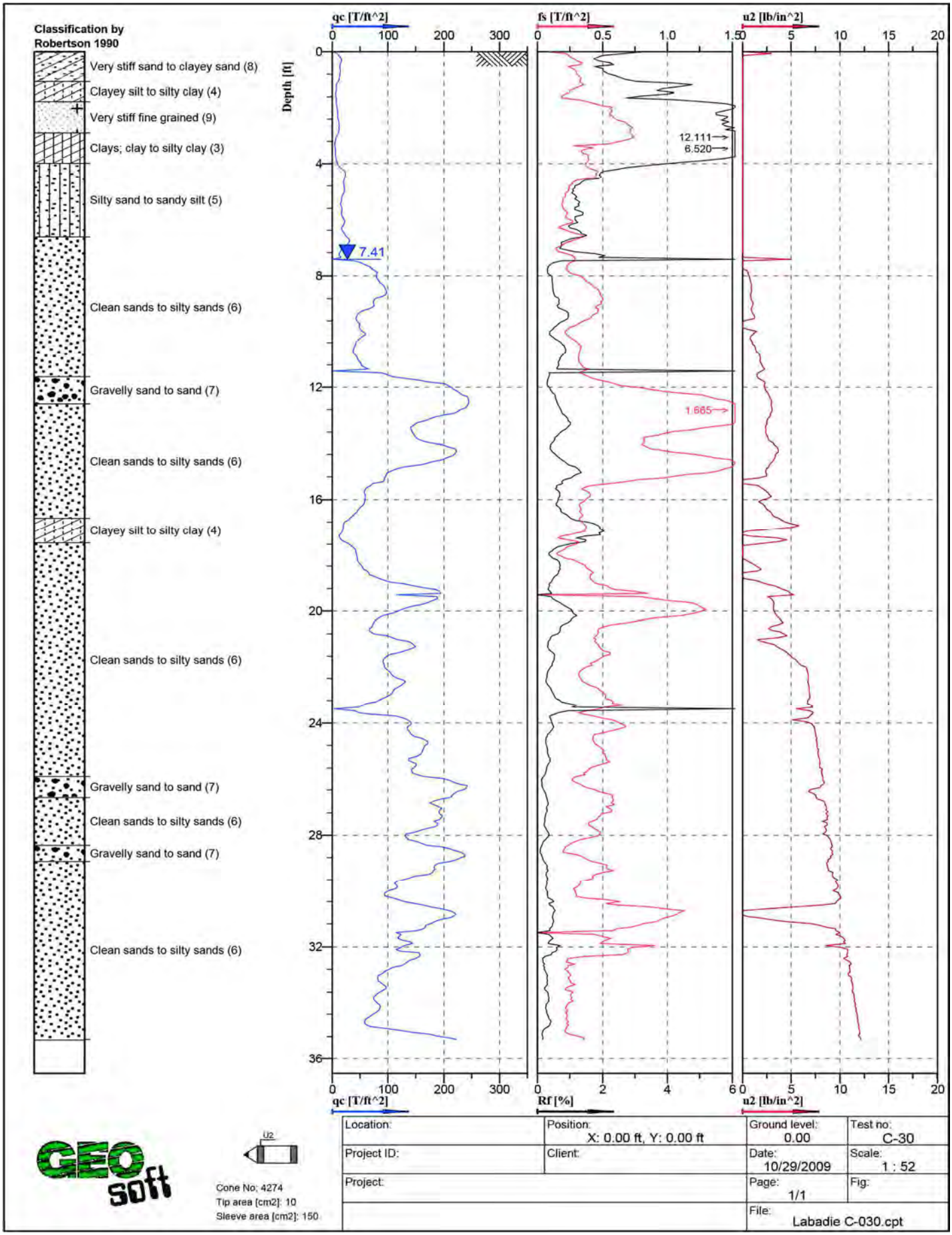

Figure A - 9: Cone Penetration Test Sounding Log, C-30

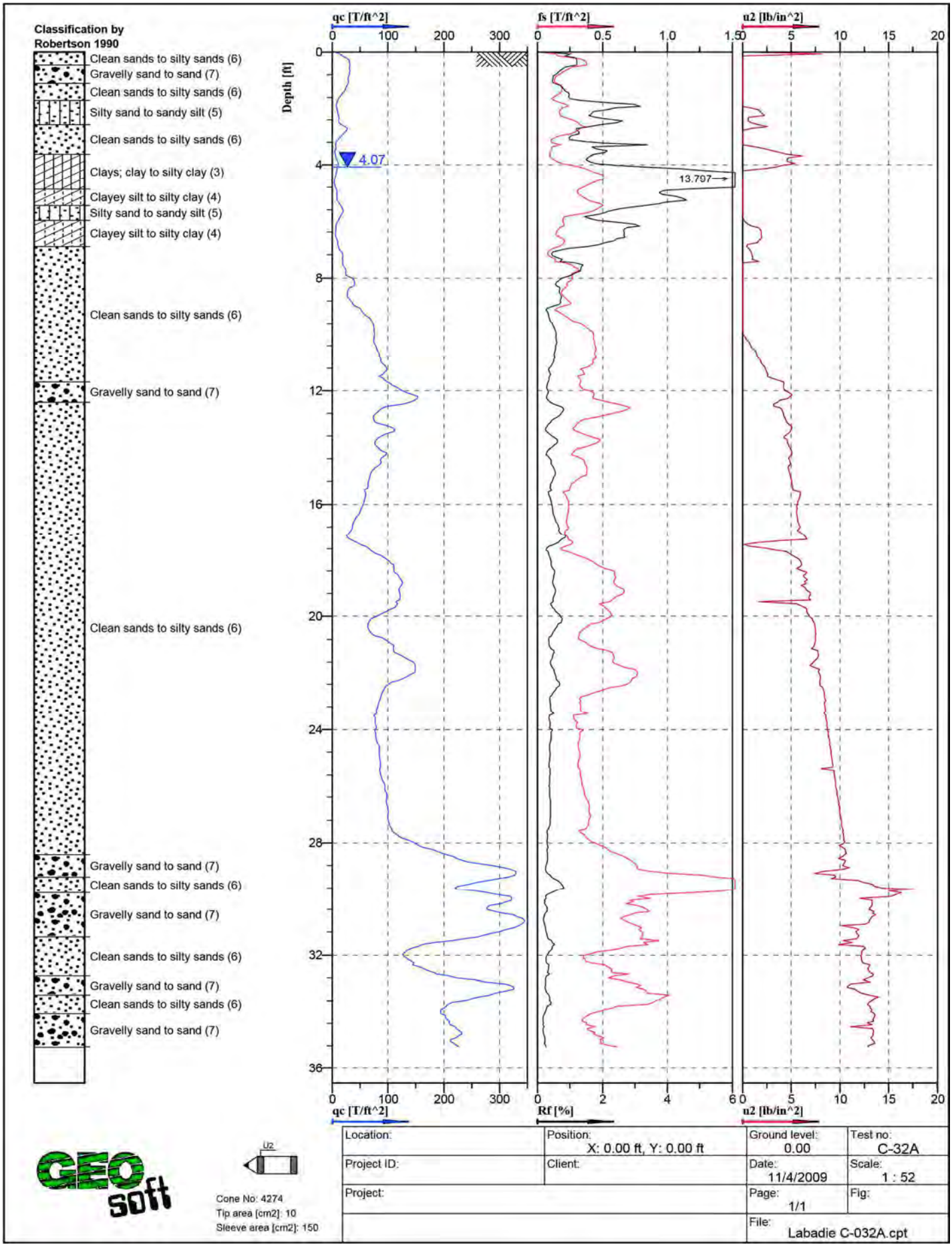
Classification by
Robertson 1990
Clean sands to silty sands (6)
Gravelly sand to sand (7)
Clean sands to silty sands (6)
Silty sand to sandy silt (5)
Clean sands to silty sands (6)
Clays; clay to silty clay (3)
Clayey silt to silty clay (4)
Silty sand to sandy silt (5)
Clayey silt to silty clay (4)
Clean sands to silty sands (6)
Gravelly sand to sand (7)
Clean sands to silty sands (6)
Gravelly sand to sand (7)
Clean sands to silty sands (6)
Gravelly sand to sand (7)
Clean sands to silty sands (6)
Gravelly sand to sand (7)
qc [T/ft^2]
fs [T/ft^2]
u2 [lb/in^2]
Depth [ft]
4.07
13.797
Rf [%]
Location:
Position:
X: 0.00 ft, Y: 0.00 ft
Ground level:
0.00
Test no:
C-32A
Project ID:
Client:
Date:
11/4/2009
Scale:
1 : 52
Project:
Page:
1/1
Fig:
File:
Labadie C-032A.cpt
Cone No: 4274
Tip area [cm2]: 10
Sleeve area [cm2]: 150

Figure A - 10: Cone Penetration Test Sounding Log, C-32A

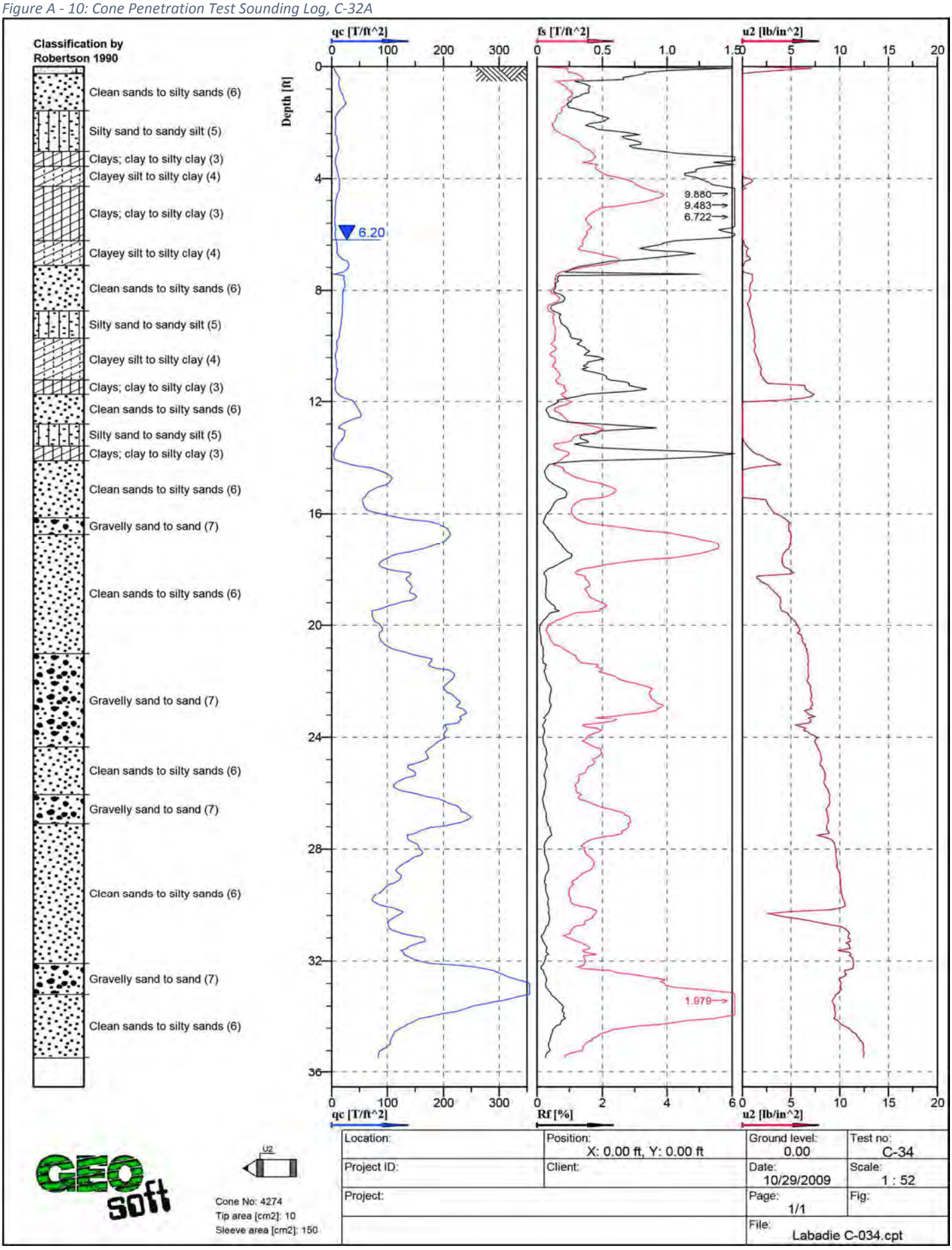

Figure A - 11: Cone Penetration Test Sounding Log, C-34

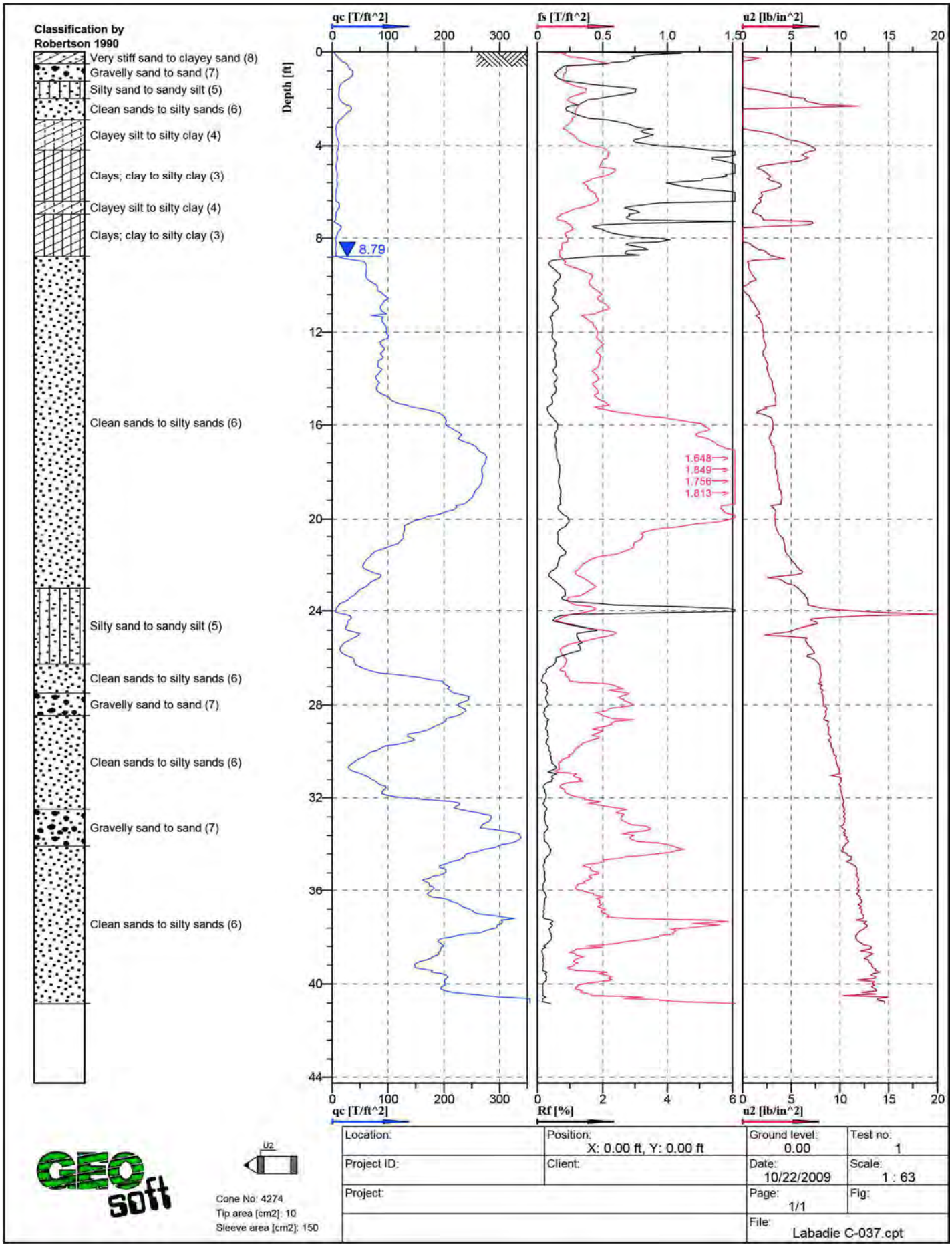

Figure A - 12: Cone Penetration Test Sounding Log, C-37

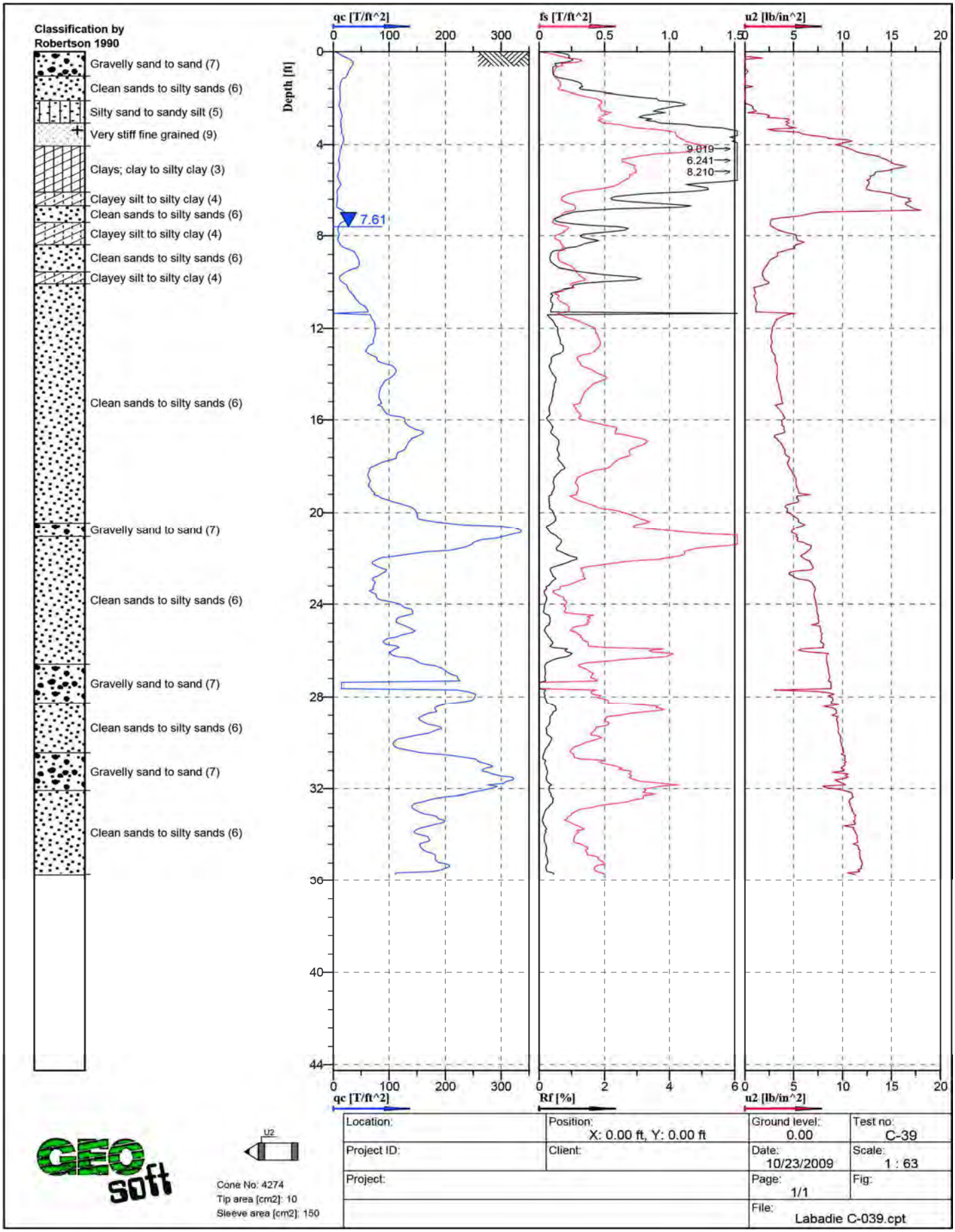

Figure A - 13: Cone Penetration Test Sounding Log, C-39

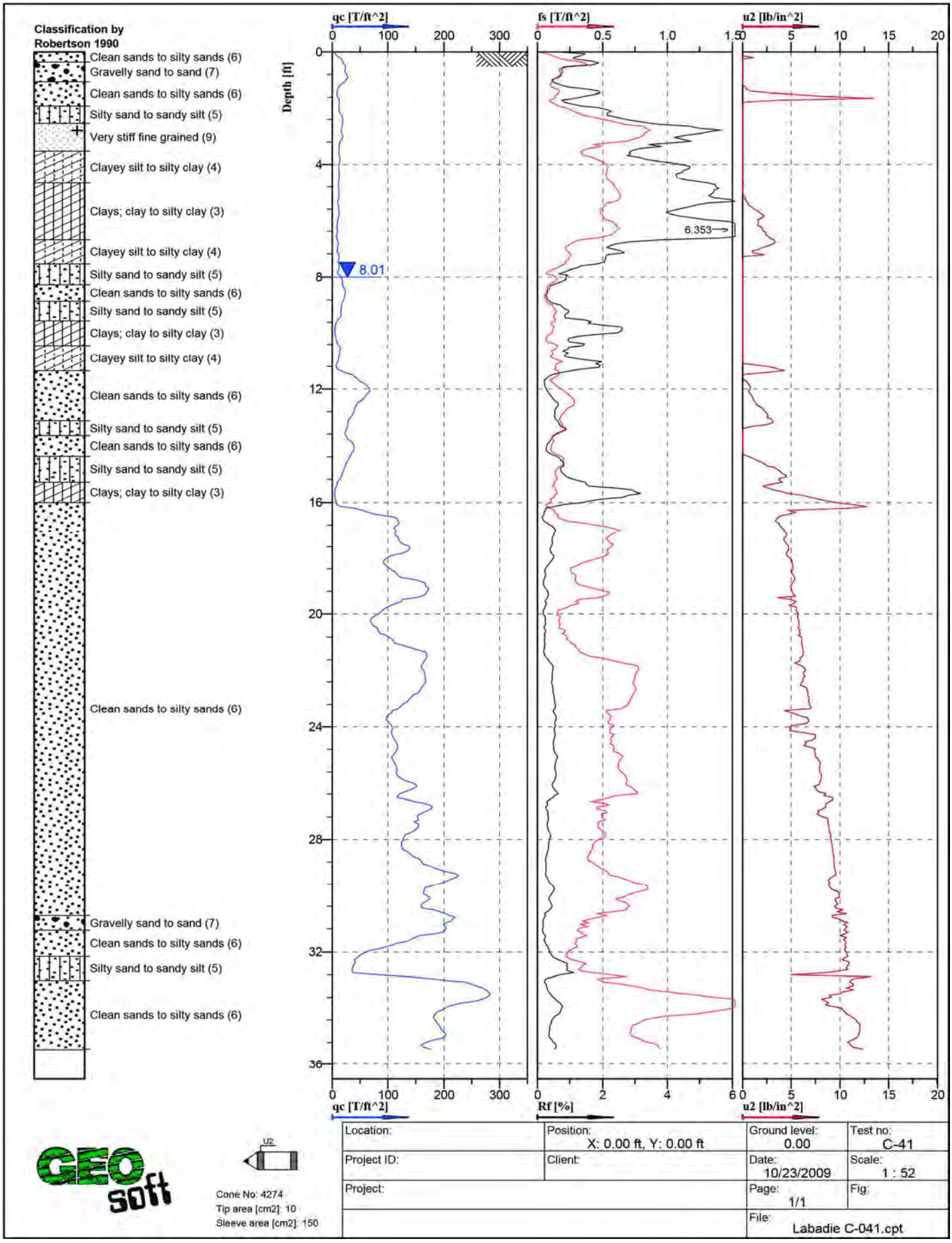

Figure A - 14: Cone Penetration Test Sounding Log, C-41

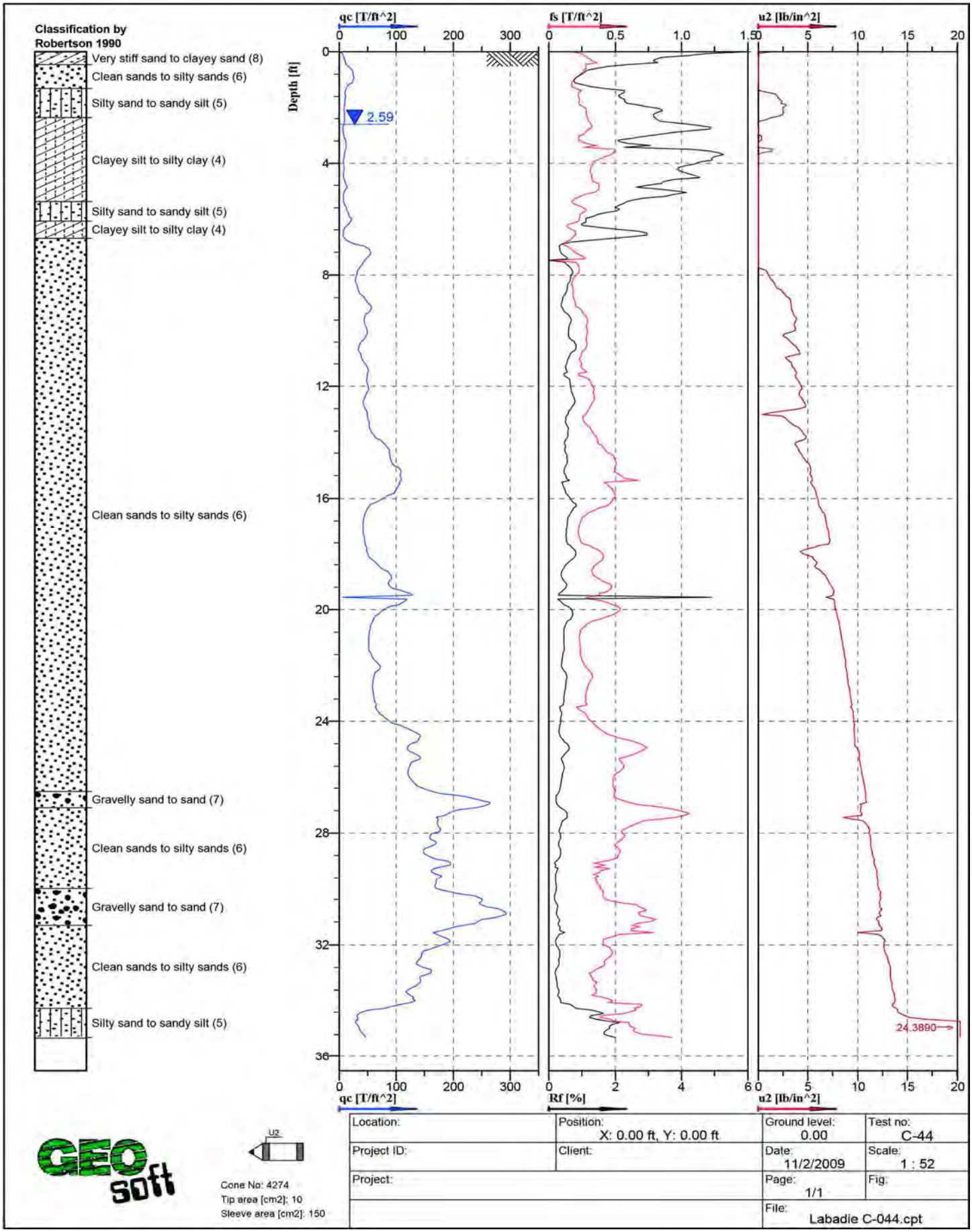

Figure A - 15: Cone Penetration Test Sounding Log, C-44

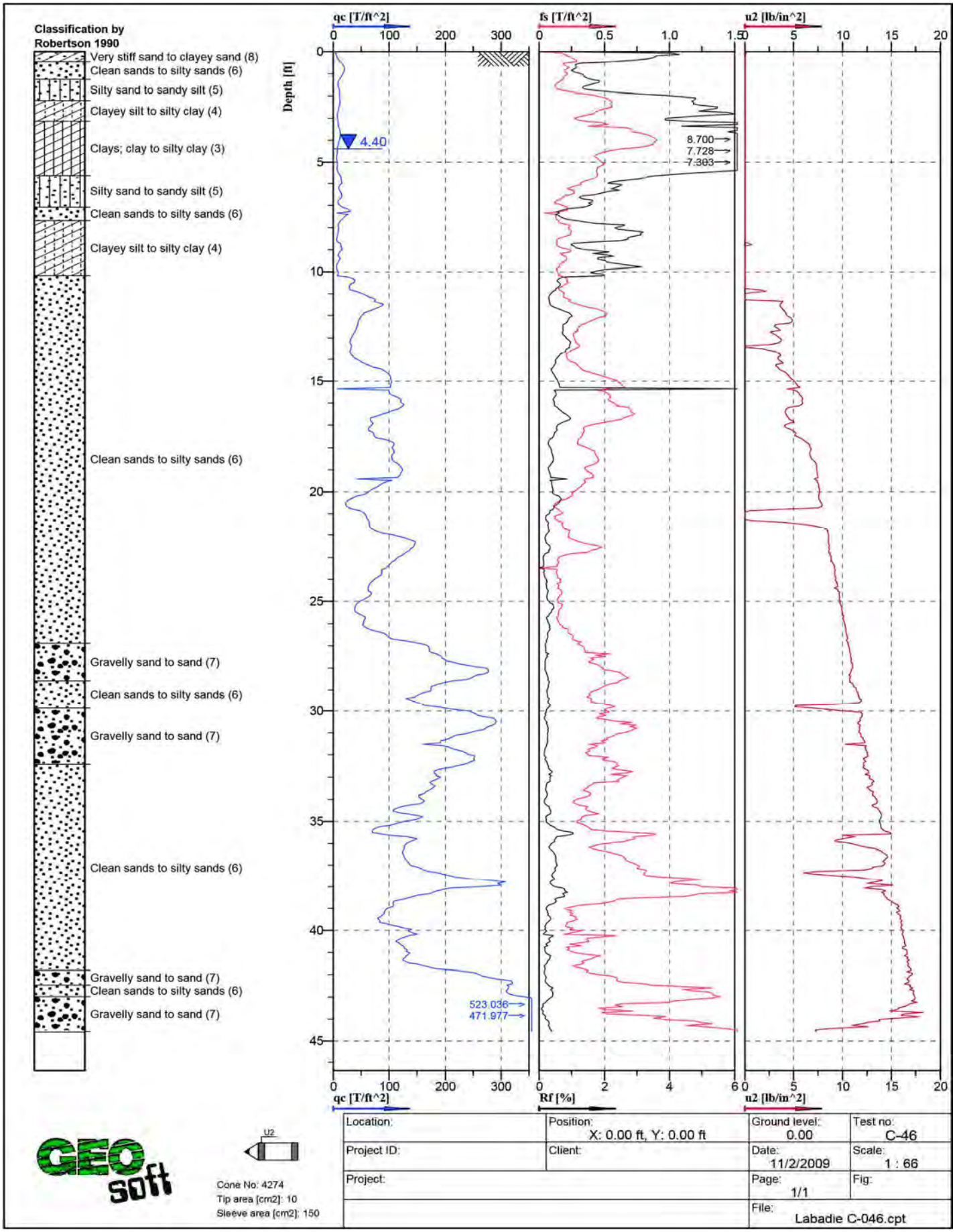

Figure A - 16: Cone Penetration Test Sounding Log, C-46

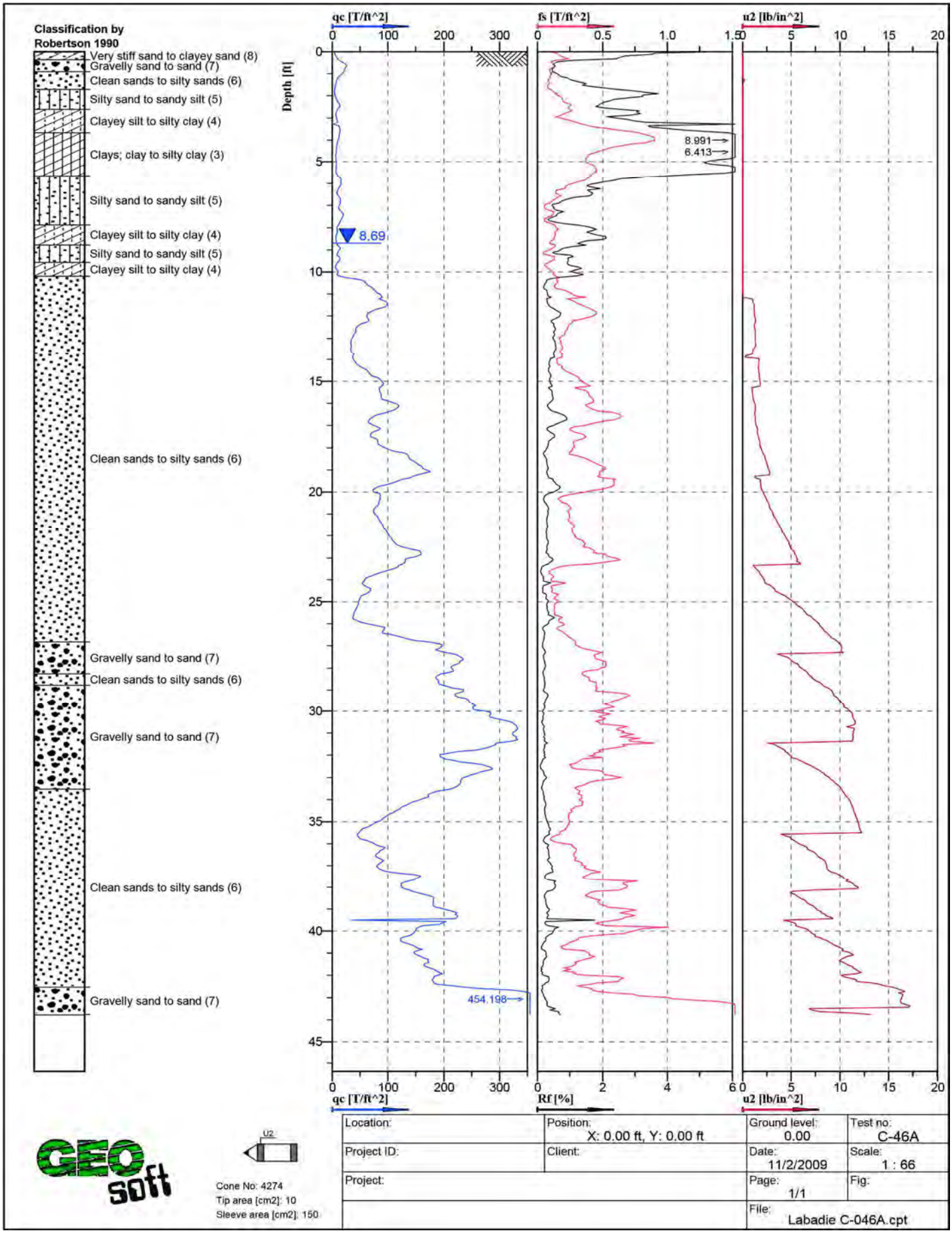

Figure A - 17: Cone Penetration Test Sounding Log, C-49A

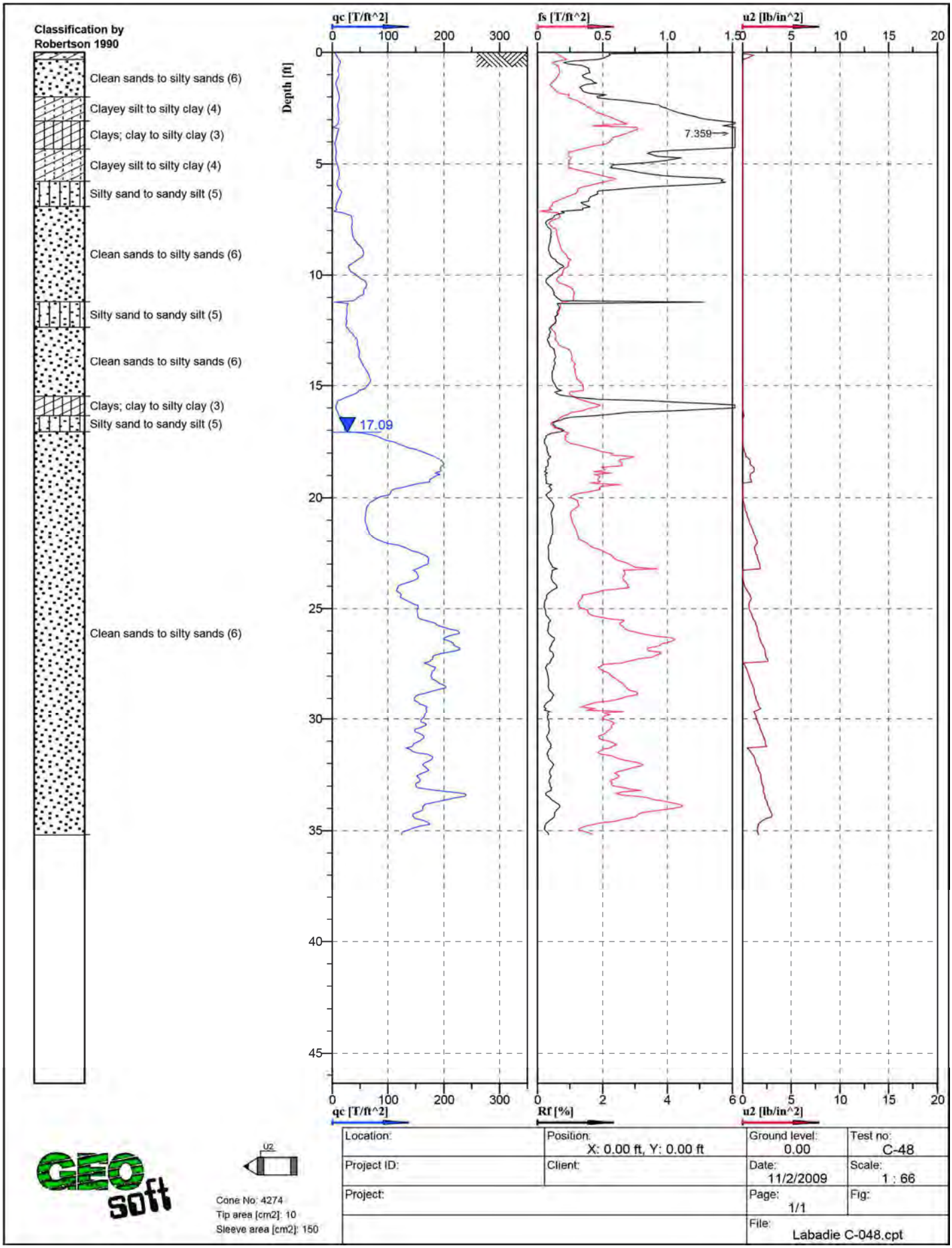

Figure A - 18: Cone Penetration Test Sounding Log, C-48

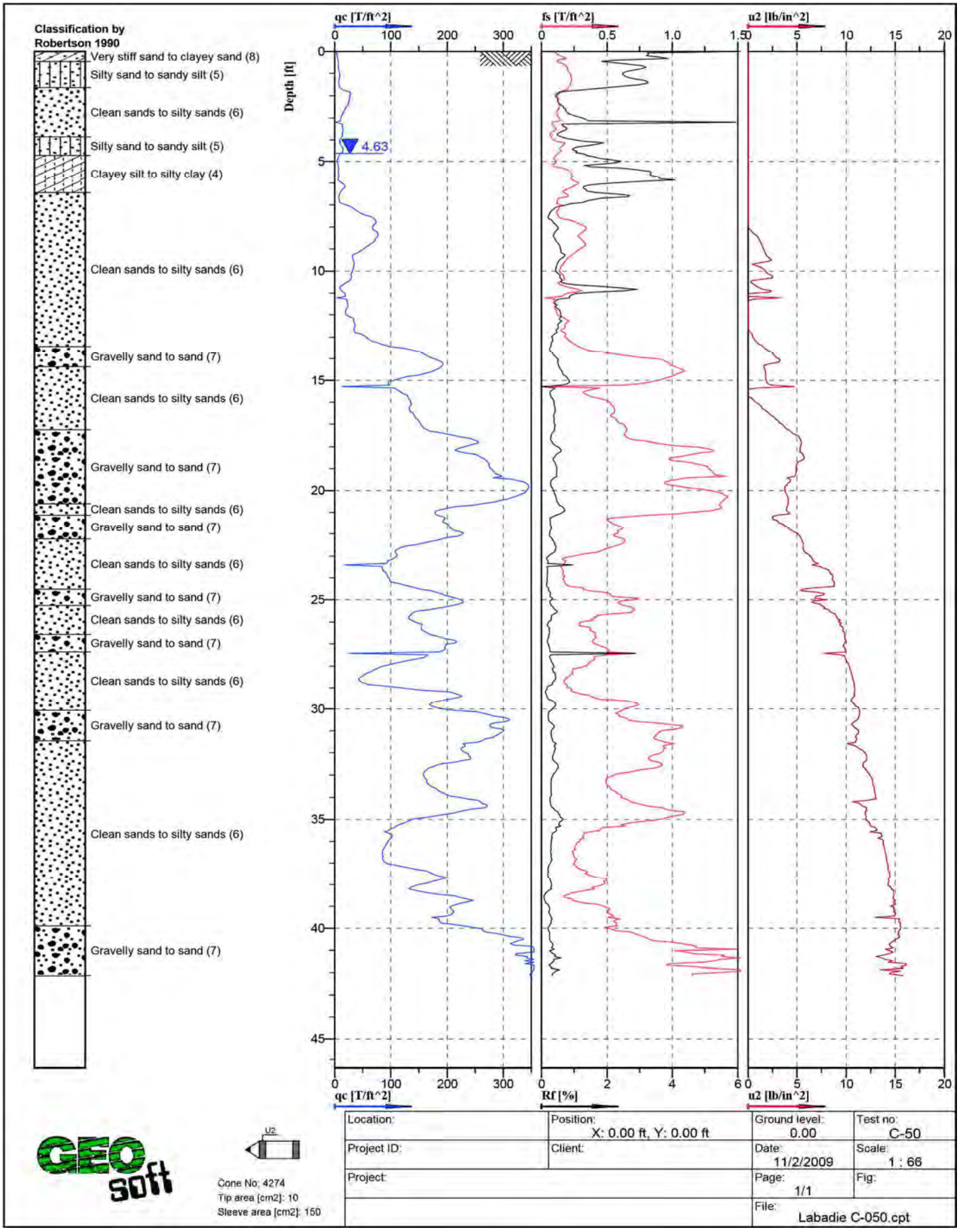

Figure A - 19: Cone Penetration Test Sounding Log, C-50

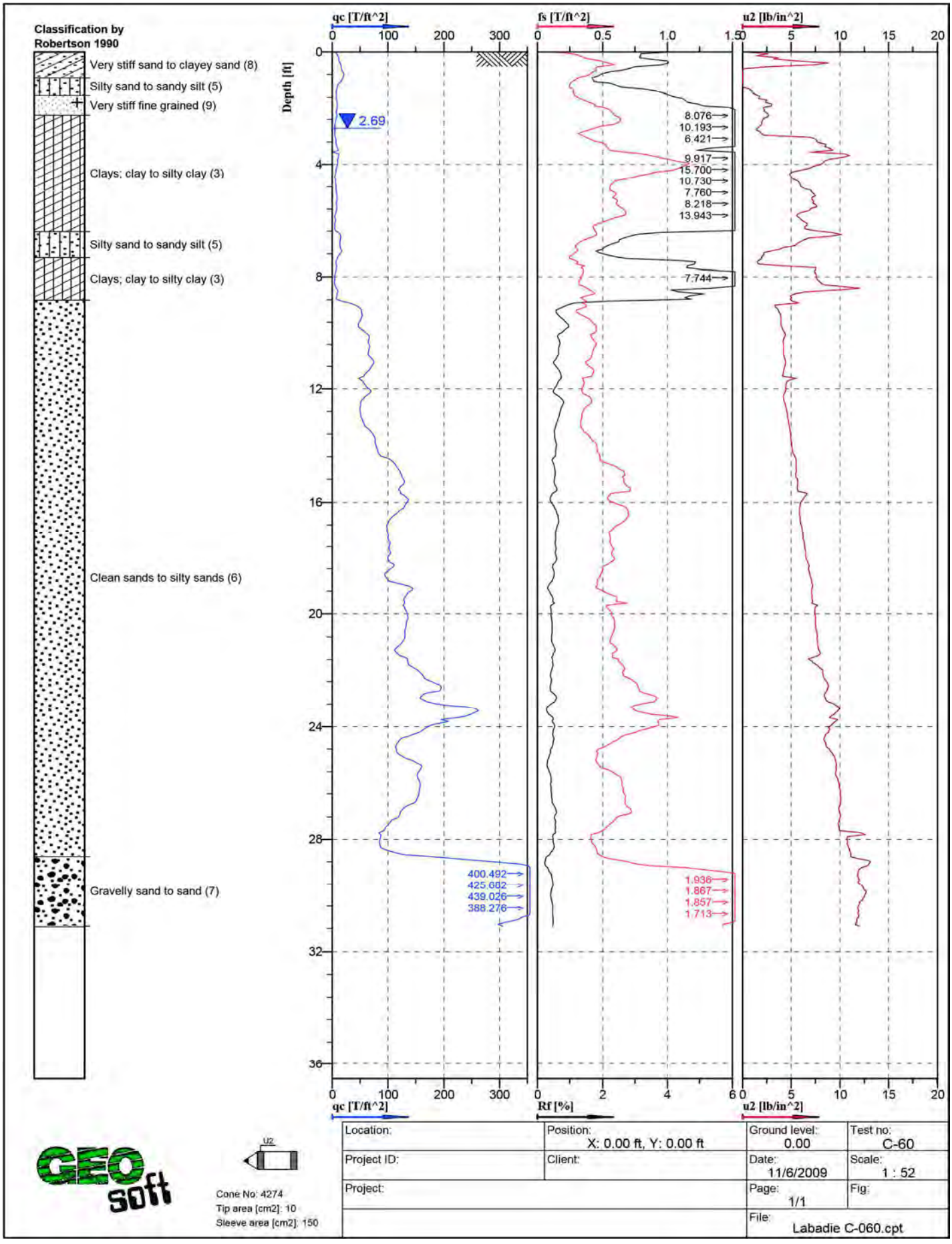

Figure A - 20: Cone Penetration Test Sounding Log, C-60

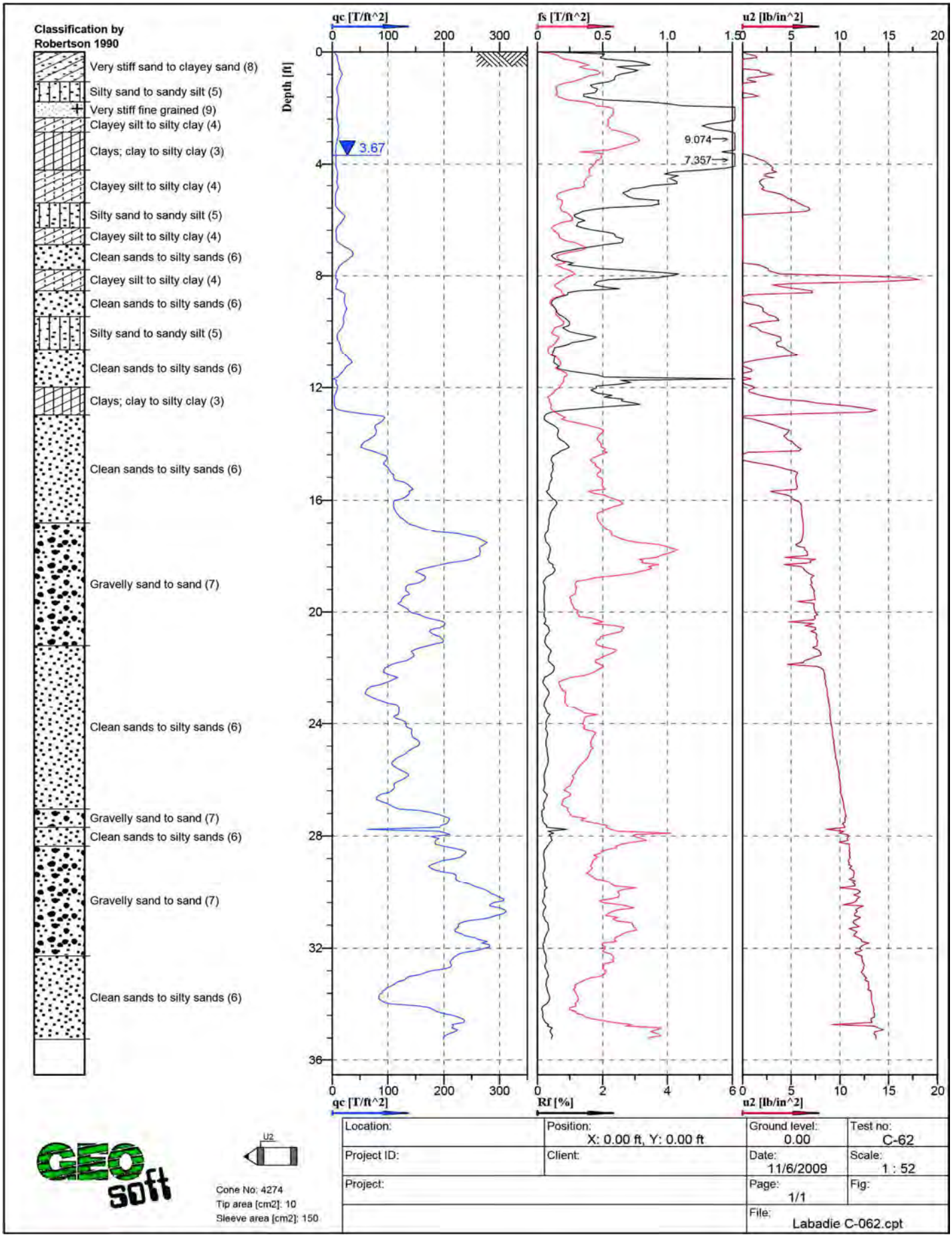

Figure A - 21: Cone Penetration Test Sounding Log, C-62

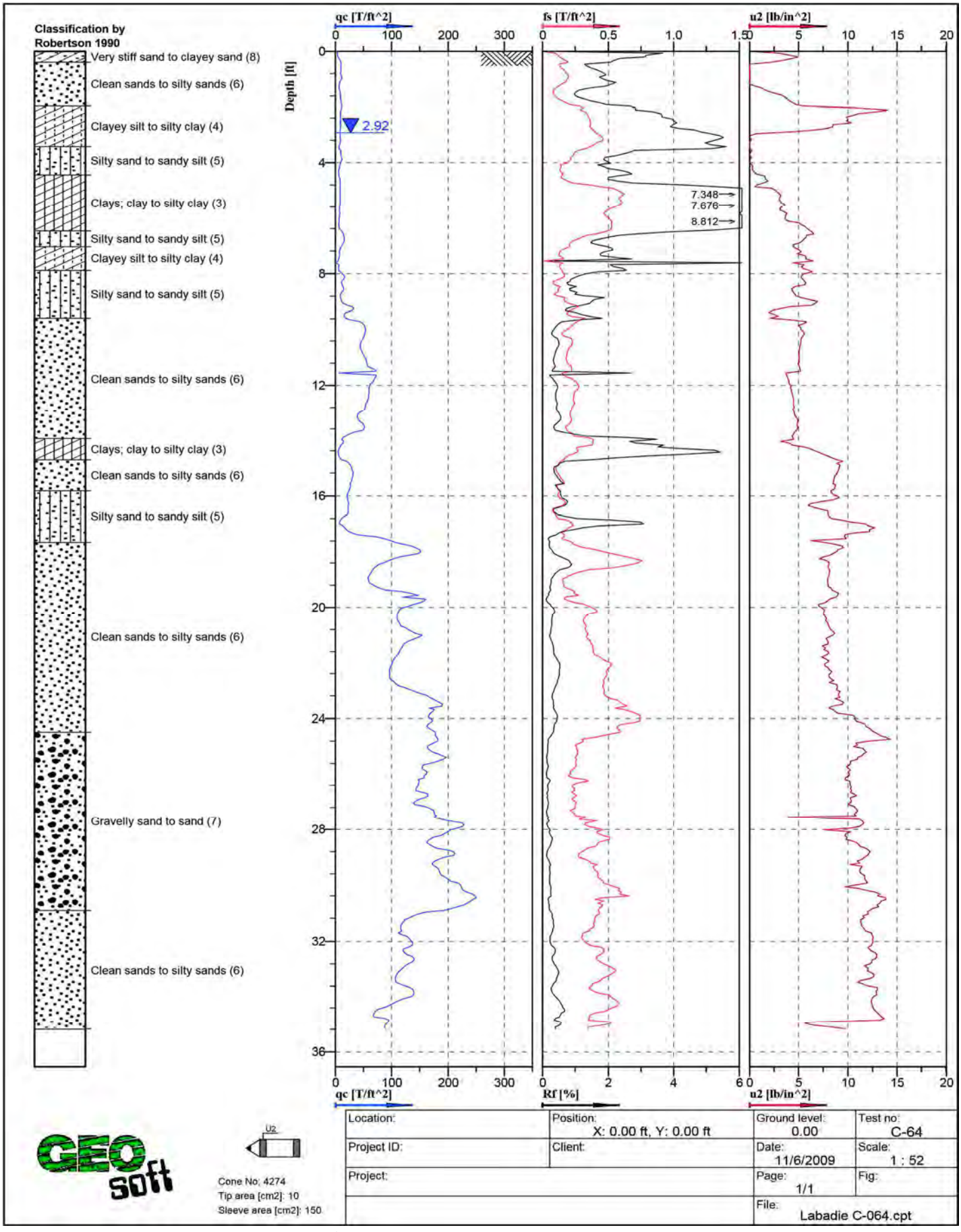

Figure A - 22: Cone Penetration Test Sounding Log, C-64

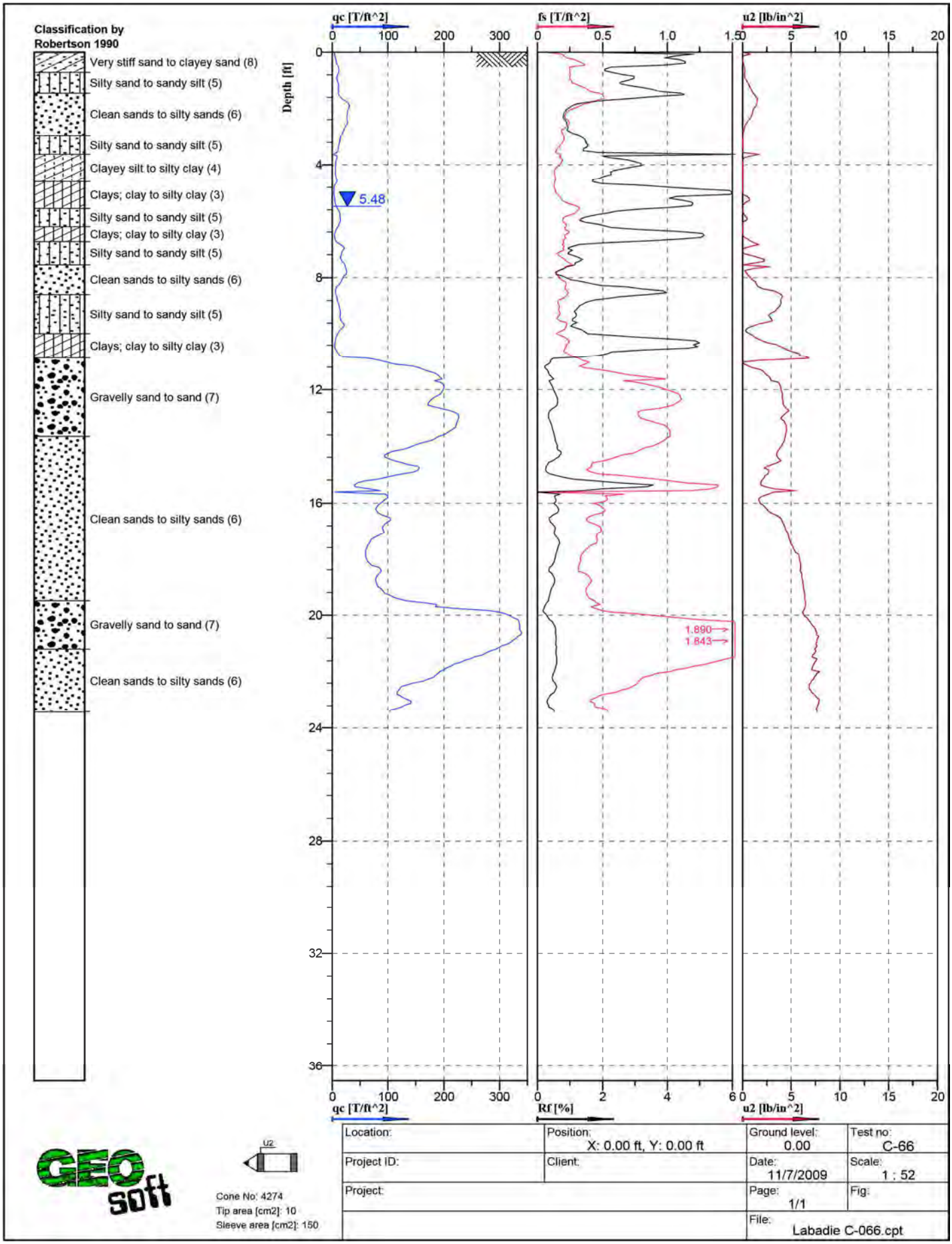

Figure A - 23: Cone Penetration Test Sounding Log, C-66

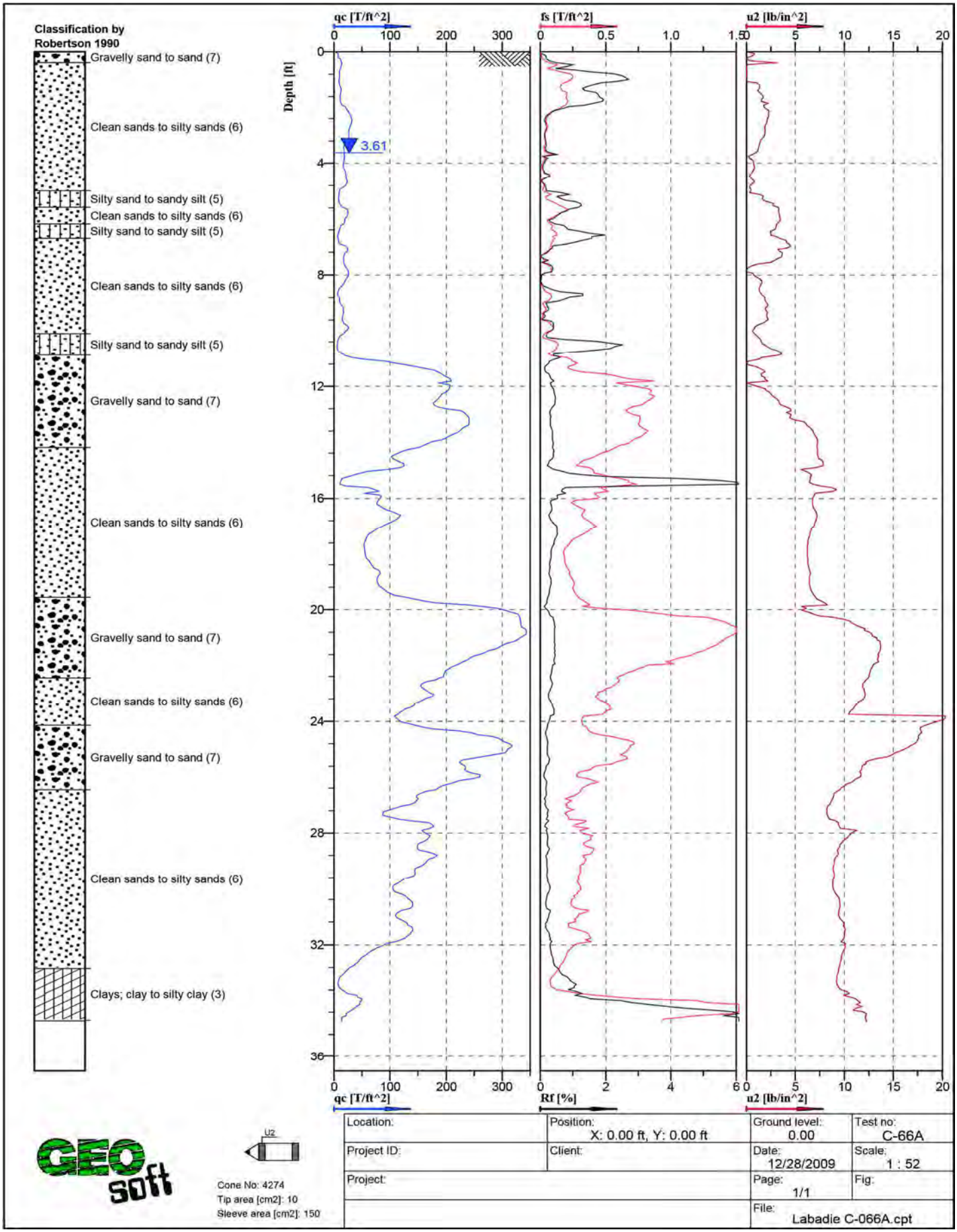

Figure A - 24: Cone Penetration Test Sounding Log, C-66A

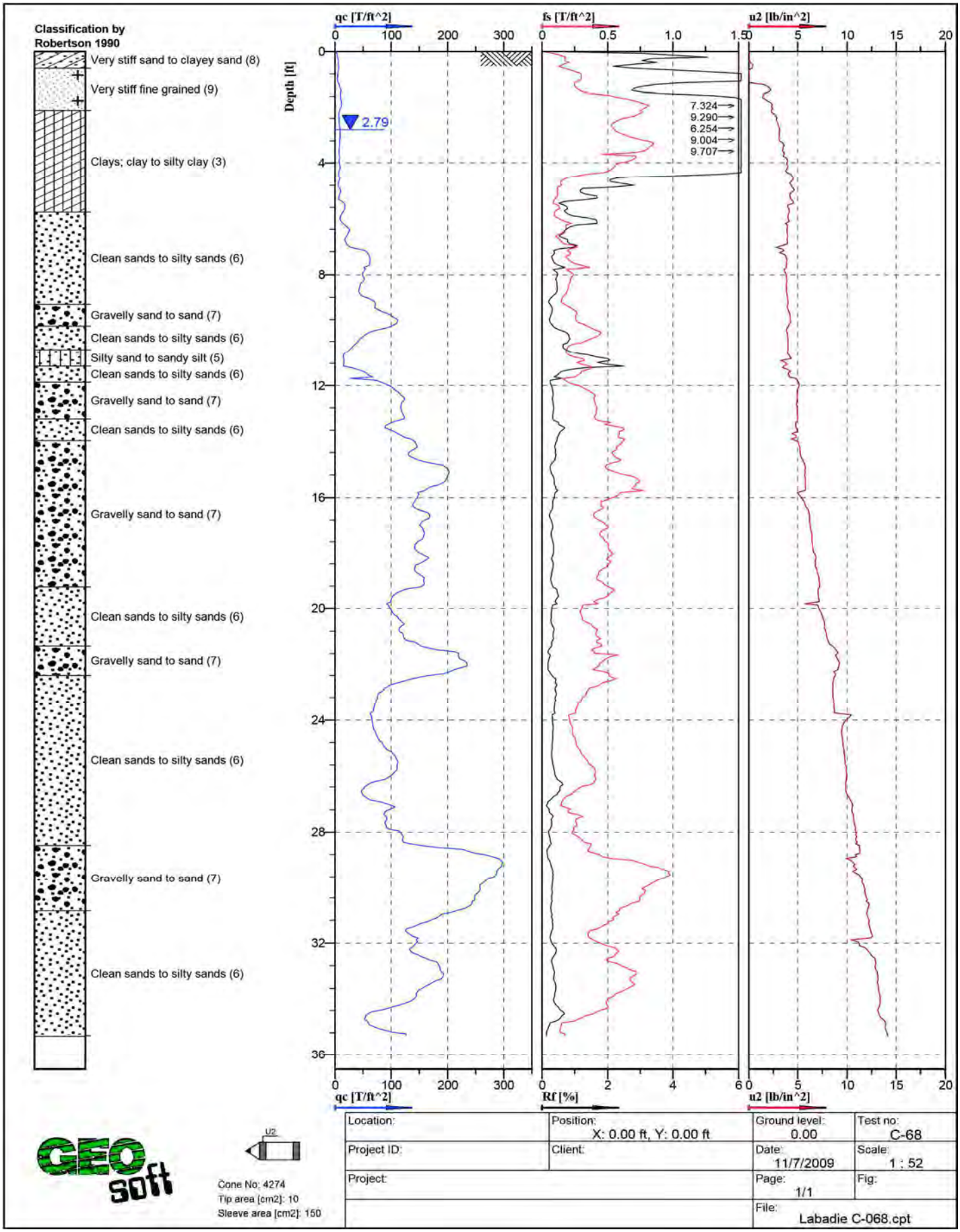

Figure A - 25: Cone Penetration Test Sounding Log, C-68

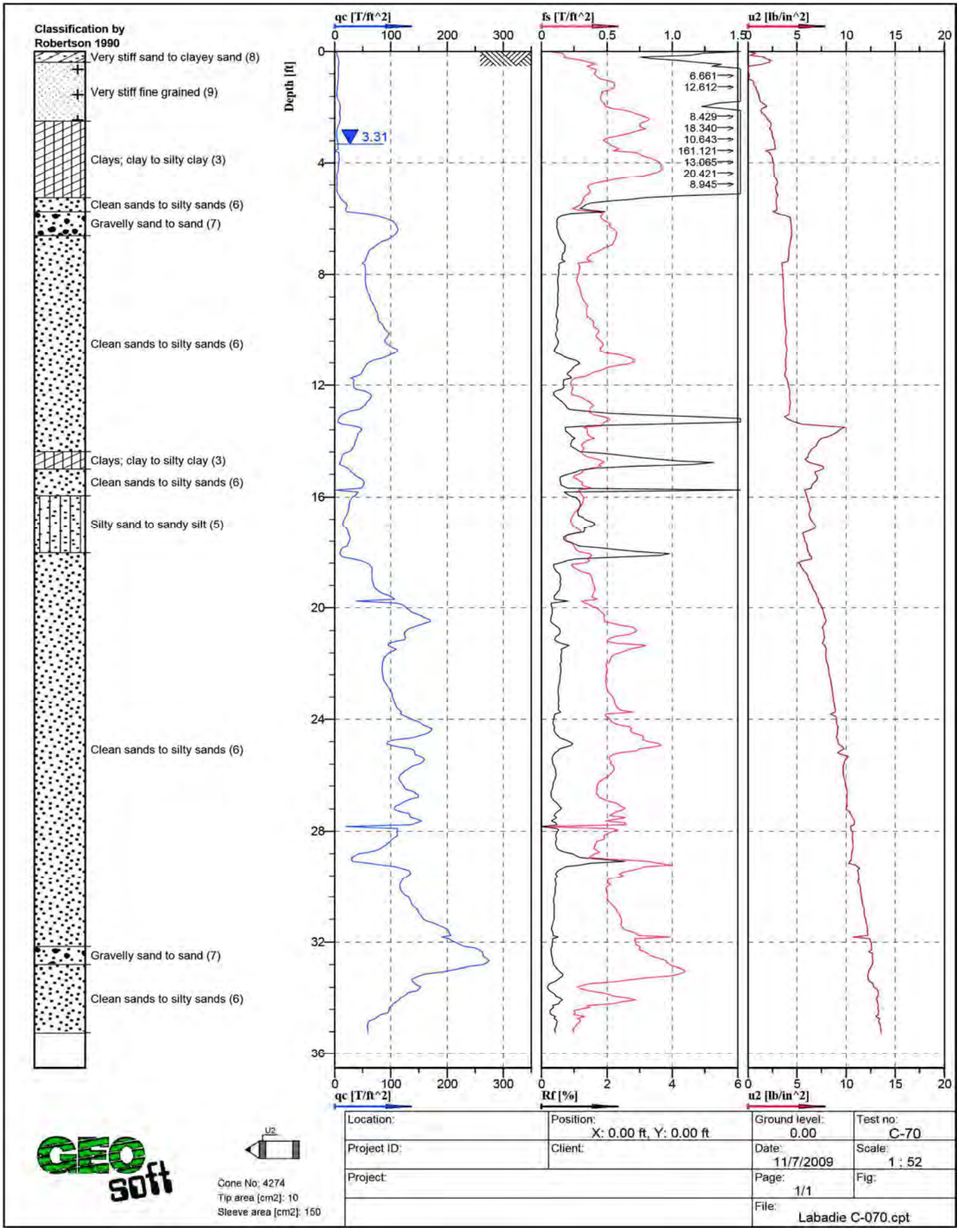

Figure A - 26: Cone Penetration Test Sounding Log, C-70

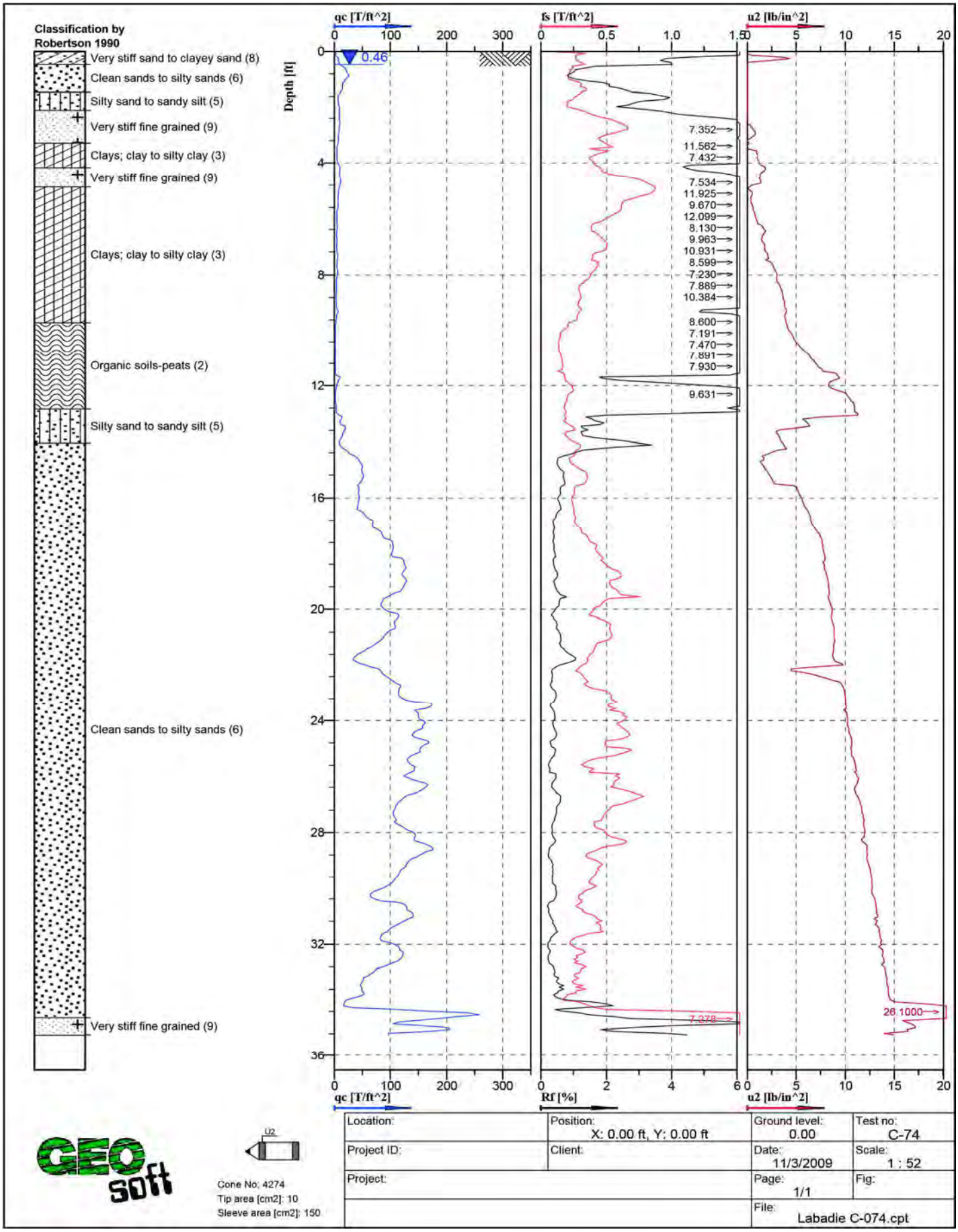

Figure A - 27: Cone Penetration Test Sounding Log, C-74

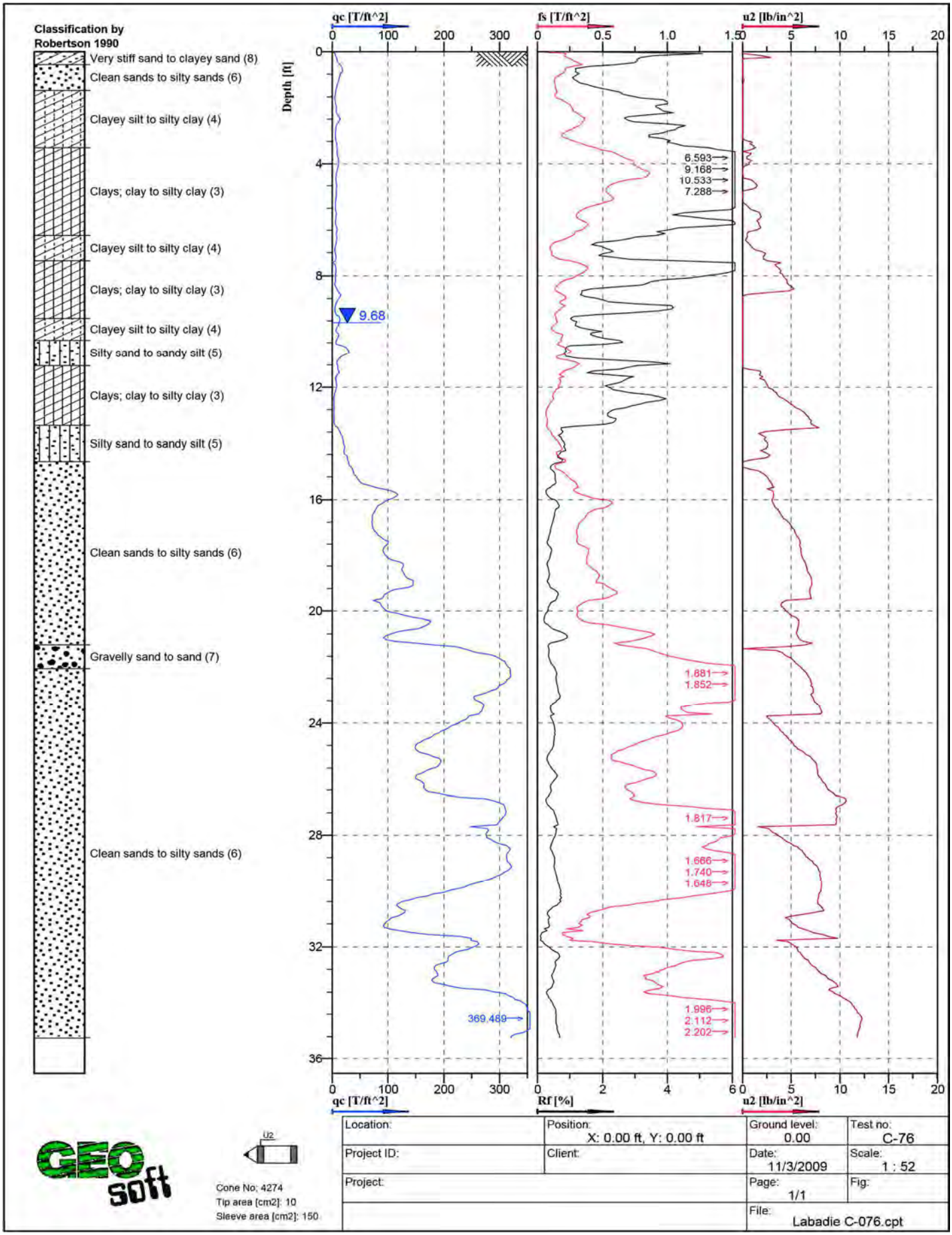

Figure A - 28: Cone Penetration Test Sounding Log, C-76

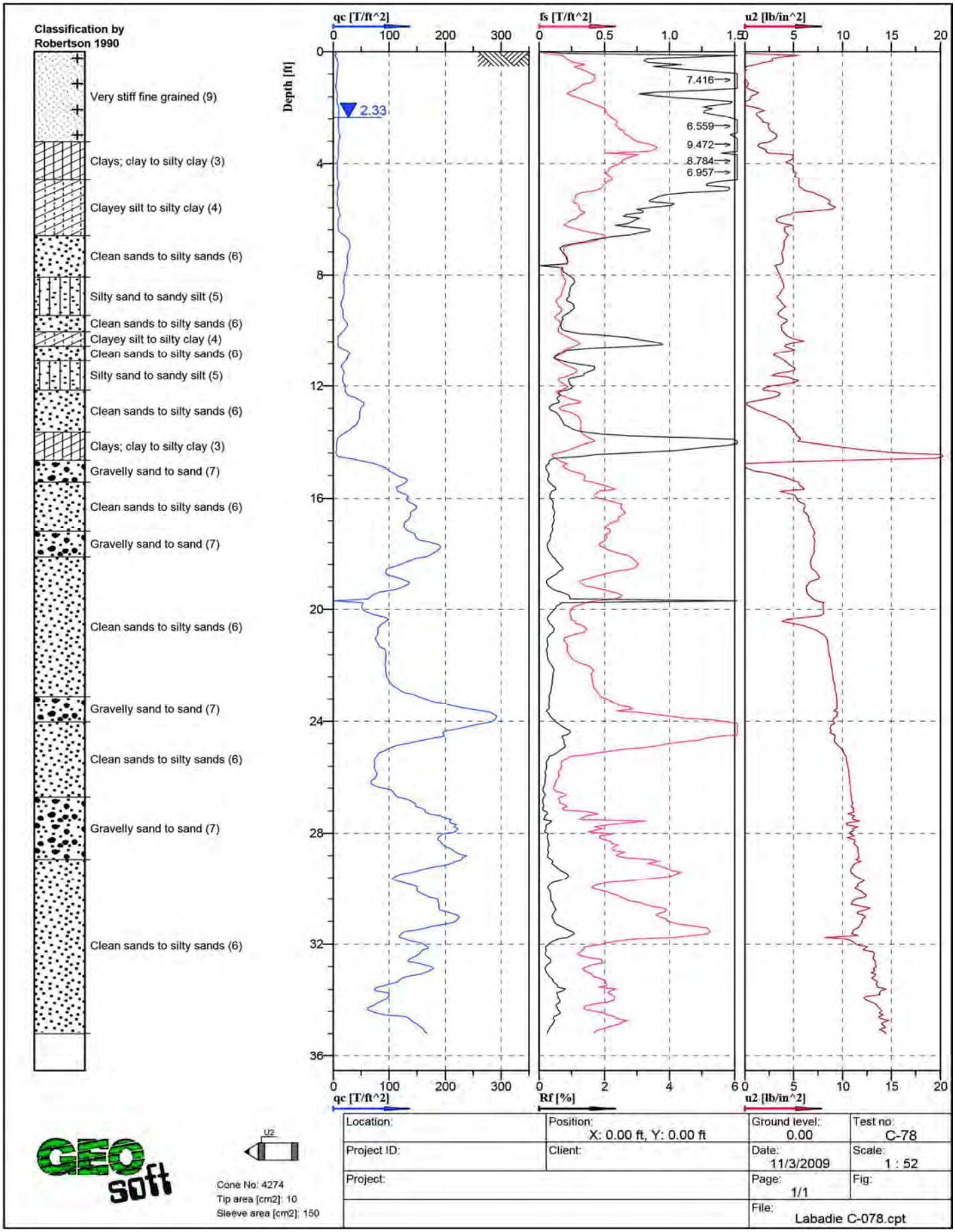

Figure A - 29: Cone Penetration Test Sounding Log, C-78

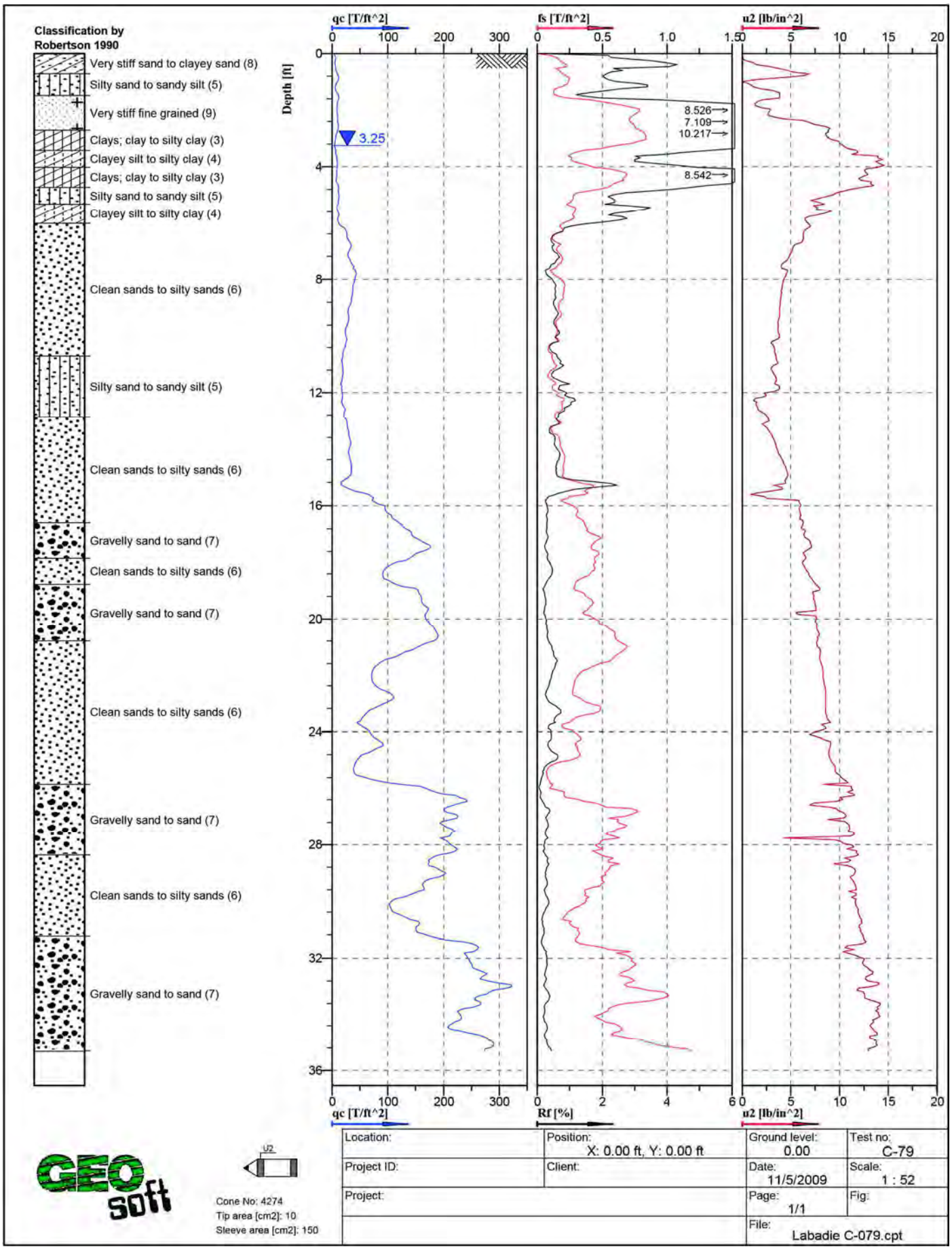

Figure A - 30: Cone Penetration Test Sounding Log, C-79

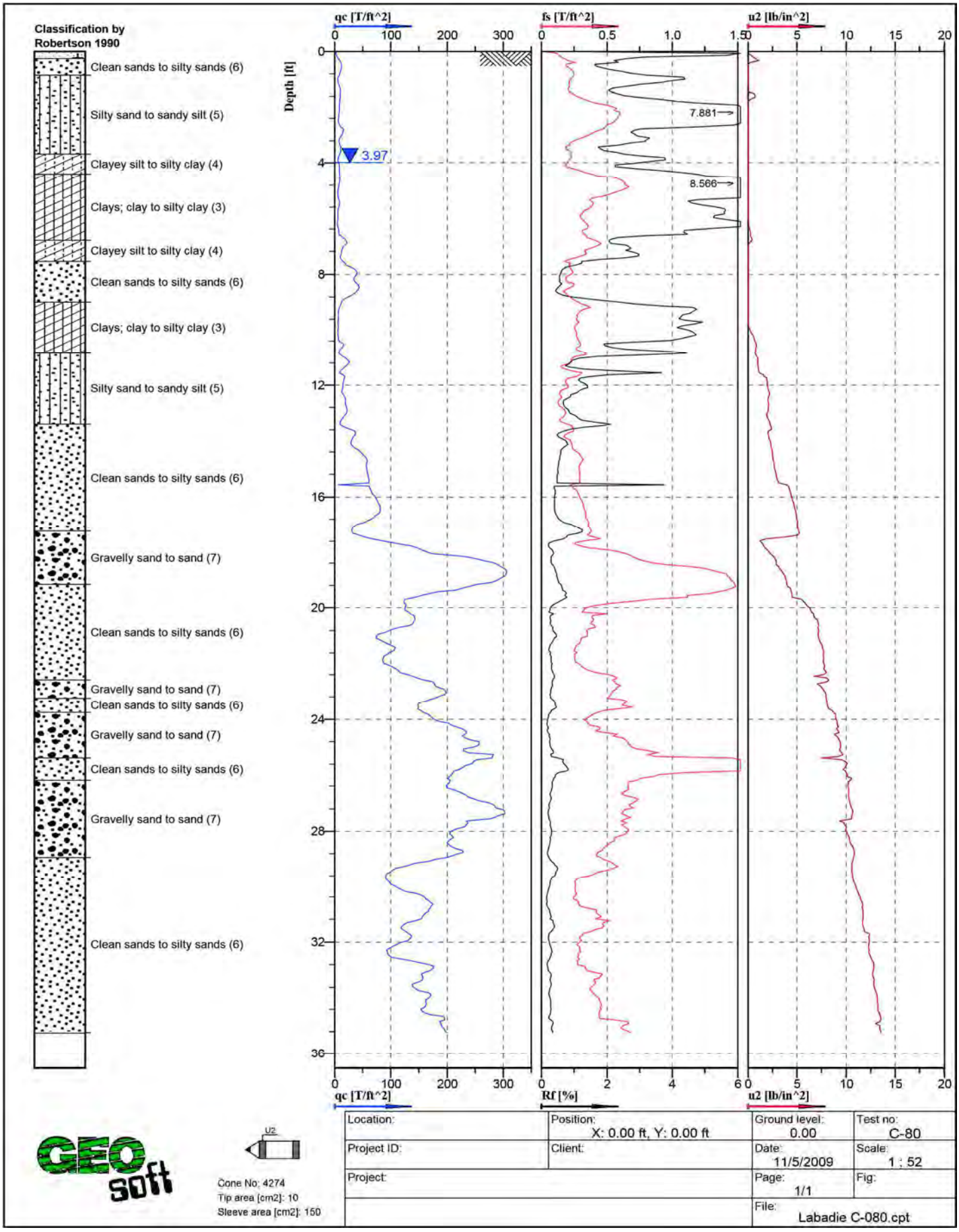

Figure A - 31: Cone Penetration Test Sounding Log, C-80

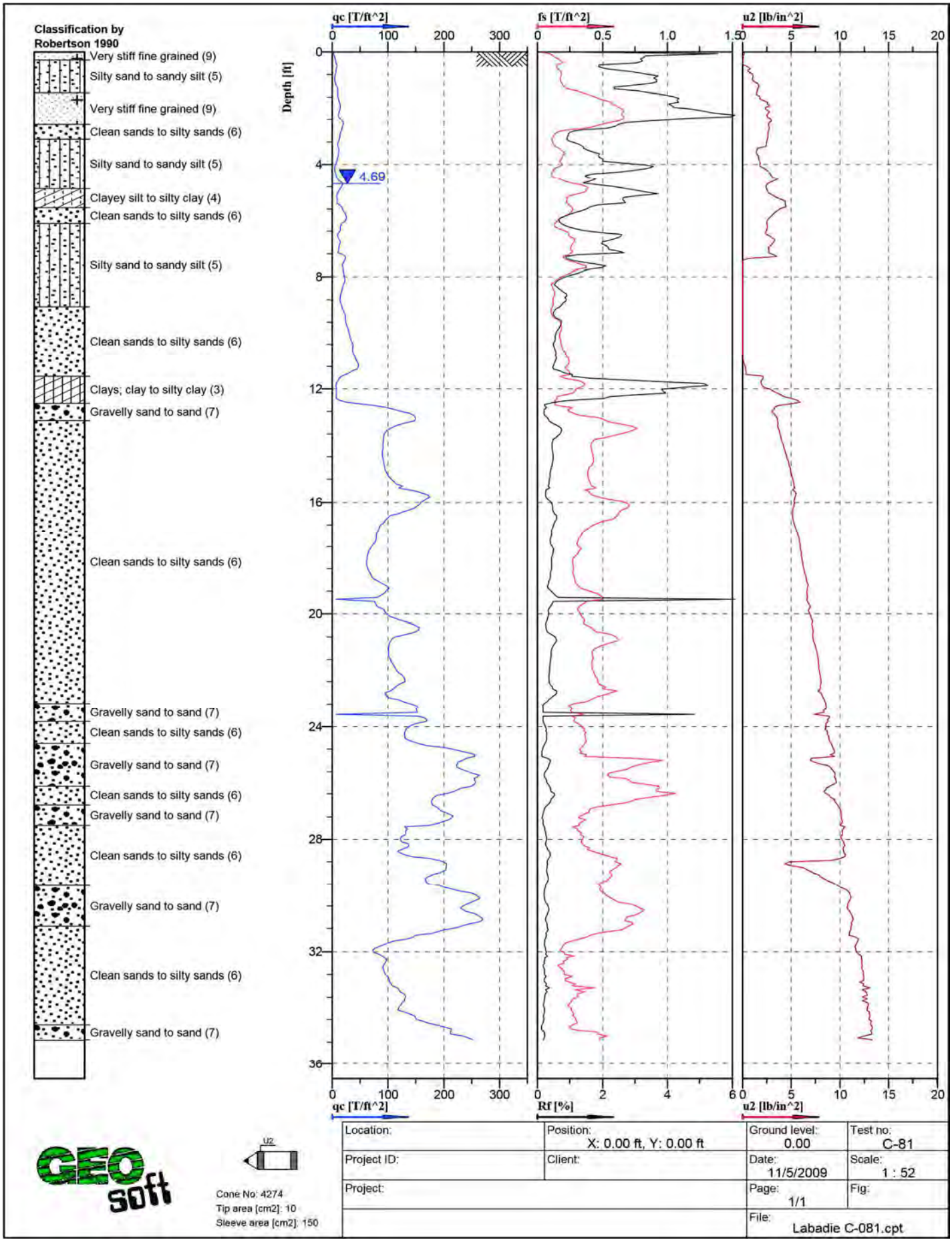

Figure A - 32: Cone Penetration Test Sounding Log, C-81

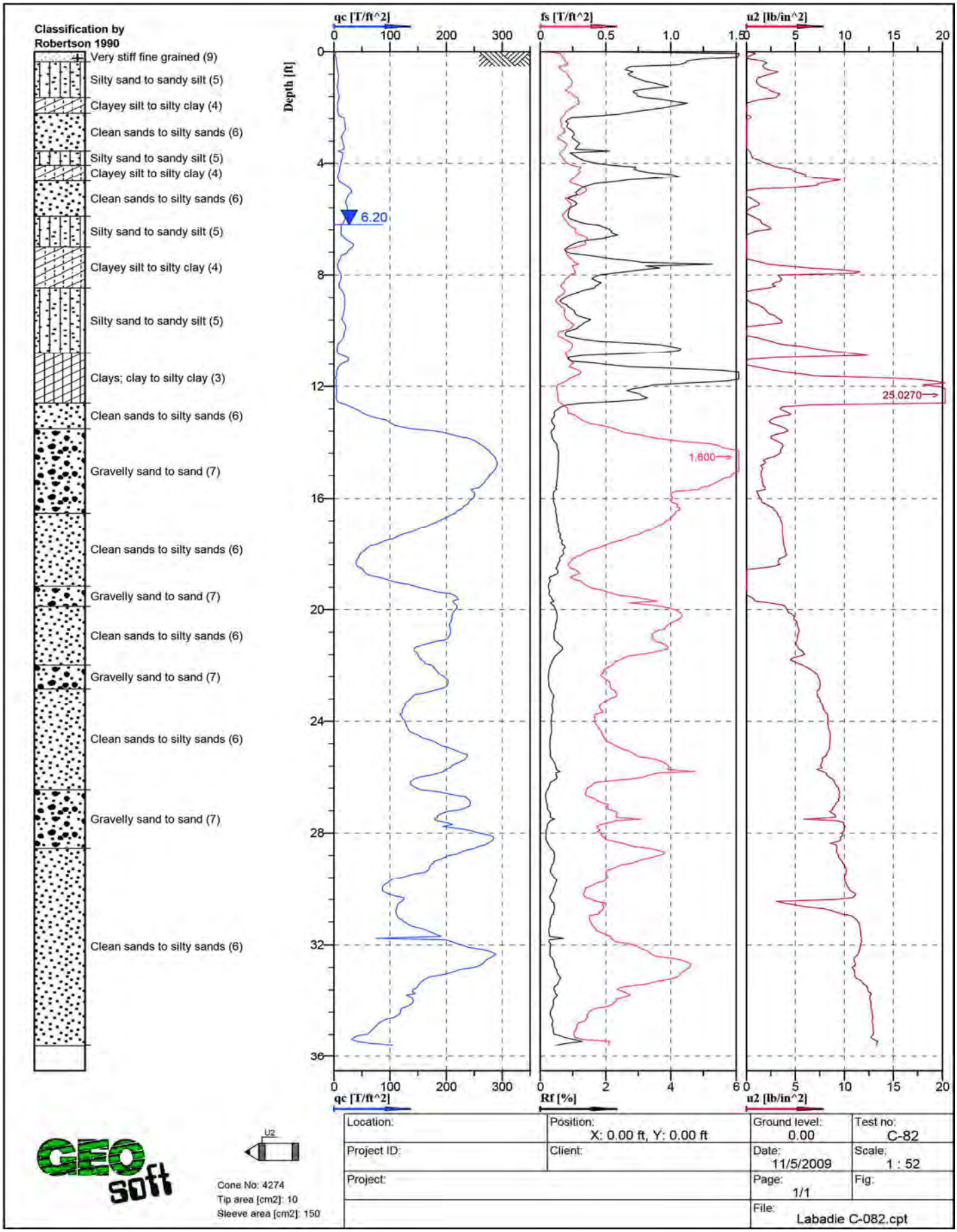

Figure A - 33: Cone Penetration Test Sounding Log, C-82

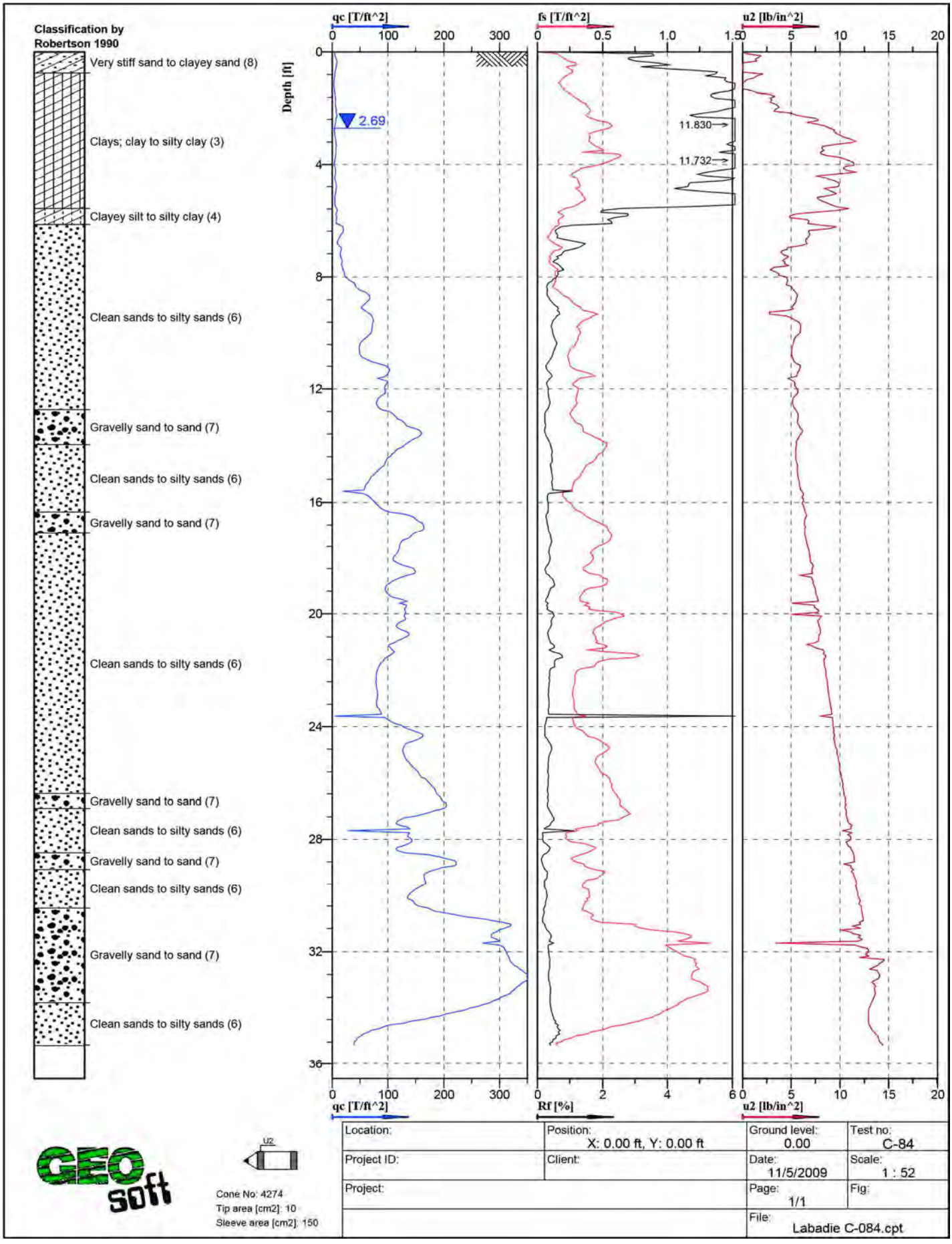

Figure A - 34: Cone Penetration Test Sounding Log, C-84

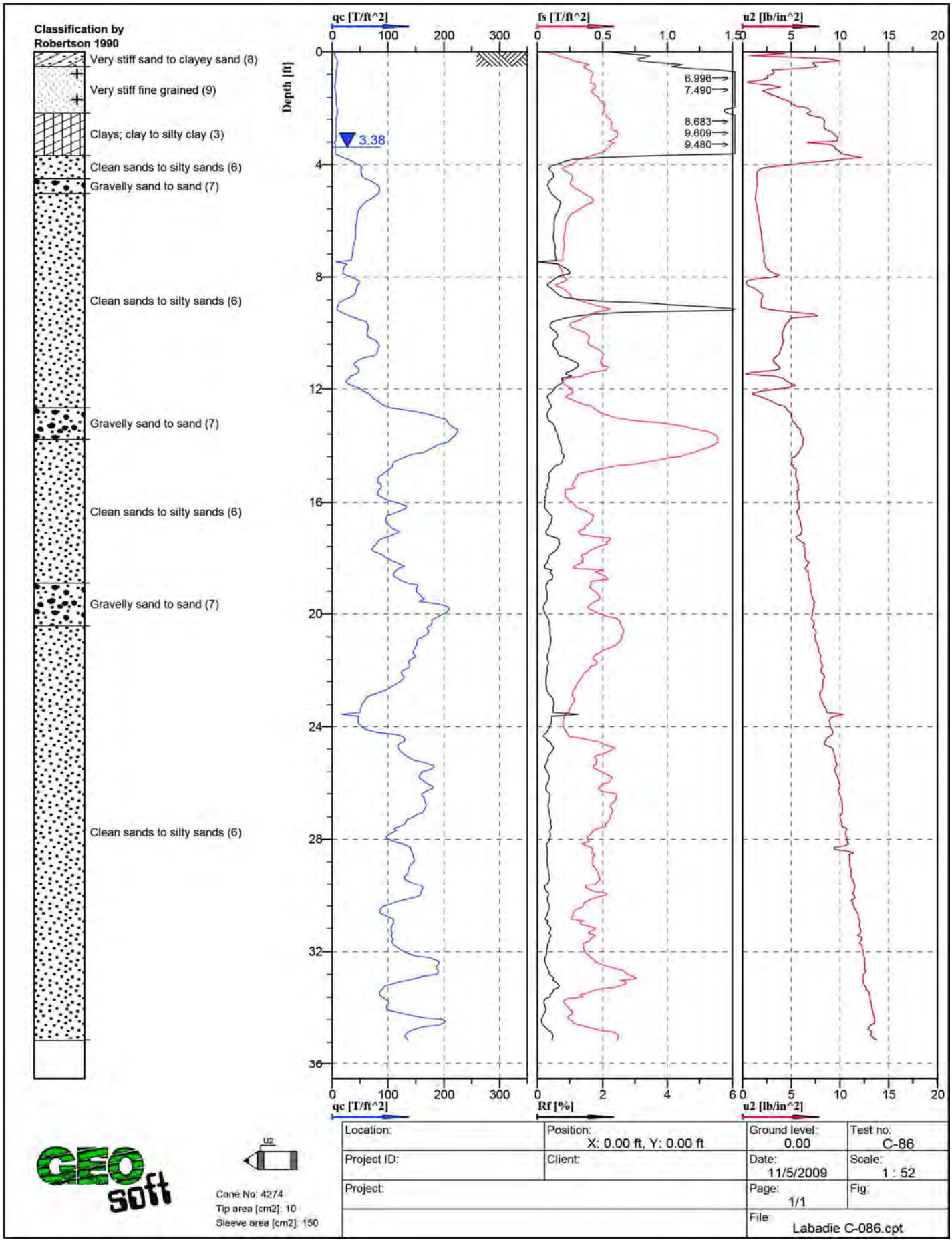

Figure A - 35: Cone Penetration Test Sounding Log, C-86

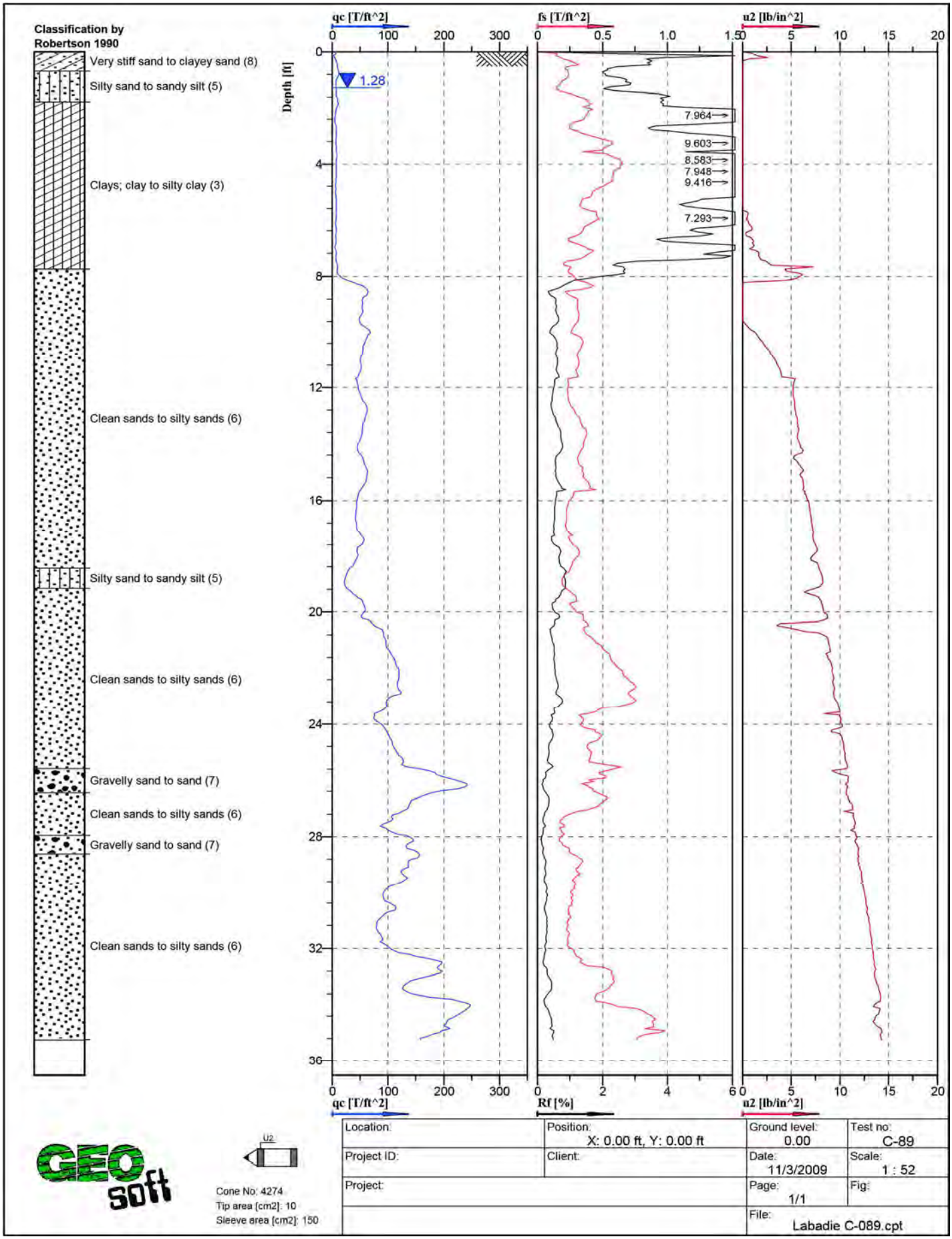

Figure A - 36: Cone Penetration Test Sounding Log, C-89

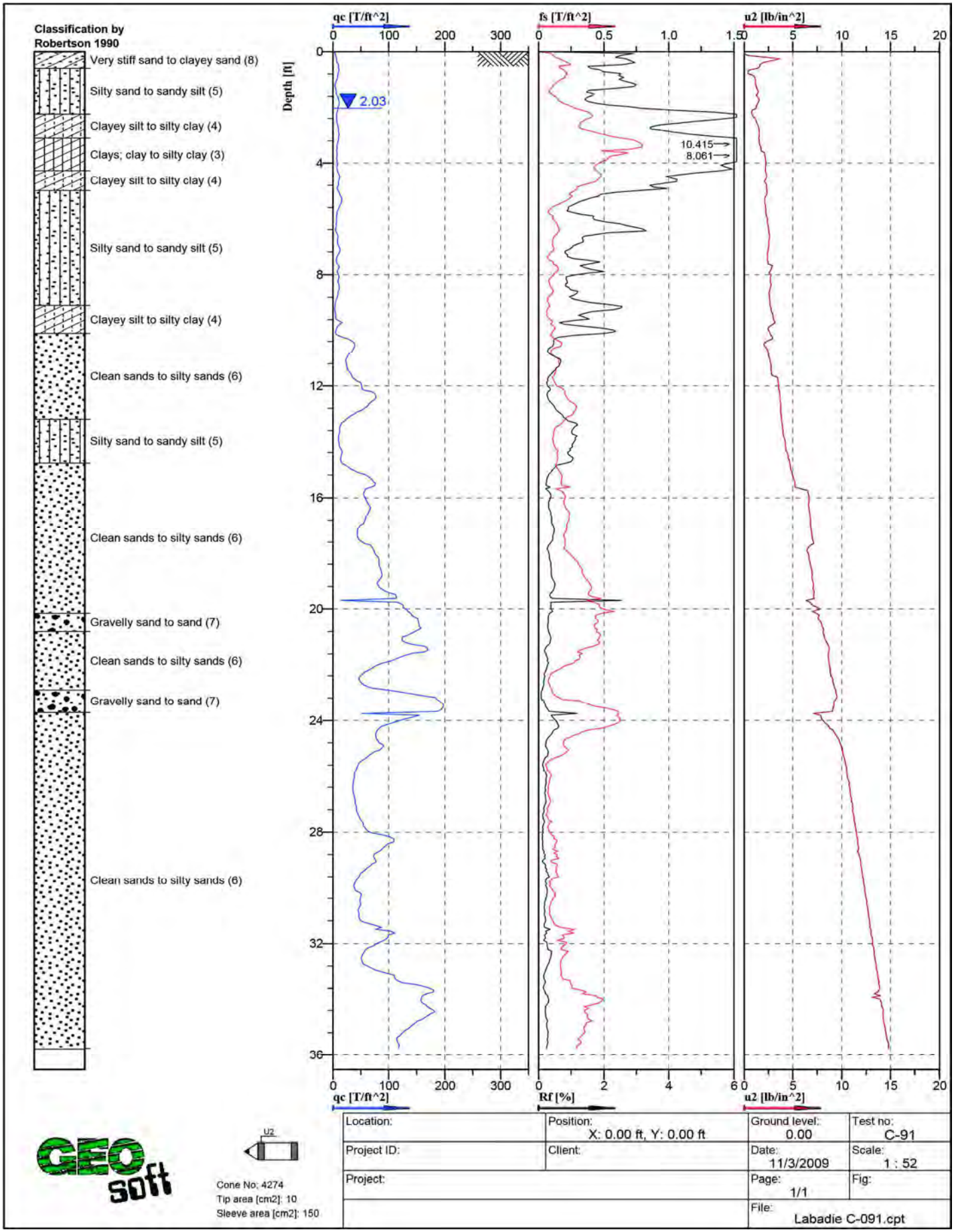

Figure A - 37: Cone Penetration Test Sounding Log, C-91

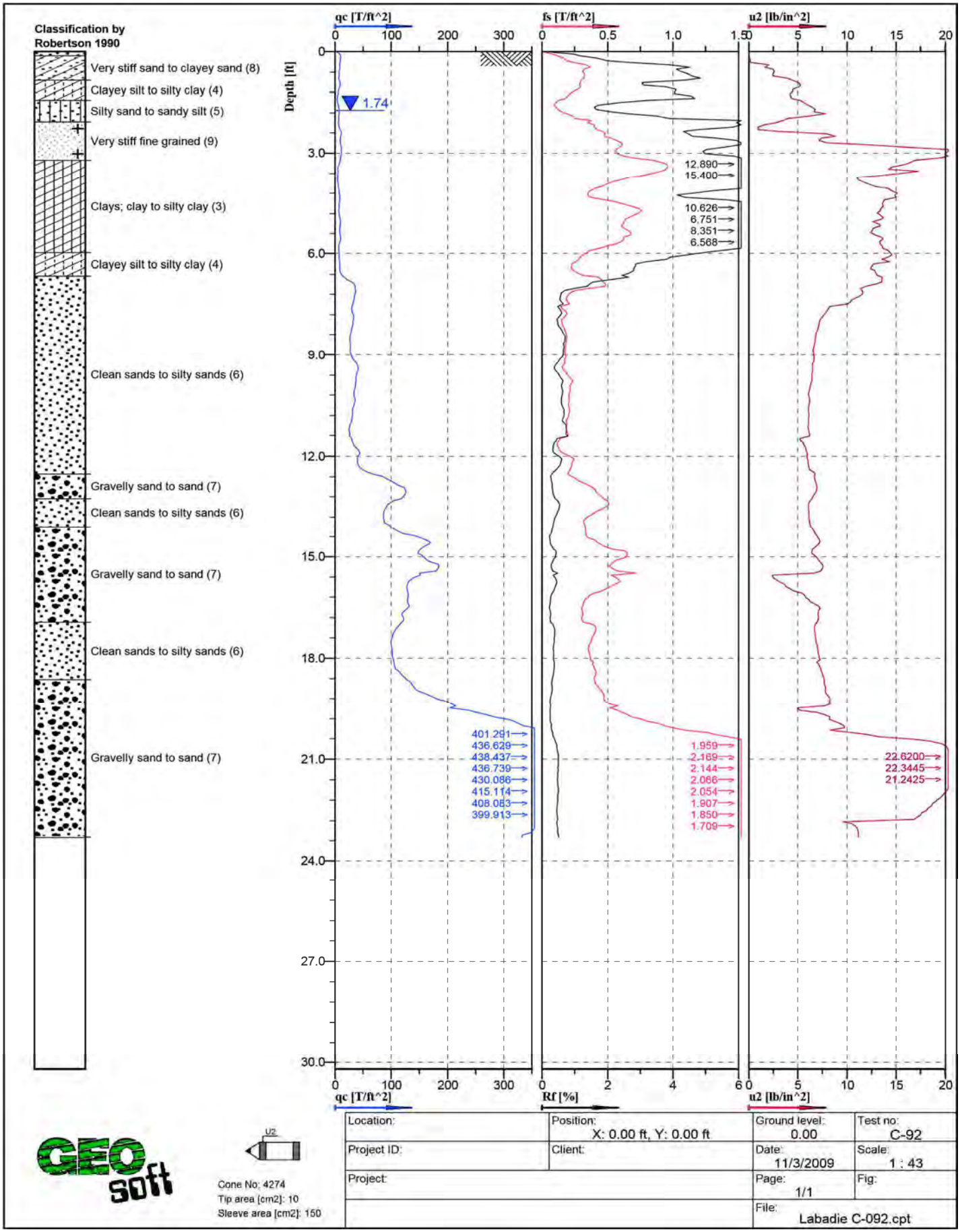

Figure A - 38: Cone Penetration Test Sounding Log, C-92

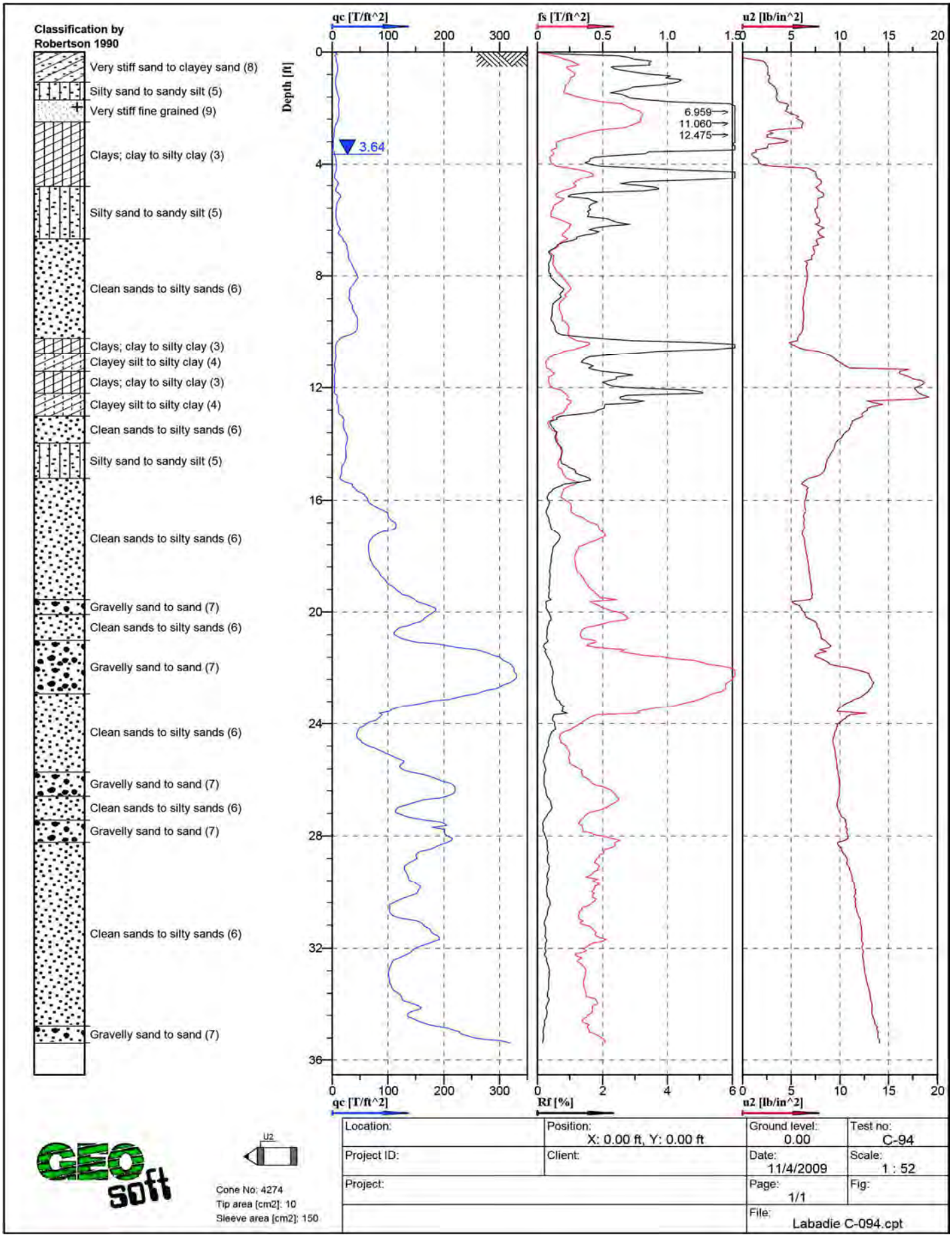

Figure A - 39: Cone Penetration Test Sounding Log, C-94

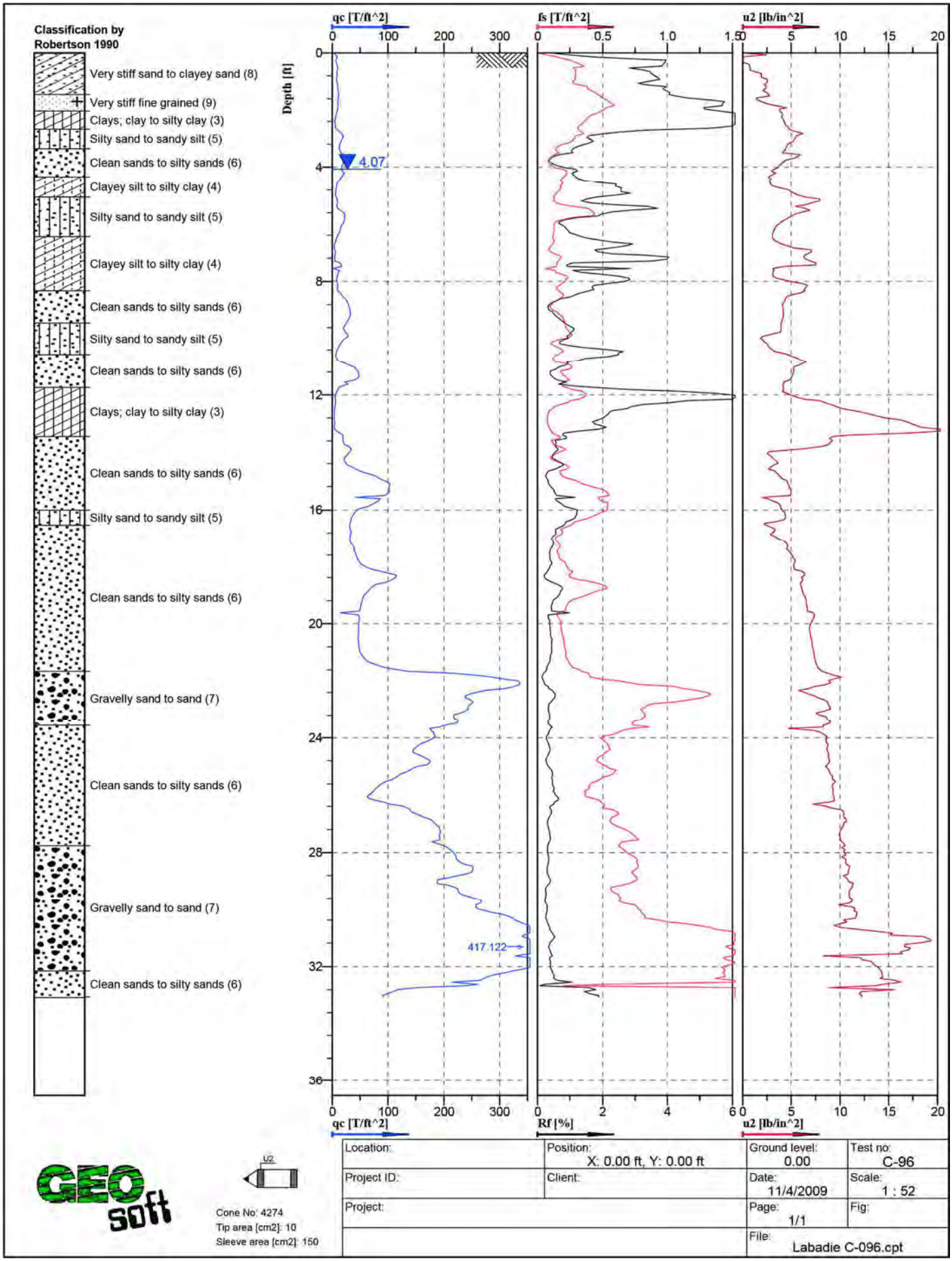

Figure A - 40: Cone Penetration Test Sounding Log, C-96

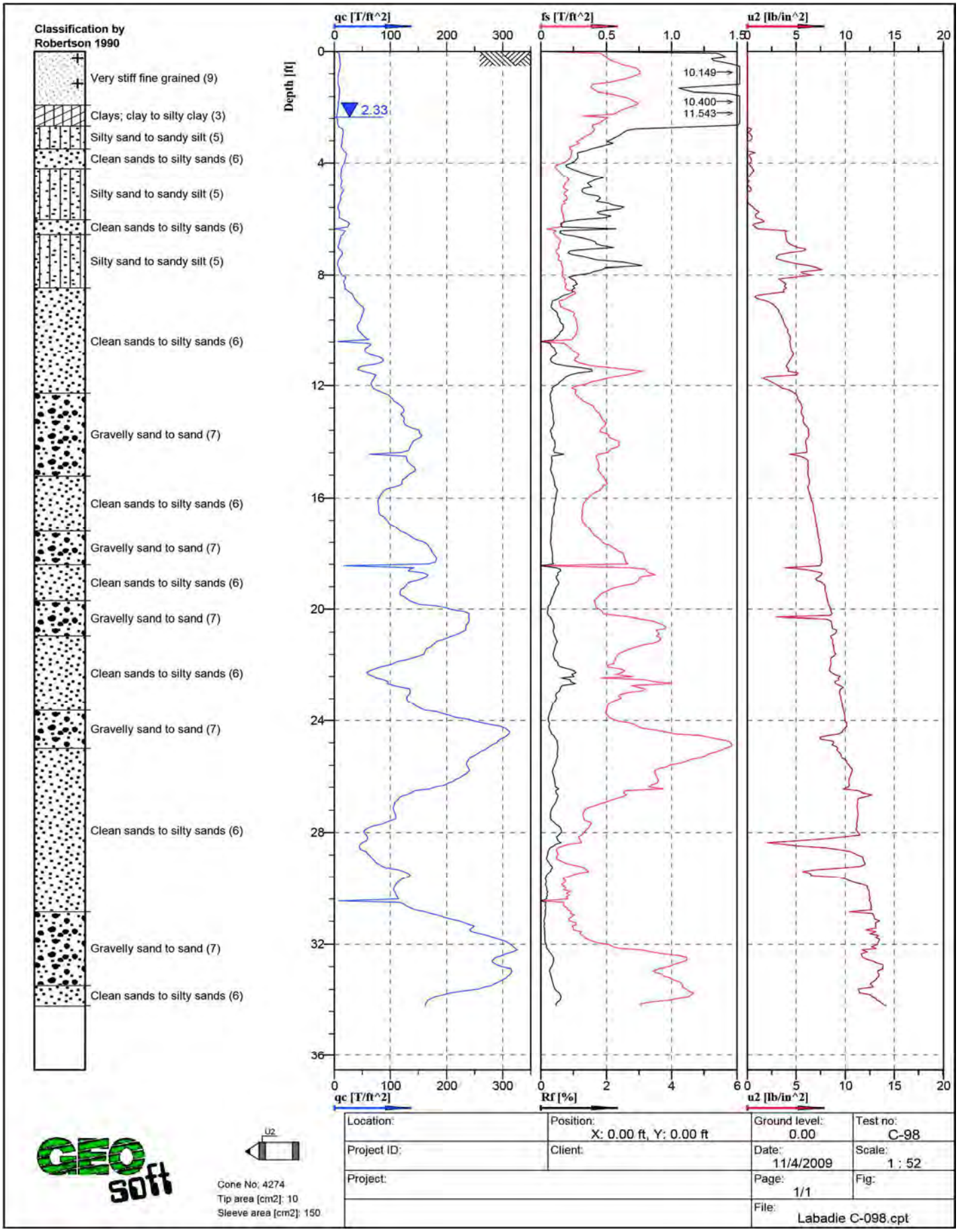

Figure A - 41: Cone Penetration Test Sounding Log, C-98

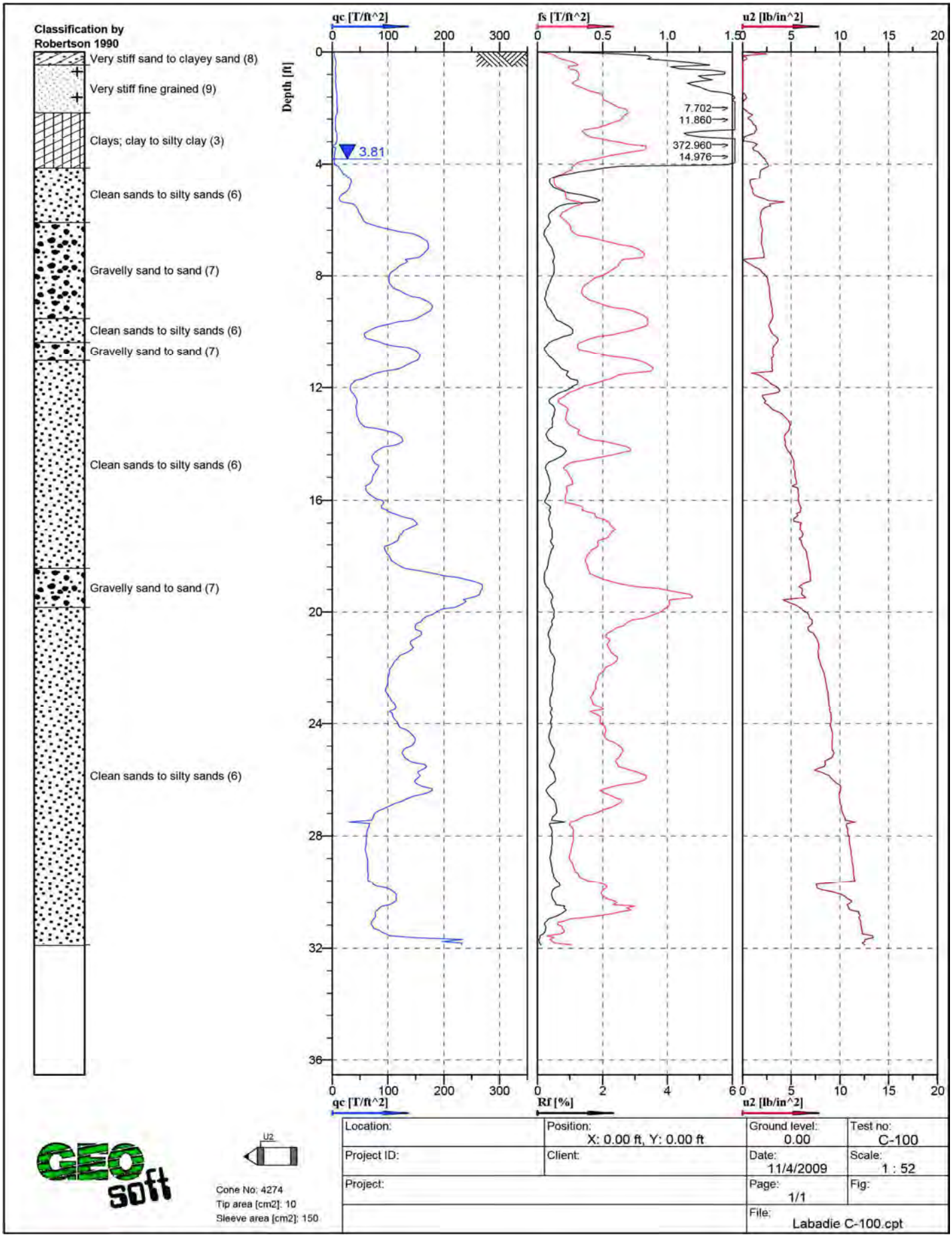

Figure A - 42: Cone Penetration Test Sounding Log, C-100

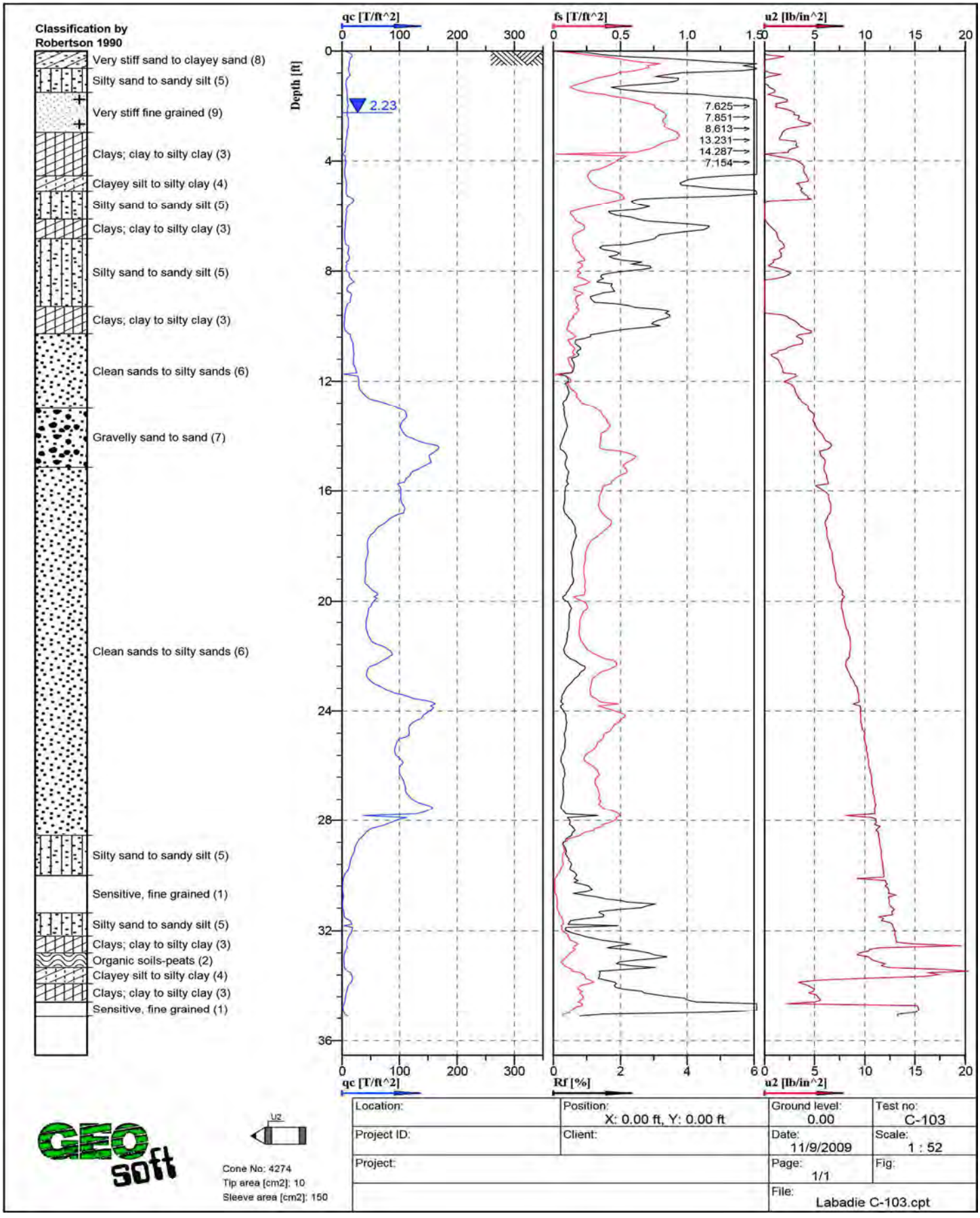

Figure A - 43: Cone Penetration Test Sounding Log, C-103

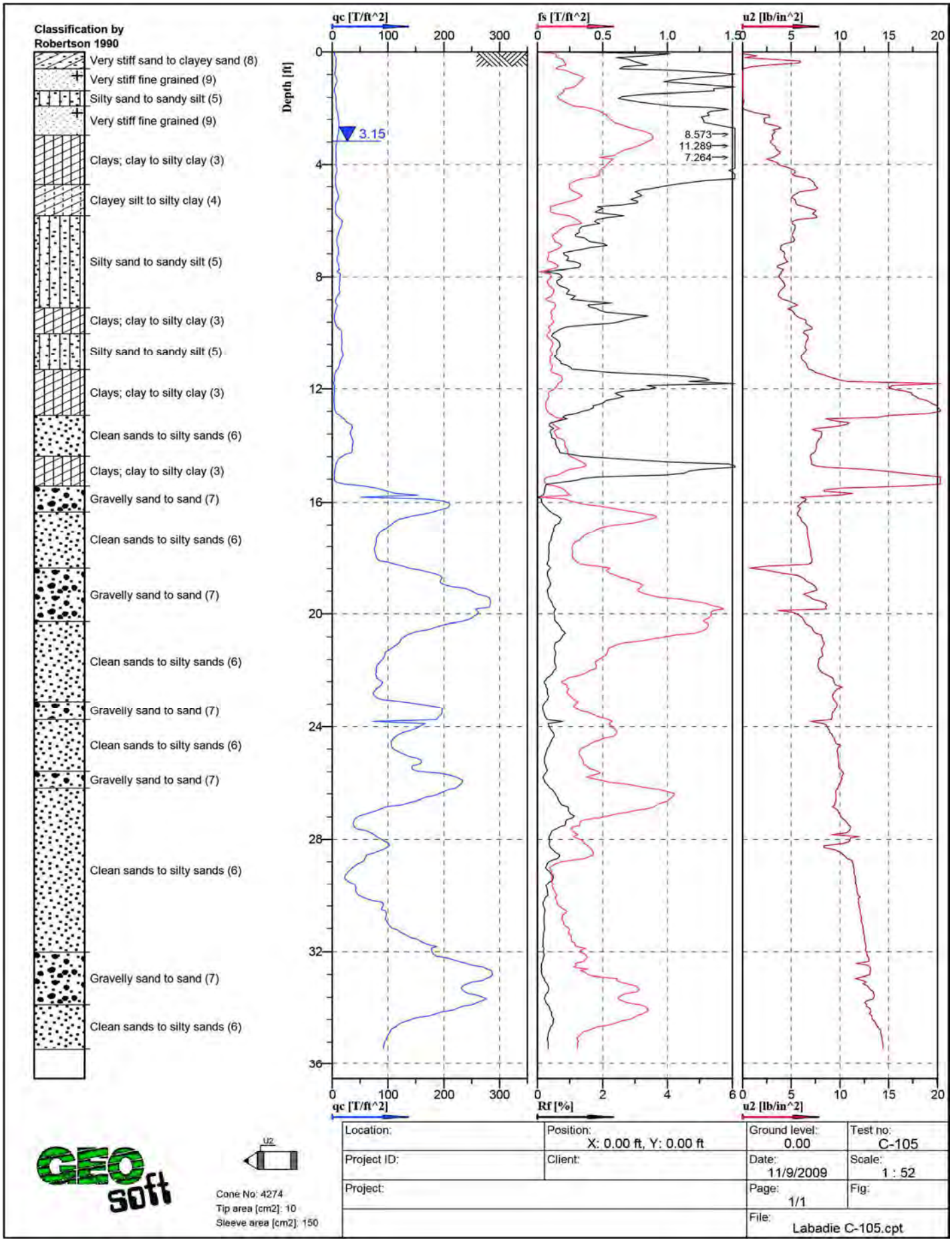

Figure A - 44: Cone Penetration Test Sounding Log, C-105

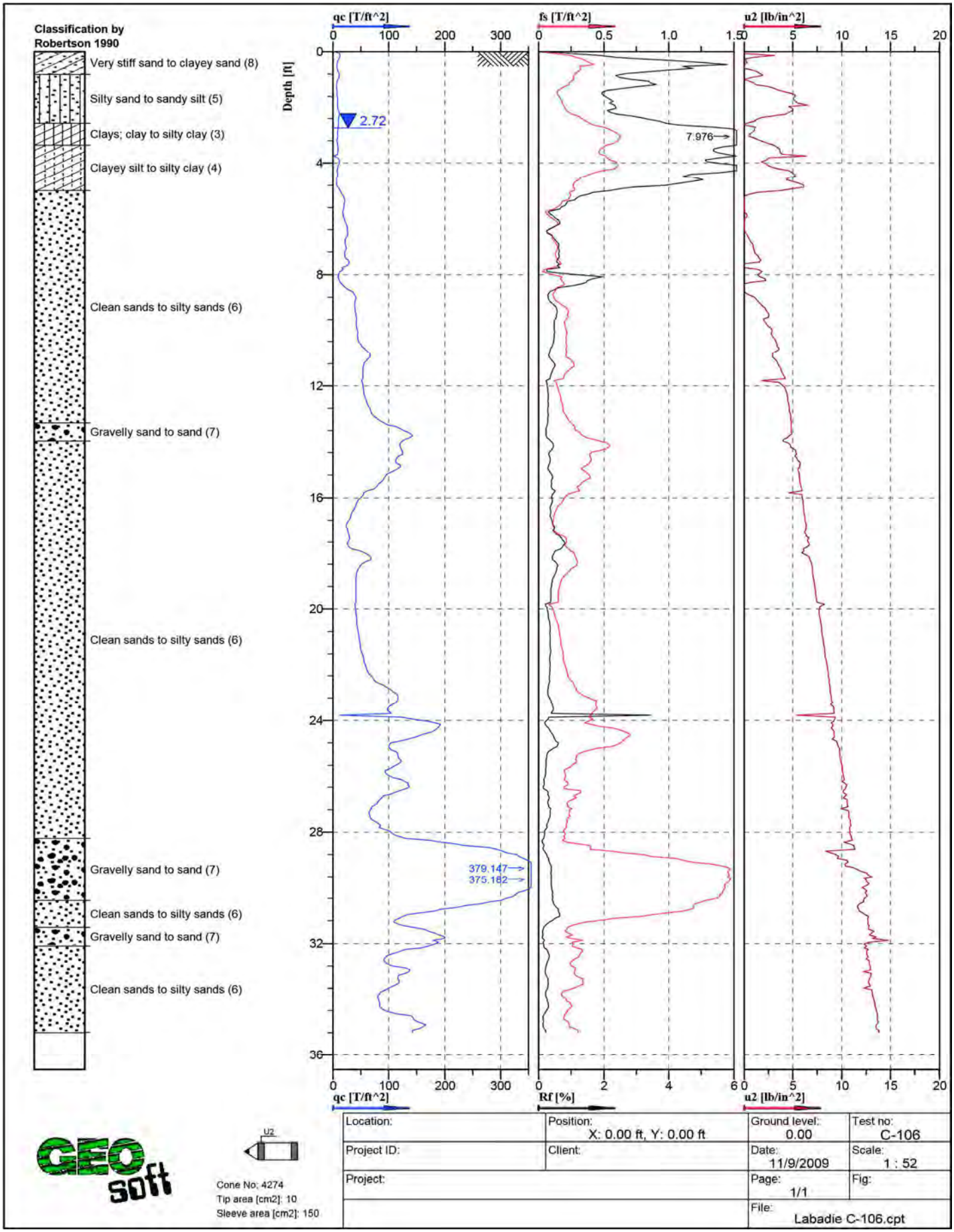

Figure A - 45: Cone Penetration Test Sounding Log, C-106

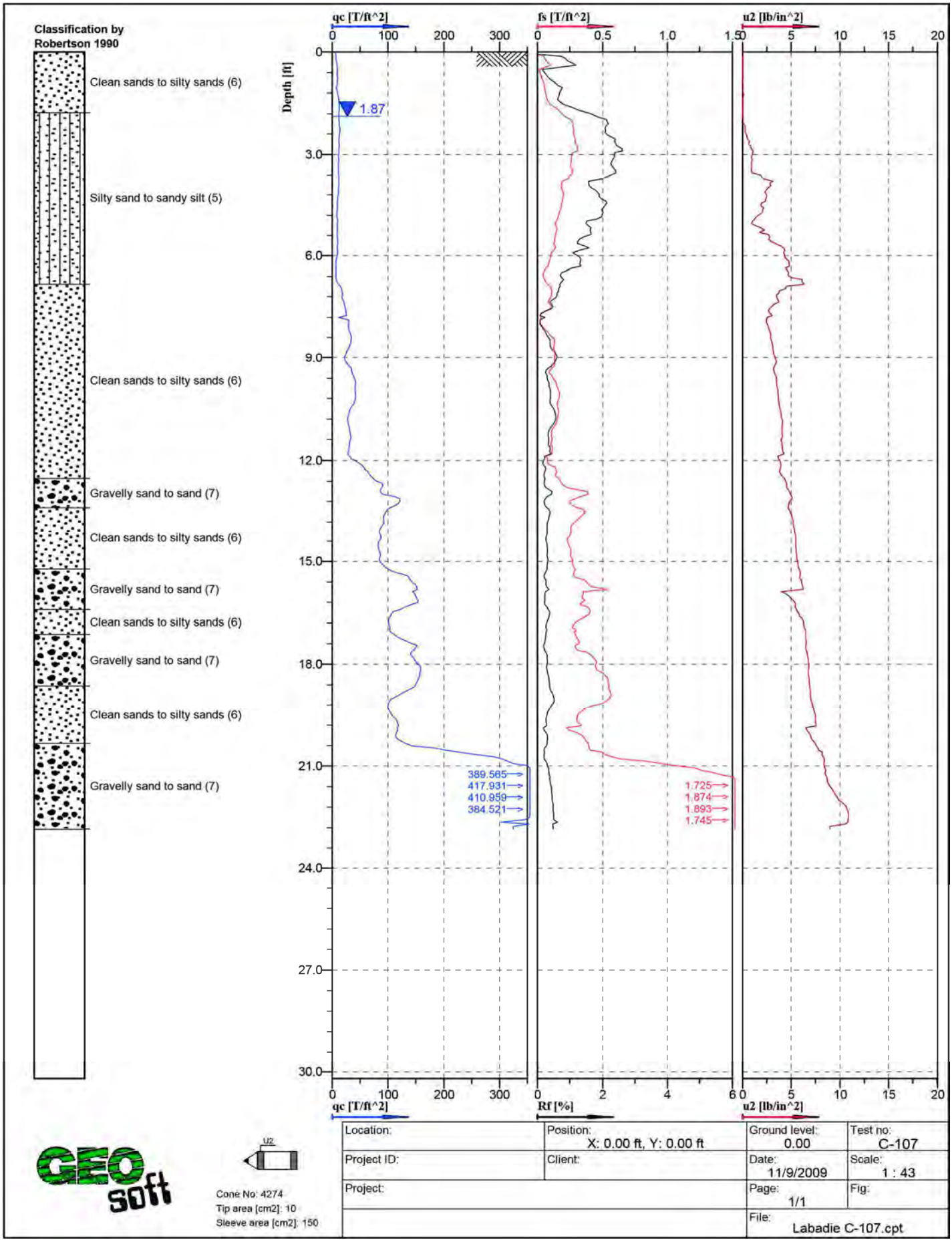

Figure A - 46: Cone Penetration Test Sounding Log, C-107

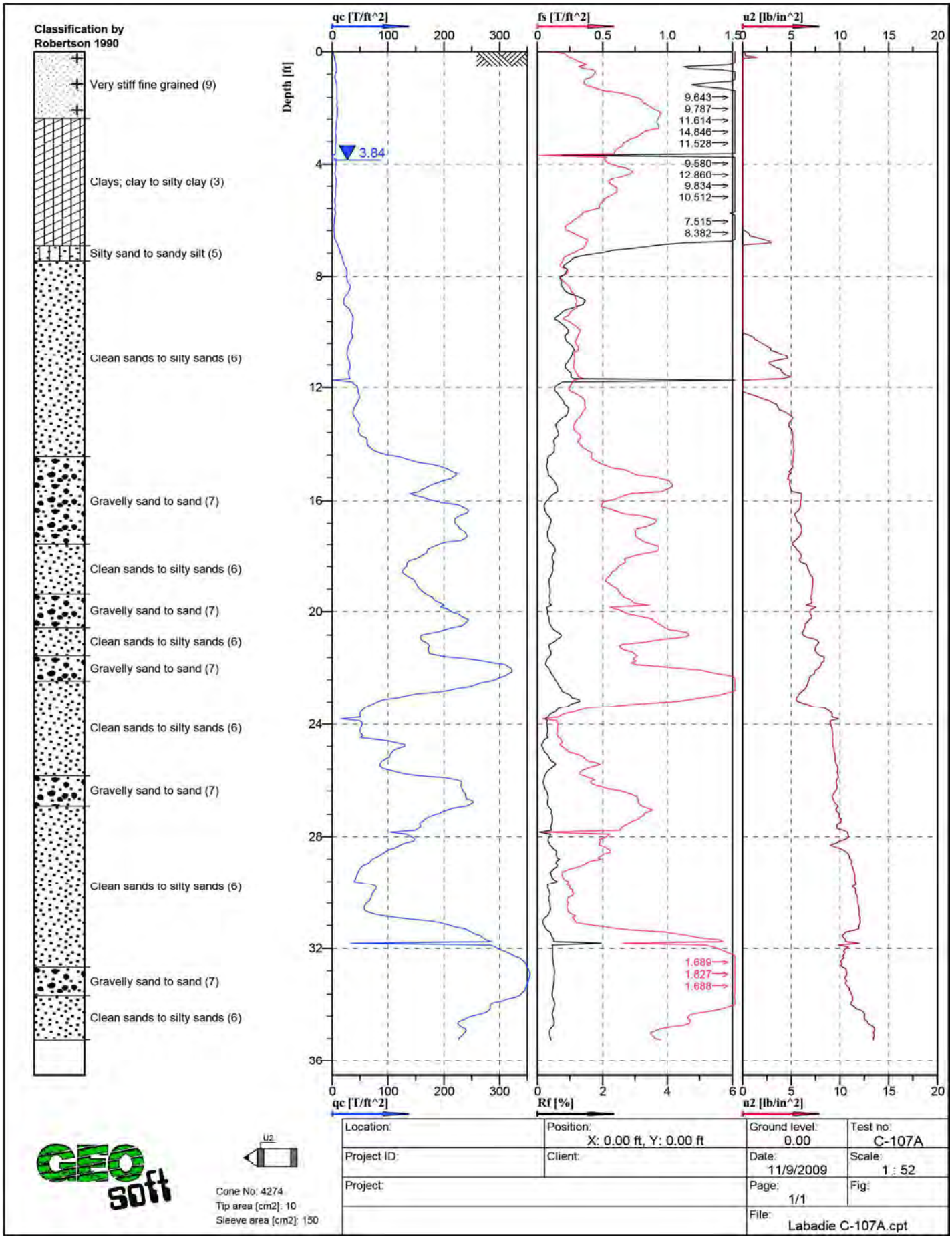

Figure A - 47: Cone Penetration Test Sounding Log, C-107A

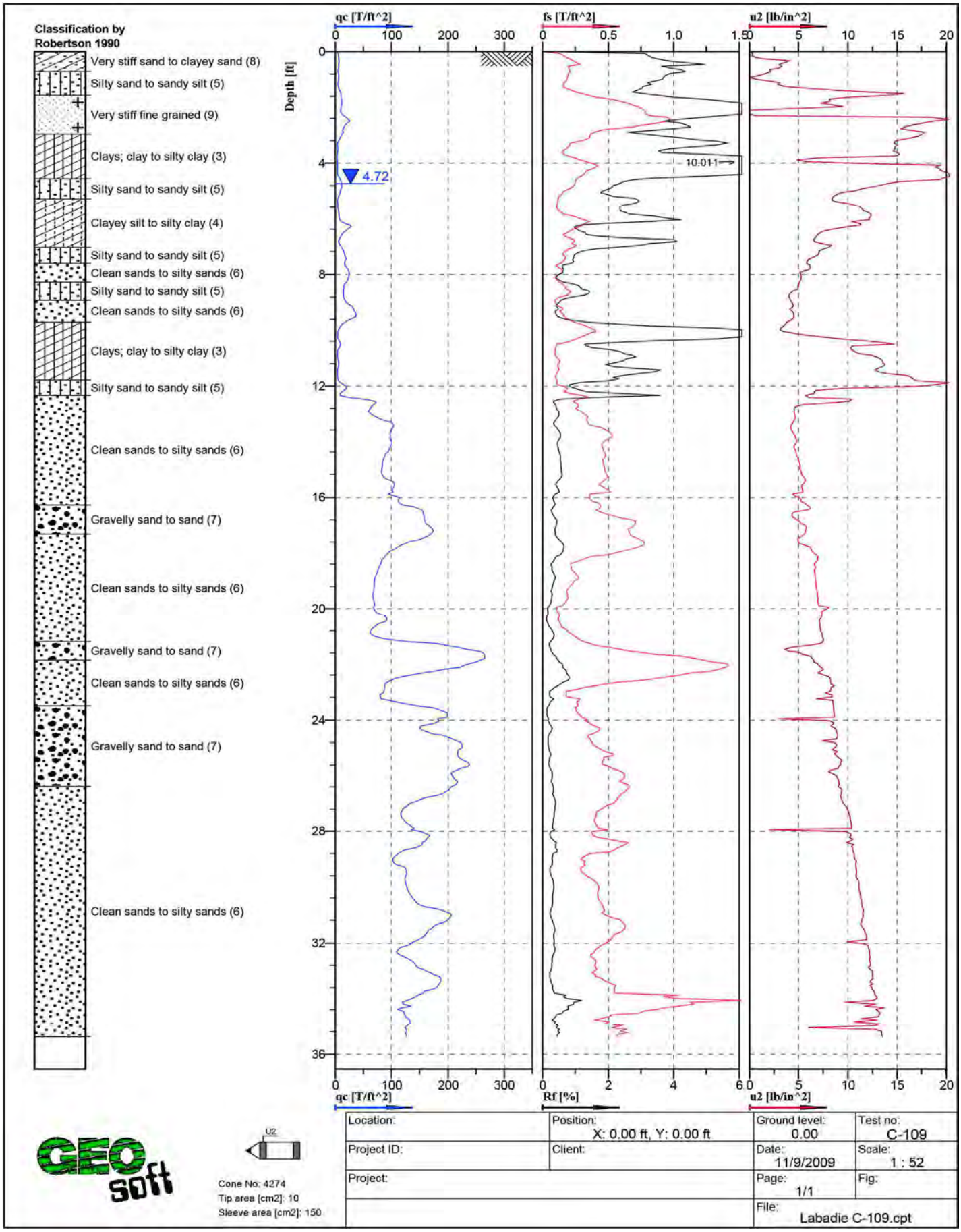

Figure A - 48: Cone Penetration Test Sounding Log, C-109

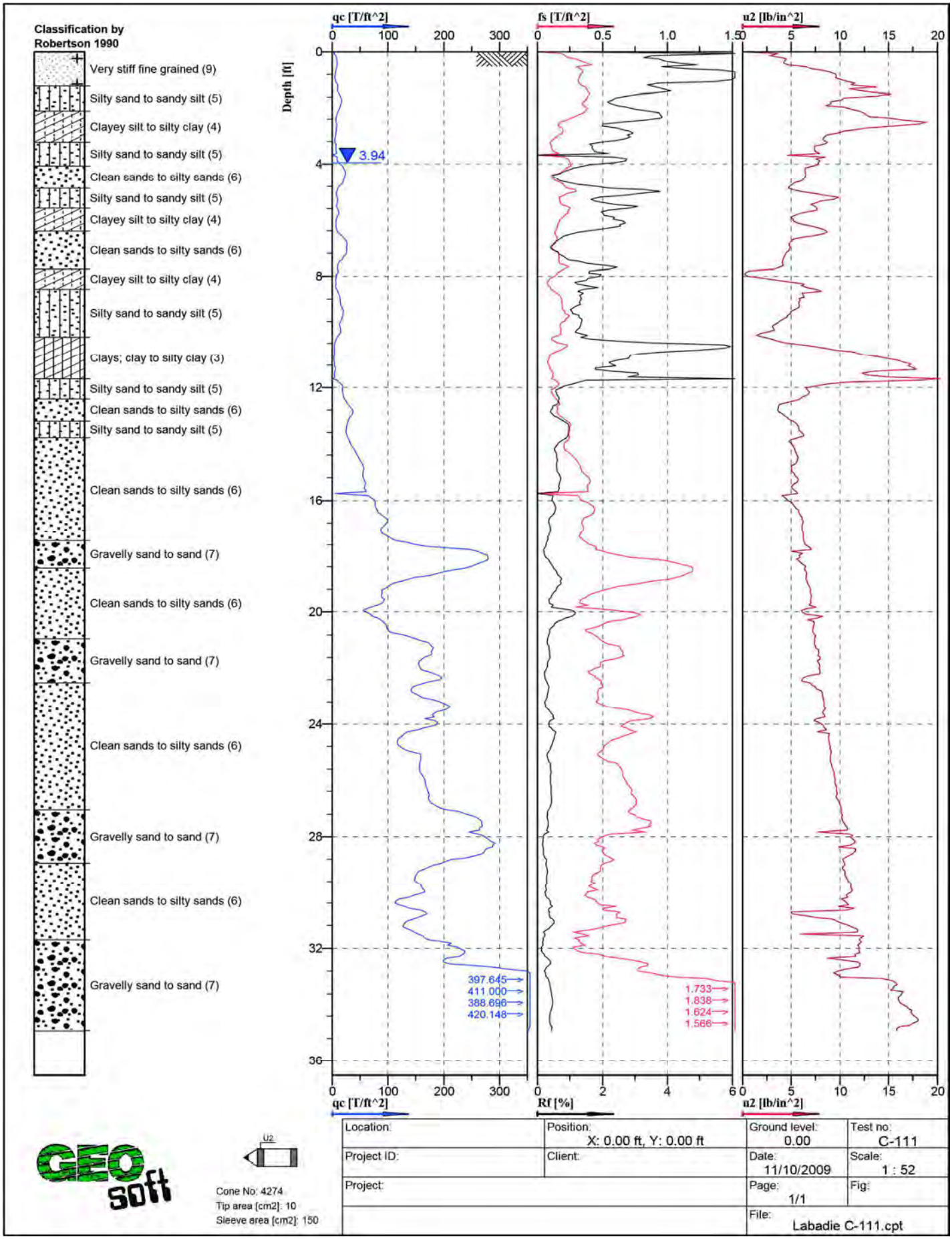

Figure A - 49: Cone Penetration Test Sounding Log, C-111

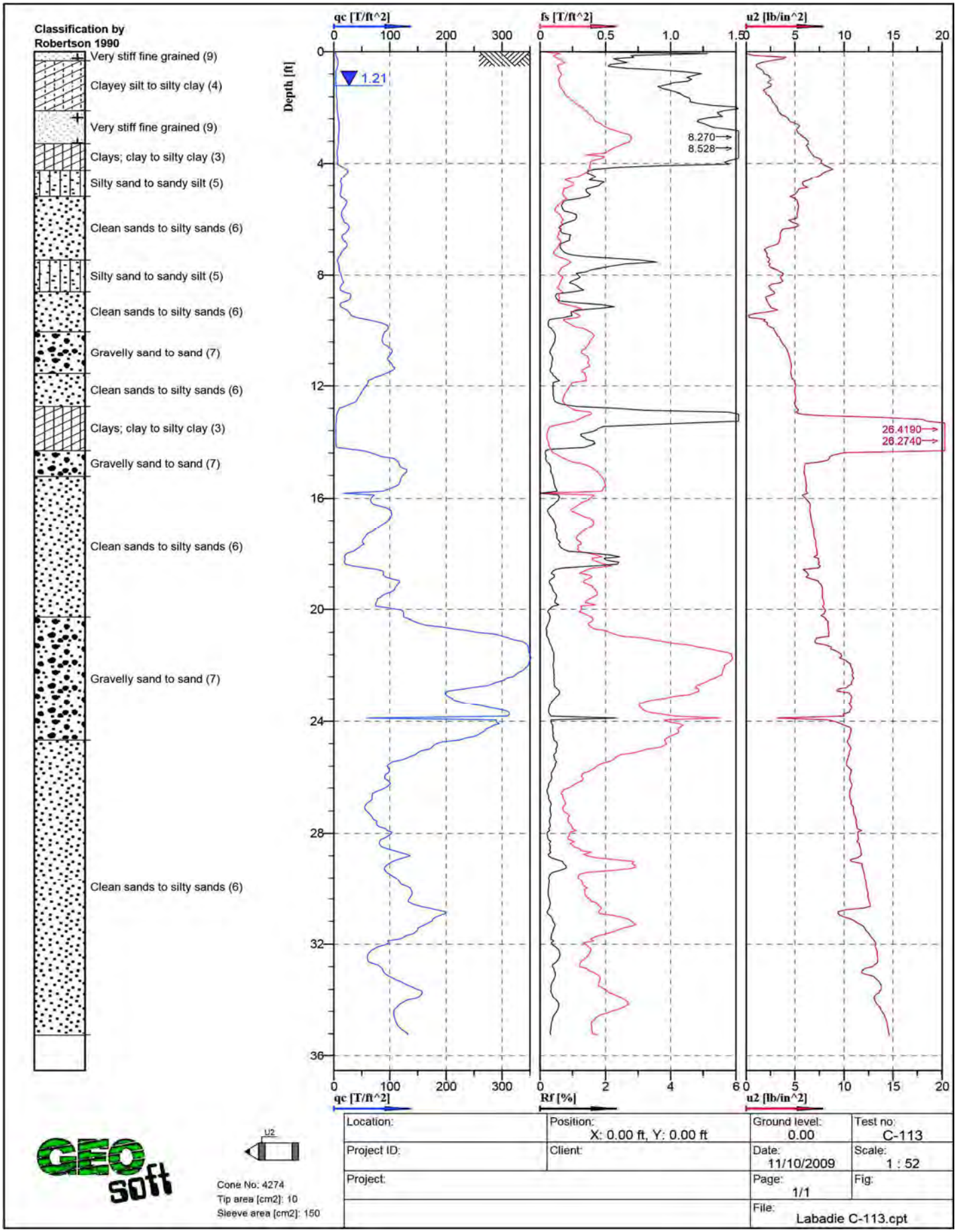

Figure A - 50: Cone Penetration Test Sounding Log, C-113

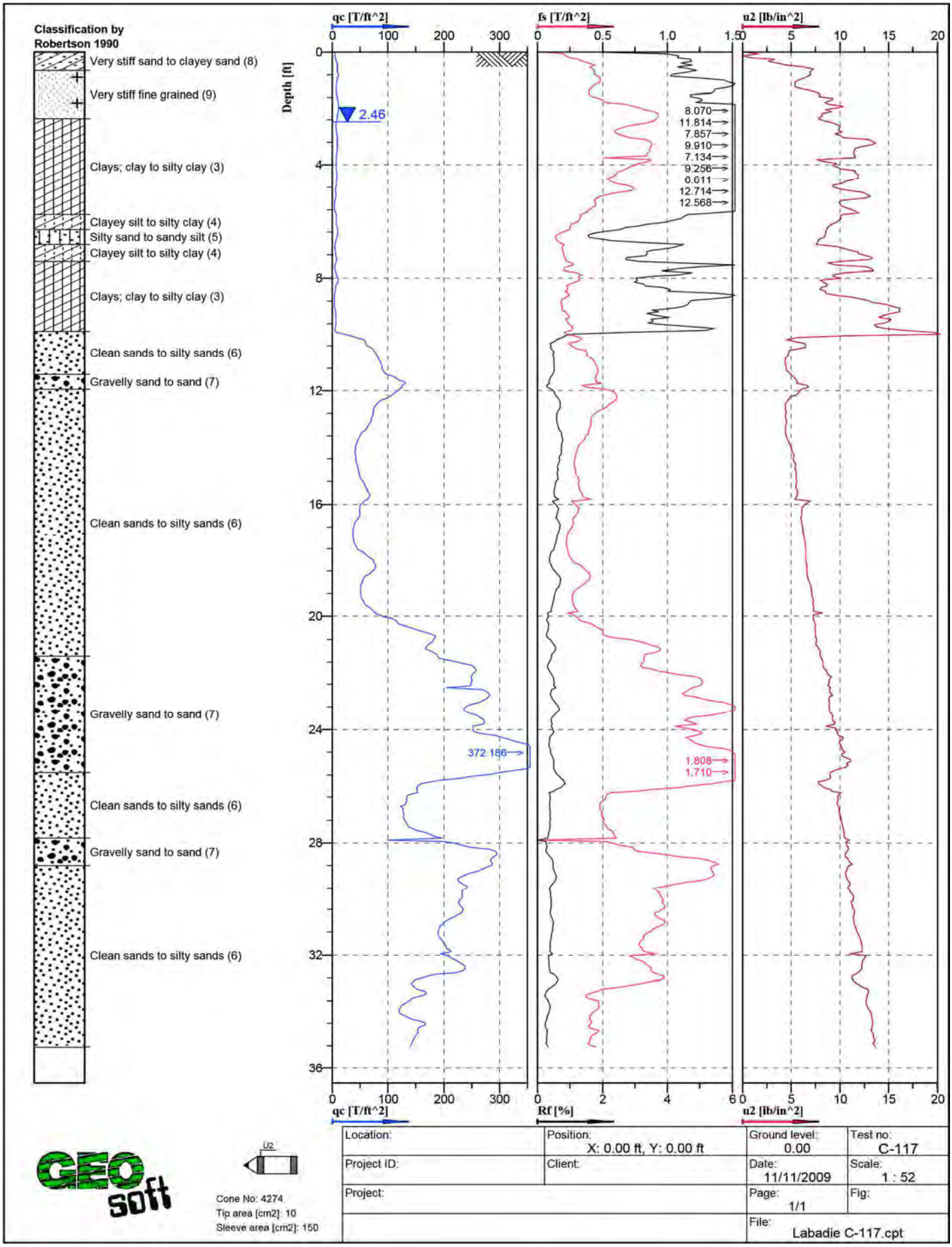

Figure A - 51: Cone Penetration Test Sounding Log, C-117

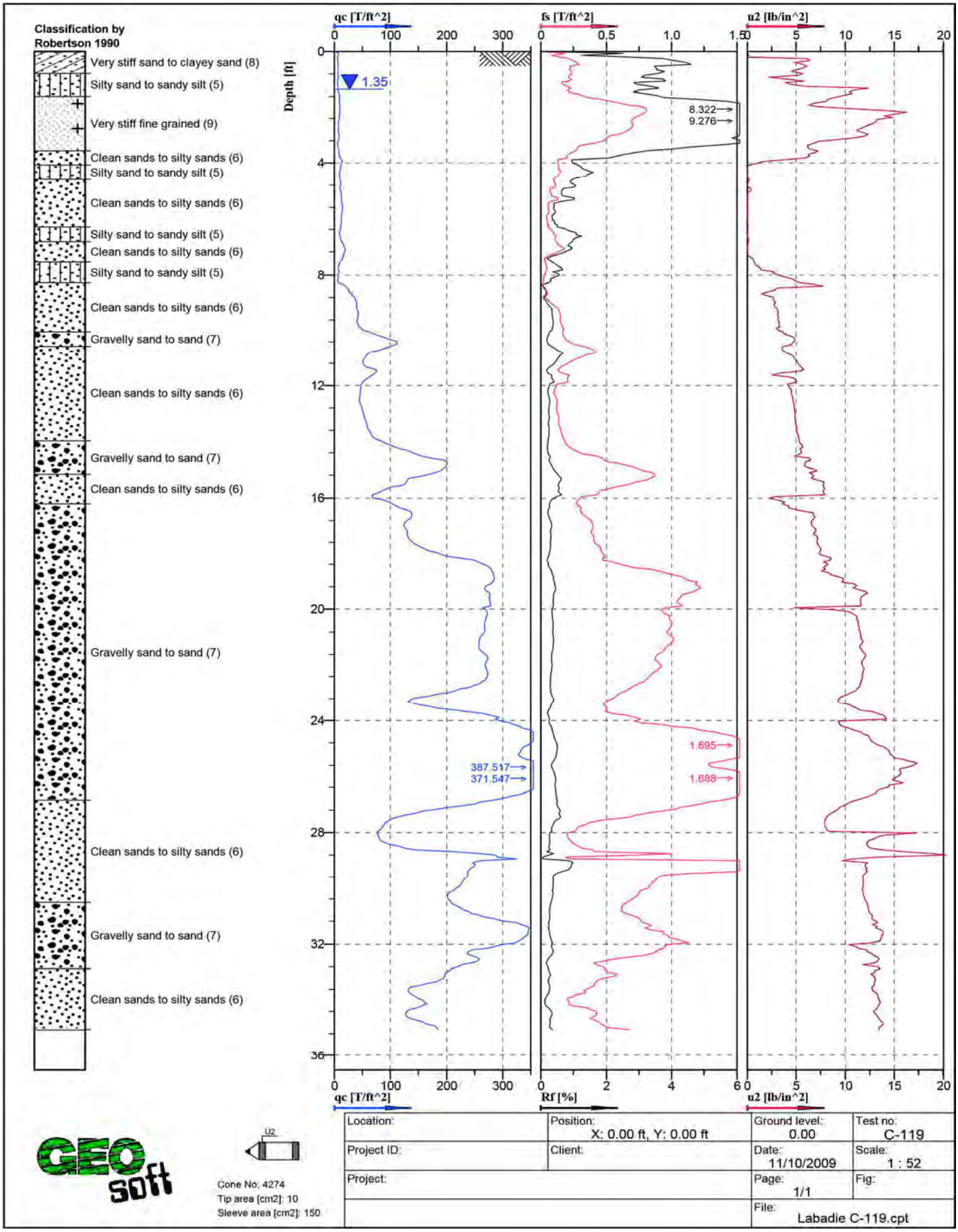

Figure A - 52: Cone Penetration Test Sounding Log, C-119

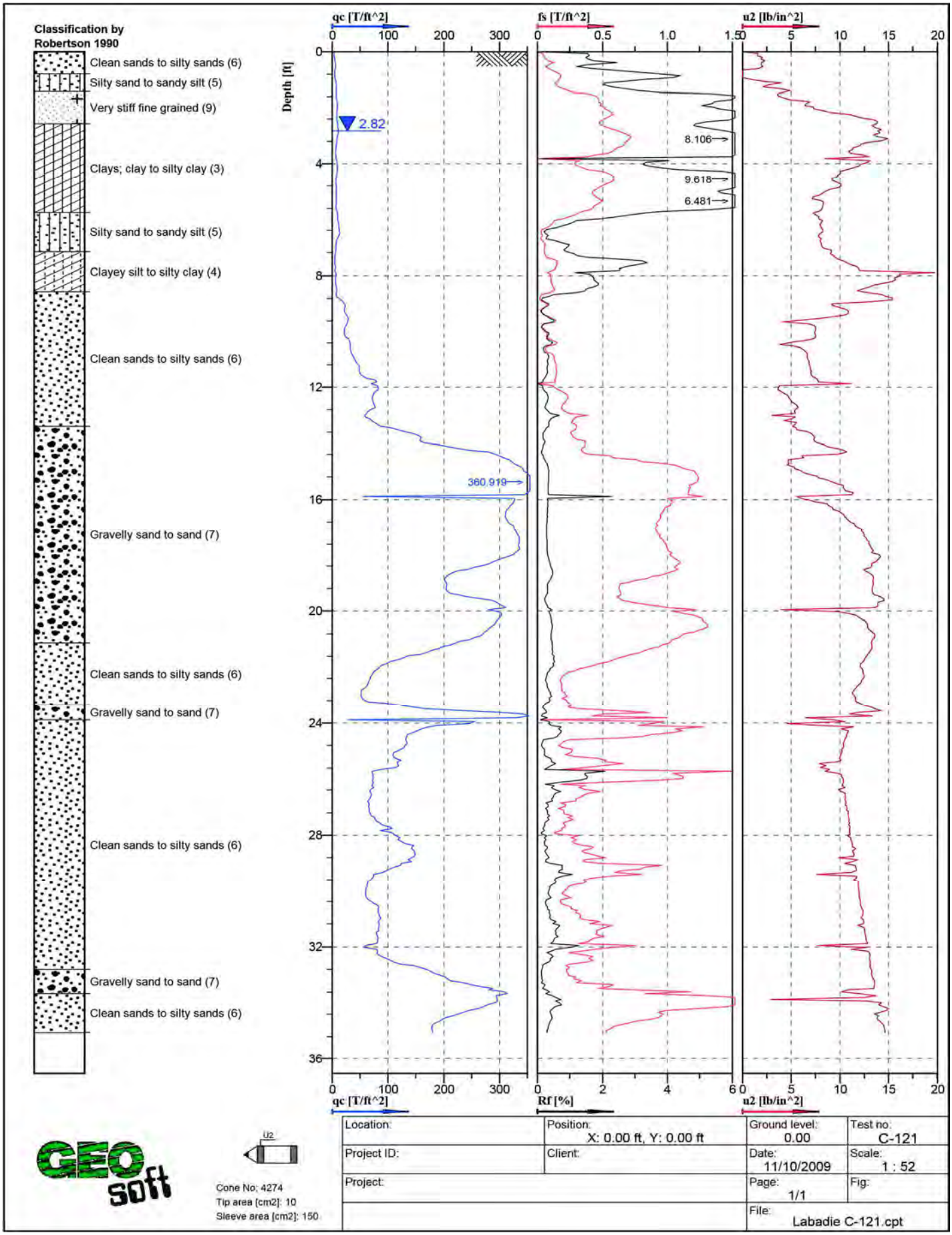

Figure A - 53: Cone Penetration Test Sounding Log, C-121

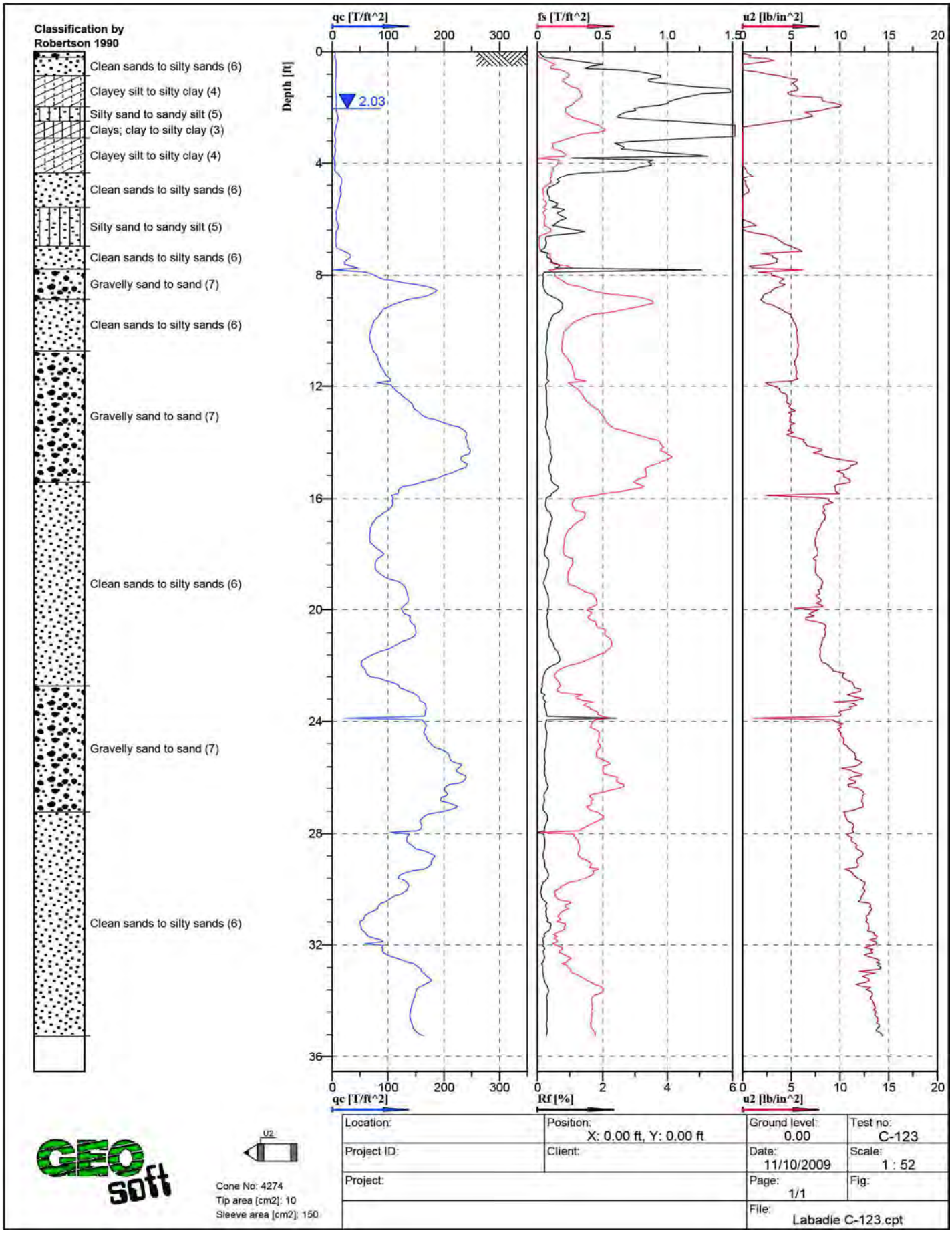

Figure A - 54: Cone Penetration Test Sounding Log, C-123

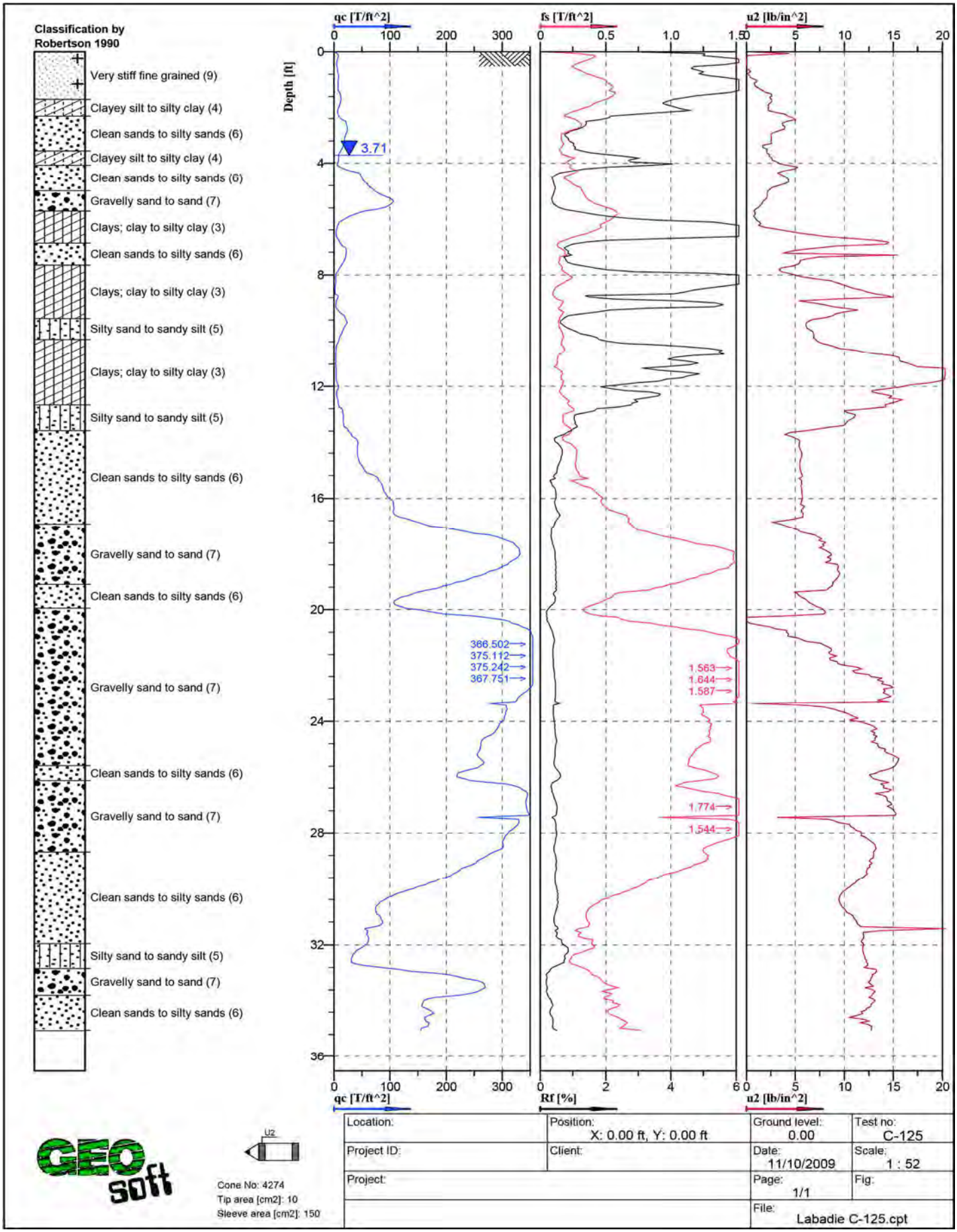

Figure A - 55: Cone Penetration Test Sounding Log, C-125

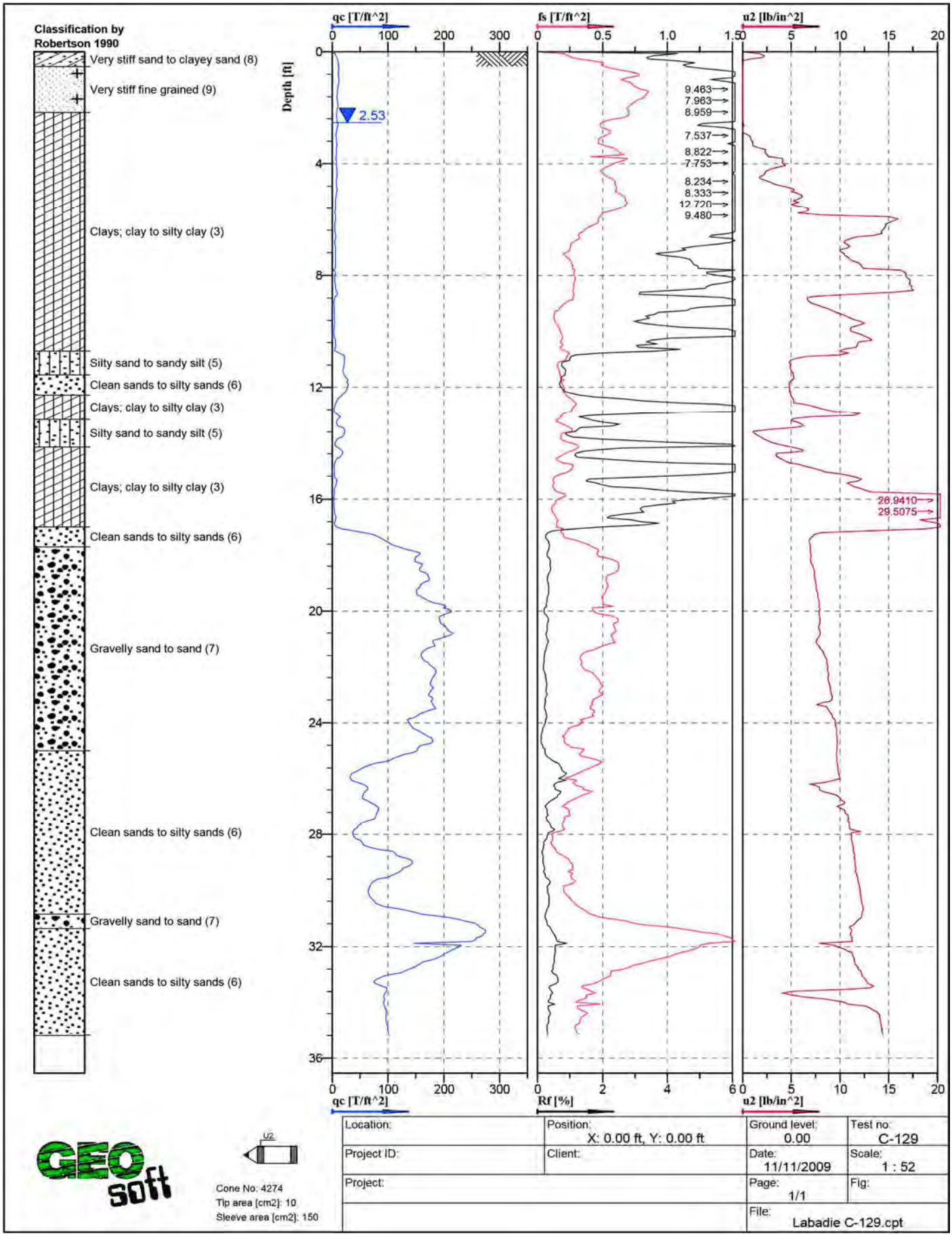

Figure A - 56: Cone Penetration Test Sounding Log, C-129

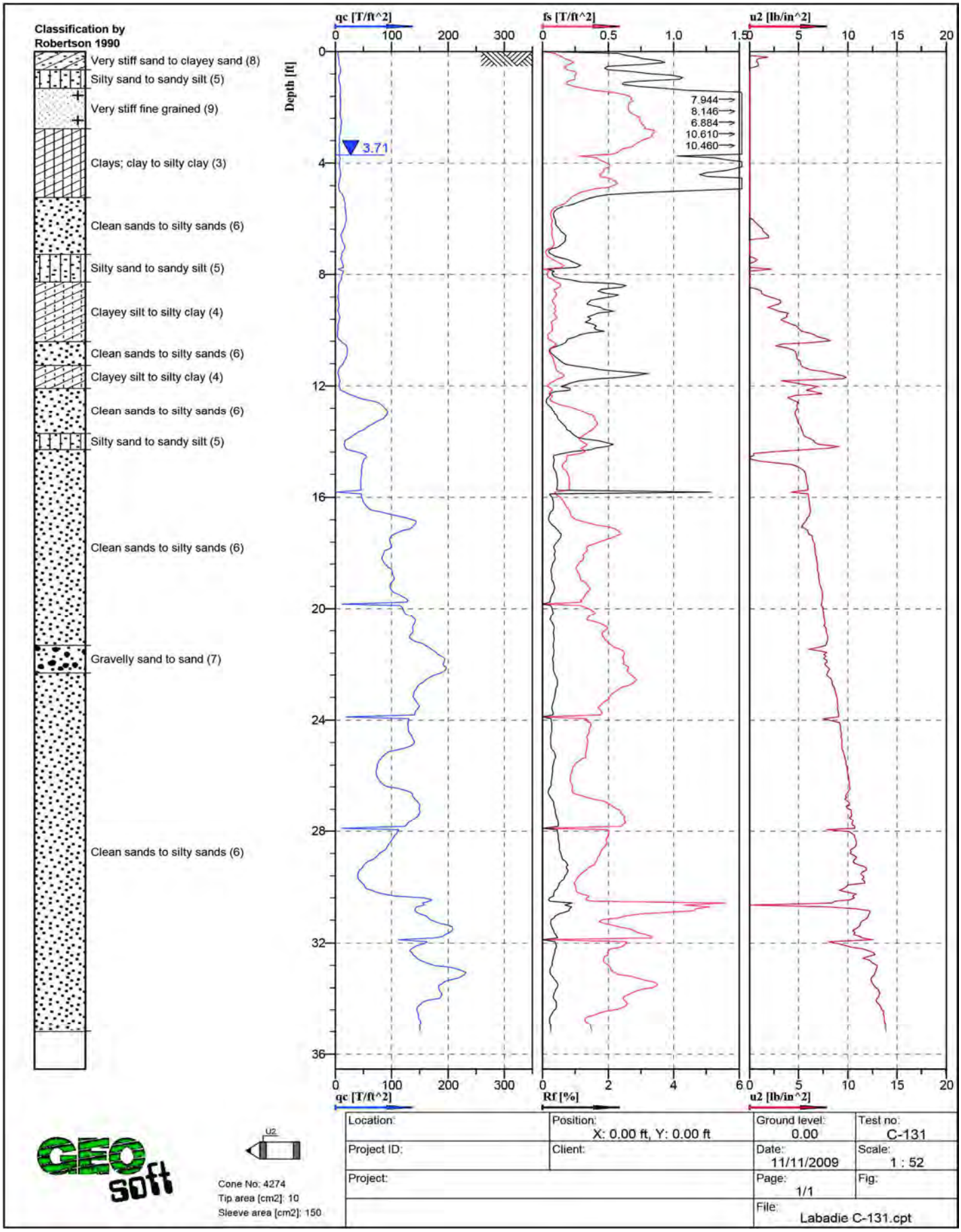

Figure A - 57: Cone Penetration Test Sounding Log, C-131

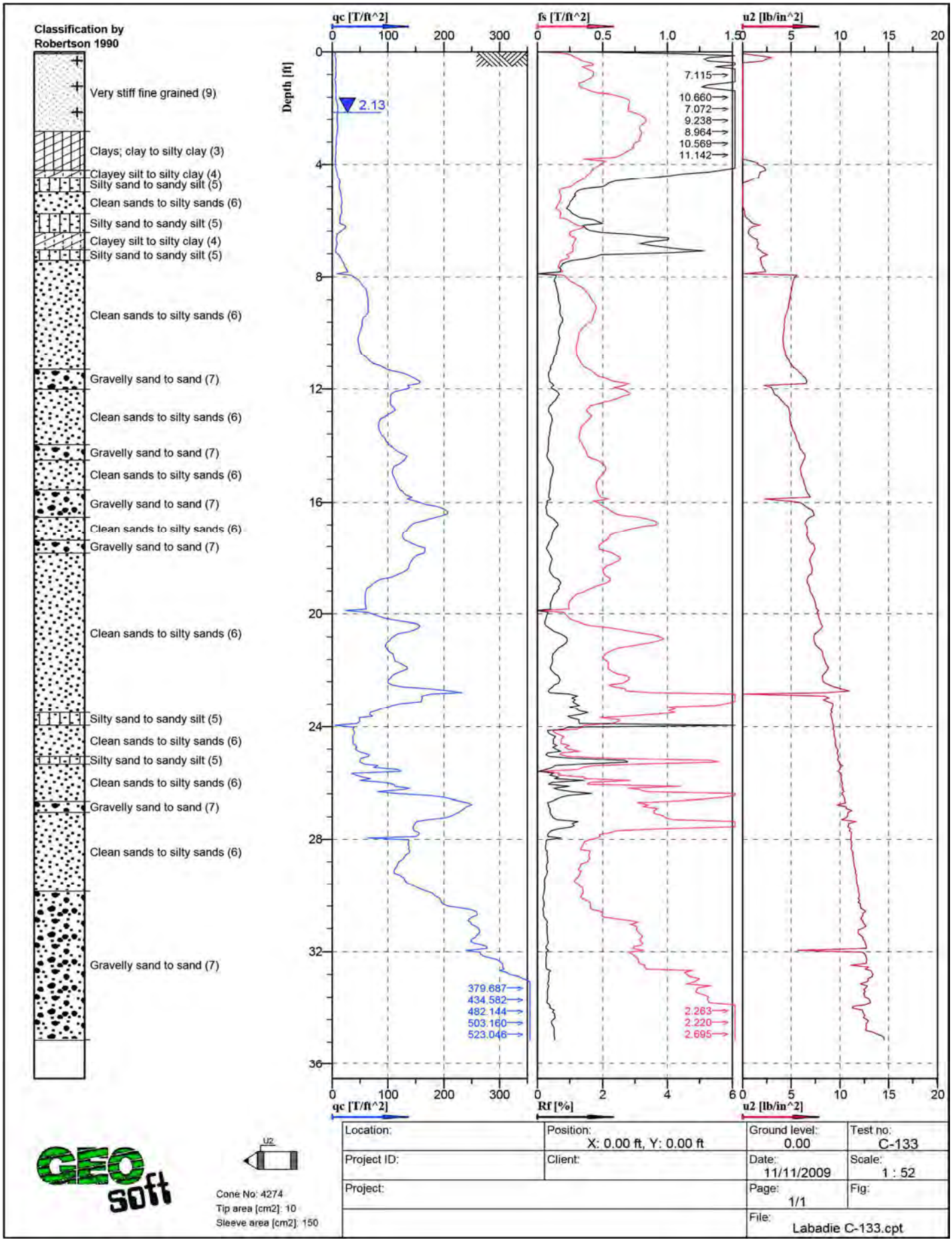

Figure A - 58: Cone Penetration Test Sounding Log, C-133

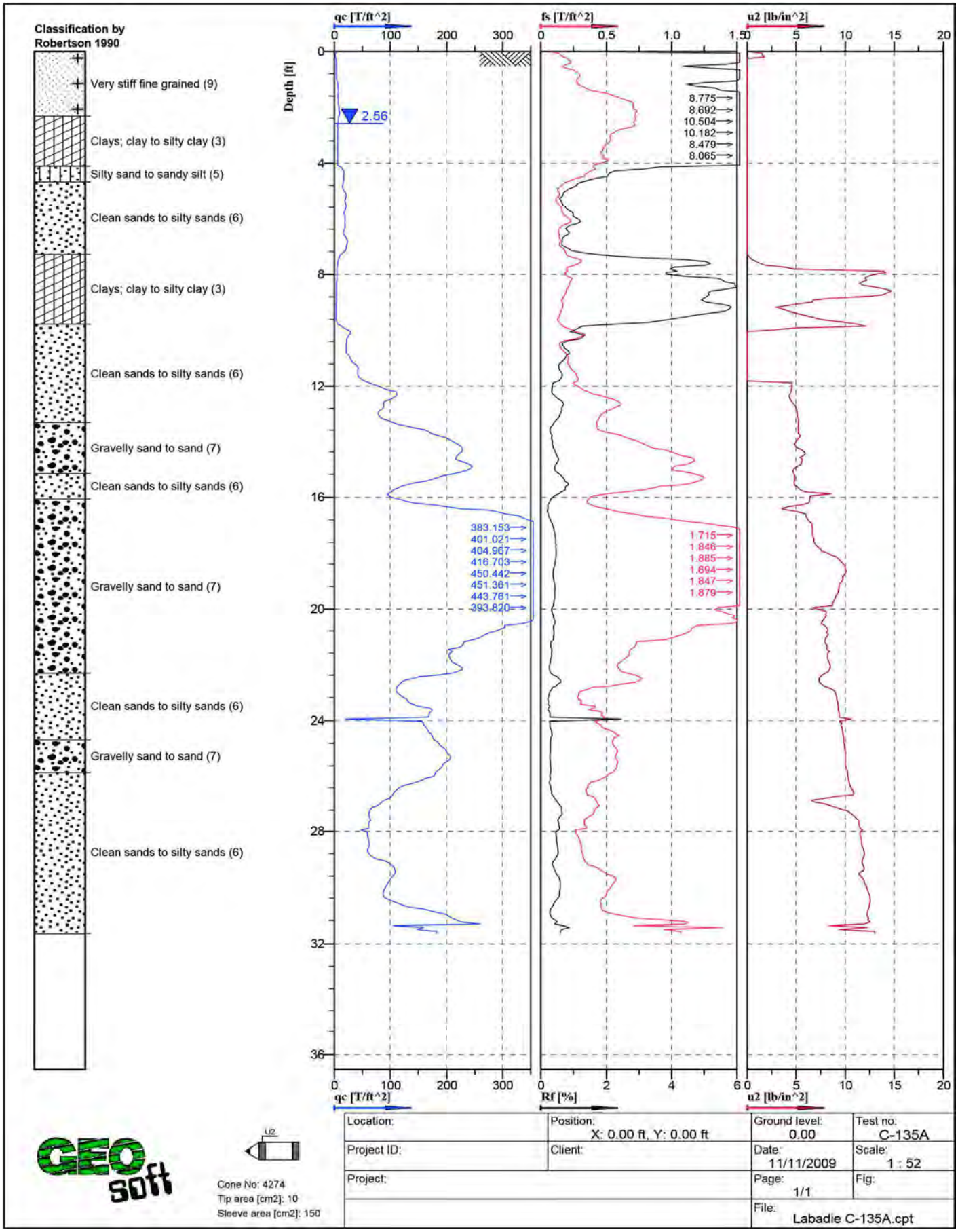

Figure A - 59: Cone Penetration Test Sounding Log, C-135A

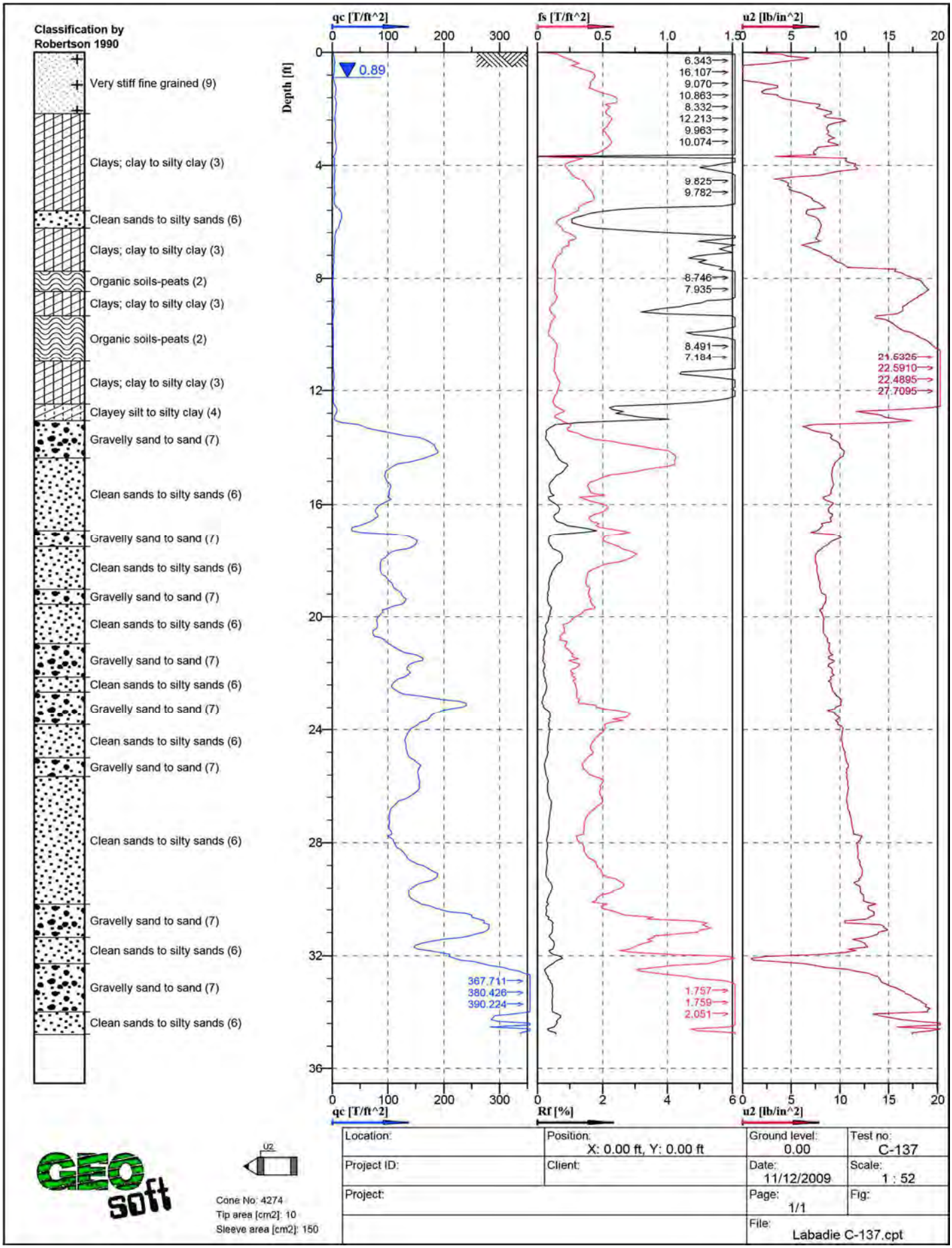

Figure A - 60: Cone Penetration Test Sounding Log, C-137

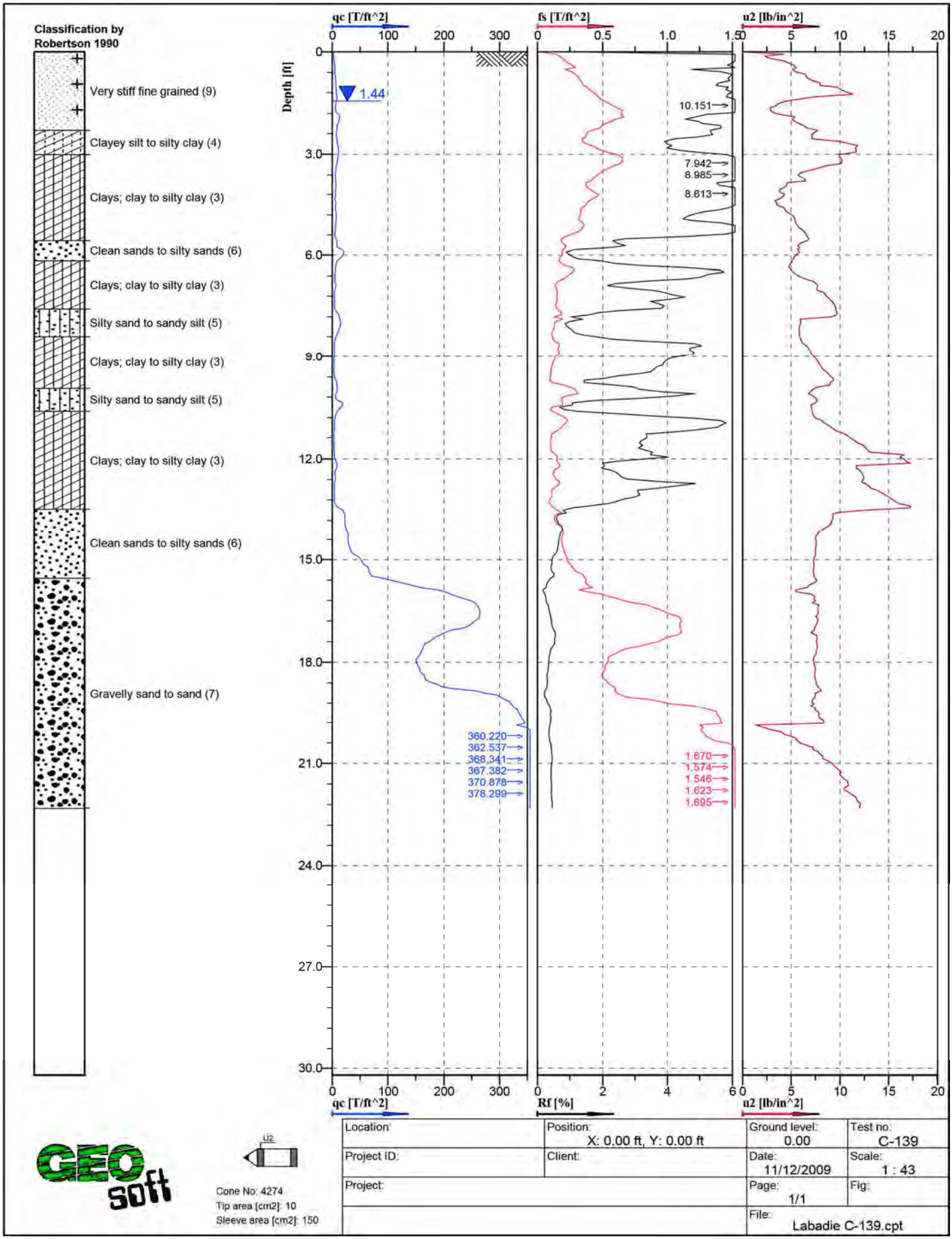

Figure A - 61: Cone Penetration Test Sounding Log, C-139

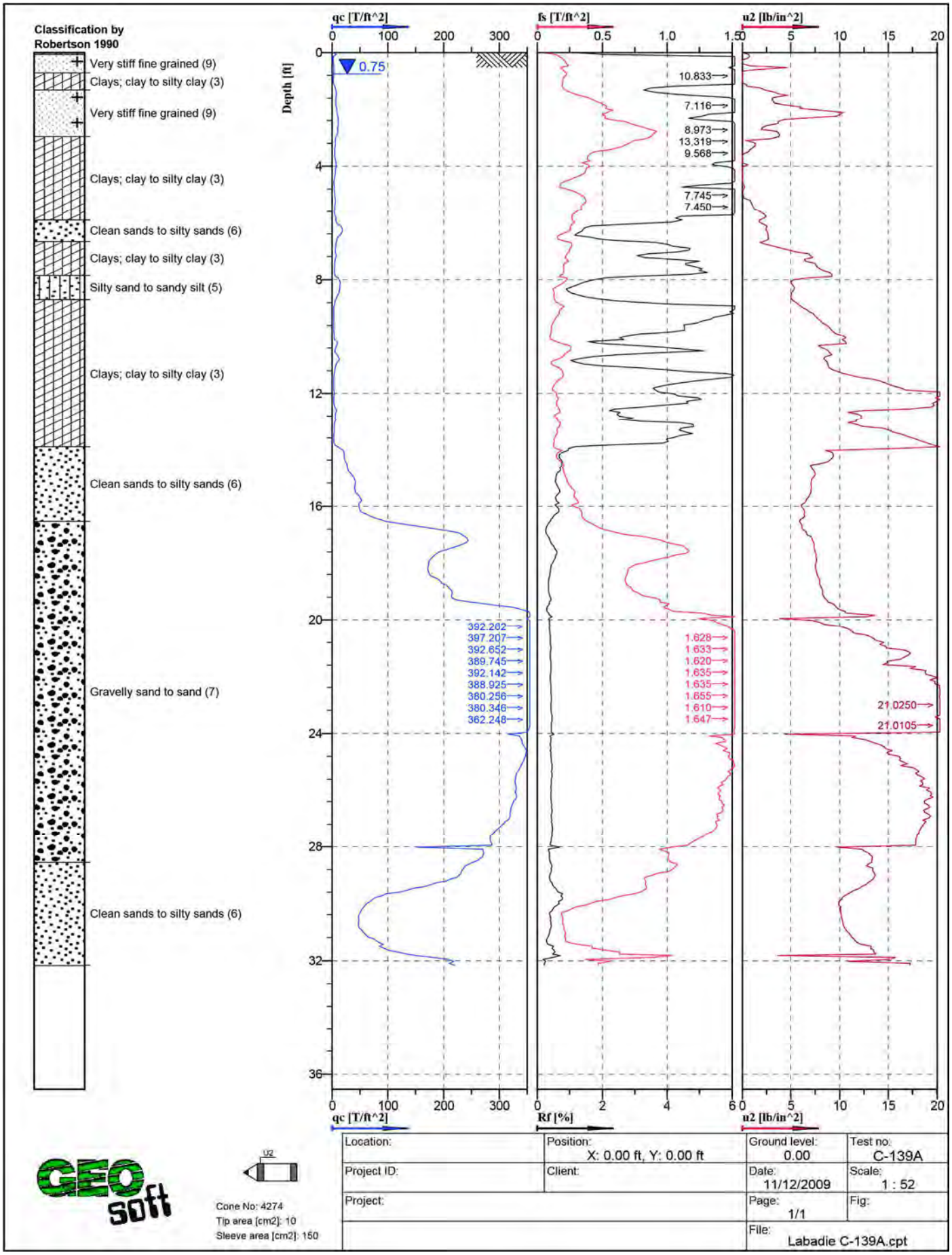

Figure A - 62: Cone Penetration Test Sounding Log, C-139A

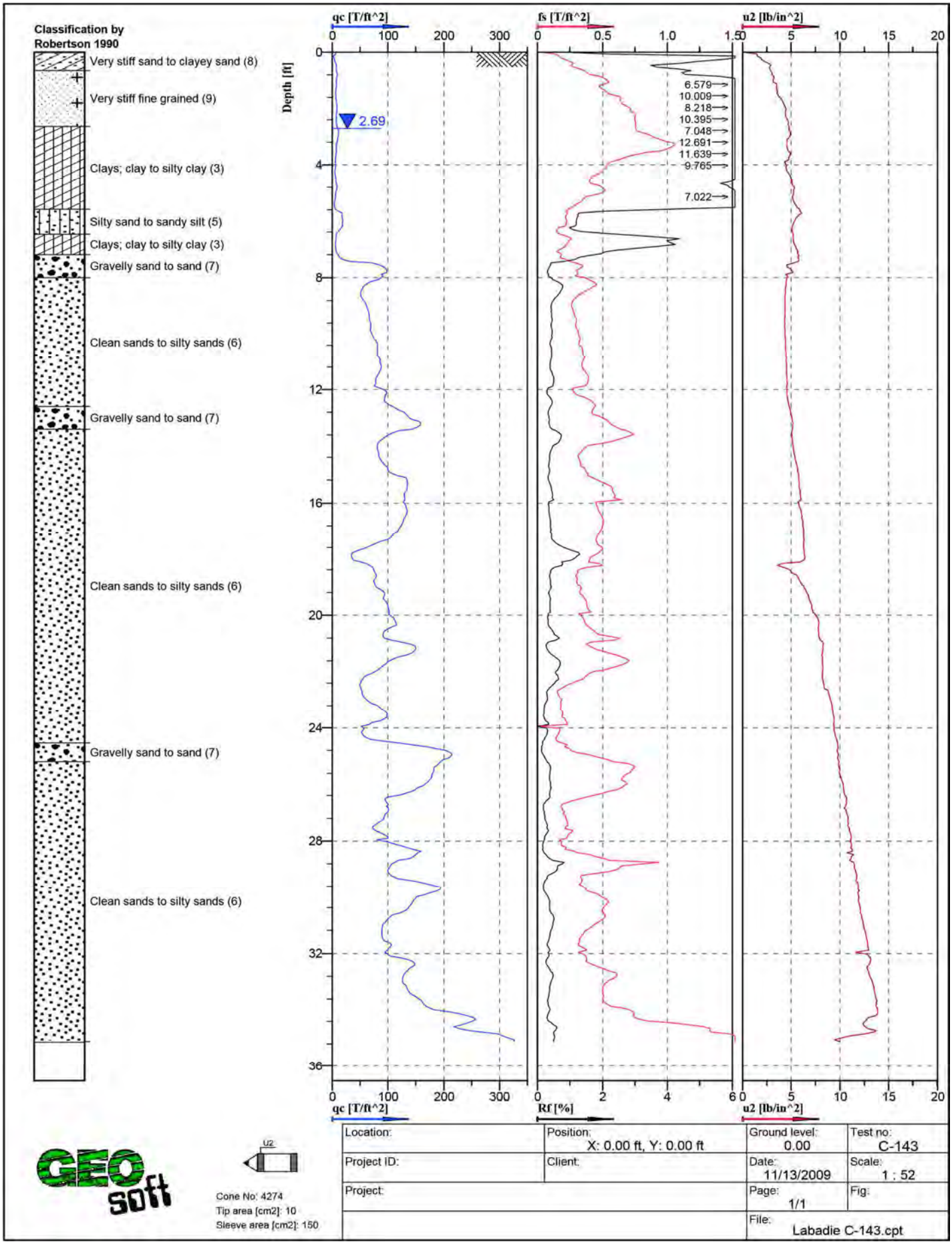

Figure A - 63: Cone Penetration Test Sounding Log, C-143

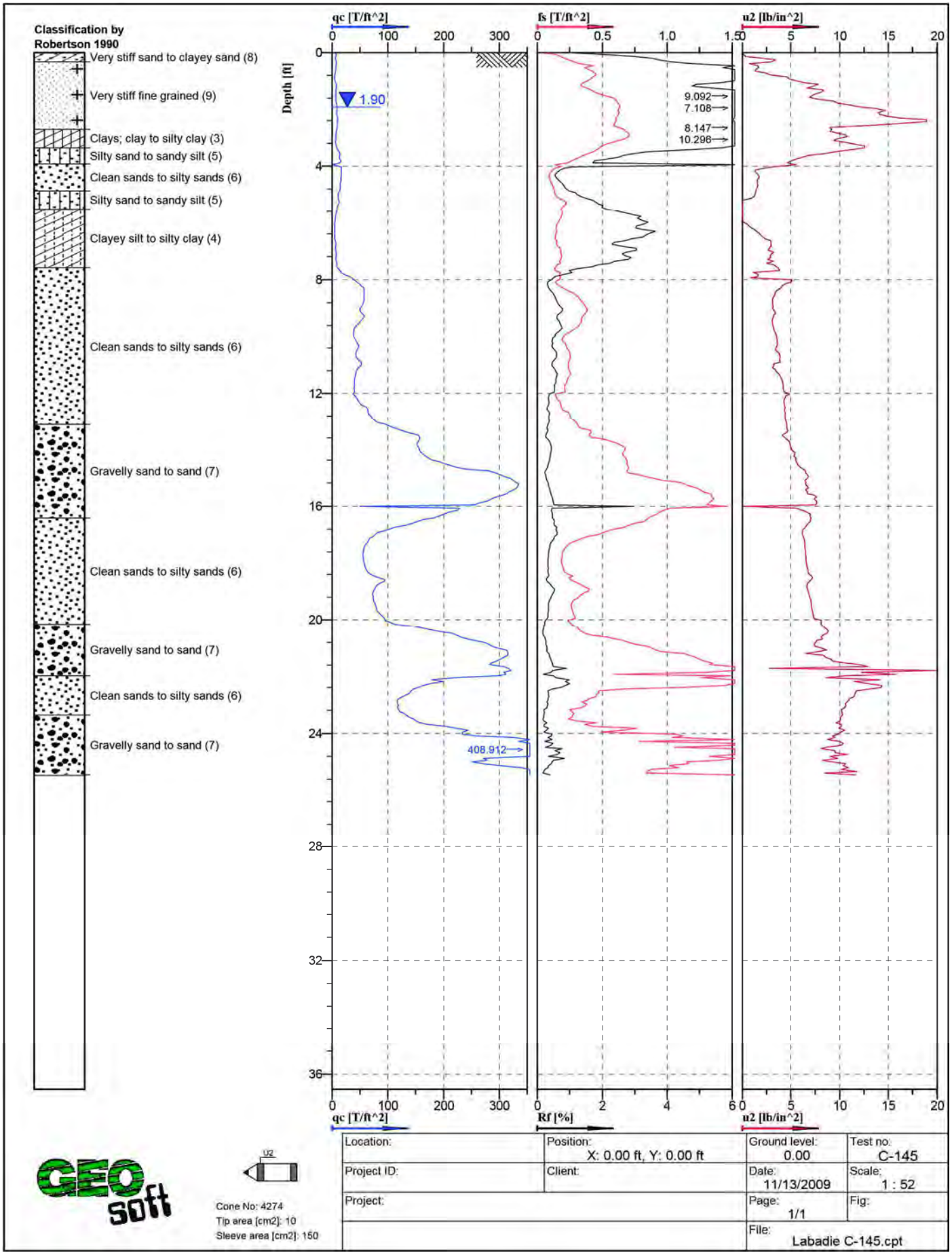

Figure A - 64: Cone Penetration Test Sounding Log, C-145

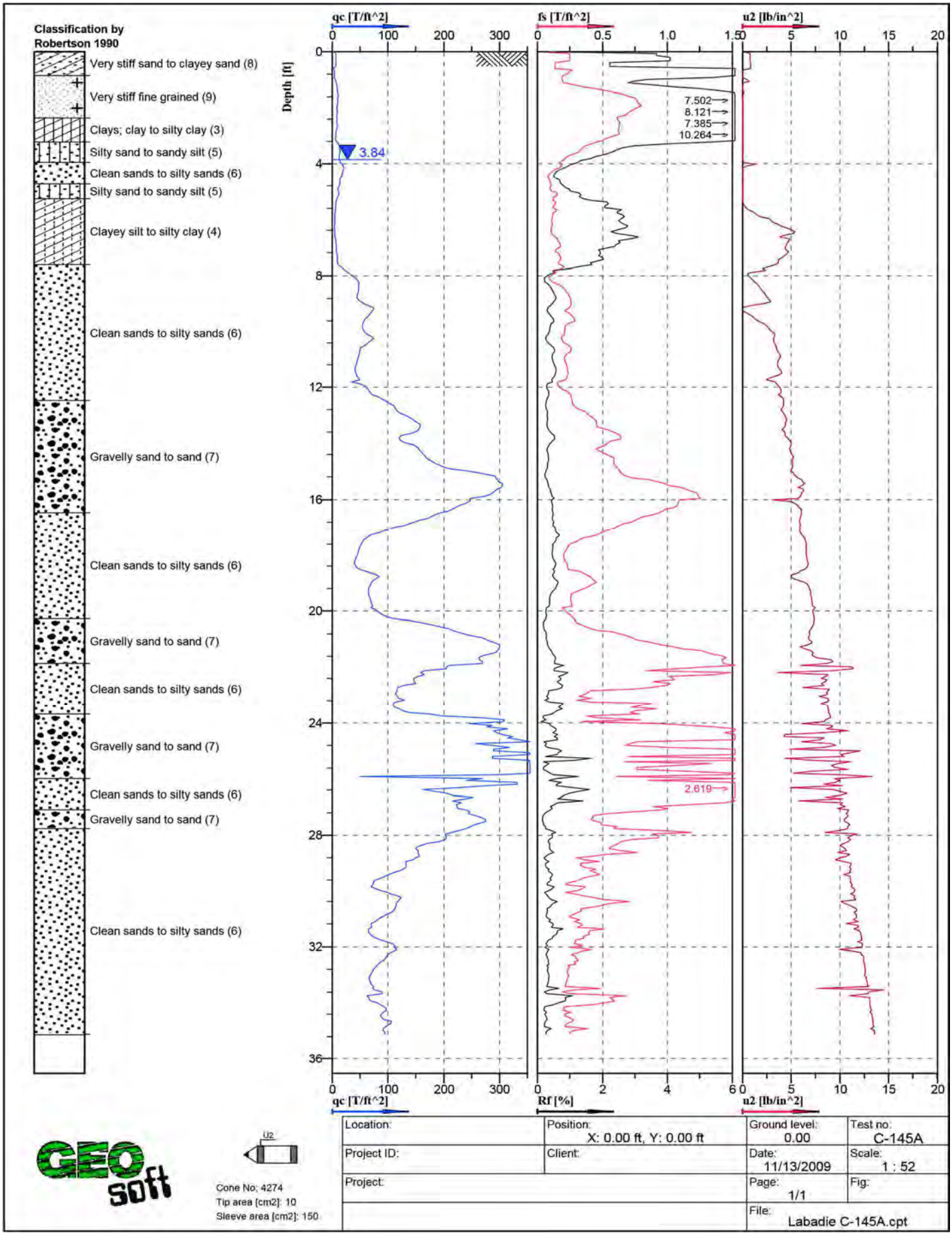

Figure A - 65: Cone Penetration Test Sounding Log, C-145A

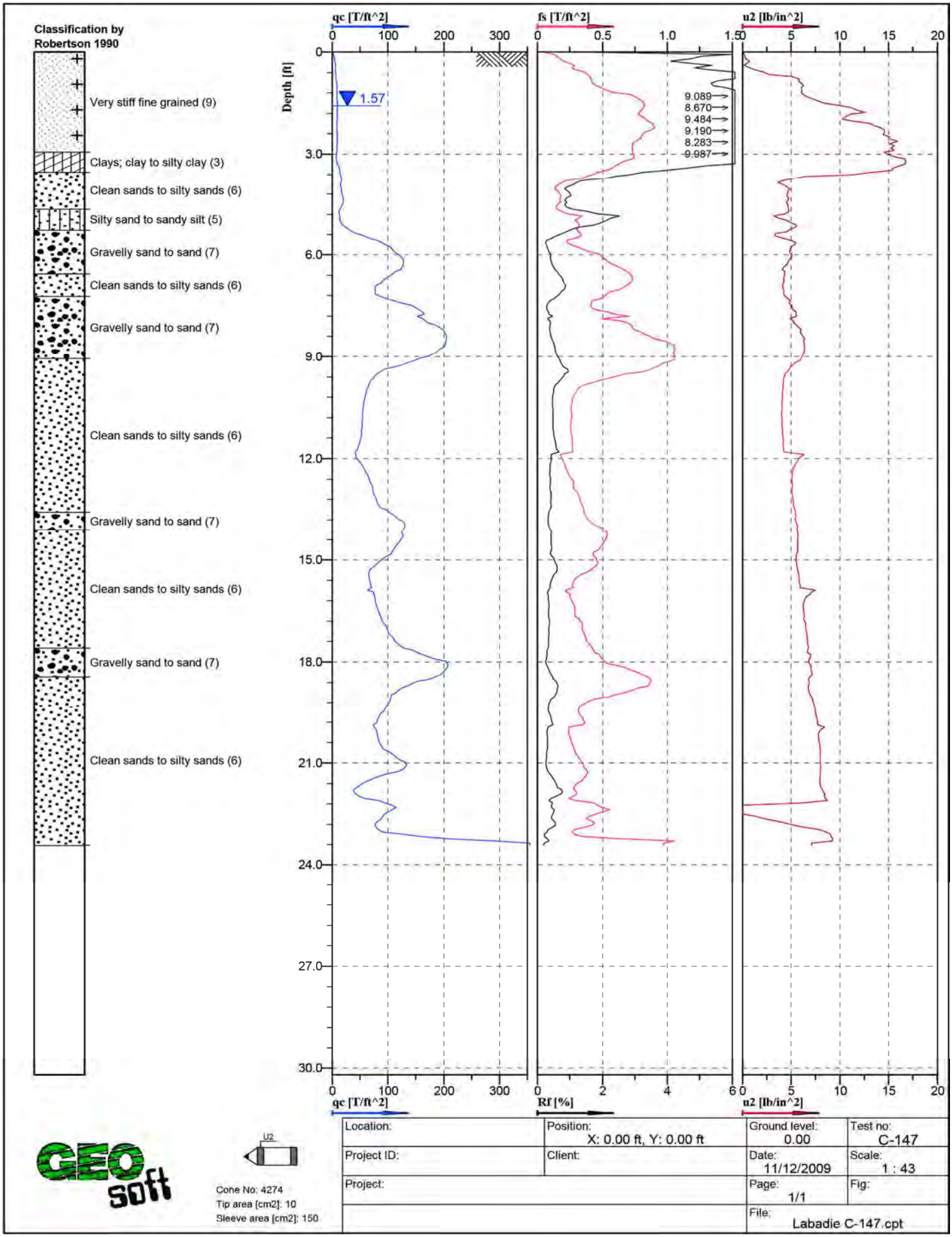

Figure A - 66: Cone Penetration Test Sounding Log, C-147

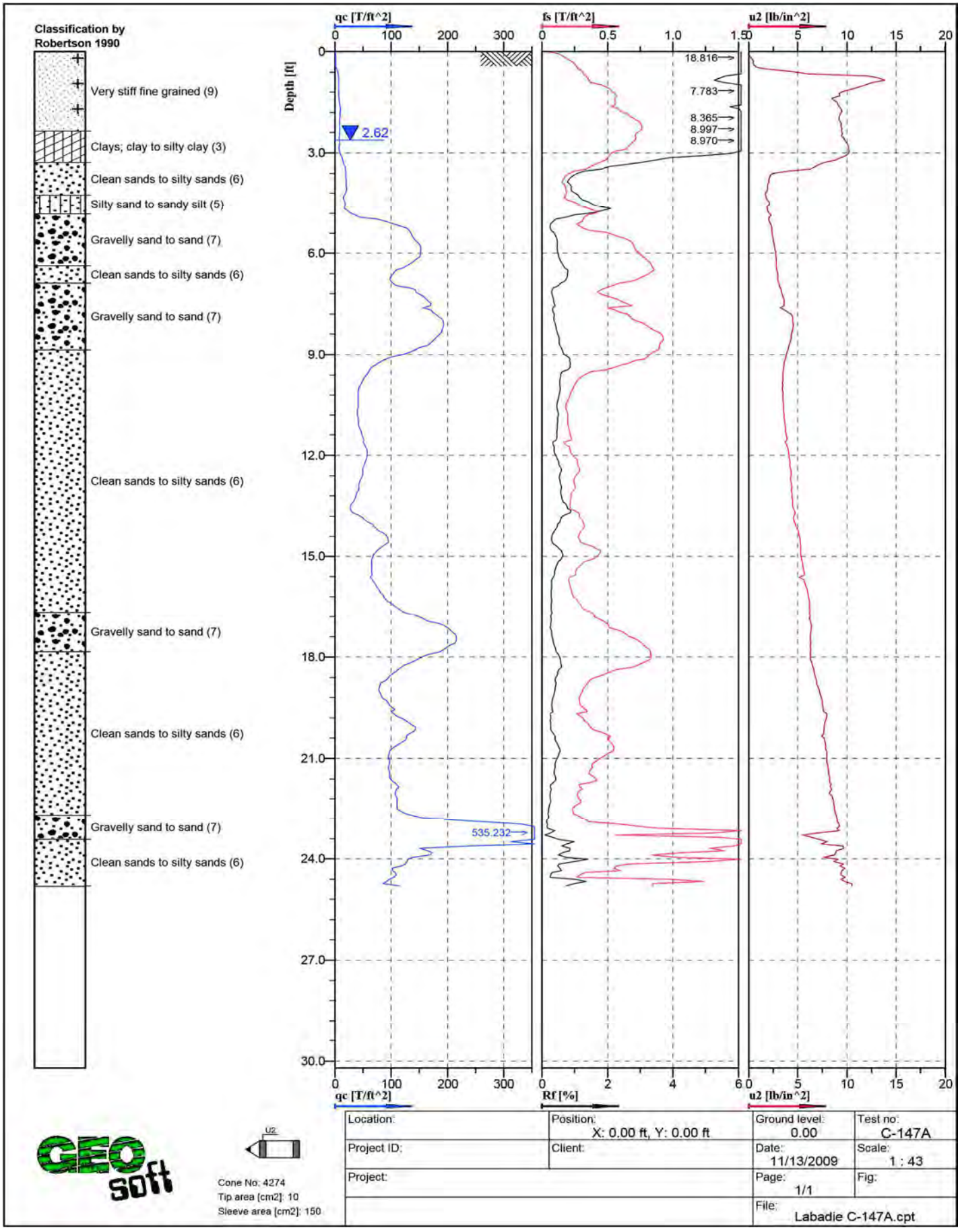

Figure A - 67: Cone Penetration Test Sounding Log, C-147A

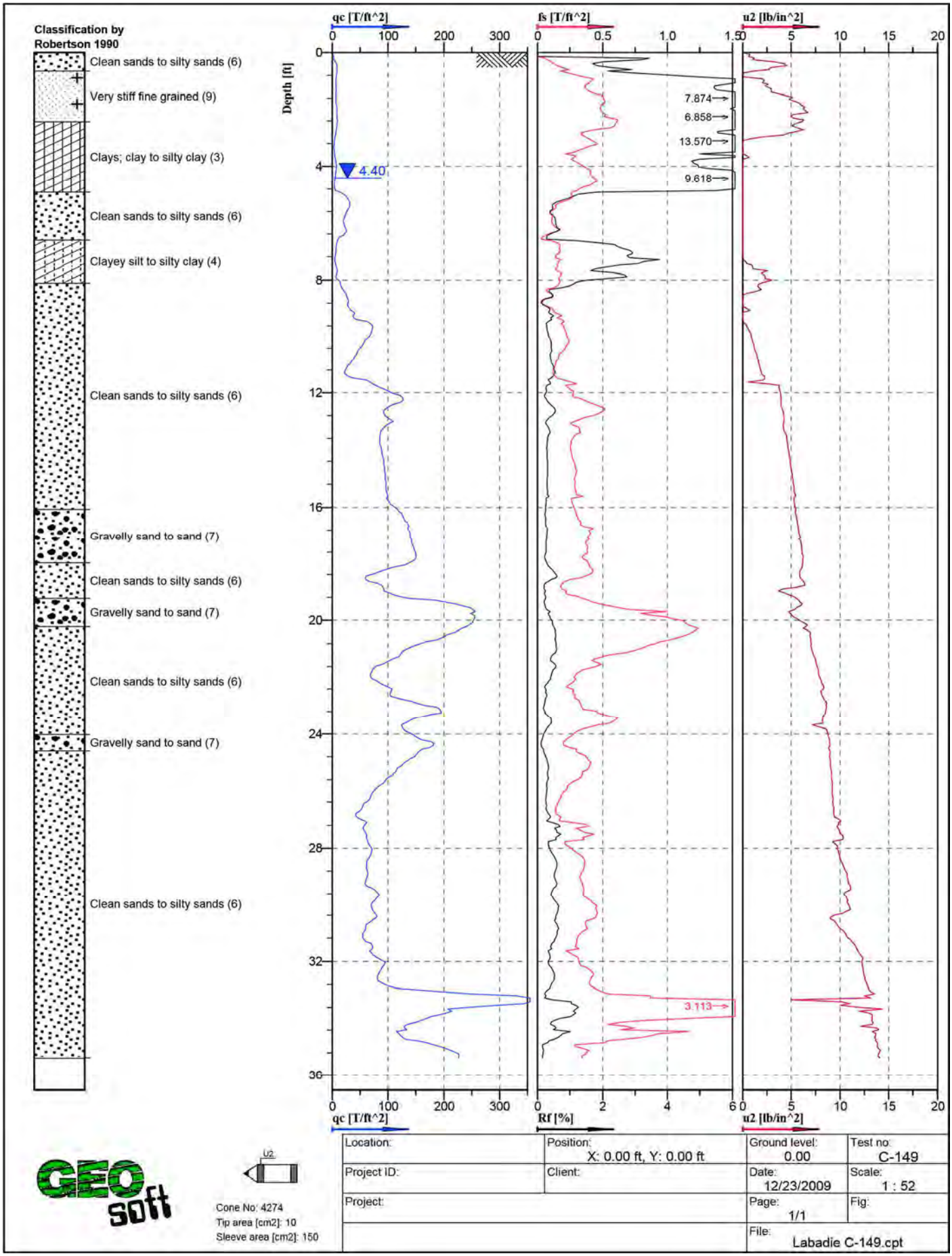

Figure A - 68: Cone Penetration Test Sounding Log, C-149

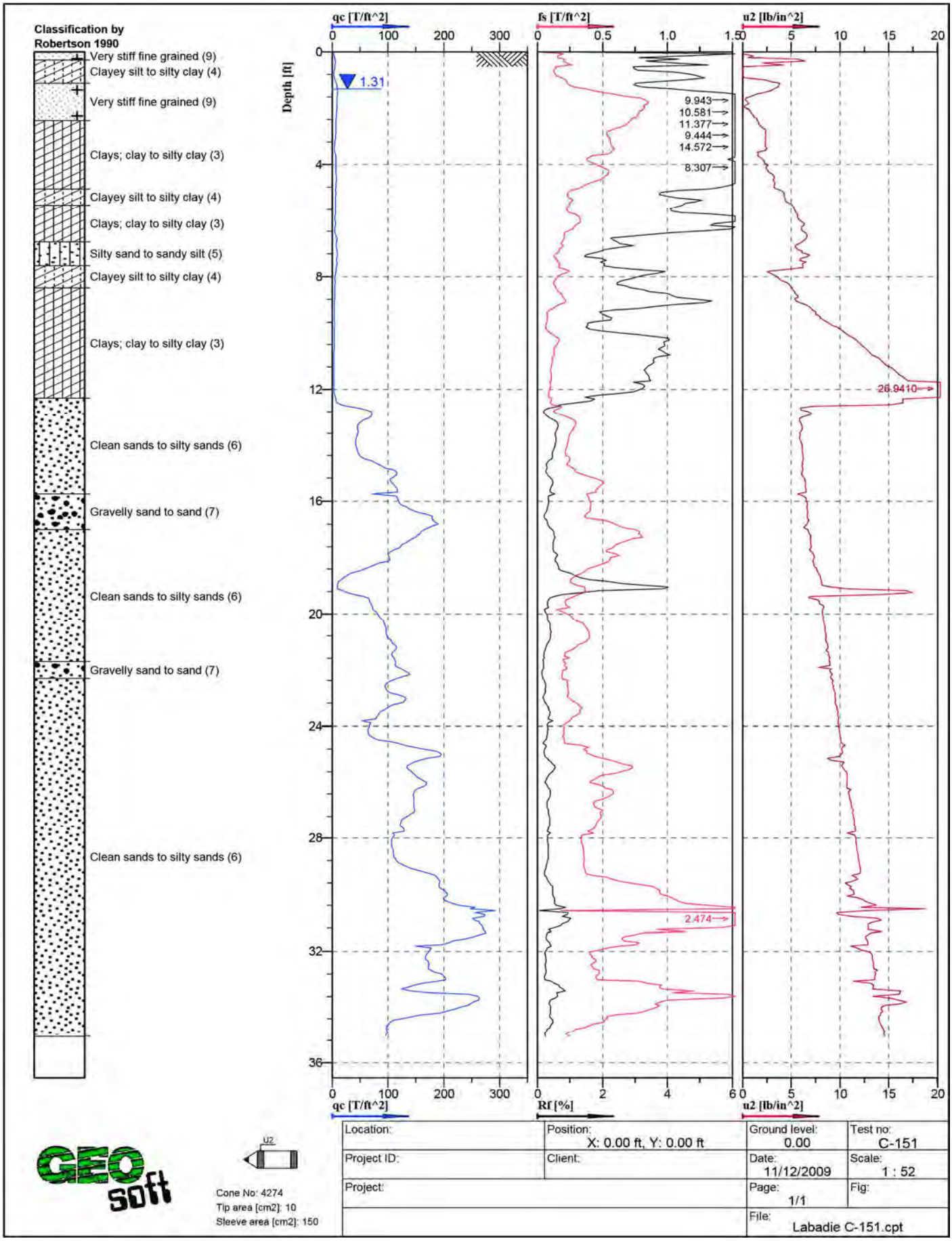

Figure A - 69: Cone Penetration Test Sounding Log, C-151

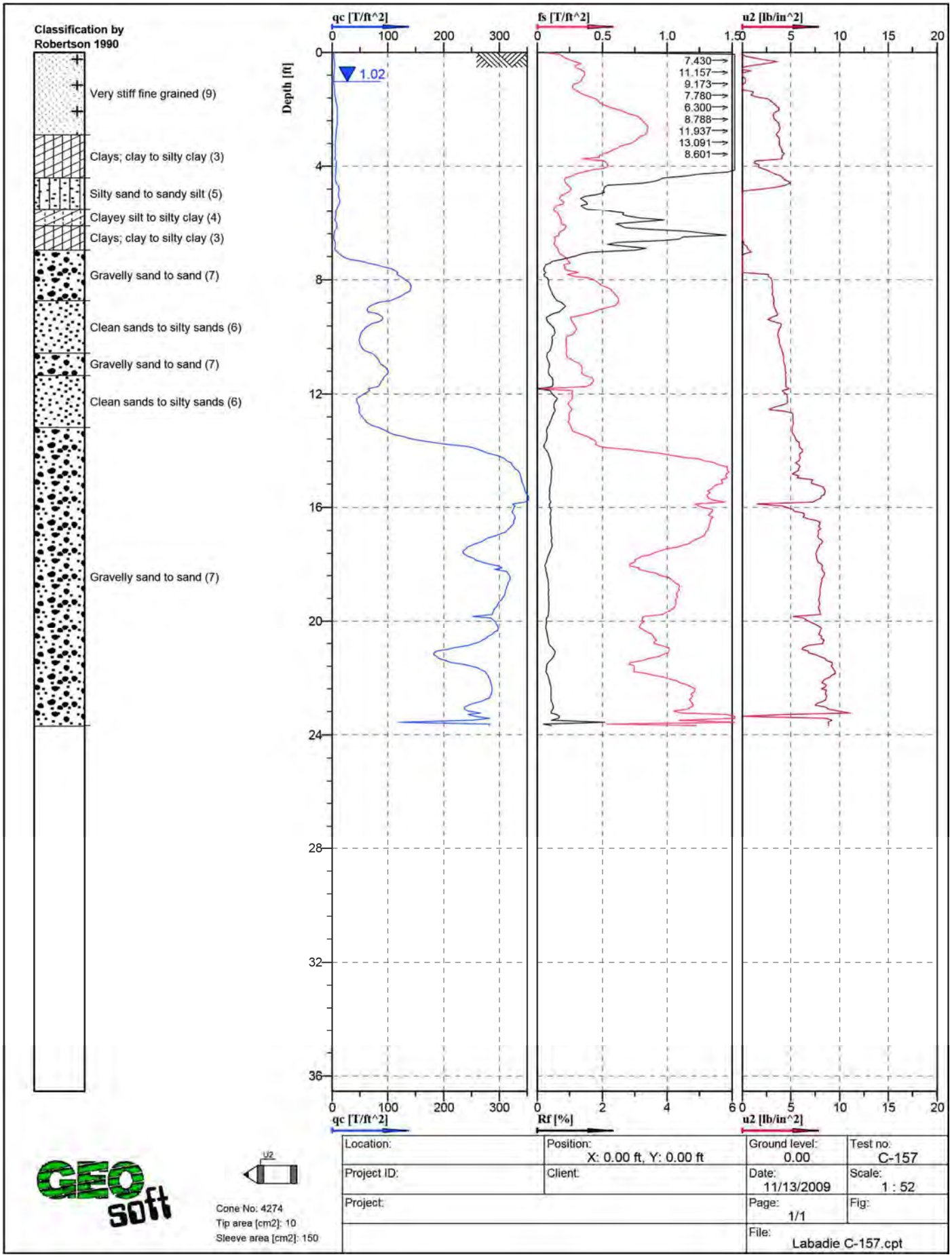

Figure A - 70: Cone Penetration Test Sounding Log, C-157

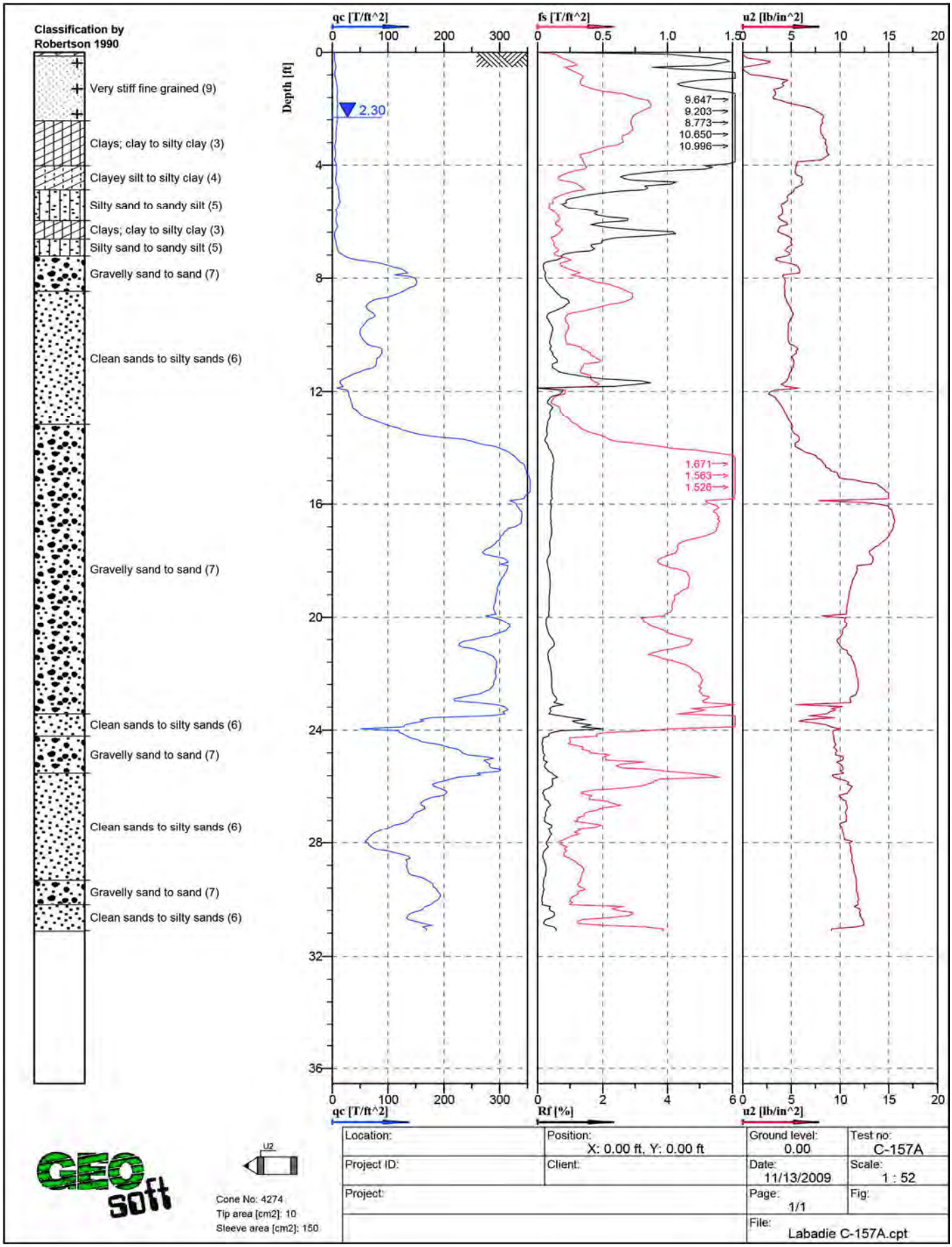

Figure A - 71: Cone Penetration Test Sounding Log, C-157A

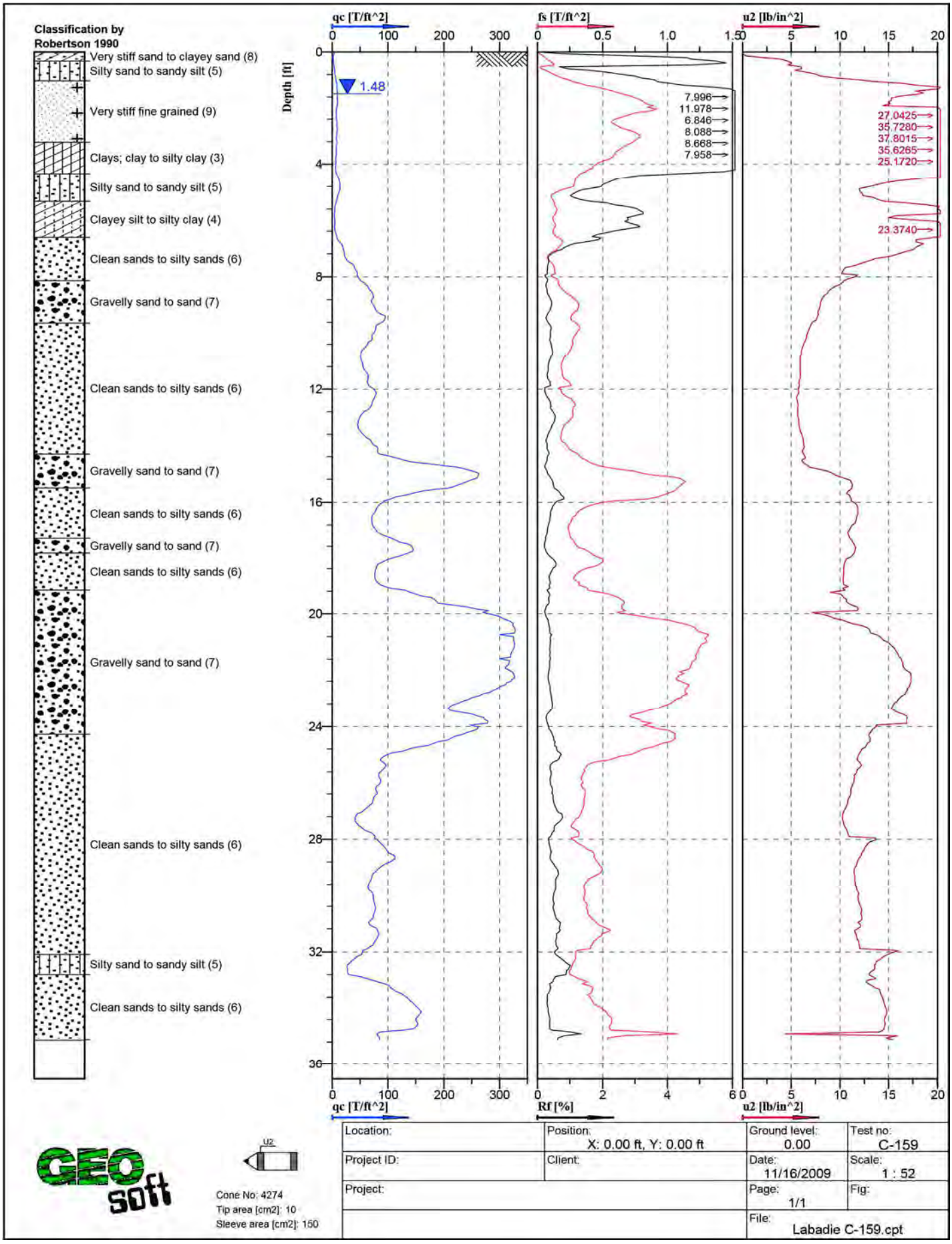

Figure A - 72: Cone Penetration Test Sounding Log, C-159

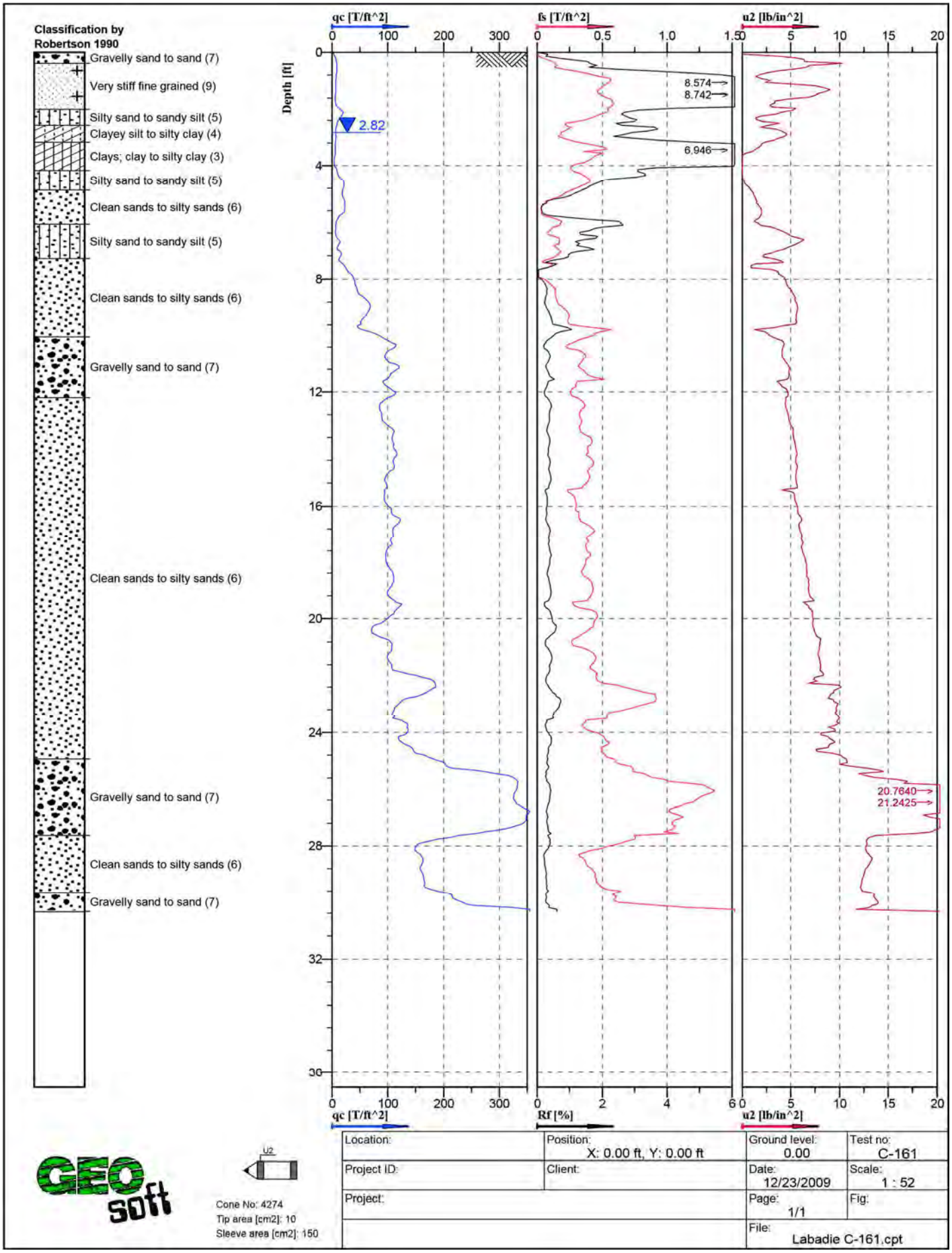

Figure A - 73: Cone Penetration Test Sounding Log, C-161

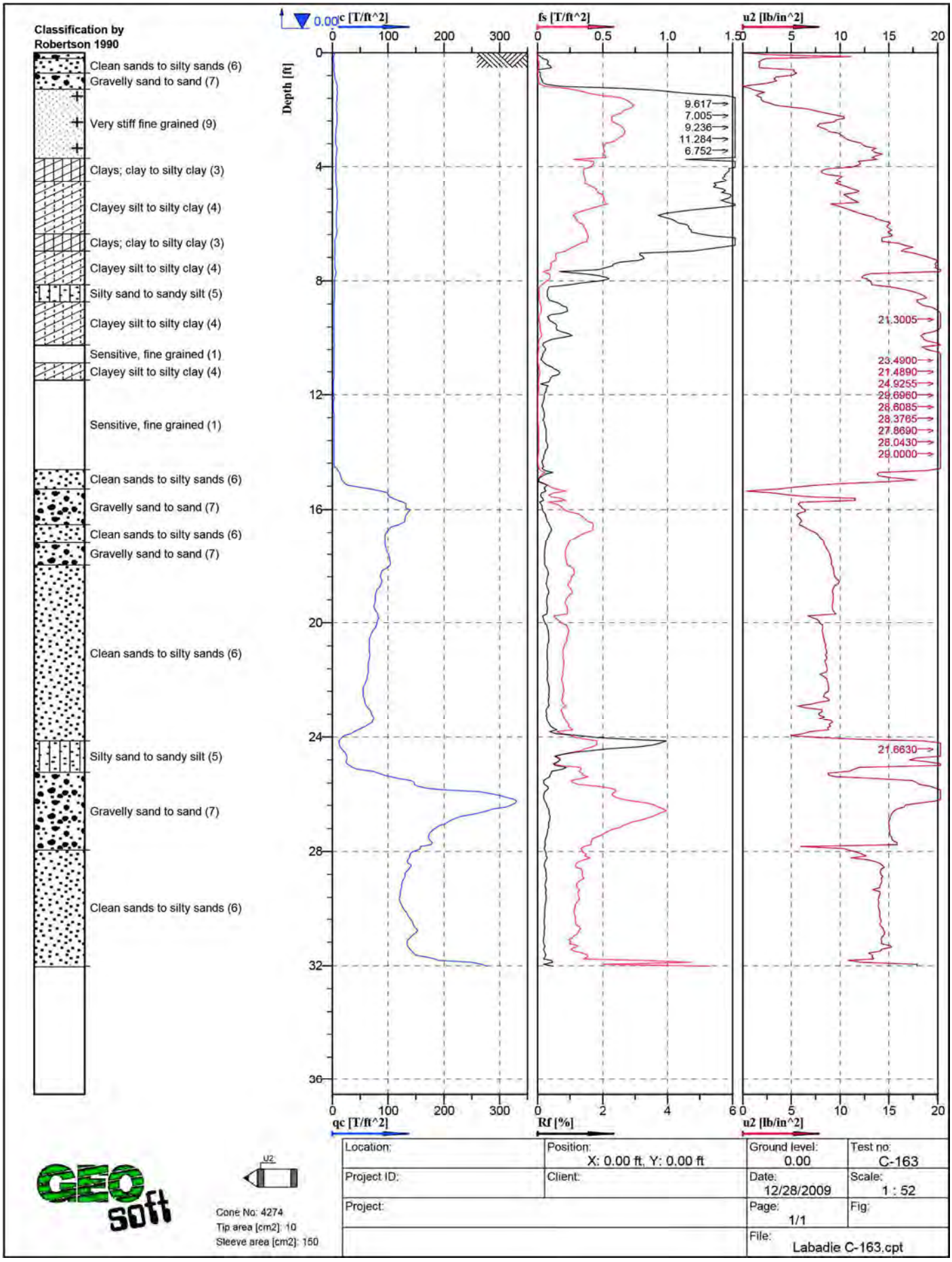

Figure A - 74: Cone Penetration Test Sounding Log, C-163

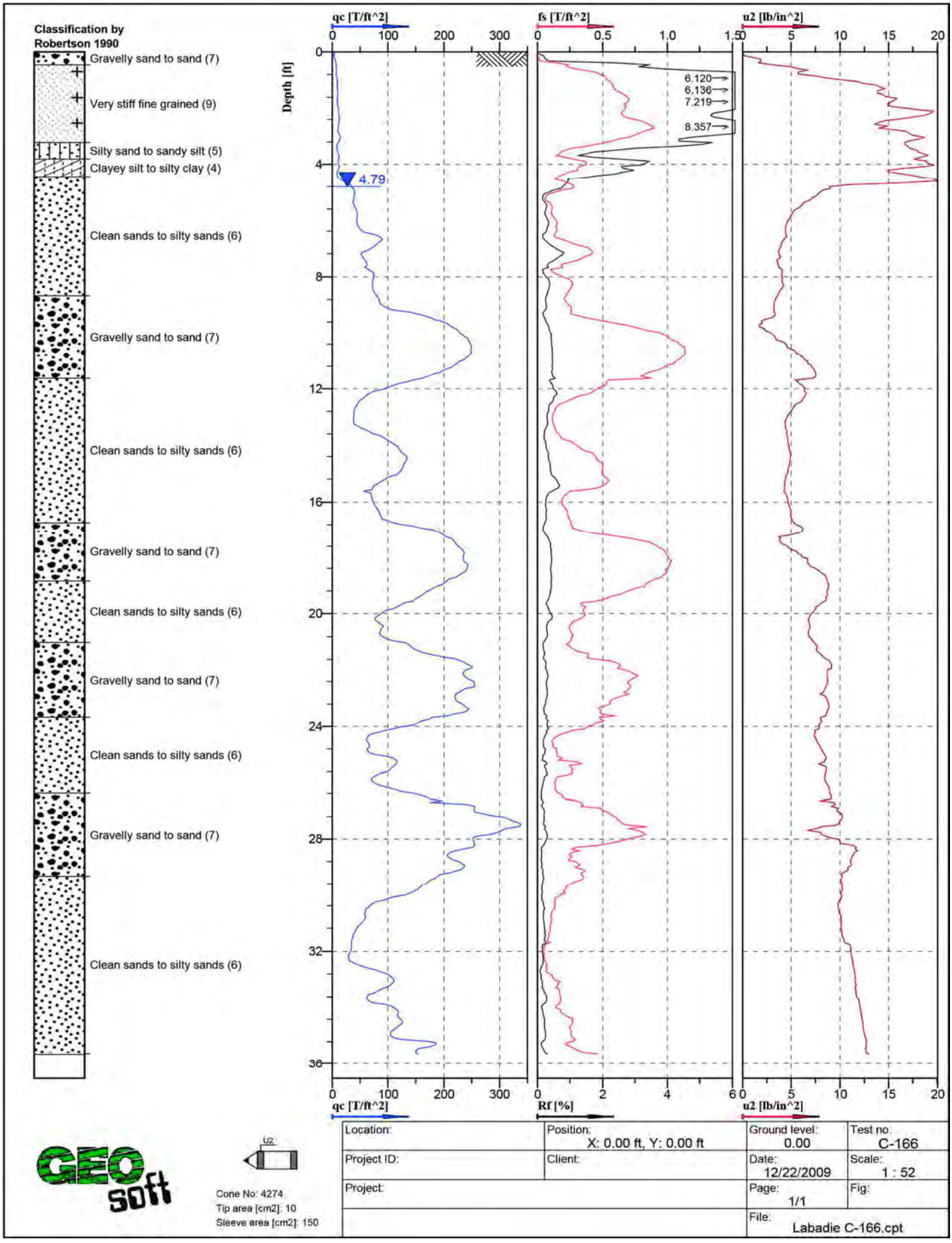

Figure A - 75: Cone Penetration Test Sounding Log, C-166

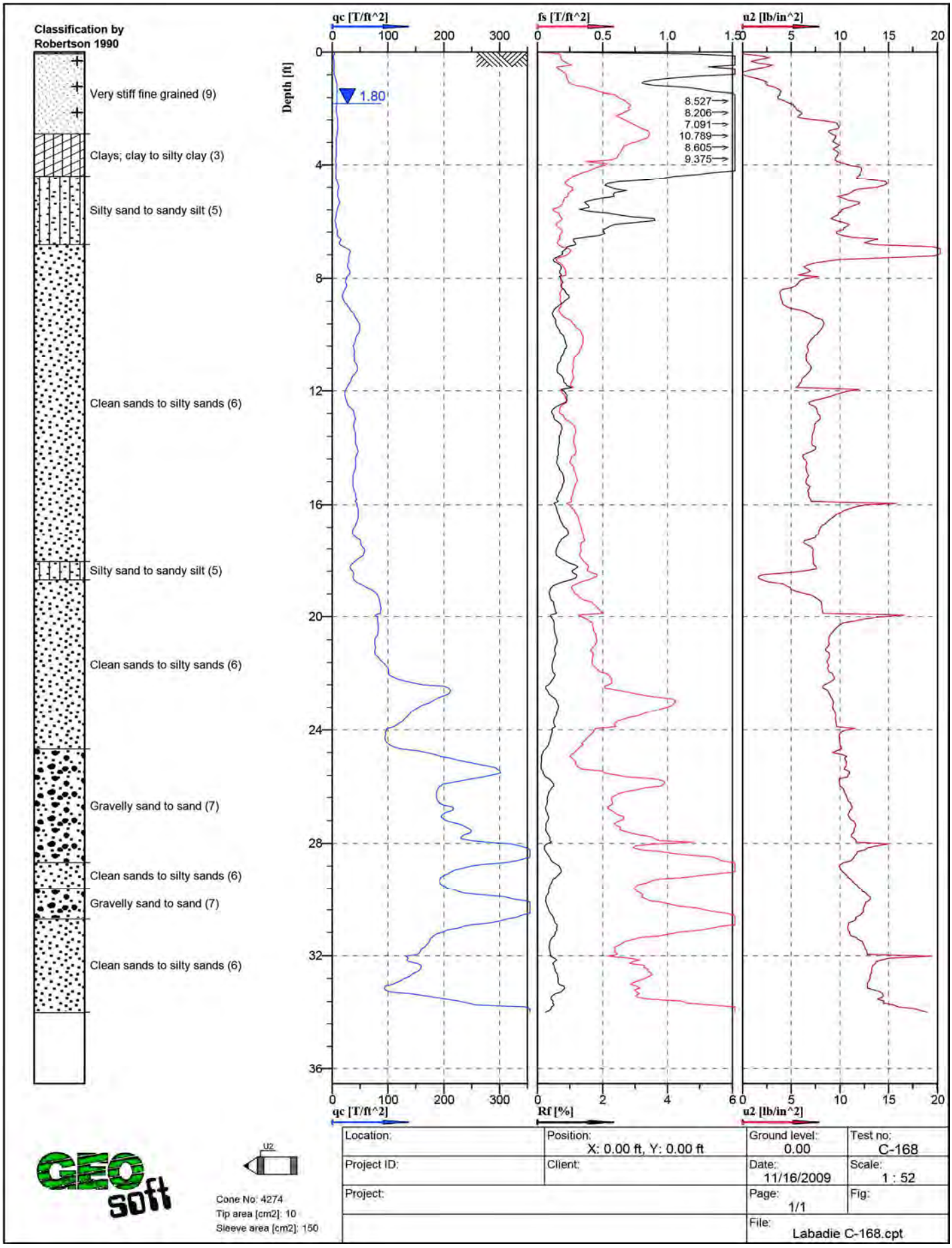

Figure A - 76: Cone Penetration Test Sounding Log, C-168

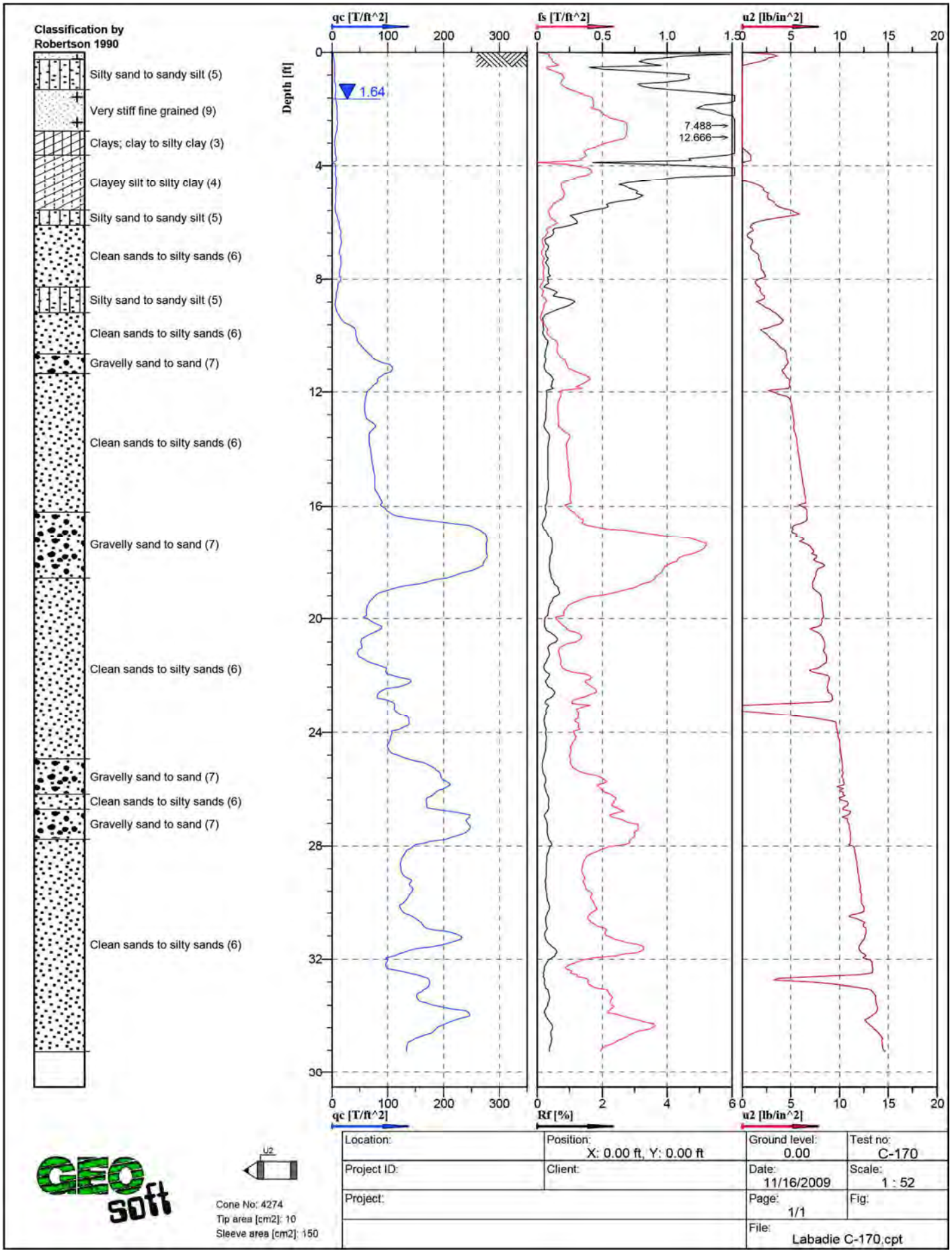

Figure A - 77: Cone Penetration Test Sounding Log, C-170

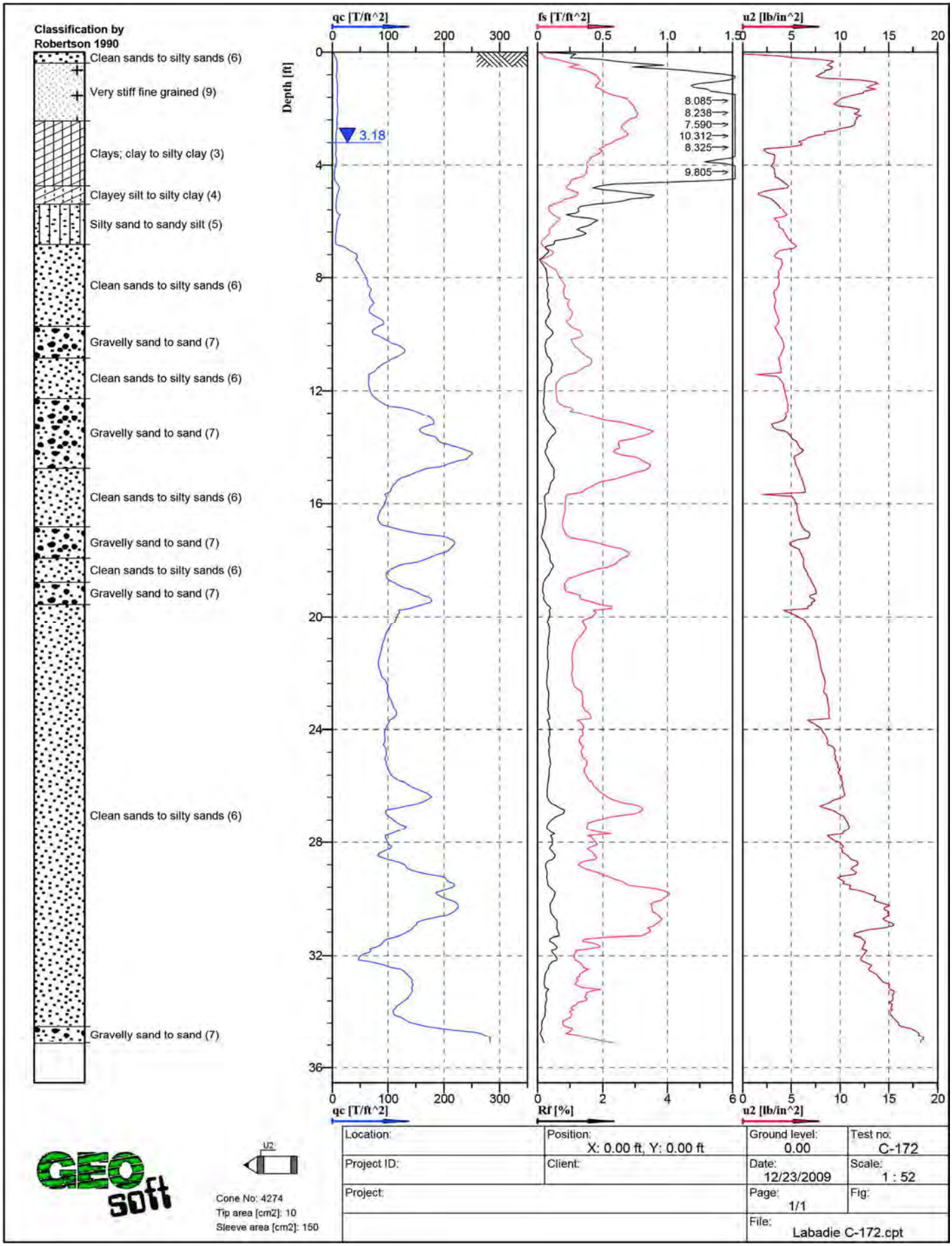

Figure A - 78: Cone Penetration Test Sounding Log, C-172

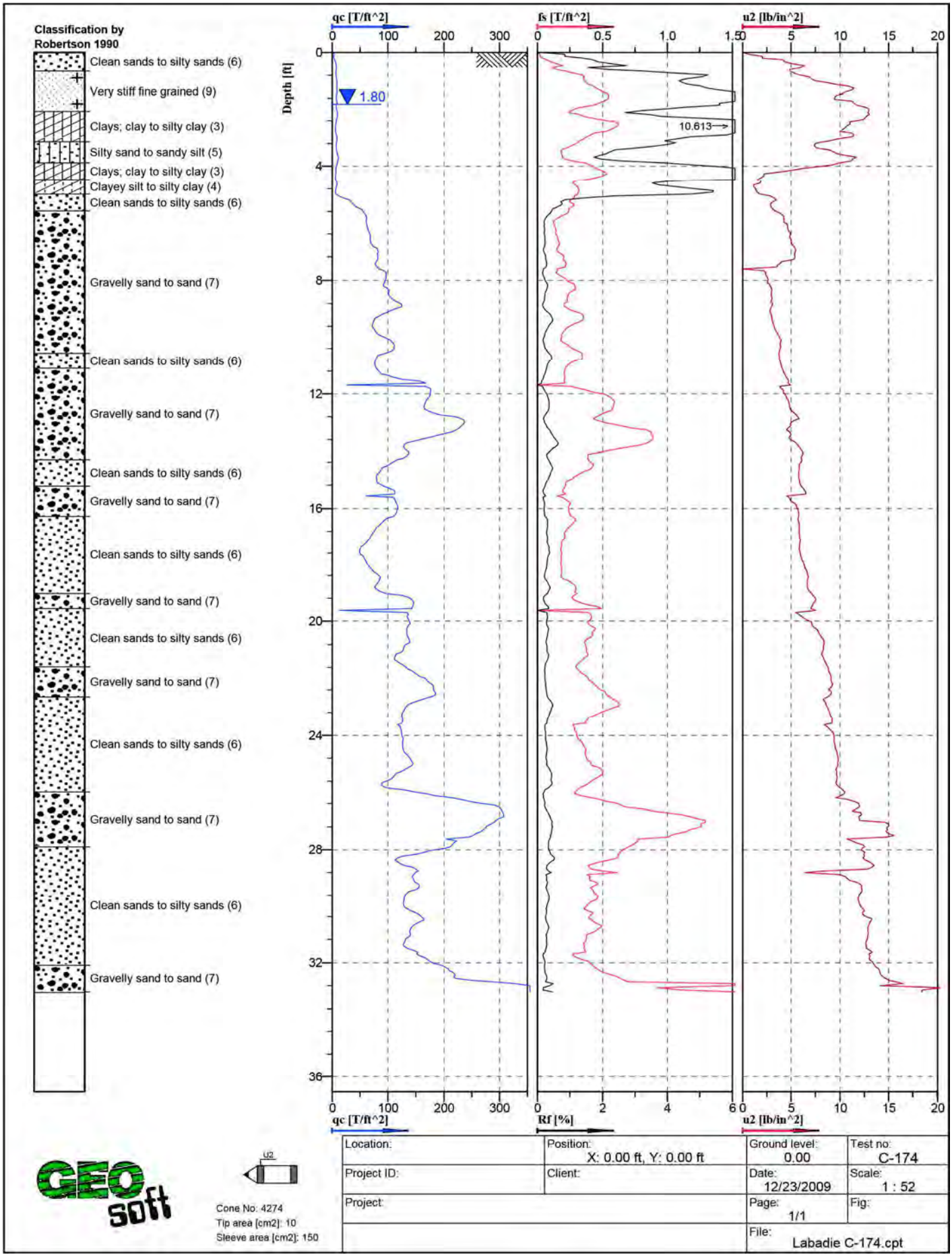

Figure A - 79: Cone Penetration Test Sounding Log, C-174

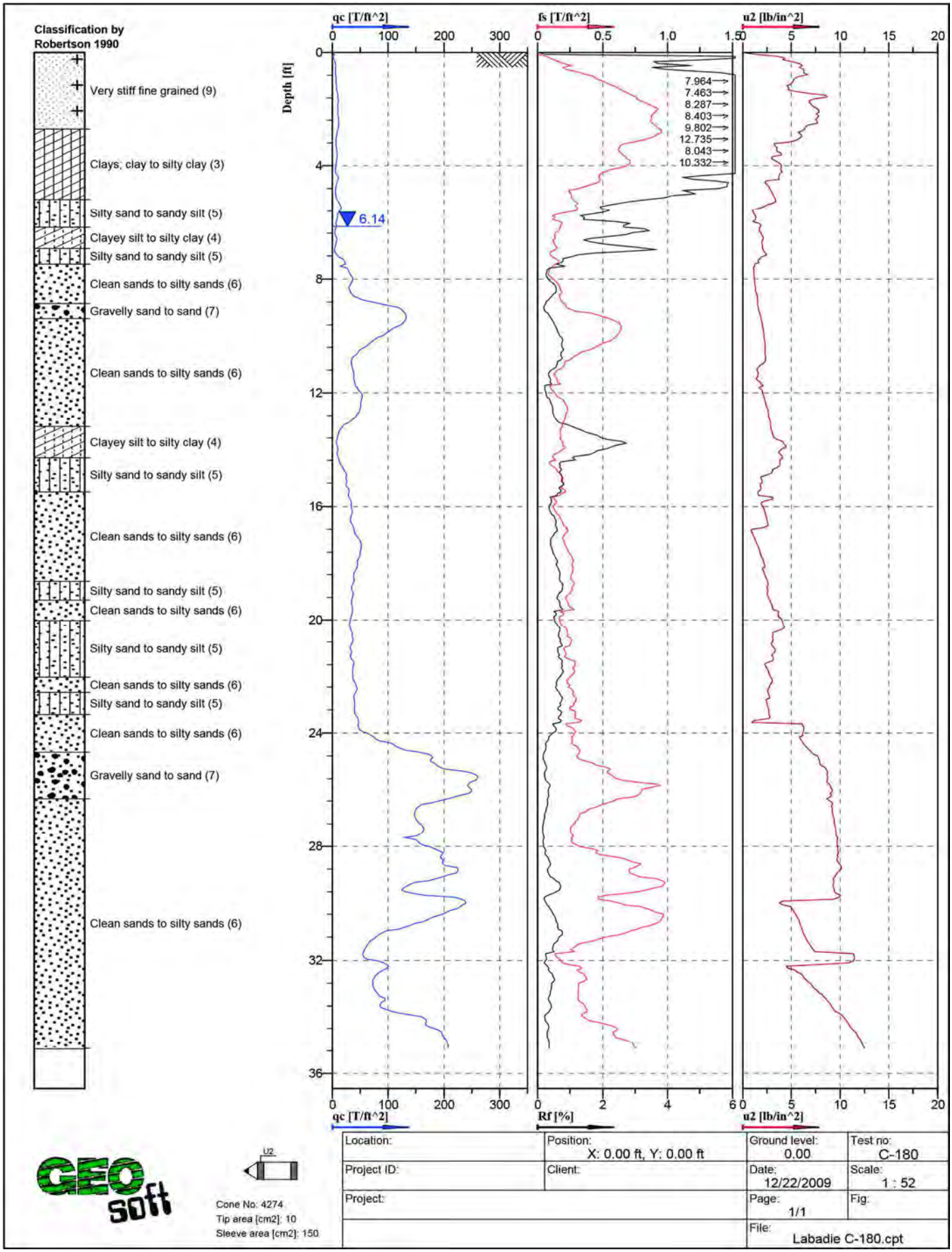

Figure A - 80: Cone Penetration Test Sounding Log, C-180

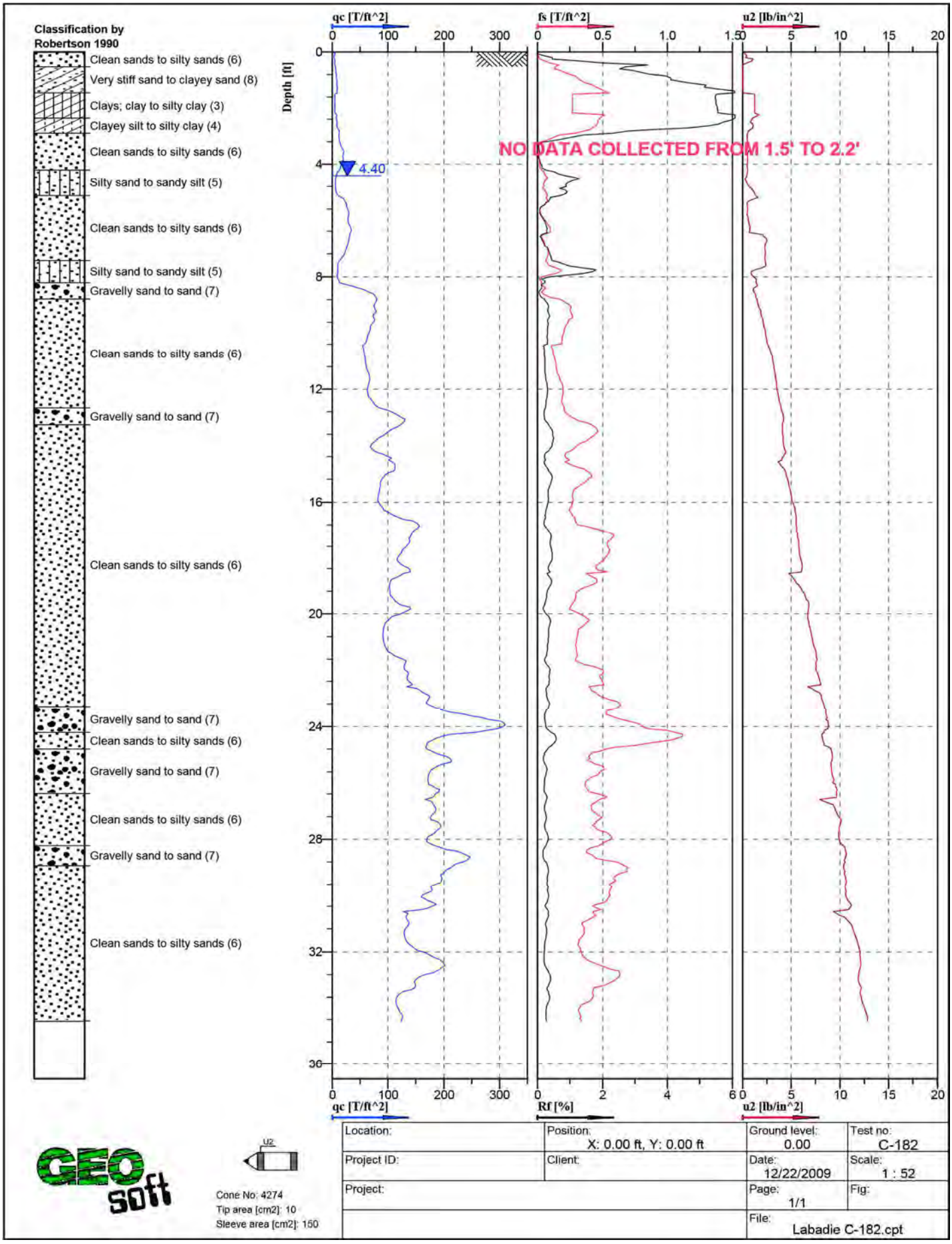

Figure A - 81: Cone Penetration Test Sounding Log, C-182

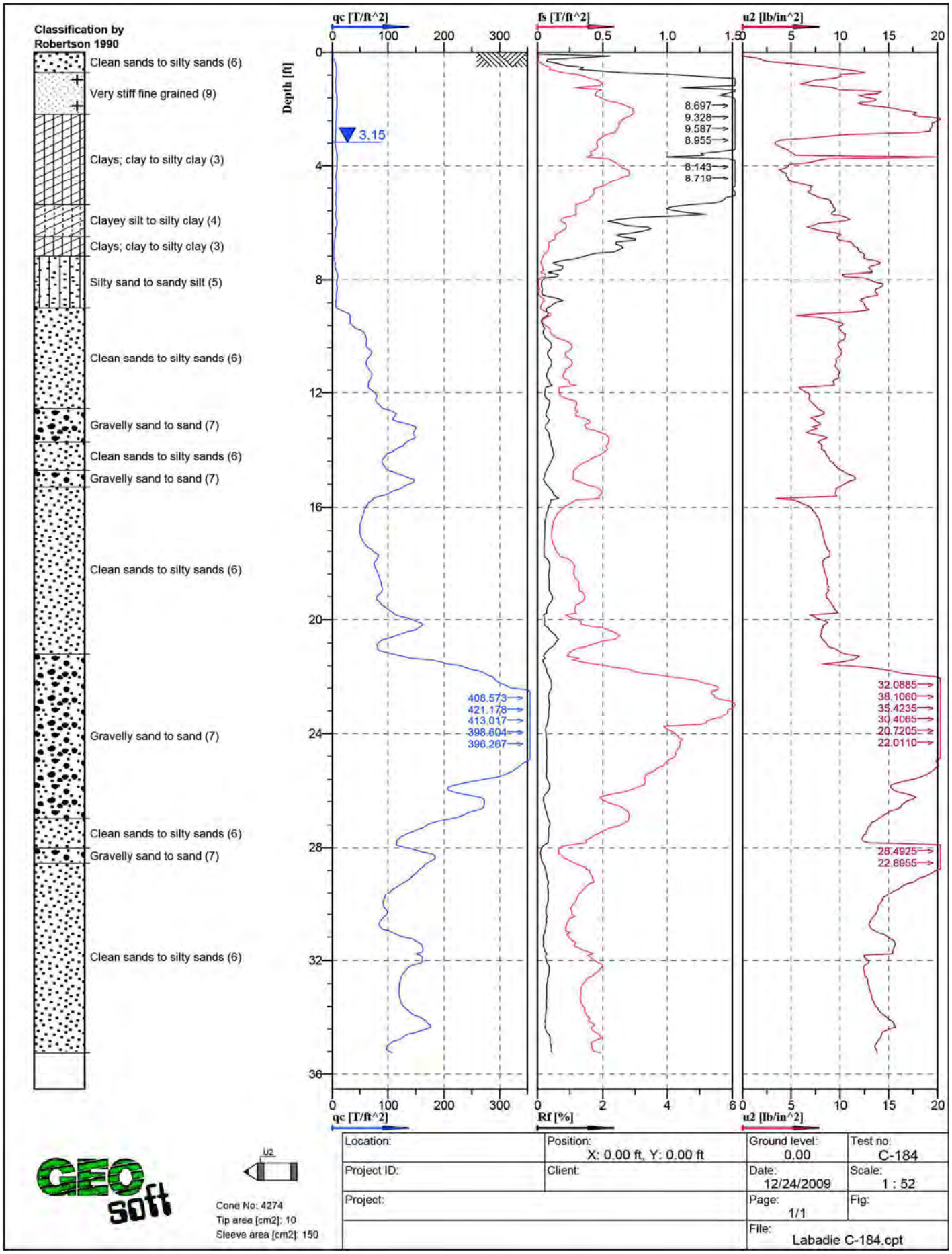

Figure A - 82: Cone Penetration Test Sounding Log, C-184

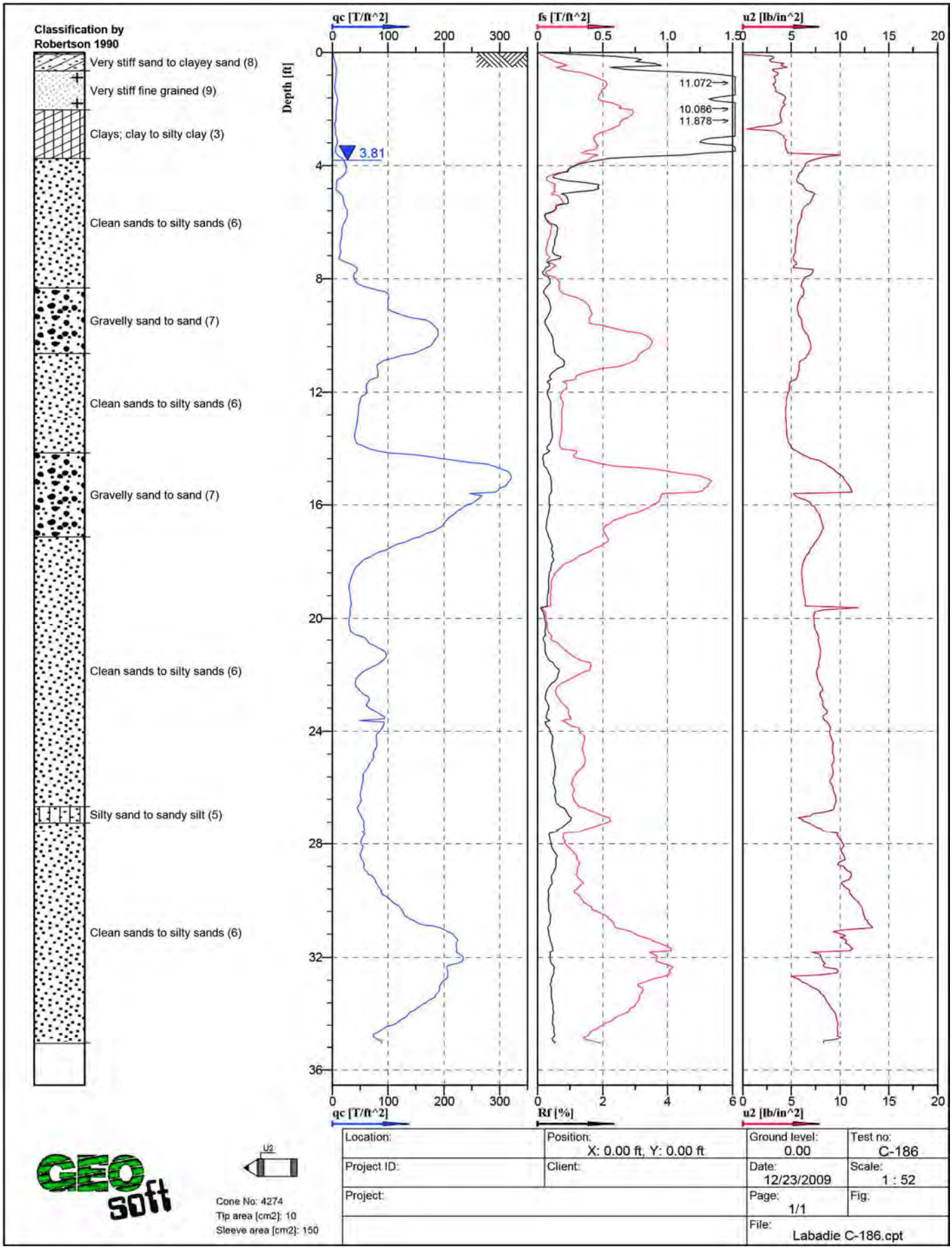

Figure A - 83: Cone Penetration Test Sounding Log, C-186

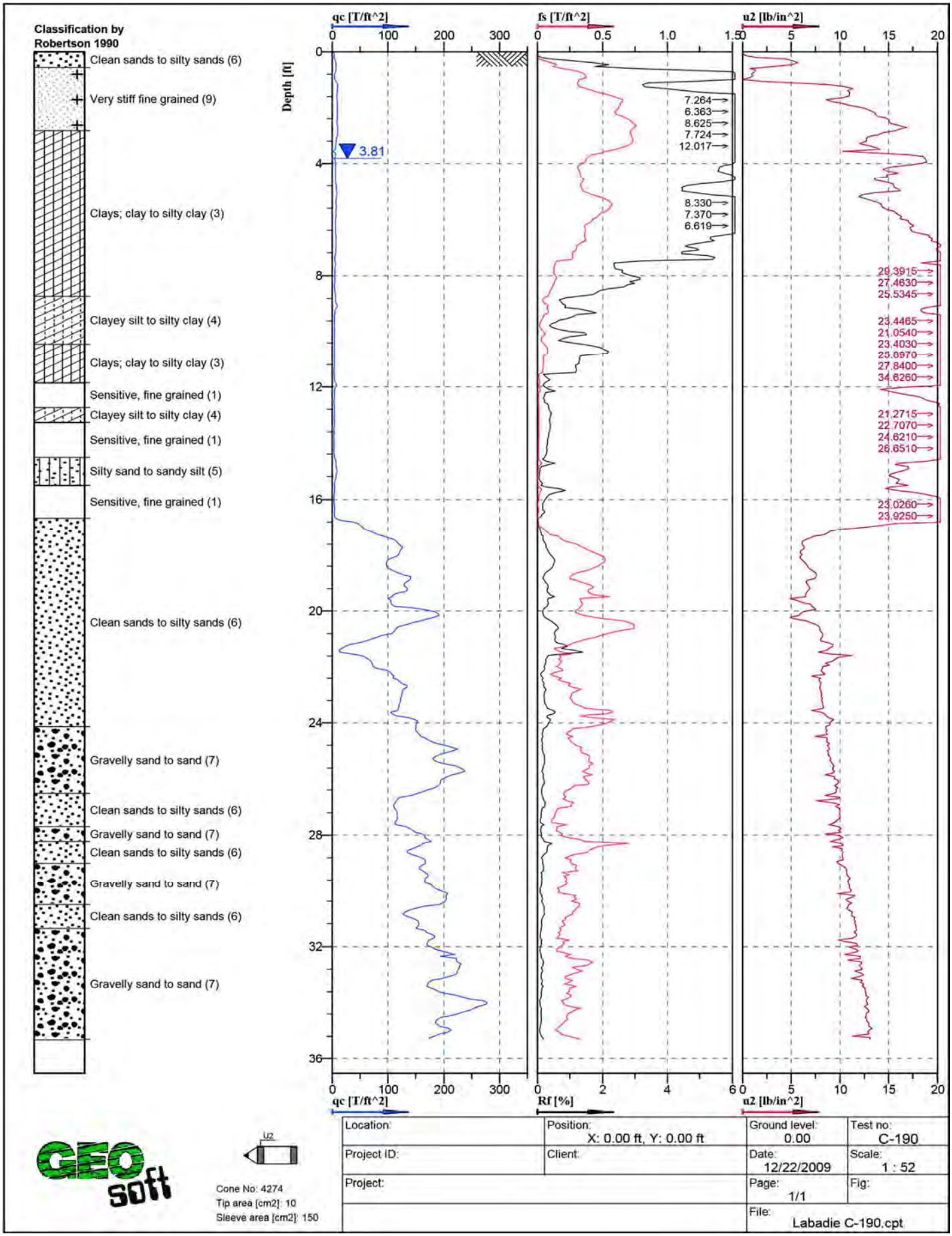

Figure A - 84: Cone Penetration Test Sounding Log, C-190

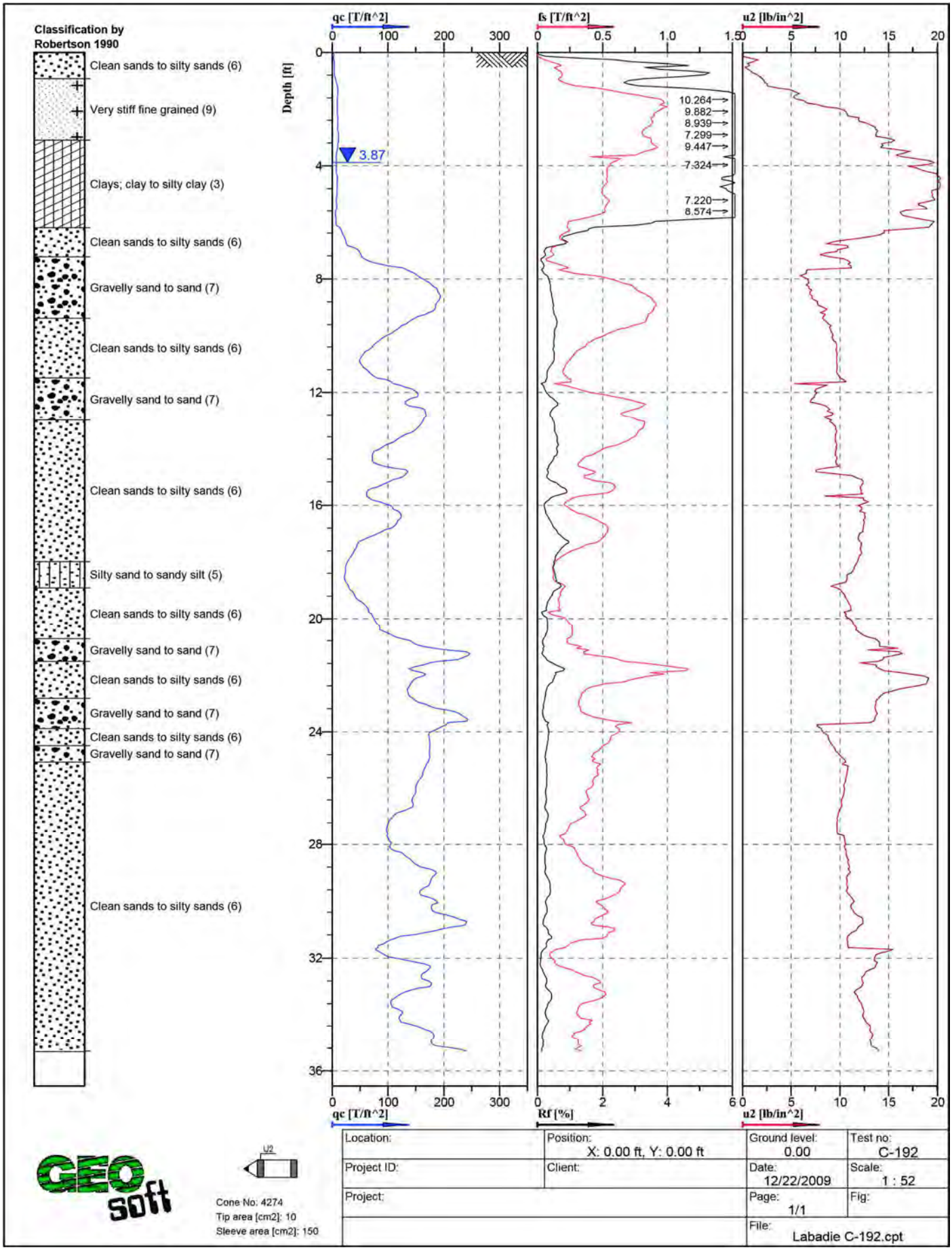

Figure A - 85: Cone Penetration Test Sounding Log, C-192

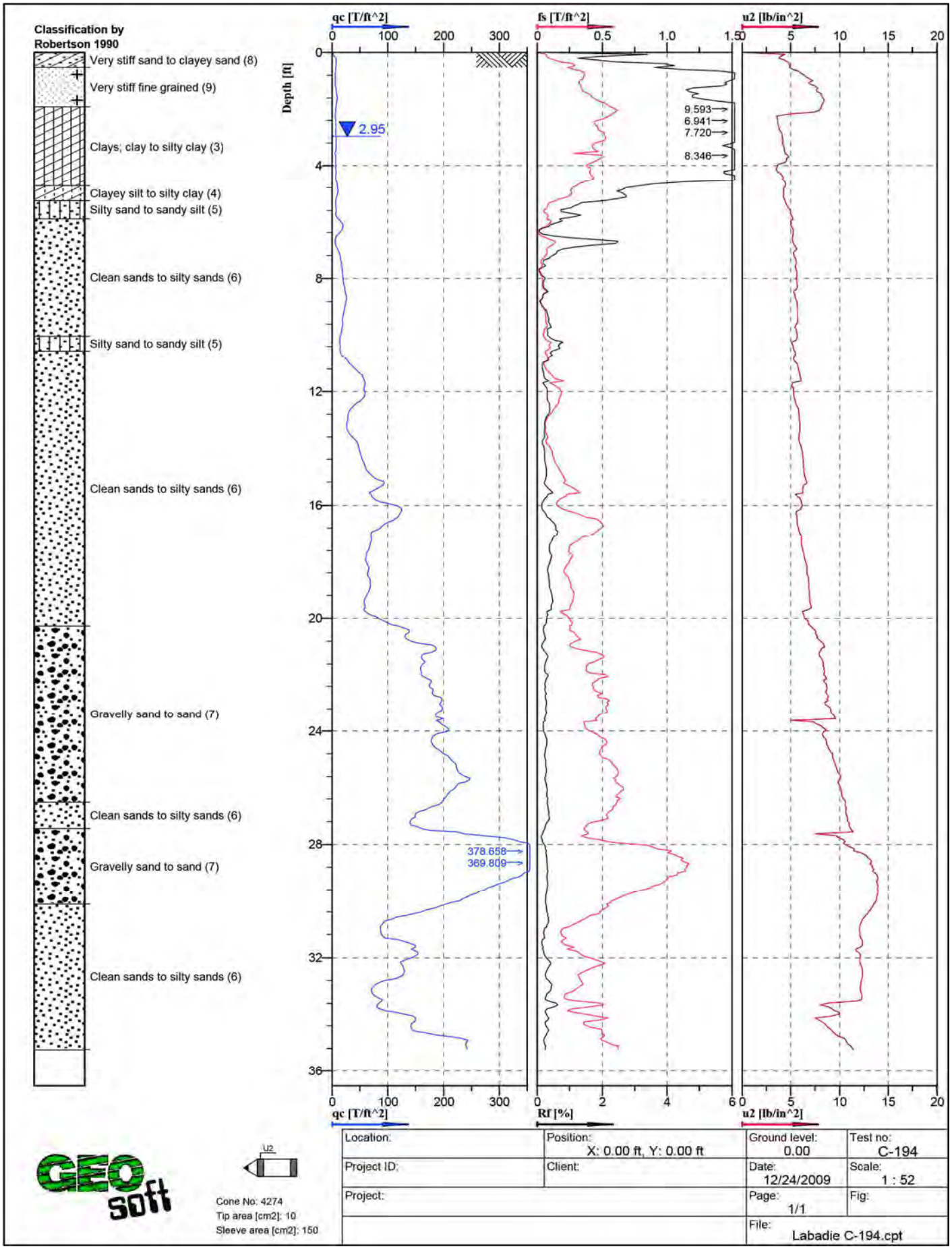

Figure A - 86: Cone Penetration Test Sounding Log, C-194

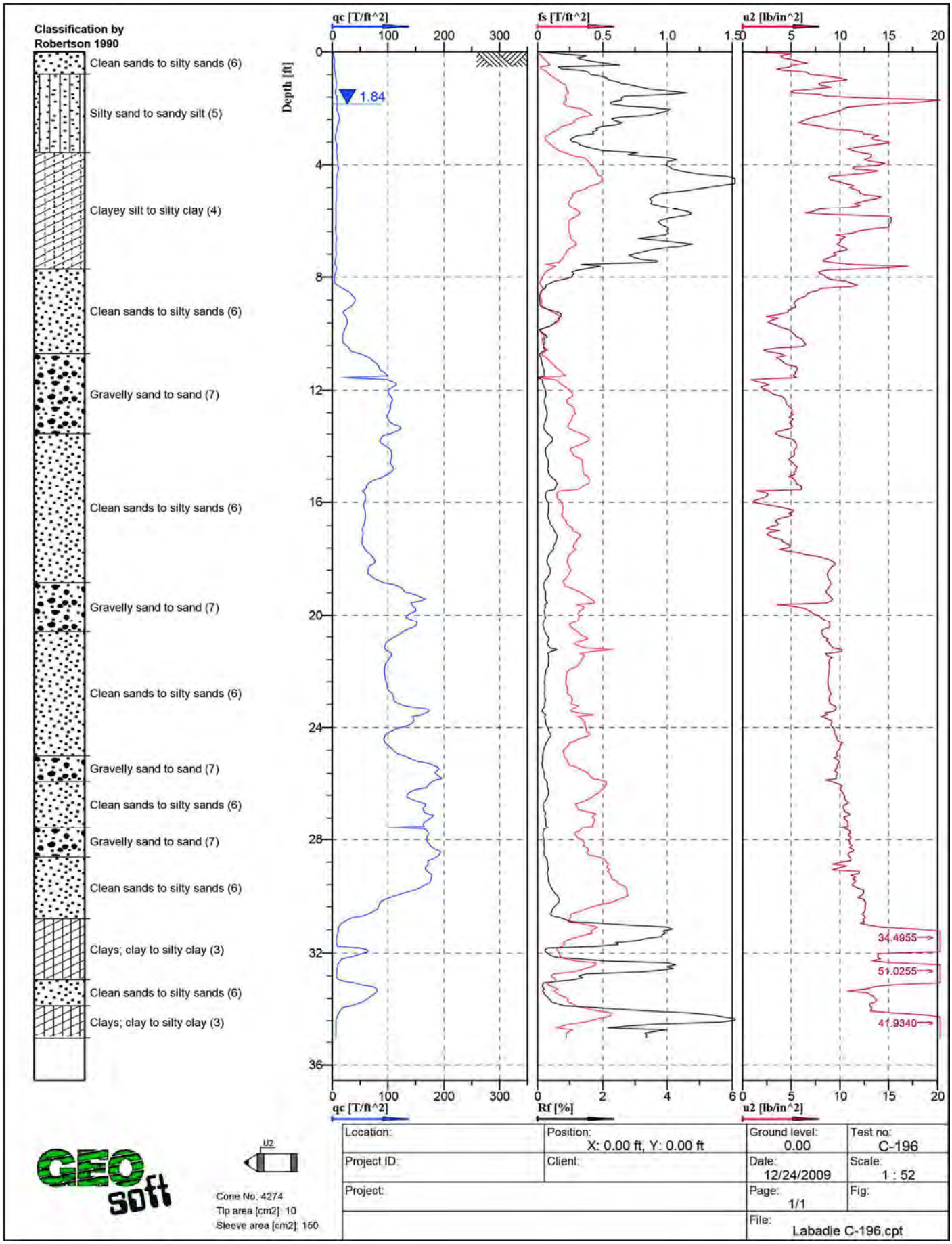

Figure A - 87: Cone Penetration Test Sounding Log, C-196

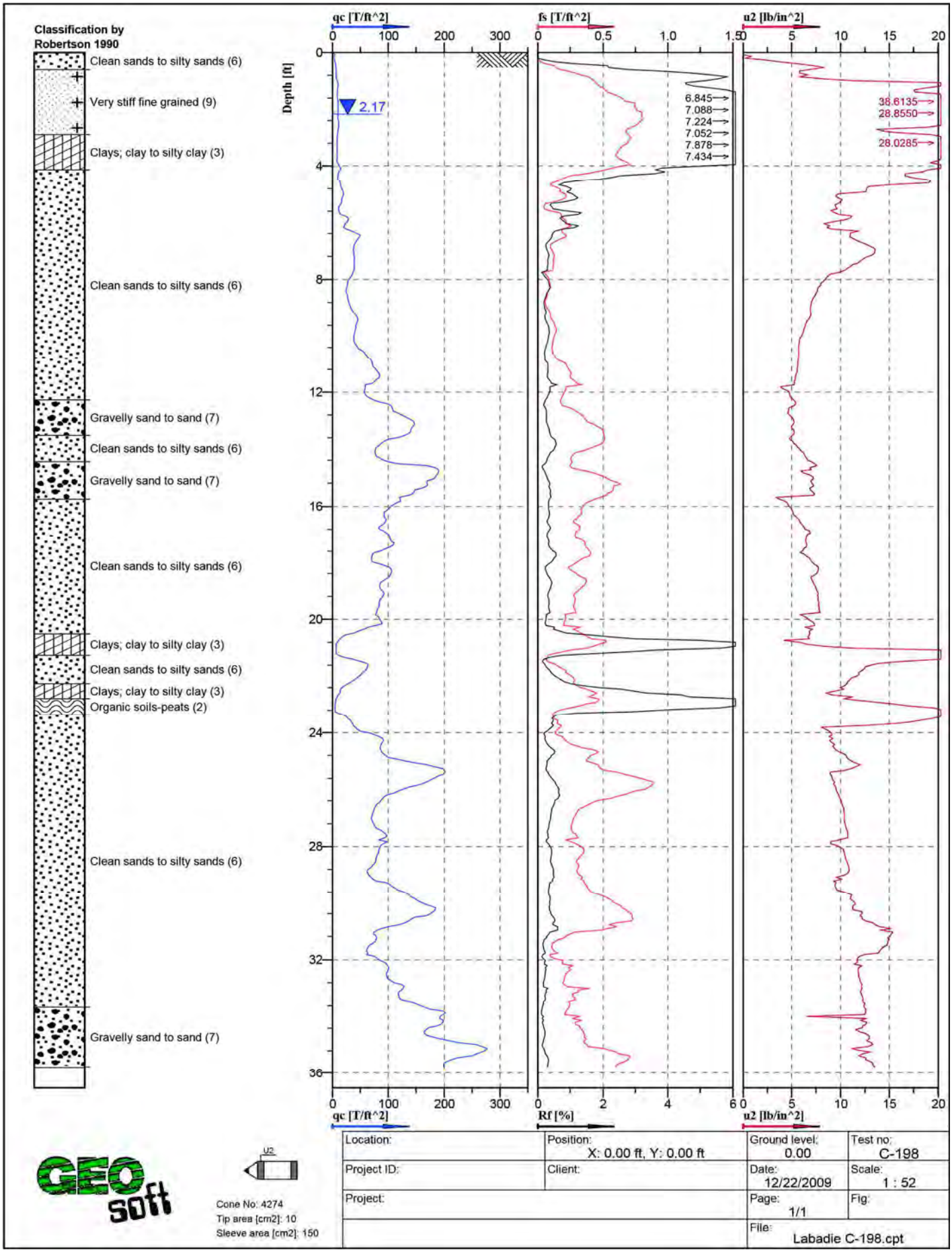

Figure A - 88: Cone Penetration Test Sounding Log, C-198

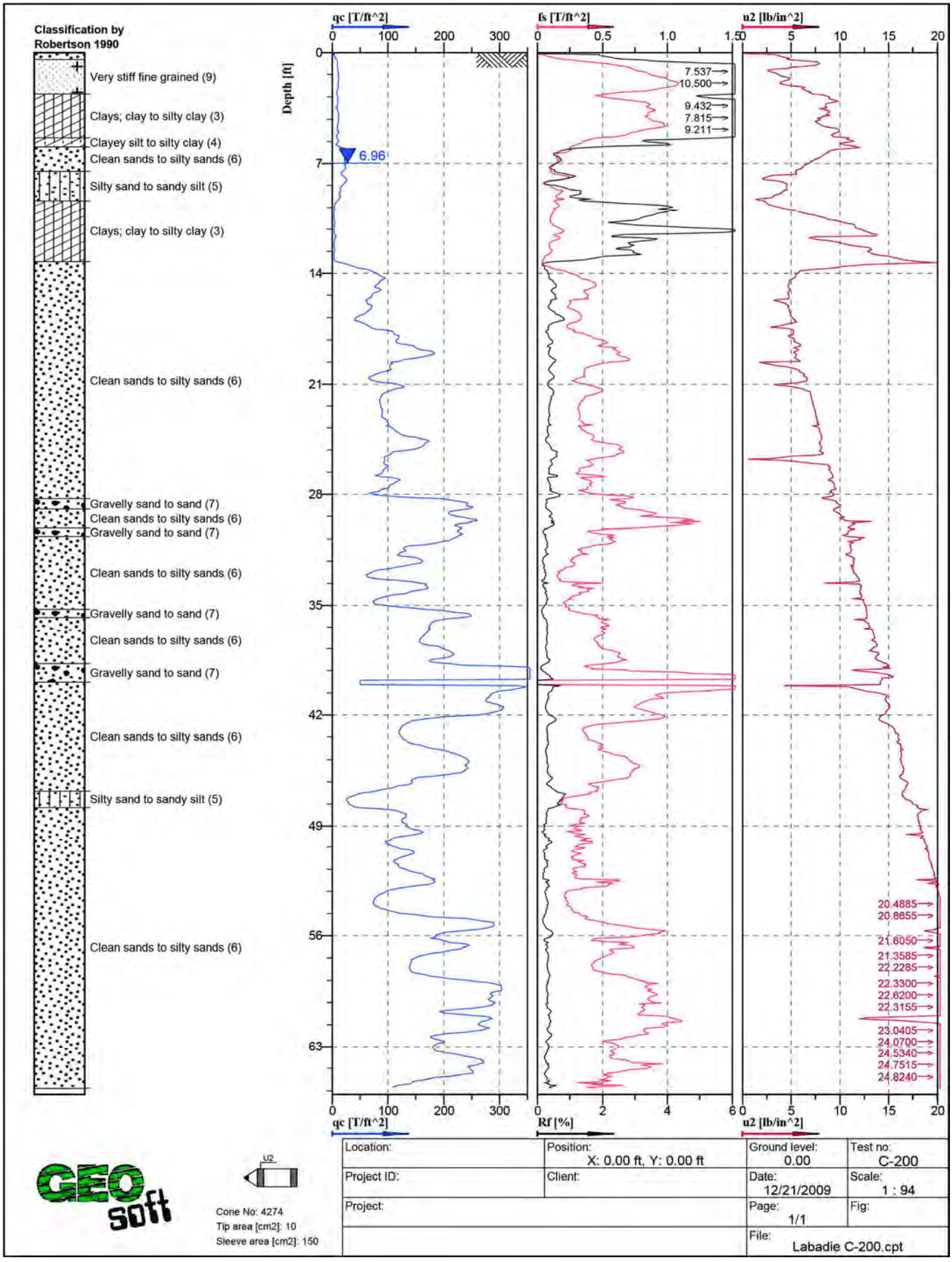

Figure A - 89: Cone Penetration Test Sounding Log, C-200

APPENDIX B

Plots to Estimate the Scale of Fluctuation
Autocorrelation Function versus Lag for
Homogeneous Soil Units

Figure B - 1: Estimation of the Scale of Fluctuation, θ = 0.9 feet, for Cone Tip Resistance Data from Sounding C-11, "Clean sands to silty sands (6)" layer from 18 to 20 feet depth. 1
Figure B - 2: Estimation of the Scale of Fluctuation, θ = 2.0 feet, for Friction Ratio Data from Sounding C-11, "Clean sands to silty sands (6)" layer from 18 to 20 feet depth. 1
Figure B - 3: Estimation of the Scale of Fluctuation, θ = 1.1 feet, for Cone Tip Resistance Data from Sounding C-13, "Clean sands to silty sands (6)" layer from 8 to 14 feet depth. 2
Figure B - 4: Estimation of the Scale of Fluctuation, θ = 0.3 feet, for Friction Ratio Data from Sounding C-13, "Clean sands to silty sands (6)" layer from 8 to 14 feet depth. 2
Figure B - 5: Estimation of the Scale of Fluctuation, θ = 2.2 feet, for Cone Tip Resistance Data from Sounding C-13, "Clean sands to silty sands (6)" layer from 15 to 40 feet depth. 3
Figure B - 6: Estimation of the Scale of Fluctuation, θ = 1.4 feet, for Friction Ratio Data from Sounding C-13, "Clean sands to silty sands (6)" layer from 15 to 40 feet depth. Data is a poor fit for the points greater than the Bartlett limit of 0.10; coefficient of determination, R^2, value is less 0.9. Therefore, these results were not included in final analysis. 3
Figure B - 7: Estimation of the Scale of Fluctuation, θ = 1.3 feet, for Cone Tip Resistance Data from Sounding C-16, "Clean sands to silty sands (6)" layer from 17 to 22 feet depth. Data is a poor fit for the points greater than the Bartlett limit of 0.21; coefficient of determination, R^2, value is less 0.9. Therefore, these results were not included in final analysis. 4
Figure B - 8: Estimation of the Scale of Fluctuation, θ = 0.9 feet, for Friction Ratio Data from Sounding C-16, "Clean sands to silty sands (6)" layer from 17 to 22 feet depth. 4
Figure B - 9: Estimation of the Scale of Fluctuation, θ = 1.2 feet, for Cone Tip Resistance Data from Sounding C-16, "Clean sands to silty sands (6)" layer from 23 to 32 feet depth. 5
Figure B - 10: Estimation of the Scale of Fluctuation, θ = 0.5 feet, for Friction Ratio Data from Sounding C-16, "Clean sands to silty sands (6)" layer from 23 to 32 feet depth. 5
Figure B - 11: Estimation of the Scale of Fluctuation, θ = 0.7 feet, for Cone Tip Resistance Data from Sounding C-16, "Clean sands to silty sands (6)" layer from 35 to 40 feet depth. 6
Figure B - 12: Estimation of the Scale of Fluctuation, θ = 0.7 feet, for Friction Ratio Data from Sounding C-16, "Clean sands to silty sands (6)" layer from 35 to 40 feet depth. 6
Figure B - 13: Estimation of the Scale of Fluctuation, θ = 1.3 feet, for Cone Tip Resistance Data from Sounding C-18, "Clean sands to silty sands (6)" layer from 11 to 26 feet depth. 7
Figure B - 14: Estimation of the Scale of Fluctuation, θ = 0.8 feet, for Friction Ratio Data from Sounding C-18, "Clean sands to silty sands (6)" layer from 11 to 26 feet depth. 7
Figure B - 15: Estimation of the Scale of Fluctuation, θ = 2.0 feet, for Cone Tip Resistance Data from Sounding C-18, "Clean sands to silty sands (6)" layer from 27 to 35 feet depth. 8
Figure B - 16: Estimation of the Scale of Fluctuation, θ = 1.0 feet, for Friction Ratio Data from Sounding C-18, "Clean sands to silty sands (6)" layer from 27 to 35 feet depth. 8
Figure B - 17: Estimation of the Scale of Fluctuation, θ = 2.3 feet, for Cone Tip Resistance Data from Sounding C-21, "Clean sands to silty sands (6)" layer from 11 to 16 feet depth. 9
Figure B - 18: Estimation of the Scale of Fluctuation, θ = 0.3 feet, for Friction Ratio Data from Sounding C-21, "Clean sands to silty sands (6)" layer from 11 to 16 feet depth. 9
Figure B - 19: Estimation of the Scale of Fluctuation, θ = 0.8 feet, for Cone Tip Resistance Data from Sounding C-21, "Clean sands to silty sands (6)" layer from 17 to 35 feet depth. 10

Figure B - 20: Estimation of the Scale of Fluctuation, θ = 0.8 feet, for Friction Ratio Data from Sounding C-21, "Clean sands to silty sands (6)" layer from 17 to 35 feet depth. Data is a poor fit for the points greater than the Bartlett limit of 0.12; coefficient of determination, R^2, value is less 0.9. Therefore, these results were not included in final analysis. 10
Figure B - 21: Estimation of the Scale of Fluctuation, θ = 2.5 feet, for Cone Tip Resistance Data from Sounding C-23, "Clean sands to silty sands (6)" layer from 9 to 18 feet depth. 11
Figure B - 22: Estimation of the Scale of Fluctuation, θ = 0.2 feet, for Friction Ratio Data from Sounding C-23, "Clean sands to silty sands (6)" layer from 9 to 18 feet depth. Data is limited to only 3 points greater than the Bartlett limit of 0.12; therefore, these results were not included in final analysis. 11
Figure B - 23: Estimation of the Scale of Fluctuation, θ = 2.4 feet, for Cone Tip Resistance Data from Sounding C-23, "Clean sands to silty sands (6)" layer from 19 to 24 feet depth. 12
Figure B - 24: Estimation of the Scale of Fluctuation, θ = 1.1 feet, for Cone Tip Resistance Data from Sounding C-23, "Clean sands to silty sands (6)" layer from 19 to 24 feet depth. 12
Figure B - 25: Estimation of the Scale of Fluctuation, θ = 0.9 feet, for Cone Tip Resistance Data from Sounding C-23, "Clean sands to silty sands (6)" layer from 26 to 31 feet depth. 13
Figure B - 26: Estimation of the Scale of Fluctuation, θ = 0.7 feet, for Friction Ratio Data from Sounding C-23, "Clean sands to silty sands (6)" layer from 26 to 31 feet depth. 13
Figure B - 27: Estimation of the Scale of Fluctuation, θ = 1.9 feet, for Cone Tip Resistance Data from Sounding C-25, "Clean sands to silty sands (6)" layer from 4 to 34 feet depth. 14
Figure B - 28: Estimation of the Scale of Fluctuation, θ = 0.4 feet, for Friction Ratio Data from Sounding C-25, "Clean sands to silty sands (6)" layer from 4 to 34 feet depth. 14
Figure B - 29: Estimation of the Scale of Fluctuation, θ = 1.3 feet, for Cone Tip Resistance Data from Sounding C-28, "Clean sands to silty sands (6)" layer from 18 to 23 feet depth. 15
Figure B - 30: Estimation of the Scale of Fluctuation, θ, for Friction Ratio Data from Sounding C-28, "Clean sands to silty sands (6)" layer from 18 to 23 feet depth. Data is limited to only 1 point greater than the Bartlett limit of 0.17; therefore, θ could not be estimated, and these results were not included in final analysis. 15
Figure B - 31: Estimation of the Scale of Fluctuation, θ = 1.2 feet, for Cone Tip Resistance Data from Sounding C-28, "Clean sands to silty sands (6)" layer from 24 to 34 feet depth. 16
Figure B - 32: Estimation of the Scale of Fluctuation, θ = 0.1 feet, for Friction Ratio Data from Sounding C-28, "Clean sands to silty sands (6)" layer from 24 to 34 feet depth. 16
Figure B - 33: Estimation of the Scale of Fluctuation, θ = 1.5 feet, for Cone Tip Resistance Data from Sounding C-30, "Clean sands to silty sands (6)" layer from 13 to 17 feet depth. 17
Figure B - 34: Estimation of the Scale of Fluctuation, θ = 0.8 feet, for Friction Ratio Data from Sounding C-30, "Clean sands to silty sands (6)" layer from 13 to 17 feet depth. 17
Figure B - 35: Estimation of the Scale of Fluctuation, θ = 1.0 feet, for Cone Tip Resistance Data from Sounding C-30, "Clean sands to silty sands (6)" layer from 18 to 26 feet depth. 18
Figure B - 36: Estimation of the Scale of Fluctuation, θ, for Friction Ratio Data from Sounding C-30, "Clean sands to silty sands (6)" layer from 18 to 26 feet depth. Data is limited to only 1 point greater than the Bartlett limit of 0.20; therefore, θ could not be estimated, and these results were not included in final analysis. 18
Figure B - 37: Estimation of the Scale of Fluctuation, θ = 1.0 feet, for Cone Tip Resistance Data from Sounding C-30, "Clean sands to silty sands (6)" layer from 29 to 35 feet depth. 19

Figure B - 38: Estimation of the Scale of Fluctuation, θ = 0.4 feet, for Friction Ratio Data from Sounding C-30, "Clean sands to silty sands (6)" layer from 29 to 35 feet depth. 19
Figure B - 39: Estimation of the Scale of Fluctuation, θ = 2.3 feet, for Cone Tip Resistance Data from Sounding C-32a, "Clean sands to silty sands (6)" layer from 7 to 12 feet depth. 20
Figure B - 40: Estimation of the Scale of Fluctuation, θ = 0.8 feet, for Friction Ratio Data from Sounding C-32a, "Clean sands to silty sands (6)" layer from 7 to 12 feet depth. 20
Figure B - 41: Estimation of the Scale of Fluctuation, θ = 1.5 feet, for Cone Tip Resistance Data from Sounding C-32a, "Clean sands to silty sands (6)" layer from 12 to 28 feet depth. 21
Figure B - 42: Estimation of the Scale of Fluctuation, θ = 0.7 feet, for Friction Ratio Data from Sounding C-32a, "Clean sands to silty sands (6)" layer from 12 to 28 feet depth. Data is a poor fit for the points greater than the Bartlett limit of 0.13; coefficient of determination, $R,^2$ value is less 0.9. Therefore, these results were not included in final analysis. 21
Figure B - 43: Estimation of the Scale of Fluctuation, θ = 1.1 feet, for Cone Tip Resistance Data from Sounding C-34, "Clean sands to silty sands (6)" layer from 27 to 32 feet depth. Data is a poor fit for the points greater than the Bartlett limit of 0.22; coefficient of determination, $R,^2$ value is less 0.9. Therefore, these results were not included in final analysis. 22
Figure B - 44: Estimation of the Scale of Fluctuation, θ = 0.5 feet, for Friction Ratio Data from Sounding C-34, "Clean sands to silty sands (6)" layer from 27 to 32 feet depth. Data is a poor fit for the points greater than the Bartlett limit of 0.22; coefficient of determination, $R,^2$ value is less 0.9. Therefore, these results were not included in final analysis. 22
Figure B - 45: Estimation of the Scale of Fluctuation, θ = 4.3 feet, for Cone Tip Resistance Data from Sounding C-37, "Clean sands to silty sands (6)" layer from 9 to 23 feet depth. Data is a poor fit for the points greater than the Bartlett limit of 0.13; coefficient of determination, $R,^2$ value is less than 0.9. Therefore, these results were not included in final analysis. 23
Figure B - 46: Estimation of the Scale of Fluctuation, θ = 0.6 feet, for Friction Ratio Data from Sounding C-37, "Clean sands to silty sands (6)" layer from 9 to 23 feet depth. 23
Figure B - 47: Estimation of the Scale of Fluctuation, θ = 0.5 feet, for Cone Tip Resistance Data from Sounding C-37, "Clean sands to silty sands (6)" layer from 34 to 41 feet depth. 24
Figure B - 48: Estimation of the Scale of Fluctuation, θ = 0.7 feet, for Friction Ratio Data from Sounding C-37, "Clean sands to silty sands (6)" layer from 34 to 41 feet depth. 24
Figure B - 49: Estimation of the Scale of Fluctuation, θ = 1.5 feet, for Cone Tip Resistance Data from Sounding C-39, "Clean sands to silty sands (6)" layer from 10 to 20 feet depth. 25
Figure B - 50: Estimation of the Scale of Fluctuation, θ, for Friction Ratio Data from Sounding C-39, "Clean sands to silty sands (6)" layer from 10 to 20 feet depth. Data is limited to only 1 point greater than the Bartlett limit of 0.16; therefore, θ could not be estimated, and these results were not included in final analysis. 25
Figure B - 51: Estimation of the Scale of Fluctuation, θ = 1.0 feet, for Cone Tip Resistance Data from Sounding C-39, "Clean sands to silty sands (6)" layer from 21 to 27 feet depth. 26
Figure B - 52: Estimation of the Scale of Fluctuation, θ = 0.9 feet, for Friction Ratio Data from Sounding C-39, "Clean sands to silty sands (6)" layer from 21 to 27 feet depth. 26
Figure B - 53: Estimation of the Scale of Fluctuation, θ = 0.35 feet, for Cone Tip Resistance Data from Sounding C-39, "Clean sands to silty sands (6)" layer from 32 to 41 feet depth. 27

Figure B - 54: Estimation of the Scale of Fluctuation, θ = 0.7 feet, for Friction Ratio Data from Sounding C-39, "Clean sands to silty sands (6)" layer from 32 to 41 feet depth. 27
Figure B - 55: Estimation of the Scale of Fluctuation, θ = 1.0 feet, for Cone Tip Resistance Data from Sounding C-41, "Clean sands to silty sands (6)" layer from 16 to 31 feet depth. 28
Figure B - 56: Estimation of the Scale of Fluctuation, θ = 1.9 feet, for Friction Ratio Data from Sounding C-41, "Clean sands to silty sands (6)" layer from 16 to 31 feet depth. 28
Figure B - 57: Estimation of the Scale of Fluctuation, θ = 2.0 feet, for Cone Tip Resistance Data from Sounding C-44, "Clean sands to silty sands (6)" layer from 7 to 27 feet depth. 29
Figure B - 59: Estimation of the Scale of Fluctuation, θ = 1.5 feet, for Cone Tip Resistance Data from Sounding C-46, "Clean sands to silty sands (6)" layer from 10 to 27 feet depth. 30
Figure B - 60: Estimation of the Scale of Fluctuation, θ = 0.13 feet, for Friction Ratio Data from Sounding C-46, "Clean sands to silty sands (6)" layer from 10 to 27 feet depth. Data is a poor fit for the points greater than the Bartlett limit of 0.12; coefficient of determination, R^2 value is less 0.9. Therefore, these results were not included in final analysis. 30
Figure B - 61: Estimation of the Scale of Fluctuation, θ = 1.2 feet, for Cone Tip Resistance Data from Sounding C-46, "Clean sands to silty sands (6)" layer from 32 to 42 feet depth. 31
Figure B - 62: Estimation of the Scale of Fluctuation, θ = 0.7 feet, for Friction Ratio Data from Sounding C-46, "Clean sands to silty sands (6)" layer from 32 to 42 feet depth. 31
Figure B - 63: Estimation of the Scale of Fluctuation, θ = 1.8 feet, for Cone Tip Resistance Data from Sounding C-46a, "Clean sands to silty sands (6)" layer from 10 to 27 feet depth. 32
Figure B - 64: Estimation of the Scale of Fluctuation, θ = 0.9 feet, for Friction Ratio Data from Sounding C-46a, "Clean sands to silty sands (6)" layer from 10 to 27 feet depth. 32
Figure B - 65: Estimation of the Scale of Fluctuation, θ = 1.1 feet, for Cone Tip Resistance Data from Sounding C-46a, "Gravelly sand to sand (7)" layer from 29 to 33 feet depth. 33
Figure B - 66: Estimation of the Scale of Fluctuation, θ = 0.5 feet, for Friction Ratio Data from Sounding C-46a, " Gravelly sand to sand (7)" layer from 29 to 33 feet depth. 33
Figure B - 67: Estimation of the Scale of Fluctuation, θ = 1.9 feet, for Cone Tip Resistance Data from Sounding C-46a, "Clean sands to silty sands (6)" layer from 32 to 42 feet depth. 34
Figure B - 68: Estimation of the Scale of Fluctuation, θ = 0.2 feet, for Friction Ratio Data from Sounding C-46a, "Clean sands to silty sands (6)" layer from 32 to 42 feet depth. 34
Figure B - 69: Estimation of the Scale of Fluctuation, θ = 1.5 feet, for Cone Tip Resistance Data from Sounding C-48, "Clean sands to silty sands (6)" layer from 17 to 35 feet depth. 35
Figure B - 70: Estimation of the Scale of Fluctuation, θ = 0.13 feet, for Friction Ratio Data from Sounding C-48, "Clean sands to silty sands (6)" layer from 17 to 35 feet depth. Data is a poor fit for the points greater than the Bartlett limit of 0.12; coefficient of determination, R^2 value is less 0.9. Therefore, these results were not included in final analysis. 35
Figure B - 71: Estimation of the Scale of Fluctuation, θ = 1.6 feet, for Cone Tip Resistance Data from Sounding C-50, "Clean sands to silty sands (6)" layer from 6 to 13 feet depth. 36
Figure B - 72: Estimation of the Scale of Fluctuation, θ = 0.6 feet, for Friction Ratio Data from Sounding C-50, "Clean sands to silty sands (6)" layer from 6 to 13 feet depth. 36
Figure B - 73: Estimation of the Scale of Fluctuation, θ = 1.6 feet, for Cone Tip Resistance Data from Sounding C-50, "Clean sands to silty sands (6)" layer from 31 to 40 feet depth. 37

Figure B - 74: Estimation of the Scale of Fluctuation, θ = 1.2 feet, for Friction Ratio Data from Sounding C-50, "Clean sands to silty sands (6)" layer from 31 to 40 feet depth. 37
Figure B - 75: Estimation of the Scale of Fluctuation, θ = 0.59 feet, for Cone Tip Resistance Data from Sounding C-60, "Clays; Clay to silty clay (3)" layer from 2 to 6 feet depth. 38
Figure B - 76: Estimation of the Scale of Fluctuation, θ, for Friction Ratio Data from Sounding C-60, "Clays; clay to silty clay (3)" layer from 2 to 6 feet depth. Data is limited to only 1 point greater than the Bartlett limit of 0.25; therefore, θ could not be estimated, and these results were not included in final analysis. 38
Figure B - 77: Estimation of the Scale of Fluctuation, θ = 3.1 feet, for Cone Tip Resistance Data from Sounding C-60, "Clean sands to silty sands (6)" layer from 9 to 29 feet depth. 39
Figure B - 78: Estimation of the Scale of Fluctuation, θ, for Cone Tip Resistance Data from Sounding C-60, "Clean sands to silty sands (6)" layer from 9 to 29 feet depth. Data is a poor fit for the points greater than the Bartlett limit of 0.12; coefficient of determination, R^2 value is less 0.9. Therefore, these results were not included in final analysis. 39
Figure B - 79: Estimation of the Scale of Fluctuation, θ = 1.4 feet, for Cone Tip Resistance Data from Sounding C-62, "Gravelly sand to sand (7)" layer from 17 to 21 feet depth. 40
Figure B - 80: Estimation of the Scale of Fluctuation, θ = 0.7 feet, for Friction Ratio Data from Sounding C-62, "Gravelly sand to sand (7)" layer from 17 to 21 feet depth. 40
Figure B - 81: Estimation of the Scale of Fluctuation, θ = 0.9 feet, for Cone Tip Resistance Data from Sounding C-62, "Clean sands to silty sands (6)" layer from 17 to 21 feet depth. 41
Figure B - 82: Estimation of the Scale of Fluctuation, θ = 0.5 feet, for Friction Ratio Data from Sounding C-62, "Clean sands to silty sands (6)" layer from 17 to 21 feet depth. 41
Figure B - 83: Estimation of the Scale of Fluctuation, θ = 0.24 feet, for Cone Tip Resistance Data from Sounding C-64, "Clean sands to silty sands (6)" layer from 10 to 14 feet depth. 42
Figure B - 84: Estimation of the Scale of Fluctuation, θ, for Friction Ratio Data from Sounding C-64, "Clean sands to silty sands (6)" layer from 10 to 14 feet depth. Data is limited to only 1 point greater than the Bartlett limit of 0.24; therefore, θ could not be estimated, and these results were not included in final analysis. 42
Figure B - 85: Estimation of the Scale of Fluctuation, θ = 1.1 feet, for Cone Tip Resistance Data from Sounding C-64, "Clean sands to silty sands (6)" layer from 18 to 24 feet depth. 43
Figure B - 86: Estimation of the Scale of Fluctuation, θ = 0.8 feet, for Friction Ratio Data from Sounding C-64, "Clean sands to silty sands (6)" layer from 18 to 24 feet depth. Data is a poor fit for the points greater than the Bartlett limit of 0.10; coefficient of determination, R^2, value is less 0.9. Therefore, these results were not included in final analysis. 43
Figure B - 87: Estimation of the Scale of Fluctuation, θ = 0.9 feet, for Cone Tip Resistance Data from Sounding C-64, "Gravelly sand to sand (7)" layer from 24 to 31 feet depth. 44
Figure B - 88: Estimation of the Scale of Fluctuation, θ = 0.5 feet, for Friction Ratio Data from Sounding C-64, "Gravelly sand to sand (7)" layer from 24 to 31 feet depth. 44
Figure B - 89: Estimation of the Scale of Fluctuation, θ = 0.7 feet, for Cone Tip Resistance Data from Sounding C-64, "Clean sands to silty sands (6)" layer from 31 to 35 feet depth. 45
Figure B - 90: Estimation of the Scale of Fluctuation, θ = 0.8 feet, for Friction Ratio Data from Sounding C-64, "Clean sands to silty sands (6)" layer from 31 to 35 feet depth. 45

Figure B - 91: Estimation of the Scale of Fluctuation, θ = 1.4 feet, for Cone Tip Resistance Data from Sounding C-66, "Clean sands to silty sands (6)" layer from 14 to 19 feet depth. 46
Figure B - 92: Estimation of the Scale of Fluctuation, θ = 0.7 feet, for Friction Ratio Data from Sounding C-66, "Clean sands to silty sands (6)" layer from 14 to 19 feet depth. 46
Figure B - 93: Estimation of the Scale of Fluctuation, θ = 1.4 feet, for the Cone Tip Resistance Data from Sounding C-66a, "Clean sands to silty sands (6)" layer from 0.4 to 5 feet depth. 47
Figure B - 94: Estimation of the Scale of Fluctuation, θ = 1.5 feet, for Friction Ratio Data from Sounding C-66a, "Clean sands to silty sands (6)" layer from 0.4 to 5 feet depth. 47
Figure B - 95: Estimation of the Scale of Fluctuation, θ = 0.6 feet, for the Cone Tip Resistance Data from Sounding C-66a, "Clean sands to silty sands (6)" layer from 14 to 19 feet depth. 48
Figure B - 96: Estimation of the Scale of Fluctuation, θ = 0.5 feet, for Friction Ratio Data from Sounding C-66a, "Clean sands to silty sands (6)" layer from 14 to 19 feet depth. 48
Figure B - 97: Estimation of the Scale of Fluctuation, θ = 0.9 feet, for Cone Tip Resistance Data from Sounding C-66a, "Clean sands to silty sands (6)" layer from 26 to 33 feet depth. 49
Figure B - 98: Estimation of the Scale of Fluctuation, θ, for Friction Ratio Data from Sounding C-66a, "Clean sands to silty sands (6)" layer from 26 to 33 feet depth 49
Figure B - 99: Estimation of the Scale of Fluctuation, θ = 1.1 feet, for Cone Tip Resistance Data from Sounding C-68, "Gravelly sand to sand (7)" layer from 14 to 19 feet depth. Data is a poor fit for the points greater than the Bartlett limit of 0.22; coefficient of determination, R^2 value is less 0.9. Therefore, these results were not included in final analysis. 50
Figure B - 100: Estimation of the Scale of Fluctuation, θ = 0.5 feet, for Friction Ratio Data from Sounding C-68, "Gravelly sand to sand (7)" layer from 14 to 19 feet depth. 50
Figure B - 101: Estimation of the Scale of Fluctuation, θ = 0.7 feet, for Cone Tip Resistance Data from Sounding C-68, "Clean sands to silty sands (6)" layer from 22 to 287 feet depth. 51
Figure B - 102: Estimation of the Scale of Fluctuation, θ = 0.9 feet, for Friction Ratio Data from Sounding C-68, "Clean sands to silty sands (6)" layer from 22 to 28 feet depth. 51
Figure B - 103: Estimation of the Scale of Fluctuation, θ = 1.3 feet, for Cone Tip Resistance Data from Sounding C-68, "Clean sands to silty sands (6)" layer from 31 to 35 feet depth. 52
Figure B - 104: Estimation of the Scale of Fluctuation, θ = 0.7 feet, for Friction Ratio Data from Sounding C-68, "Clean sands to silty sands (6)" layer from 31 to 35 feet depth. 52
Figure B - 105: Estimation of the Scale of Fluctuation, θ = 1.7 feet, for Cone Tip Resistance Data from Sounding C-70, "Clean sands to silty sands (6)" layer from 7 to 14 feet depth. 53
Figure B - 106: Estimation of the Scale of Fluctuation, θ = 0.5 feet, for Friction Ratio Data from Sounding C-70, "Clean sands to silty sands (6)" layer from 7 to 14 feet depth. 53
Figure B - 107: Estimation of the Scale of Fluctuation, θ = 1.1 feet, for Cone Tip Resistance Data from Sounding C-70, "Clean sands to silty sands (6)" layer from 18 to 32 feet depth. 54
Figure B - 108: Estimation of the Scale of Fluctuation, θ = 0.3 feet, for Friction Ratio Data from Sounding C-70, "Clean sands to silty sands (6)" layer from 18 to 32 feet depth sis. 54
Figure B - 109: Estimation of the Scale of Fluctuation, θ = 0.7 feet, for Cone Tip Resistance Data from Sounding C-74, "Clays; clay to silty clay (3)" layer from 5 to 10 feet depth. 55
Figure B - 110: θ = 0.4 feet, for Friction Ratio Data from Sounding C-74, "Clays; clay to silty clay (3)" layer from 5 to 10 feet depth. Data is a poor fit for the points greater than the Bartlett limit of 0.23;

coefficient of determination, R^2 value is less 0.9. Therefore, these results were not included in final analysis 55
Figure B - 111: Estimation of the Scale of Fluctuation, θ = 1.8 feet, for Cone Tip Resistance Data from Sounding C-74, "Clean sands to silty sands (6)" layer from 14 to 35 feet depth. 56
Figure B - 112: Estimation of the Scale of Fluctuation, θ = 0.5 feet, for Friction Ratio Data from Sounding C-74, "Clean sands to silty sands (6)" layer from 14 to 35 feet depth. 56
Figure B - 113: Estimation of the Scale of Fluctuation, θ = 0.9 feet, for Cone Tip Resistance Data from Sounding C-76, "Clean sands to silty sands (6)" layer from 15 to 21 feet depth. 57
Figure B - 114: Estimation of the Scale of Fluctuation, θ = 0.6 feet, for Friction Ratio Data from Sounding C-76, "Clean sands to silty sands (6)" layer from 15 to 21 feet depth. 57
Figure B - 115: Estimation of the Scale of Fluctuation, θ = 1.8 feet, for Cone Tip Resistance Data from Sounding C-76, "Clean sands to silty sands (6)" layer from 22 to 35 feet depth. 58
Figure B - 116: Estimation of the Scale of Fluctuation, θ = 0.9 feet, for Friction Ratio Data from Sounding C-76, "Clean sands to silty sands (6)" layer from 22 to 35 feet depth. 58
Figure B - 117: Estimation of the Scale of Fluctuation, θ = 0.7 feet, for Cone Tip Resistance Data from Sounding C-78, "Clean sands to silty sands (6)" layer from 18 to 23 feet depth. 59
Figure B - 118: Estimation of the Scale of Fluctuation, θ = 0.6 feet, for Friction Ratio Data from Sounding C-78, "Clean sands to silty sands (6)" layer from 18 to 23 feet depth. 59
Figure B - 119: Estimation of the Scale of Fluctuation, θ = 1.0 feet, for Cone Tip Resistance Data from Sounding C-78, "Clean sands to silty sands (6)" layer from 29 to 35 feet depth. 60
Figure B - 120: Estimation of the Scale of Fluctuation, θ = 0.6 feet, for Friction Ratio Data from Sounding C-78, "Clean sands to silty sands (6)" layer from 29 to 35 feet depth. Data is a poor fit for the points greater than the Bartlett limit of 0.20; coefficient of determination, R^2 value is less 0.9. Therefore, these results were not included in final analysis. 60
Figure B - 121: Estimation of the Scale of Fluctuation, θ = 1.2 feet, for Cone Tip Resistance Data from Sounding C-79, "Clean sands to silty sands (6)" layer from 6 to 11 feet depth. 61
Figure B - 122: Estimation of the Scale of Fluctuation, θ = 0.4 feet, for Friction Ratio Data from Sounding C-79, "Clean sands to silty sands (6)" layer from 6 to 11 feet depth. 61
Figure B - 123: Estimation of the Scale of Fluctuation, θ = 0.9 feet, for Cone Tip Resistance Data from Sounding C-79, "Clean sands to silty sands (6)" layer from 21 to 26 feet depth. 62
Figure B - 124: Estimation of the Scale of Fluctuation, θ = 0.7 feet, for Friction Ratio Data from Sounding C-79, "Clean sands to silty sands (6)" layer from 21 to 26 feet depth. 62
Figure B - 125: Estimation of the Scale of Fluctuation, θ = 0.6 feet, for Cone Tip Resistance Data from Sounding C-79, "Gravelly sand to sand (7)" layer from 31 to 34 feet depth. 63
Figure B - 126: Estimation of the Scale of Fluctuation, θ = 0.5 feet, for Friction Ratio Data from Sounding C-79, "Gravelly sand to sand (7)" layer from 31 to 34 feet depth. 63
Figure B - 127: Estimation of the Scale of Fluctuation, θ = 0.9 feet, for Cone Tip Resistance Data from Sounding C-80, "Clean sands to silty sands (6)" layer from 29 to 35 feet depth. 64
Figure B - 128: Estimation of the Scale of Fluctuation, θ = 0.7 feet, for Friction Ratio Data from Sounding C-80, "Clean sands to silty sands (6)" layer from 29 to 35 feet depth. 64
Figure B - 129: Estimation of the Scale of Fluctuation, θ = 1.2 feet, for Cone Tip Resistance Data from Sounding C-81, " Clean sands to silty sands (6)" layer from 13 to 23 feet depth. 65

Figure B - 130: Estimation of the Scale of Fluctuation, θ, for Friction Ratio Data from Sounding C-81, " Clean sands to silty sands (6)" layer from 13 to 23 feet depth. Data is limited to only 1 point greater than the Bartlett limit of 0.16; therefore, θ could not be estimated, and these results were not included in final analysis. 65
Figure B - 131: Estimation of the Scale of Fluctuation, θ = 1.5 feet, for Cone Tip Resistance Data from Sounding C-82, "Clean sands to silty sands (6)" layer from 29 to 36 feet depth. 66
Figure B - 132: Estimation of the Scale of Fluctuation, θ = 0.4 feet, for Friction Ratio Data from Sounding C-82, "Clean sands to silty sands (6)" layer from 29 to 36 feet depth. 66
Figure B - 133: Estimation of the Scale of Fluctuation, θ = 0.7 feet, for Cone Tip Resistance Data from Sounding C-84, "Clays; clay to silty clay (3)" layer from 1 to 6 feet depth. 67
Figure B - 134: Estimation of the Scale of Fluctuation, θ = 0.6 feet, for Friction Ratio Data from Sounding C-84, "Clays; clay to silty clay (3)" layer from 1 to 6 feet depth. 67
Figure B - 135: Estimation of the Scale of Fluctuation, θ = 2.4 feet, for Cone Tip Resistance Data from Sounding C-84, "Clean sands to silty sands (6)" layer from 6 to 13 feet depth. 68
Figure B - 136: Estimation of the Scale of Fluctuation, θ = 0.9 feet, for Friction Ratio Data from Sounding C-84, "Clean sands to silty sands (6)" layer from 6 to 13 feet depth. 68
Figure B - 137: Estimation of the Scale of Fluctuation, θ = 1.4 feet, for Cone Tip Resistance Data from Sounding C-84, "Clean sands to silty sands (6)" layer from 17 to 26 feet depth. 69
Figure B - 138: Estimation of the Scale of Fluctuation, θ, for Friction Ratio Data from Sounding C-84, "Clean sands to silty sands (6)" layer from 17 to 26 feet depth. Data is limited to only 1 point greater than the Bartlett limit of 0.17; therefore, θ could not be estimated, and these results were not included in final analysis. 69
Figure B - 139: Estimation of the Scale of Fluctuation, θ = 0.9 feet, for Cone Tip Resistance Data from Sounding C-86, "Clean sands to silty sands (6)" layer from 5 to 13 feet depth. 70
Figure B - 140: Estimation of the Scale of Fluctuation, θ = 1.0 feet, for Friction Ratio Data from Sounding C-86, "Clean sands to silty sands (6)" layer from 5 to 13 feet depth. 70
Figure B - 141: Estimation of the Scale of Fluctuation, θ = 0.8 feet, for Cone Tip Resistance Data from Sounding C-86, "Clean sands to silty sands (6)" layer from 14 to 19 feet depth. 71
Figure B - 142: Estimation of the Scale of Fluctuation, θ = 1.0 feet, for Friction Ratio Data from Sounding C-86, "Clean sands to silty sands (6)" layer from 14 to 19 feet depth. 71
Figure B - 143: Estimation of the Scale of Fluctuation, θ = 1.2 feet, for Cone Tip Resistance Data from Sounding C-86, "Clean sands to silty sands (6)" layer from 20 to 36 feet depth. 72
Figure B - 144: Estimation of the Scale of Fluctuation, θ = 0.5 feet, for Friction Ratio Data from Sounding C-86, "Clean sands to silty sands (6)" layer from 20 to 36 feet depth. 72
Figure B - 145: Estimation of the Scale of Fluctuation, θ = 0.4 feet, for Friction Ratio Data from Sounding C-89, "Clays; clay to silty clay (3)" layer from 2 to 8 feet depth. 73
Figure B - 146: Estimation of the Scale of Fluctuation, θ = 0.5 feet, for Friction Ratio Data from Sounding C-89, "Clays; clay to silty clay (3)" layer from 2 to 8 feet depth. 73
Figure B - 147: Estimation of the Scale of Fluctuation, θ = 0.8 feet, for Cone Tip Resistance Data from Sounding C-89, "Clean sands to silty sands (6)" layer from 8 to 18 feet depth. 74
Figure B - 148: Estimation of the Scale of Fluctuation, θ = 0.5 feet, for Friction Ratio Data from Sounding C-89, "Clean sands to silty sands (6)" layer from 8 to 18 feet depth. 74

Figure B - 149: Estimation of the Scale of Fluctuation, θ = 1.6 feet, for Cone Tip Resistance Data from Sounding C-89, "Clean sands to silty sands (6)" layer from 19 to 26 feet depth. 75
Figure B - 150: Estimation of the Scale of Fluctuation, θ = 0.8 feet, for Friction Ratio Data from Sounding C-89, "Clean sands to silty sands (6)" layer from 19 to 26 feet depth. 75
Figure B - 151: Estimation of the Scale of Fluctuation, θ = 1.7 feet, for Cone Tip Resistance Data from Sounding C-89, "Clean sands to silty sands (6)" layer from 29 to 35 feet depth. 76
Figure B - 152: Estimation of the Scale of Fluctuation, θ = 0.9 feet, for Friction Ratio Data from Sounding C-89, "Clean sands to silty sands (6)" layer from 29 to 35 feet depth. 76
Figure B - 153: Estimation of the Scale of Fluctuation, θ = 0.5 feet, for Cone Tip Resistance Data from Sounding C-91, "Silty sand to sandy silt (5)" layer from 5 to 9 feet depth. 77
Figure B - 154: Estimation of the Scale of Fluctuation, θ = 0.5 feet, for Friction Ratio Data from Sounding C-91, "Silty sand to sandy silt (5)" layer from 5 to 9 feet depth. 77
Figure B - 155: Estimation of the Scale of Fluctuation, θ = 0.6 feet, for Cone Tip Resistance Data from Sounding C-91, "Clean sands to silty sands (6)" layer from 15 to 20 feet depth. 78
Figure B - 156: Estimation of the Scale of Fluctuation, θ, for Friction Ratio Data from Sounding C-91, "Clean sands to silty sands (6)" layer from 15 to 20 feet depth. Data is limited to only 1 point greater than the Bartlett limit of 0.22; therefore, θ could not be estimated, and these results were not included in final analysis. 78
Figure B - 157: Estimation of the Scale of Fluctuation, θ = 2.2 feet, for Cone Tip Resistance Data from Sounding C-91, "Clean sands to silty sands (6)" layer from 24 to 36 feet depth. 79
Figure B - 158: Estimation of the Scale of Fluctuation, θ = 0.8 feet, for Friction Ratio Data from Sounding C-91, "Clean sands to silty sands (6)" layer from 24 to 36 feet depth. 79
Figure B - 159: Estimation of the Scale of Fluctuation, θ = 0.6 feet, for Cone Tip Resistance Data from Sounding C-92, "Clean sands to silty sands (6)" layer from 7 to 12 feet depth. 80
Figure B - 160: Estimation of the Scale of Fluctuation, θ = 0.4 feet, for Friction Ratio Data from Sounding C-92, "Clean sands to silty sands (6)" layer from 7 to 12 feet depth. 80
Figure B - 161: Estimation of the Scale of Fluctuation, θ = 1.8 feet, for Cone Tip Resistance Data from Sounding C-92, "Clean sands to silty sands (6)" layer from 19 to 23 feet depth. 81
Figure B - 162: Estimation of the Scale of Fluctuation, θ = 2.0 feet, for Friction Ratio Data from Sounding C-92, "Gravelly sand to sand (7)" layer from 19 to 23 feet depth. Data is a poor fit for the points greater than the Bartlett limit of 0.23; coefficient of determination, R^2 value is less 0.9. Therefore, these results were not included in final analysis. 81
Figure B - 163: Estimation of the Scale of Fluctuation, θ = 0.9 feet, for Cone Tip Resistance Data from Sounding C-94, "Clean sands to silty sands (6)" layer from 15 to 19 feet depth. 82
Figure B - 164: Estimation of the Scale of Fluctuation, θ = 0.4 feet, for Friction Ratio Data from Sounding C-94, "Clean sands to silty sands (6)" layer from 15 to 19 feet depth. 82
Figure B - 165: Estimation of the Scale of Fluctuation, θ = 1.0 feet, for Cone Tip Resistance Data from Sounding C-94, "Clean sands to silty sands (6)" layer from 28 to 35 feet depth. 83
Figure B - 166: Estimation of the Scale of Fluctuation, θ = 0.7 feet, for Friction Ratio Data from Sounding C-94, "Clean sands to silty sands (6)" layer from 28 to 35 feet depth. 83
Figure B - 167: Estimation of the Scale of Fluctuation, θ = 0.9 feet, for Cone Tip Resistance Data from Sounding C-96, "Clean sands to silty sands (6)" layer from 17 to 22 feet depth. 84

Figure B - 168: Estimation of the Scale of Fluctuation, θ = 0.3 feet, for Friction Ratio Data from Sounding C-96, "Clean sands to silty sands (6)" layer from 17 to 22 feet depth. 84
Figure B - 169: Estimation of the Scale of Fluctuation, θ = 1.4 feet, for Cone Tip Resistance Data from Sounding C-96, "Clean sands to silty sands (6)" layer from 24 to 28 feet depth. 85
Figure B - 170: Estimation of the Scale of Fluctuation, θ = 0.9 feet, for Friction Ratio Data from Sounding C-96, "Clean sands to silty sands (6)" layer from 24 to 28 feet depth. 85
Figure B - 171: Estimation of the Scale of Fluctuation, θ = 2.2 feet, for Cone Tip Resistance Data from Sounding C-96, "Gravelly sand to sand (7)" layer from 28 to 32 feet depth. 86
Figure B - 172: Estimation of the Scale of Fluctuation, θ = 0.8 feet, for Friction Ratio Data from Sounding C-96, "Gravelly sand to sand (7)" layer from 28 to 32 feet depth. 86
Figure B - 173: Estimation of the Scale of Fluctuation, θ = 2.1 feet, for Cone Tip Resistance Data from Sounding C-98, "Clean sands to silty sands (6)" layer from 25 to 31 feet depth. 87
Figure B - 174: Estimation of the Scale of Fluctuation, θ = 1.0 feet, for Friction Ratio Data from Sounding C-98, "Clean sands to silty sands (6)" layer from 25 to 31 feet depth. 87
Figure B - 175: Estimation of the Scale of Fluctuation, θ = 1.0 feet, for Cone Tip Resistance Data from Sounding C-100, "Clean sands to silty sands (6)" layer from 11 to 18 feet depth. 88
Figure B - 176: Estimation of the Scale of Fluctuation, θ = 1.0 feet, for Friction Ratio Data from Sounding C-100, "Clean sands to silty sands (6)" layer from 11 to 18 feet depth. 88
Figure B - 177: Estimation of the Scale of Fluctuation, θ = 2.0 feet, for Cone Tip Resistance Data from Sounding C-100, "Clean sands to silty sands (6)" layer from 20 to 32 feet depth. 89
Figure B - 179: Estimation of the Scale of Fluctuation, θ = 0.6 feet, for Friction Ratio Data from Sounding C-100, "Clean sands to silty sands (6)" layer from 20 to 32 feet depth. 89
Figure B - 179: Estimation of the Scale of Fluctuation, θ = 1.8 feet, for Cone Tip Resistance Data from Sounding C-103, "Clean sands to silty sands (6)" layer from 15 to 28 feet depth. 90
Figure B - 180: Estimation of the Scale of Fluctuation, θ = 0.9 feet, for Friction Ratio Data from Sounding C-103, "Clean sands to silty sands (6)" layer from 15 to 28 feet depth. 90
Figure B - 181: Estimation of the Scale of Fluctuation, θ = 1.1 feet, for Cone Tip Resistance Data from Sounding C-105, "Clean sands to silty sands (6)" layer from 26 to 32 feet depth. 91
Figure B - 182: Estimation of the Scale of Fluctuation, θ = 1.5 feet, for Friction Ratio Data from Sounding C-105, "Clean sands to silty sands (6)" layer from 26 to 32 feet depth. 91
Figure B - 183: Estimation of the Scale of Fluctuation, θ = 0.5 feet, for Cone Tip Resistance Data from Sounding C-106, "Clean sands to silty sands (6)" layer from 5 to 13 feet depth. 92
Figure B - 184: Estimation of the Scale of Fluctuation, θ = 0.5 feet, for Friction Ratio Data from Sounding C-106, "Clean sands to silty sands (6)" layer from 5 to 13 feet depth. 92
Figure B - 185: Estimation of the Scale of Fluctuation, θ = 2.4 feet, for Cone Tip Resistance Data from Sounding C-106, "Clean sands to silty sands (6)" layer from 14 to 28 feet depth. 93
Figure B - 186: Estimation of the Scale of Fluctuation, θ = 0.1 feet, for Friction Ratio Data from Sounding C-106, "Clean sands to silty sands (6)" layer from 14 to 28 feet depth. 93
Figure B - 187: Estimation of the Scale of Fluctuation, θ = 1.6 feet, for Cone Tip Resistance Data from Sounding C-107, "Silty sand to sandy silt (5)" layer from 2 to 7 feet depth. 94
Figure B - 188: Estimation of the Scale of Fluctuation, θ = 1.5 feet, for Friction Ratio Data from Sounding C-107, "Silty sand to sandy silt (5)" layer from 2 to 7 feet depth. 94

Figure B - 189: Estimation of the Scale of Fluctuation, θ = 0.8 feet, for Cone Tip Resistance Data from Sounding C-107, "Clean sands to silty sands (6)" layer from 7 to 12 feet depth. 95
Figure B - 190: Estimation of the Scale of Fluctuation, θ = 0.8 feet, for Friction Ratio Data from Sounding C-107, "Clean sands to silty sands (6)" layer from 7 to 12 feet depth. 95
Figure B - 191: Estimation of the Scale of Fluctuation, θ = 1.5 feet, for Cone Tip Resistance Data from Sounding C-107, "Clean sands to silty sands (6)" layer from 29 to 36 feet depth. 96
Figure B - 192: Estimation of the Scale of Fluctuation, θ = 0.4 feet, for Friction Ratio Data from Sounding C-107, "Clean sands to silty sands (6)" layer from 29 to 36 feet depth. 96
Figure B - 193: Estimation of the Scale of Fluctuation, θ = 0.3 feet, for Cone Tip Resistance Data from Sounding C-107a, "Clays; clay to silty clay (3)" layer from 2 to 7 feet depth. 97
Figure B - 194: Estimation of the Scale of Fluctuation, θ, for Friction Ratio Data from Sounding C-107a, "Clays; clay to silty clay (3)" layer from 2 to 7 feet depth. Data is limited to only 1 point greater than the Bartlett limit of 0.23; therefore, θ could not be estimated, and these results were not included in final analysis. 97
Figure B - 195: Estimation of the Scale of Fluctuation, θ = 0.9 feet, for Cone Tip Resistance Data from Sounding C-107a, "Clean sands to silty sands (6)" layer from 7 to 14 feet depth. 98
Figure B - 196: Estimation of the Scale of Fluctuation, θ, for Friction Ratio Data from Sounding C-107a, " Clean sands to silty sands (6)" layer from 7 to 14 feet depth. Data is limited to only 1 point greater than the Bartlett limit of 0.19; therefore, θ could not be estimated, and these results were not included in final analysis. 98
Figure B - 197: Estimation of the Scale of Fluctuation, θ = 1.7 feet, for Cone Tip Resistance Data from Sounding C-107a, "Clean sands to silty sands (6)" layer from 27 to 33 feet depth. 99
Figure B - 198: Estimation of the Scale of Fluctuation, θ, for Friction Ratio Data from Sounding C-107a, "Clean sands to silty sands (6)" layer from 27 to 33 feet depth. Data is limited to only 3 points greater than the Bartlett limit of 0.21; therefore, θ could not be estimated, and these results were not included in final analysis. 99
Figure B - 199: Estimation of the Scale of Fluctuation, θ = 0.9 feet, for Cone Tip Resistance Data from Sounding C-109, "Clean sands to silty sands (6)" layer from 26 to 36 feet depth. 100
Figure B - 200: Estimation of the Scale of Fluctuation, θ = 0.6 feet, for Friction Ratio Data from Sounding C-109, "Clean sands to silty sands (6)" layer from 26 to 36 feet depth. 100
Figure B - 201: Estimation of the Scale of Fluctuation, θ =0.9 feet, for Cone Tip Resistance Data from Sounding C-111, "Clean sands to silty sands (6)" layer from 23 to 27 feet depth. 101
Figure B - 202: Estimation of the Scale of Fluctuation, θ = 0.6 feet, for Friction Ratio Data from Sounding C-111, "Clean sands to silty sands (6)" layer from 23 to 27 feet depth. 101
Figure B - 203: Estimation of the Scale of Fluctuation, θ = 0.8 feet, for Cone Tip Resistance Data from Sounding C-113, "Clean sands to silty sands (6)" layer from 15 to 20 feet depth. 102
Figure B - 204: Estimation of the Scale of Fluctuation, θ = 0.8 feet, for Friction Ratio Data from Sounding C-113, "Clean sands to silty sands (6)" layer from 15 to 20 feet depth. 102
Figure B - 205: Estimation of the Scale of Fluctuation, θ = 0.7 feet, for Cone Tip Resistance Data from Sounding C-113, "Gravelly sand to sand (7)" layer from 20 to 25 feet depth. 103
Figure B - 206: Estimation of the Scale of Fluctuation, θ, for Friction Ratio Data from Sounding C-113, "Gravelly sand to sand (7)" layer from 20 to 25 feet depth. Data is limited to only 1 point greater than

the Bartlett limit of 0.24; therefore, θ could not be estimated, and these results were not included in final analysis. 103
Figure B - 207: Estimation of the Scale of Fluctuation, θ = 1.1 feet, for Cone Tip Resistance Data from Sounding C-113, "Clean sands to silty sands (6)" layer from 25 to 36 feet depth. 104
Figure B - 208: Estimation of the Scale of Fluctuation, θ = 0.5 feet, for Friction Ratio Data from Sounding C-113, "Clean sands to silty sands (6)" layer from 25 to 36 feet depth. 104
Figure B - 209: Estimation of the Scale of Fluctuation, θ = 1.6 feet, for Cone Tip Resistance Data from Sounding C-117, "Clean sands to silty sands (6)" layer from 12 to 21 feet depth. 105
Figure B - 210: Estimation of the Scale of Fluctuation, θ = 1.4 feet, for Friction Ratio Data from Sounding C-117, "Clean sands to silty sands (6)" layer from 12 to 21 feet depth. 105
Figure B - 211: Estimation of the Scale of Fluctuation, θ = 1.2 feet, for Cone Tip Resistance Data from Sounding C-117, "Gravelly sand to sand (7)" layer from 21 to 25 feet depth. 106
Figure B - 212: Estimation of the Scale of Fluctuation, θ = 0.6 feet, for Friction Ratio Data from Sounding C-117, "Gravelly sand to sand (7)" layer from 21 to 25 feet depth. 106
Figure B - 213: Estimation of the Scale of Fluctuation, θ = 2.3 feet, for Cone Tip Resistance Data from Sounding C-117, "Clean sands to silty sands (6)" layer from 29 to 35 feet depth. 107
Figure B - 214: Estimation of the Scale of Fluctuation, θ = 10.8 feet, for Friction Ratio Data from Sounding C-117, "Clean sands to silty sands (6)" layer from 29 to 35 feet depth. Data is a poor fit for the points greater than the Bartlett limit of 0.20; coefficient of determination, R^2 value is less 0.9. Therefore, these results were not included in final analysis 107
Figure B - 215: Estimation of the Scale of Fluctuation, θ = 1.9 feet, for Cone Tip Resistance Data from Sounding C-119, "Gravelly sand to sand (7)" layer from 16 to 27 feet depth. 108
Figure B - 216: Estimation of the Scale of Fluctuation, θ = 1.1 feet, for Friction Ratio Data from Sounding C-119, "Gravelly sand to sand (7)" layer from 16 to 27 feet depth. 108
Figure B - 217: Estimation of the Scale of Fluctuation, θ = 2.3 feet, for Cone Tip Resistance Data from Sounding C-121, "Clean sands to silty sands (6)" layer from 9 to 13 feet depth. 109
Figure B - 218: Estimation of the Scale of Fluctuation, θ, for Friction Ratio Data from Sounding C-121, "Clean sands to silty sands (6)" layer from 9 to 13 feet depth. Data is limited to only 2 points greater than the Bartlett limit of 0.23; therefore, θ could not be estimated, and these results were not included in final analysis. 109
Figure B - 219: Estimation of the Scale of Fluctuation, θ = 1.2 feet, for Cone Tip Resistance Data from Sounding C-121, "Gravelly sand to sand (7)" layer from 13 to 21 feet depth. 110
Figure B - 220: Estimation of the Scale of Fluctuation, θ, for Friction Ratio Data from Sounding C-121, "Clean sands to silty sands (6)" layer from 13 to 21 feet depth. Data is limited to only 1 point greater than the Bartlett limit of 0.18; therefore, θ could not be estimated, and these results were not included in final analysis. 110
Figure B - 221: Estimation of the Scale of Fluctuation, θ = 1.0 feet, for Cone Tip Resistance Data from Sounding C-121, "Clean sands to silty sands (6)" layer from 24 to 23 feet depth. 111
Figure B - 222: Estimation of the Scale of Fluctuation, θ = 0.5 feet, for Friction Ratio Data from Sounding C-121, "Clean sands to silty sands (6)" layer from 24 to 33 feet depth. 111
Figure B - 223: Estimation of the Scale of Fluctuation, θ = 2.6 feet, for Cone Tip Resistance Data from Sounding C-123, "Gravelly sand to sand (7)" layer from 11 to 15 feet depth. 112

Figure B - 224: Estimation of the Scale of Fluctuation, θ = 1.4 feet, for Friction Ratio Data from Sounding C-123, “Gravelly sand to sand (7)" layer from 11 to 15 feet depth. 112
Figure B - 225: Estimation of the Scale of Fluctuation, θ = 1.5 feet, for Cone Tip Resistance Data from Sounding C-123, "Clean sands to silty sands (6)" layer from 15 to 23 feet depth. 113
Figure B - 226: Estimation of the Scale of Fluctuation, θ = 0.8 feet, for Friction Ratio Data from Sounding C-123, "Clean sands to silty sands (6)" layer from 15 to 23 feet depth. Data is a poor fit for the points greater than the Bartlett limit of 0.19; coefficient of determination, R^2, value is less 0.9. Therefore, these results were not included in final analysis. 113
Figure B - 227: Estimation of the Scale of Fluctuation, θ = 1.1 feet, for Cone Tip Resistance Data from Sounding C-123, "Gravelly sand to sand (7)" layer from 23 to 27 feet depth. Data is a poor fit for the points greater than the Bartlett limit of 0.24; coefficient of determination, R^2, value is less 0.9. Therefore, these results were not included in final analysis. 114
Figure B - 228: Estimation of the Scale of Fluctuation, θ, for Friction Ratio Data from Sounding C-123, "Gravelly sand to sand (7)" layer from 23 to 27 feet depth. Data is limited to only 1 point greater than the Bartlett limit of 0.24; therefore, θ could not be estimated, and these results were not included in final analysis. 114
Figure B - 229: Estimation of the Scale of Fluctuation, θ = 1.5 feet, for Cone Tip Resistance Data from Sounding C-123, "Clean sands to silty sands (6)" layer from 27 to 35 feet depth. 115
Figure B - 230: Estimation of the Scale of Fluctuation, θ = 0.4 feet, for Friction Ratio Data from Sounding C-123, "Clean sands to silty sands (6)" layer from 27 to 35 feet depth. 115
Figure B - 231: Estimation of the Scale of Fluctuation, θ = 1.4 feet, for Cone Tip Resistance Data from Sounding C-125, "Gravelly sand to sand (7)" layer from 20 to 26 feet depth. 116
Figure B - 232: Estimation of the Scale of Fluctuation, θ = 1.1 feet, for Friction Ratio Data from Sounding C-125, "Gravelly sand to sand (7)" layer from 20 to 26 feet depth. 116
Figure B - 233: Estimation of the Scale of Fluctuation, θ = 1.9 feet, for Cone Tip Resistance Data from Sounding C-129, "Clays; clay to silty clay (3)" layer from 2 to 11 feet depth. Data is a poor fit for the points greater than the Bartlett limit of 0.17; coefficient of determination, R^2, value is less 0.9. Therefore, these results were not included in final analysis. 117
Figure B - 234: Estimation of the Scale of Fluctuation, θ = 0.5 feet, for Friction Ratio Data from Sounding C-129, "Clays; clay to silty clay (3)" layer from 2 to 11 feet depth. Data is a poor fit for the points greater than the Bartlett limit of 0.17; coefficient of determination, R^2, value is less 0.9. Therefore, these results were not included in final analysis 117
Figure B - 235: Estimation of the Scale of Fluctuation, θ = 1.2 feet, for Cone Tip Resistance Data from Sounding C-129, "Gravelly sand to sand (7)" layer from 18 to 25 feet depth. 118
Figure B - 236: Estimation of the Scale of Fluctuation, θ = 1.2 feet, for Friction Ratio Data from Sounding C-129, "Gravelly sand to sand (7)" layer from 18 to 25 feet depth. 118
Figure B - 237: Estimation of the Scale of Fluctuation, θ = 0.8 feet, for Cone Tip Resistance Data from Sounding C-129, "Clean sands to silty sands (6)" layer from 25 to 31 feet depth. 119
Figure B - 238: Estimation of the Scale of Fluctuation, θ = 1.2 feet, for Friction Ratio Data from Sounding C-129, "Clean sands to silty sands (6)" layer from 25 to 31 feet depth. 119
Figure B - 239: Estimation of the Scale of Fluctuation, θ = 1.3 feet, for Cone Tip Resistance Data from Sounding C-131, "Clean sands to silty sands (6)" layer from 14 to 21 feet depth. 120

Figure B - 240: Estimation of the Scale of Fluctuation, θ, for Friction Ratio Data from Sounding C-131, " Clean sands to silty sands (6)" layer from 14 to 21 feet depth. Data is limited to only 1 point greater than the Bartlett limit of 0.19; therefore, θ could not be estimated, and these results were not included in final analysis. 120
Figure B - 241: Estimation of the Scale of Fluctuation, θ = 1.6 feet, for Cone Tip Resistance Data from Sounding C-131, "Clean sands to silty sands (6)" layer from 22 to 35 feet depth. 121
Figure B - 242: Estimation of the Scale of Fluctuation, θ = 1.2 feet, for Friction Ratio Data from Sounding C-131, "Clean sands to silty sands (6)" layer from 22 to 35 feet depth. Data is a poor fit for the points greater than the Bartlett limit of 0.14; coefficient of determination, R^2 value is less 0.9. Therefore, these results were not included in final analysis. 121
Figure B - 243: Estimation of the Scale of Fluctuation, θ = 1.0 feet, for Friction Ratio Data from Sounding C-133, "Clean sands to silty sands (6)" layer from 7 to 11 feet depth. 122
Figure B - 244: Estimation of the Scale of Fluctuation, θ = 0.2 feet, for Friction Ratio Data from Sounding C-133, "Clean sands to silty sands (6)" layer from 7 to 11 feet depth. 122
Figure B - 245: Estimation of the Scale of Fluctuation, θ = 1.3 feet, for Cone Tip Resistance Data from Sounding C-133, "Clean sands to silty sands (6)" layer from 17 to 30 feet depth. 123
Figure B - 246: Estimation of the Scale of Fluctuation, θ, for Friction Ratio Data from Sounding C-133, " Clean sands to silty sands (6)" layer from 17 to 30 feet depth. Data is limited to only 3 points greater than the Bartlett limit of 0.14; therefore, θ could not be estimated, and these results were not included in final analysis. 123
Figure B - 247: Estimation of the Scale of Fluctuation, θ = 2.5 feet, for Cone Tip Resistance Data from Sounding C-133, "Gravelly sand to sand (7)" layer from 30 to 35 feet depth. 124
Figure B - 248: Estimation of the Scale of Fluctuation, θ = 1.5 feet, for Friction Ratio Data from Sounding C-133, "Gravelly sand to sand (7)" layer from 30 to 35 feet depth. 124
Figure B - 249: Estimation of the Scale of Fluctuation, θ = 1.9 feet, for Cone Tip Resistance Data from Sounding C-135a, "Gravelly sand to sand (7)" layer from 16 to 22 feet depth. 125
Figure B - 250: Estimation of the Scale of Fluctuation, θ = 1.1 feet, for Friction Ratio Data from Sounding C-135a, "Gravelly sand to sand (7)" layer from 16 to 22 feet depth. 125
Figure B - 251: Estimation of the Scale of Fluctuation, θ = 1.2 feet, for Cone Tip Resistance Data from Sounding C-135a, "Clean sands to silty sands (6)" layer from 26 to 32 feet depth. 126
Figure B - 252: Estimation of the Scale of Fluctuation, θ = 0.7 feet, for Friction Ratio Data from Sounding C-135a, "Clean sands to silty sands (6)" layer from 26 to 32 feet depth. 126
Figure B - 253: Estimation of the Scale of Fluctuation, θ = 1.4 feet, for Cone Tip Resistance Data from Sounding C-137, "Clean sands to silty sands (6)" layer from 26 to 30 feet depth. 127
Figure B - 254: Estimation of the Scale of Fluctuation, θ = 0.8 feet, for Friction Ratio Data from Sounding C-137, "Clean sands to silty sands (6)" layer from 26 to 30 feet depth. 127
Figure B - 255: Estimation of the Scale of Fluctuation, θ = 2.0 feet, for Cone Tip Resistance Data from Sounding C-139, "Gravelly sand to sand (7)" layer from 16 to 22 feet depth. 128
Figure B - 256: Estimation of the Scale of Fluctuation, θ = 1.1 feet, for Cone Tip Resistance Data from Sounding C-139, "Gravelly sand to sand (7)" layer from 16 to 22 feet depth analysis 128
Figure B - 257: Estimation of the Scale of Fluctuation, θ = 0.5 feet, for Cone Tip Resistance Data from Sounding C-139, "Clays; clay to silty clay (3)" layer from 9 to 14 feet depth. 129

Figure B - 258: Estimation of the Scale of Fluctuation, θ = 0.5 feet, for Friction Ratio Data from Sounding C-139, "Clays; clay to silty clay (3)" layer from 9 to 14 feet depth. 129
Figure B - 259: Estimation of the Scale of Fluctuation, θ = 3.5 feet, for Cone Tip Resistance Data from Sounding C-139a, "Gravelly sand to sand (7)" layer from 17 to 28 feet depth. 130
Figure B - 260: Estimation of the Scale of Fluctuation, θ = 0.6 feet, for Friction Ratio Data from Sounding C-139a, "Gravelly sand to sand (7)" layer from 17 to 28 feet depth. 130
Figure B - 261: Estimation of the Scale of Fluctuation, θ = 1.2 feet, for Cone Tip Resistance Data from Sounding C-143, "Clean sands to silty sands (6)" layer from 8 to 13 feet depth. 131
Figure B - 262: Estimation of the Scale of Fluctuation, θ = 1.0 feet, for Friction Ratio Data from Sounding C-143, "Clean sands to silty sands (6)" layer from 8 to 13 feet depth. Data is a poor fit for the points greater than the Bartlett limit of 0.23; coefficient of determination, R^2 value is less 0.9. Therefore, these results were not included in final analysis. 131
Figure B - 263: Estimation of the Scale of Fluctuation, θ = 1.6 feet, for Cone Tip Resistance Data from Sounding C-143, "Clean sands to silty sands (6)" layer from 13 to 24 feet depth. 132
Figure B - 264: Estimation of the Scale of Fluctuation, θ = 0.9 feet, for Friction Ratio Data from Sounding C-143, "Clean sands to silty sands (6)" layer from 13 to 24 feet depth. 132
Figure B - 265: Estimation of the Scale of Fluctuation, θ = 1.3 feet, for Cone Tip Resistance Data from Sounding C-143, "Clean sands to silty sands (6)" layer from 25 to 35 feet depth. 133
Figure B - 266: Estimation of the Scale of Fluctuation, θ = 0.7 feet, for Friction Ratio Data from Sounding C-143, "Clean sands to silty sands (6)" layer from 25 to 35 feet depth. 133
Figure B - 267: Estimation of the Scale of Fluctuation, θ = 0.7 feet, for Cone Tip Resistance Data from Sounding C-145, "Clean sands to silty sands (6)" layer from 8 to 13 feet depth. 134
Figure B - 268: Estimation of the Scale of Fluctuation, θ = 0.5 feet, for Friction Ratio Data from Sounding C-145, "Clean sands to silty sands (6)" layer from 8 to 13 feet depth. 134
Figure B - 269: Estimation of the Scale of Fluctuation, θ = 0.7 feet, for Cone Tip Resistance Data from Sounding C-145a, "Clean sands to silty sands (6)" layer from 8 to 12 feet depth. 135
Figure B - 270: Estimation of the Scale of Fluctuation, θ, for Friction Ratio Data from Sounding C-145a, "Clean sands to silty sands (6)" layer from 8 to 12 feet depth. Data is limited to only 3 points greater than the Bartlett limit of 0.23; therefore, θ could not be estimated, and these results were not included in final analysis. 135
Figure B - 271: Estimation of the Scale of Fluctuation, θ = 1.8 feet, for Cone Tip Resistance Data from Sounding C-145a, "Gravelly sand to sand (7)" layer from 12 to 16 feet depth. 136
Figure B - 272: Estimation of the Scale of Fluctuation, θ = 0.7 feet, for Friction Ratio Data from Sounding C-145a, "Gravelly sand to sand (7)" layer from 12 to 16 feet depth. 136
Figure B - 273: Estimation of the Scale of Fluctuation, θ = 1.3 feet, for Cone Tip Resistance Data from Sounding C-145a, "Clean sands to silty sands (6)" layer from 28 to 35 feet depth. 137
Figure B - 274: Estimation of the Scale of Fluctuation, θ = 0.3 feet, for Friction Ratio Data from Sounding C-145a, "Clean sands to silty sands (6)" layer from 28 to 35 feet depth. 137
Figure B - 275: Estimation of the Scale of Fluctuation, θ = 0.7 feet, for Cone Tip Resistance Data from Sounding C-147, "Clean sands to silty sands (6)" layer from 9 to 14 feet depth. 138
Figure B - 276: Estimation of the Scale of Fluctuation, θ = 1.1 feet, for Friction Ratio Data from Sounding C-147, "Clean sands to silty sands (6)" layer from 9 to 14 feet depth. 138

Figure B - 277: Estimation of the Scale of Fluctuation, θ = 0.3 feet, for Cone Tip Resistance Data from Sounding C-147, "Clean sands to silty sands (6)" layer from 18 to 23 feet depth. 139
Figure B - 278: Estimation of the Scale of Fluctuation, θ = 0.7 feet, for Friction Ratio Data from Sounding C-147, "Clean sands to silty sands (6)" layer from 18 to 23 feet depth. 139
Figure B - 279: Estimation of the Scale of Fluctuation, θ = 0.8 feet, for Cone Tip Resistance Data from Sounding C-147a, "Clean sands to silty sands (6)" layer from 9 to 17 feet depth. 140
Figure B - 280: Estimation of the Scale of Fluctuation, θ = 1.0 feet, for Friction Ratio Data from Sounding C-147a, "Clean sands to silty sands (6)" layer from 9 to 17 feet depth. 140
Figure B - 281: Estimation of the Scale of Fluctuation, θ = 0.8 feet, for Cone Tip Resistance Data from Sounding C-147a, "Clean sands to silty sands (6)" layer from 18 to 23 feet depth. 141
Figure B - 282: Estimation of the Scale of Fluctuation, θ = 1.2 feet, for Friction Ratio Data from Sounding C-147a, "Clean sands to silty sands (6)" layer from 18 to 23 feet depth. 141
Figure B - 283: Estimation of the Scale of Fluctuation, θ = 1.6 feet, for Cone Tip Resistance Data from Sounding C-149, "Clean sands to silty sands (6)" layer from 8 to 16 feet depth. 142
Figure B - 284: Estimation of the Scale of Fluctuation, θ = 0.3 feet, for Friction Ratio Data from Sounding C-149, "Clean sands to silty sands (6)" layer from 8 to 16 feet depth. 142
Figure B - 285: Estimation of the Scale of Fluctuation, θ = 1.6 feet, for Cone Tip Resistance Data from Sounding C-149, "Clean sands to silty sands (6)" layer from 25 to 35 feet depth. Data is a poor fit for the points greater than the Bartlett limit of 0.15; coefficient of determination, R^2, value is less 0.9. Therefore, these results were not included in final analysis. 143
Figure B - 286: Estimation of the Scale of Fluctuation, θ = 0.7 feet, for Friction Ratio Data from Sounding C-146, "Clean sands to silty sands (6)" layer from 25 to 35 feet depth. 143
Figure B - 287: Estimation of the Scale of Fluctuation, θ = 1.4 feet, for Cone Tip Resistance Data from Sounding C-151, "Clean sands to silty sands (6)" layer from 17 to 22 feet depth. 144
Figure B – 288: Estimation of the Scale of Fluctuation, θ = 0.7 feet, for Friction Ratio Data from Sounding C-151, "Clean sands to silty sands (6)" layer from 17 to 22 feet depth. 144
Figure B - 289: Estimation of the Scale of Fluctuation, θ = 1.6 feet, for Cone Tip Resistance Data from Sounding C-151, "Clean sands to silty sands (6)" layer from 22 to 35 feet depth. 145
Figure B - 290: Estimation of the Scale of Fluctuation, θ = 0.5 feet, for Friction Ratio Data from Sounding C-151, "Clean sands to silty sands (6)" layer from 22 to 35 feet depth. 145
Figure B - 291: Estimation of the Scale of Fluctuation, θ = 1.4 feet, for Cone Tip Resistance Data from Sounding C-157, "Gravelly sand to sand (7)" layer from 13 to 24 feet depth. 146
Figure B - 292: Estimation of the Scale of Fluctuation, θ = 0.2 feet, for Friction Ratio Data from Sounding C-157, "Gravelly sand to sand (7)" layer from 13 to 24 feet depth. Data is a poor fit for the points greater than the Bartlett limit of 0.15; coefficient of determination, R^2, value is less 0.9. Therefore, these results were not included in final analysis. 146
Figure B - 293: Estimation of the Scale of Fluctuation, θ = 1.4 feet, for Cone Tip Resistance Data from Sounding C-157, "Clean sands to silty sands (6)" layer from 24 to 35 feet depth. 147
Figure B - 294: Estimation of the Scale of Fluctuation, θ = 0.5 feet, for Friction Ratio Data from Sounding C-157, "Clean sands to silty sands (6)" layer from 24 to 35 feet depth. 147
Figure B - 295: Estimation of the Scale of Fluctuation, θ = 0.9 feet, for Cone Tip Resistance Data from Sounding C-157a, "Clean sands to silty sands (6)" layer from 8 to 13 feet depth. 148

Figure B - 296: Estimation of the Scale of Fluctuation, θ = 0.5 feet, for Friction Ratio Data from Sounding C-157a, "Clean sands to silty sands (6)" layer from 8 to 13 feet depth. 148
Figure B - 297: Estimation of the Scale of Fluctuation, θ = 1.5 feet, for Cone Tip Resistance Data from Sounding C-157a, "Gravelly sand to sand (7)" layer from 13 to 23 feet depth. 149
Figure B - 298: Estimation of the Scale of Fluctuation, θ = 0.8 feet, for Friction Ratio Data from Sounding C-157a, "Gravelly sand to sand (7)" layer from 13 to 23 feet depth. 149
Figure B - 299: Estimation of the Scale of Fluctuation, θ = 0.9 feet, for Cone Tip Resistance Data from Sounding C-157a, "Clean sands to silty sands (6)" layer from 30 to 35 feet depth. 150
Figure B - 300: Estimation of the Scale of Fluctuation, θ = 0.4 feet, for Friction Ratio Data from Sounding C-157a, "Clean sands to silty sands (6)" layer from 30 to 35 feet depth. 150
Figure B - 301: Estimation of the Scale of Fluctuation, θ = 1.0 feet, for Cone Tip Resistance Data from Sounding C-159, "Clean sands to silty sands (6)" layer from 10 to 14 feet depth. 151
Figure B - 302: Estimation of the Scale of Fluctuation, θ = 0.8 feet, for Friction Ratio Data from Sounding C-159, "Clean sands to silty sands (6)" layer from 10 to 14 feet depth. 151
Figure B - 303: Estimation of the Scale of Fluctuation, θ = 1.2 feet, for Cone Tip Resistance Data from Sounding C-159, "Gravelly sand to sand (7)" layer from 19 to 24 feet depth. 152
Figure B - 304: Estimation of the Scale of Fluctuation, θ = 0.8 feet, for Friction Ratio Data from Sounding C-159, "Gravelly sand to sand (7)" layer from 19 to 24 feet depth. 152
Figure B - 305: Estimation of the Scale of Fluctuation, θ = 0.9 feet, for Cone Tip Resistance Data from Sounding C-159, "Clean sands to silty sands (6)" layer from 24 to 32 feet depth. 153
Figure B - 306: Estimation of the Scale of Fluctuation, θ = 0.8 feet, for Friction Ratio Data from Sounding C-159, "Clean sands to silty sands (6)" layer from 24 to 32 feet depth. 153
Figure B - 307: Estimation of the Scale of Fluctuation, θ = 1.0 feet, for Cone Tip Resistance Data from Sounding C-161, "Clean sands to silty sands (6)" layer from 12 to 25 feet depth. 154
Figure B - 308: Estimation of the Scale of Fluctuation, θ = 0.7 feet, for Friction Ratio Data from Sounding C-161, "Clean sands to silty sands (6)" layer from 12 to 25 feet depth. Data is a poor fit for the points greater than the Bartlett limit of 0.14; coefficient of determination, R^2, value is less 0.9. Therefore, these results were not included in final analysis. 154
Figure B - 309: Estimation of the Scale of Fluctuation, θ = 1.6 feet, for Cone Tip Resistance Data from Sounding C-163, "Clean sands to silty sands (6)" layer from 18 to 24 feet depth. Data is a poor fit for the points greater than the Bartlett limit of 0.20; coefficient of determination, R^2, value is less 0.9. Therefore, these results were not included in final analysis. 155
Figure B - 310: Estimation of the Scale of Fluctuation, θ, for Friction Ratio Data from Sounding C-163, "Clean sands to silty sands (6)" layer from 18 to 24 feet depth. Data is limited to only 3 points greater than the Bartlett limit of 0.20; therefore, θ could not be estimated, and these results were not included in final analysis. 155
Figure B - 311: Estimation of the Scale of Fluctuation, θ = 1.7 feet, for Cone Tip Resistance Data from Sounding C-163, "Clean sands to silty sands (6)" layer from 28 to 35 feet depth. 156
Figure B - 312: Estimation of the Scale of Fluctuation, θ = 0.8 feet, for Friction Ratio Data from Sounding C-163, "Clean sands to silty sands (6)" layer from 28 to 35 feet depth. 156
Figure B - 313: Estimation of the Scale of Fluctuation, θ = 1.0 feet, for Cone Tip Resistance Data from Sounding C-166, "Clean sands to silty sands (6)" layer from 4 to 9 feet depth. 157

Figure B - 314: Estimation of the Scale of Fluctuation, θ = 0.6 feet, for Friction Ratio Data from Sounding C-166, "Clean sands to silty sands (6)" layer from 4 to 9 feet depth. 157
Figure B - 315: Estimation of the Scale of Fluctuation, θ = 1.2 feet, for Cone Tip Resistance Data from Sounding C-166, "Clean sands to silty sands (6)" layer from 12 to 17 feet depth. 158
Figure B - 316: Estimation of the Scale of Fluctuation, θ = 0.9 feet, for Friction Ratio Data from Sounding C-166, "Clean sands to silty sands (6)" layer from 12 to 17 feet depth. 158
Figure B - 317: Estimation of the Scale of Fluctuation, θ = 1.2 feet, for Cone Tip Resistance Data from Sounding C-166, "Clean sands to silty sands (6)" layer from 29 to 36 feet depth. 159
Figure B - 318: Estimation of the Scale of Fluctuation, θ = 0.5 feet, for Friction Ratio Data from Sounding C-166, "Clean sands to silty sands (6)" layer from 29 to 36 feet depth. 159
Figure B - 319: Estimation of the Scale of Fluctuation, θ = 1.1 feet, for Cone Tip Resistance Data from Sounding C-168, "Clean sands to silty sands (6)" layer from 7 to 18 feet depth. 160
Figure B - 320: Estimation of the Scale of Fluctuation, θ = 0.6 feet, for Friction Ratio Data from Sounding C-168, "Clean sands to silty sands (6)" layer from 7 to 18 feet depth. 160
Figure B - 321: Estimation of the Scale of Fluctuation, θ = 1.5 feet, for Cone Tip Resistance Data from Sounding C-168, "Clean sands to silty sands (6)" layer from 19 to 25 feet depth. 161
Figure B - 322: Estimation of the Scale of Fluctuation, θ = 0.4 feet, for Friction Ratio Data from Sounding C-168, "Clean sands to silty sands (6)" layer from 19 to 25 feet depth. 161
Figure B - 323: Estimation of the Scale of Fluctuation, θ = 0.8 feet, for Cone Tip Resistance Data from Sounding C-168, "Gravelly sand to sand (7)" layer from 25 to 29 feet depth. 162
Figure B - 324: Estimation of the Scale of Fluctuation, θ = 0.7 feet, for Friction Ratio Data from Sounding C-168, "Gravelly sand to sand (7)" layer from 25 to 29 feet depth. 162
Figure B - 325: Estimation of the Scale of Fluctuation, θ = 0.7 feet, for Cone Tip Resistance Data from Sounding C-170, "Clean sands to silty sands (6)" layer from 11 to 16 feet depth. 163
Figure B - 326: Estimation of the Scale of Fluctuation, θ = 0.7 feet, for Friction Ratio Data from Sounding C-170, "Clean sands to silty sands (6)" layer from 11 to 16 feet depth. 163
Figure B - 327: Estimation of the Scale of Fluctuation, θ = 0.7 feet, for Cone Tip Resistance Data from Sounding C-170, "Clean sands to silty sands (6)" layer from 19 to 25 feet depth. 164
Figure B - 328: Estimation of the Scale of Fluctuation, θ = 0.7 feet, for Friction Ratio Data from Sounding C-170, "Clean sands to silty sands (6)" layer from 19 to 25 feet depth. 164
Figure B - 329: Estimation of the Scale of Fluctuation, θ = 0.8 feet, for Cone Tip Resistance Data from Sounding C-170, "Clean sands to silty sands (6)" layer from 28 to 35 feet depth. 165
Figure B - 330: Estimation of the Scale of Fluctuation, θ = 0.4 feet, for Friction Ratio Data from Sounding C-170, "Clean sands to silty sands (6)" layer from 28 to 35 feet depth. 165
Figure B - 331: Estimation of the Scale of Fluctuation, θ = 1.5 feet, for Cone Tip Resistance Data from Sounding C-172, "Clean sands to silty sands (6)" layer from 20 to 34 feet depth. 166
Figure B - 332: Estimation of the Scale of Fluctuation, θ = 0.9 feet, for Friction Ratio Data from Sounding C-172, "Clean sands to silty sands (6)" layer from 20 to 34 feet depth. 166
Figure B - 333: Estimation of the Scale of Fluctuation, θ = 1.1 feet, for Cone Tip Resistance Data from Sounding C-174, "Gravelly sand to sand (7)" layer from 6 to 10 feet depth. 167
Figure B - 334: Estimation of the Scale of Fluctuation, θ = 0.6 feet, for Friction Ratio Data from Sounding C-174, "Gravelly sand to sand (7)" layer from 6 to 10 feet depth. 167

Figure B - 335: Estimation of the Scale of Fluctuation, θ = 0.4 feet, for Cone Tip Resistance Data from Sounding C-174, "Clean sands to silty sands (6)" layer from 28 to 32 feet depth. 168
Figure B - 336: Estimation of the Scale of Fluctuation, θ = 0.6 feet, for Friction Ratio Data from Sounding C-174, "Clean sands to silty sands (6)" layer from 28 to 32 feet depth. 168
Figure B - 337: Estimation of the Scale of Fluctuation, θ = 1.9 feet, for Cone Tip Resistance Data from Sounding C-180, "Clean sands to silty sands (6)" layer from 26 to 35 feet depth. 169
Figure B - 338: Estimation of the Scale of Fluctuation, θ = 1.0 feet, for Friction Ratio Data from Sounding C-180, "Clean sands to silty sands (6)" layer from 26 to 35 feet depth. 169
Figure B - 339: Estimation of the Scale of Fluctuation, θ = 1.1 feet, for Cone Tip Resistance Data from Sounding C-182, "Clean sands to silty sands (6)" layer from 13 to 23 feet depth. 170
Figure B - 340: Estimation of the Scale of Fluctuation, θ = 0.8 feet, for Friction Ratio Data from Sounding C-182, "Clean sands to silty sands (6)" layer from 13 to 23 feet depth. Data is a poor fit for the points greater than the Bartlett limit of 0.16; coefficient of determination, R^2, value is less 0.9. Therefore, these results were not included in final analysis. 170
Figure B - 341: Estimation of the Scale of Fluctuation, θ = 1.4 feet, for Cone Tip Resistance Data from Sounding C-182, "Clean sands to silty sands (6)" layer from 29 to 34 feet depth. 171
Figure B - 342: Estimation of the Scale of Fluctuation, θ = 0.7 feet, for Friction Ratio Data from Sounding C-182, "Clean sands to silty sands (6)" layer from 29 to 34 feet depth. 171
Figure B - 343: Estimation of the Scale of Fluctuation, θ = 1.1 feet, for Cone Tip Resistance Data from Sounding C-184, "Clean sands to silty sands (6)" layer from 15 to 21 feet depth. 172
Figure B - 344: Estimation of the Scale of Fluctuation, θ = 0.8 feet, for Friction Ratio Data from Sounding C-184, "Clean sands to silty sands (6)" layer from 15 to 21 feet depth. 172
Figure B - 345: Estimation of the Scale of Fluctuation, θ = 1.3 feet, for Cone Tip Resistance Data from Sounding C-184, "Gravelly sand to sand (7)" layer from 21 to 27 feet depth. 173
Figure B - 346: Estimation of the Scale of Fluctuation, θ = 0.8 feet, for Friction Ratio Data from Sounding C-184, "Gravelly sand to sand (7)" layer from 21 to 27 feet depth. Data is a poor fit for the points greater than the Bartlett limit of 0.21; coefficient of determination, R^2, value is less 0.9. Therefore, these results were not included in final analysis 173
Figure B - 347: Estimation of the Scale of Fluctuation, θ = 1.0 feet, for Cone Tip Resistance Data from Sounding C-184, "Clean sands to silty sands (6)" layer from 29 to 35 feet depth. Data is a poor fit for the points greater than the Bartlett limit of 0.19; coefficient of determination, R^2, value is less 0.9. Therefore, these results were not included in final analysis. 174
Figure B - 348: Estimation of the Scale of Fluctuation, θ = 0.9 feet, for Friction Ratio Data from Sounding C-184, "Clean sands to silty sands (6)" layer from 29 to 35 feet depth. 174
Figure B - 349: Estimation of the Scale of Fluctuation, θ = 0.9 feet, for Cone Tip Resistance Data from Sounding C-186, "Clean sands to silty sands (6)" layer from 4 to 8 feet depth. 175
Figure B - 350: Estimation of the Scale of Fluctuation, θ = 0.6 feet, for Friction Ratio Data from Sounding C-186, "Clean sands to silty sands (6)" layer from 4 to 8 feet depth. 175
Figure B - 351: Estimation of the Scale of Fluctuation, θ = 1.1 feet, for Cone Tip Resistance Data from Sounding C-186, "Clean sands to silty sands (6)" layer from 17 to 27 feet depth. 176
Figure B - 352: Estimation of the Scale of Fluctuation, θ = 1.3 feet, for Friction Ratio Data from Sounding C-186, "Clean sands to silty sands (6)" layer from 17 to 27 feet depth. 176

Figure B - 353: Estimation of the Scale of Fluctuation, θ = 3.3 feet, for Cone Tip Resistance Data from Sounding C-186, "Clean sands to silty sands (6)" layer from 27 to 35 feet depth. Data is a poor fit for the points greater than the Bartlett limit of 0.18; coefficient of determination, R^2, value is less 0.9. Therefore, these results were not included in final analysis. 177
Figure B - 354: Estimation of the Scale of Fluctuation, θ = 0.6 feet, for Friction Ratio Data from Sounding C-186, "Clean sands to silty sands (6)" layer from 27 to 35 feet depth. 177
Figure B - 355: Estimation of the Scale of Fluctuation, θ = 0.6 feet, for Cone Tip Resistance Data from Sounding C-190, "Clays; clay to silty clay (3)" layer from 3 to 9 feet depth. 178
Figure B - 356: Estimation of the Scale of Fluctuation, θ, for Friction Ratio Data from Sounding C-190, " Clays; clay to silty clay (3)" layer from 3 to 9 feet depth. Data is limited to only 1 point greater than the Bartlett limit of 0.21; therefore, θ could not be estimated, and these results were not included in final analysis. 178
Figure B - 357: Estimation of the Scale of Fluctuation, θ = 1.0 feet, for Cone Tip Resistance Data from Sounding C-190, "Clean sands to silty sands (6)" layer from 17 to 24 feet depth. 179
Figure B - 358: Estimation of the Scale of Fluctuation, θ = 0.7 feet, for Friction Ratio Data from Sounding C-190, "Clean sands to silty sands (6)" layer from 17 to 24 feet depth. 179
Figure B - 359: Estimation of the Scale of Fluctuation, θ = 0.7 feet, for Cone Tip Resistance Data from Sounding C-190, "Gravelly sand to sand (7)" layer from 31 to 35 feet depth. 180
Figure B - 360: Estimation of the Scale of Fluctuation, θ, for Friction Ratio Data from Sounding C-190, "Gravelly sand to sand (7)" layer from 31 to 35 feet depth. Data is limited to only 3 points greater than the Bartlett limit of 0.25; therefore, θ could not be estimated, and these results were not included in final analysis. 180
Figure B - 361: Estimation of the Scale of Fluctuation, θ = 0.9 feet, for Cone Tip Resistance Data from Sounding C-192, "Clean sands to silty sands (6)" layer from 13 to 18 feet depth. 181
Figure B - 362: Estimation of the Scale of Fluctuation, θ = 0.8 feet, for Friction Ratio Data from Sounding C-192, "Clean sands to silty sands (6)" layer from 13 to 18 feet depth. Data is a poor fit for the points greater than the Bartlett limit of 0.22; coefficient of determination, R^2 value is less 0.9. Therefore, these results were not included in final analysis. 181
Figure B - 363: Estimation of the Scale of Fluctuation, θ = 0.8 feet, for Cone Tip Resistance Data from Sounding C-192, "Clean sands to silty sands (6)" layer from 25 to 36 feet depth. 182
Figure B - 364: Estimation of the Scale of Fluctuation, θ = 0.3 feet, for Friction Ratio Data from Sounding C-192, "Clean sands to silty sands (6)" layer from 25 to 36 feet depth. 182
Figure B - 365: Estimation of the Scale of Fluctuation, θ = 1.3 feet, for Cone Tip Resistance Data from Sounding C-194, "Clean sands to silty sands (6)" layer from 6 to 10 feet depth. 183
Figure B - 366: Estimation of the Scale of Fluctuation, θ = 0.6 feet, for Friction Ratio Data from Sounding C-194, "Clean sands to silty sands (6)" layer from 6 to 10 feet depth. 183
Figure B - 367: Estimation of the Scale of Fluctuation, θ = 1.5 feet, for Cone Tip Resistance Data from Sounding C-194, "Clean sands to silty sands (6)" layer from 11 to 20 feet depth. 184
Figure B - 368: Estimation of the Scale of Fluctuation, θ = 0.9 feet, for Friction Ratio Data from Sounding C-194, "Clean sands to silty sands (6)" layer from 11 to 20 feet depth. 184
Figure B - 370: Estimation of the Scale of Fluctuation, θ = 1.0 feet, for Cone Tip Resistance Data from Sounding C-194, "Gravelly sand to sand (7)" layer from 20 to 26 feet depth. 185

Figure B - 371: Estimation of the Scale of Fluctuation, θ = 0.5 feet, for Friction Ratio Data from Sounding C-194, "Gravelly sand to sand (7)" layer from 20 to 26 feet depth. 185
Figure B - 371: Estimation of the Scale of Fluctuation, θ = 0.9 feet, for Cone Tip Resistance Data from Sounding C-194, "Clean sands to silty sands (6)" layer from 30 to 35 feet depth. 186
Figure B - 372: Estimation of the Scale of Fluctuation, θ = 0.4 feet, for Friction Ratio Data from Sounding C-194, "Clean sands to silty sands (6)" layer from 30 to 35 feet depth. 186
Figure B - 373: Estimation of the Scale of Fluctuation, θ = 0.9 feet, for Cone Tip Resistance Data from Sounding C-196, "Clayey silt to silty clay (4)" layer from 4 to 8 feet depth. 187
Figure B - 374: Estimation of the Scale of Fluctuation, θ = 0.5 feet, for Friction Ratio Data from Sounding C-196, "Clayey silt to silty clay (4)" layer from 4 to 8 feet depth. 187
Figure B - 375: Estimation of the Scale of Fluctuation, θ = 2.1 feet, for Cone Tip Resistance Data from Sounding C-196, "Clean sands to silty sands (6)" layer from 14 to 19 feet depth. 188
Figure B - 376: Estimation of the Scale of Fluctuation, θ = 0.7 feet, for Friction Ratio Data from Sounding C-196, "Clean sands to silty sands (6)" layer from 14 to 19 feet depth. 188
Figure B - 377: Estimation of the Scale of Fluctuation, θ = 0.9 feet, for Cone Tip Resistance Data from Sounding C-196, "Clean sands to silty sands (6)" layer from 21 to 25 feet depth. 189
Figure B - 378: Estimation of the Scale of Fluctuation, θ = 0.6 feet, for Friction Ratio Data from Sounding C-196, "Clean sands to silty sands (6)" layer from 21 to 25 feet depth. 189
Figure B - 379: Estimation of the Scale of Fluctuation, θ = 2.2 feet, for Cone Tip Resistance Data from Sounding C-198, "Clean sands to silty sands (6)" layer from 4 to 12 feet depth. 190
Figure B - 380: Estimation of the Scale of Fluctuation, θ = 0.8 feet, for Friction Ratio Data from Sounding C-198, "Clean sands to silty sands (6)" layer from 4 to 12 feet depth. Data is a poor fit for the points greater than the Bartlett limit of 0.18; coefficient of determination, R^2, value is less 0.9. Therefore, these results were not included in final analysis. 190
Figure B - 381: Estimation of the Scale of Fluctuation, θ = 0.5 feet, for Cone Tip Resistance Data from Sounding C-198, "Clean sands to silty sands (6)" layer from 16 to 20 feet depth. 191
Figure B - 382: Estimation of the Scale of Fluctuation, θ = 0.3 feet, for Friction Ratio Data from Sounding C-198, "Clean sands to silty sands (6)" layer from 16 to 20 feet depth. 191
Figure B - 383: Estimation of the Scale of Fluctuation, θ = 1.3 feet, for Cone Tip Resistance Data from Sounding C-198, "Clean sands to silty sands (6)" layer from 23 to 34 feet depth. Data is a poor fit for the points greater than the Bartlett limit of 0.16; coefficient of determination, R^2, value is less 0.9. Therefore, these results were not included in final analysis. 192
Figure B - 384: Estimation of the Scale of Fluctuation, θ = 0.9 feet, for Friction Ratio Data from Sounding C-198, "Clean sands to silty sands (6)" layer from 23 to 34 feet depth. 192
Figure B - 385: Estimation of the Scale of Fluctuation, θ = 1.3 feet, for Cone Tip Resistance Data from Sounding C-200, "Clean sands to silty sands (6)" layer from 13 to 28 feet depth. 193
Figure B - 386: Estimation of the Scale of Fluctuation, θ = 0.6 feet, for Friction Ratio Data from Sounding C-200, "Clean sands to silty sands (6)" layer from 13 to 28 feet depth. 193
Figure B - 387: Estimation of the Scale of Fluctuation, θ = 0.8 feet, for Cone Tip Resistance Data from Sounding C-200, "Clean sands to silty sands (6)" layer from 31 to 35 feet depth. 194
Figure B – 388: Estimation of the Scale of Fluctuation, θ = 0.5 feet, for Friction Ratio Data from Sounding C-200, "Clean sands to silty sands (6)" layer from 31 to 35 feet depth. 194

Figure B – 389: Estimation of the Scale of Fluctuation, θ = 1.1 feet, for Cone Tip Resistance Data from Sounding C-200, "Clean sands to silty sands (6)" layer from 40 to 47 feet depth. 195
Figure B - 390: Estimation of the Scale of Fluctuation, θ, for Friction Ratio Data from Sounding C-200, "Clean sands to silty sands (6)" layer from 40 to 47 feet depth. Data is limited to only 3 points greater than the Bartlett limit of 0.19; therefore, θ could not be estimated, and these results were not included in final analysis. 195
Figure B - 391: Estimation of the Scale of Fluctuation, θ = 3.1 feet, for Cone Tip Resistance Data from Sounding C-200, "Clean sands to silty sands (6)" layer from 48 to 66 feet depth. Data is a poor fit for the points greater than the Bartlett limit of 0.12; coefficient of determination, R^2, value is less 0.9. Therefore, these results were not included in final analysis. 196
Figure B - 392: Estimation of the Scale of Fluctuation, θ = 1.1 feet, for Friction Ratio Data from Sounding C-200, Clean sands to silty sands (6)" layer from 48 to 66 feet depth. 196

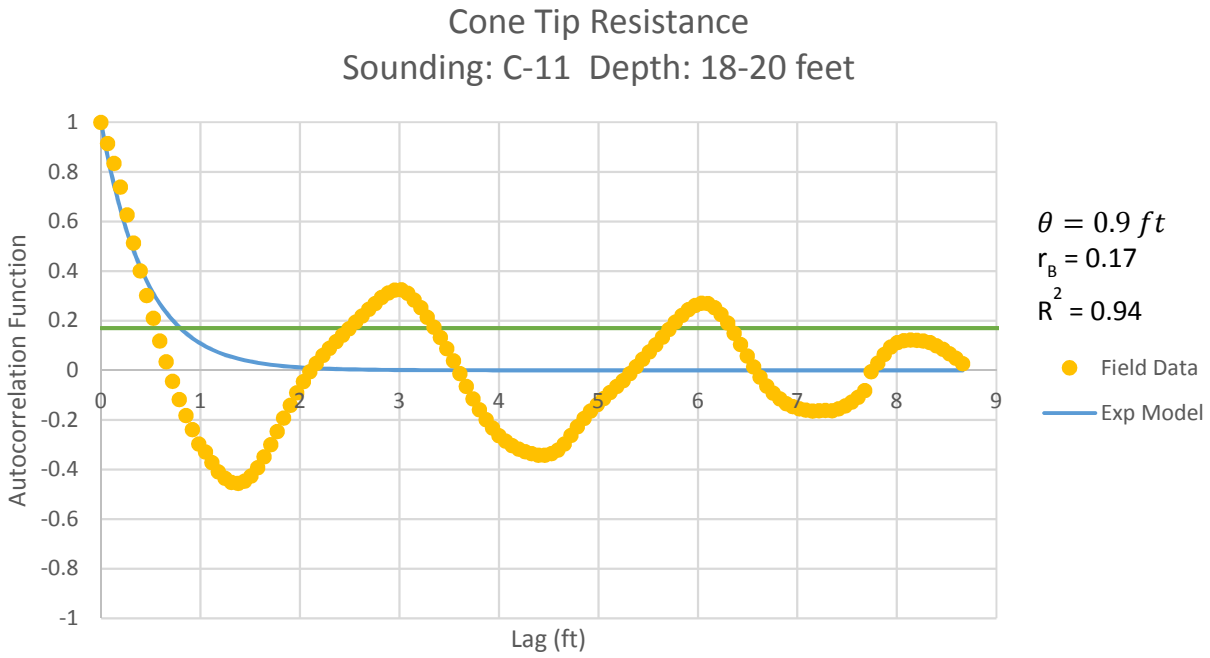

Figure B - 1: Estimation of the Scale of Fluctuation, θ = 0.9 feet, for Cone Tip Resistance Data from Sounding C-11, "Clean sands to silty sands (6)" layer from 18 to 20 feet depth.

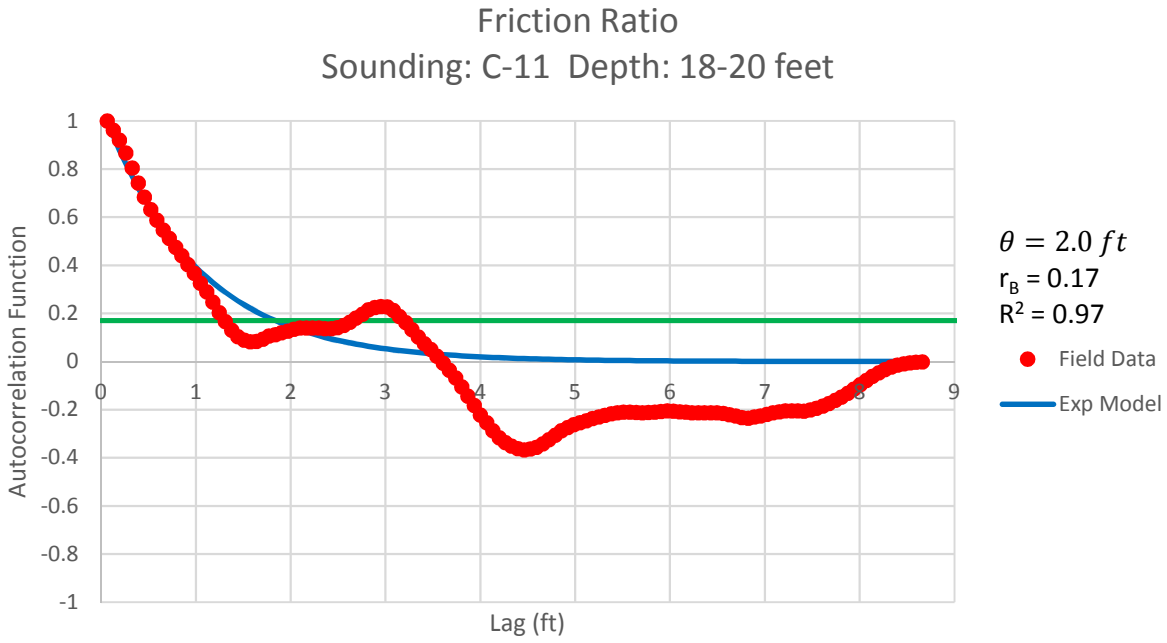

Figure B - 2: Estimation of the Scale of Fluctuation, θ = 2.0 feet, for Friction Ratio Data from Sounding C-11, "Clean sands to silty sands (6)" layer from 18 to 20 feet depth.

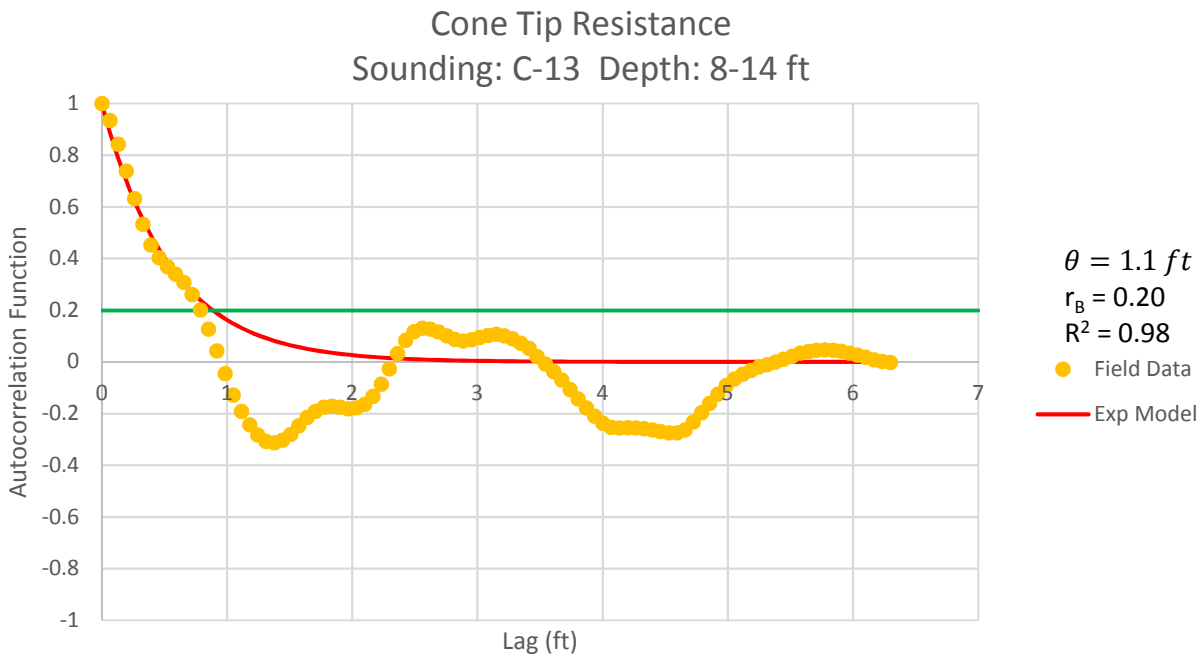

Figure B - 3: Estimation of the Scale of Fluctuation, $\theta = 1.1$ feet, for Cone Tip Resistance Data from Sounding C-13, "Clean sands to silty sands (6)" layer from 8 to 14 feet depth.

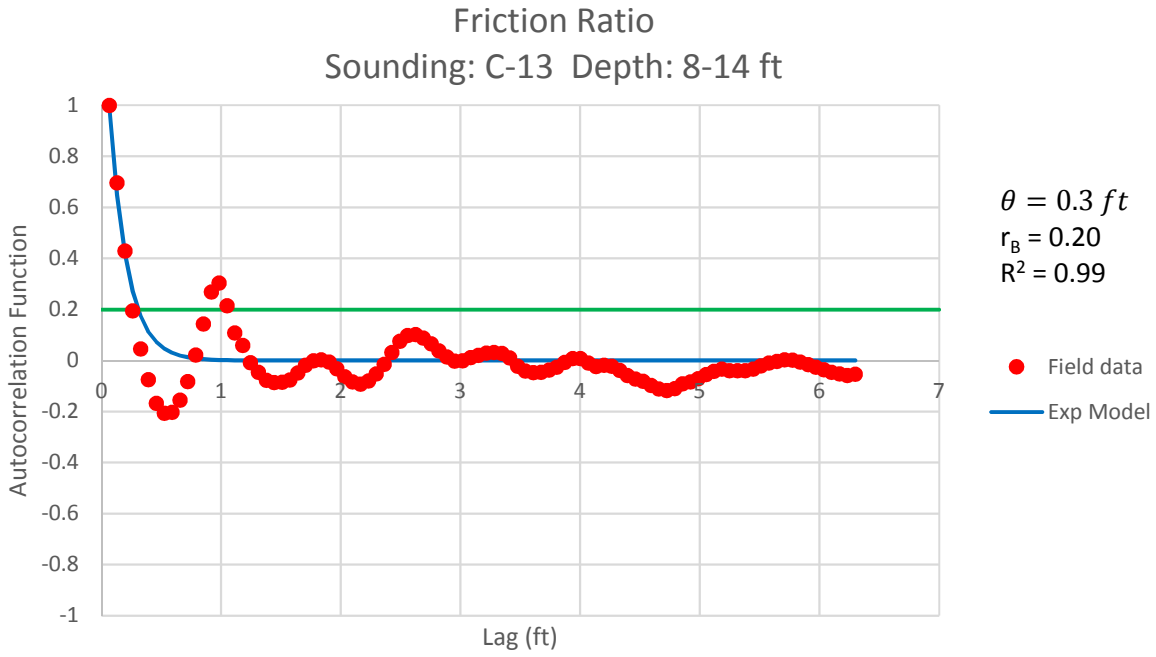

Figure B - 4: Estimation of the Scale of Fluctuation, $\theta = 0.3$ feet, for Friction Ratio Data from Sounding C-13, "Clean sands to silty sands (6)" layer from 8 to 14 feet depth.

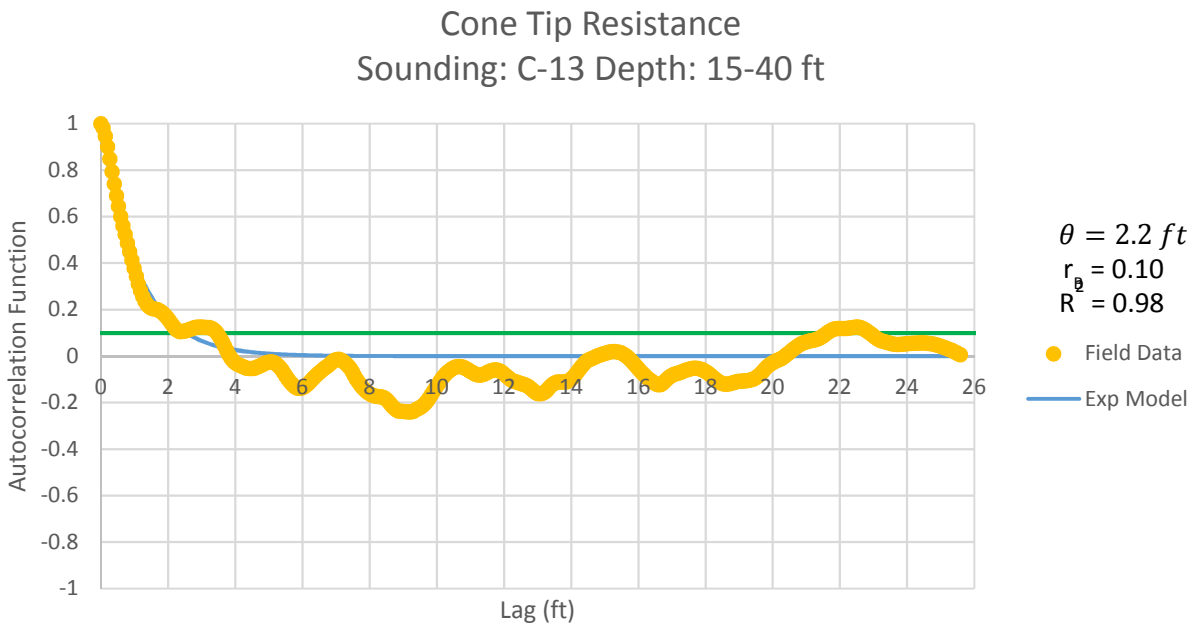

Figure B - 5: Estimation of the Scale of Fluctuation, θ = 2.2 feet, for Cone Tip Resistance Data from Sounding C-13, "Clean sands to silty sands (6)" layer from 15 to 40 feet depth.

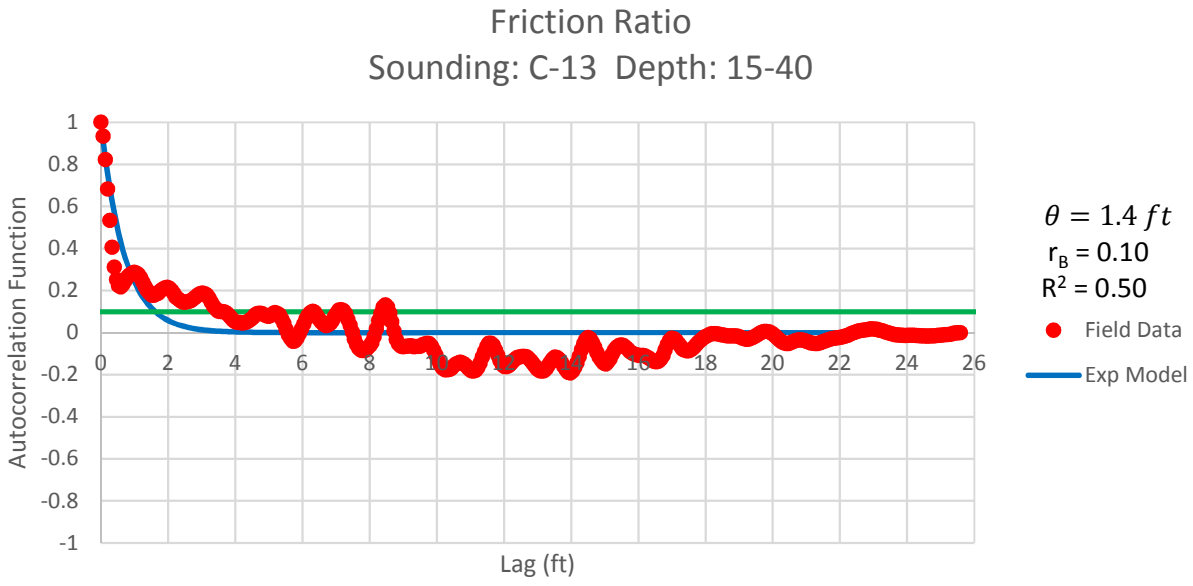

Figure B - 6: Estimation of the Scale of Fluctuation, θ = 1.4 feet, for Friction Ratio Data from Sounding C-13, "Clean sands to silty sands (6)" layer from 15 to 40 feet depth. Data is a poor fit for the points greater than the Bartlett limit of 0.10; coefficient of determination, R^2, value is less 0.9. Therefore, these results were not included in final analysis.

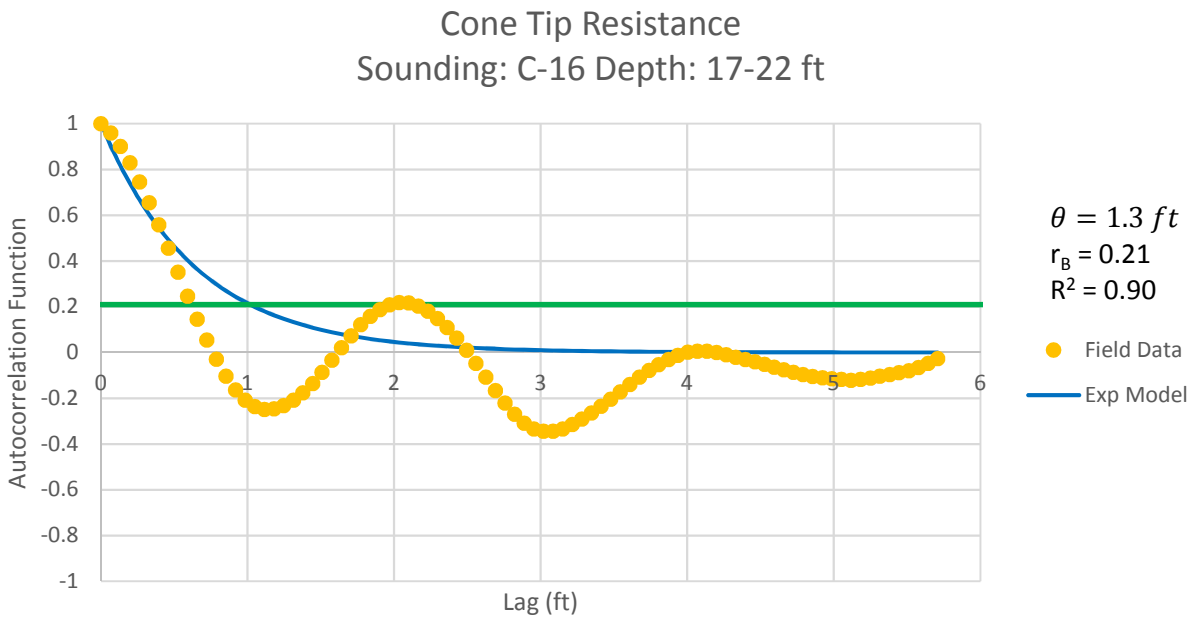

Figure B - 7: Estimation of the Scale of Fluctuation, $\theta = 1.3$ feet, for Cone Tip Resistance Data from Sounding C-16, "Clean sands to silty sands (6)" layer from 17 to 22 feet depth. Data is a poor fit for the points greater than the Bartlett limit of 0.21; coefficient of determination, R^2, value is less 0.9. Therefore, these results were not included in final analysis.

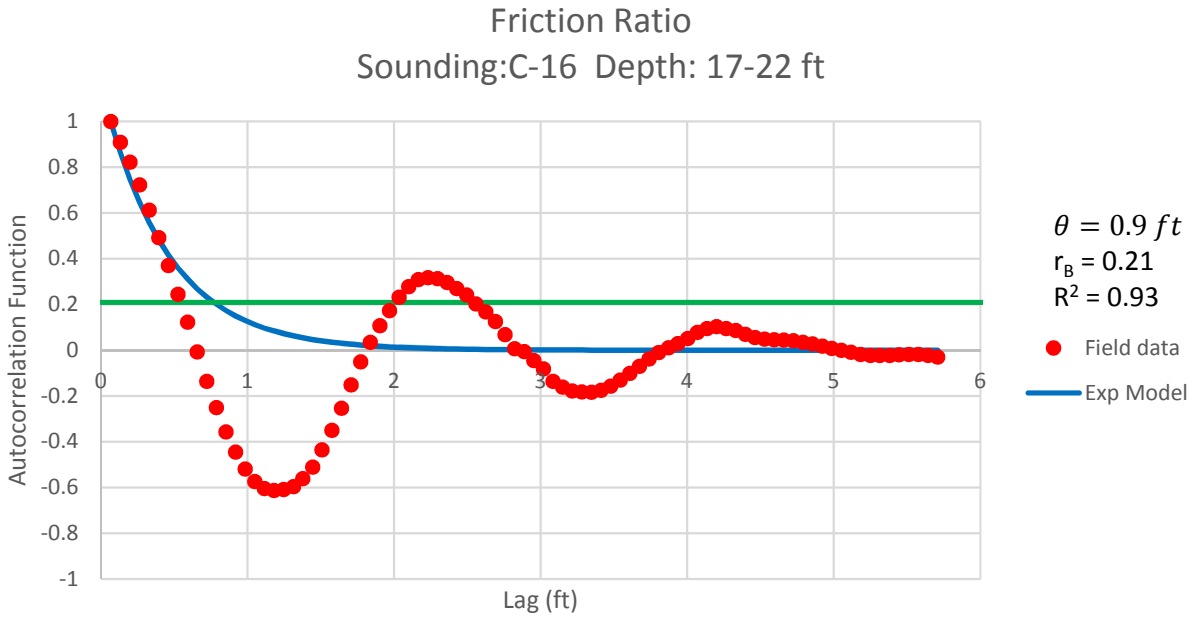

Figure B - 8: Estimation of the Scale of Fluctuation, $\theta = 0.9$ feet, for Friction Ratio Data from Sounding C-16, "Clean sands to silty sands (6)" layer from 17 to 22 feet depth.

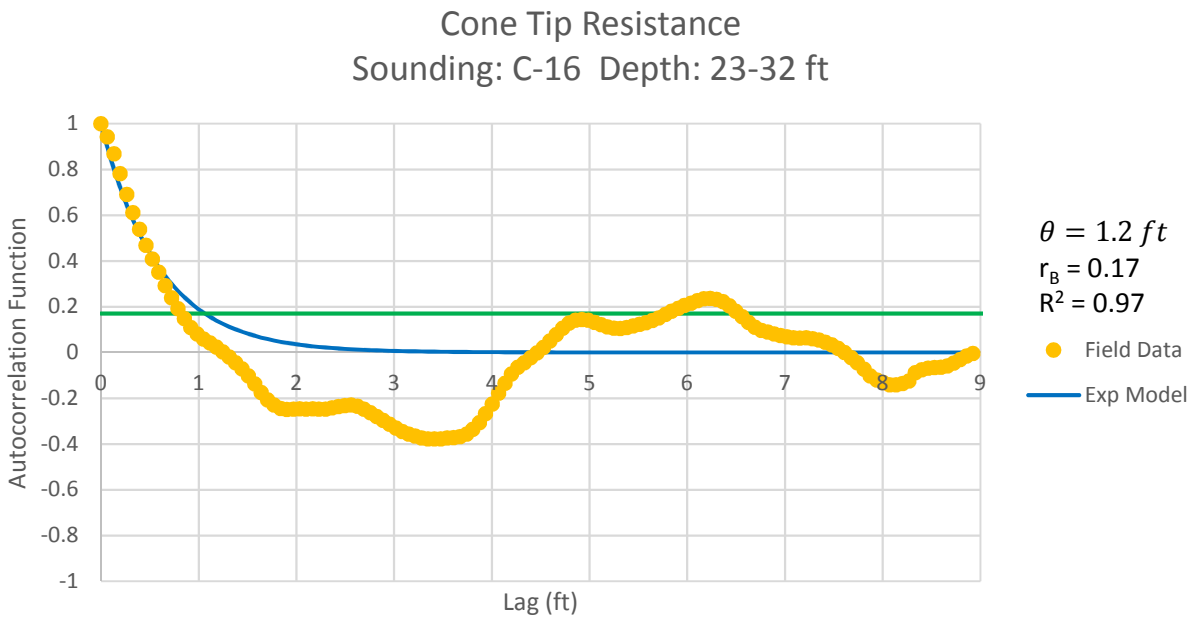

Figure B - 9: Estimation of the Scale of Fluctuation, θ = 1.2 feet, for Cone Tip Resistance Data from Sounding C-16, "Clean sands to silty sands (6)" layer from 23 to 32 feet depth.

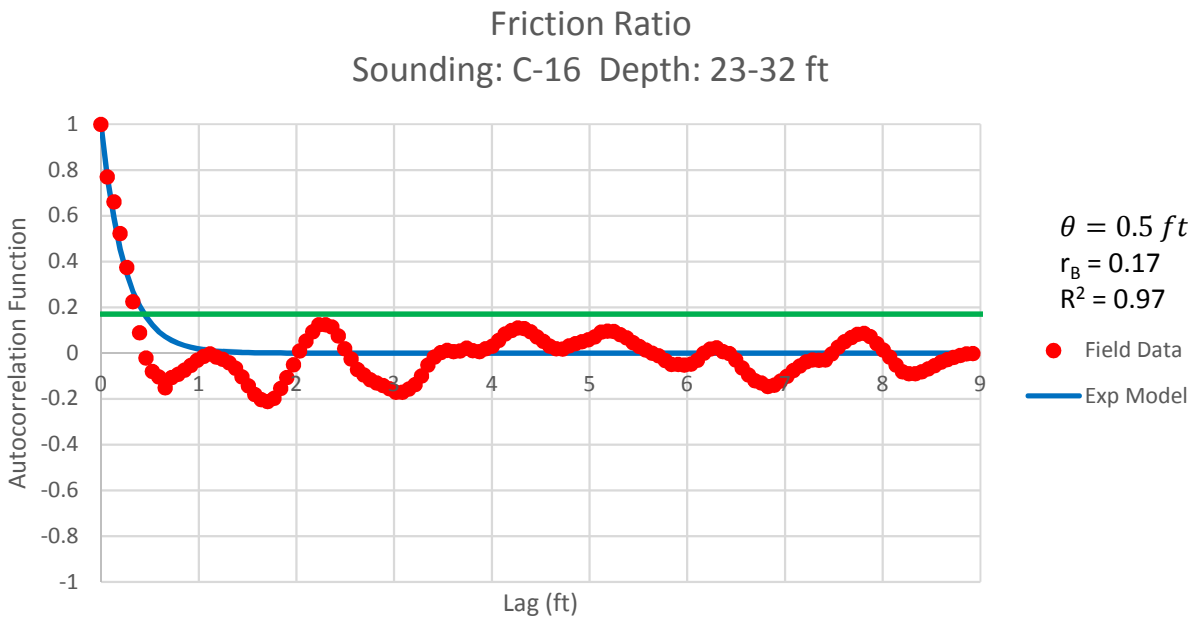

Figure B - 10: Estimation of the Scale of Fluctuation, θ = 0.5 feet, for Friction Ratio Data from Sounding C-16, "Clean sands to silty sands (6)" layer from 23 to 32 feet depth.

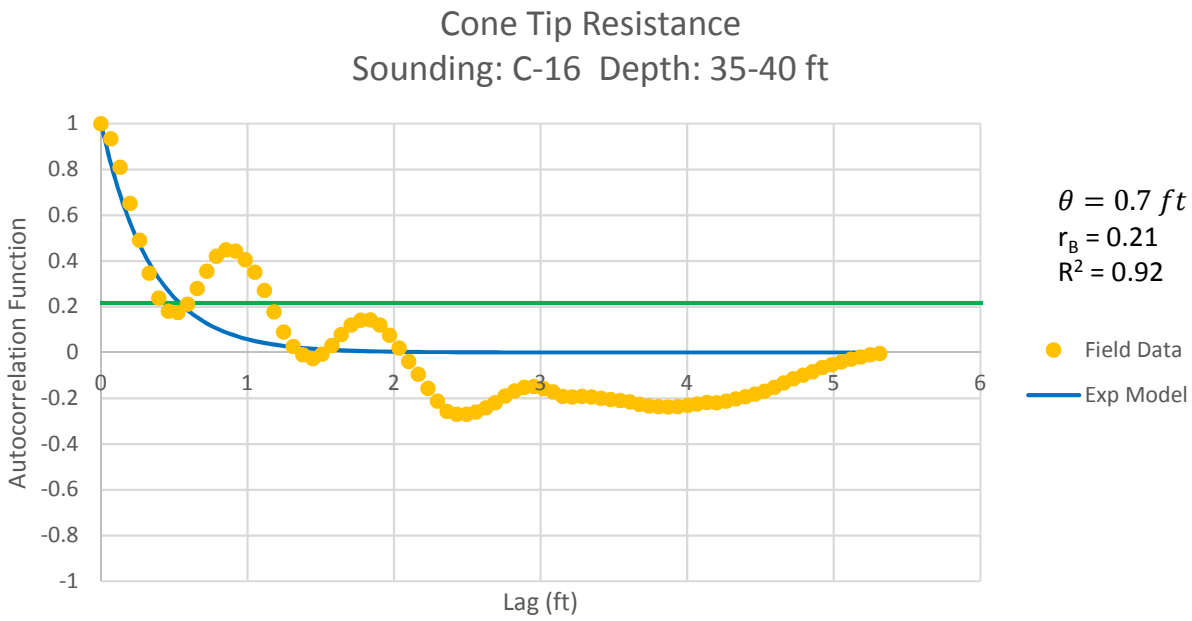

Figure B - 11: Estimation of the Scale of Fluctuation, $\theta = 0.7$ feet, for Cone Tip Resistance Data from Sounding C-16, "Clean sands to silty sands (6)" layer from 35 to 40 feet depth.

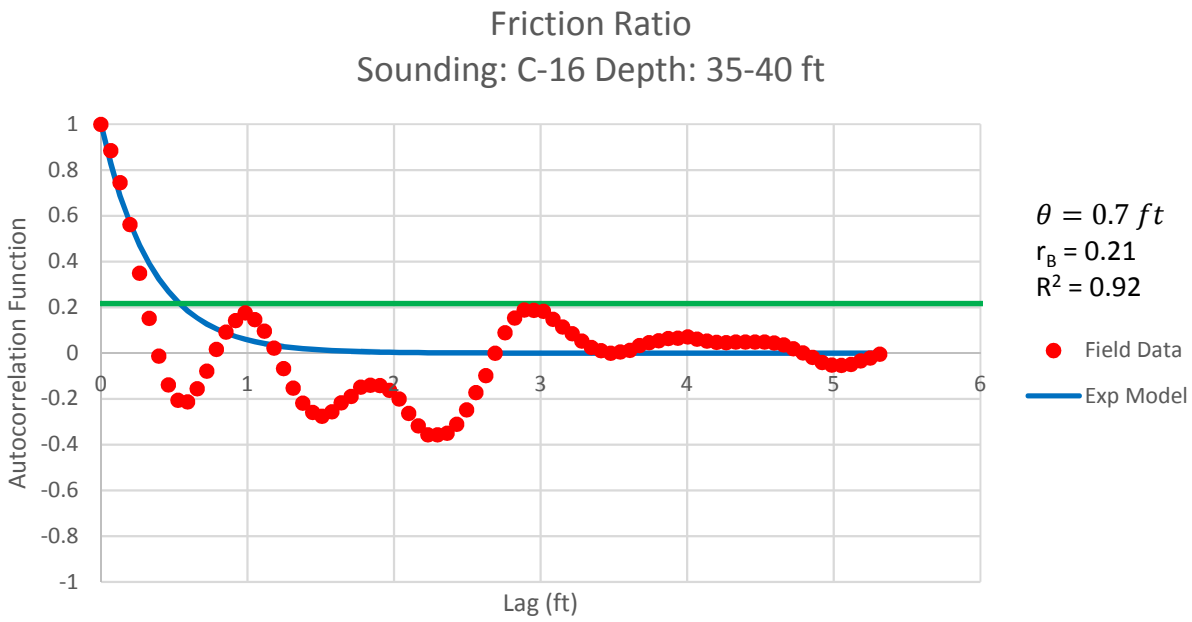

Figure B - 12: Estimation of the Scale of Fluctuation, $\theta = 0.7$ feet, for Friction Ratio Data from Sounding C-16, "Clean sands to silty sands (6)" layer from 35 to 40 feet depth.

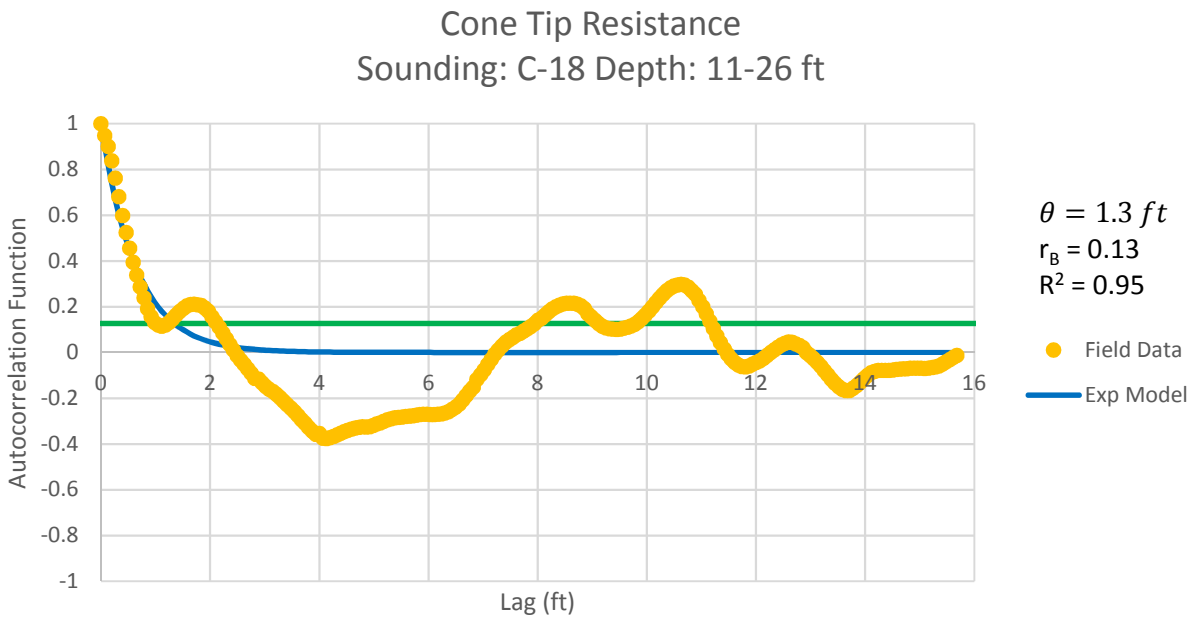

Figure B - 13: Estimation of the Scale of Fluctuation, $\theta = 1.3$ feet, for Cone Tip Resistance Data from Sounding C-18, "Clean sands to silty sands (6)" layer from 11 to 26 feet depth.

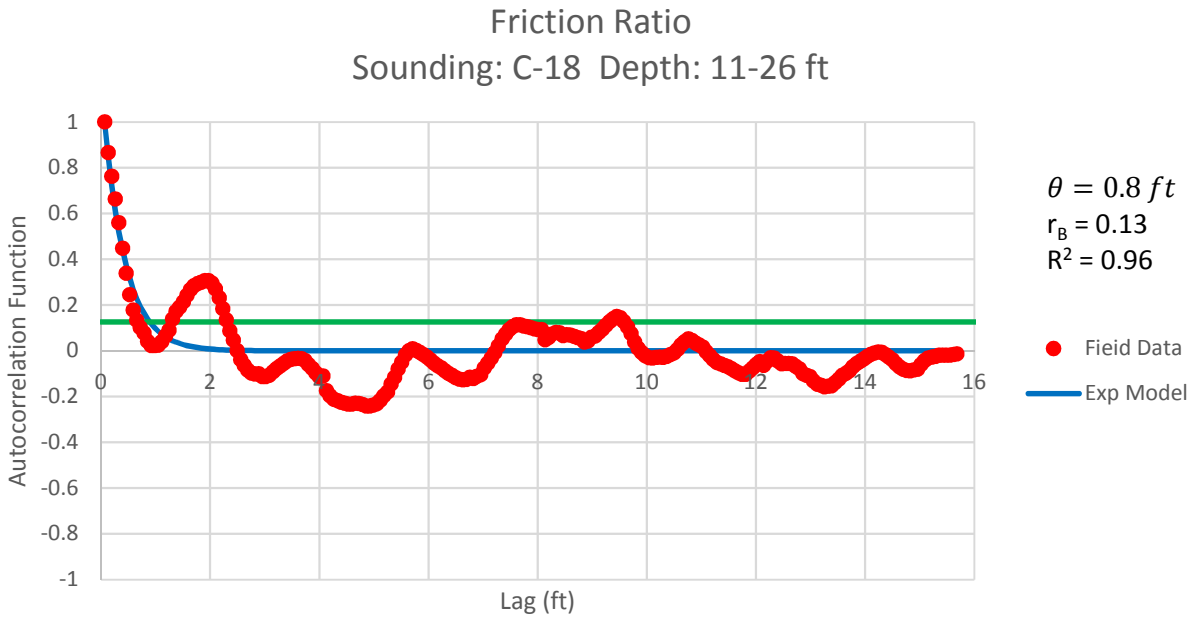

Figure B - 14: Estimation of the Scale of Fluctuation, $\theta = 0.8$ feet, for Friction Ratio Data from Sounding C-18, "Clean sands to silty sands (6)" layer from 11 to 26 feet depth.

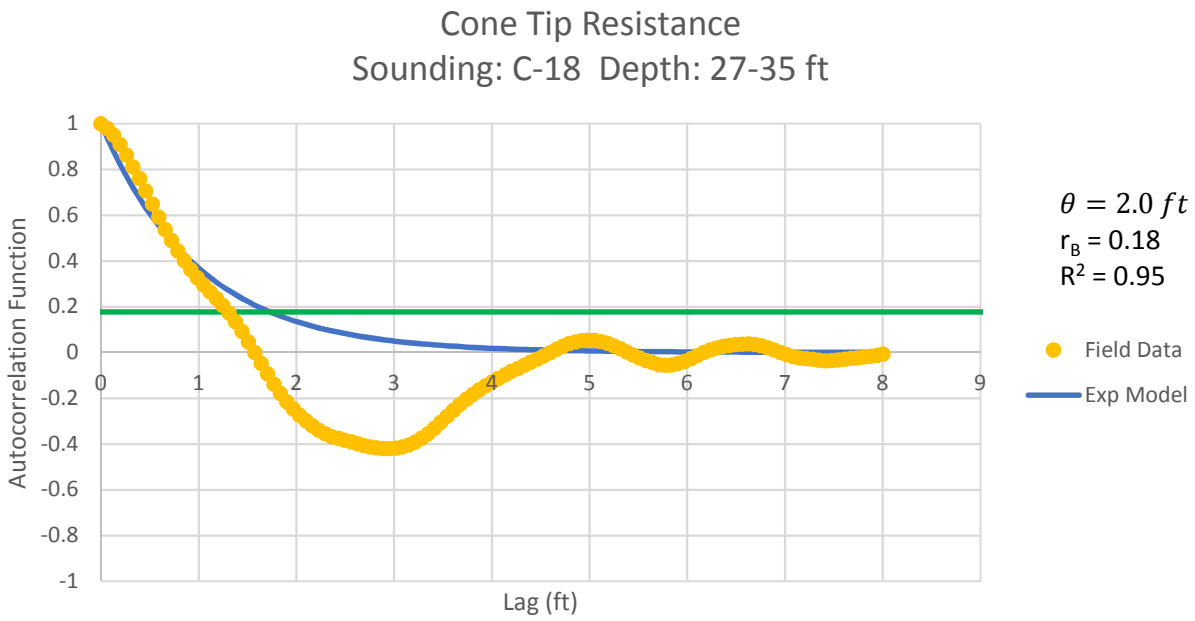

Figure B - 15: Estimation of the Scale of Fluctuation, $\theta = 2.0$ feet, for Cone Tip Resistance Data from Sounding C-18, "Clean sands to silty sands (6)" layer from 27 to 35 feet depth.

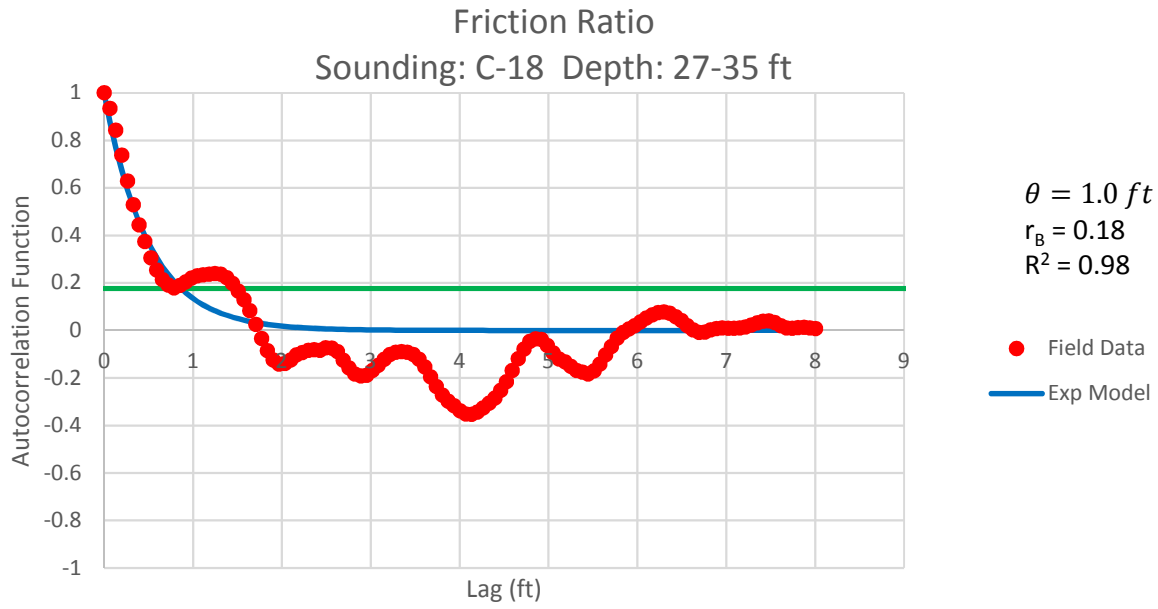

Figure B - 16: Estimation of the Scale of Fluctuation, $\theta = 1.0$ feet, for Friction Ratio Data from Sounding C-18, "Clean sands to silty sands (6)" layer from 27 to 35 feet depth.

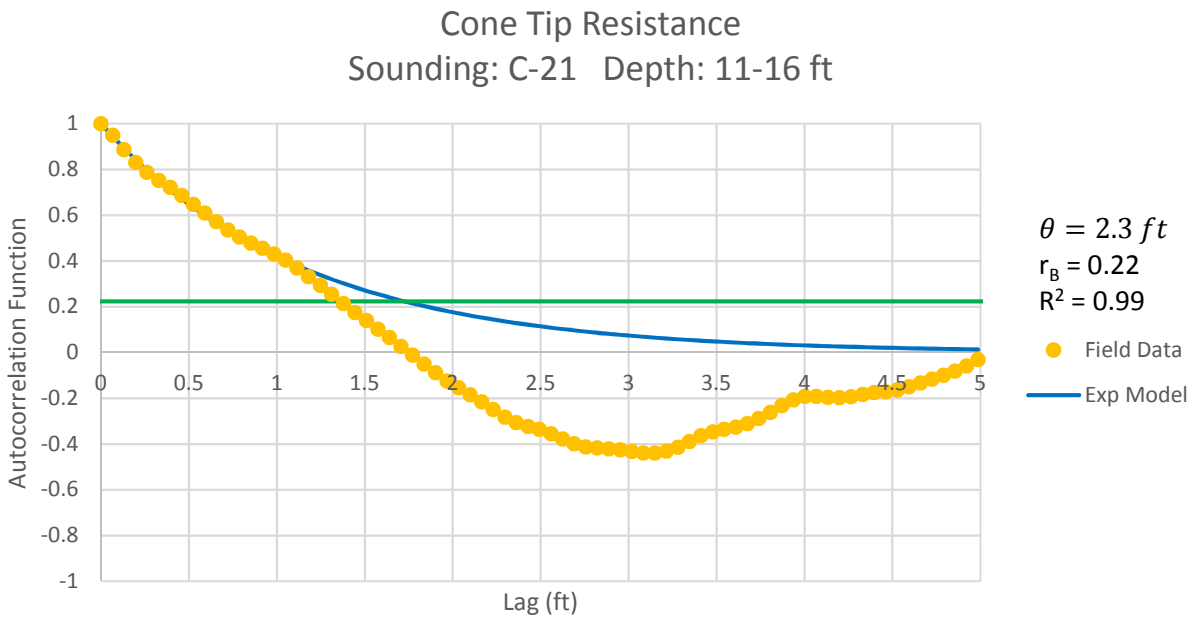

Figure B - 17: Estimation of the Scale of Fluctuation, θ = 2.3 feet, for Cone Tip Resistance Data from Sounding C-21, "Clean sands to silty sands (6)" layer from 11 to 16 feet depth.

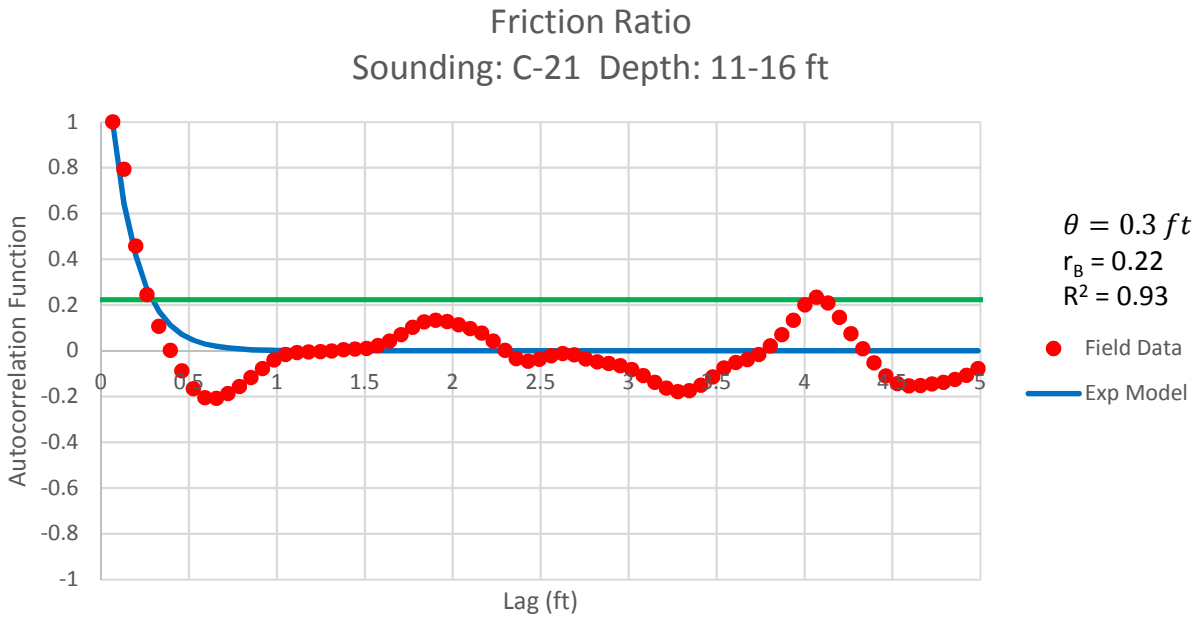

Figure B - 18: Estimation of the Scale of Fluctuation, θ = 0.3 feet, for Friction Ratio Data from Sounding C-21, "Clean sands to silty sands (6)" layer from 11 to 16 feet depth.

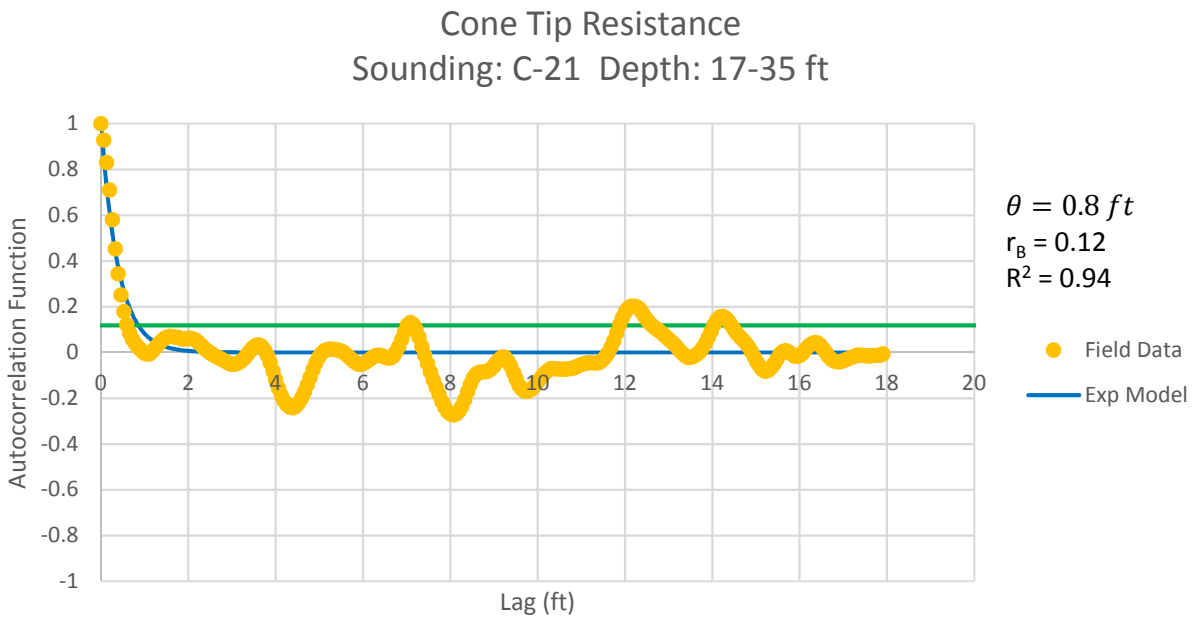

Figure B - 19: Estimation of the Scale of Fluctuation, $\theta = 0.8$ feet, for Cone Tip Resistance Data from Sounding C-21, "Clean sands to silty sands (6)" layer from 17 to 35 feet depth.

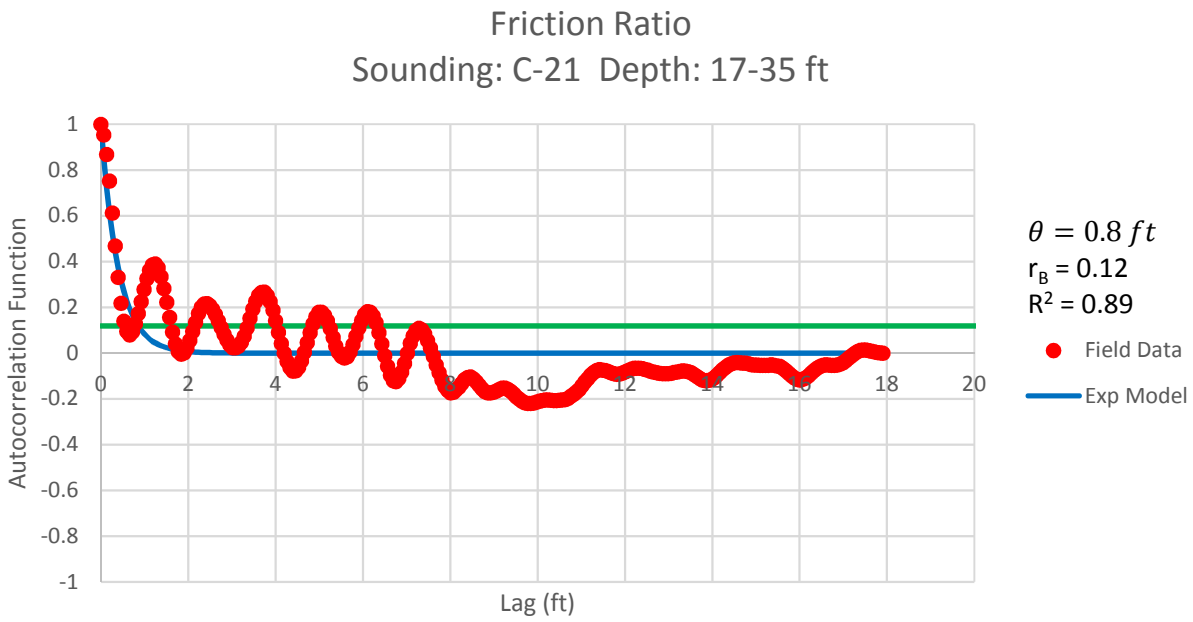

Figure B - 20: Estimation of the Scale of Fluctuation, $\theta = 0.8$ feet, for Friction Ratio Data from Sounding C-21, "Clean sands to silty sands (6)" layer from 17 to 35 feet depth. Data is a poor fit for the points greater than the Bartlett limit of 0.12; coefficient of determination, R^2, value is less 0.9. Therefore, these results were not included in final analysis.

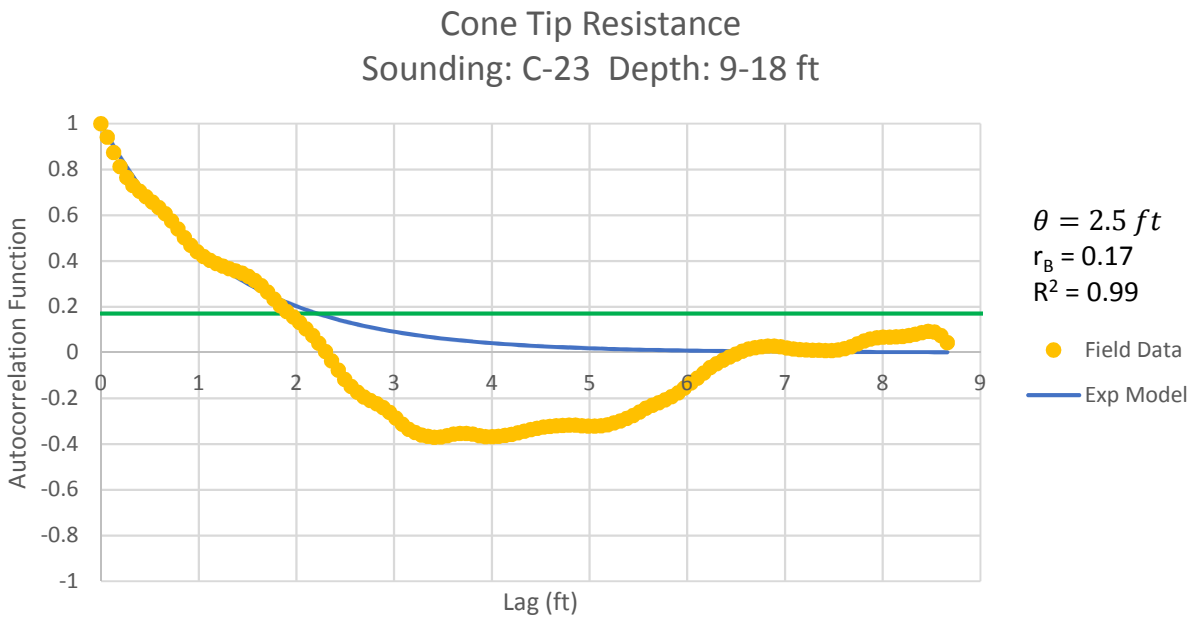

Figure B - 21: Estimation of the Scale of Fluctuation, θ = 2.5 feet, for Cone Tip Resistance Data from Sounding C-23, "Clean sands to silty sands (6)" layer from 9 to 18 feet depth.

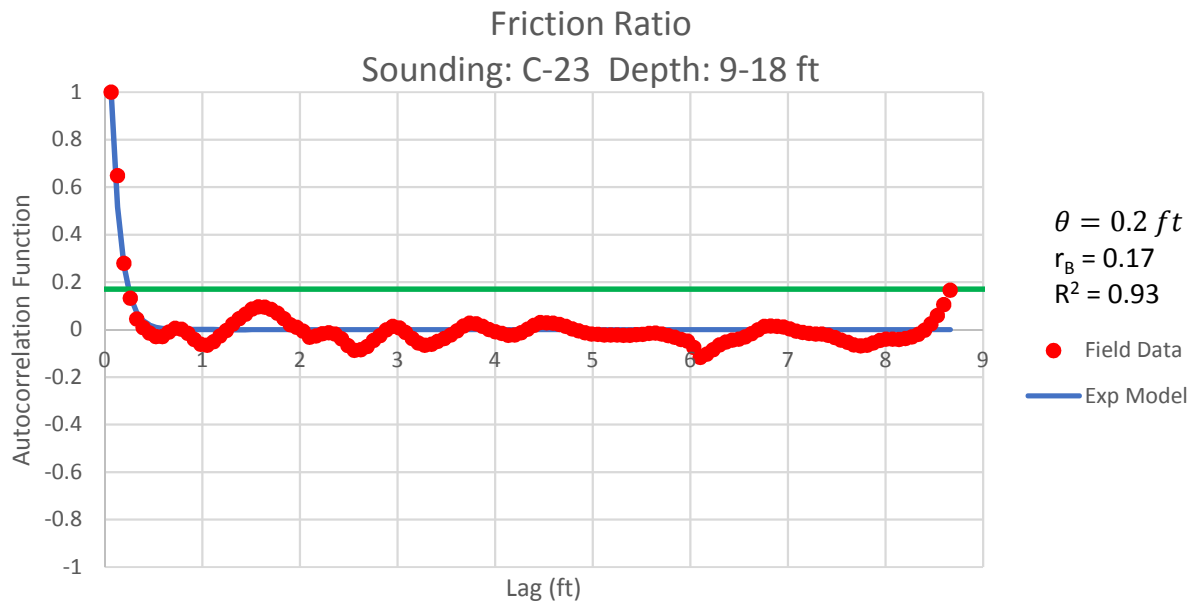

Figure B - 22: Estimation of the Scale of Fluctuation, θ = 0.2 feet, for Friction Ratio Data from Sounding C-23, "Clean sands to silty sands (6)" layer from 9 to 18 feet depth. Data is limited to only 3 points greater than the Bartlett limit of 0.17; therefore, these results were not included in final analysis.

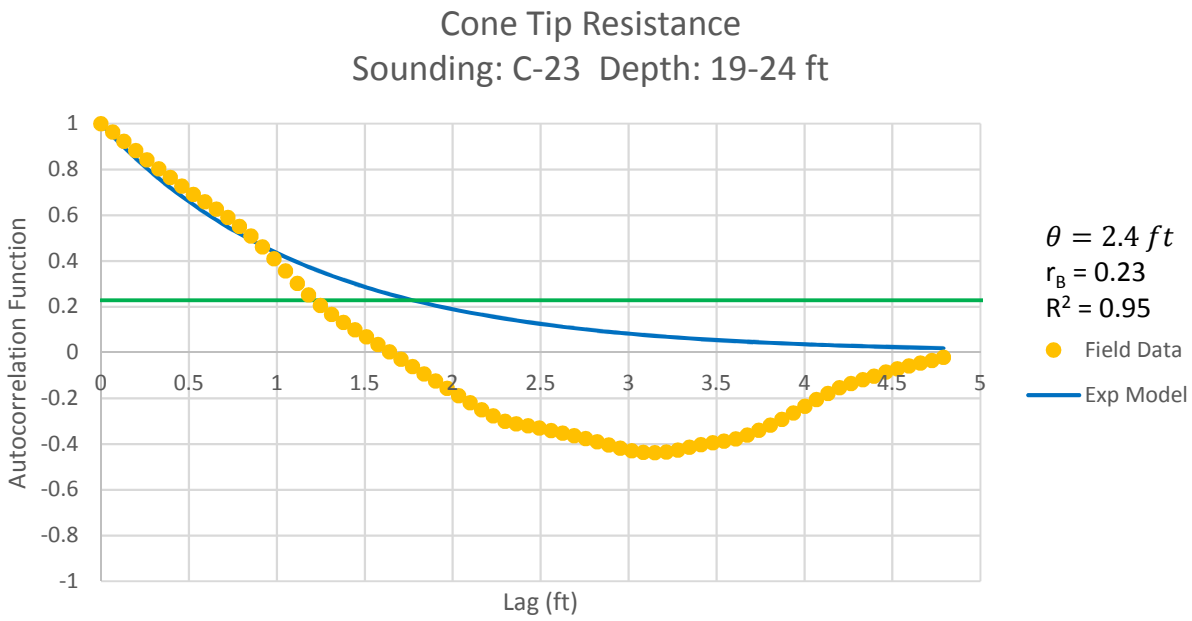

Figure B - 23: Estimation of the Scale of Fluctuation, θ = 2.4 feet, for Cone Tip Resistance Data from Sounding C-23, "Clean sands to silty sands (6)" layer from 19 to 24 feet depth.

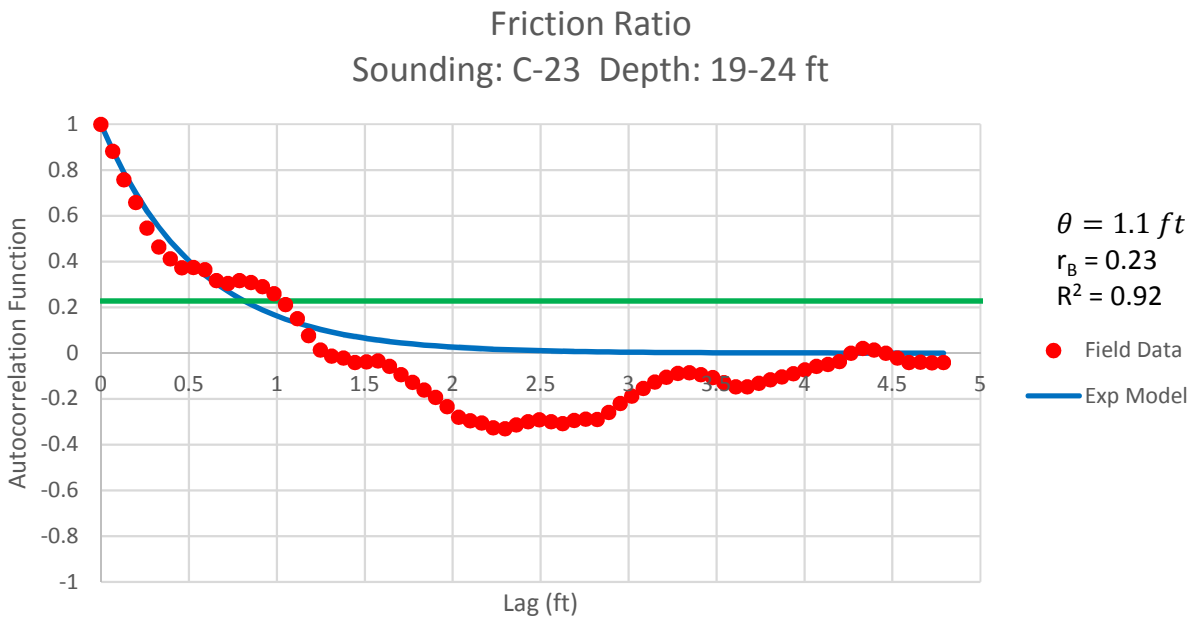

Figure B - 24: Estimation of the Scale of Fluctuation, θ = 1.1 feet, for Cone Tip Resistance Data from Sounding C-23, "Clean sands to silty sands (6)" layer from 19 to 24 feet depth.

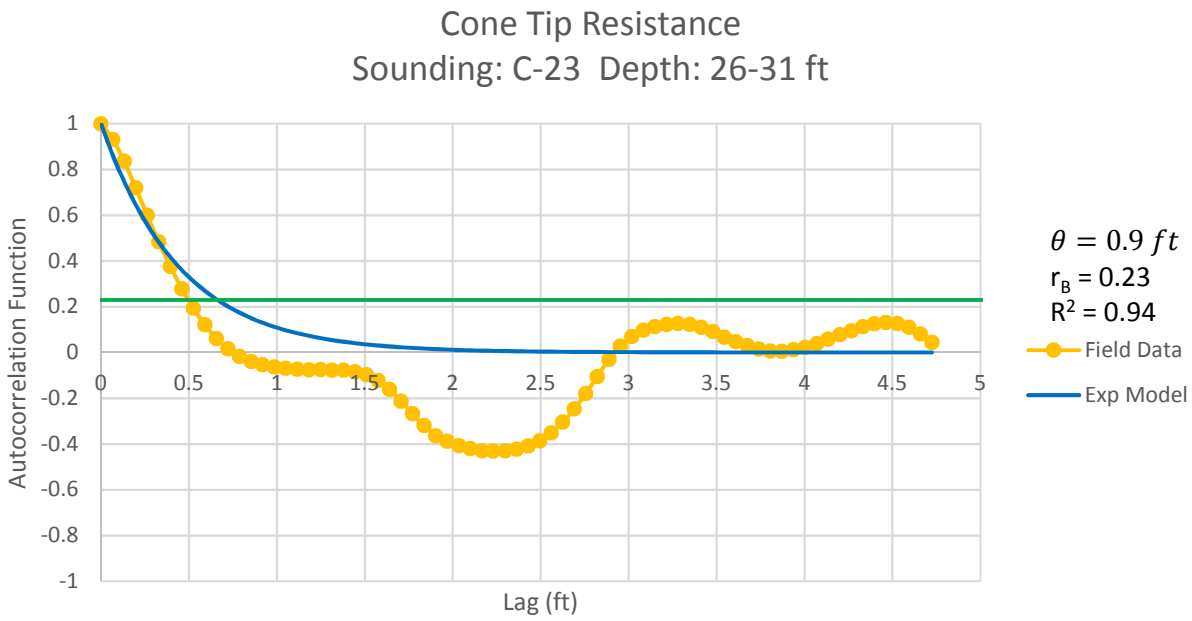

Figure B - 25: Estimation of the Scale of Fluctuation, $\theta = 0.9$ feet, for Cone Tip Resistance Data from Sounding C-23, "Clean sands to silty sands (6)" layer from 26 to 31 feet depth.

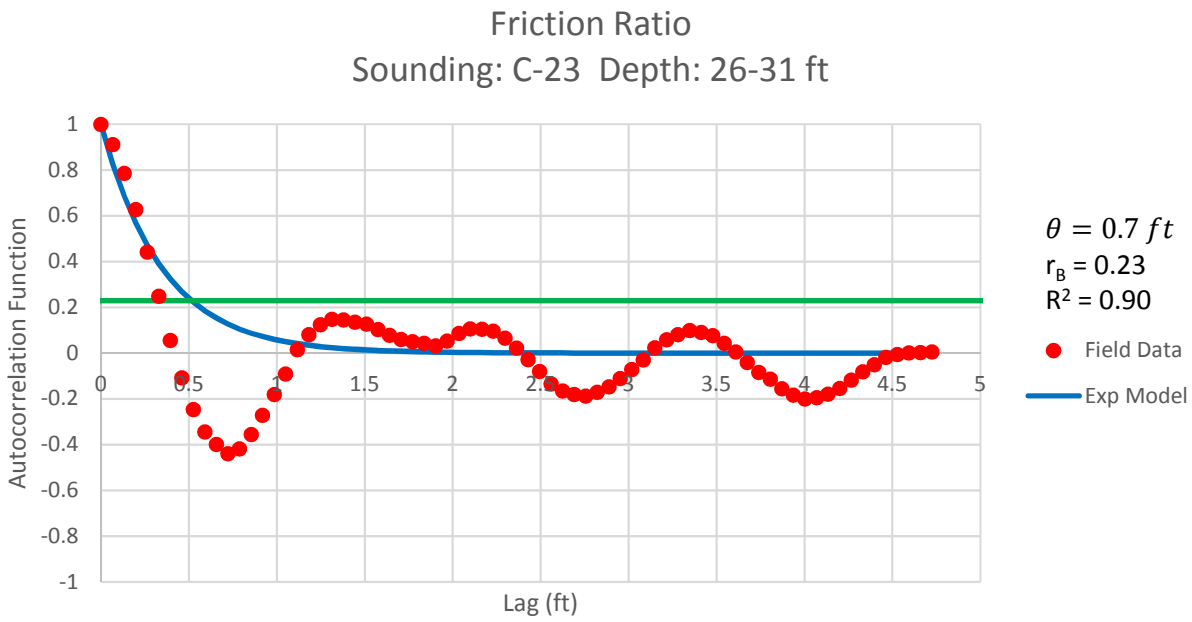

Figure B - 26: Estimation of the Scale of Fluctuation, $\theta = 0.7$ feet, for Friction Ratio Data from Sounding C-23, "Clean sands to silty sands (6)" layer from 26 to 31 feet depth.

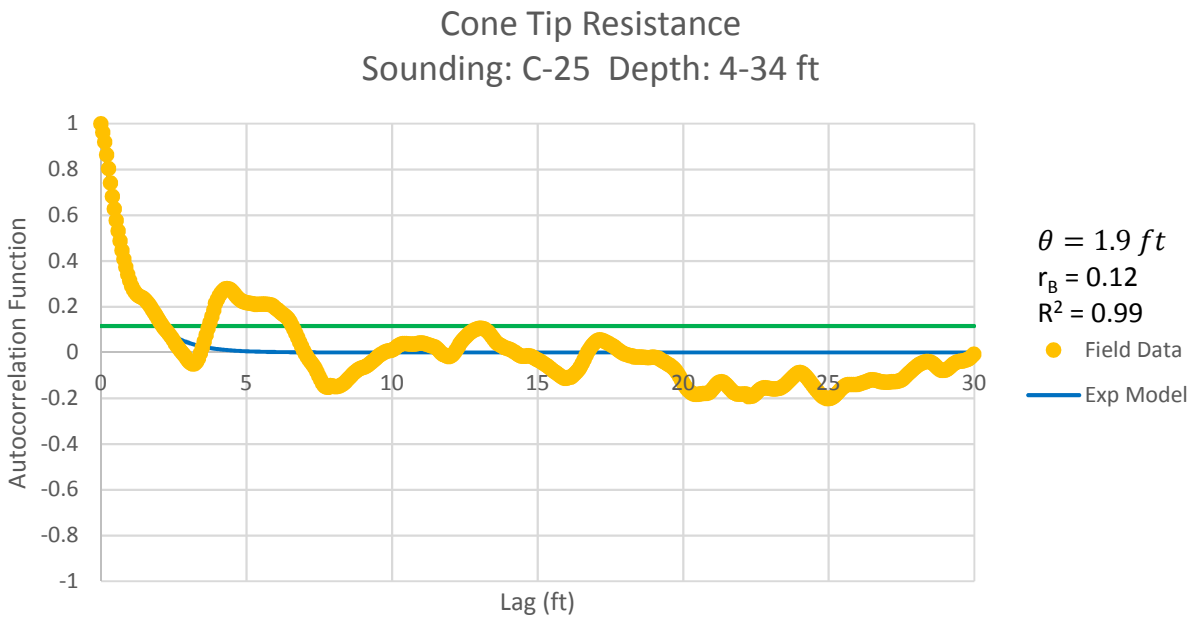

Figure B - 27: Estimation of the Scale of Fluctuation, $\theta = 1.9$ feet, for Cone Tip Resistance Data from Sounding C-25, "Clean sands to silty sands (6)" layer from 4 to 34 feet depth.

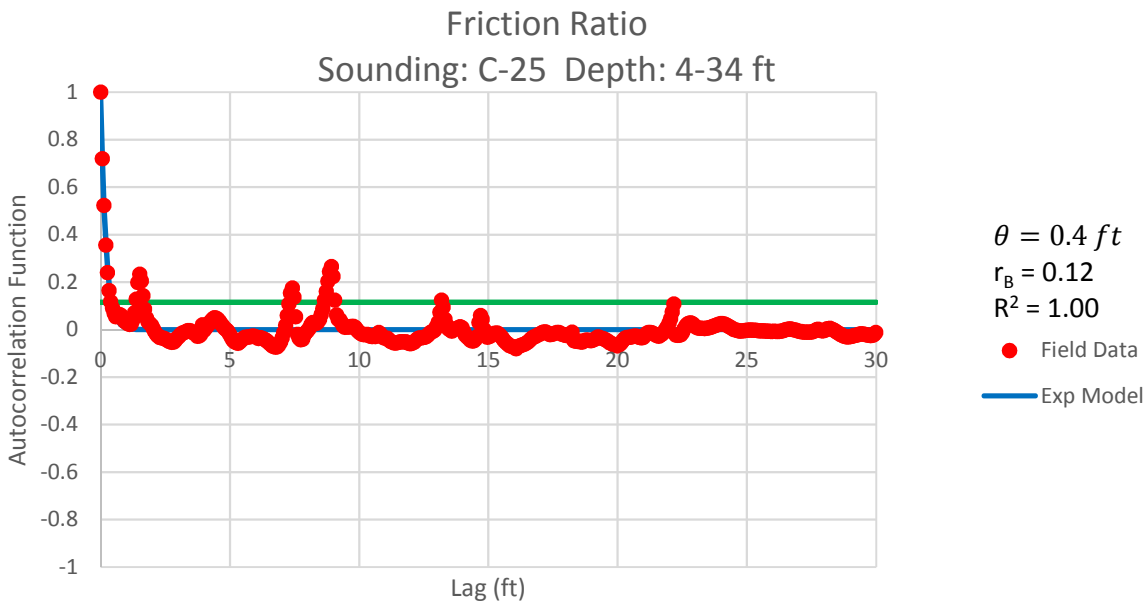

Figure B - 28: Estimation of the Scale of Fluctuation, $\theta = 0.4$ feet, for Friction Ratio Data from Sounding C-25, "Clean sands to silty sands (6)" layer from 4 to 34 feet depth.

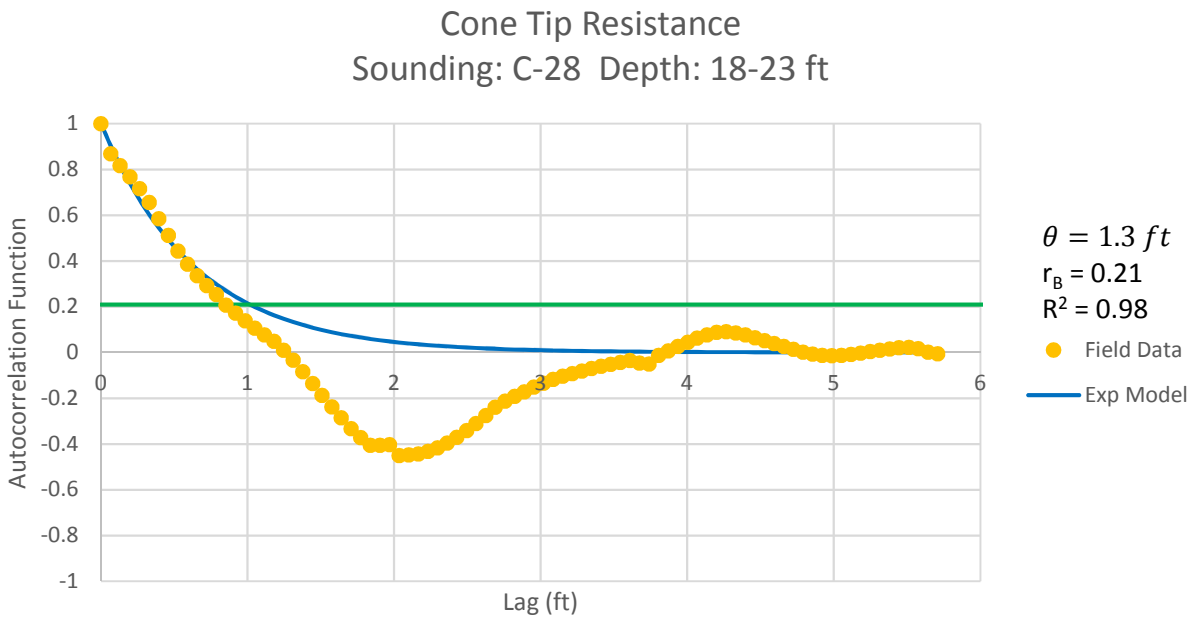

Figure B - 29: Estimation of the Scale of Fluctuation, θ = 1.3 feet, for Cone Tip Resistance Data from Sounding C-28, "Clean sands to silty sands (6)" layer from 18 to 23 feet depth.

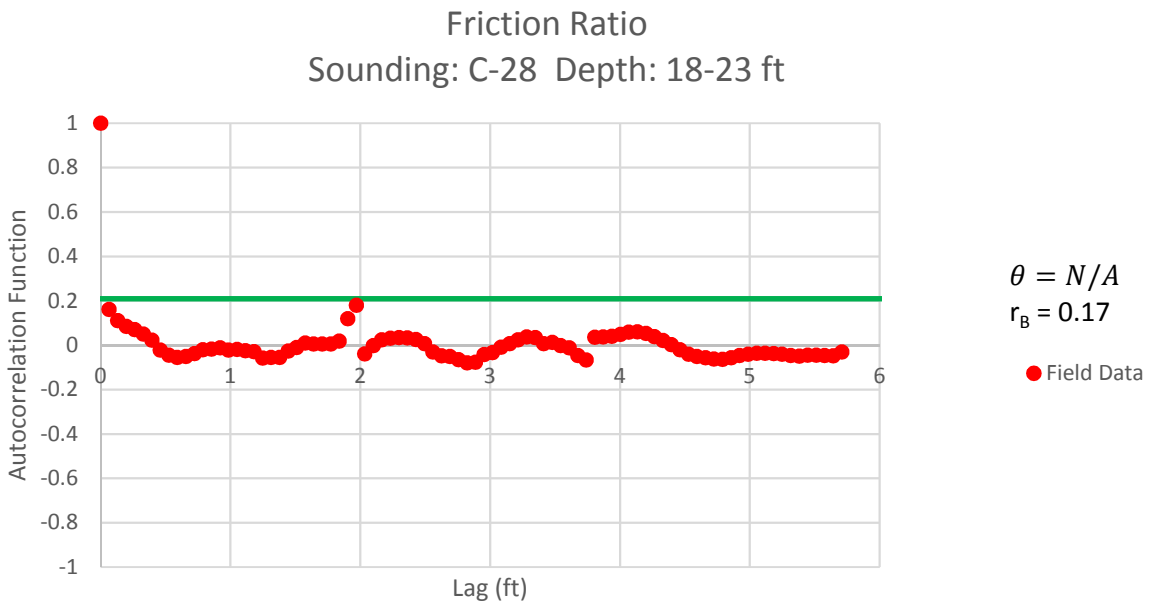

Figure B - 30: Estimation of the Scale of Fluctuation, θ, for Friction Ratio Data from Sounding C-28, "Clean sands to silty sands (6)" layer from 18 to 23 feet depth. Data is limited to only 1 point greater than the Bartlett limit of 0.17; therefore, θ could not be estimated, and these results were not included in final analysis.

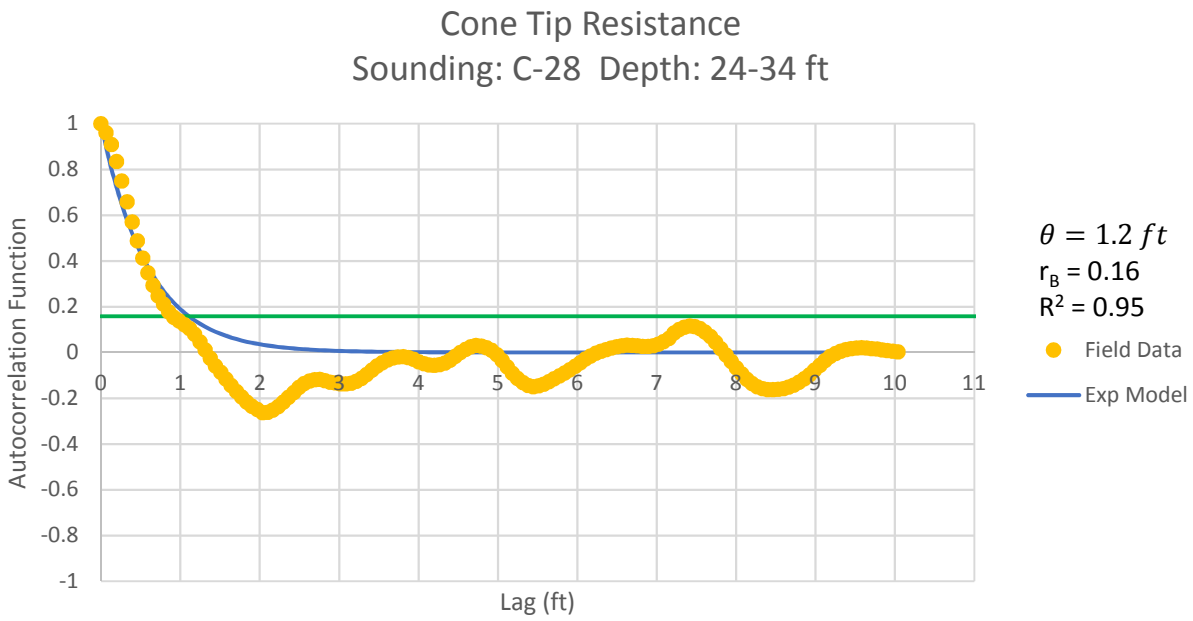

Figure B - 31: Estimation of the Scale of Fluctuation, $\theta = 1.2$ feet, for Cone Tip Resistance Data from Sounding C-28, "Clean sands to silty sands (6)" layer from 24 to 34 feet depth.

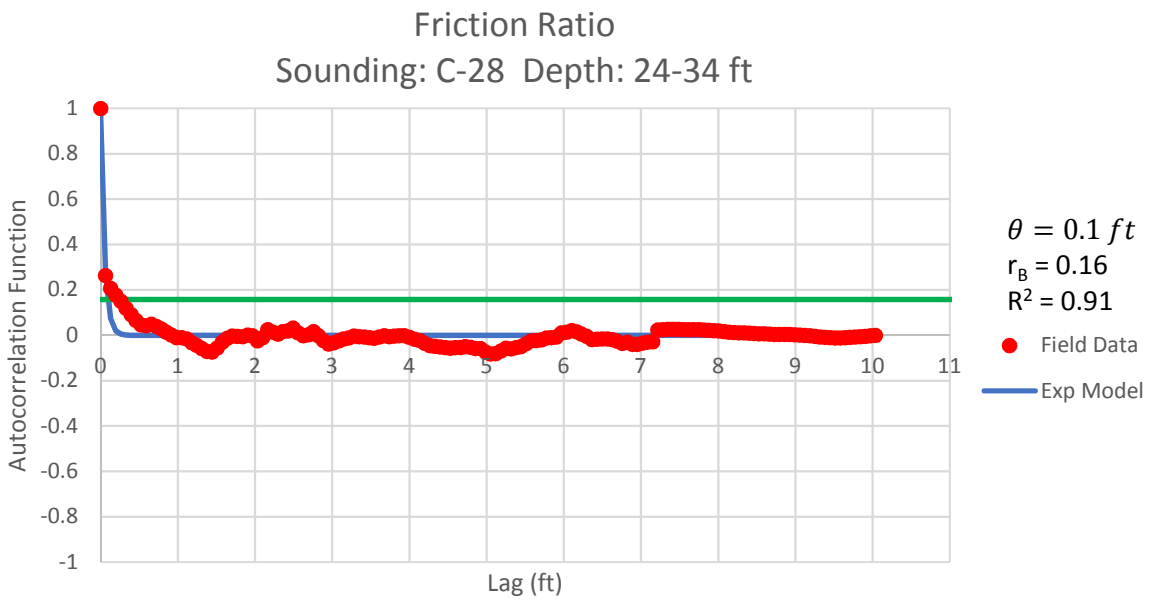

Figure B - 32: Estimation of the Scale of Fluctuation, $\theta = 0.1$ feet, for Friction Ratio Data from Tip Sounding C-28, "Clean sands to silty sands (6)" layer from 24 to 34 feet depth.

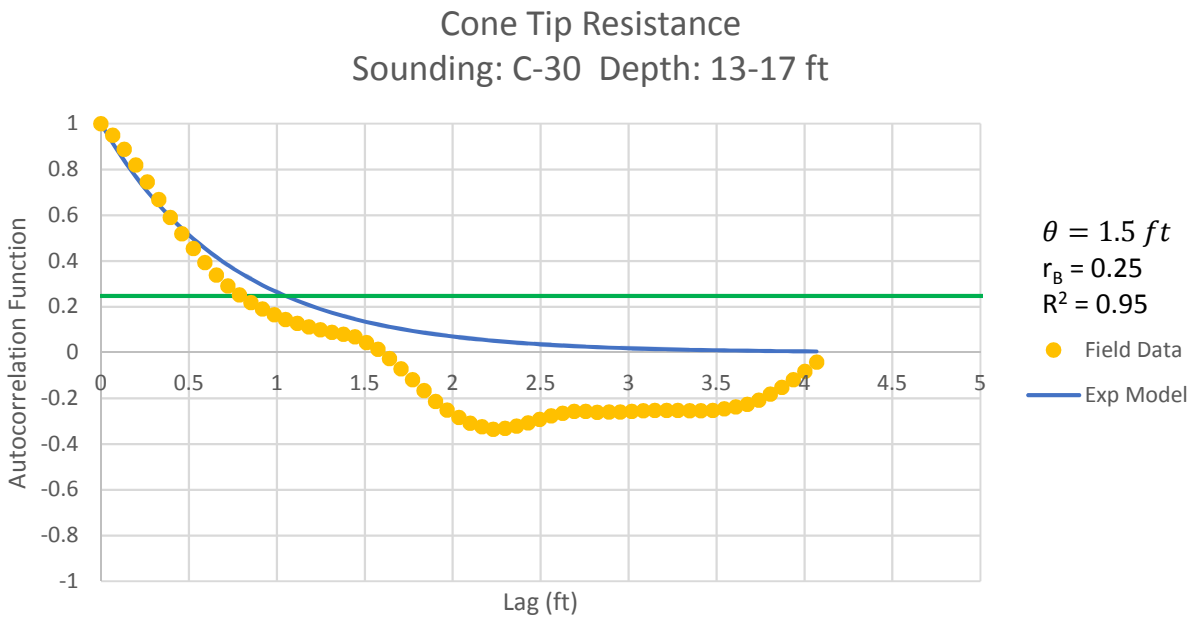

Figure B - 33: Estimation of the Scale of Fluctuation, $\theta = 1.5$ feet, for Cone Tip Resistance Data from Sounding C-30, "Clean sands to silty sands (6)" layer from 13 to 17 feet depth.

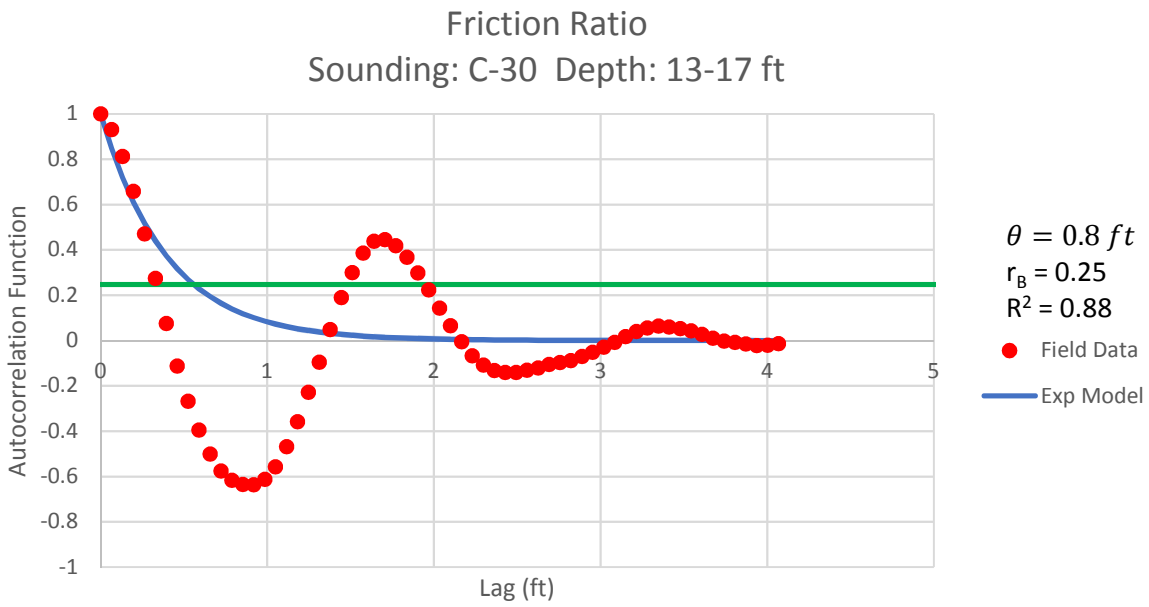

Figure B - 34: Estimation of the Scale of Fluctuation, $\theta = 0.8$ feet, for Friction Ratio Data from Sounding C-30, "Clean sands to silty sands (6)" layer from 13 to 17 feet depth. Data is a poor fit for the points greater than the Bartlett limit of 0.25; coefficient of determination, R^2, value is less 0.9. Therefore, these results were not included in final analysis.

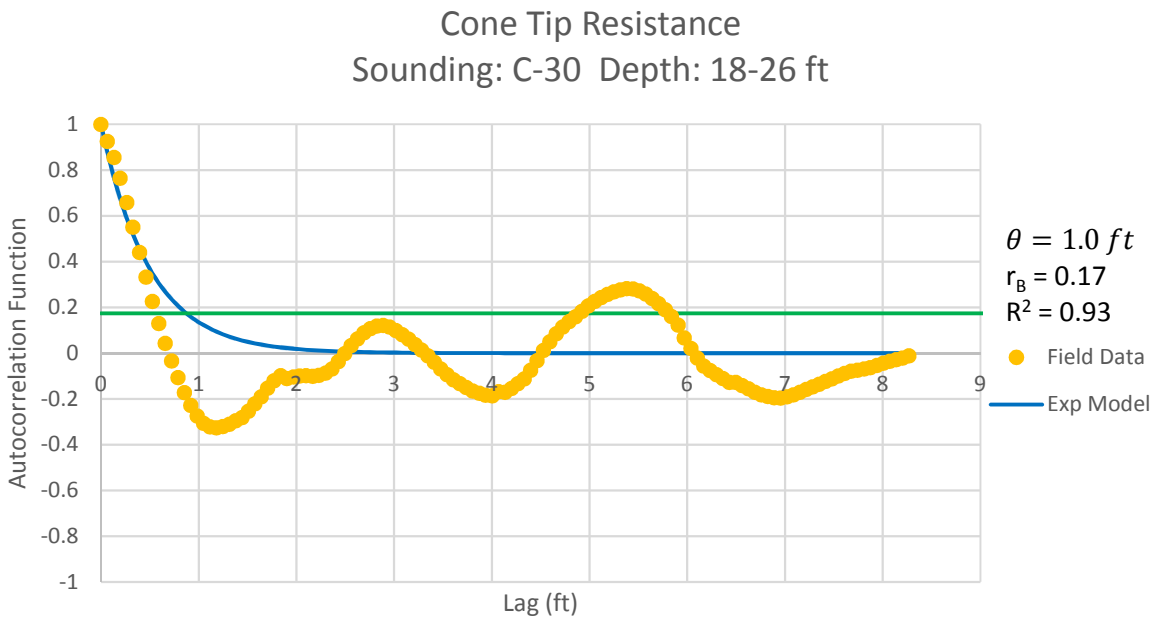

Figure B - 35: Estimation of the Scale of Fluctuation, θ = 1.0 feet, for Cone Tip Resistance Data from Sounding C-30, "Clean sands to silty sands (6)" layer from 18 to 26 feet depth.

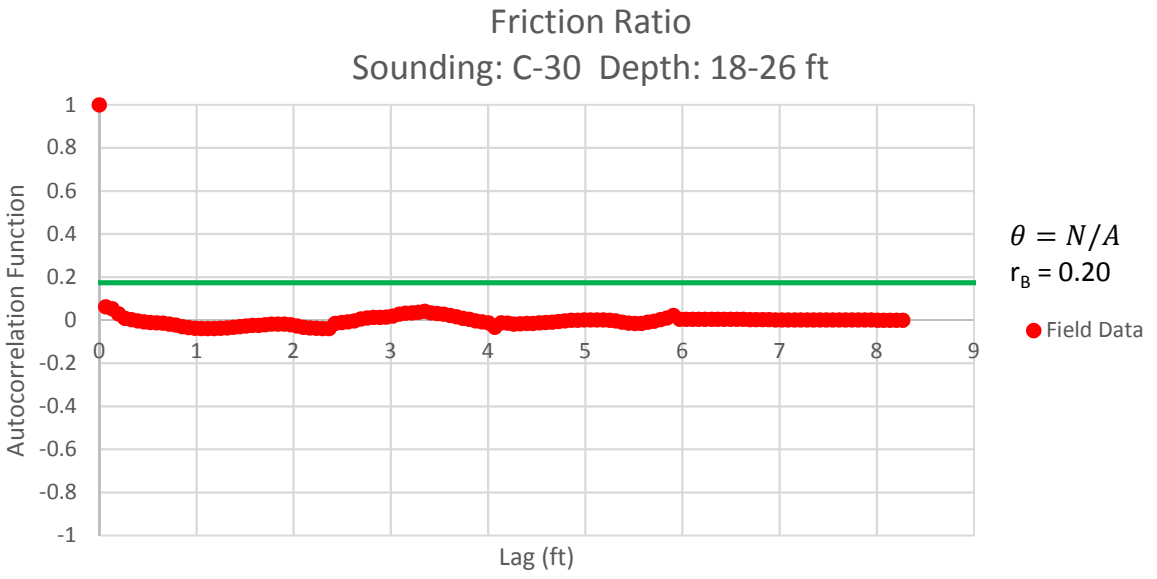

Figure B - 36: Estimation of the Scale of Fluctuation, θ, for Friction Ratio Data from Sounding C-30, "Clean sands to silty sands (6)" layer from 18 to 26 feet depth. Data is limited to only 1 point greater than the Bartlett limit of 0.20; therefore, θ could not be estimated, and these results were not included in final analysis.

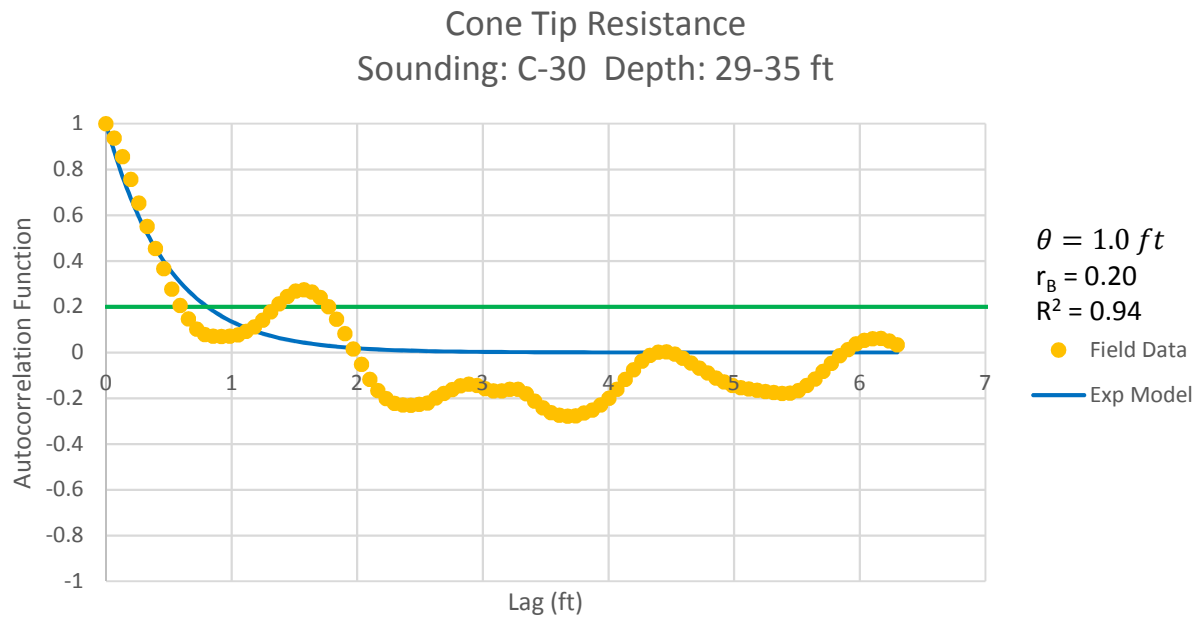

Figure B - 37: Estimation of the Scale of Fluctuation, θ = 1.0 feet, for Cone Tip Resistance Data from Sounding C-30, "Clean sands to silty sands (6)" layer from 29 to 35 feet depth.

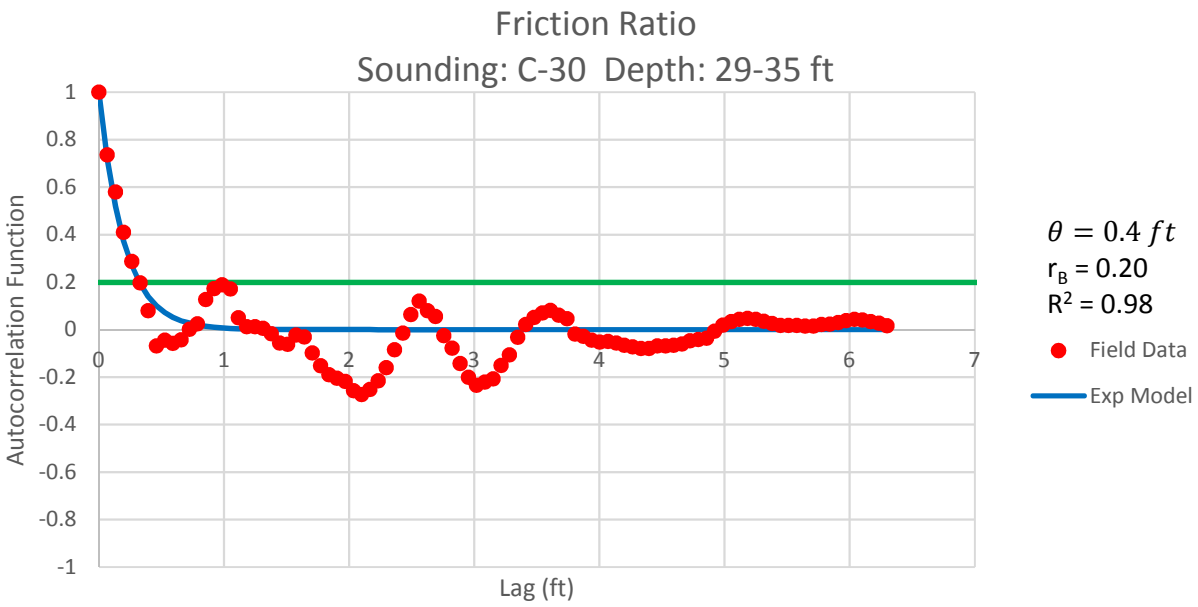

Figure B - 38: Estimation of the Scale of Fluctuation, θ = 0.4 feet, for Friction Ratio Data from Sounding C-30, "Clean sands to silty sands (6)" layer from 29 to 35 feet depth.

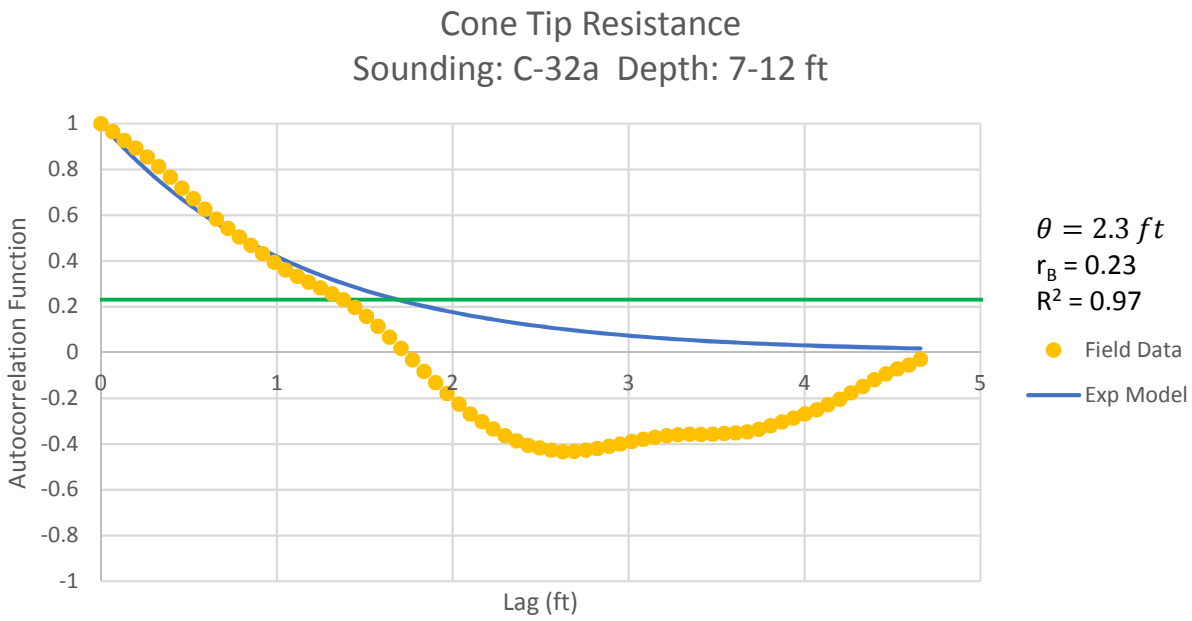

Figure B - 39: Estimation of the Scale of Fluctuation, $\theta = 2.3$ feet, for Cone Tip Resistance Data from Sounding C-32a, "Clean sands to silty sands (6)" layer from 7 to 12 feet depth.

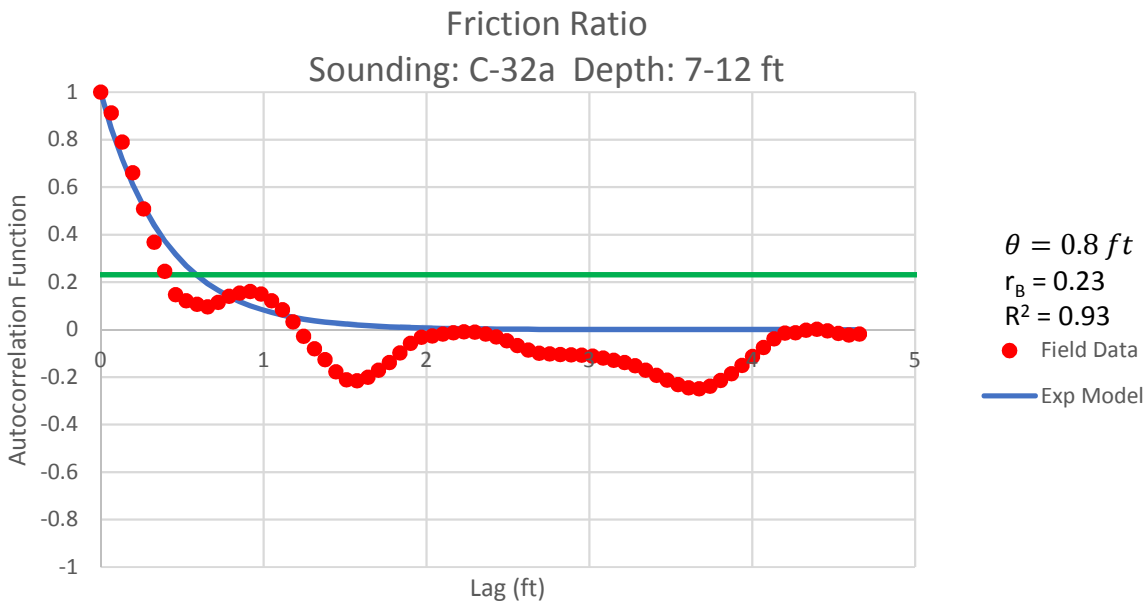

Figure B - 40: Estimation of the Scale of Fluctuation, $\theta = 0.8$ feet, for Friction Ratio Data from Sounding C-32a, "Clean sands to silty sands (6)" layer from 7 to 12 feet depth.

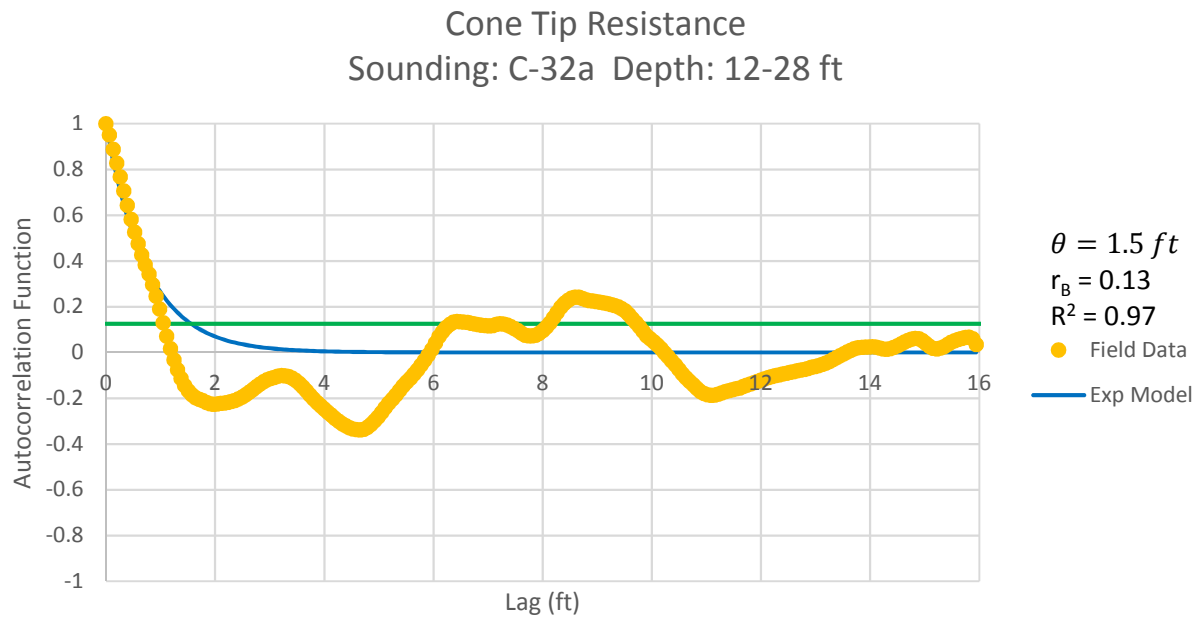

Figure B - 41: Estimation of the Scale of Fluctuation, $\theta = 1.5$ feet, for Cone Tip Resistance Data from Sounding C-32a, "Clean sands to silty sands (6)" layer from 12 to 28 feet depth.

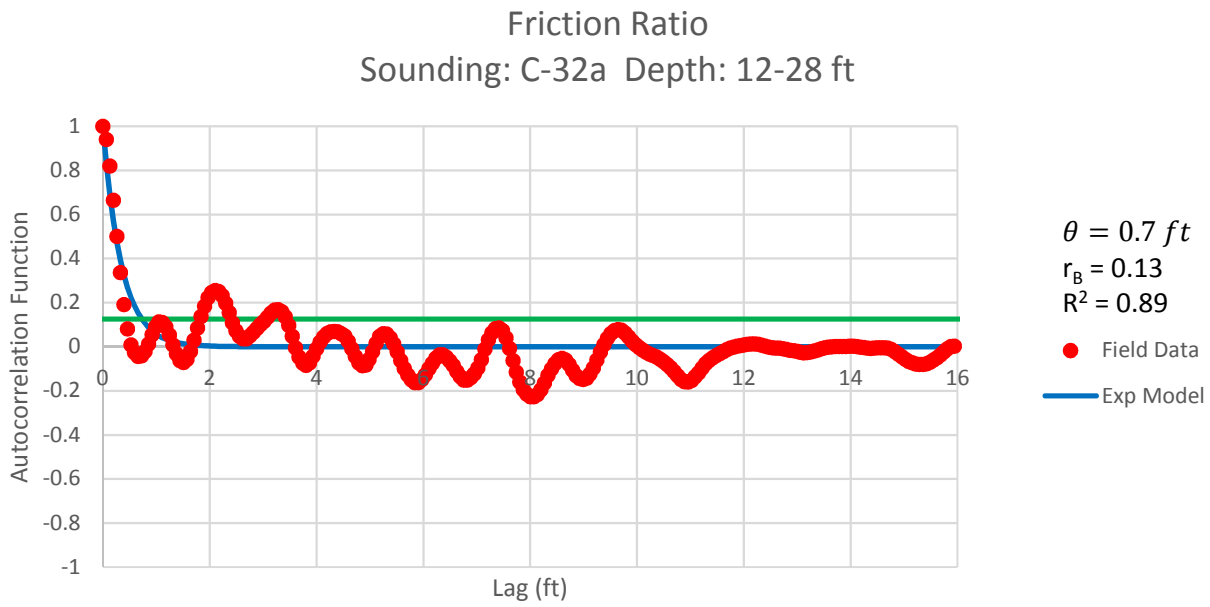

Figure B - 42: Estimation of the Scale of Fluctuation, $\theta = 0.7$ feet, for Friction Ratio Data from Sounding C-32a, "Clean sands to silty sands (6)" layer from 12 to 28 feet depth. Data is a poor fit for the points greater than the Bartlett limit of 0.13; coefficient of determination, R^2, value is less 0.9. Therefore, these results were not included in final analysis.

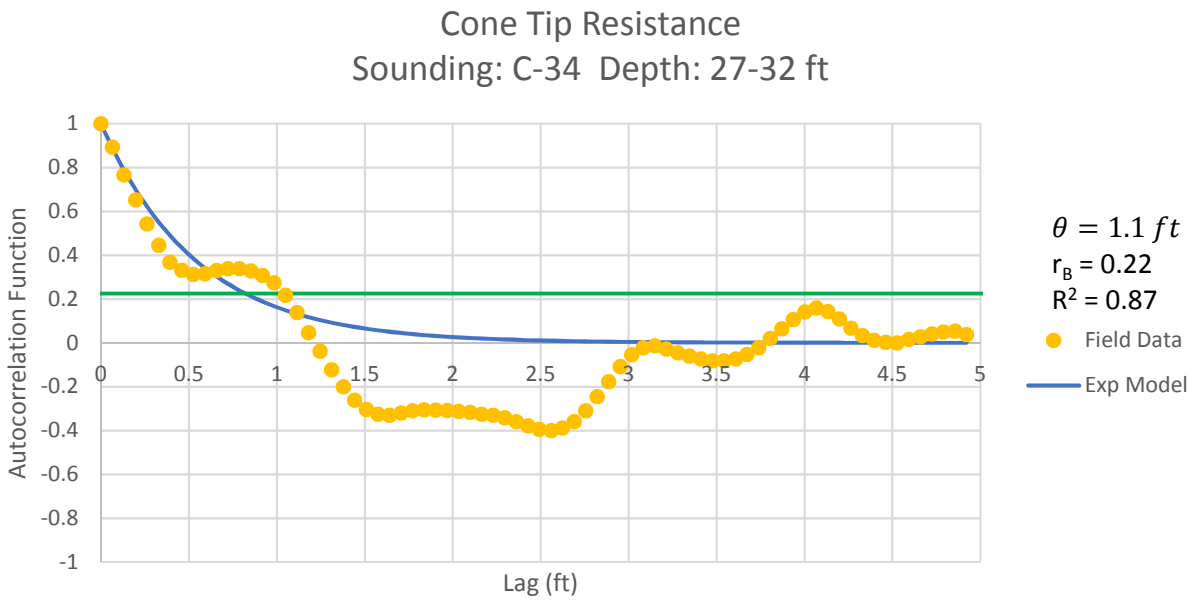

Figure B - 43: Estimation of the Scale of Fluctuation, $\theta = 1.1$ feet, for Cone Tip Resistance Data from Sounding C-34, "Clean sands to silty sands (6)" layer from 27 to 32 feet depth. Data is a poor fit for the points greater than the Bartlett limit of 0.22; coefficient of determination, R^2, value is less 0.9. Therefore, these results were not included in final analysis.

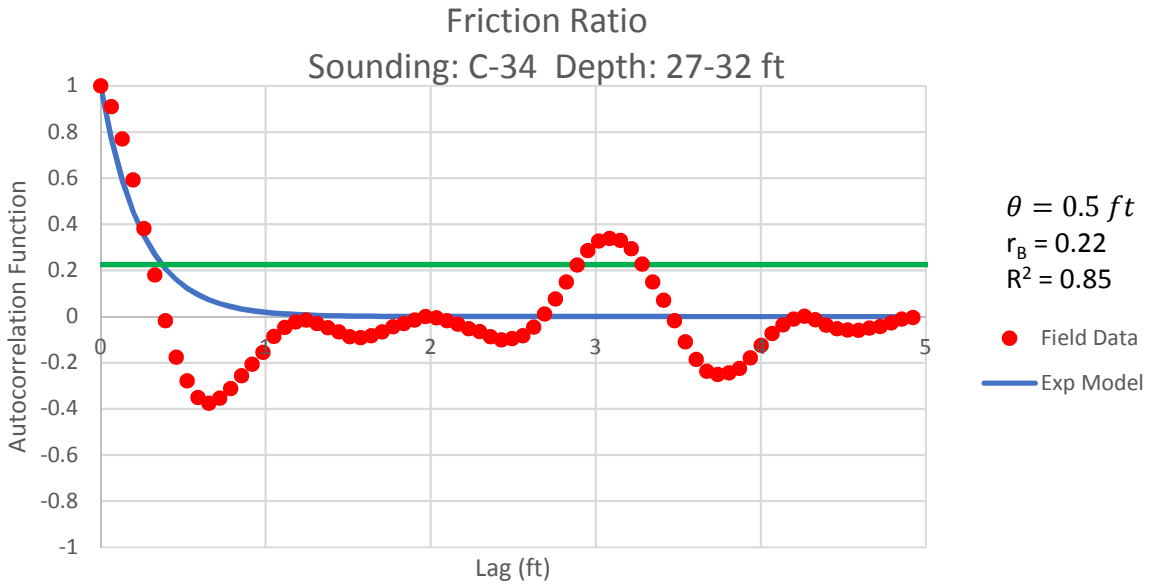

Figure B - 44: Estimation of the Scale of Fluctuation, $\theta = 0.5$ feet, for Friction Ratio Data from Sounding C-34, "Clean sands to silty sands (6)" layer from 27 to 32 feet depth. Data is a poor fit for the points greater than the Bartlett limit of 0.22; coefficient of determination, R^2, value is less 0.9. Therefore, these results were not included in final analysis.

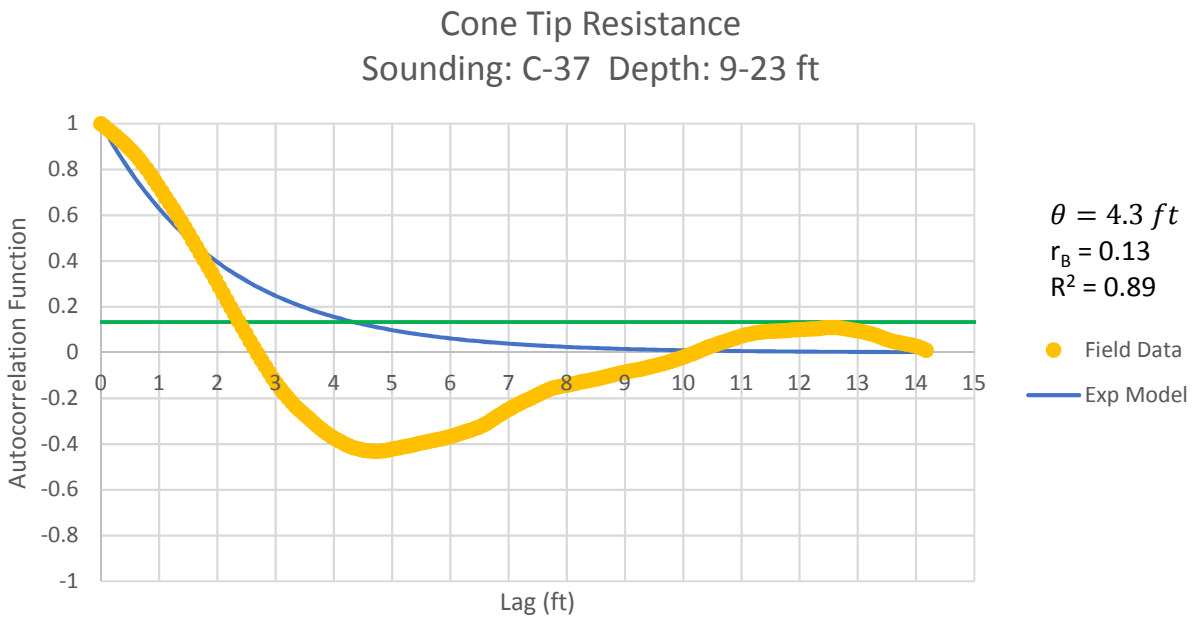

Figure B - 45: Estimation of the Scale of Fluctuation, $\theta = 4.3$ feet, for Cone Tip Resistance Data from Sounding C-37, "Clean sands to silty sands (6)" layer from 9 to 23 feet depth. Data is a poor fit for the points greater than the Bartlett limit of 0.13; coefficient of determination, R^2 value is less than 0.9. Therefore, these results were not included in final analysis.

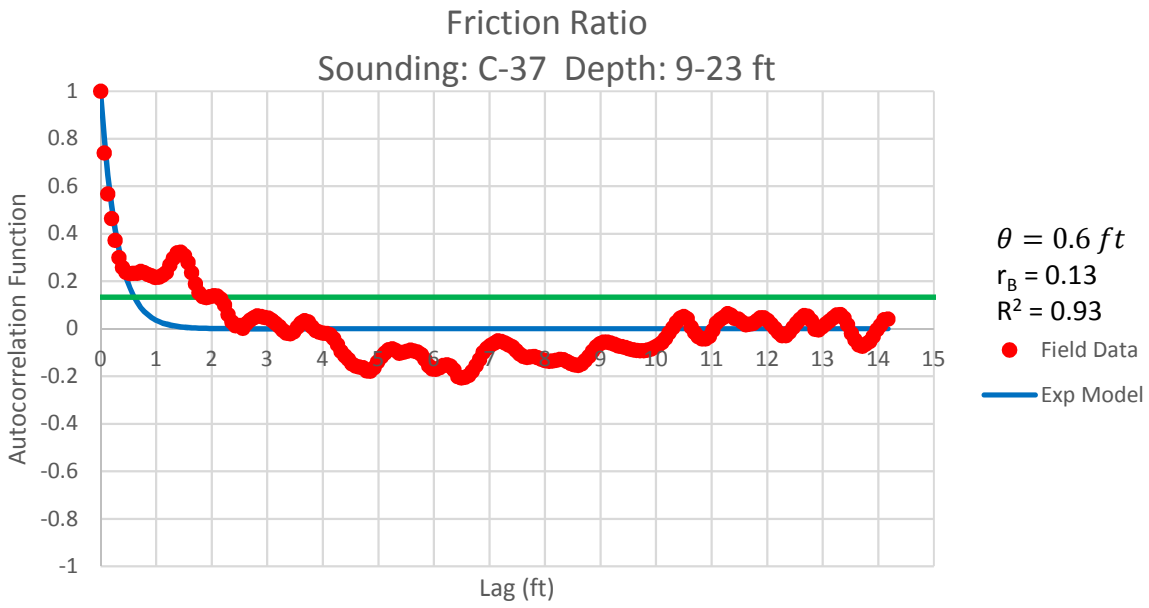

Figure B - 46: Estimation of the Scale of Fluctuation, $\theta = 0.6$ feet, for Friction Ratio Data from Sounding C-37, "Clean sands to silty sands (6)" layer from 9 to 23 feet depth.

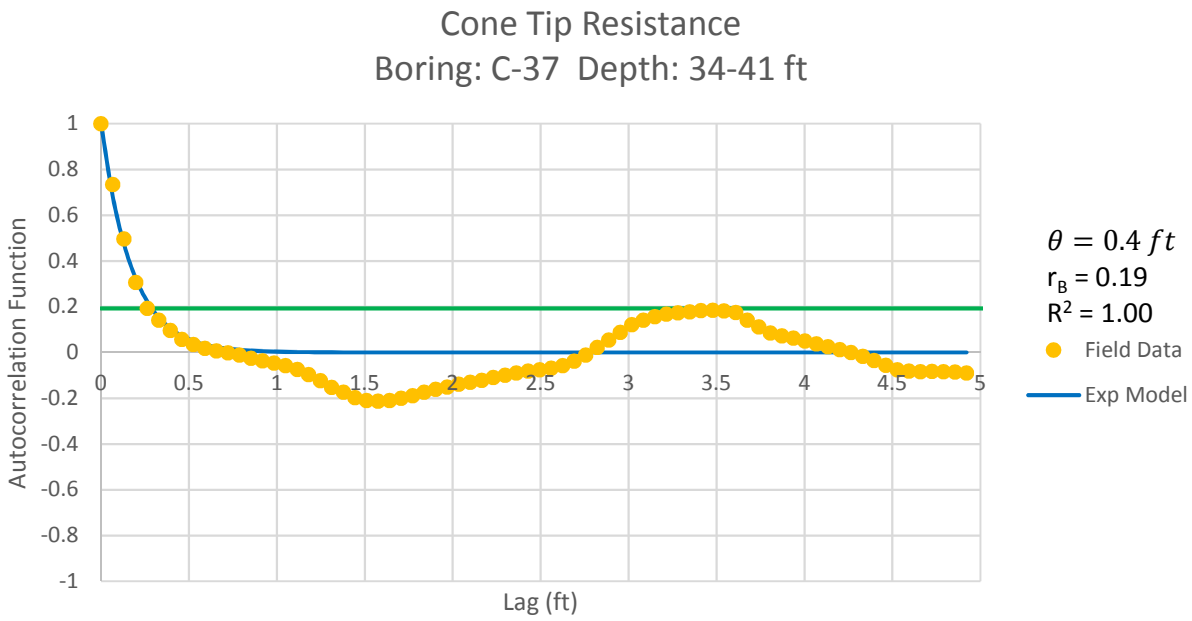

Figure B - 47: Estimation of the Scale of Fluctuation, $\theta = 0.4$ feet, for Cone Tip Resistance Data from Sounding C-37, "Clean sands to silty sands (6)" layer from 34 to 41 feet depth.

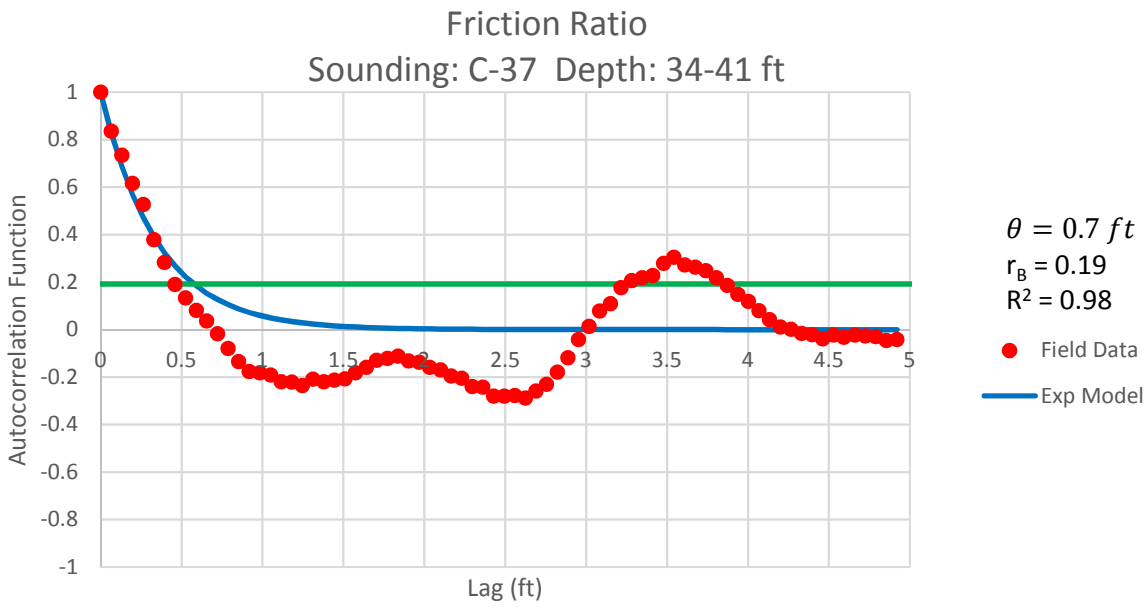

Figure B - 48: Estimation of the Scale of Fluctuation, $\theta = 0.7$ feet, for Friction Ratio Data from Sounding C-37, "Clean sands to silty sands (6)" layer from 34 to 41 feet depth.

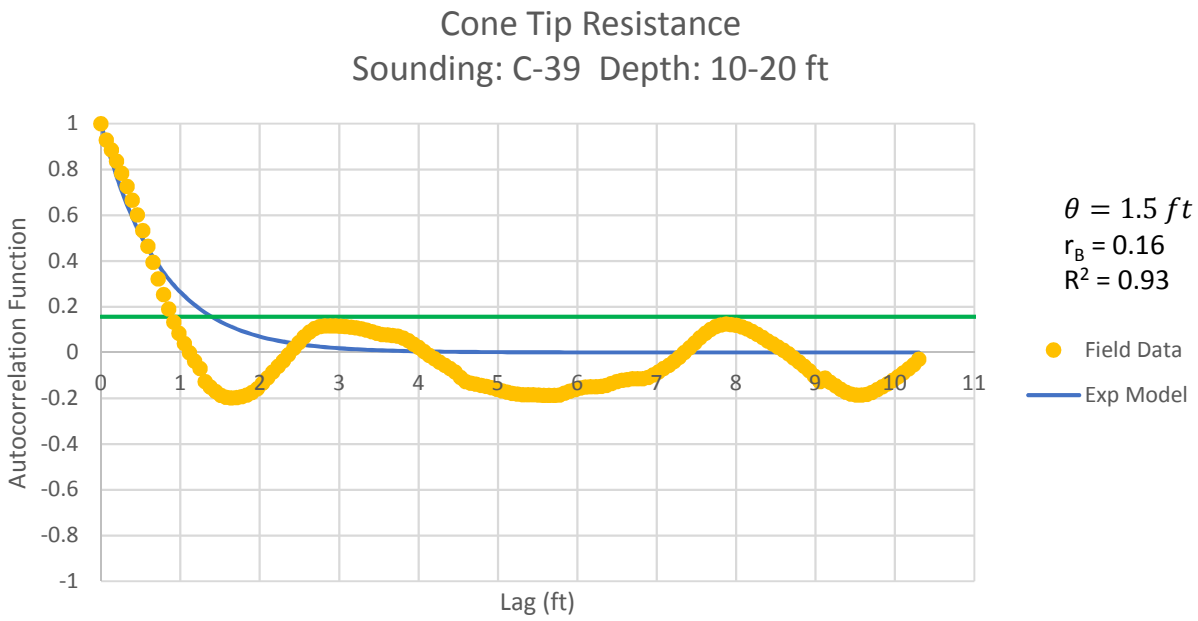

Figure B - 49: Estimation of the Scale of Fluctuation, θ = 1.5 feet, for Cone Tip Resistance Data from Sounding C-39, "Clean sands to silty sands (6)" layer from 10 to 20 feet depth.

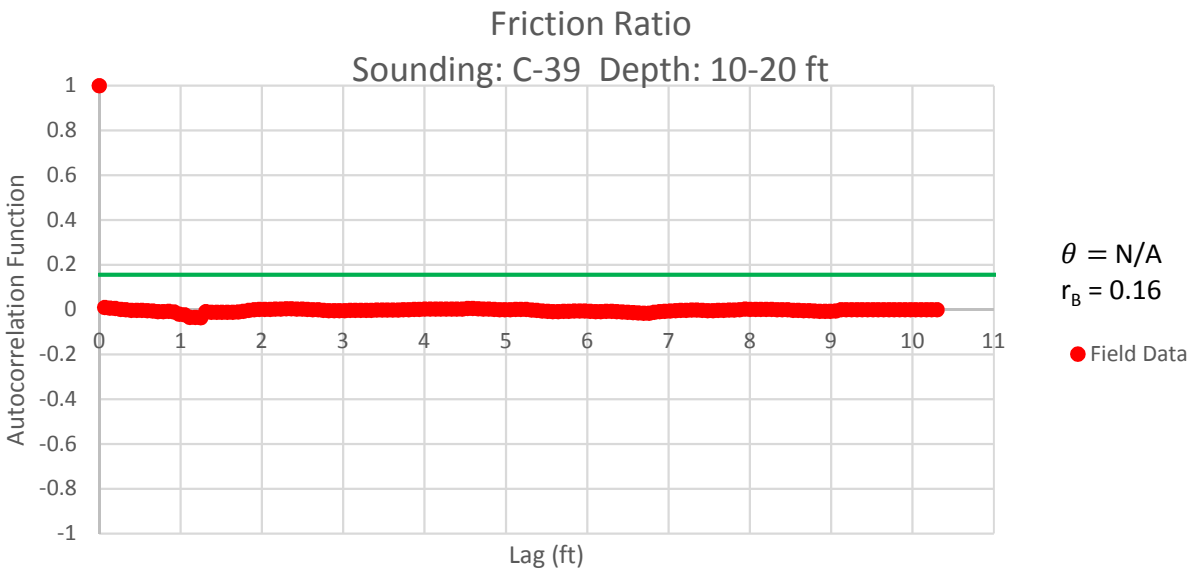

Figure B - 50: Estimation of the Scale of Fluctuation, θ, for Friction Ratio Data from Sounding C-39, "Clean sands to silty sands (6)" layer from 10 to 20 feet depth. Data is limited to only 1 point greater than the Bartlett limit of 0.16; therefore, θ could not be estimated, and these results were not included in final analysis.

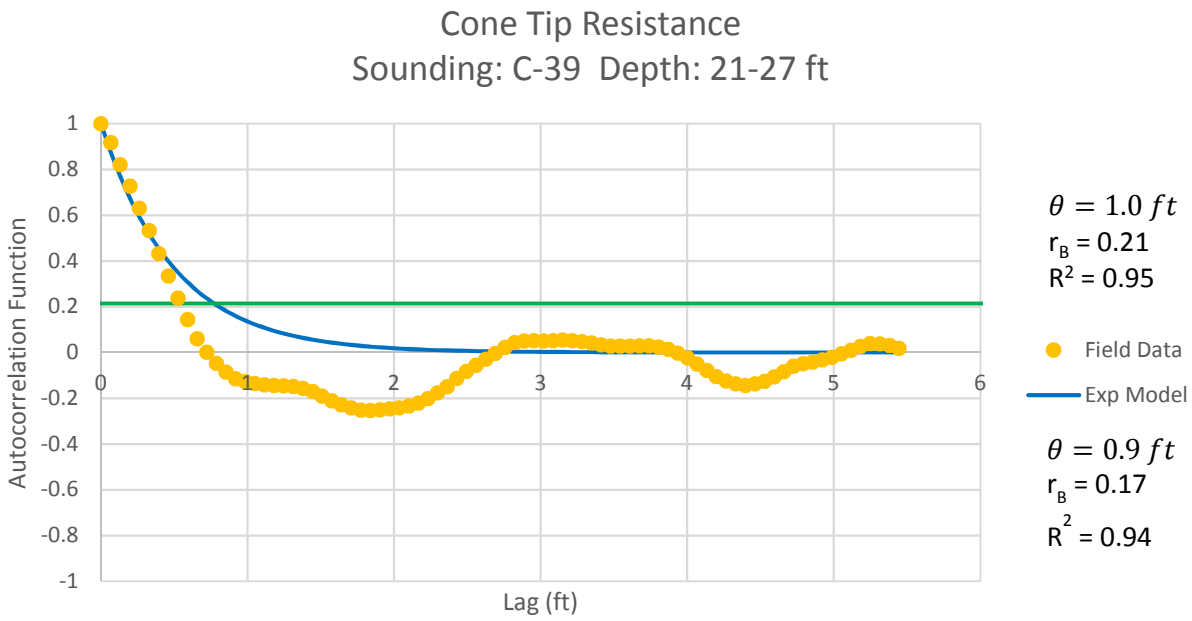

Figure B - 51: Estimation of the Scale of Fluctuation, $\theta = 1.0$ feet, for Cone Tip Resistance Data from Sounding C-39, "Clean sands to silty sands (6)" layer from 21 to 27 feet depth.

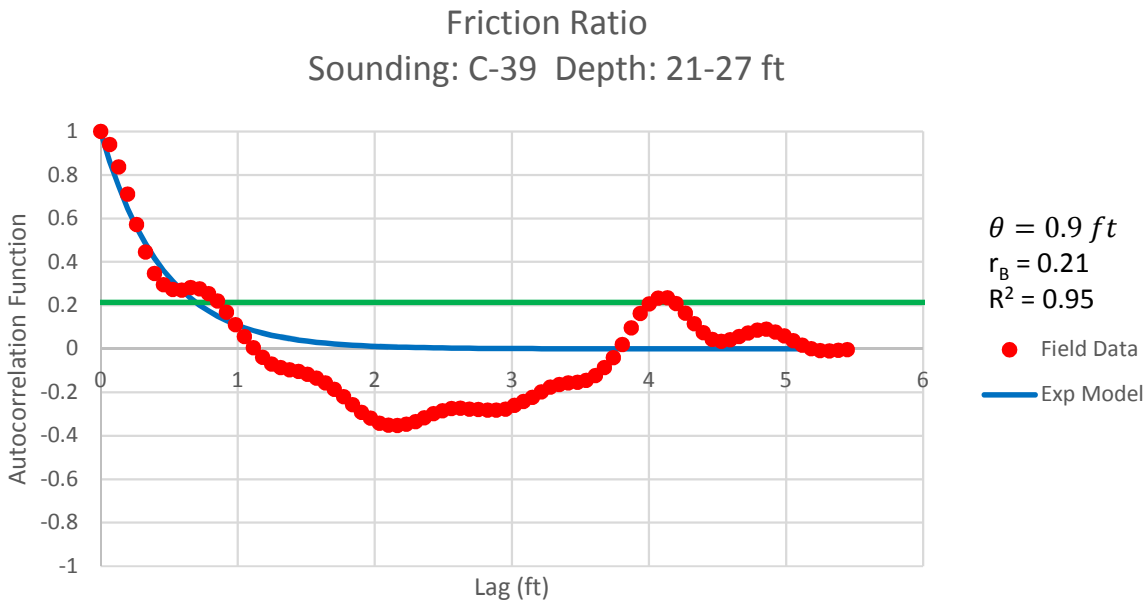

Figure B - 52: Estimation of the Scale of Fluctuation, $\theta = 0.9$ feet, for Friction Ratio Data from Sounding C-39, "Clean sands to silty sands (6)" layer from 21 to 27 feet depth.

$\theta = 2.2\ ft$
$r_B = 0.10$
$R^2 = 0.98$

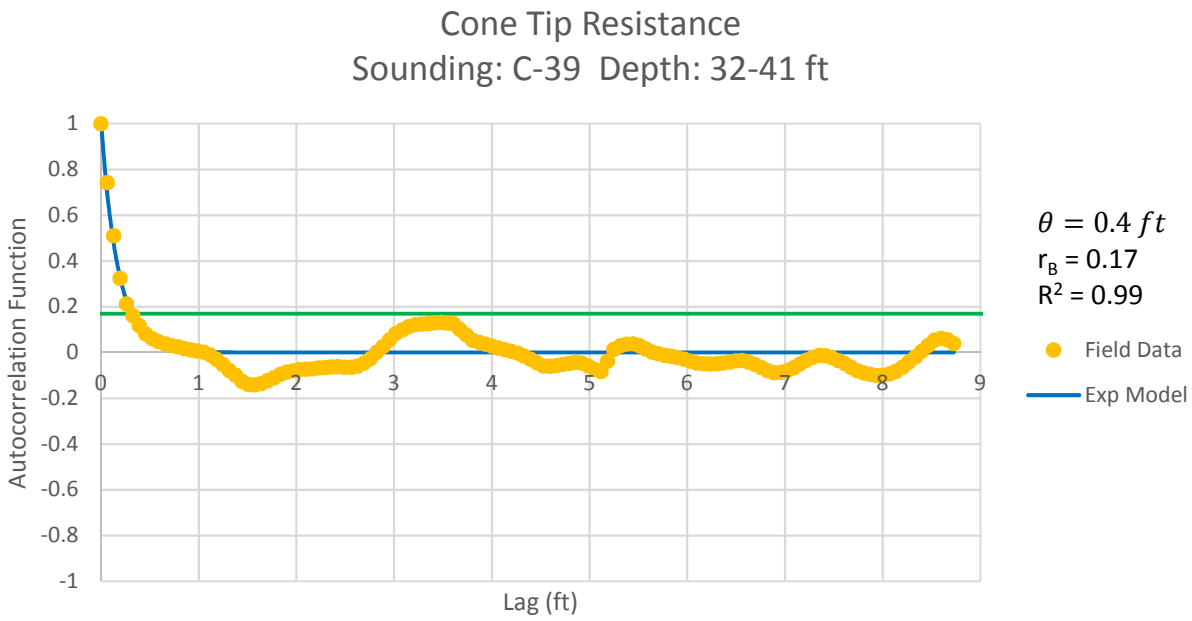

Figure B - 53: Estimation of the Scale of Fluctuation, $\theta = 0.4$ feet, for Cone Tip Resistance Data from Sounding C-39, "Clean sands to silty sands (6)" layer from 32 to 41 feet depth.

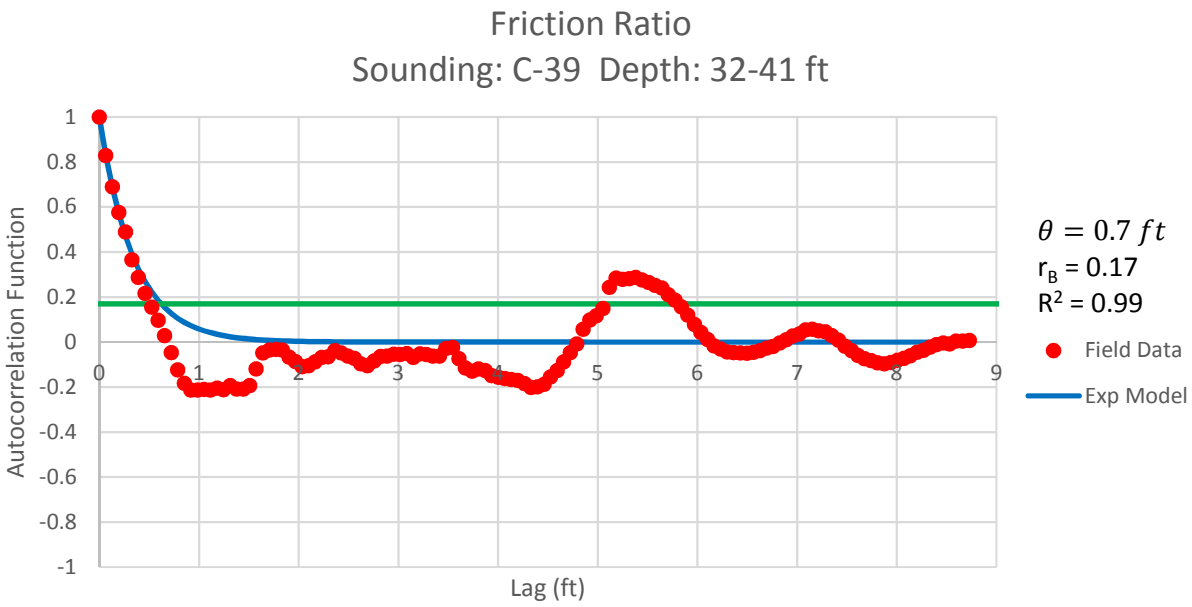

Figure B - 54: Estimation of the Scale of Fluctuation, $\theta = 0.7$ feet, for Friction Ratio Data from Sounding C-39, "Clean sands to silty sands (6)" layer from 32 to 41 feet depth.

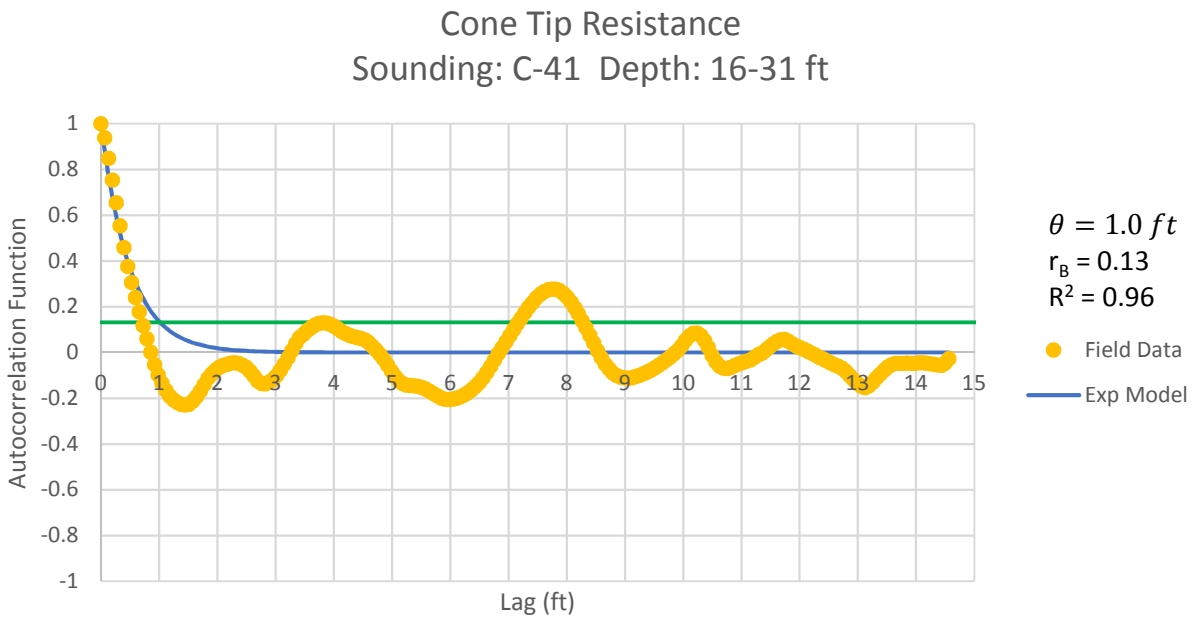

Figure B - 55: Estimation of the Scale of Fluctuation, $\theta = 1.0$ feet, for Cone Tip Resistance Data from Sounding C-41, "Clean sands to silty sands (6)" layer from 16 to 31 feet depth.

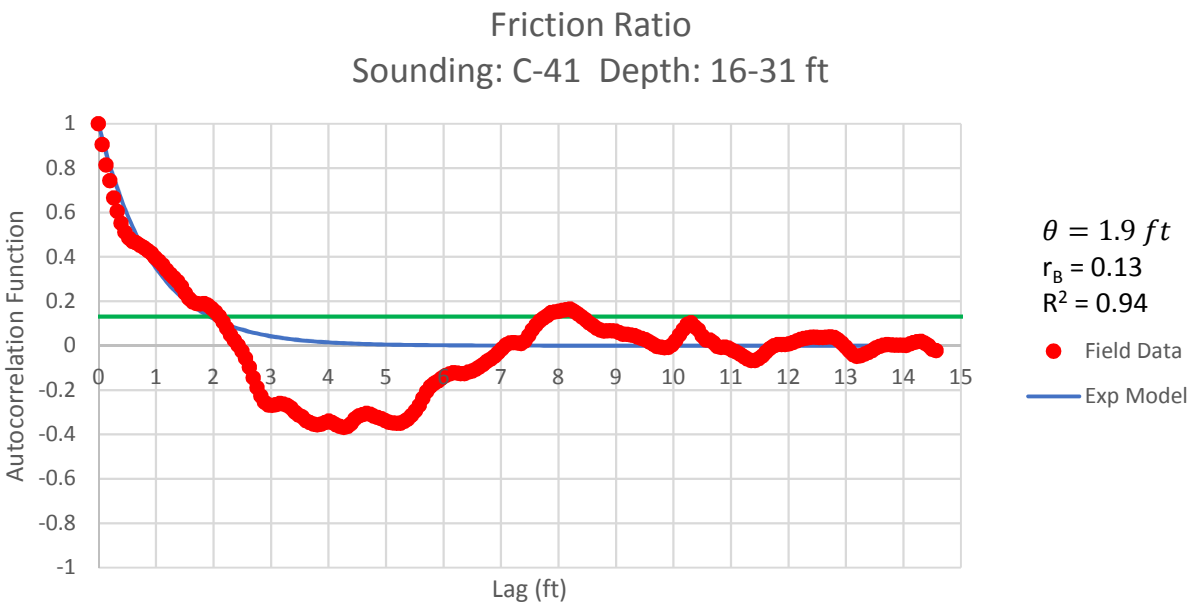

Figure B - 56: Estimation of the Scale of Fluctuation, $\theta = 1.9$ feet, for Friction Ratio Data from Sounding C-41, "Clean sands to silty sands (6)" layer from 16 to 31 feet depth.

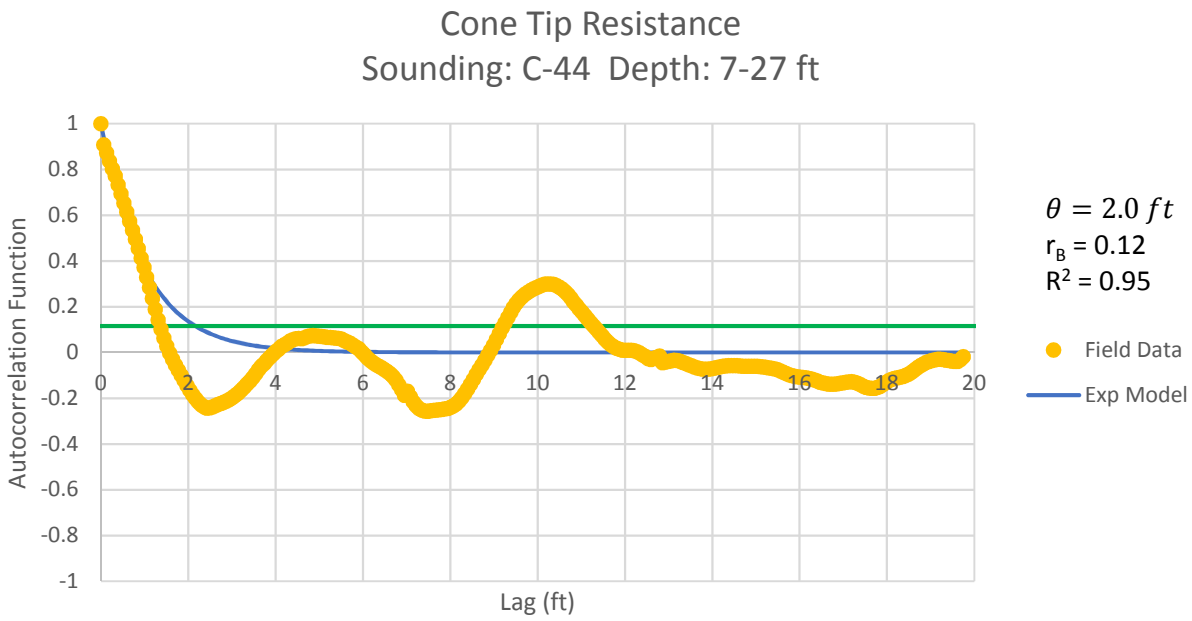

Figure B - 57: Estimation of the Scale of Fluctuation, θ = 2.0 feet, for Cone Tip Resistance Data from Sounding C-44, "Clean sands to silty sands (6)" layer from 7 to 27 feet depth.

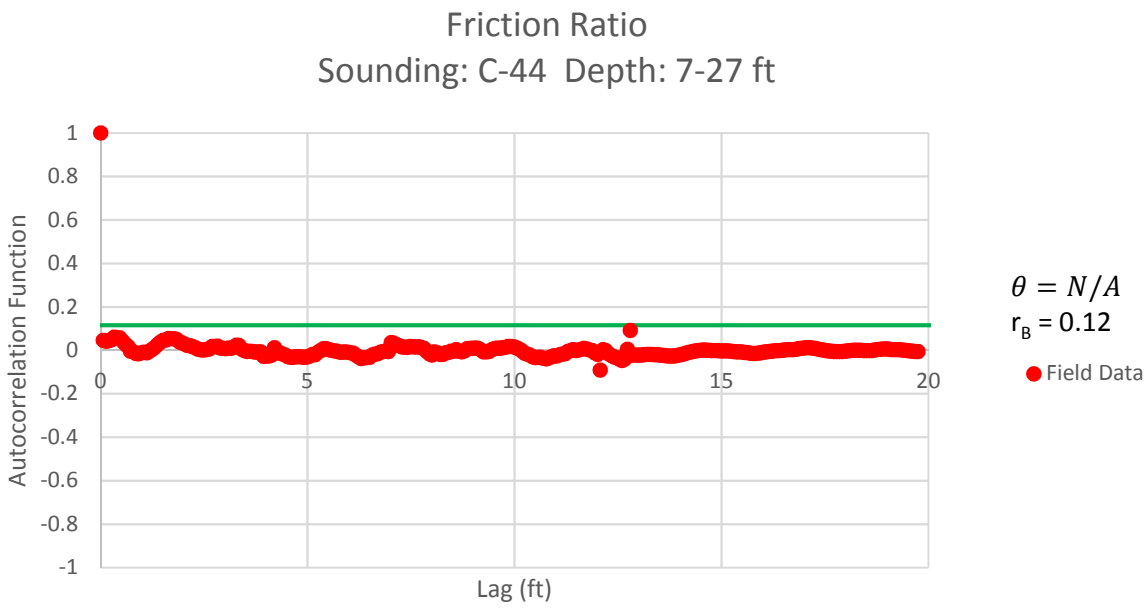

Figure B -58: Estimation of the Scale of Fluctuation, θ, for Friction Ratio Data from Sounding C-44, "Clean sands to silty sands (6)" layer from 7 to 27 feet depth. Data is limited to only 1 point greater than the Bartlett limit of 0.12; therefore, θ could not be estimated, and these results were not included in final analysis.

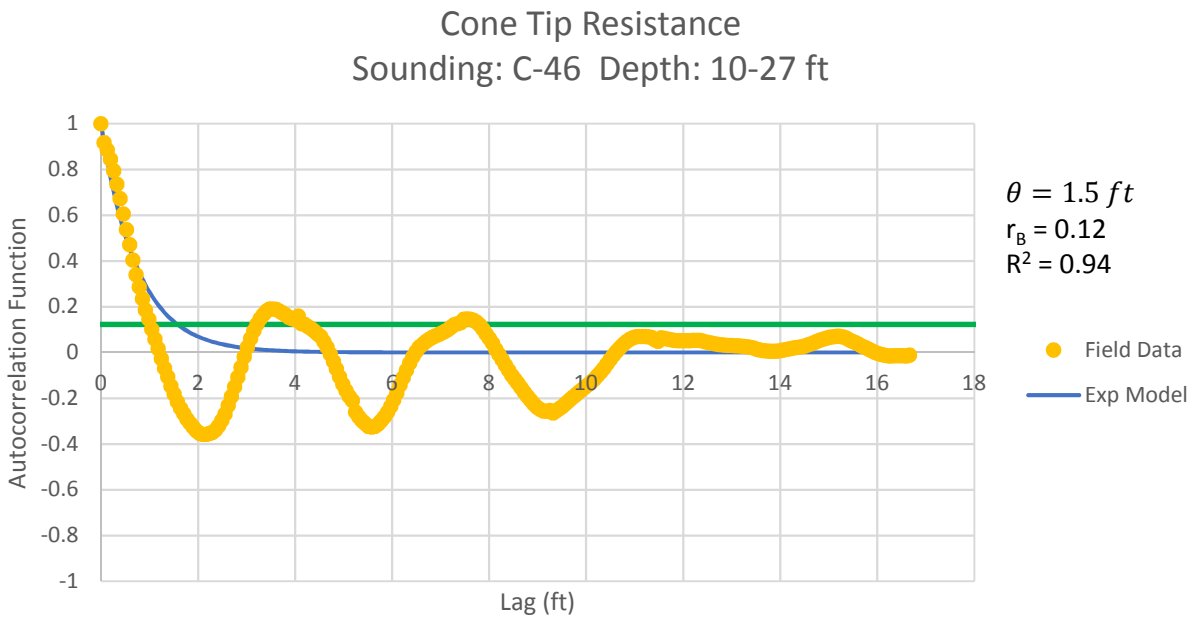

Figure B - 58: Estimation of the Scale of Fluctuation, θ = 1.5 feet, for Cone Tip Resistance Data from Sounding C-46, "Clean sands to silty sands (6)" layer from 10 to 27 feet depth.

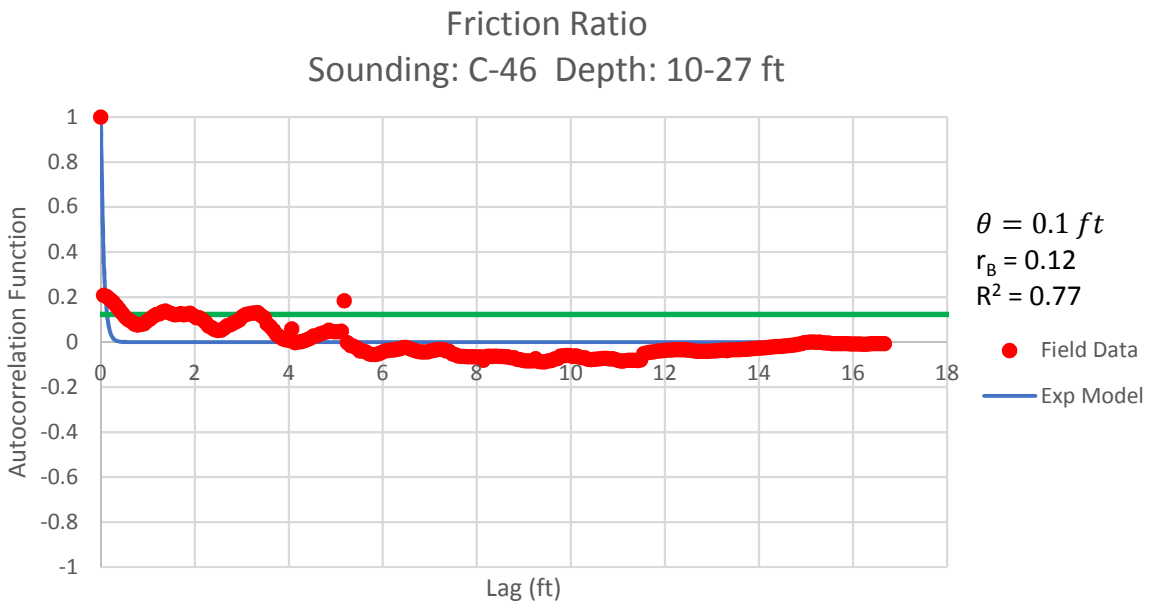

Figure B - 59: Estimation of the Scale of Fluctuation, θ = 0.1 feet, for Friction Ratio Data from Sounding C-46, "Clean sands to silty sands (6)" layer from 10 to 27 feet depth. Data is a poor fit for the points greater than the Bartlett limit of 0.12; coefficient of determination, R^2, value is less 0.9. Therefore, these results were not included in final analysis.

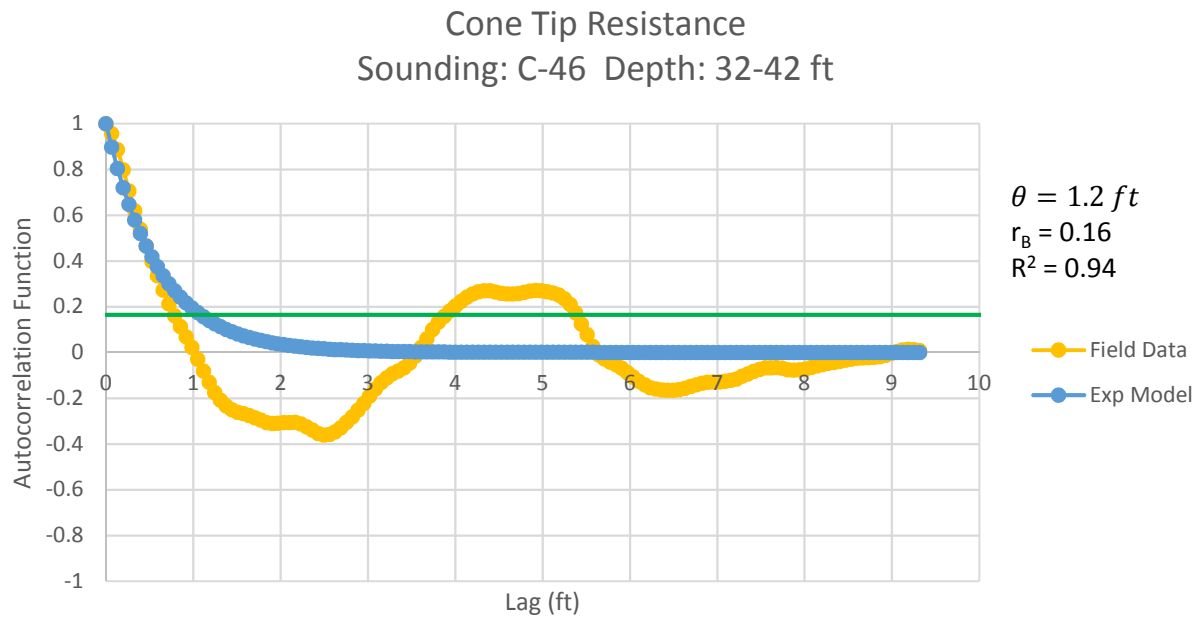

Figure B - 60: Estimation of the Scale of Fluctuation, θ = 1.2 feet, for Cone Tip Resistance Data from Sounding C-46, "Clean sands to silty sands (6)" layer from 32 to 42 feet depth.

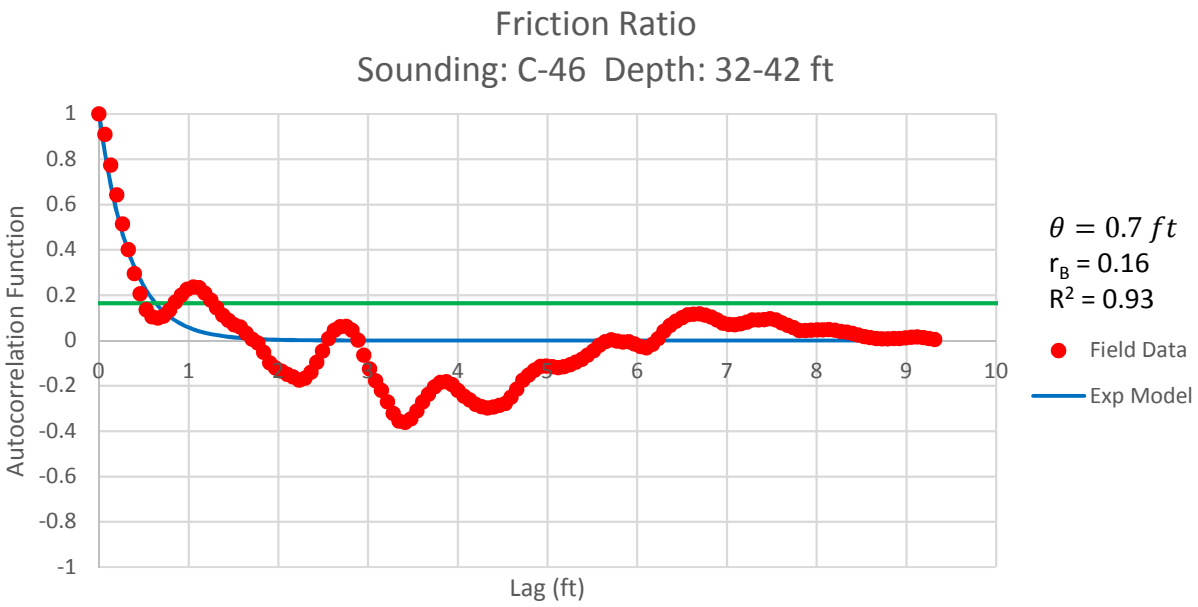

Figure B - 61: Estimation of the Scale of Fluctuation, θ = 0.7 feet, for Friction Ratio Data from Sounding C-46, "Clean sands to silty sands (6)" layer from 32 to 42 feet depth.

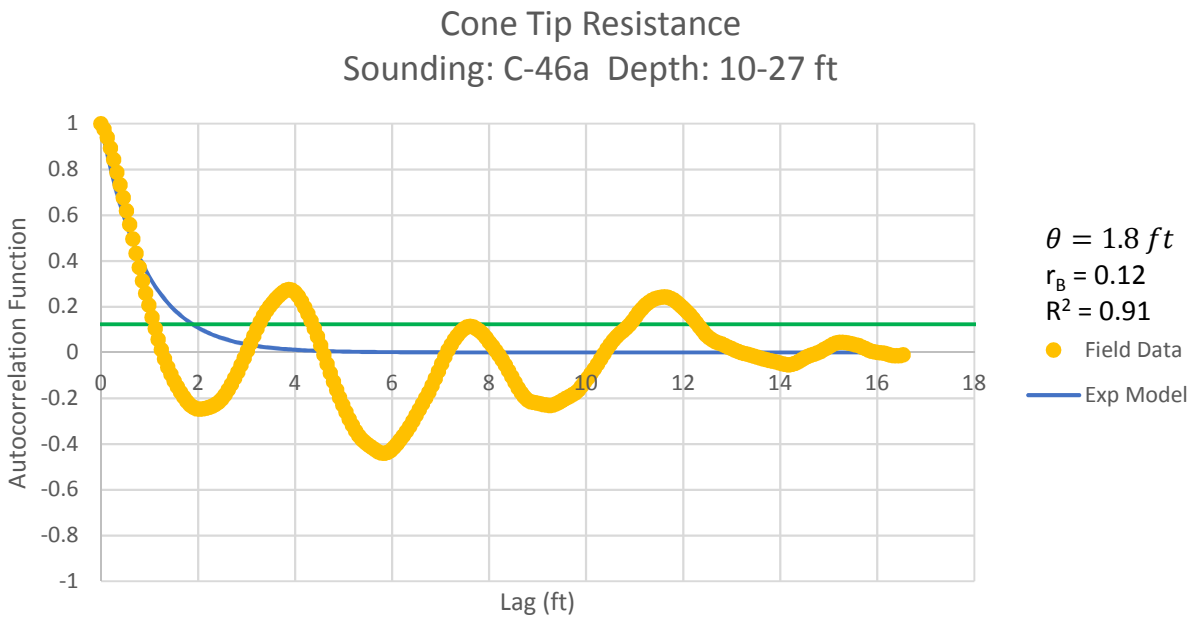

Figure B - 62: Estimation of the Scale of Fluctuation, $\theta = 1.8$ feet, for Cone Tip Resistance Data from Sounding C-46a, "Clean sands to silty sands (6)" layer from 10 to 27 feet depth.

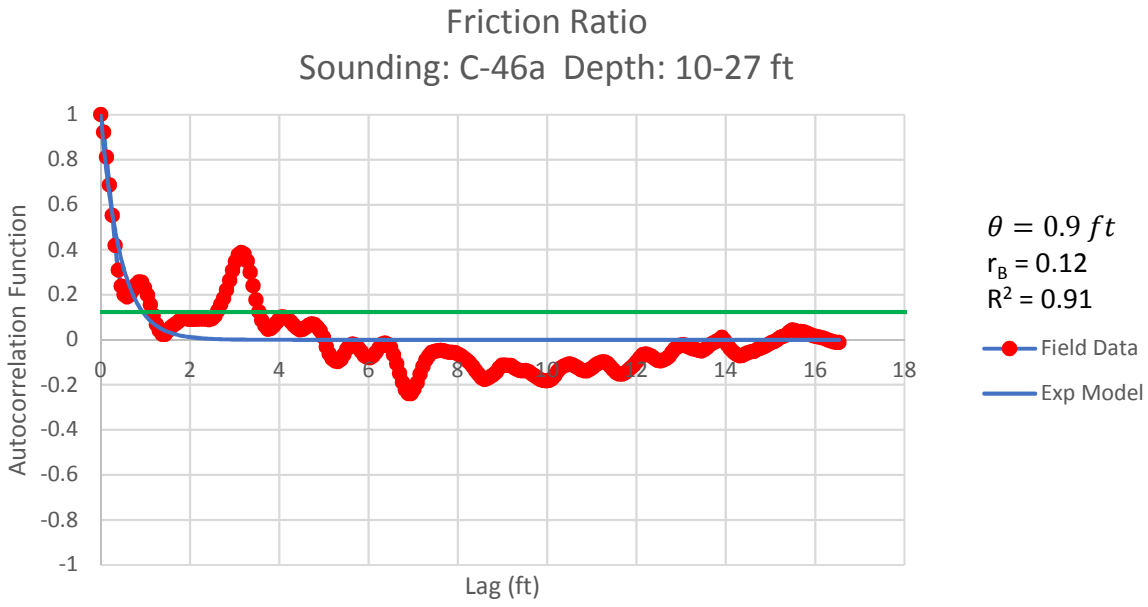

Figure B - 63: Estimation of the Scale of Fluctuation, $\theta = 0.9$ feet, for Friction Ratio Data from Sounding C-46a, "Clean sands to silty sands (6)" layer from 10 to 27 feet depth.

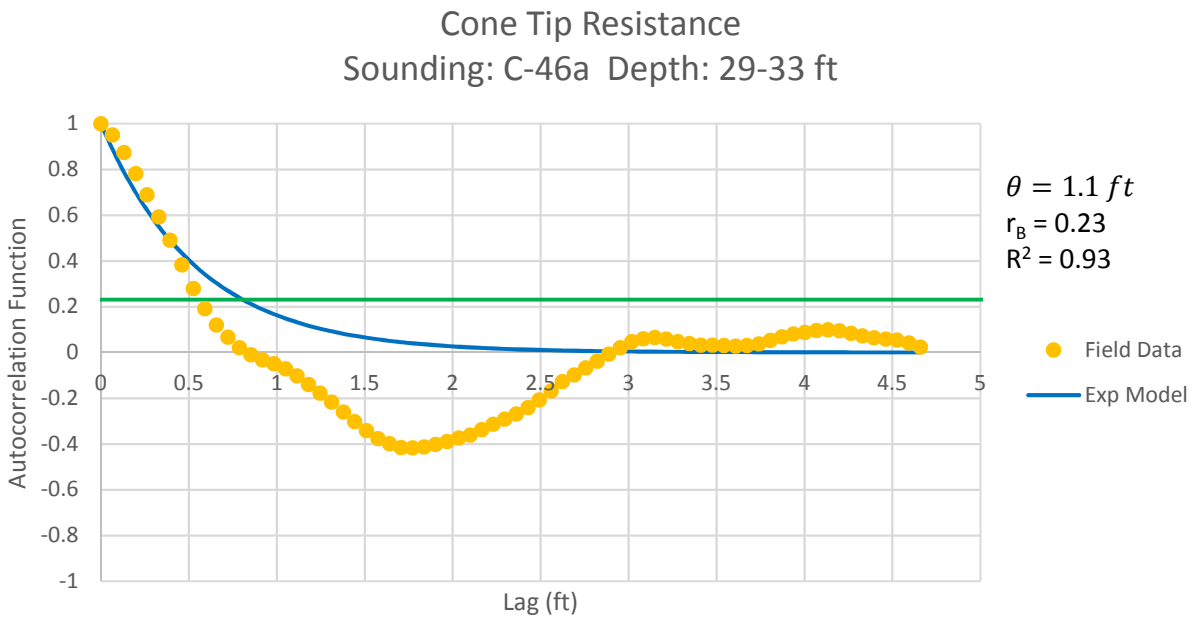

Figure B - 64: Estimation of the Scale of Fluctuation, θ = 1.1 feet, for Cone Tip Resistance Data from Sounding C-46a, "Gravelly sand to sand (7)" layer from 29 to 33 feet depth.

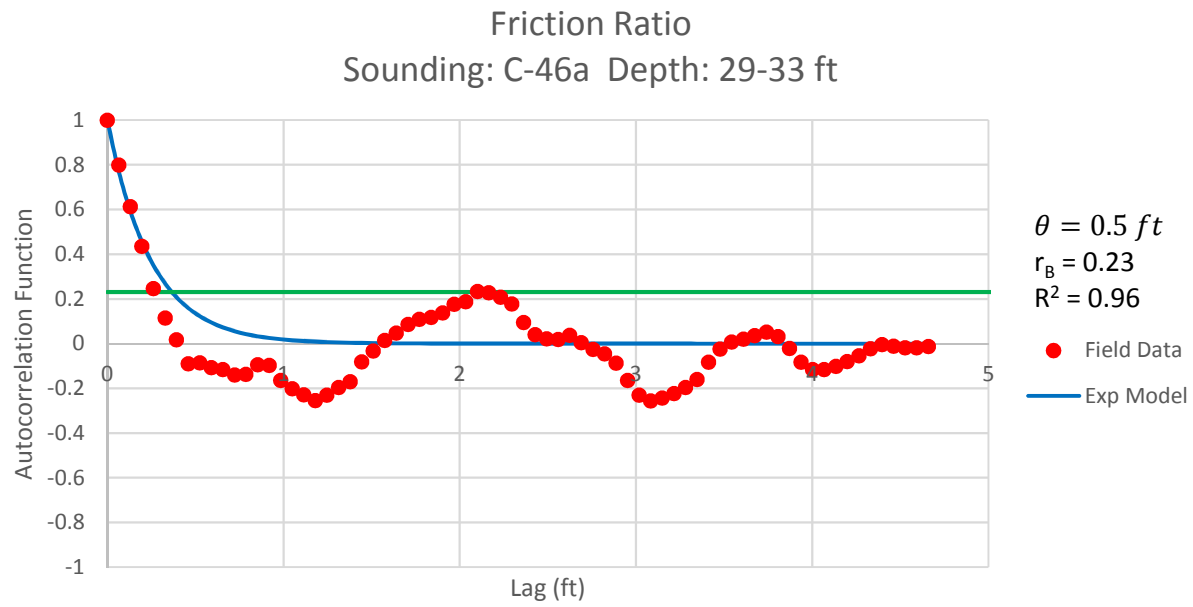

Figure B - 65: Estimation of the Scale of Fluctuation, θ = 0.5 feet, for Friction Ratio Data from Sounding C-46a, " Gravelly sand to sand (7)" layer from 29 to 33 feet depth.

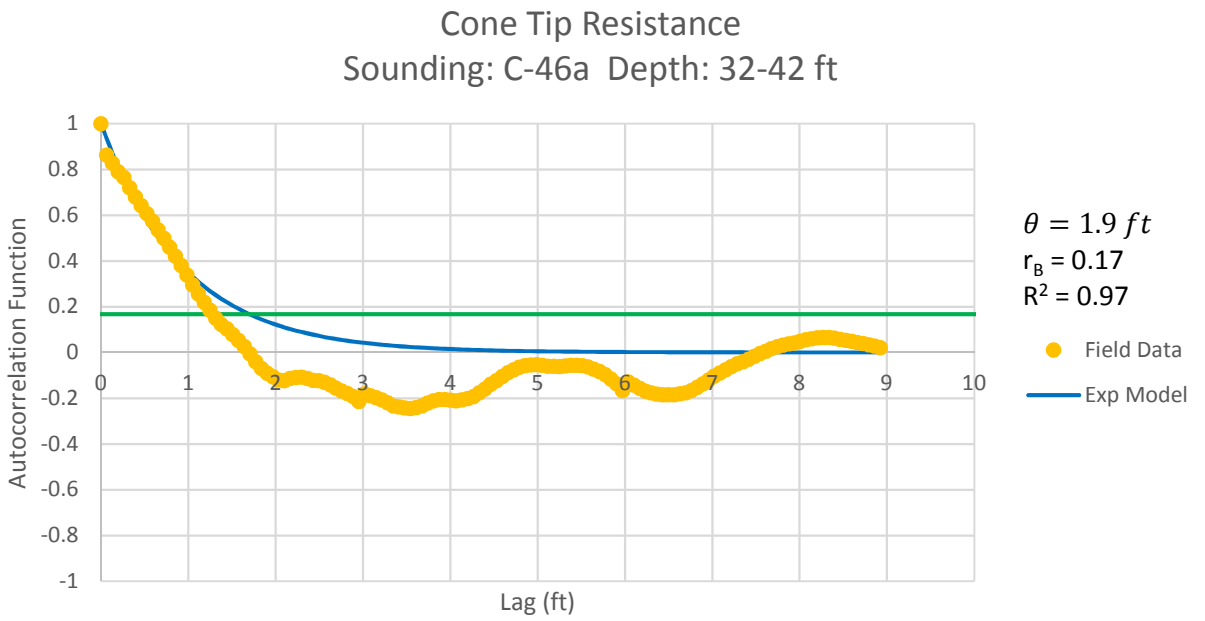

Figure B - 66: Estimation of the Scale of Fluctuation, $\theta = 1.9$ feet, for Cone Tip Resistance Data from Sounding C-46a, "Clean sands to silty sands (6)" layer from 32 to 42 feet depth.

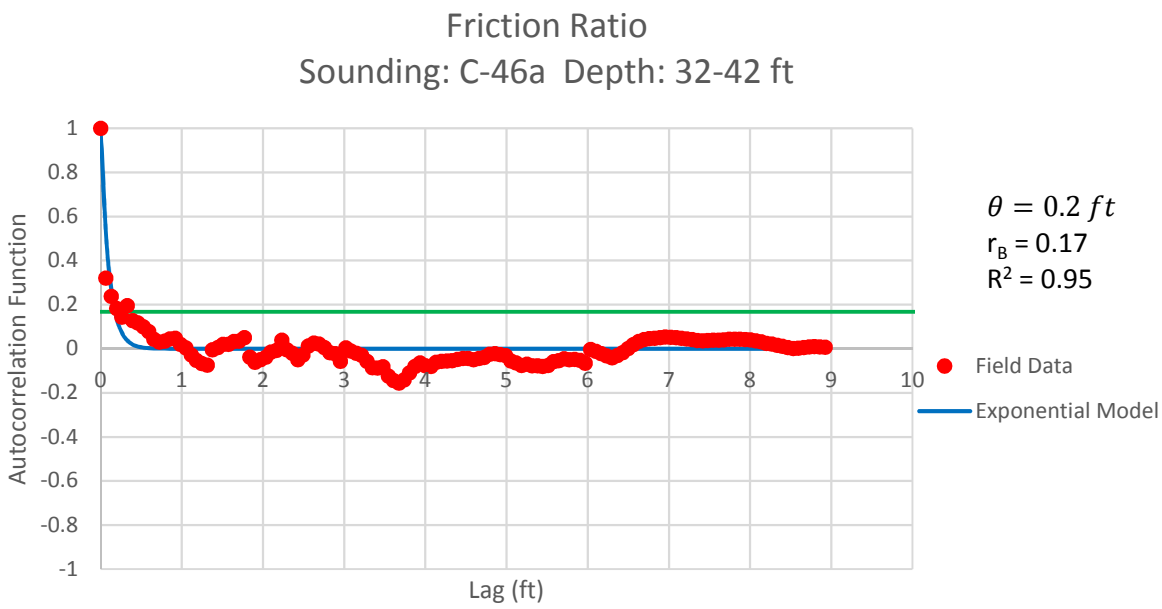

Figure B - 67: Estimation of the Scale of Fluctuation, $\theta = 0.2$ feet, for Friction Ratio Data from Sounding C-46a, "Clean sands to silty sands (6)" layer from 32 to 42 feet depth.

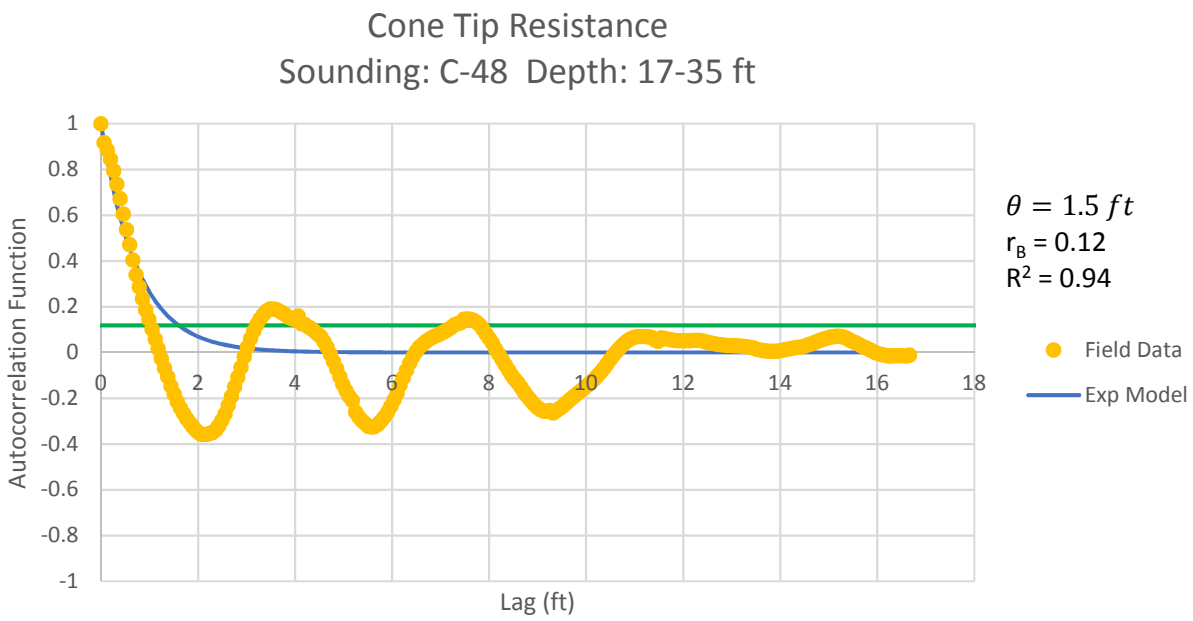

Figure B - 68: Estimation of the Scale of Fluctuation, $\theta = 1.5$ feet, for Cone Tip Resistance Data from Sounding C-48, "Clean sands to silty sands (6)" layer from 17 to 35 feet depth.

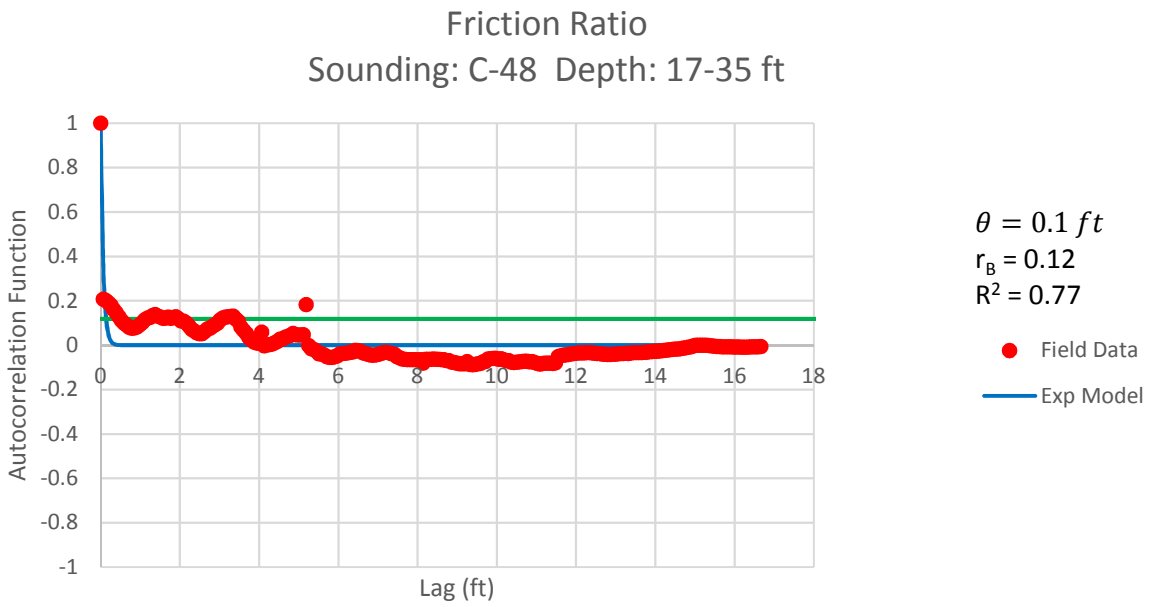

Figure B - 69: Estimation of the Scale of Fluctuation, $\theta = 0.1$ feet, for Friction Ratio Data from Sounding C-48, "Clean sands to silty sands (6)" layer from 17 to 35 feet depth. Data is a poor fit for the points greater than the Bartlett limit of 0.12; coefficient of determination, R^2, value is less 0.9. Therefore, these results were not included in final analysis.

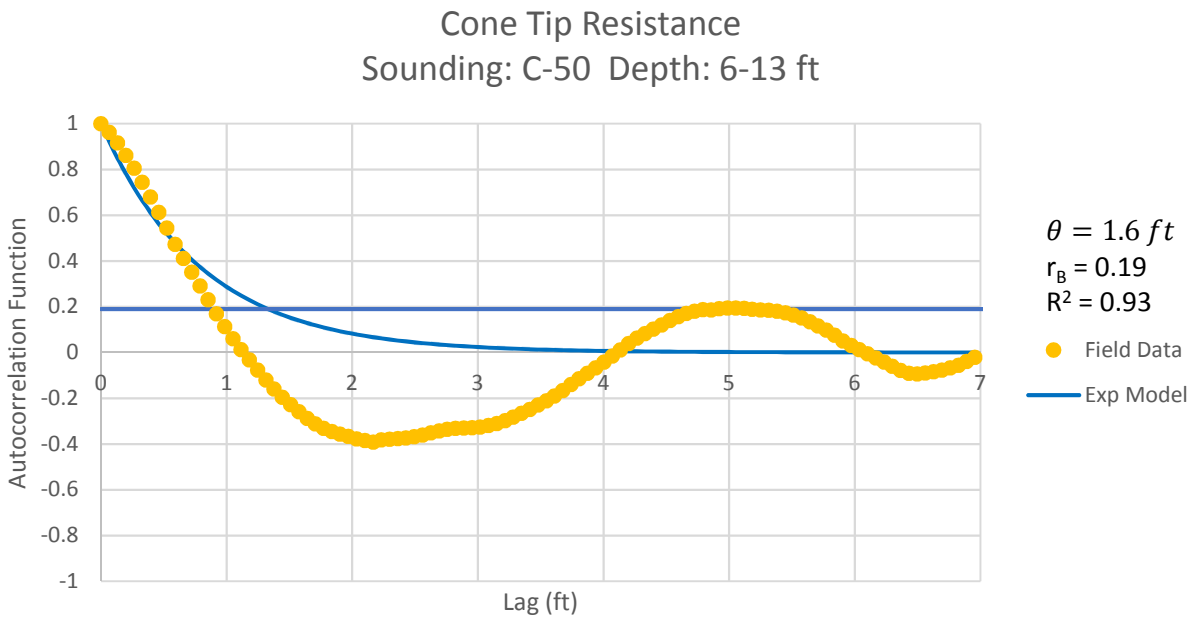

Figure B - 70: Estimation of the Scale of Fluctuation, θ = 1.6 feet, for Cone Tip Resistance Data from Sounding C-50, "Clean sands to silty sands (6)" layer from 6 to 13 feet depth.

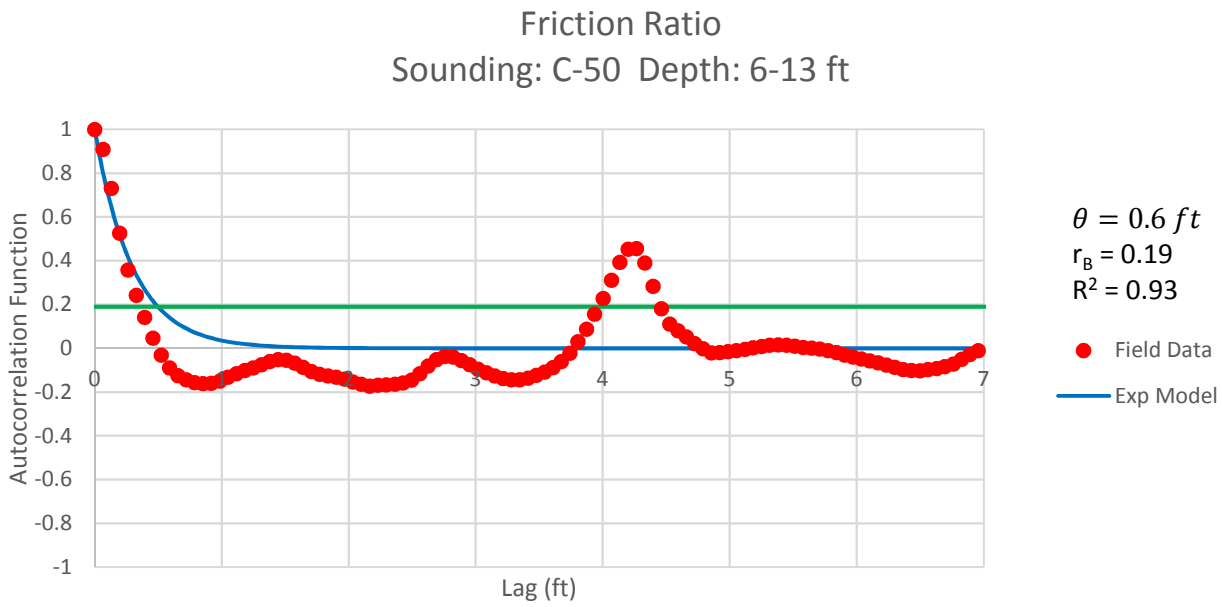

Figure B - 71: Estimation of the Scale of Fluctuation, θ = 0.6 feet, for Friction Ratio Data from Sounding C-50, "Clean sands to silty sands (6)" layer from 6 to 13 feet depth.

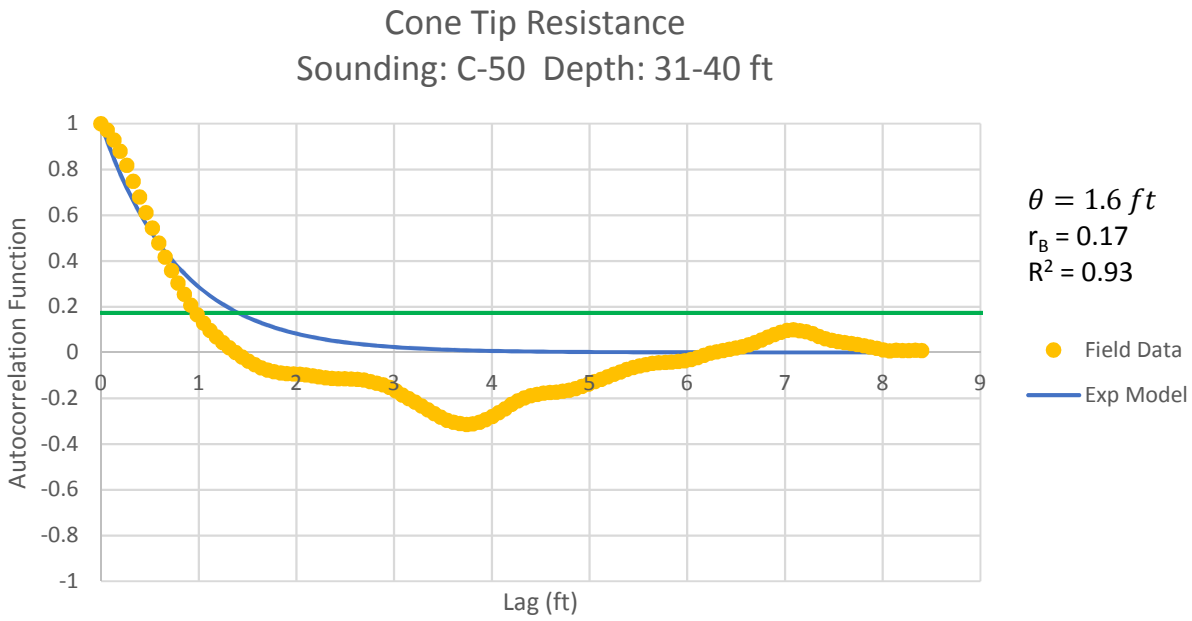

Figure B - 72: Estimation of the Scale of Fluctuation, θ = 1.6 feet, for Cone Tip Resistance Data from Sounding C-50, "Clean sands to silty sands (6)" layer from 31 to 40 feet depth.

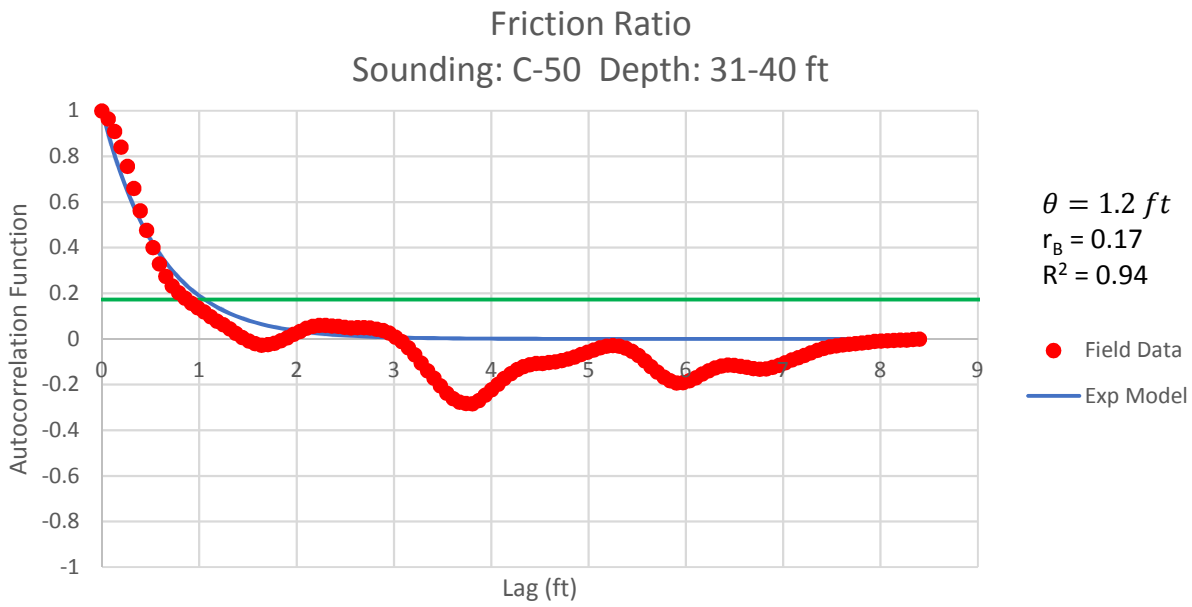

Figure B - 73: Estimation of the Scale of Fluctuation, θ = 1.2 feet, for Friction Ratio Data from Sounding C-50, "Clean sands to silty sands (6)" layer from 31 to 40 feet depth.

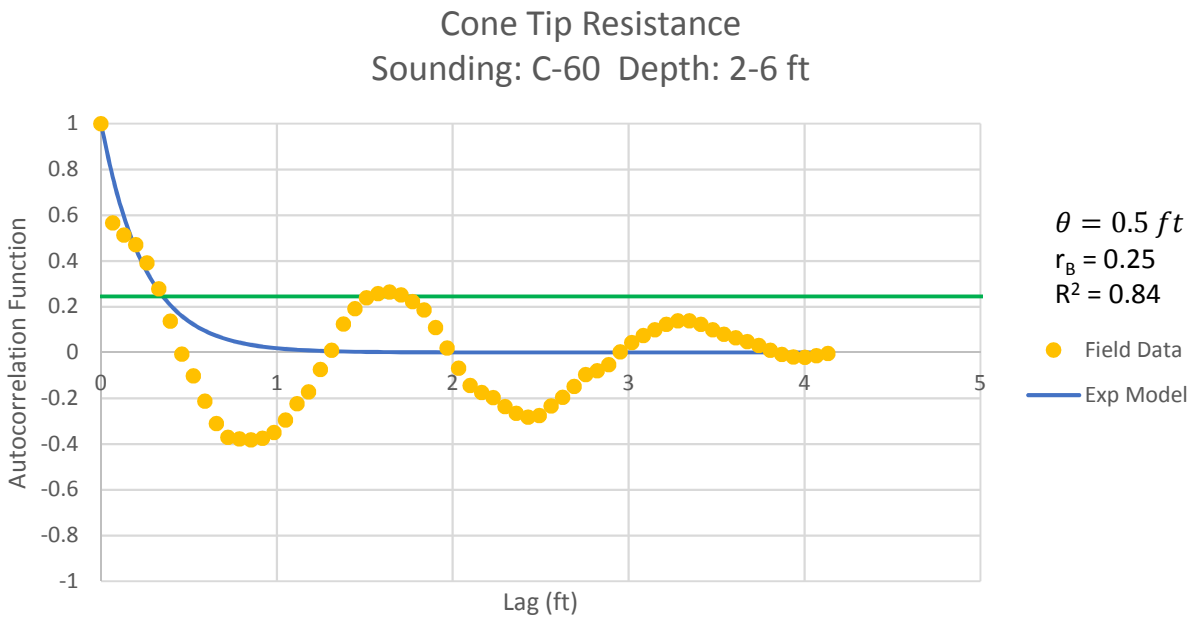

Figure B - 74: Estimation of the Scale of Fluctuation, θ = 0.5 feet, for Cone Tip Resistance Data from Sounding C-60, "Clays; Clay to silty clay (3)" layer from 2 to 6 feet depth. Data is a poor fit for the points greater than the Bartlett limit of 0.25; coefficient of determination, R^2, value is less 0.9. Therefore, these results were not included in final analysis.

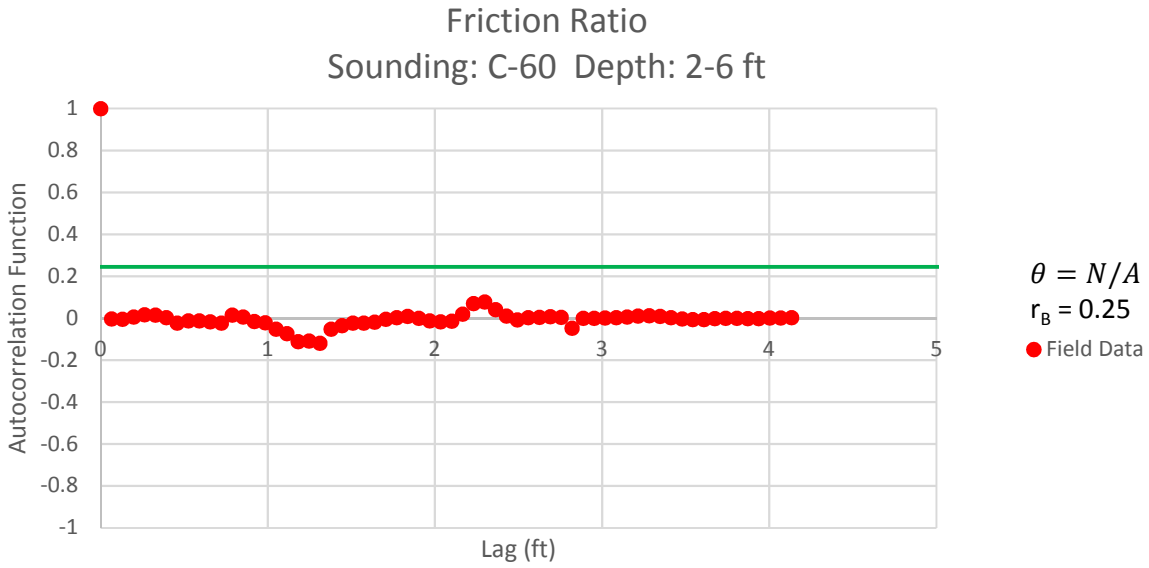

Figure B - 75: Estimation of the Scale of Fluctuation, θ, for Friction Ratio Data from Sounding C-60, "Clays; clay to silty clay (3)" layer from 2 to 6 feet depth. Data is limited to only 1 point greater than the Bartlett limit of 0.25; therefore, θ could not be estimated, and these results were not included in final analysis.

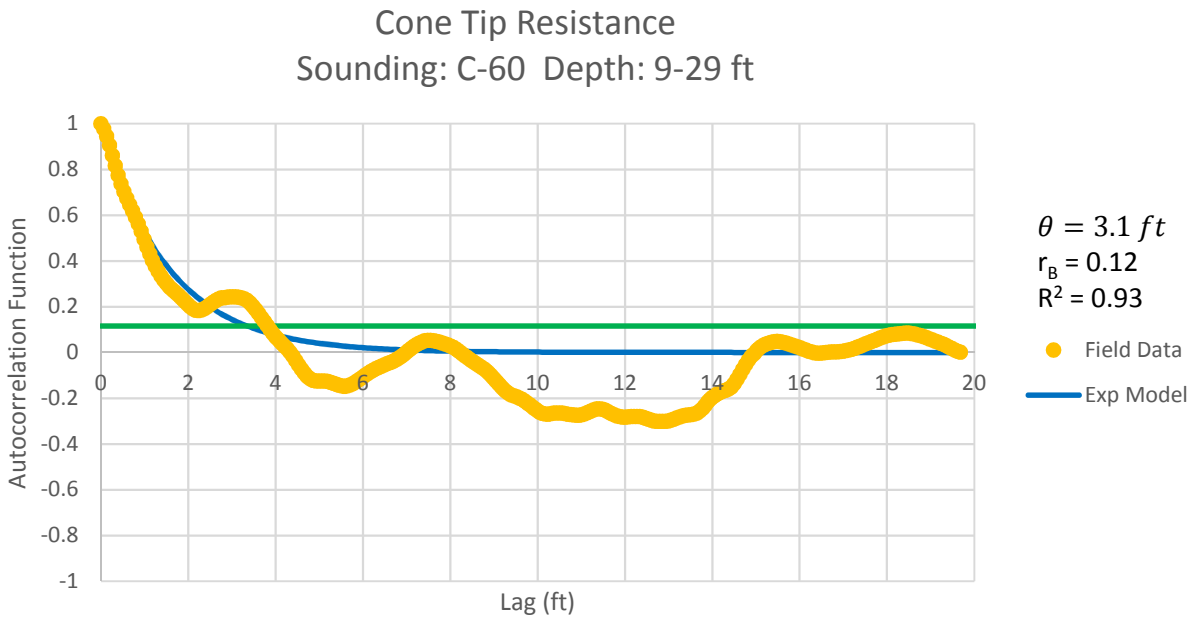

Figure B - 76: Estimation of the Scale of Fluctuation, θ = 3.1 feet, for Cone Tip Resistance Data from Sounding C-60, "Clean sands to silty sands (6)" layer from 9 to 29 feet depth.

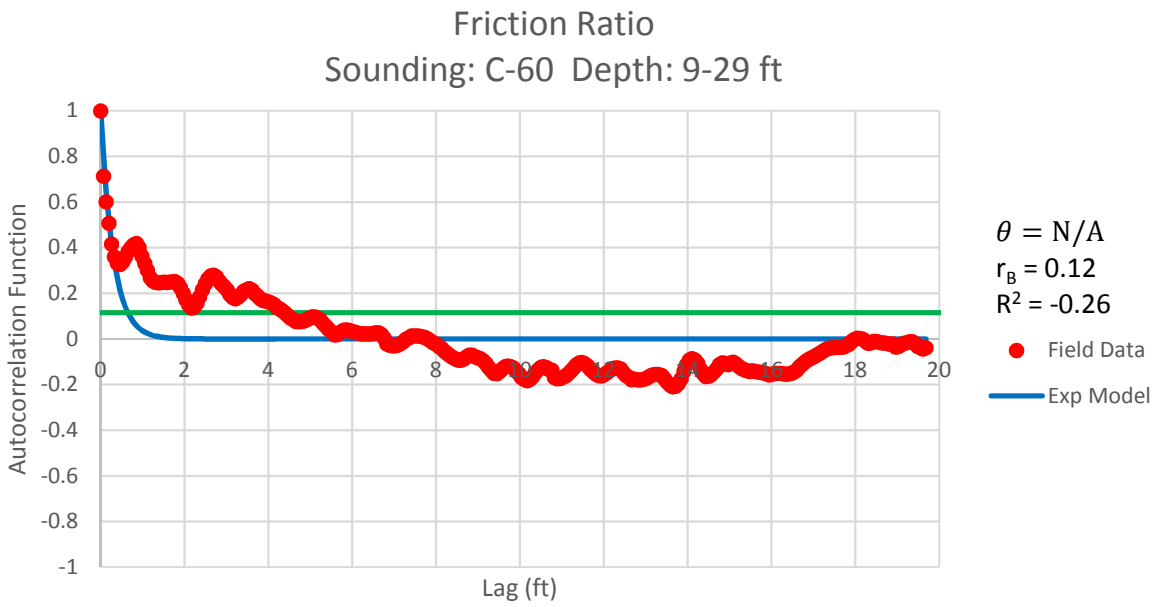

Figure B - 77: Estimation of the Scale of Fluctuation, θ, for Friction Ratio Data from Sounding C-60, "Clean sands to silty sands (6)" layer from 9 to 29 feet depth. Data is a poor fit for the points greater than the Bartlett limit of 0.12; coefficient of determination, R^2, value is less 0.9. Therefore, these results were not included in final analysis

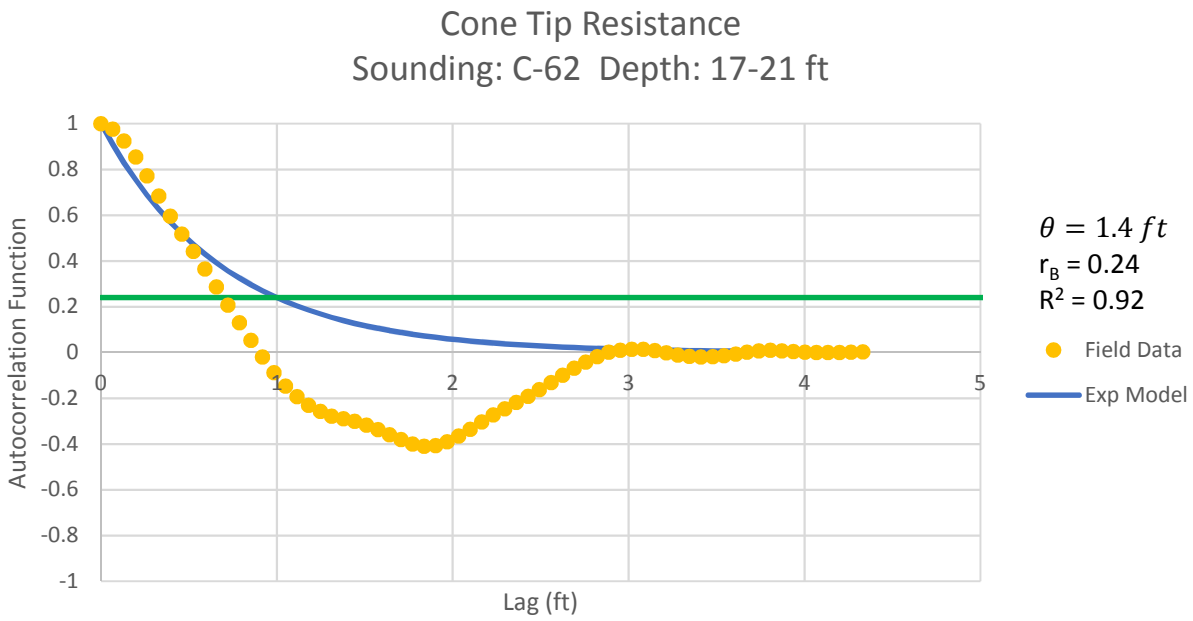

Figure B - 78: Estimation of the Scale of Fluctuation, θ = 1.4 feet, for Cone Tip Resistance Data from Sounding C-62, "Gravelly sand to sand (7)" layer from 17 to 21 feet depth.

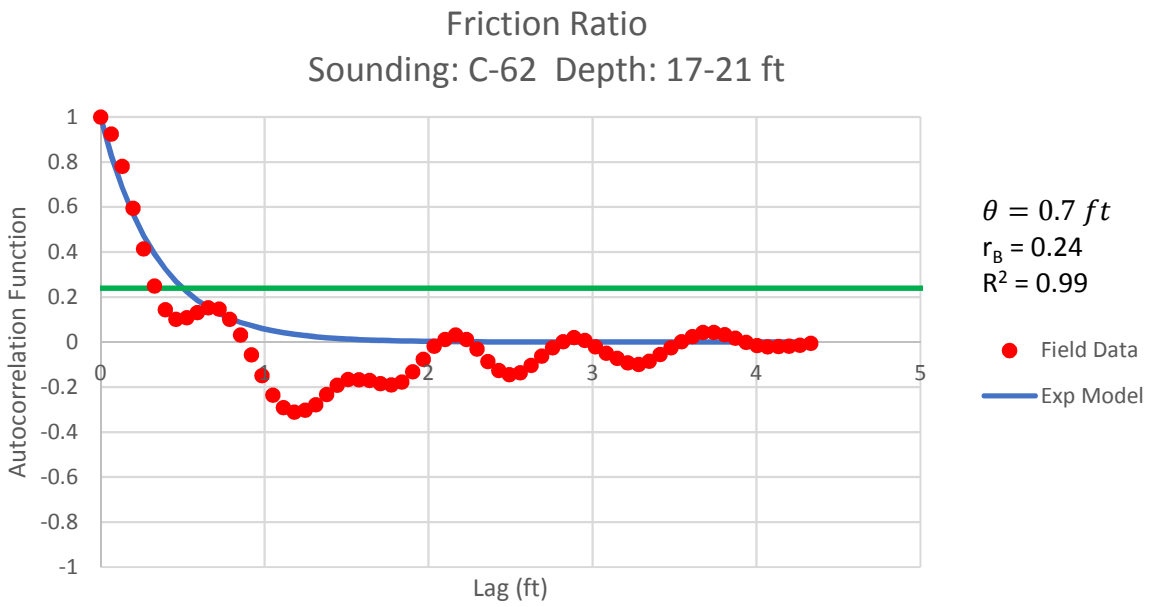

Figure B - 79: Estimation of the Scale of Fluctuation, θ = 0.7 feet, for Friction Ratio Data from Sounding C-62, "Gravelly sand to sand (7)" layer from 17 to 21 feet depth.

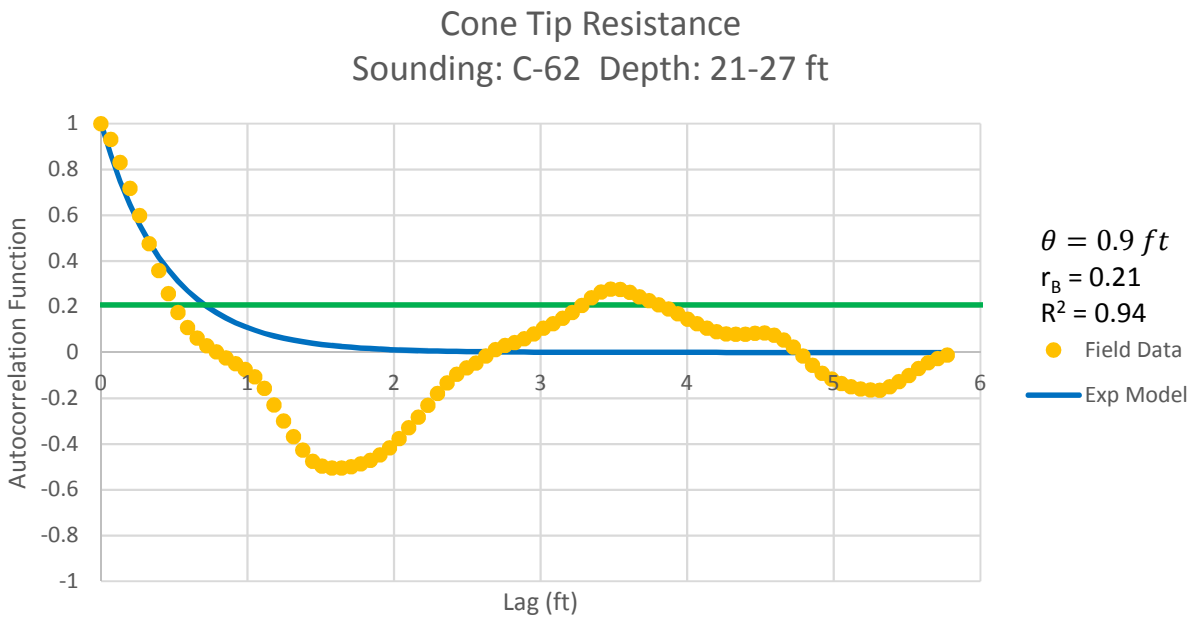

Figure B - 80: Estimation of the Scale of Fluctuation, $\theta = 0.9$ feet, for Cone Tip Resistance Data from Sounding C-62, "Clean sands to silty sands (6)" layer from 21 to 27 feet depth.

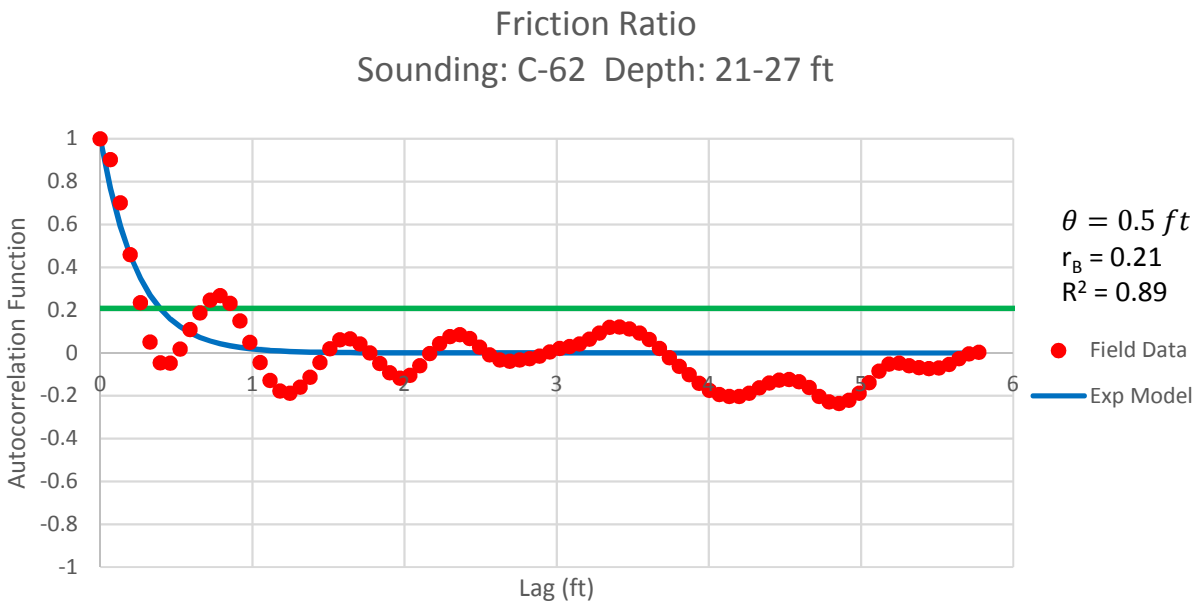

Figure B - 81: Estimation of the Scale of Fluctuation, $\theta = 0.5$ feet, for Friction Ratio Data from Sounding C-62, "Clean sands to silty sands (6)" layer from 21 to 27 feet depth. Data is a poor fit for the points greater than the Bartlett limit of 0.21; coefficient of determination, R^2, value is less 0.9. Therefore, these results were not included in final analysis.

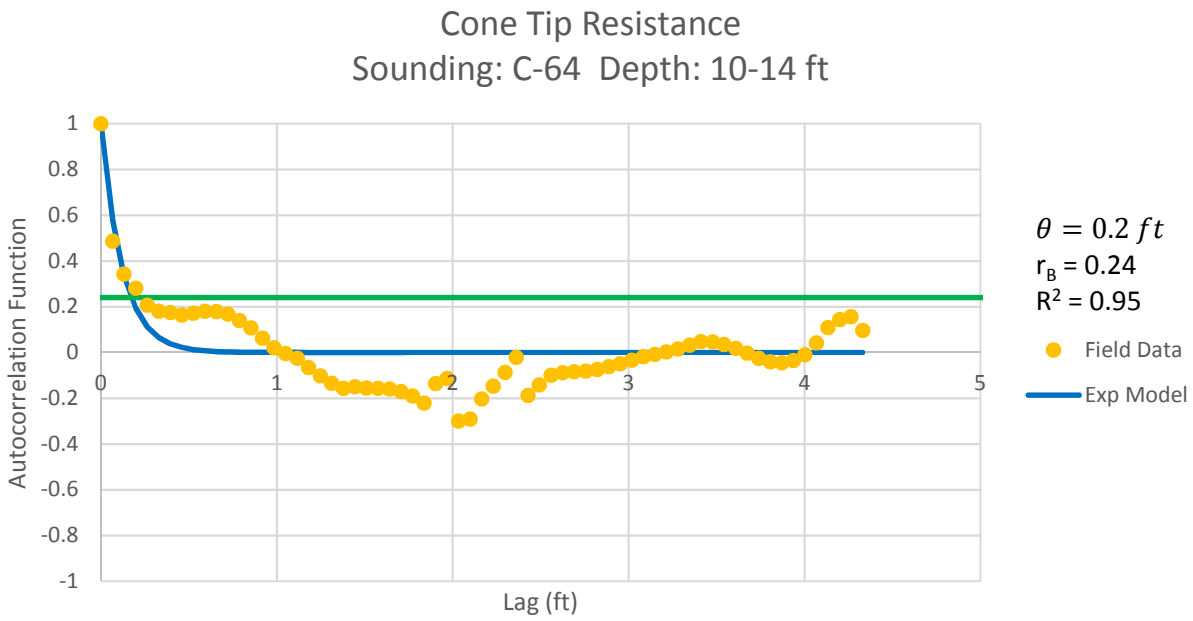

Figure B - 82: Estimation of the Scale of Fluctuation, θ = 0.2 feet, for Cone Tip Resistance Data from Sounding C-64, "Clean sands to silty sands (6)" layer from 10 to 14 feet depth.

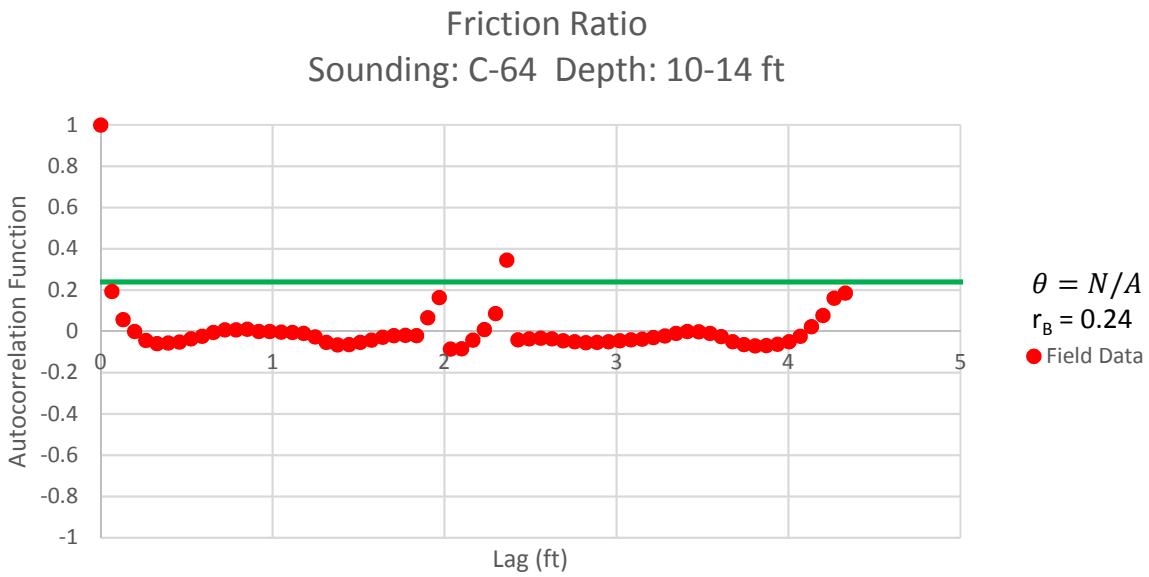

Figure B - 83: Estimation of the Scale of Fluctuation, θ, for Friction Ratio Data from Sounding C-64, "Clean sands to silty sands (6)" layer from 10 to 14 feet depth. Data is limited to only 1 point greater than the Bartlett limit of 0.24; therefore, θ could not be estimated, and these results were not included in final analysis.

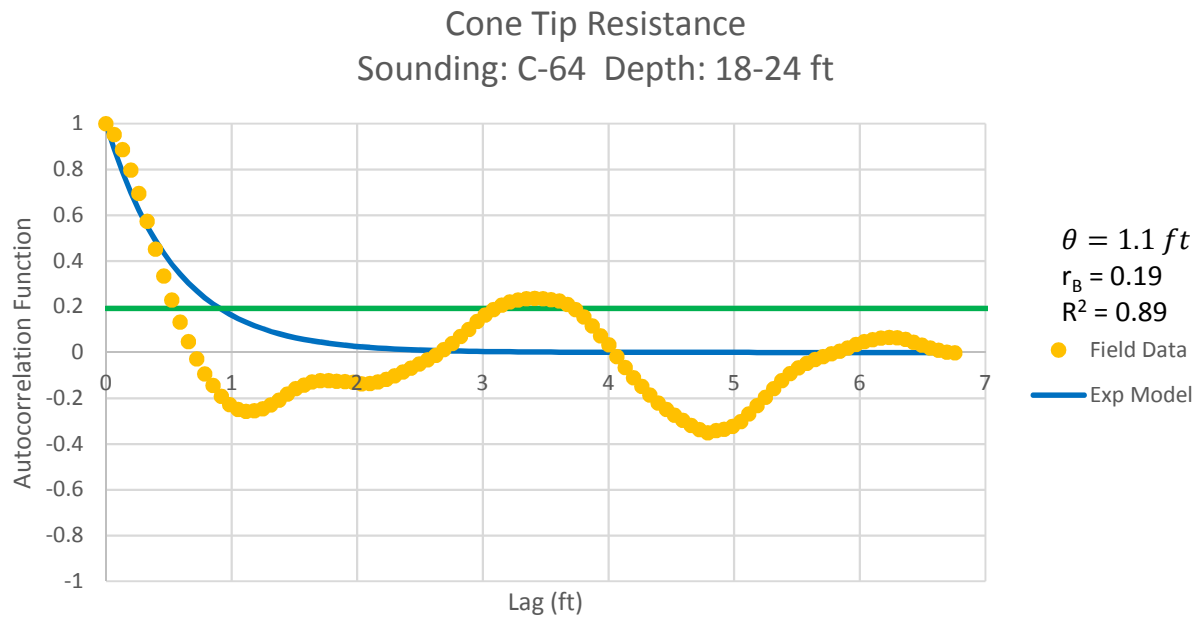

Figure B - 84: Estimation of the Scale of Fluctuation, $\theta = 1.1$ feet, for Cone Tip Resistance Data from Sounding C-64, "Clean sands to silty sands (6)" layer from 18 to 24 feet depth. Data is a poor fit for the points greater than the Bartlett limit of 0.19; coefficient of determination, R^2, value is less 0.9. Therefore, these results were not included in final analysis

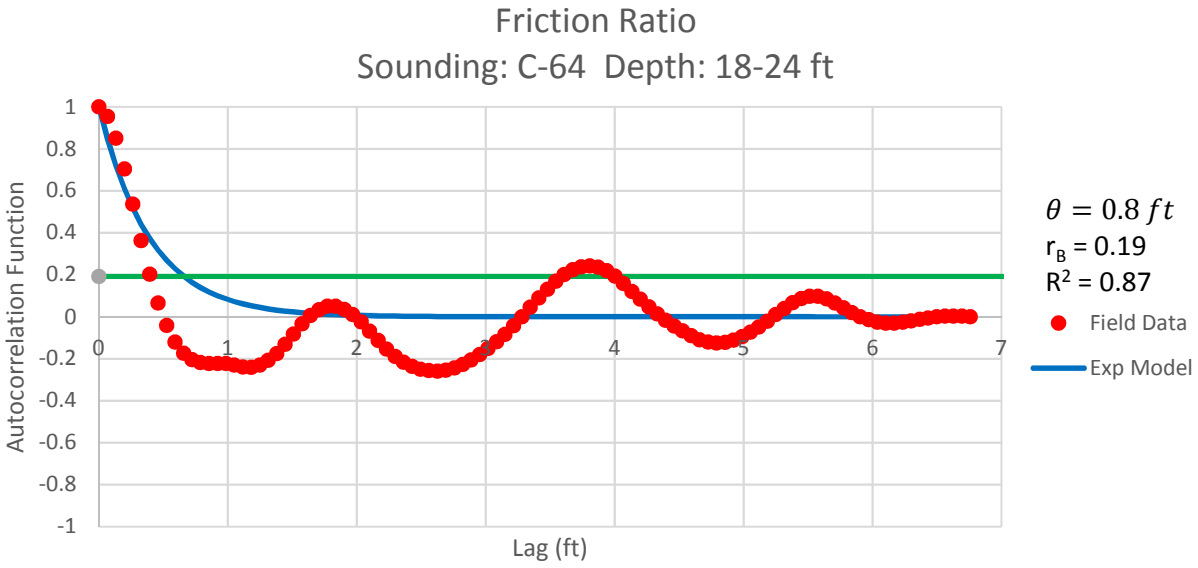

Figure B - 85: Estimation of the Scale of Fluctuation, $\theta = 0.8$ feet, for Friction Ratio Data from Sounding C-64, "Clean sands to silty sands (6)" layer from 18 to 24 feet depth. Data is a poor fit for the points greater than the Bartlett limit of 0.10; coefficient of determination, R^2, value is less 0.9. Therefore, these results were not included in final analysis.

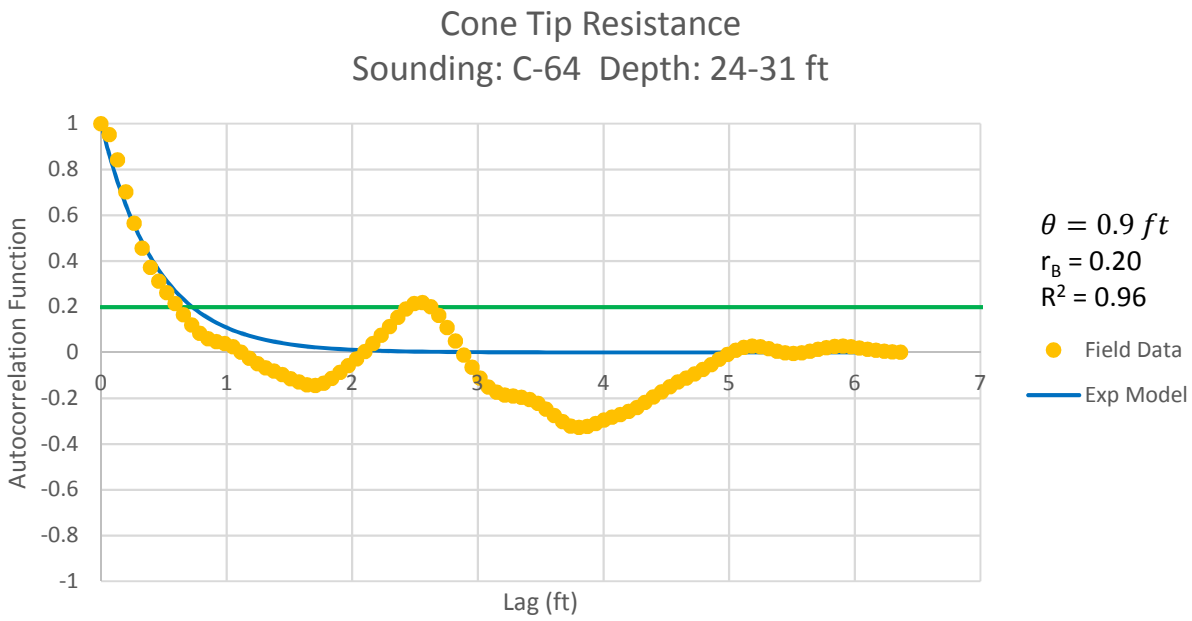

Figure B - 86: Estimation of the Scale of Fluctuation, $\theta = 0.9$ feet, for Cone Tip Resistance Data from Sounding C-64, "Gravelly sand to sand (7)" layer from 24 to 31 feet depth.

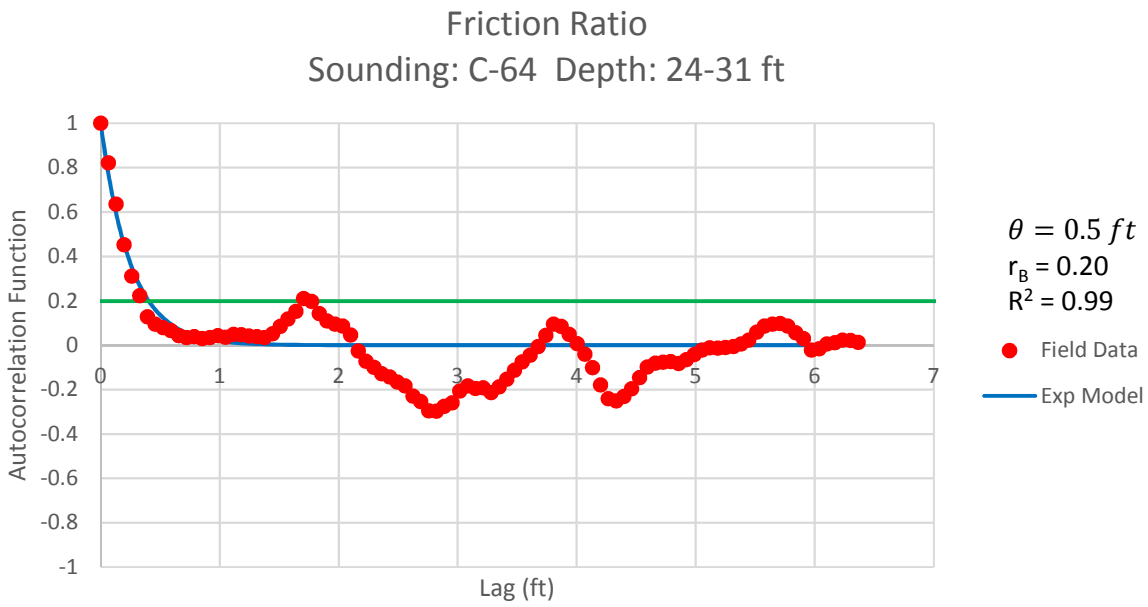

Figure B - 87: Estimation of the Scale of Fluctuation, $\theta = 0.5$ feet, for Friction Ratio Data from Sounding C-64, "Gravelly sand to sand (7)" layer from 24 to 31 feet depth.

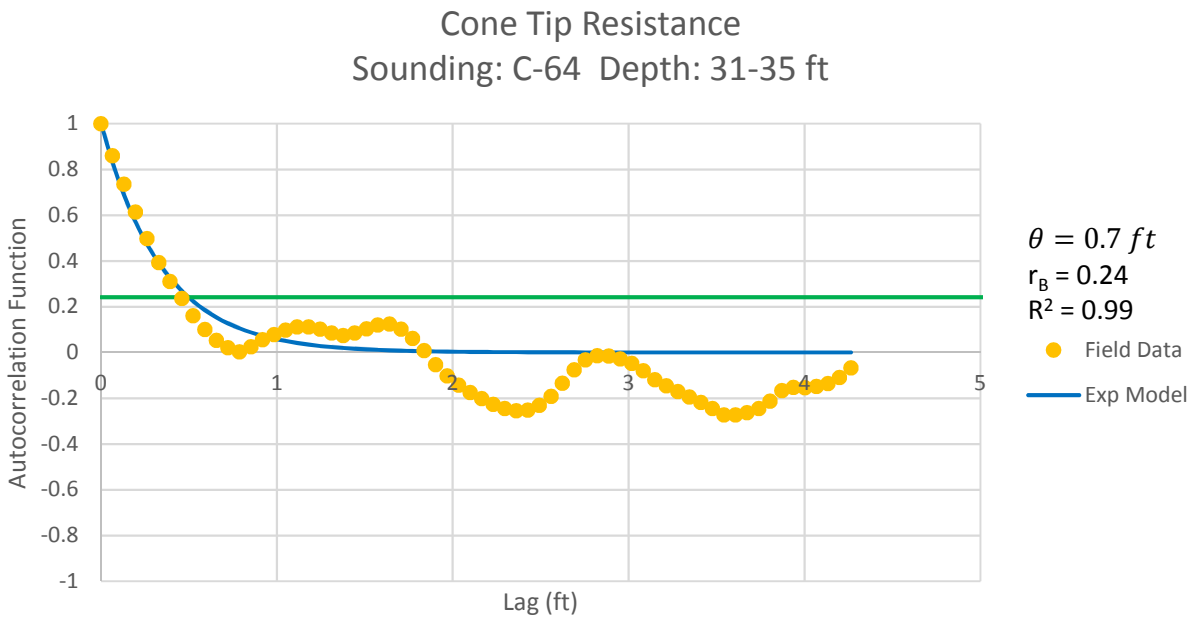

Figure B - 88: Estimation of the Scale of Fluctuation, $\theta = 0.7$ feet, for Cone Tip Resistance Data from Sounding C-64, "Clean sands to silty sands (6)" layer from 31 to 35 feet depth.

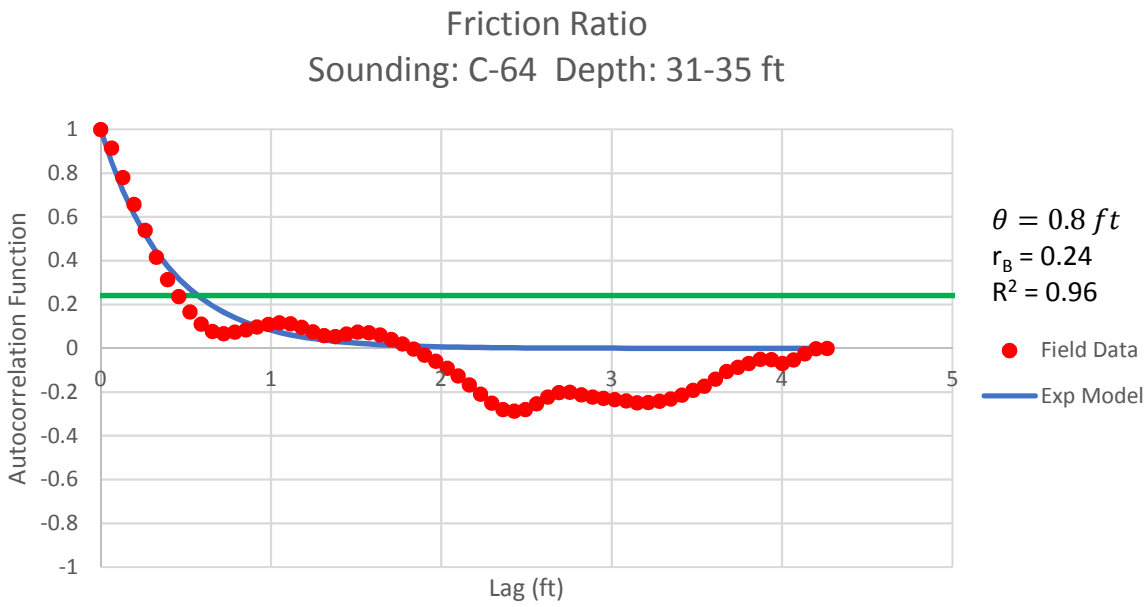

Figure B - 89: Estimation of the Scale of Fluctuation, $\theta = 0.8$ feet, for Friction Ratio Data from Sounding C-64, "Clean sands to silty sands (6)" layer from 31 to 35 feet depth.

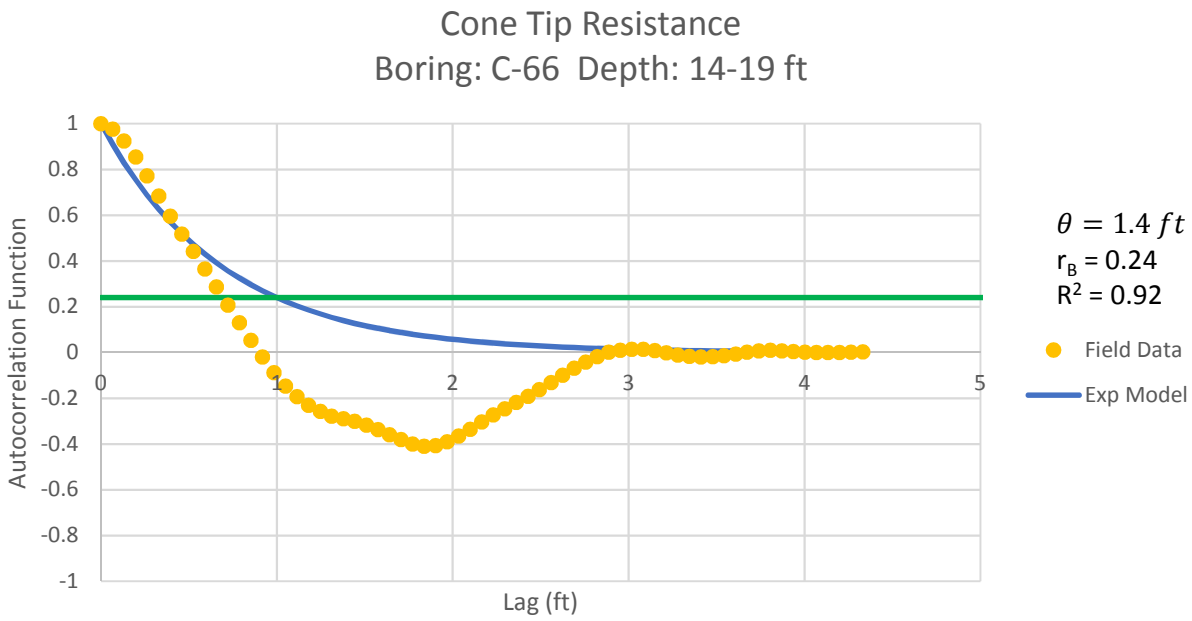

Figure B - 90: Estimation of the Scale of Fluctuation, $\theta = 1.4$ feet, for Cone Tip Resistance Data from Sounding C-66, "Clean sands to silty sands (6)" layer from 14 to 19 feet depth.

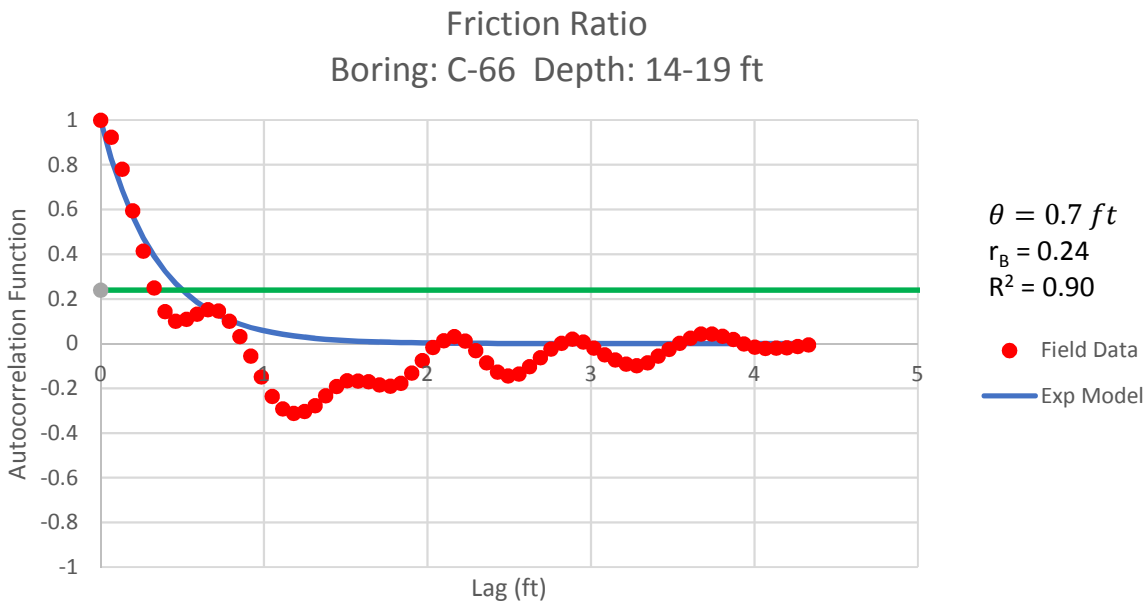

Figure B - 91: Estimation of the Scale of Fluctuation, $\theta = 0.7$ feet, for Friction Ratio Data from Sounding C-66, "Clean sands to silty sands (6)" layer from 14 to 19 feet depth.

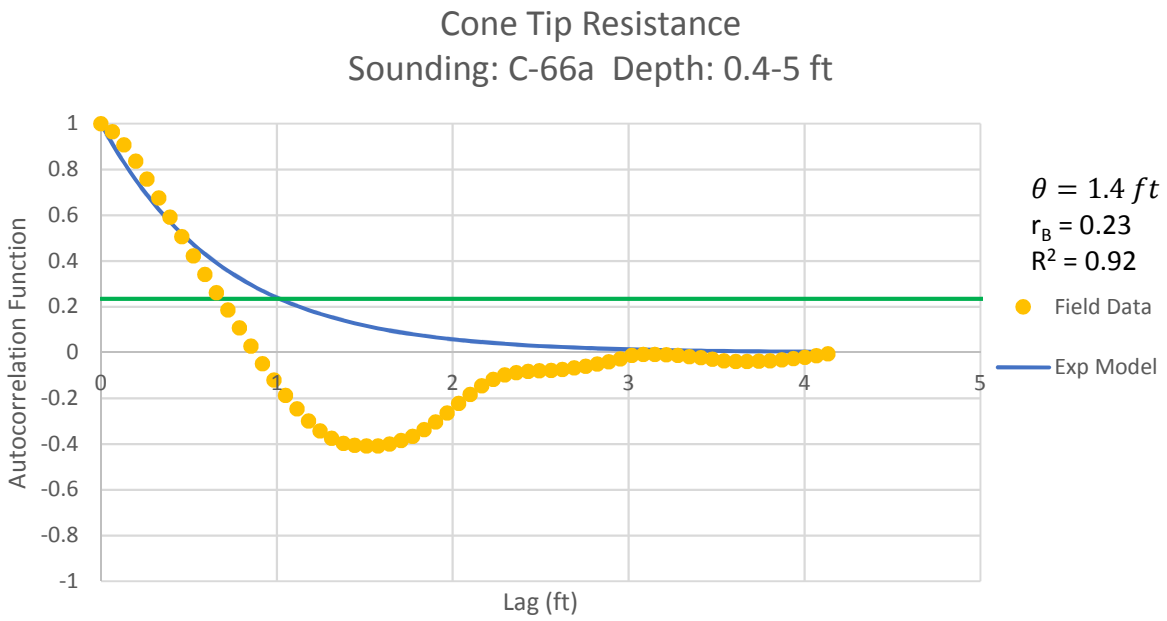

Figure B - 92: Estimation of the Scale of Fluctuation, $\theta = 1.4$ feet, for the Cone Tip Resistance Data from Sounding C-66a, "Clean sands to silty sands (6)" layer from 0.4 to 5 feet depth.

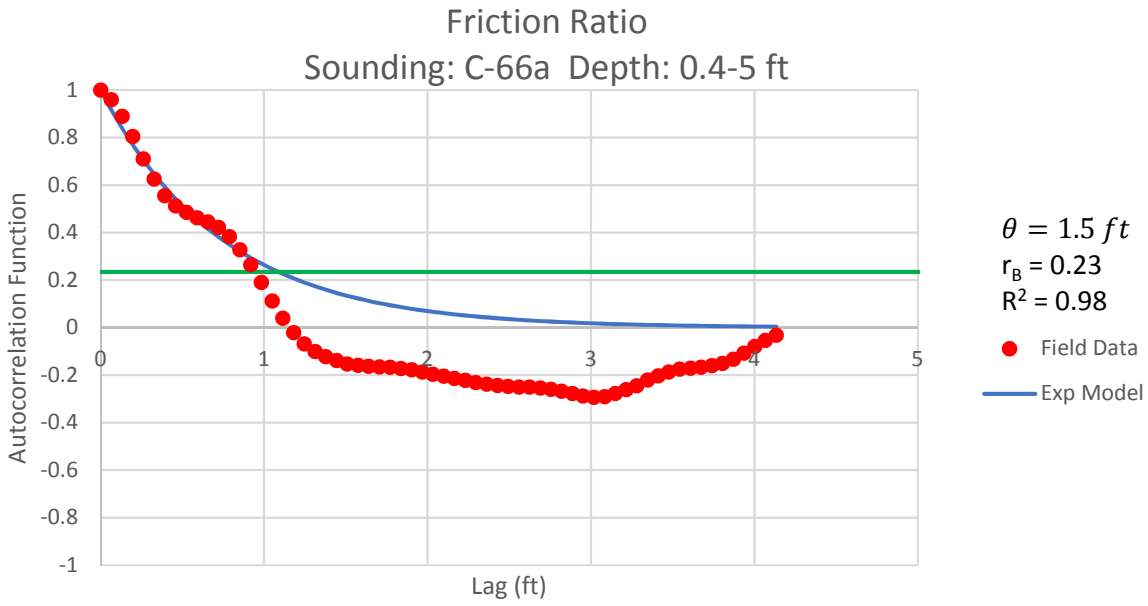

Figure B - 93: Estimation of the Scale of Fluctuation, $\theta = 1.5$ feet, for Friction Ratio Data from Sounding C-66a, "Clean sands to silty sands (6)" layer from 0.4 to 5 feet depth.

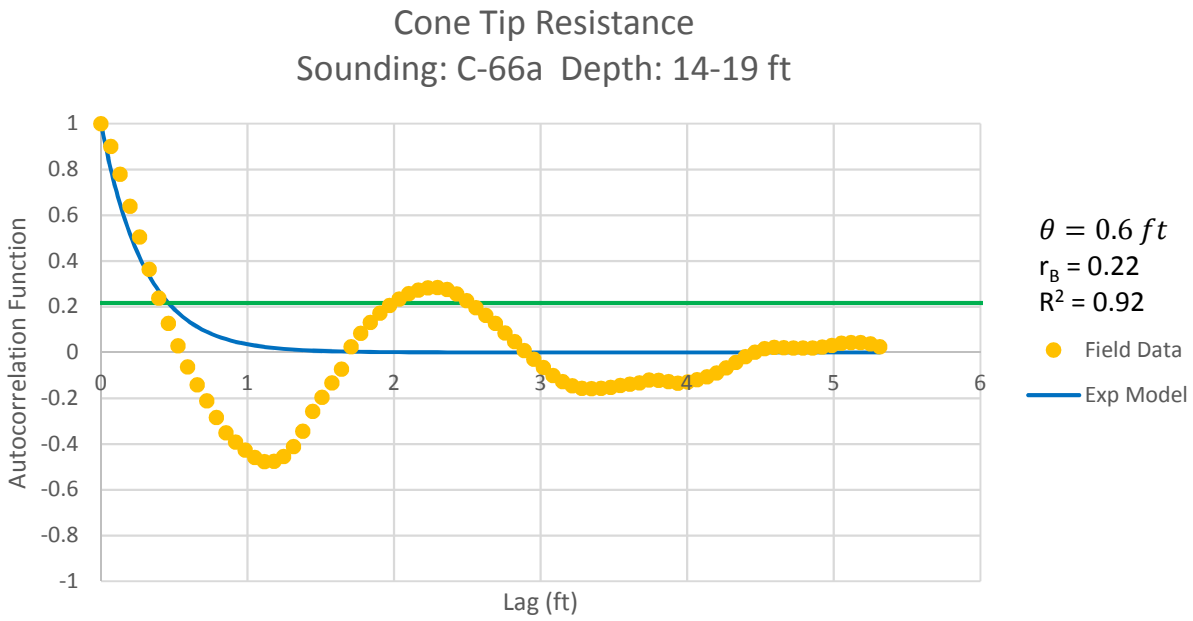

Figure B - 94: Estimation of the Scale of Fluctuation, $\theta = 0.6$ feet, for the Cone Tip Resistance Data from Sounding C-66a, "Clean sands to silty sands (6)" layer from 14 to 19 feet depth.

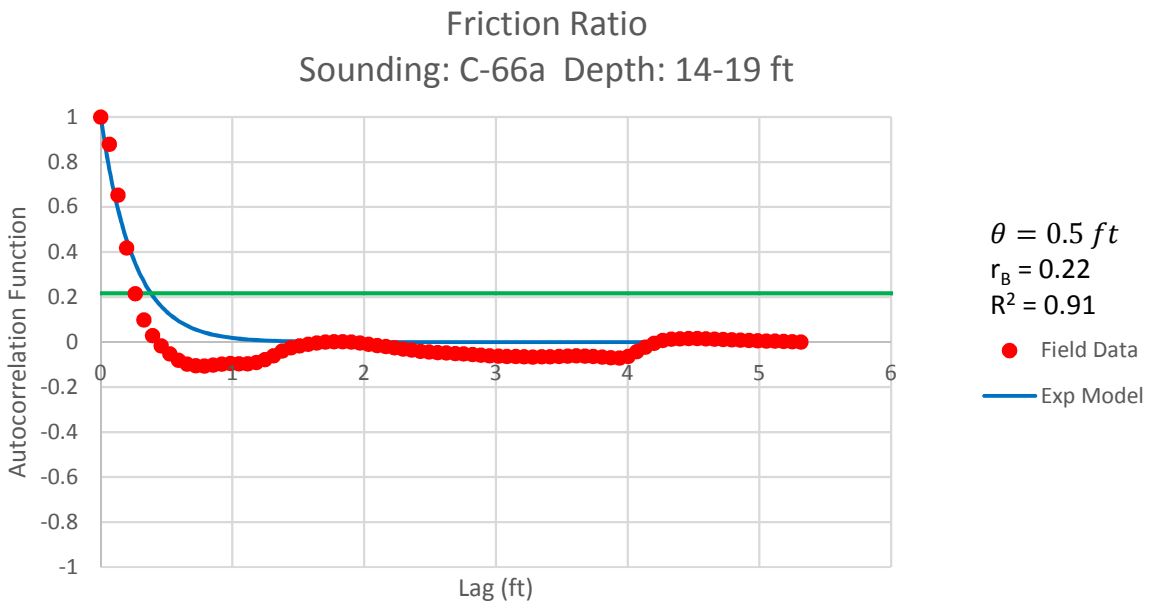

Figure B - 95: Estimation of the Scale of Fluctuation, $\theta = 0.5$ feet, for Friction Ratio Data from Sounding C-66a, "Clean sands to silty sands (6)" layer from 14 to 19 feet depth.

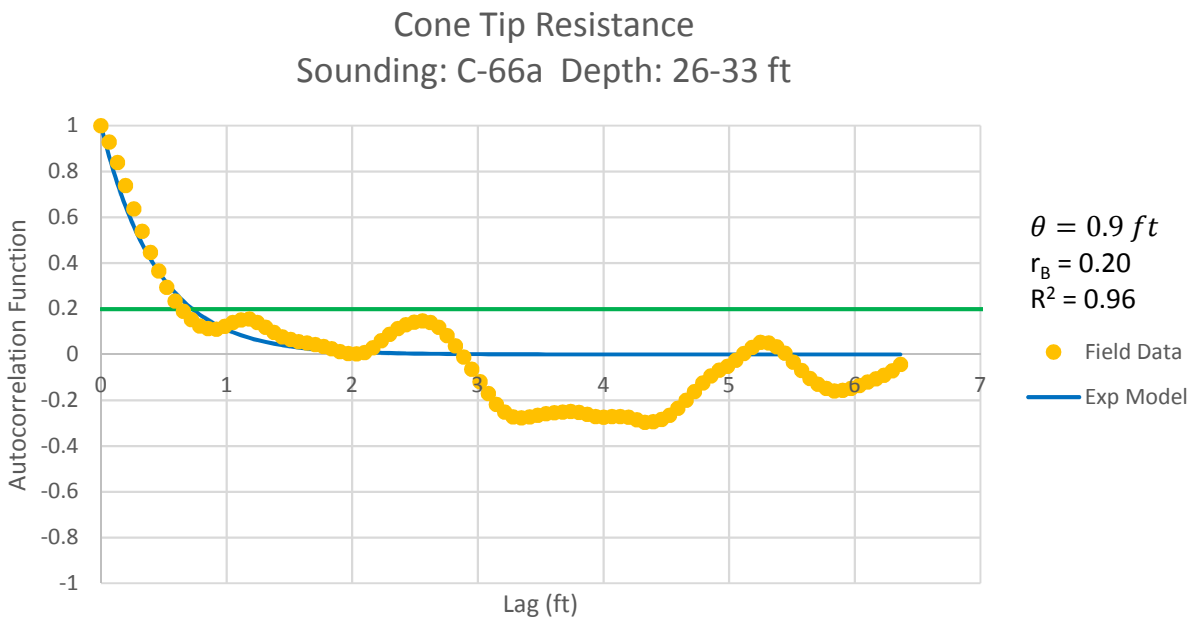

Figure B - 96: Estimation of the Scale of Fluctuation, θ = 0.9 feet, for Cone Tip Resistance Data from Sounding C-66a, "Clean sands to silty sands (6)" layer from 26 to 33 feet depth.

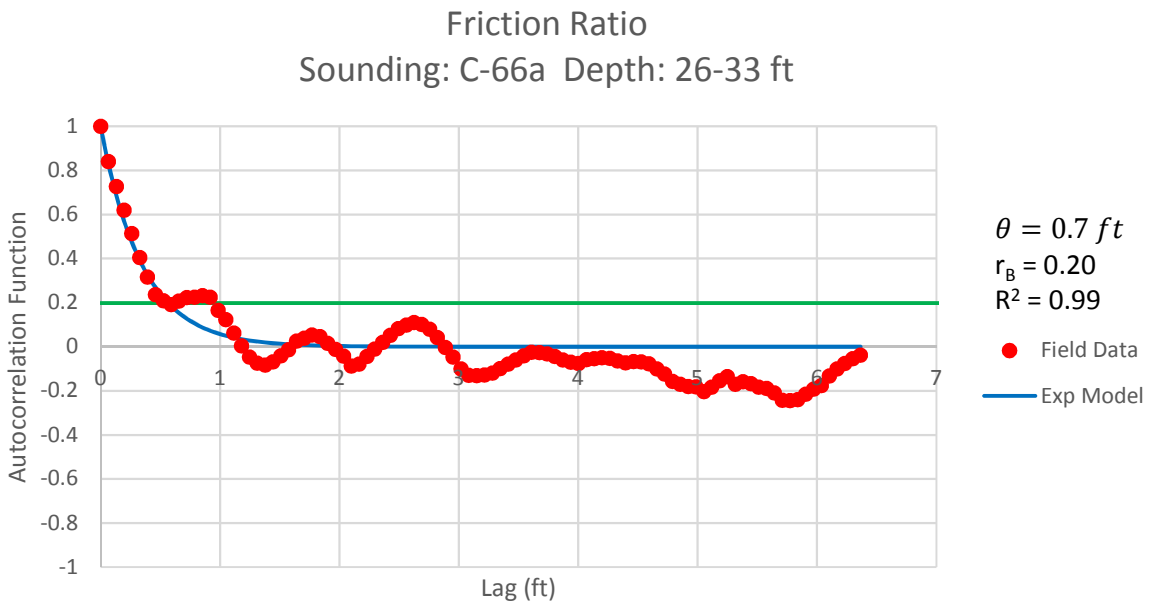

Figure B - 97: Estimation of the Scale of Fluctuation, θ, for Friction Ratio Data from Sounding C-66a, "Clean sands to silty sands (6)" layer from 26 to 33 feet depth

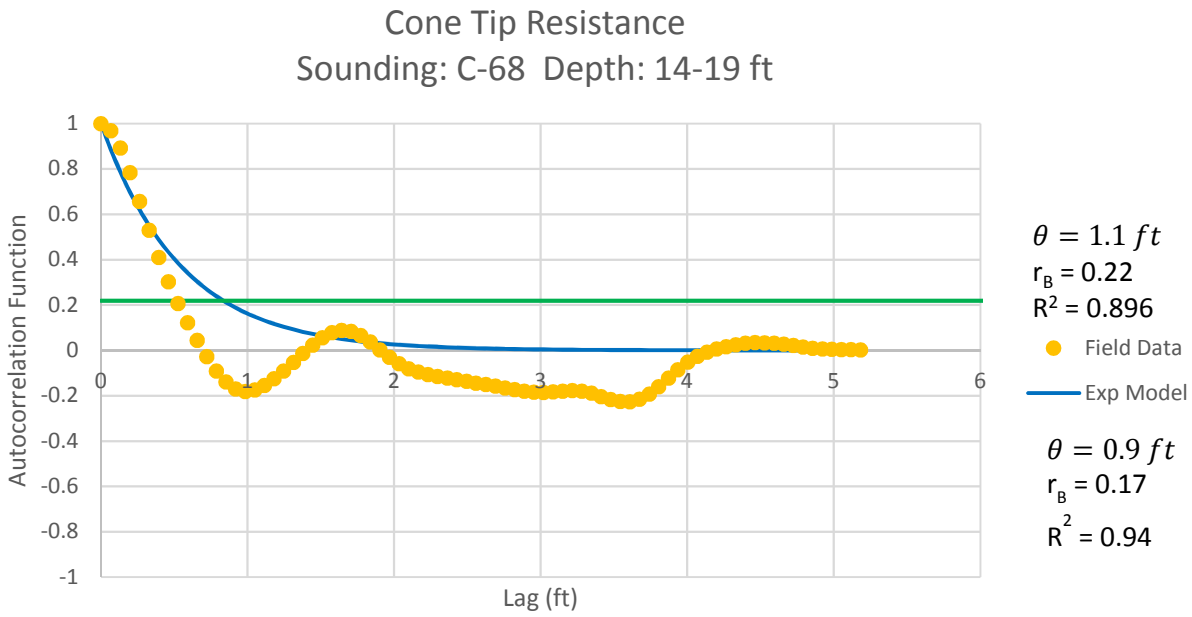

Figure B - 98: Estimation of the Scale of Fluctuation, θ = 1.1 feet, for Cone Tip Resistance Data from Sounding C-68, "Gravelly sand to sand (7)" layer from 14 to 19 feet depth. Data is a poor fit for the points greater than the Bartlett limit of 0.22; coefficient of determination, R^2 value is less 0.9. Therefore, these results were not included in final analysis.

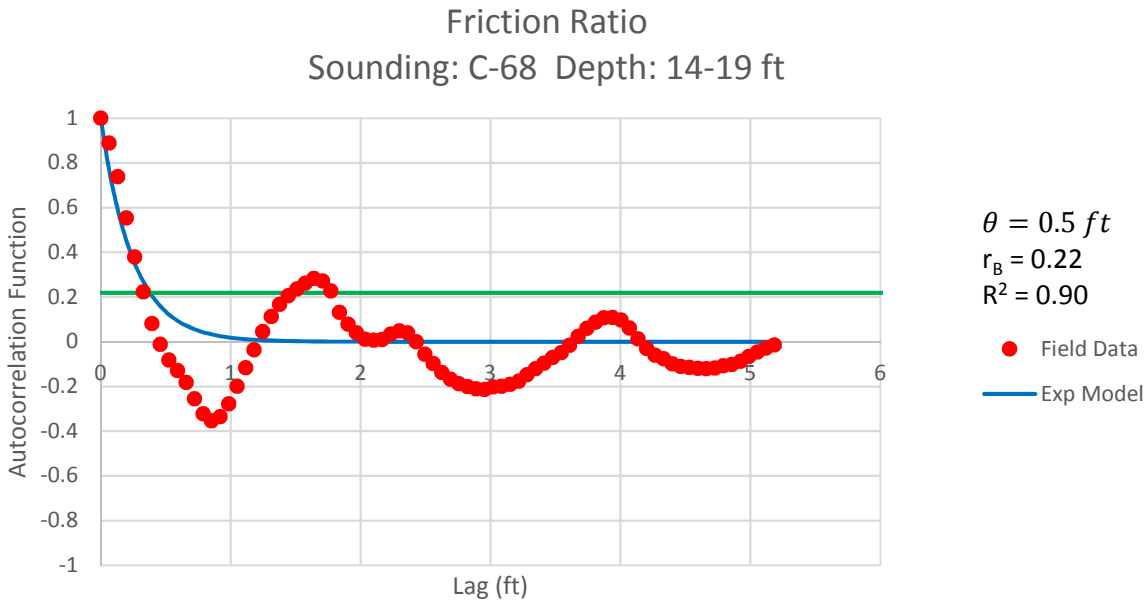

Figure B - 99: Estimation of the Scale of Fluctuation, θ = 0.5 feet, for Friction Ratio Data from Sounding C-68, "Gravelly sand to sand (7)" layer from 14 to 19 feet depth.

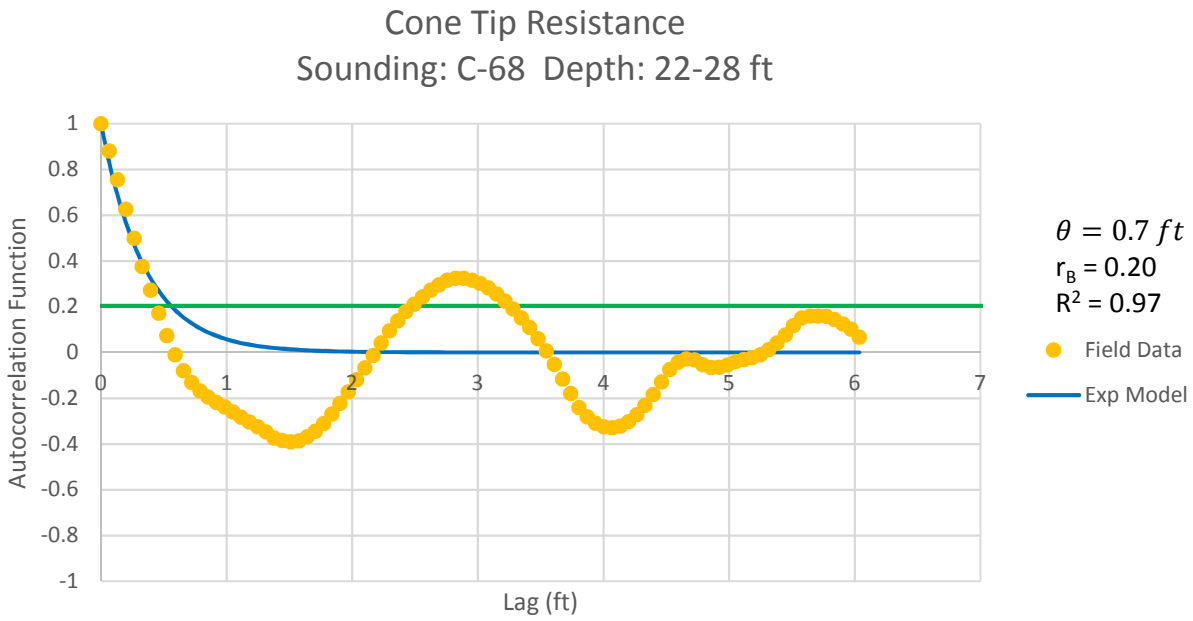

Figure B - 100: Estimation of the Scale of Fluctuation, $\theta = 0.7$ feet, for Cone Tip Resistance Data from Sounding C-68, "Clean sands to silty sands (6)" layer from 22 to 28 feet depth.

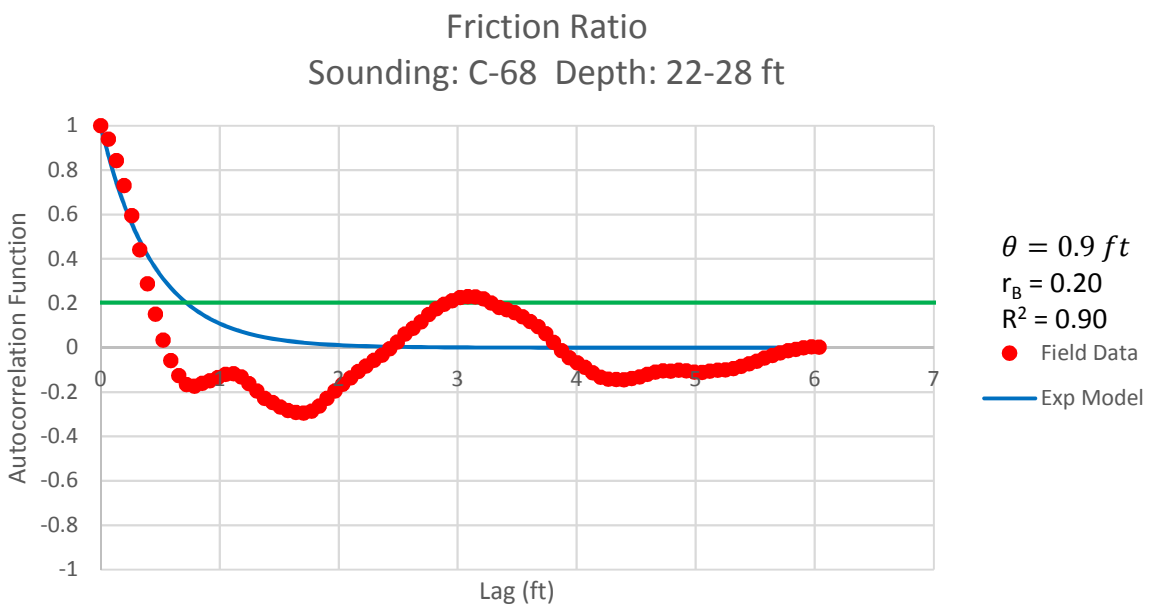

Figure B - 101: Estimation of the Scale of Fluctuation, $\theta = 0.9$ feet, for Friction Ratio Data from Sounding C-68, "Clean sands to silty sands (6)" layer from 22 to 28 feet depth.

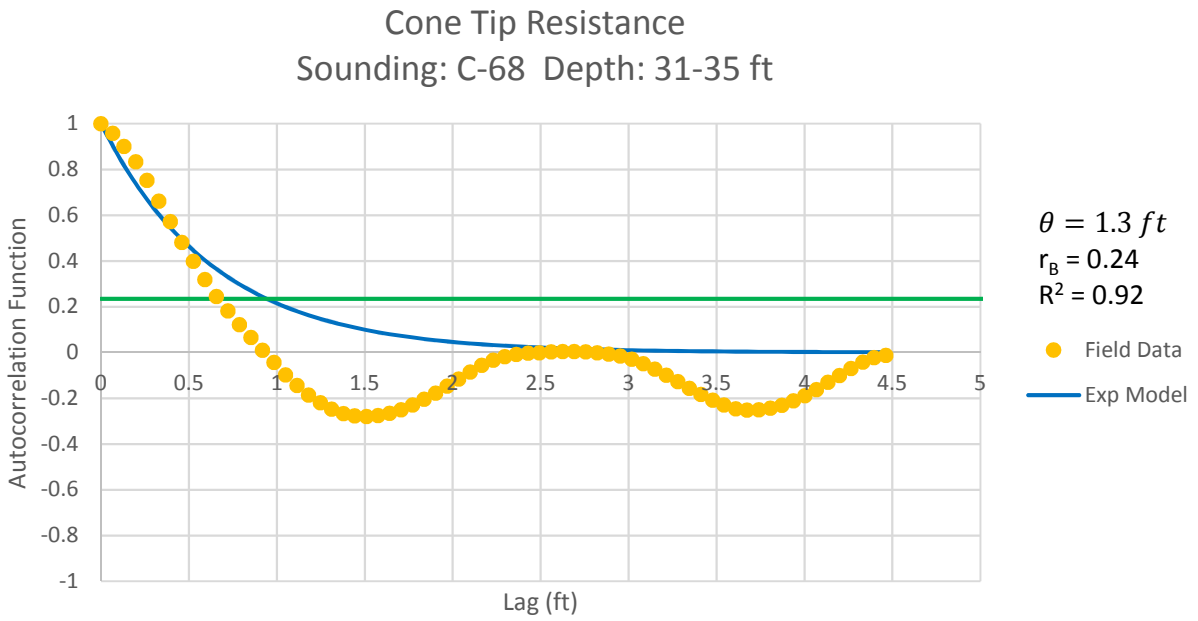

Figure B - 102: Estimation of the Scale of Fluctuation, θ = 1.3 feet, for Cone Tip Resistance Data from Sounding C-68, "Clean sands to silty sands (6)" layer from 31 to 35 feet depth.

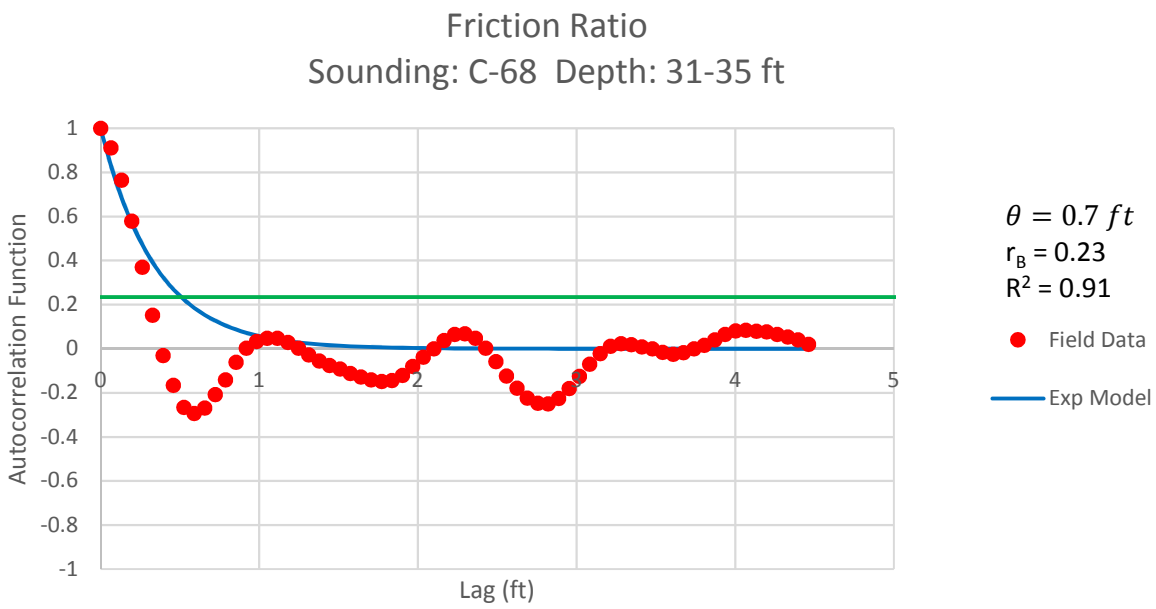

Figure B - 103: Estimation of the Scale of Fluctuation, θ = 0.7 feet, for Friction Ratio Data from Sounding C-68, "Clean sands to silty sands (6)" layer from 31 to 35 feet depth.

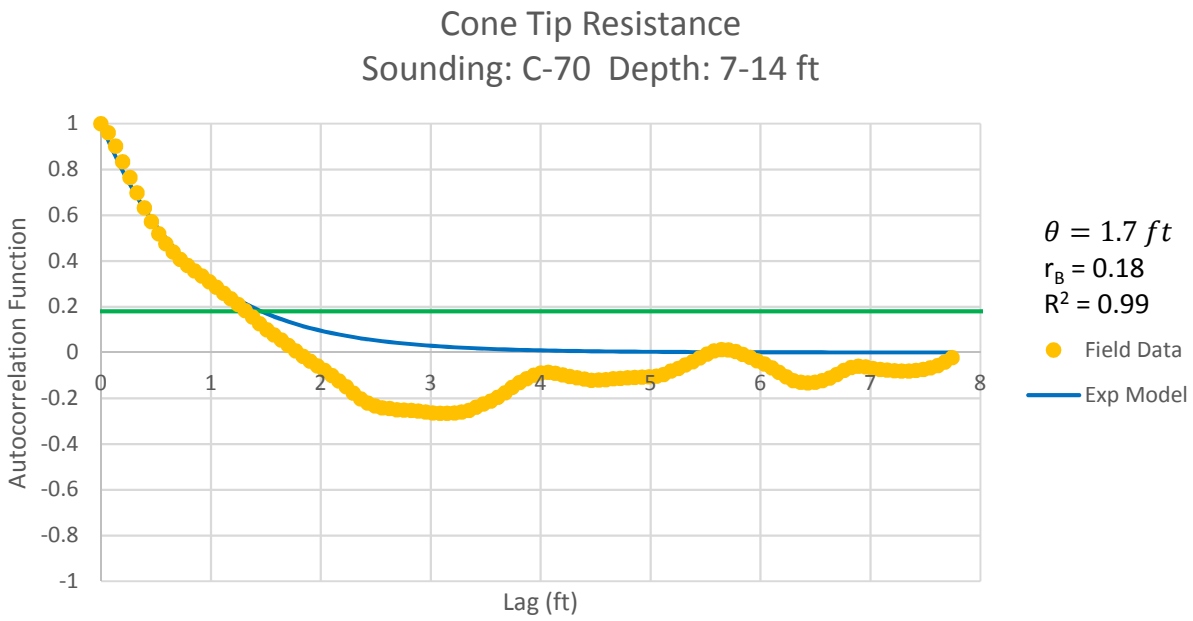

Figure B - 104: Estimation of the Scale of Fluctuation, $\theta = 1.7$ feet, for Cone Tip Resistance Data from Sounding C-70, "Clean sands to silty sands (6)" layer from 7 to 14 feet depth.

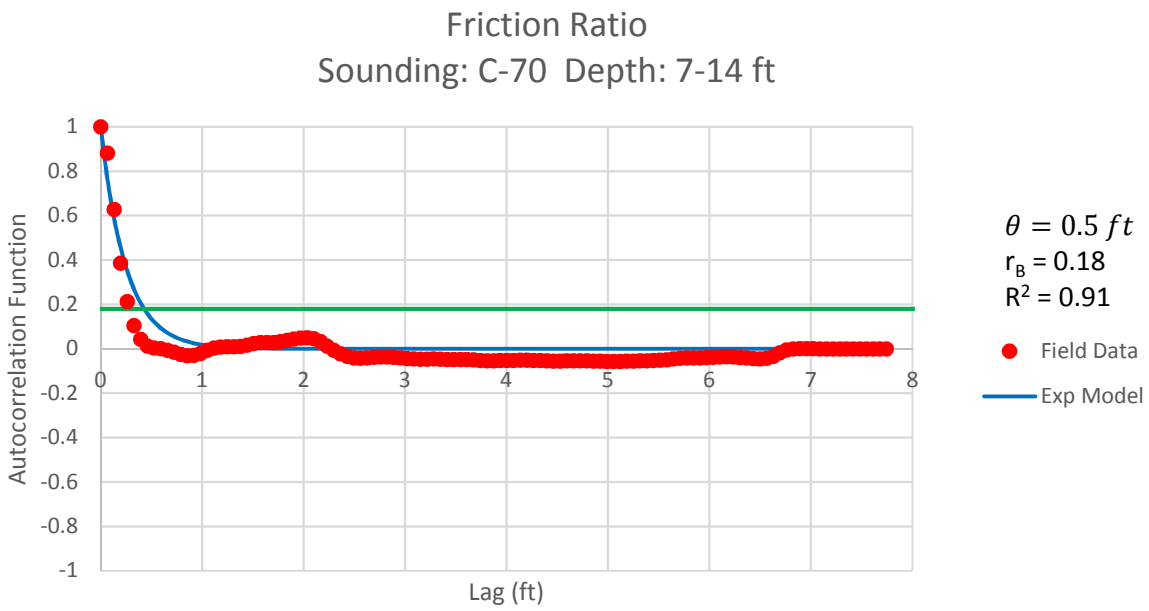

Figure B - 105: Estimation of the Scale of Fluctuation, $\theta = 0.5$ feet, for Friction Ratio Data from Sounding C-70, "Clean sands to silty sands (6)" layer from 7 to 14 feet depth.

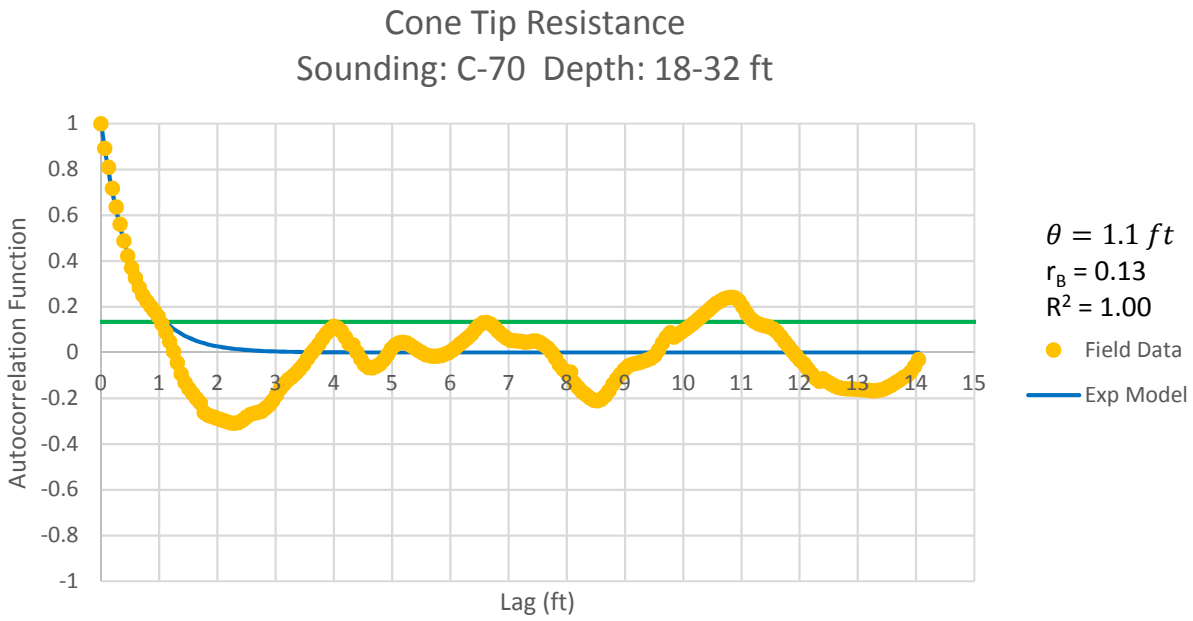

Figure B - 106: Estimation of the Scale of Fluctuation, $\theta = 1.1$ feet, for Cone Tip Resistance Data from Sounding C-70, "Clean sands to silty sands (6)" layer from 18 to 32 feet depth.

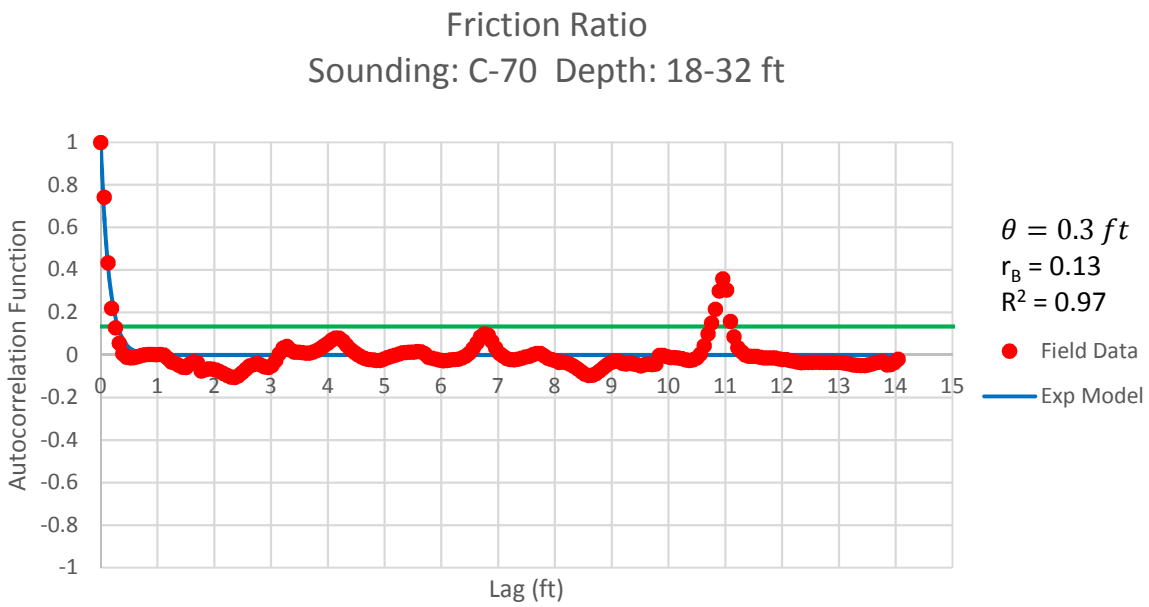

Figure B - 107: Estimation of the Scale of Fluctuation, $\theta = 0.3$ feet, for Friction Ratio Data from Sounding C-70, "Clean sands to silty sands (6)" layer from 18 to 32 feet depth.

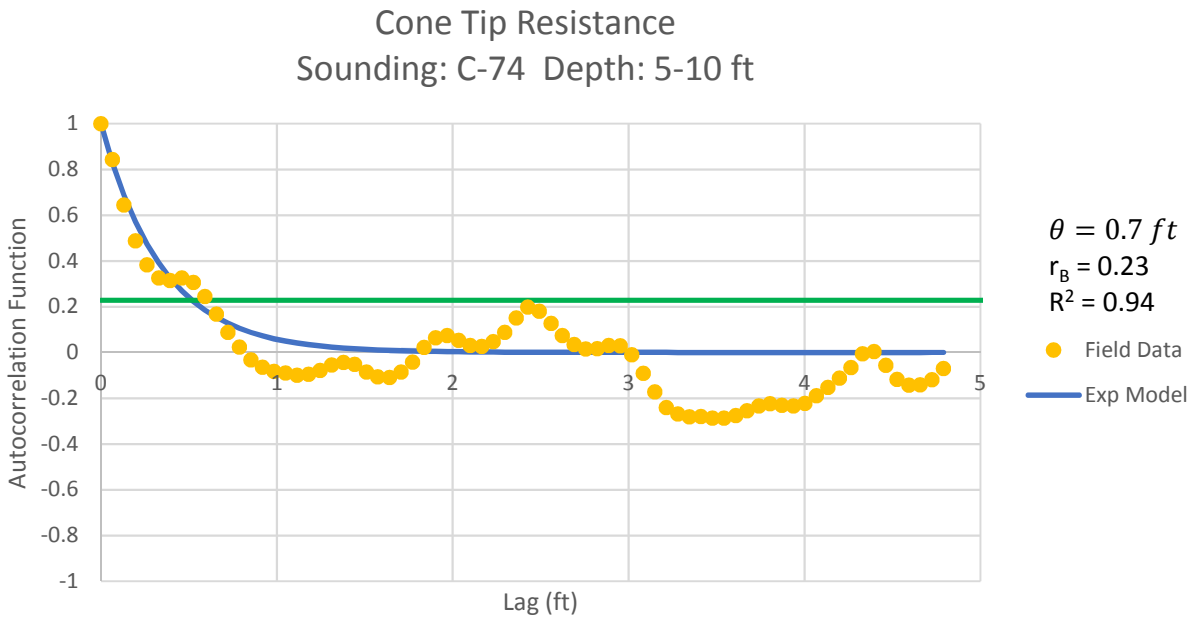

Figure B - 108: Estimation of the Scale of Fluctuation, $\theta = 0.7$ feet, for Cone Tip Resistance Data from Sounding C-74, "Clays; clay to silty clay (3)" layer from 5 to 10 feet depth.

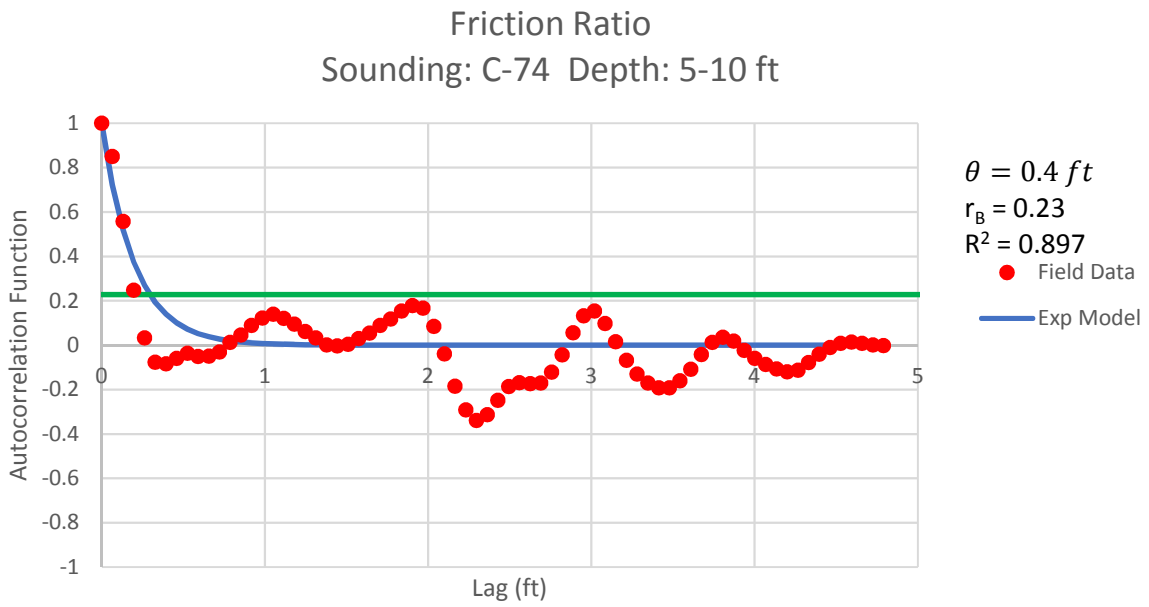

Figure B - 1090: $\theta = 0.4$ feet, for Friction Ratio Data from Sounding C-74, "Clays; clay to silty clay (3)" layer from 5 to 10 feet depth. Data is a poor fit for the points greater than the Bartlett limit of 0.23; coefficient of determination, R^2, value is less 0.9. Therefore, these results were not included in final analysis

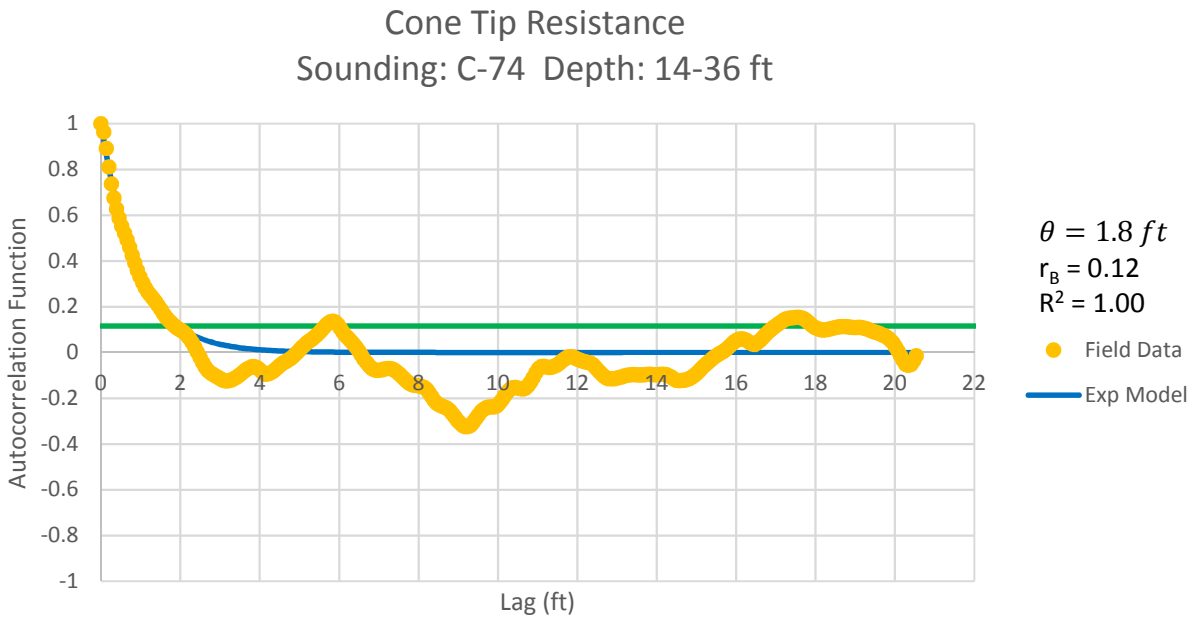

Figure B - 110: Estimation of the Scale of Fluctuation, $\theta = 1.8$ feet, for Cone Tip Resistance Data from Sounding C-74, "Clean sands to silty sands (6)" layer from 14 to 36 feet depth.

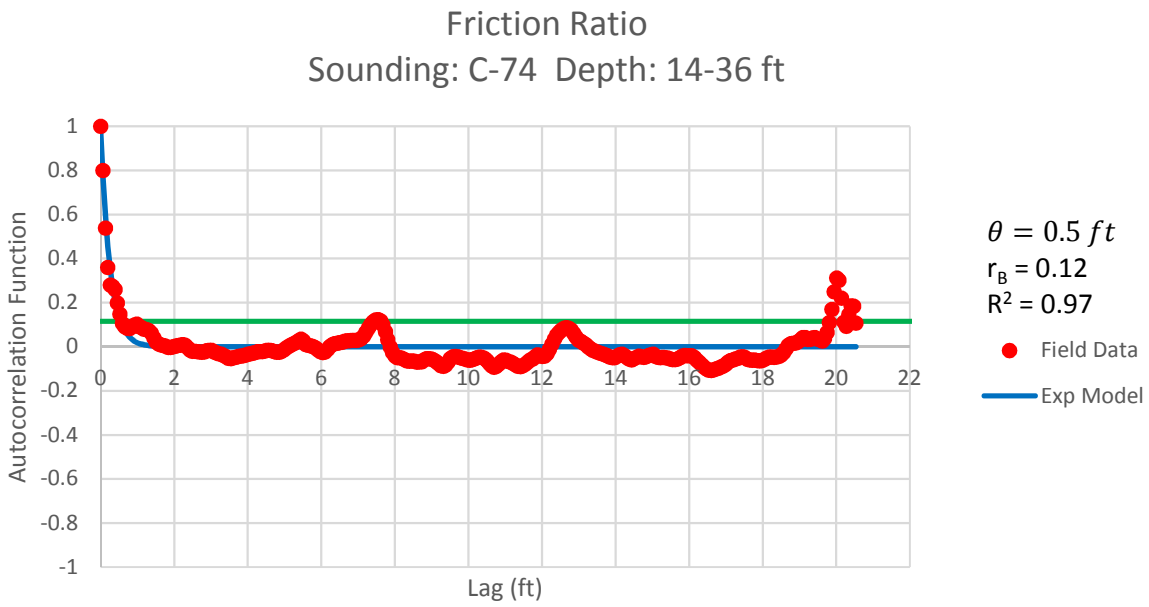

Figure B - 111: Estimation of the Scale of Fluctuation, $\theta = 0.5$ feet, for Friction Ratio Data from Sounding C-74, "Clean sands to silty sands (6)" layer from 14 to 36 feet depth.

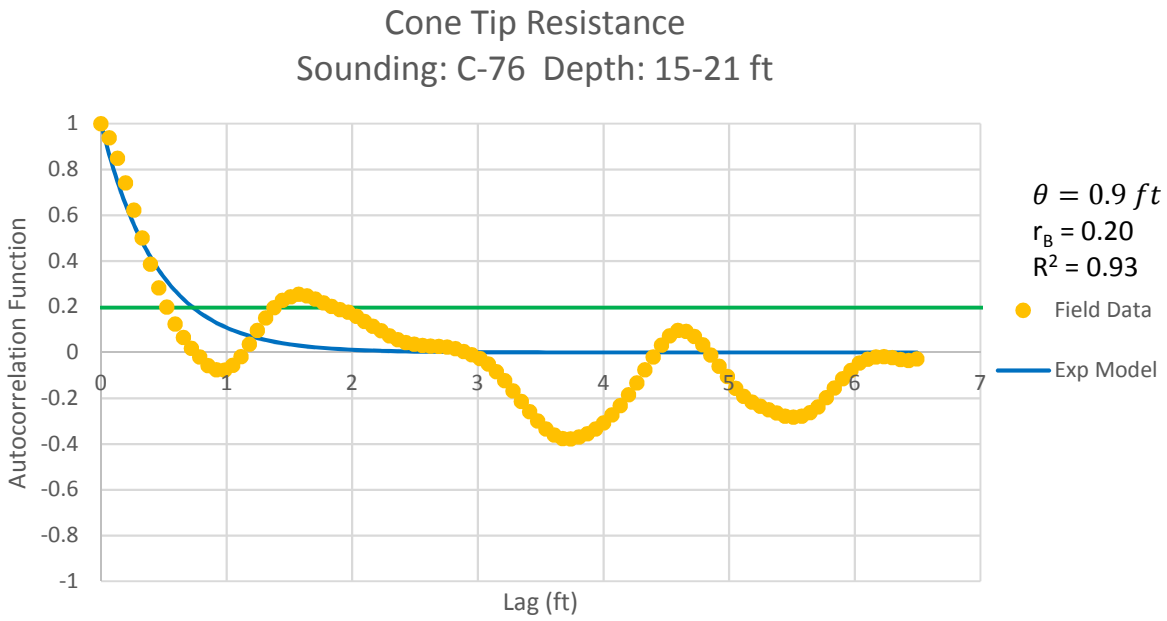

Figure B - 112: Estimation of the Scale of Fluctuation, $\theta = 0.9$ feet, for Cone Tip Resistance Data from Sounding C-76, "Clean sands to silty sands (6)" layer from 15 to 21 feet depth.

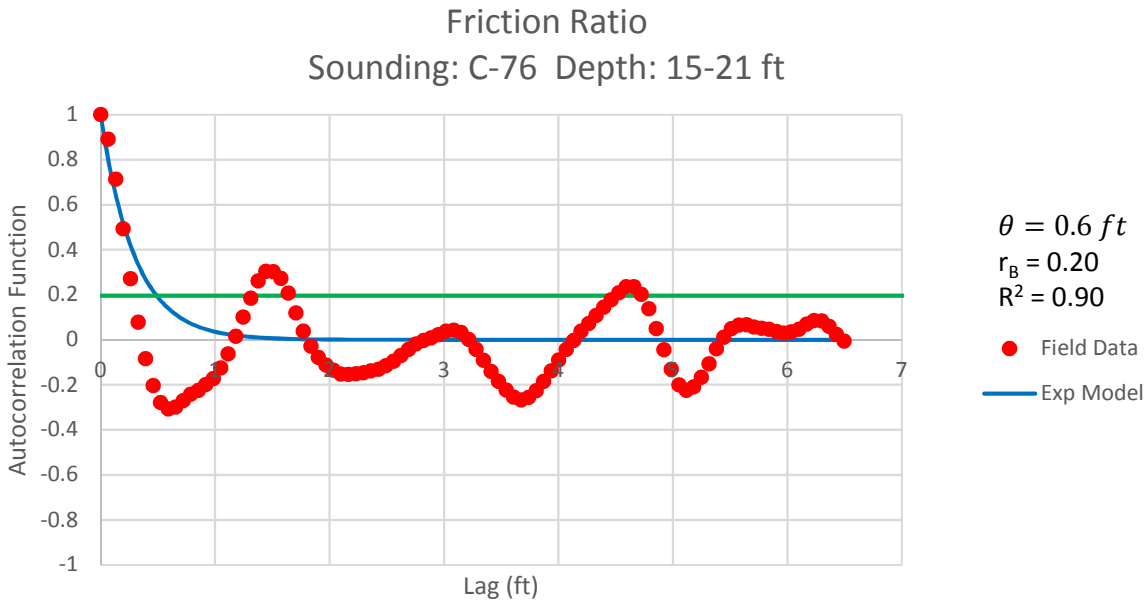

Figure B - 113: Estimation of the Scale of Fluctuation, $\theta = 0.6$ feet, for Friction Ratio Data from Sounding C-76, "Clean sands to silty sands (6)" layer from 15 to 21 feet depth.

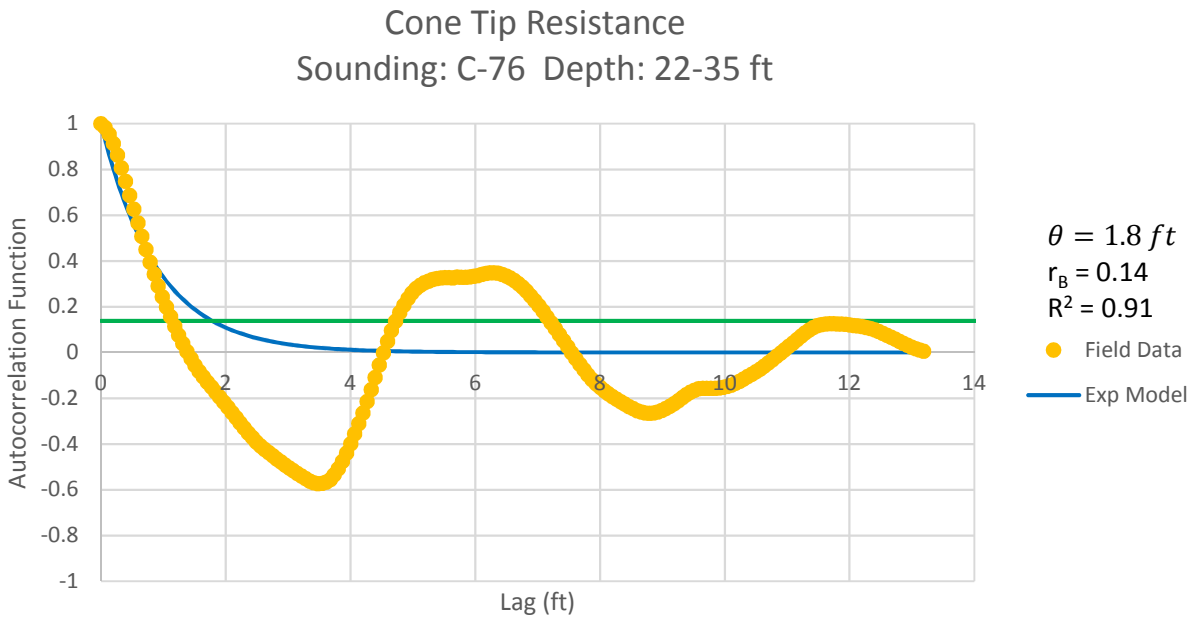

Figure B - 114: Estimation of the Scale of Fluctuation, $\theta = 1.8$ feet, for Cone Tip Resistance Data from Sounding C-76, "Clean sands to silty sands (6)" layer from 22 to 35 feet depth.

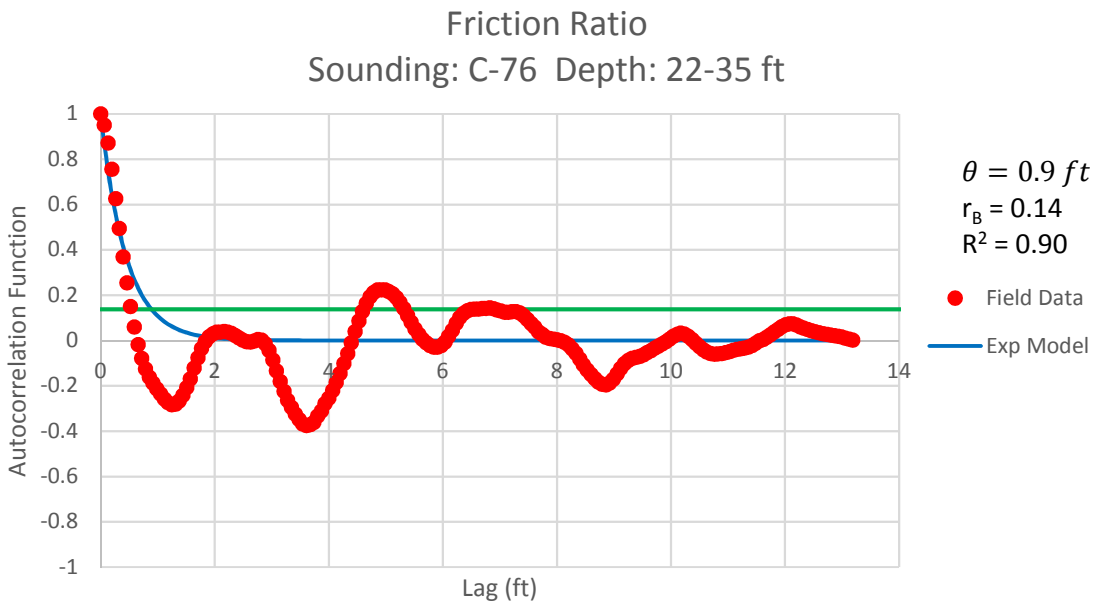

Figure B - 115: Estimation of the Scale of Fluctuation, $\theta = 0.9$ feet, for Friction Ratio Data from Sounding C-76, "Clean sands to silty sands (6)" layer from 22 to 35 feet depth.

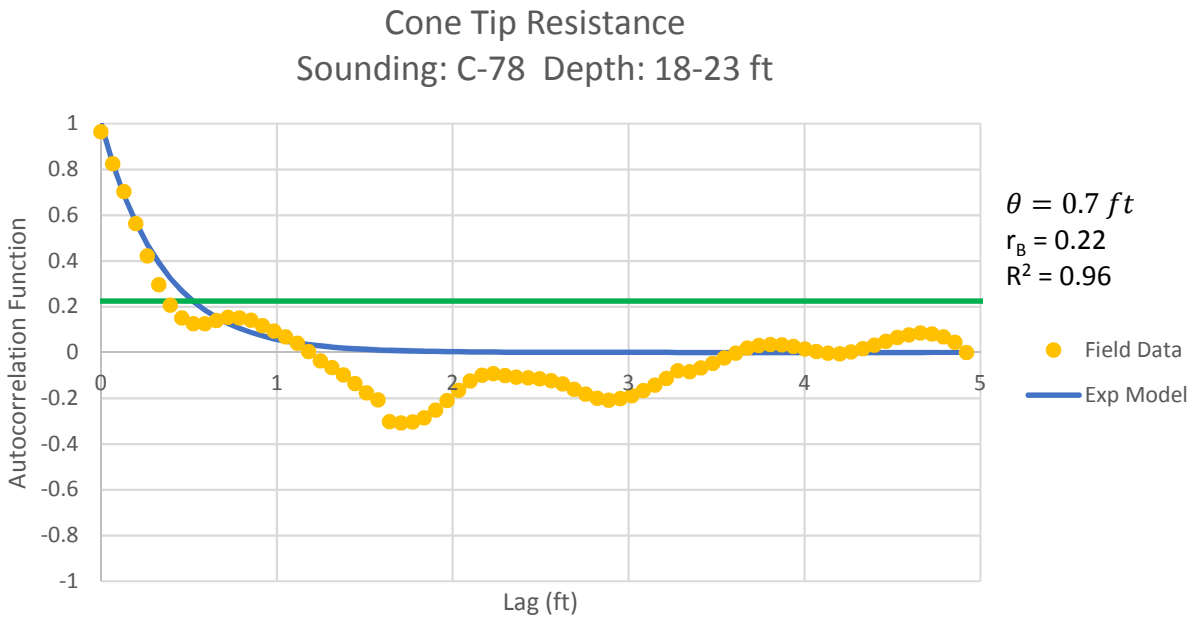

Figure B - 116: Estimation of the Scale of Fluctuation, $\theta = 0.7$ feet, for Cone Tip Resistance Data from Sounding C-78, "Clean sands to silty sands (6)" layer from 18 to 23 feet depth.

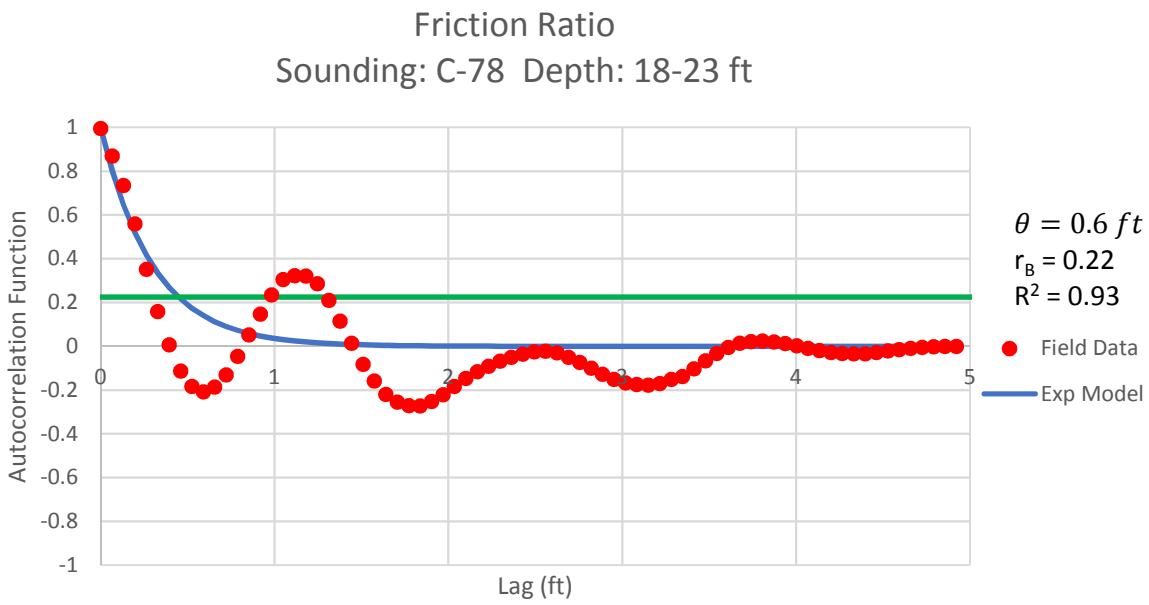

Figure B - 117: Estimation of the Scale of Fluctuation, $\theta = 0.6$ feet, for Friction Ratio Data from Sounding C-78, "Clean sands to silty sands (6)" layer from 18 to 23 feet depth.

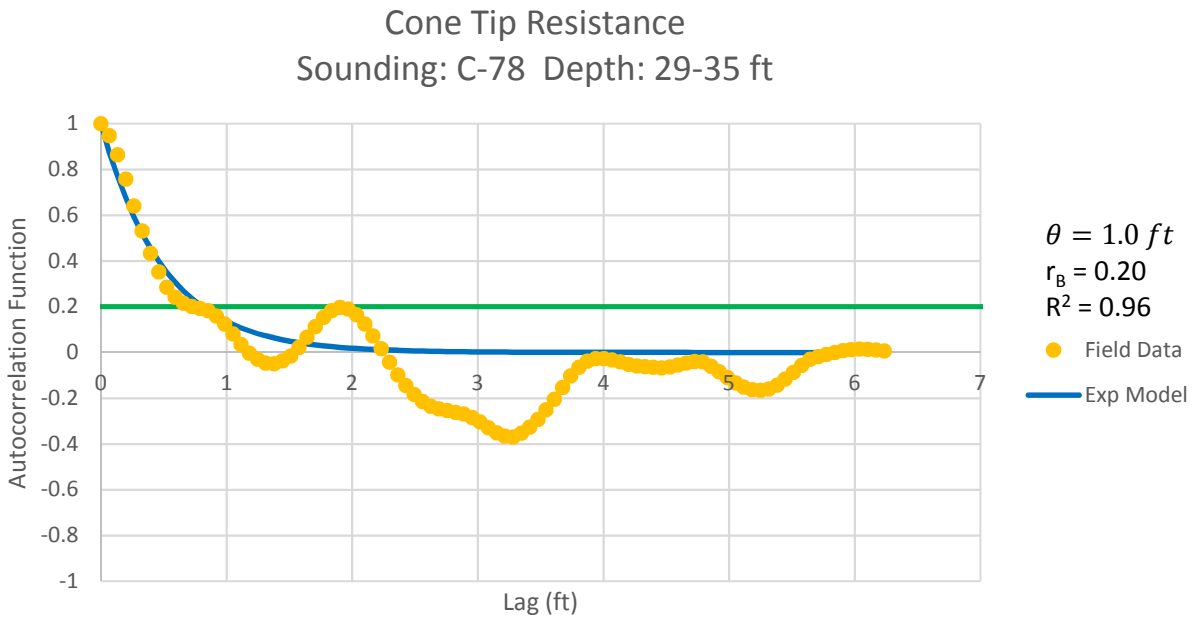

Figure B - 118: Estimation of the Scale of Fluctuation, θ = 1.0 feet, for Cone Tip Resistance Data from Sounding C-78, "Clean sands to silty sands (6)" layer from 29 to 35 feet depth.

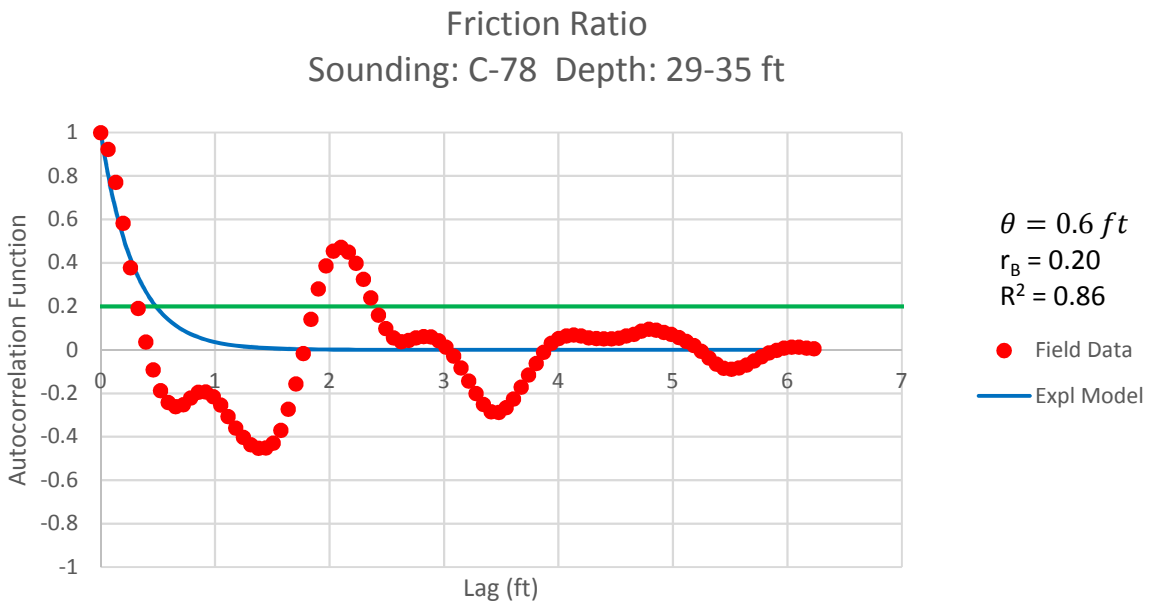

Figure B - 119: Estimation of the Scale of Fluctuation, θ = 0.6 feet, for Friction Ratio Data from Sounding C-78, "Clean sands to silty sands (6)" layer from 29 to 35 feet depth. Data is a poor fit for the points greater than the Bartlett limit of 0.20; coefficient of determination, R^2, value is less 0.9. Therefore, these results were not included in final analysis.

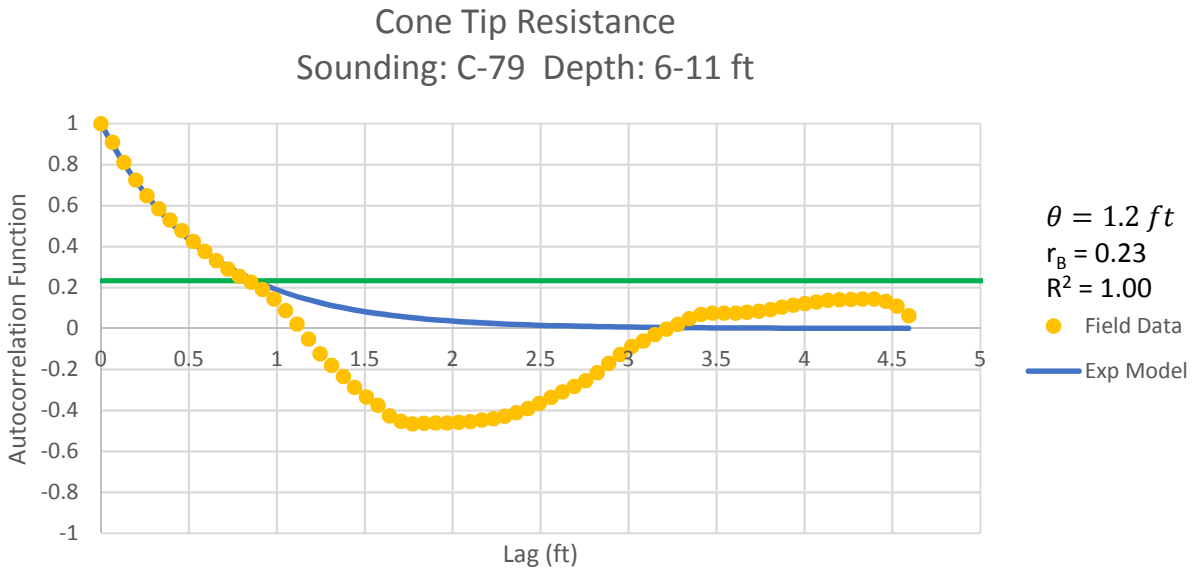

Figure B - 120: Estimation of the Scale of Fluctuation, $\theta = 1.2$ feet, for Cone Tip Resistance Data from Sounding C-79, "Clean sands to silty sands (6)" layer from 6 to 11 feet depth.

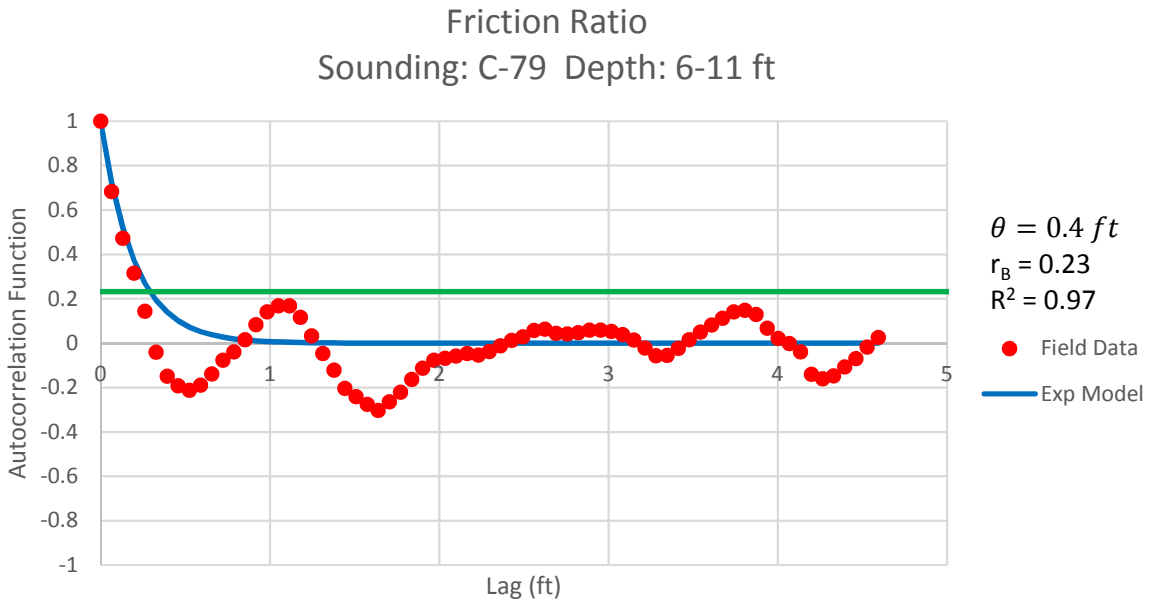

Figure B - 121: Estimation of the Scale of Fluctuation, $\theta = 0.4$ feet, for Friction Ratio Data from Sounding C-79, "Clean sands to silty sands (6)" layer from 6 to 11 feet depth.

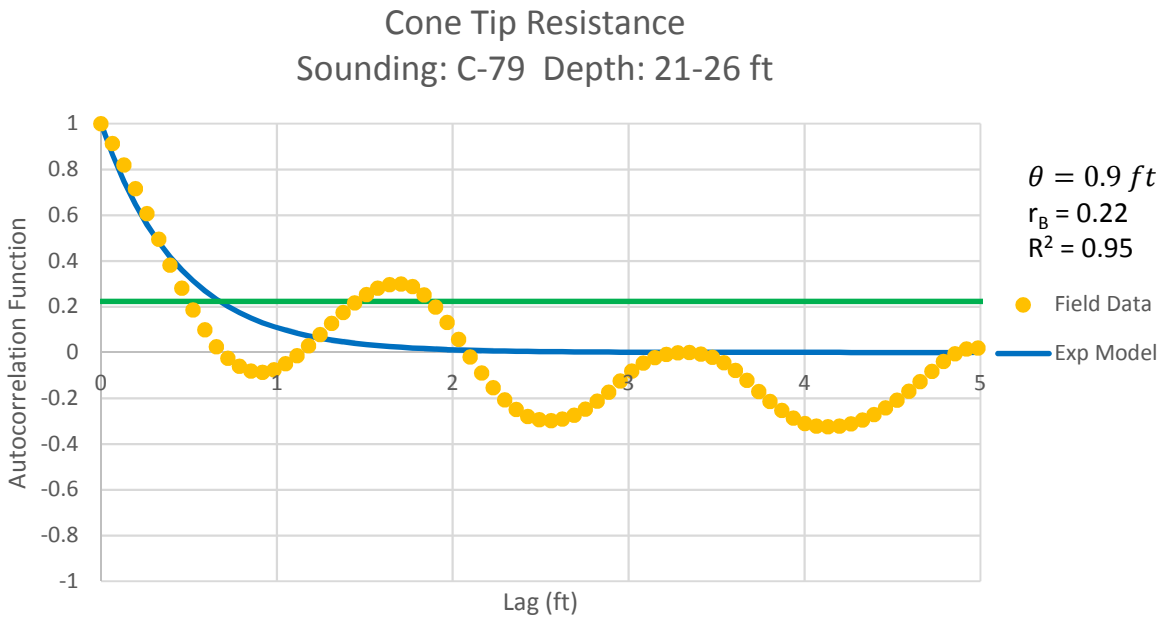

Figure B - 122: Estimation of the Scale of Fluctuation, $\theta = 0.9$ feet, for Cone Tip Resistance Data from Sounding C-79, "Clean sands to silty sands (6)" layer from 21 to 26 feet depth.

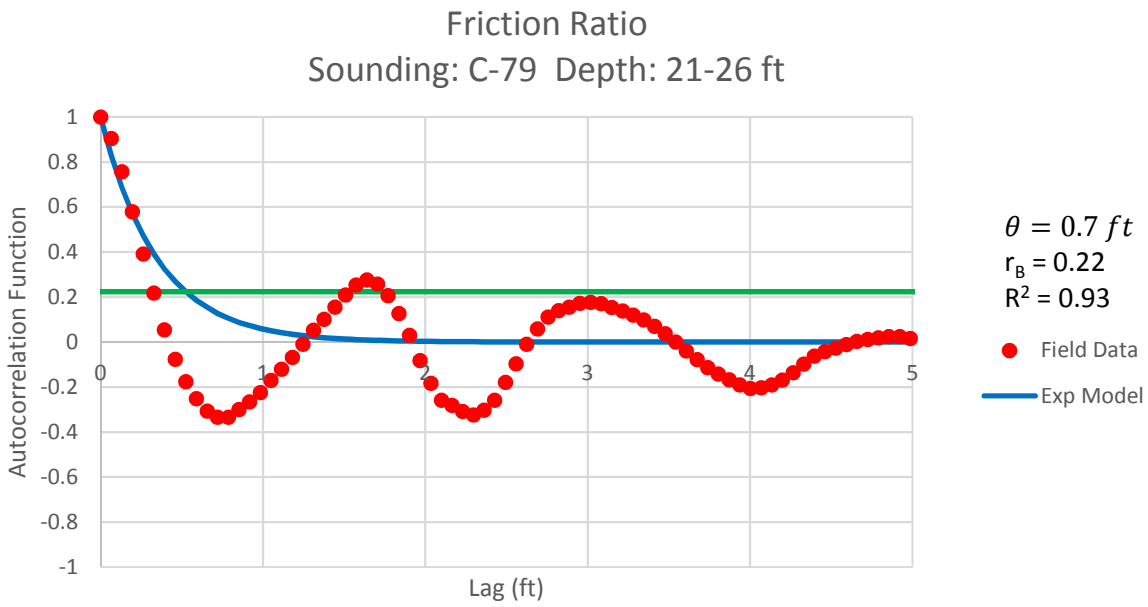

Figure B - 123: Estimation of the Scale of Fluctuation, $\theta = 0.7$ feet, for Friction Ratio Data from Sounding C-79, "Clean sands to silty sands (6)" layer from 21 to 26 feet depth.

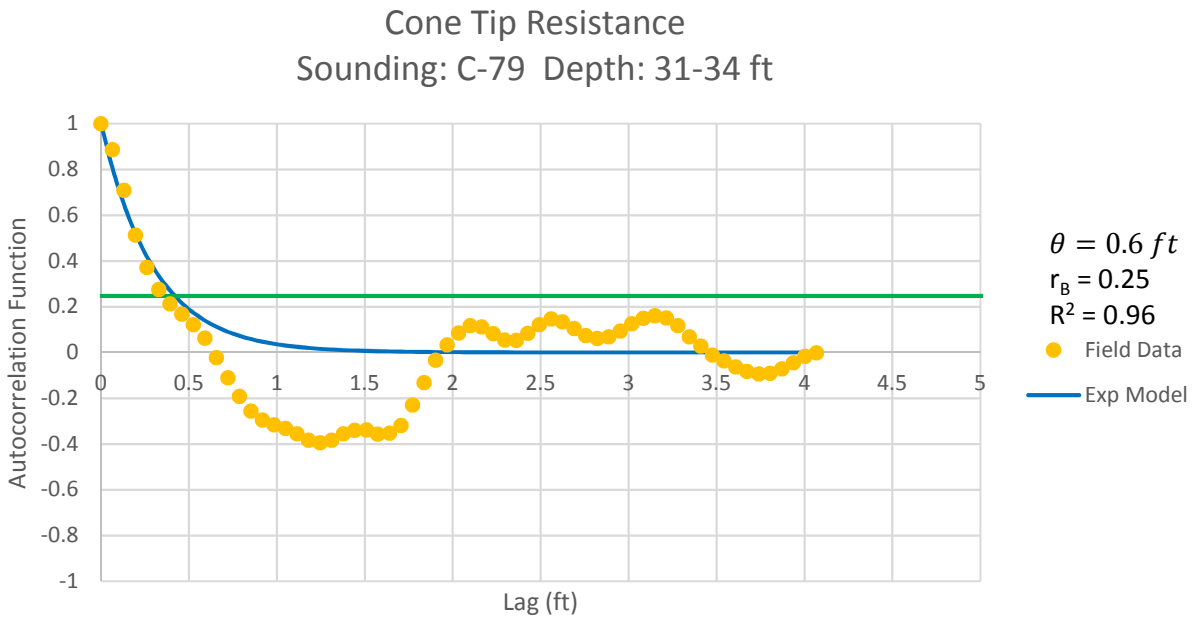

Figure B - 124: Estimation of the Scale of Fluctuation, $\theta = 0.6$ feet, for Cone Tip Resistance Data from Sounding C-79, "Gravelly sand to sand (7)" layer from 31 to 34 feet depth.

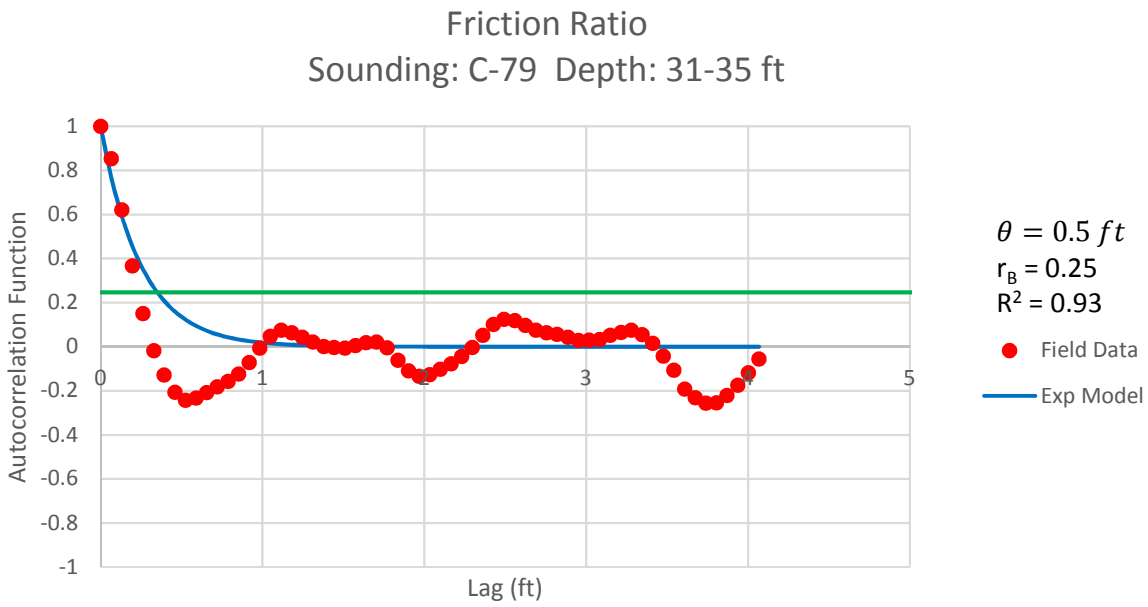

Figure B - 125: Estimation of the Scale of Fluctuation, $\theta = 0.5$ feet, for Friction Ratio Data from Sounding C-79, "Gravelly sand to sand (7)" layer from 31 to 34 feet depth.

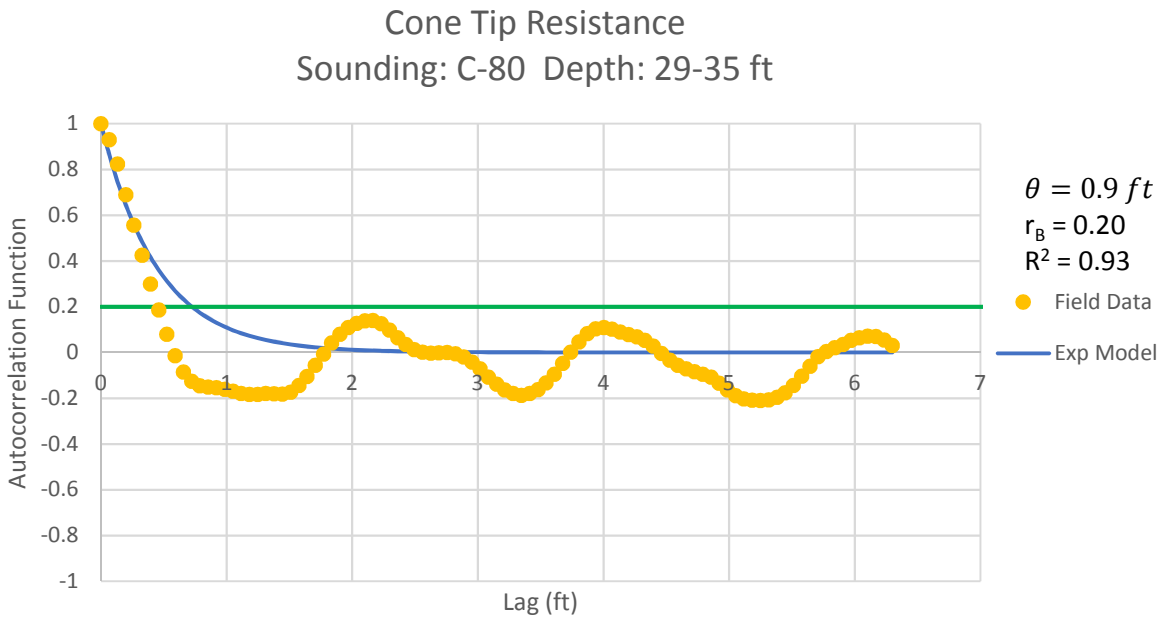

Figure B - 126: Estimation of the Scale of Fluctuation, $\theta = 0.9$ feet, for Cone Tip Resistance Data from Sounding C-80, "Clean sands to silty sands (6)" layer from 29 to 35 feet depth.

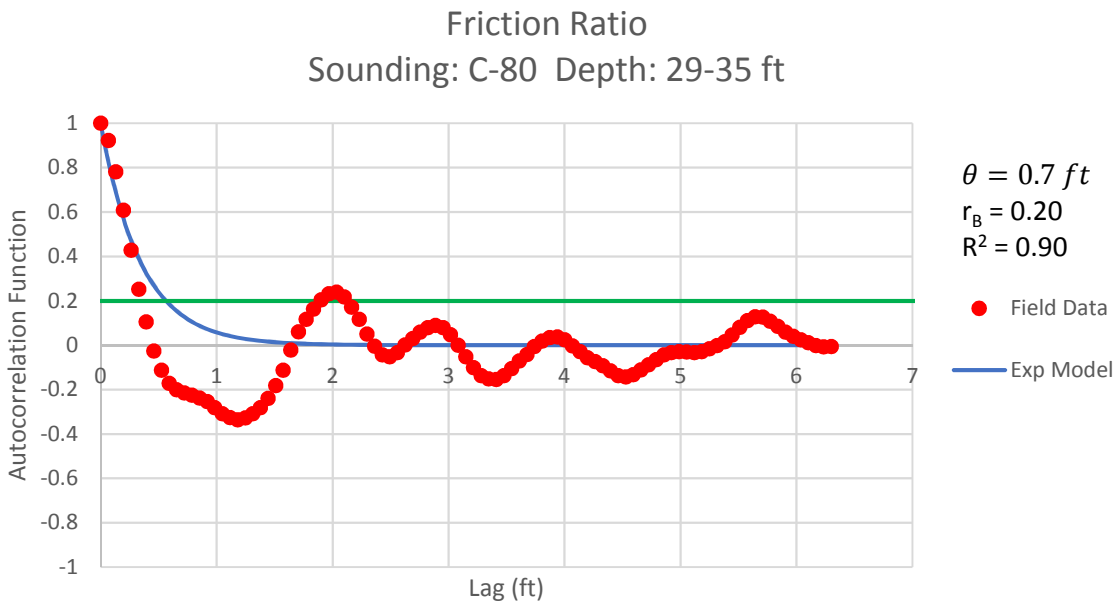

Figure B - 127: Estimation of the Scale of Fluctuation, $\theta = 0.7$ feet, for Friction Ratio Data from Sounding C-80, "Clean sands to silty sands (6)" layer from 29 to 35 feet depth.

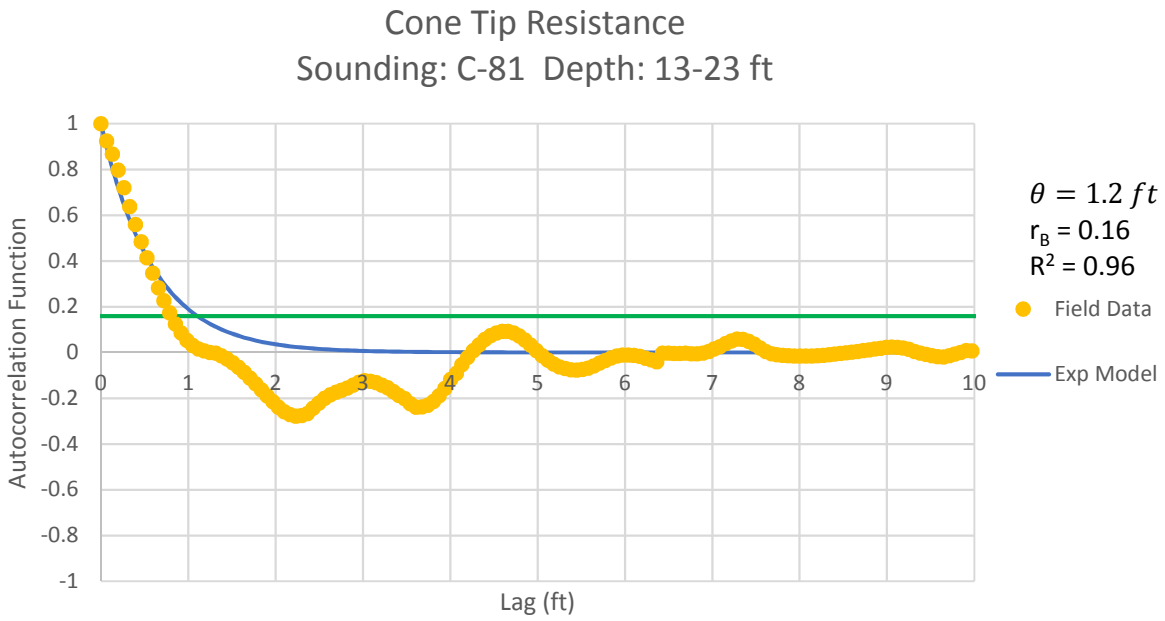

Figure B - 128: Estimation of the Scale of Fluctuation, θ = 1.2 feet, for Cone Tip Resistance Data from Sounding C-81, " Clean sands to silty sands (6)" layer from 13 to 23 feet depth.

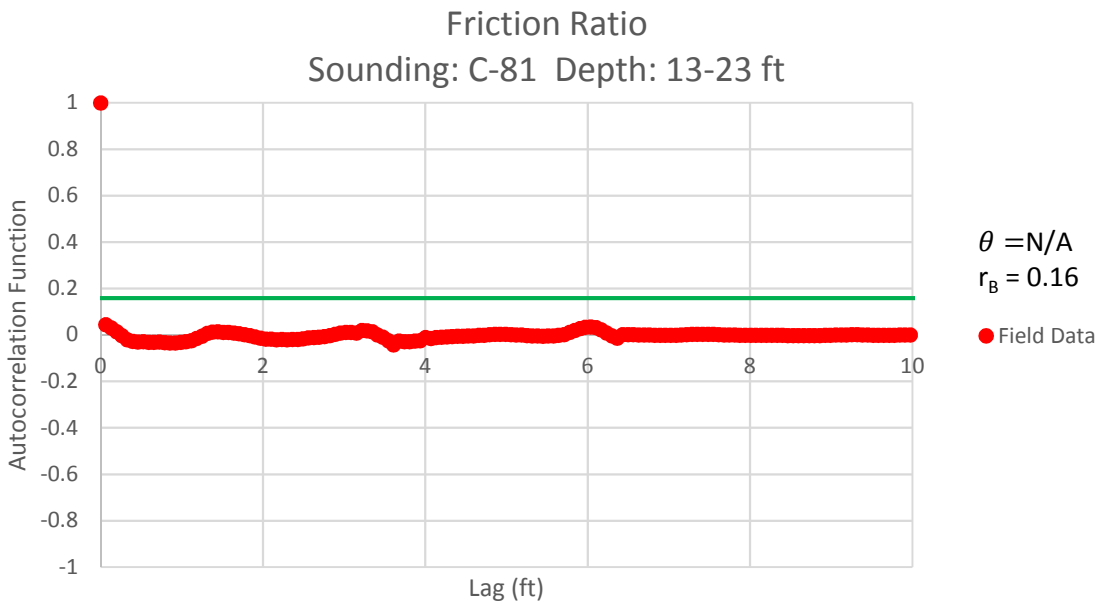

Figure B - 129: Estimation of the Scale of Fluctuation, θ, for Friction Ratio Data from Sounding C-81, " Clean sands to silty sands (6)" layer from 13 to 23 feet depth. Data is limited to only 1 point greater than the Bartlett limit of 0.16; therefore, θ could not be estimated, and these results were not included in final analysis.

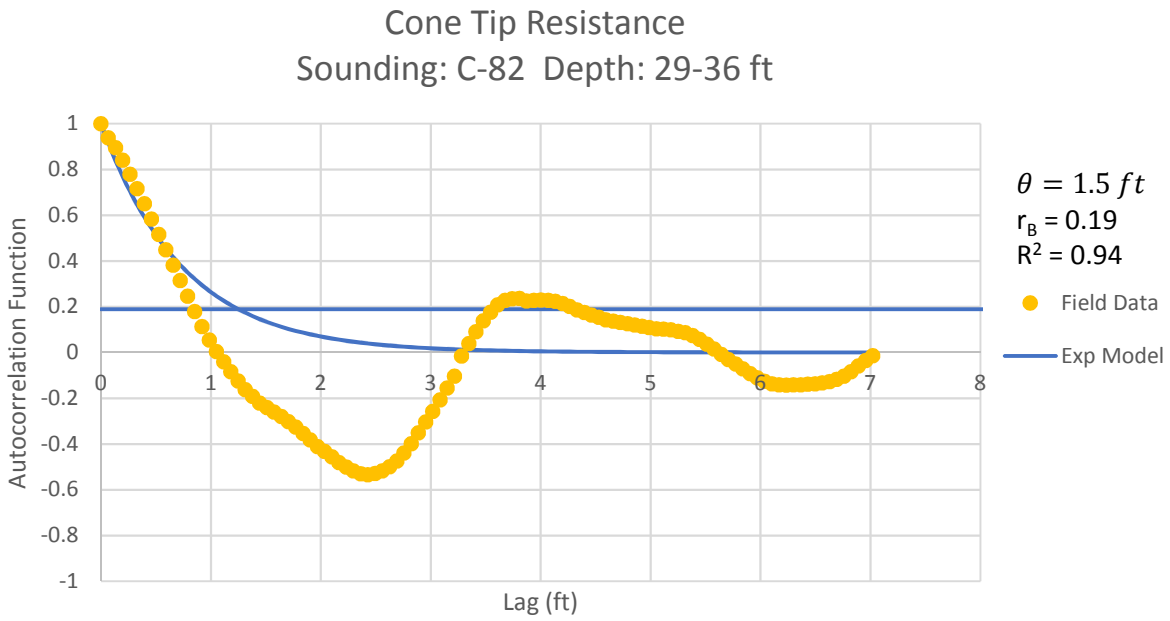

Figure B - 1301: Estimation of the Scale of Fluctuation, $\theta = 1.5$ feet, for Cone Tip Resistance Data from Sounding C-82, "Clean sands to silty sands (6)" layer from 29 to 36 feet depth.

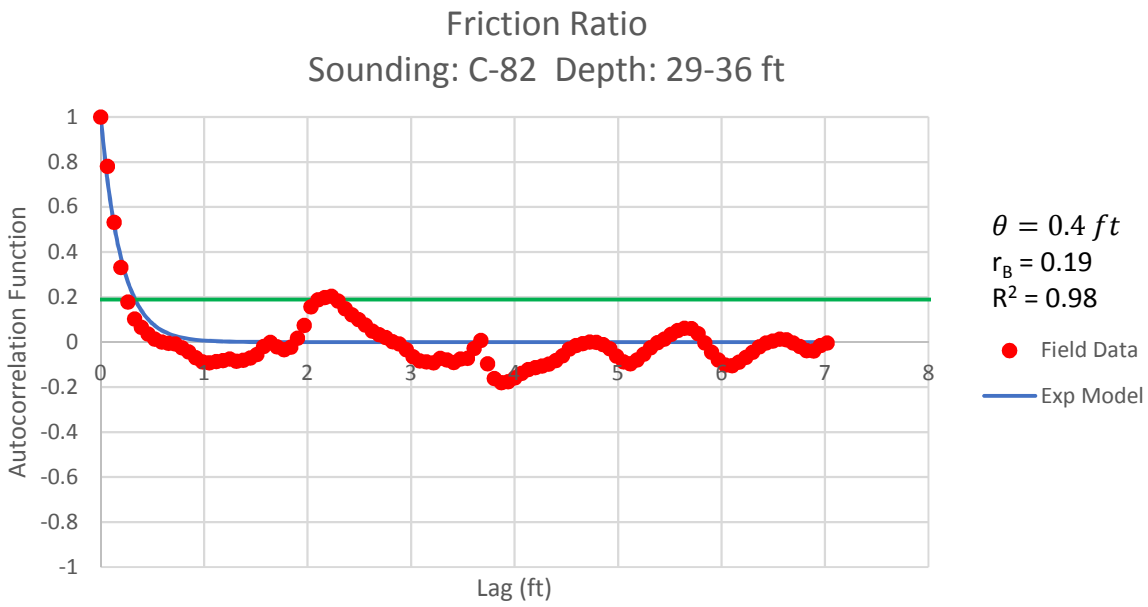

Figure B - 131: Estimation of the Scale of Fluctuation, $\theta = 0.4$ feet, for Friction Ratio Data from Sounding C-82, "Clean sands to silty sands (6)" layer from 29 to 36 feet depth.

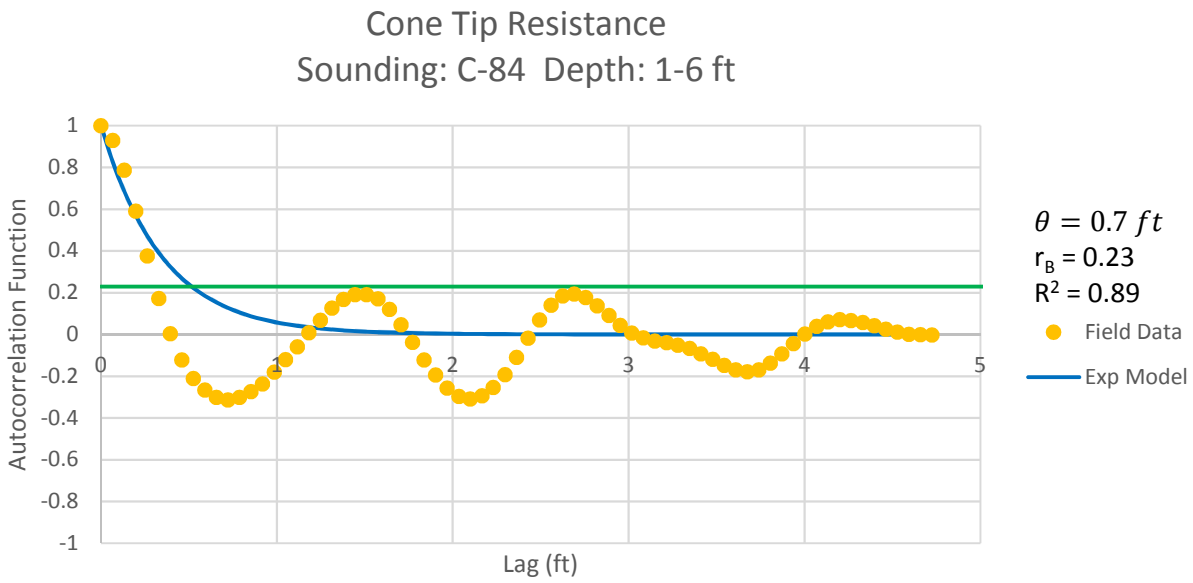

Figure B - 132: Estimation of the Scale of Fluctuation, θ = 0.7 feet, for Cone Tip Resistance Data from Sounding C-84, "Clays; clay to silty clay (3)" layer from 1 to 6 feet depth. Data is a poor fit for the points greater than the Bartlett limit of 0.23; coefficient of determination, R^2, value is less 0.9. Therefore, these results were not included in final analysis.

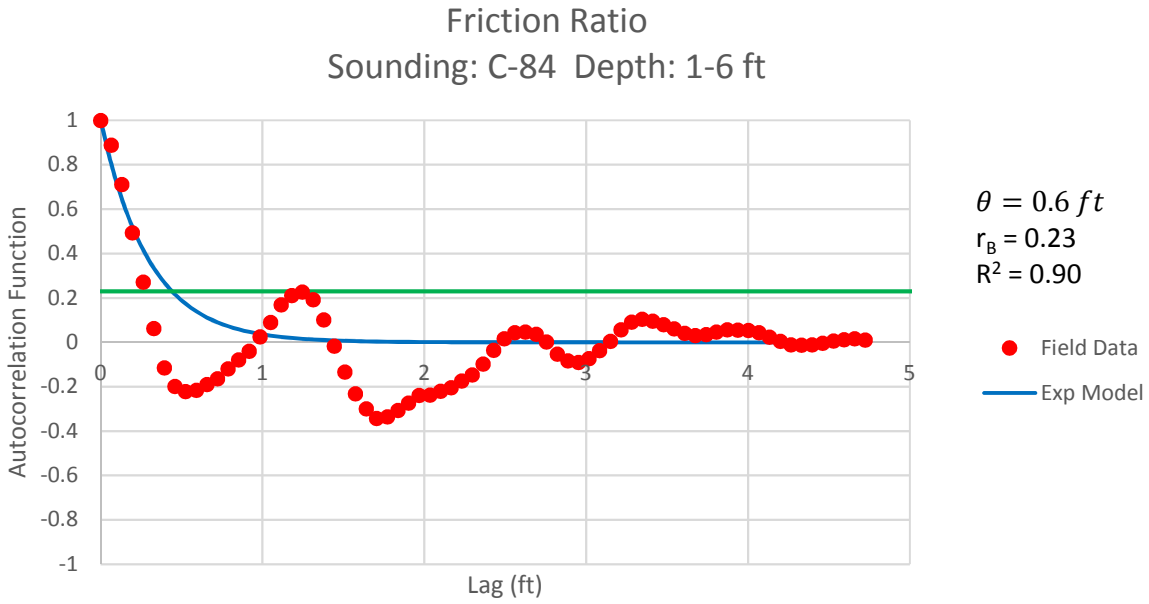

Figure B - 133: Estimation of the Scale of Fluctuation, θ = 0.6 feet, for Friction Ratio Data from Sounding C-84, "Clays; clay to silty clay (3)" layer from 1 to 6 feet depth.

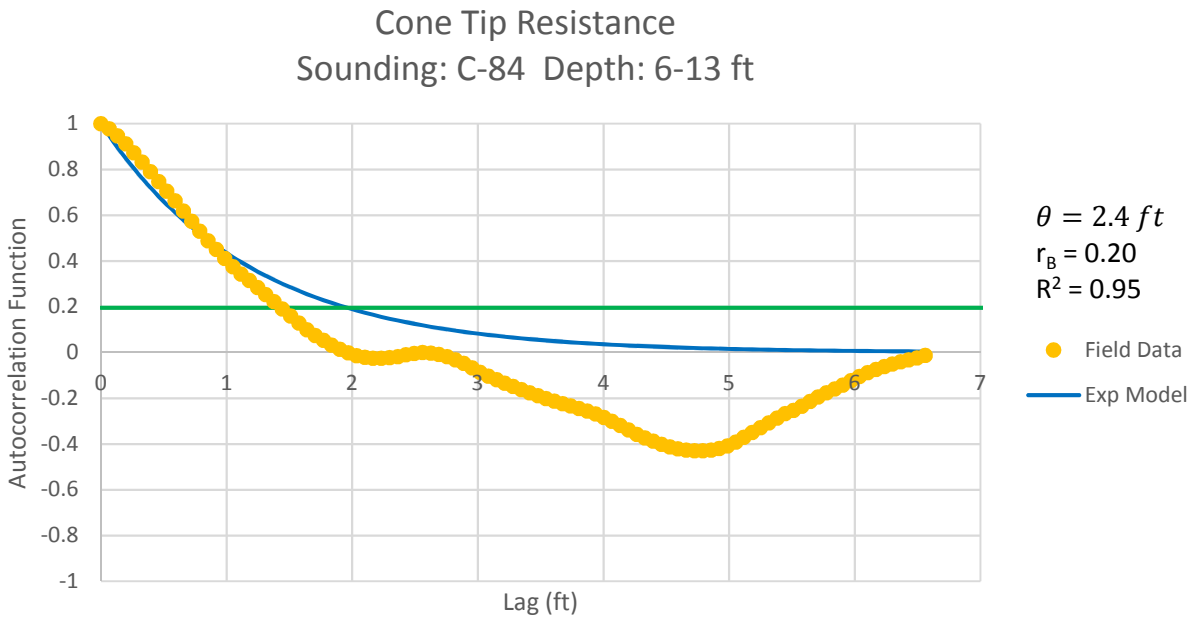

Figure B - 134: Estimation of the Scale of Fluctuation, $\theta = 2.4$ feet, for Cone Tip Resistance Data from Sounding C-84, "Clean sands to silty sands (6)" layer from 6 to 13 feet depth.

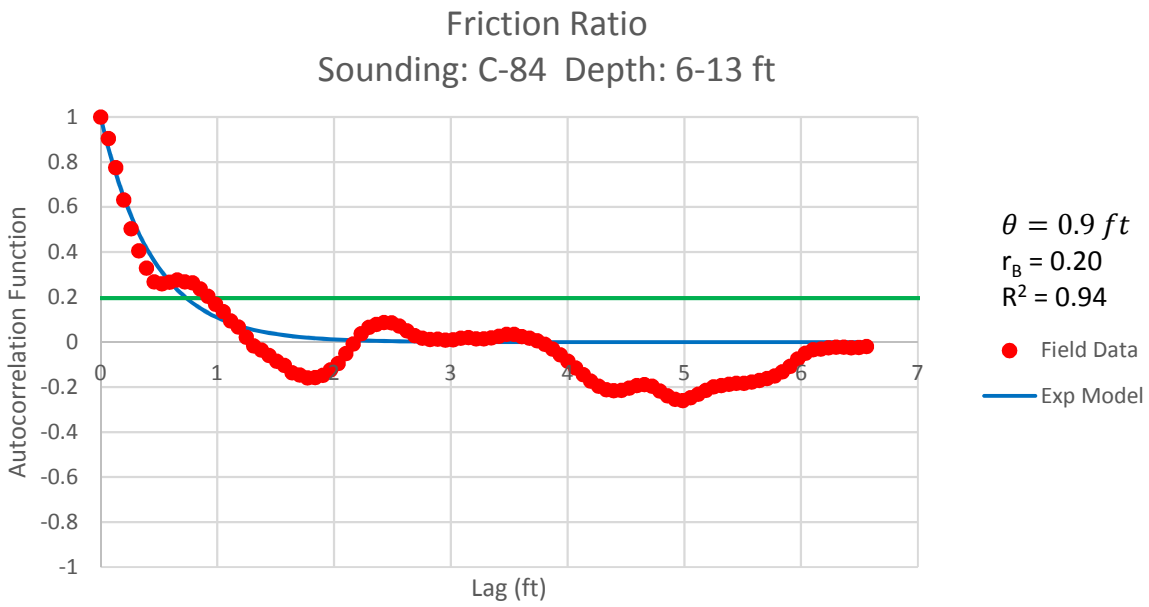

Figure B - 1356: Estimation of the Scale of Fluctuation, $\theta = 0.9$ feet, for Friction Ratio Data from Sounding C-84, "Clean sands to silty sands (6)" layer from 6 to 13 feet depth.

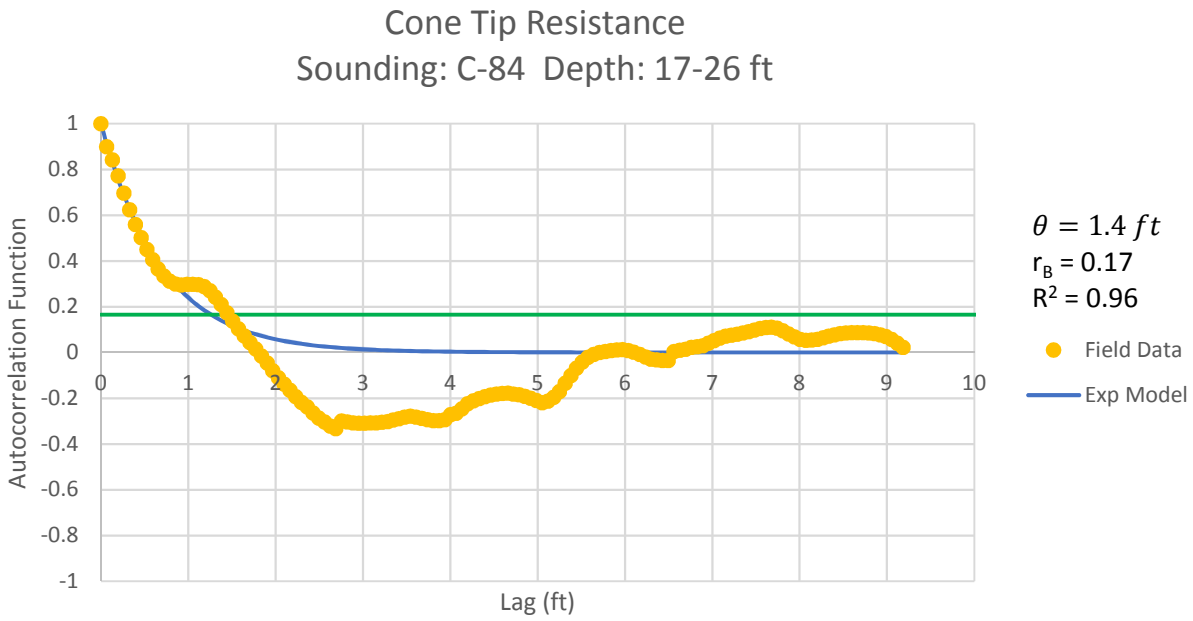

Figure B - 136: Estimation of the Scale of Fluctuation, θ = 1.4 feet, for Cone Tip Resistance Data from Sounding C-84, "Clean sands to silty sands (6)" layer from 17 to 26 feet depth.

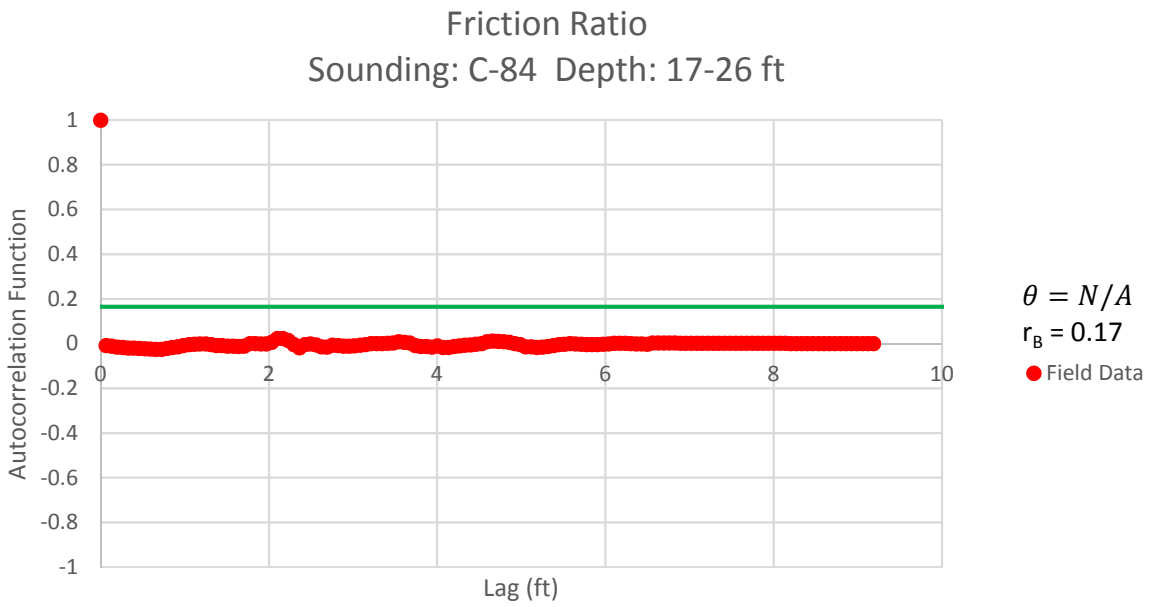

Figure B - 137: Estimation of the Scale of Fluctuation, θ, for Friction Ratio Data from Sounding C-84, "Clean sands to silty sands (6)" layer from 17 to 26 feet depth. Data is limited to only 1 point greater than the Bartlett limit of 0.17; therefore, θ could not be estimated, and these results were not included in final analysis.

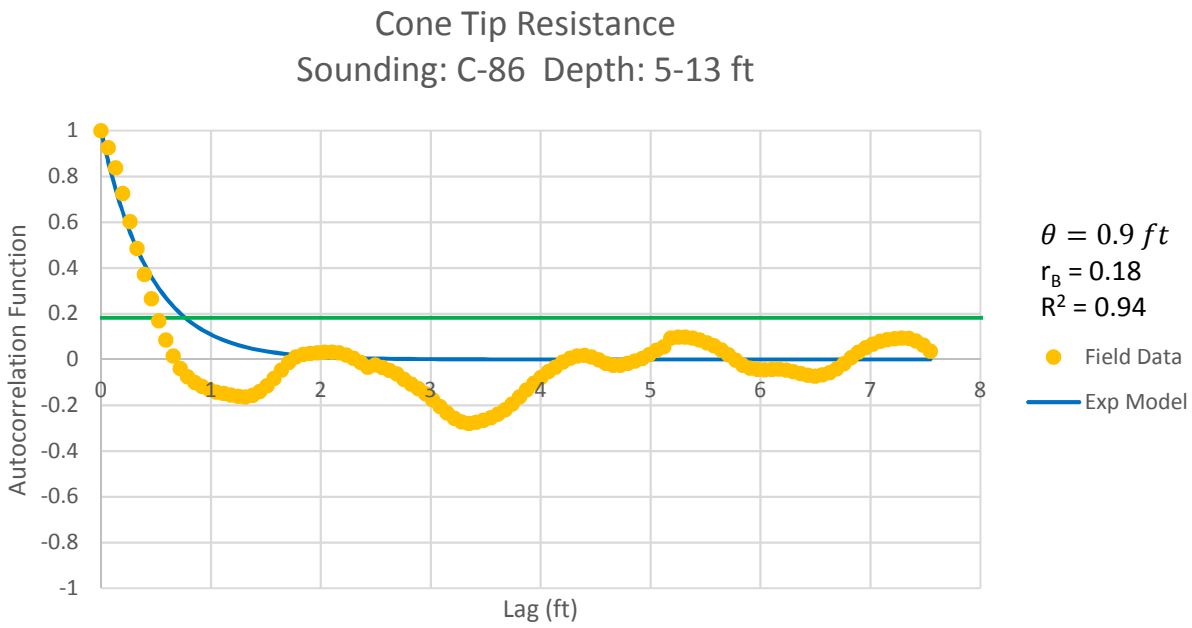

Figure B - 13839: Estimation of the Scale of Fluctuation, $\theta = 0.9$ feet, for Cone Tip Resistance Data from Sounding C-86, "Clean sands to silty sands (6)" layer from 5 to 13 feet depth.

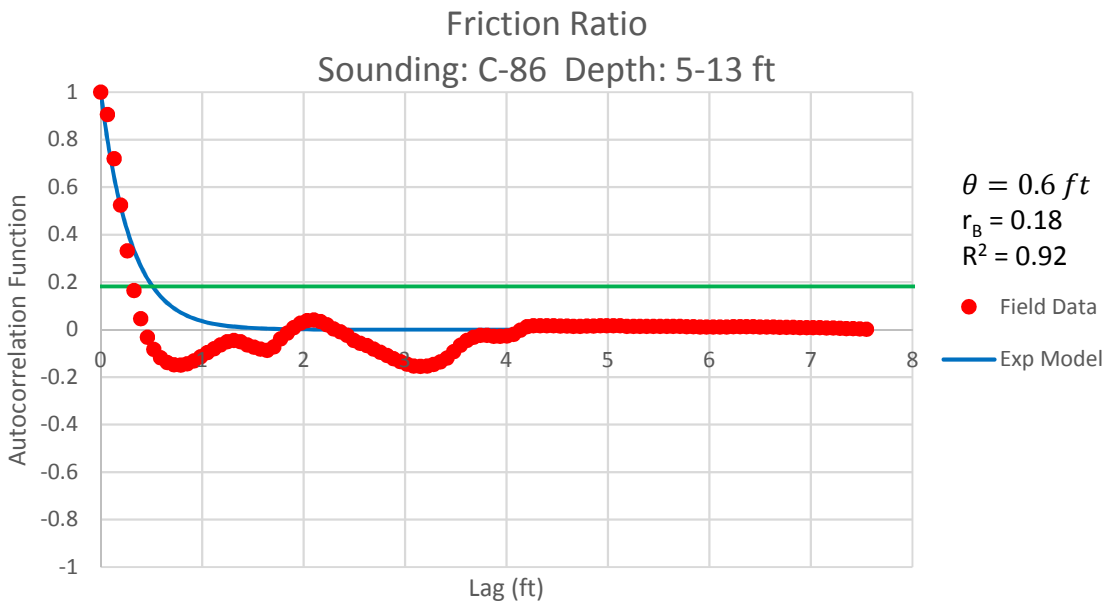

Figure B - 139: Estimation of the Scale of Fluctuation, $\theta = 0.6$ feet, for Friction Ratio Data from Sounding C-86, "Clean sands to silty sands (6)" layer from 5 to 13 feet depth.

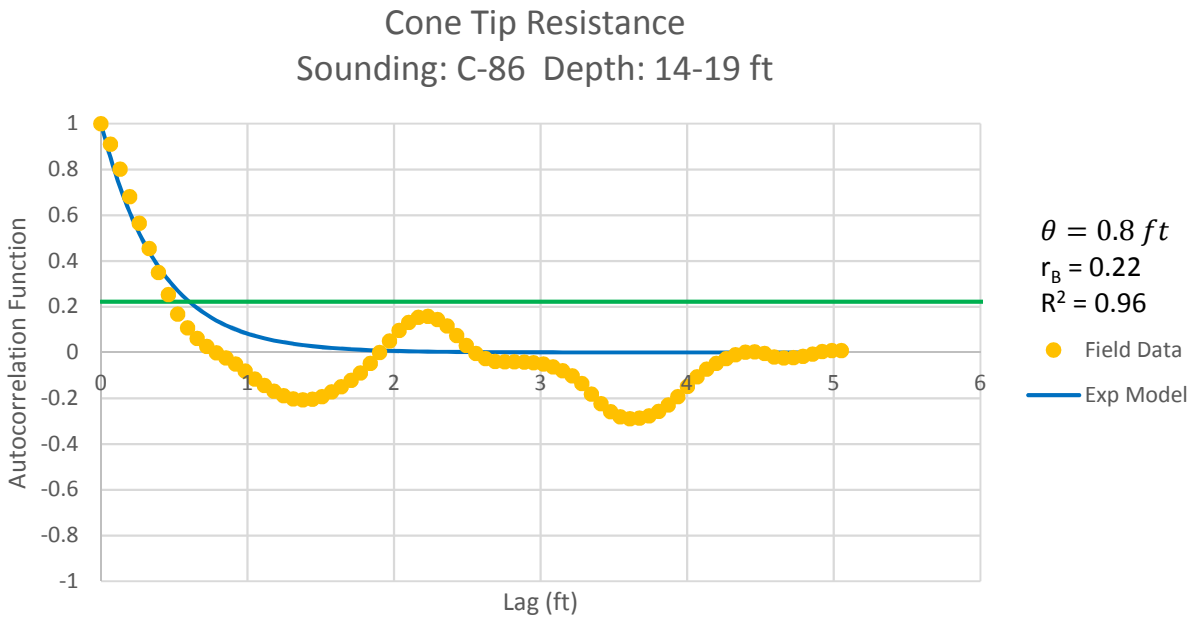

Figure B - 140: Estimation of the Scale of Fluctuation, $\theta = 0.8$ feet, for Cone Tip Resistance Data from Sounding C-86, "Clean sands to silty sands (6)" layer from 14 to 19 feet depth.

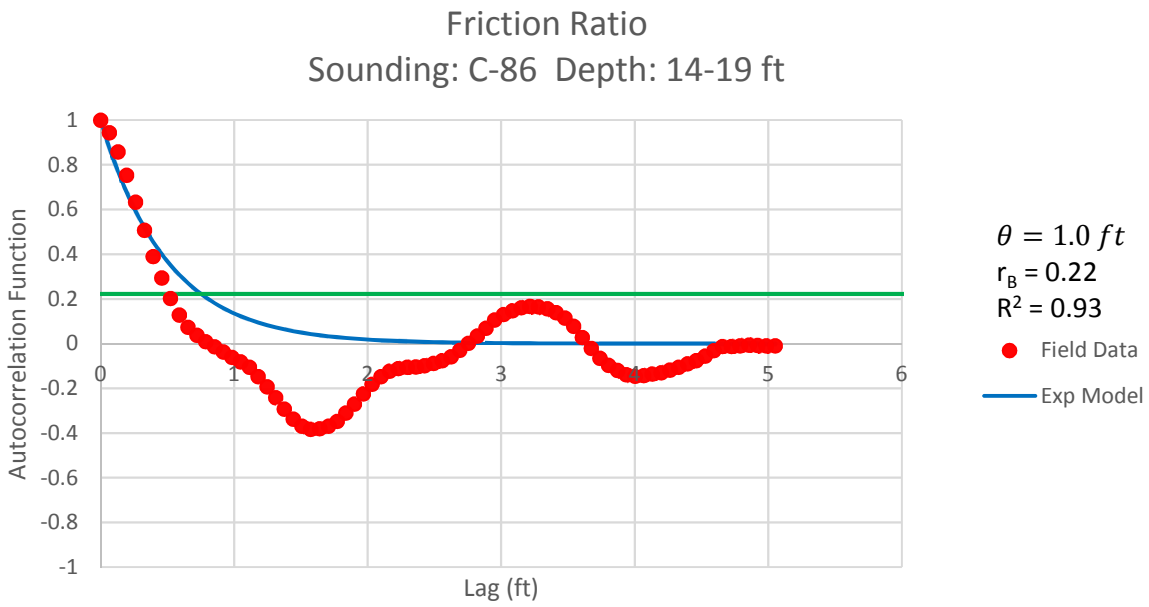

Figure B - 141: Estimation of the Scale of Fluctuation, $\theta = 1.0$ feet, for Friction Ratio Data from Sounding C-86, "Clean sands to silty sands (6)" layer from 14 to 19 feet depth.

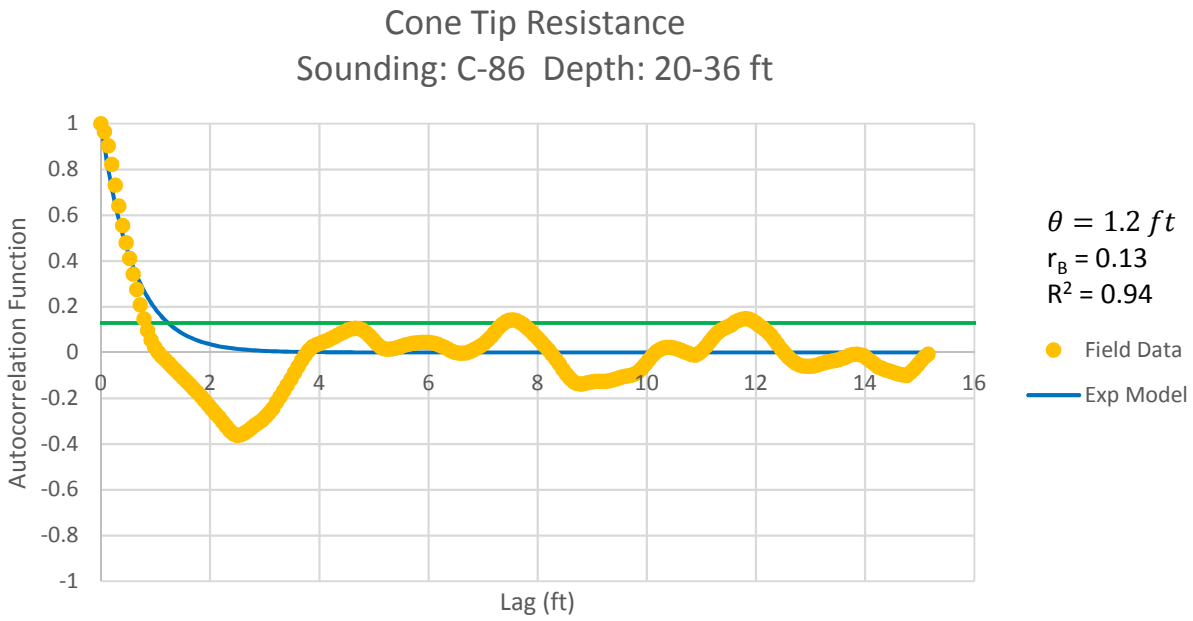

Figure B - 142: Estimation of the Scale of Fluctuation, θ = 1.2 feet, for Cone Tip Resistance Data from Sounding C-86, "Clean sands to silty sands (6)" layer from 20 to 36 feet depth.

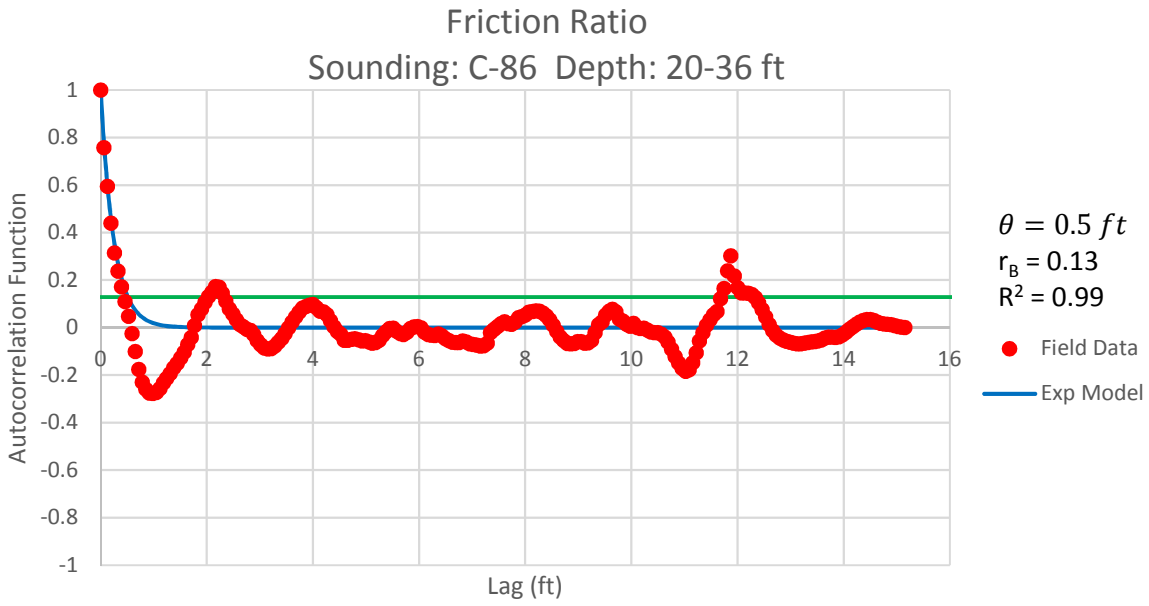

Figure B - 143: Estimation of the Scale of Fluctuation, θ = 0.5 feet, for Friction Ratio Data from Sounding C-86, "Clean sands to silty sands (6)" layer from 20 to 36 feet depth.

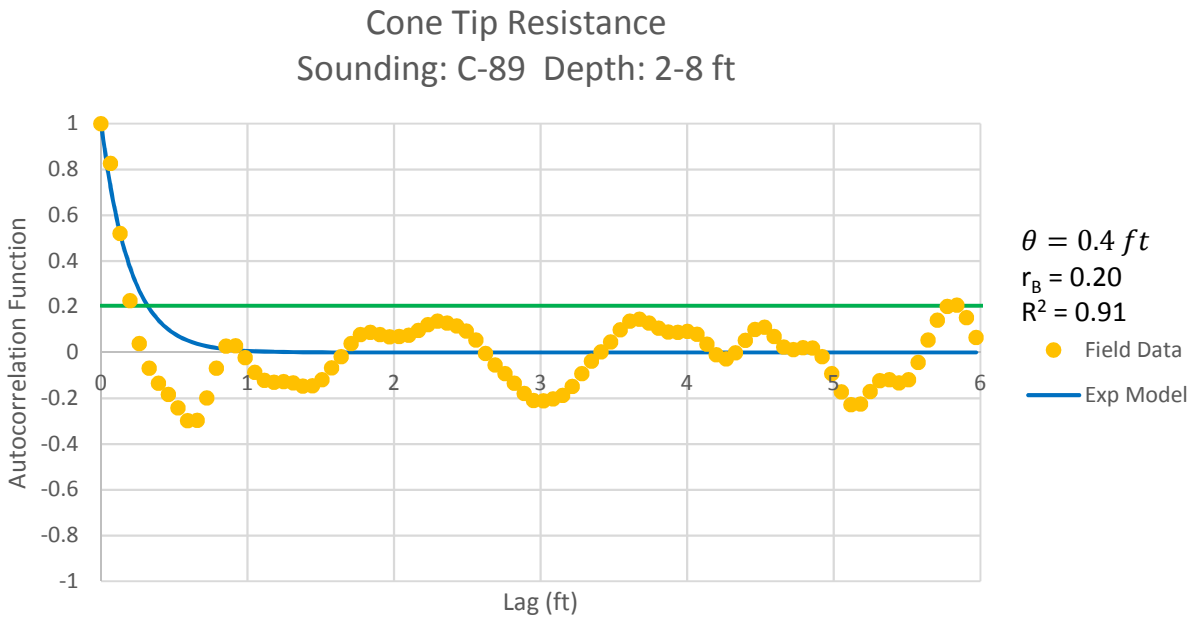

Figure B - 144: Estimation of the Scale of Fluctuation, $\theta = 0.4$ feet, for Friction Ratio Data from Sounding C-89, "Clays; clay to silty clay (3)" layer from 2 to 8 feet depth.

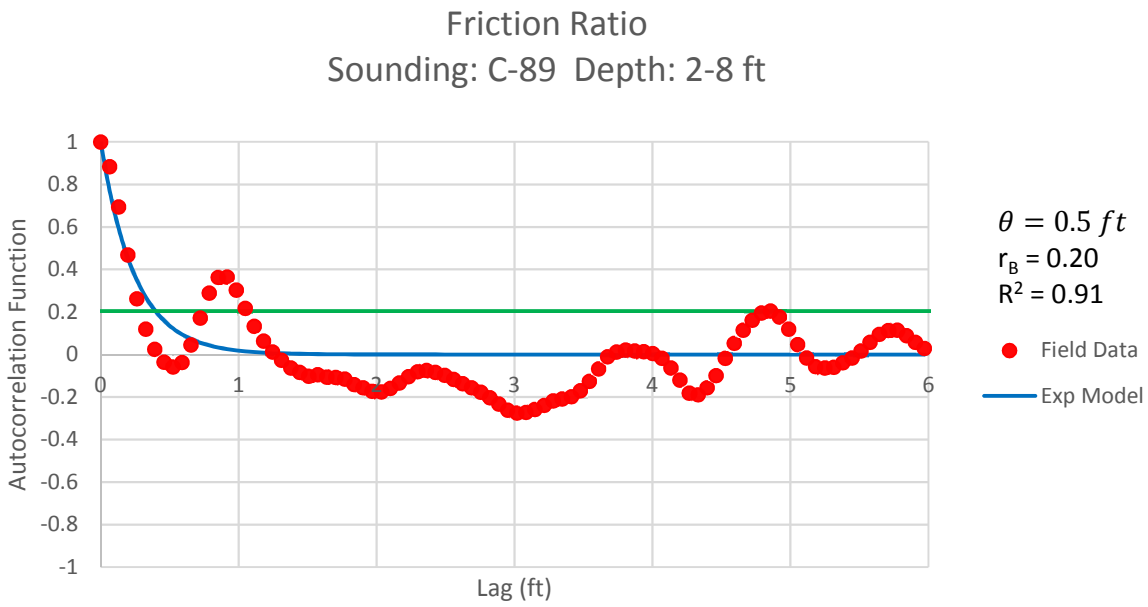

Figure B - 145: Estimation of the Scale of Fluctuation, $\theta = 0.5$ feet, for Friction Ratio Data from Sounding C-89, "Clays; clay to silty clay (3)" layer from 2 to 8 feet depth.

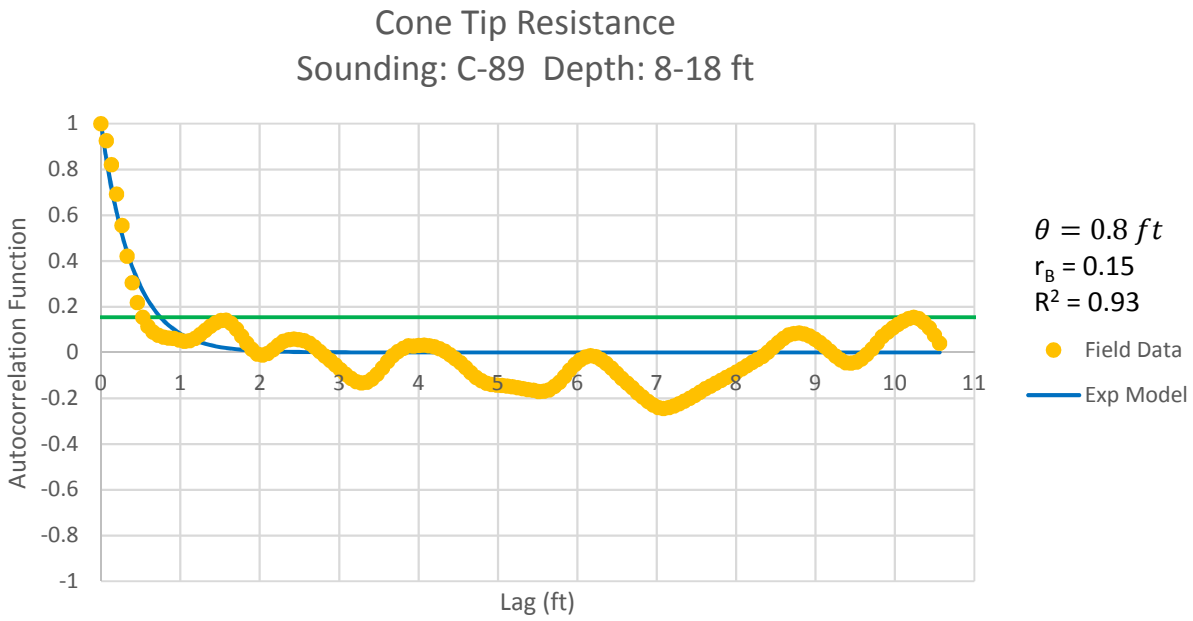

Figure B - 146: Estimation of the Scale of Fluctuation, $\theta = 0.8$ feet, for Cone Tip Resistance Data from Sounding C-89, "Clean sands to silty sands (6)" layer from 8 to 18 feet depth.

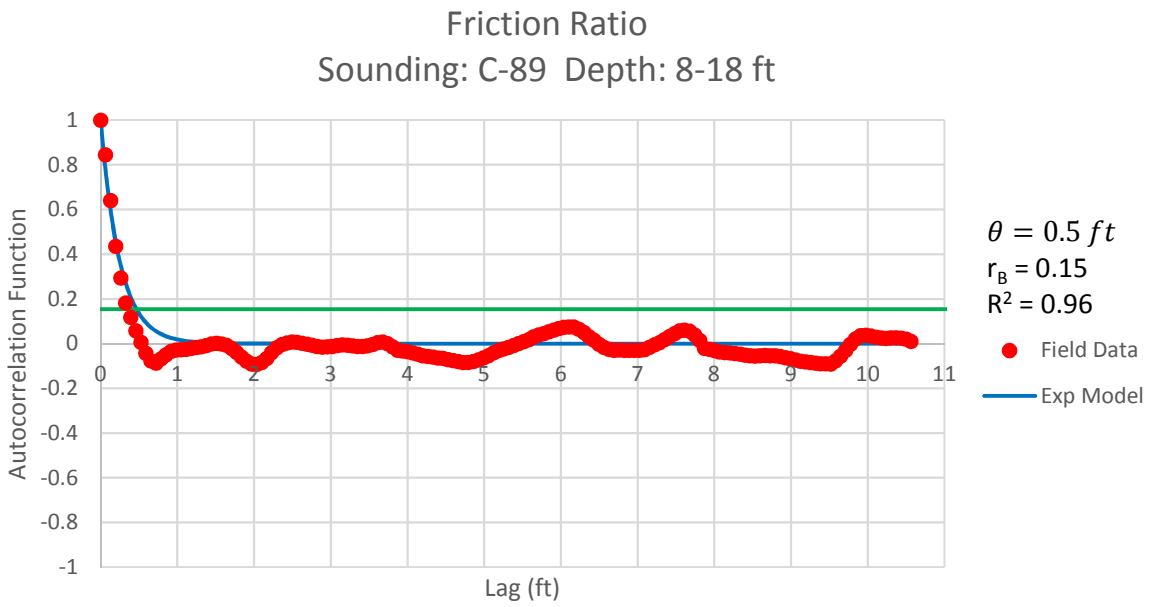

Figure B - 14748: Estimation of the Scale of Fluctuation, $\theta = 0.5$ feet, for Friction Ratio Data from Sounding C-89, "Clean sands to silty sands (6)" layer from 8 to 18 feet depth.

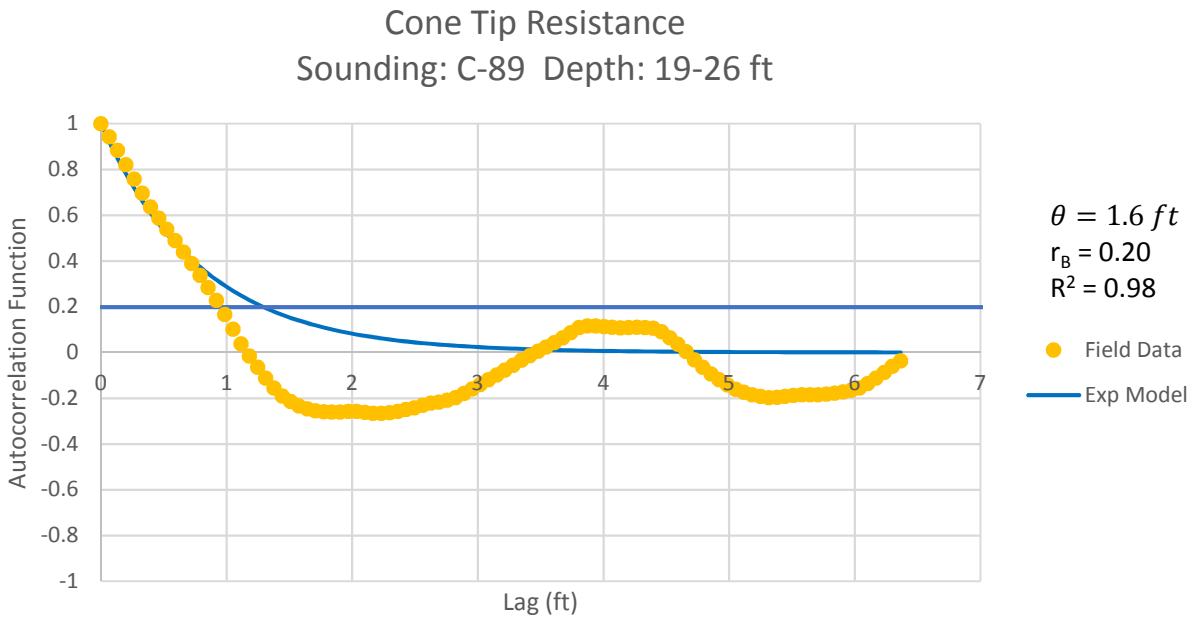

Figure B - 14849: Estimation of the Scale of Fluctuation, $\theta = 1.6$ feet, for Cone Tip Resistance Data from Sounding C-89, "Clean sands to silty sands (6)" layer from 19 to 26 feet depth.

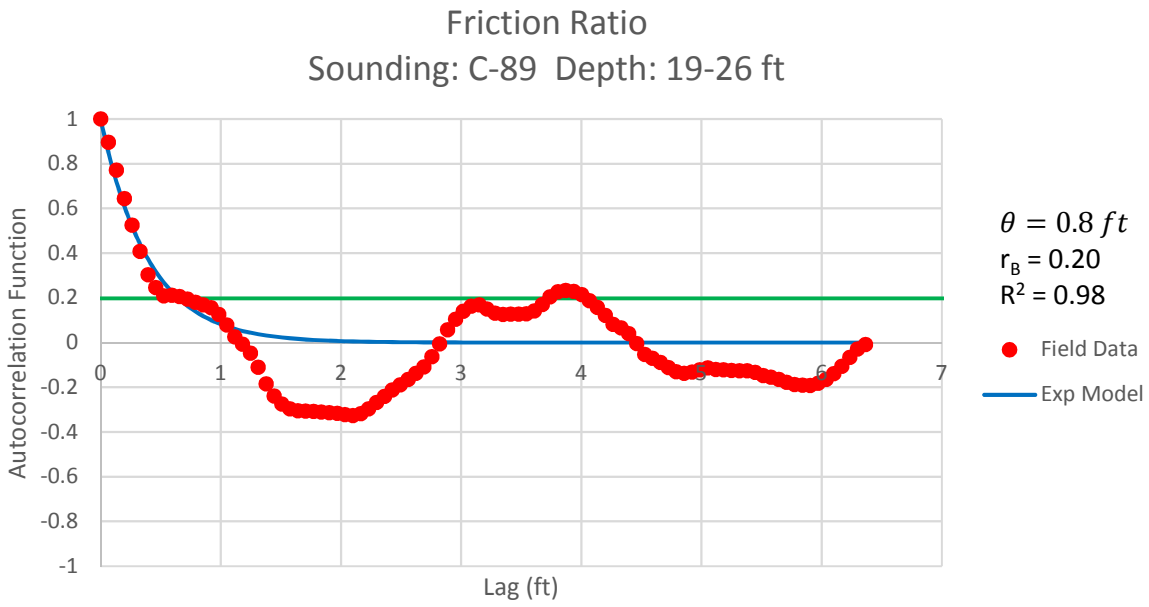

Figure B - 1490: Estimation of the Scale of Fluctuation, $\theta = 0.8$ feet, for Friction Ratio Data from Sounding C-89, "Clean sands to silty sands (6)" layer from 19 to 26 feet depth.

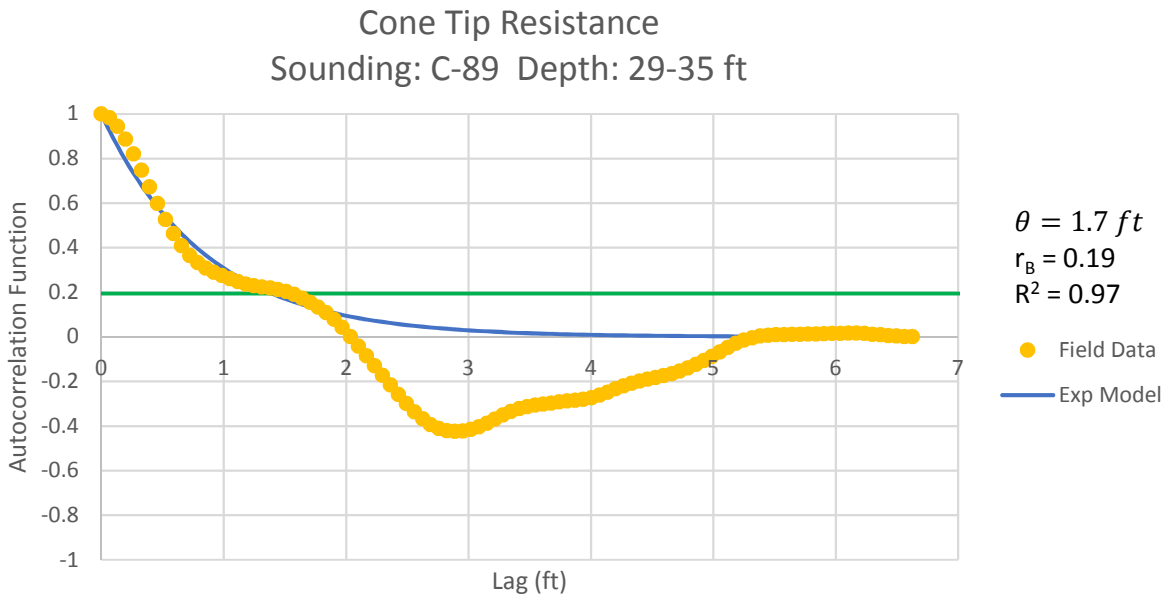

Figure B - 1501: Estimation of the Scale of Fluctuation, $\theta = 1.7$ feet, for Cone Tip Resistance Data from Sounding C-89, "Clean sands to silty sands (6)" layer from 29 to 35 feet depth.

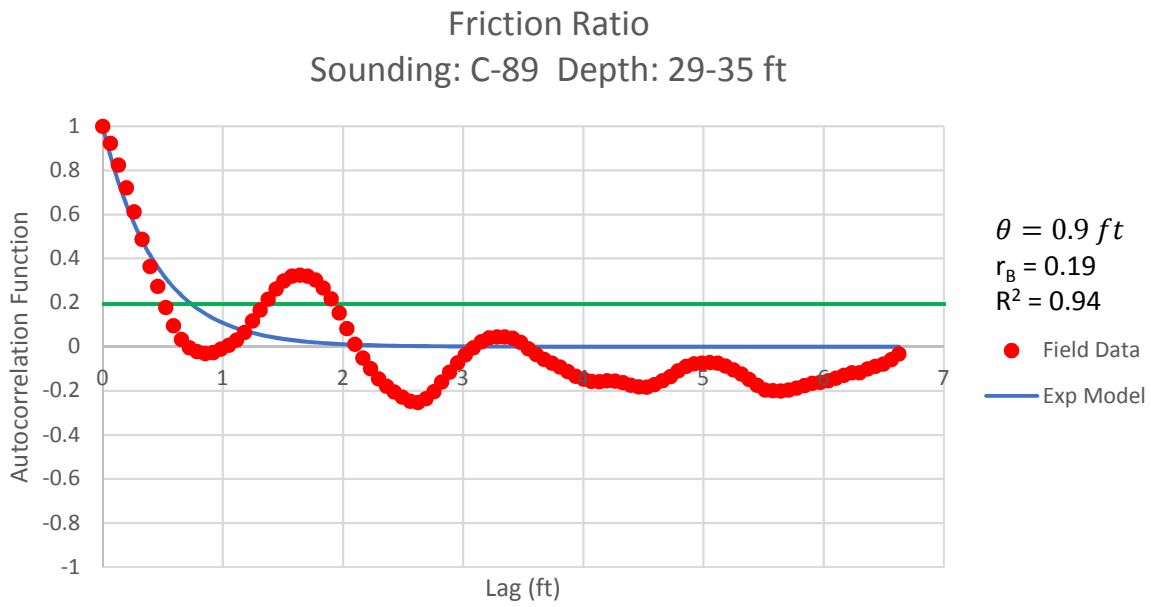

Figure B - 151: Estimation of the Scale of Fluctuation, $\theta = 0.9$ feet, for Friction Ratio Data from Sounding C-89, "Clean sands to silty sands (6)" layer from 29 to 35 feet depth.

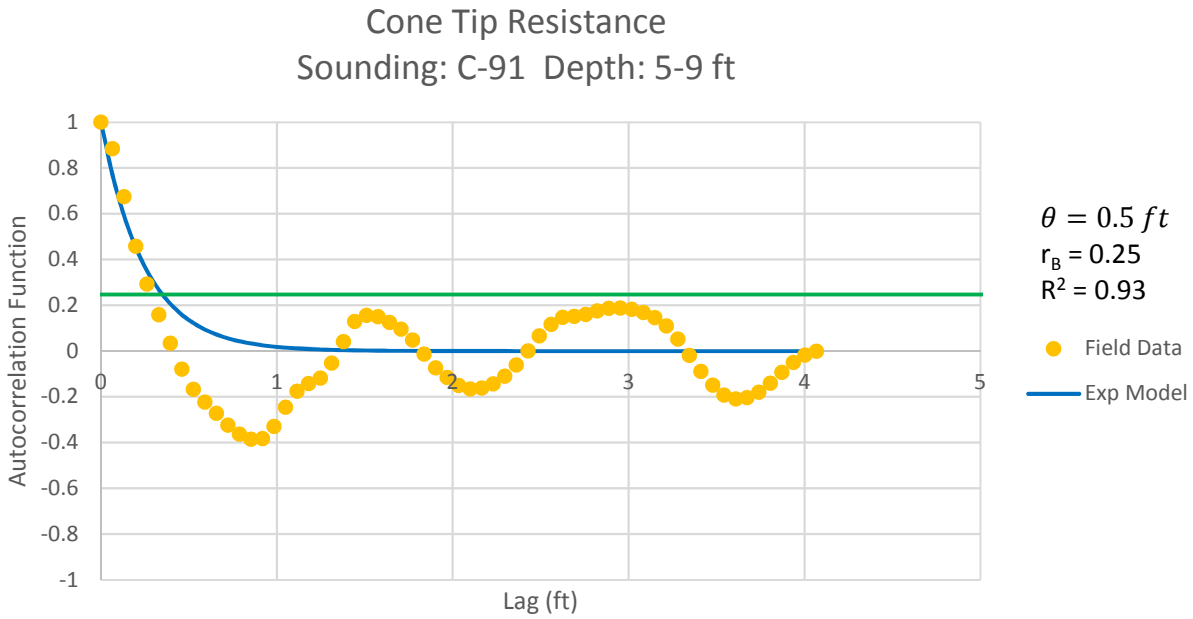

Figure B - 152: Estimation of the Scale of Fluctuation, $\theta = 0.5$ feet, for Cone Tip Resistance Data from Sounding C-91, "Silty sand to sandy silt (5)" layer from 5 to 9 feet depth.

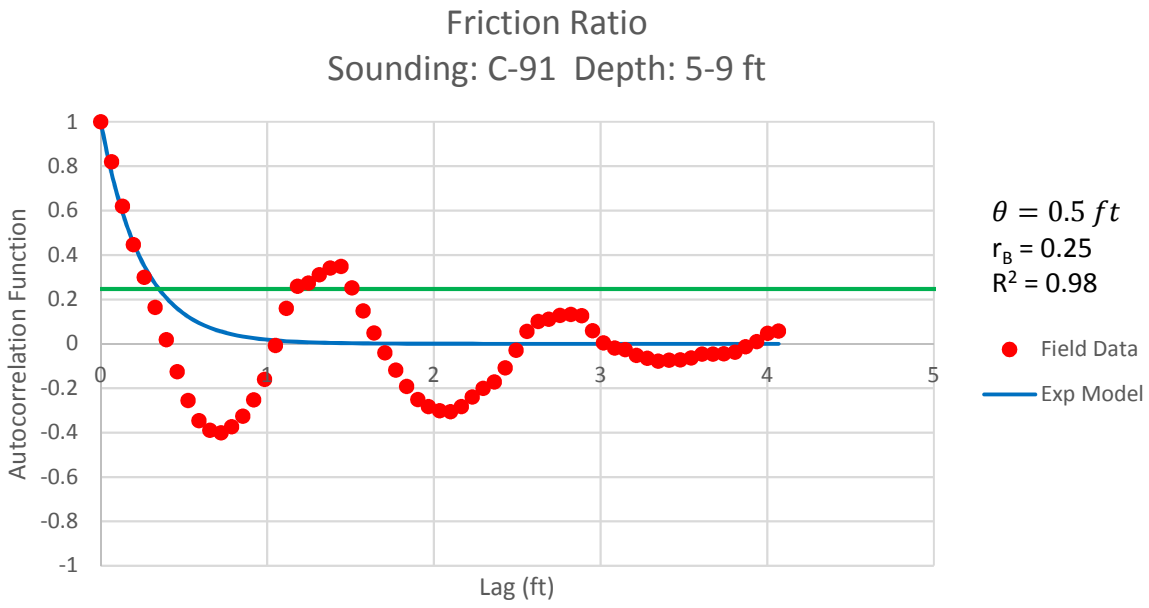

Figure B - 153: Estimation of the Scale of Fluctuation, $\theta = 0.5$ feet, for Friction Ratio Data from Sounding C-91, "Silty sand to sandy silt (5)" layer from 5 to 9 feet depth.

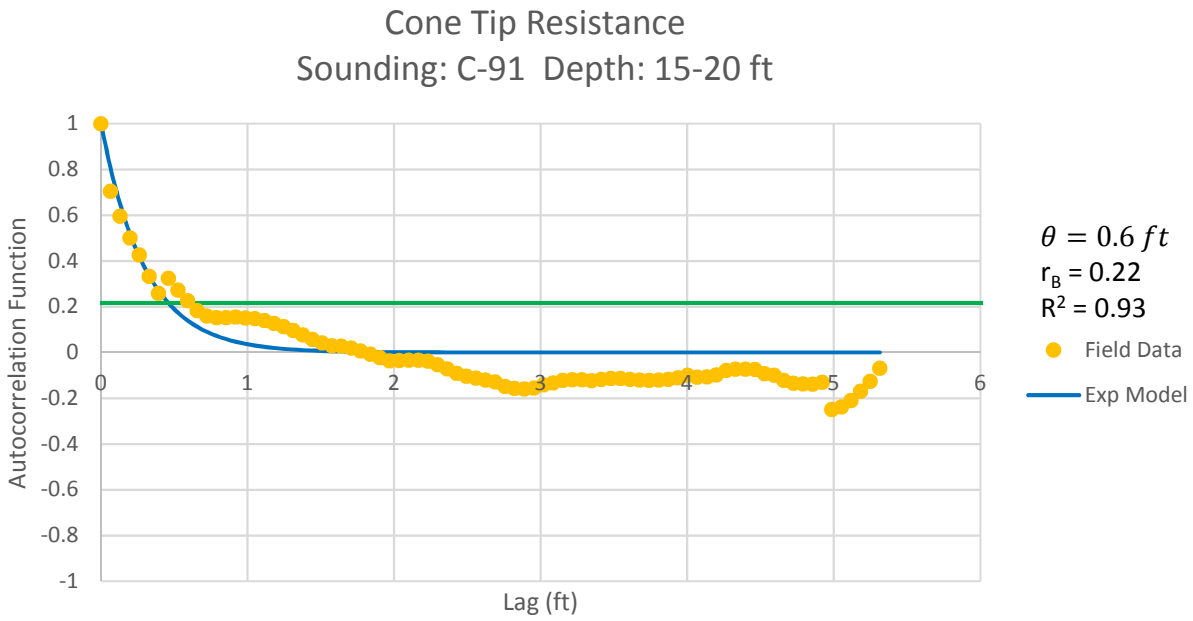

Figure B - 154: Estimation of the Scale of Fluctuation, θ = 0.6 feet, for Cone Tip Resistance Data from Sounding C-91, "Clean sands to silty sands (6)" layer from 15 to 20 feet depth.

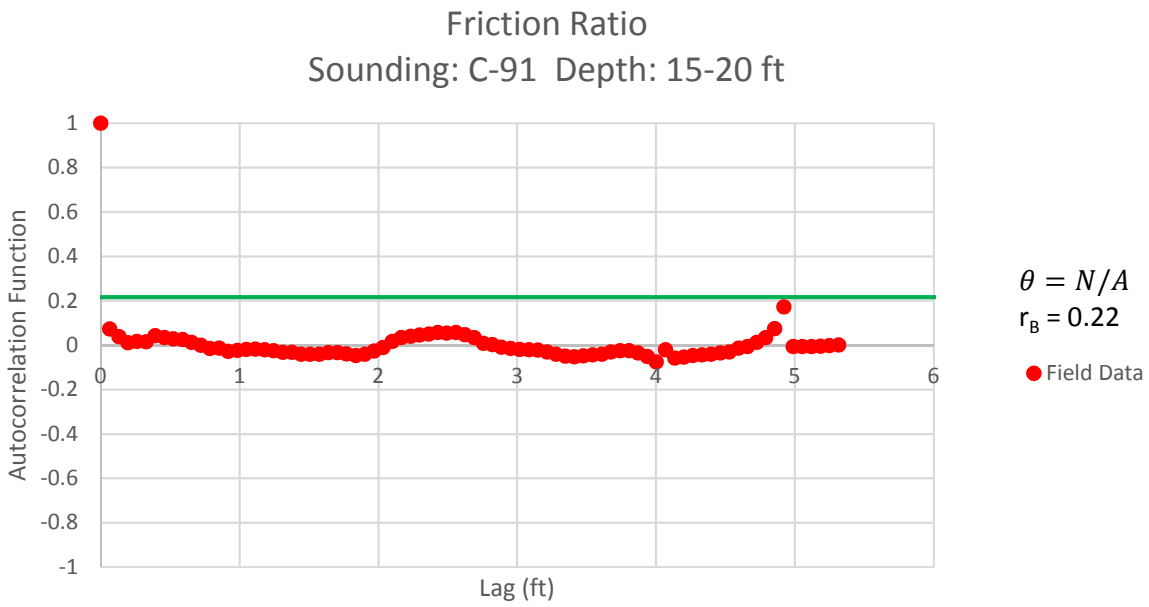

Figure B - 155: Estimation of the Scale of Fluctuation, θ, for Friction Ratio Data from Sounding C-91, "Clean sands to silty sands (6)" layer from 15 to 20 feet depth. Data is limited to only 1 point greater than the Bartlett limit of 0.22; therefore, θ could not be estimated, and these results were not included in final analysis.

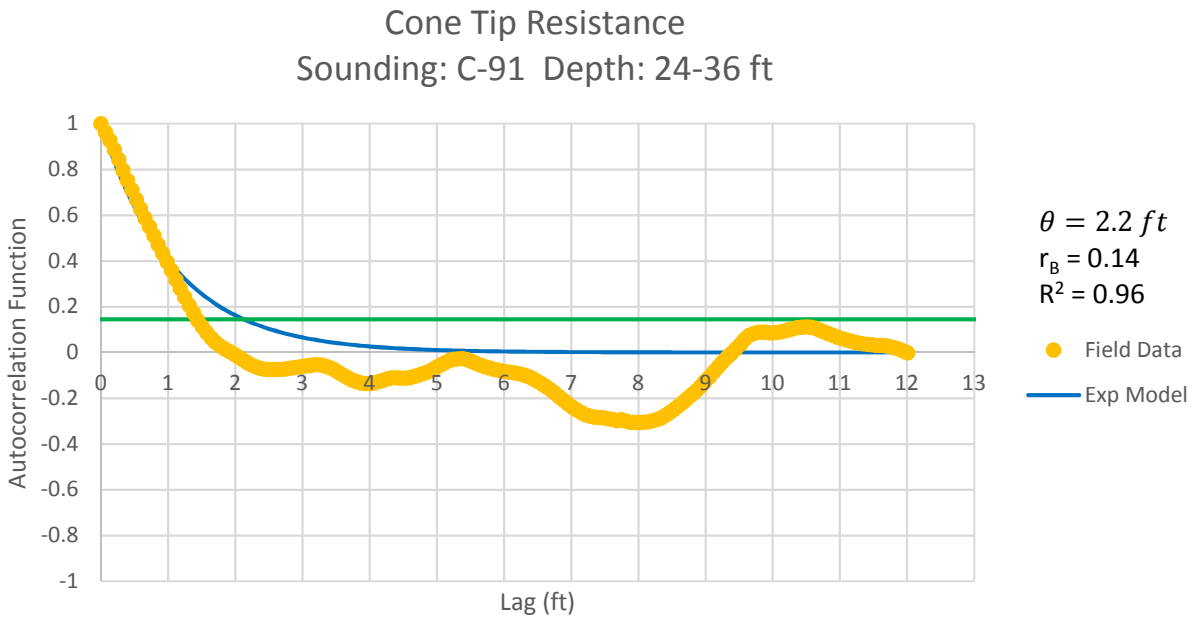

Figure B - 156: Estimation of the Scale of Fluctuation, θ = 2.2 feet, for Cone Tip Resistance Data from Sounding C-91, "Clean sands to silty sands (6)" layer from 24 to 36 feet depth.

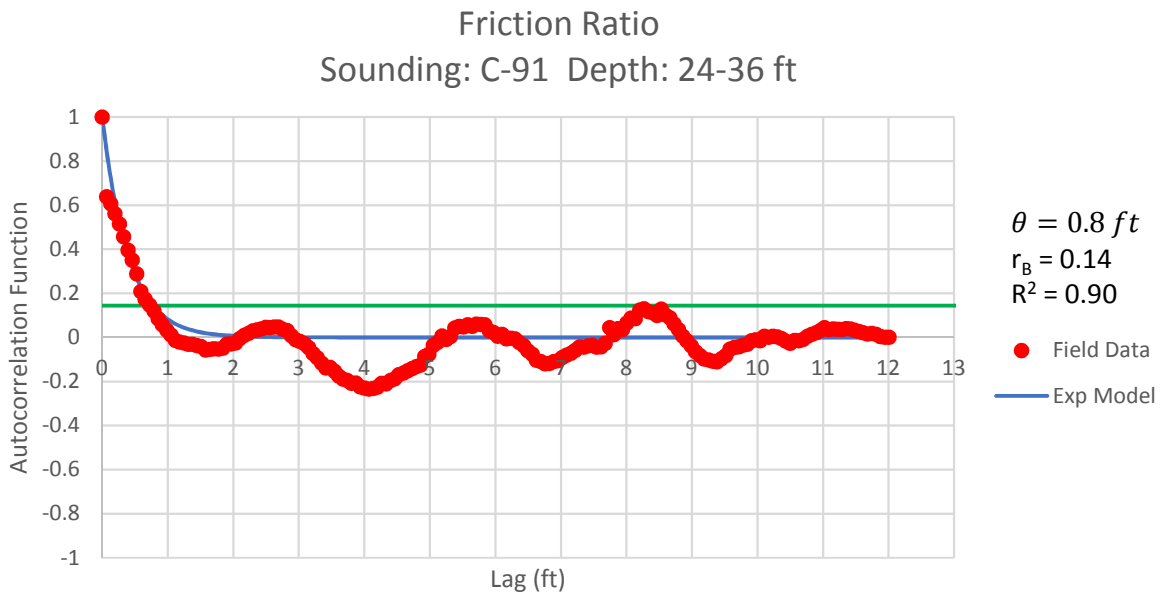

Figure B - 15758: Estimation of the Scale of Fluctuation, θ = 0.8 feet, for Friction Ratio Data from Sounding C-91, "Clean sands to silty sands (6)" layer from 24 to 36 feet depth.

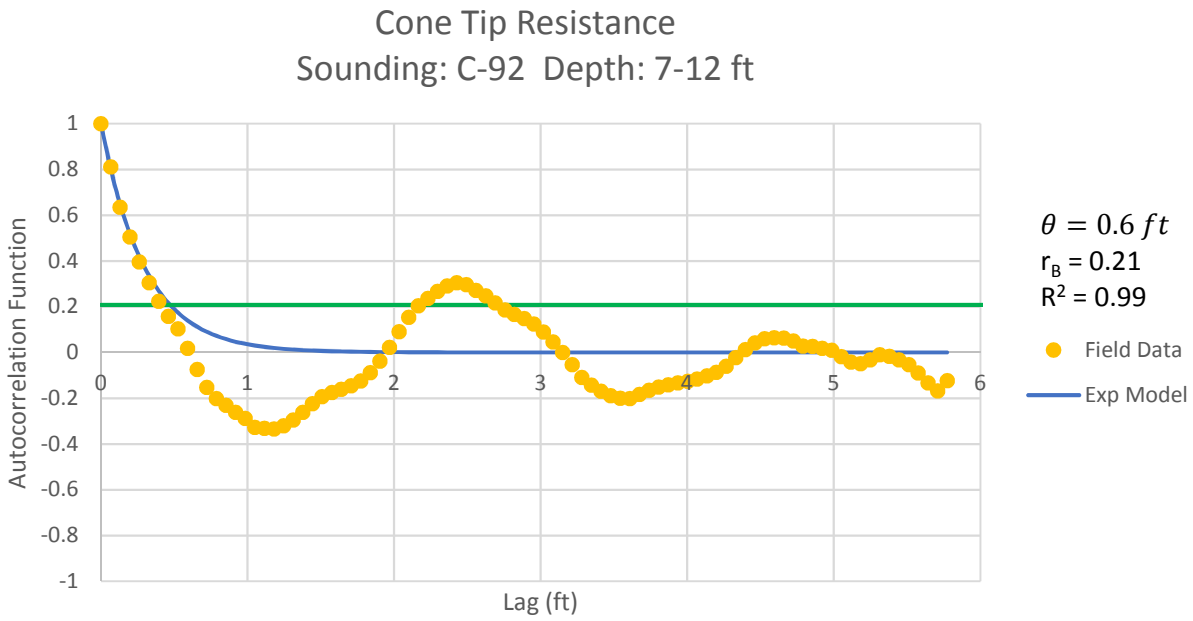

Figure B - 158: Estimation of the Scale of Fluctuation, $\theta = 0.6$ feet, for Cone Tip Resistance Data from Sounding C-92, "Clean sands to silty sands (6)" layer from 7 to 12 feet depth.

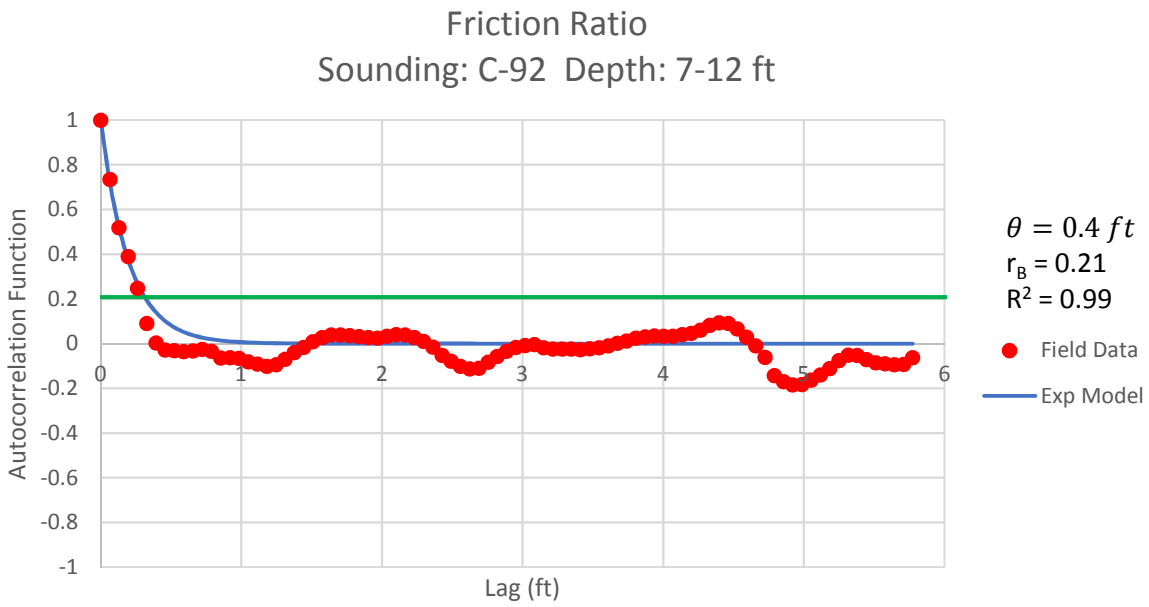

Figure B - 159: Estimation of the Scale of Fluctuation, $\theta = 0.4$ feet, for Friction Ratio Data from Sounding C-92, "Clean sands to silty sands (6)" layer from 7 to 12 feet depth.

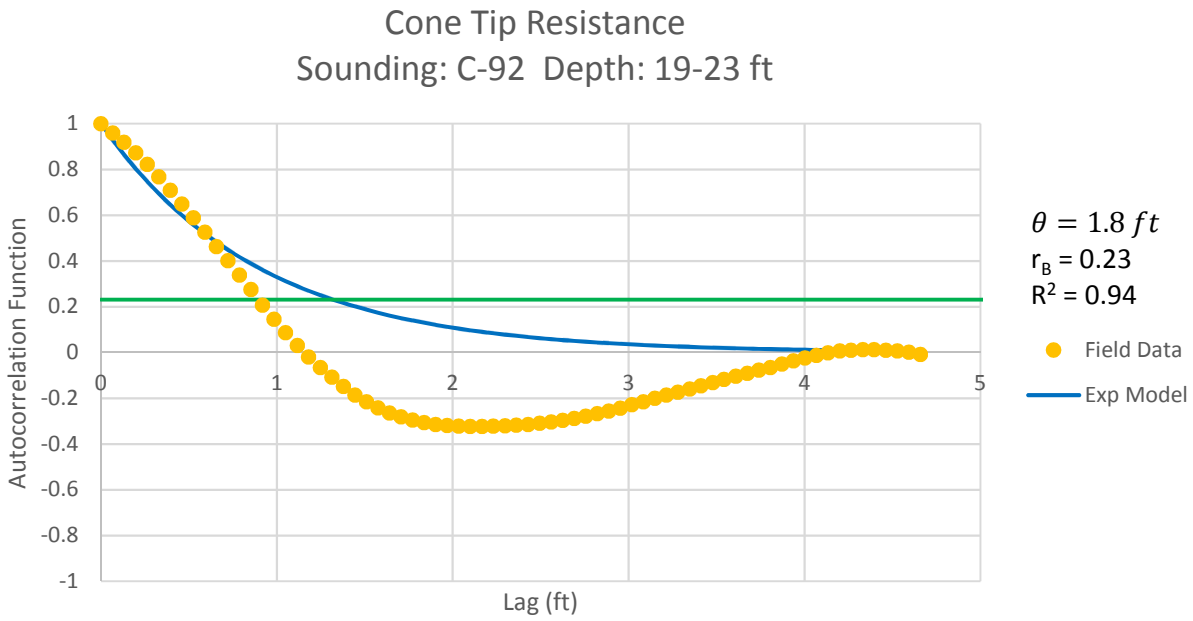

Figure B - 160: Estimation of the Scale of Fluctuation, $\theta = 1.8$ feet, for Cone Tip Resistance Data from Sounding C-92, "Gravelly sand to sand (7)" layer from 19 to 23 feet depth.

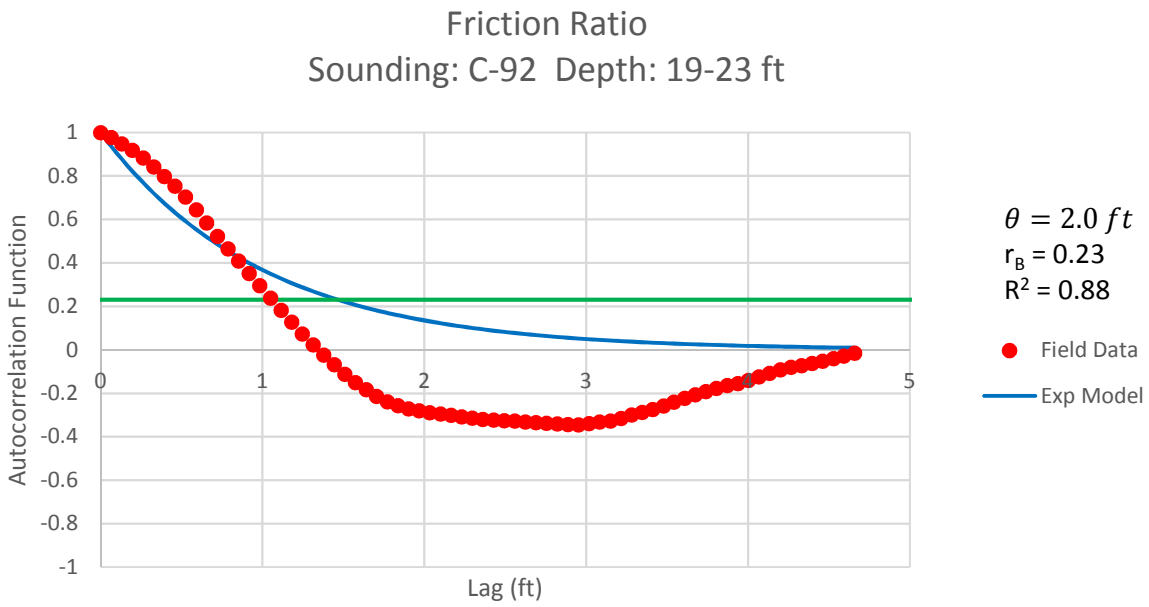

Figure B - 161: Estimation of the Scale of Fluctuation, $\theta = 2.0$ feet, for Friction Ratio Data from Sounding C-92, "Gravelly sand to sand (7)" layer from 19 to 23 feet depth. Data is a poor fit for the points greater than the Bartlett limit of 0.23; coefficient of determination, R^2, value is less 0.9. Therefore, these results were not included in final analysis.

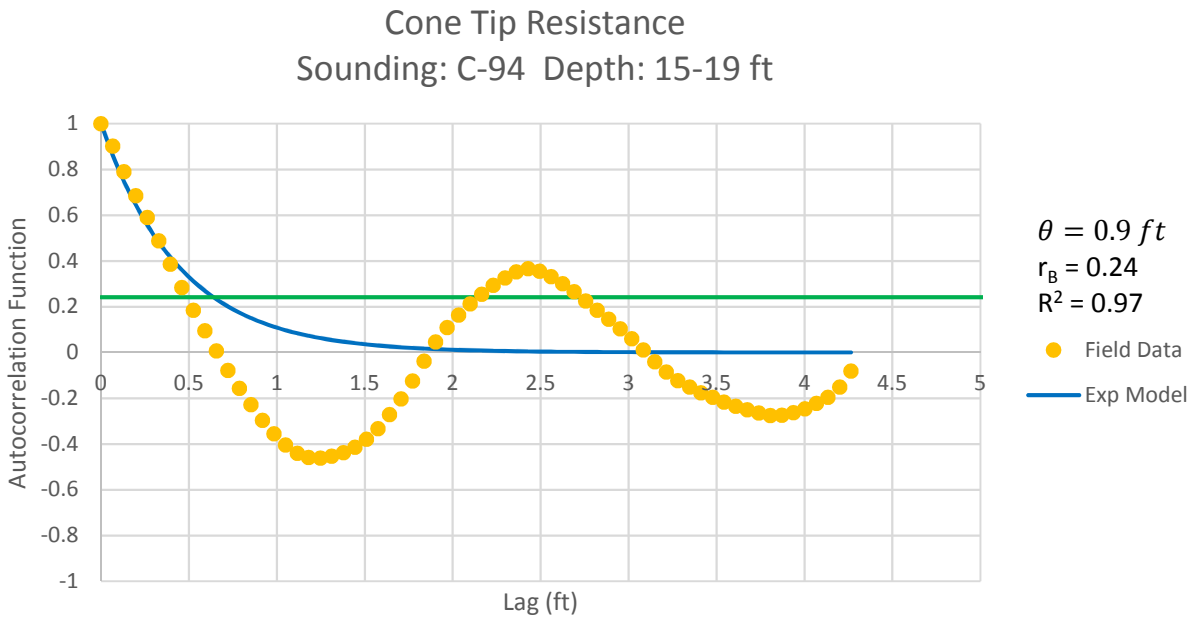

Figure B - 162: Estimation of the Scale of Fluctuation, $\theta = 0.9$ feet, for Cone Tip Resistance Data from Sounding C-94, "Clean sands to silty sands (6)" layer from 15 to 19 feet depth.

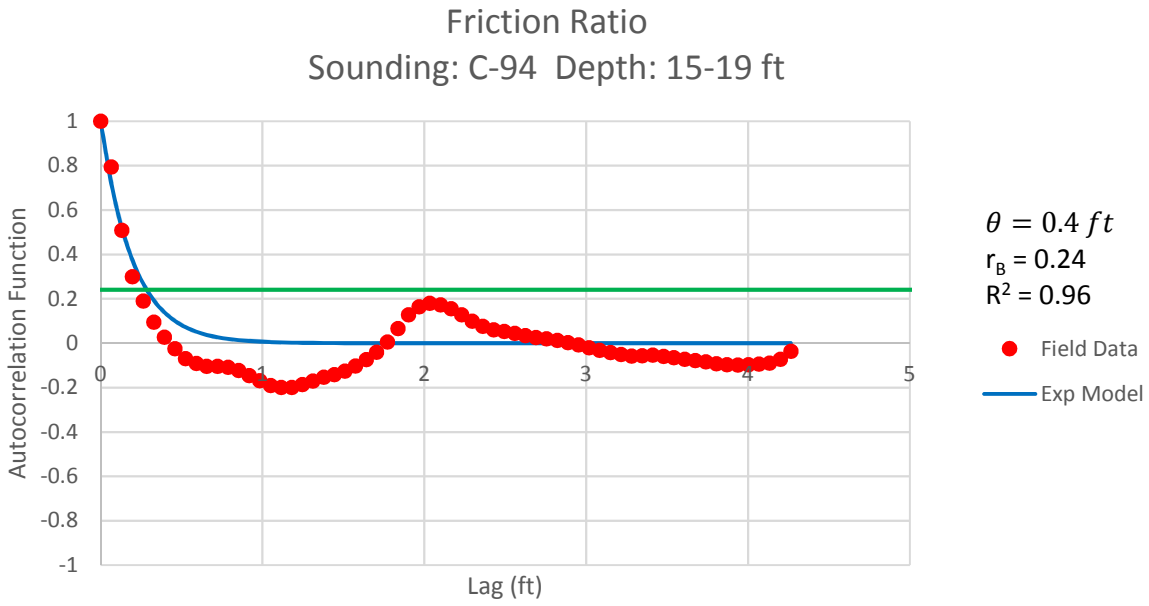

Figure B - 163: Estimation of the Scale of Fluctuation, $\theta = 0.4$ feet, for Friction Ratio Data from Sounding C-94, "Clean sands to silty sands (6)" layer from 15 to 19 feet depth.

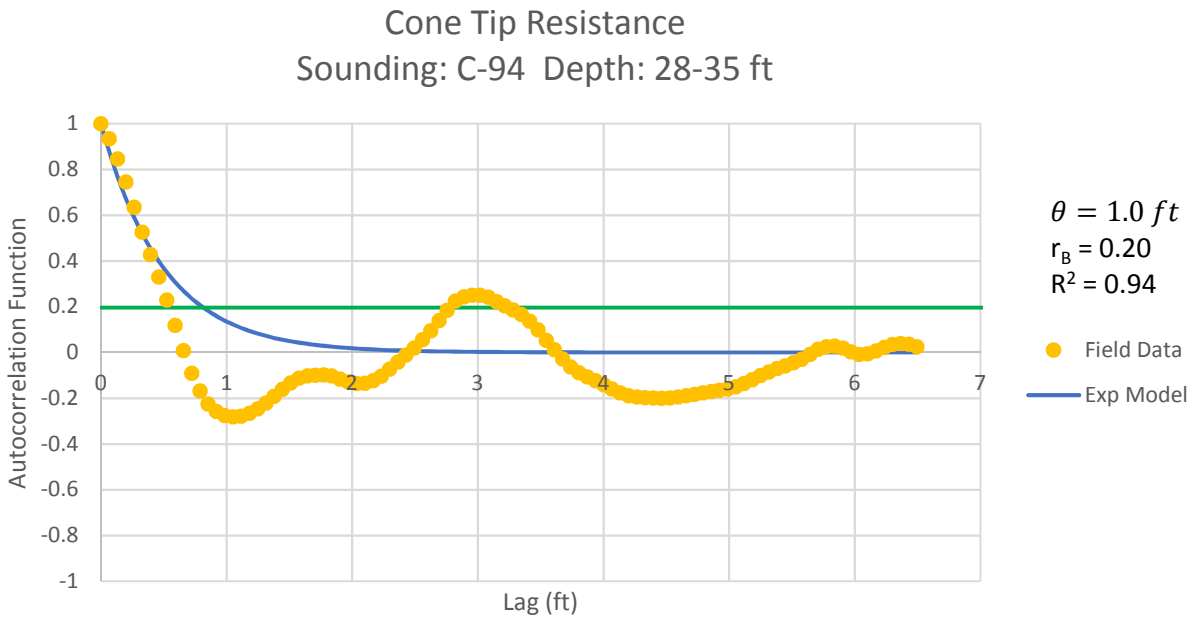

Figure B - 164: Estimation of the Scale of Fluctuation, $\theta = 1.0$ feet, for Cone Tip Resistance Data from Sounding C-94, "Clean sands to silty sands (6)" layer from 28 to 35 feet depth.

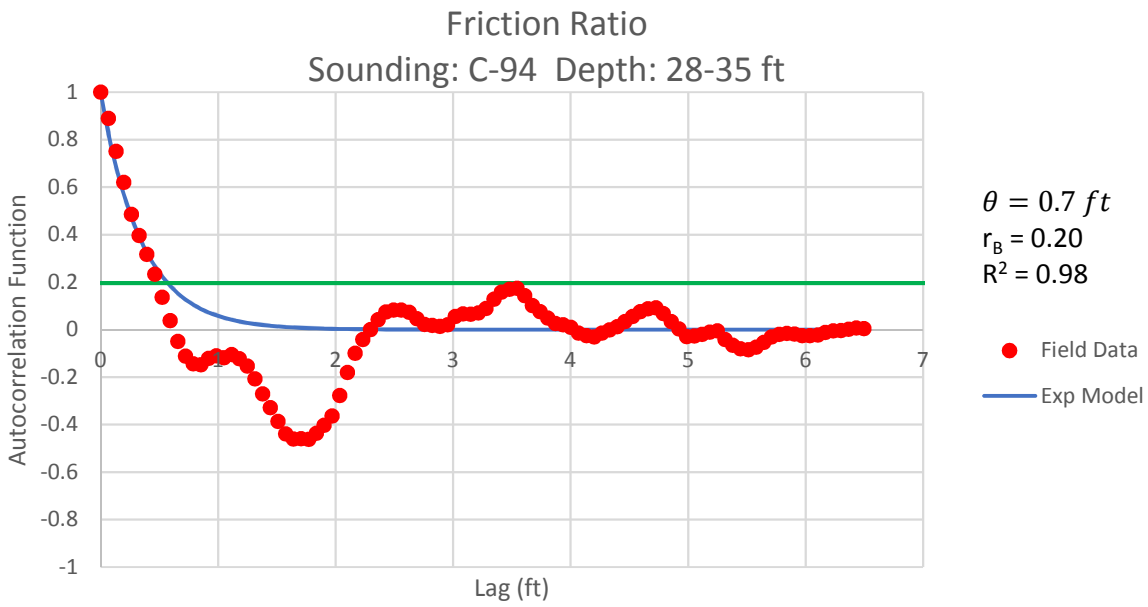

Figure B - 165: Estimation of the Scale of Fluctuation, $\theta = 0.7$ feet, for Friction Ratio Data from Sounding C-94, "Clean sands to silty sands (6)" layer from 28 to 35 feet depth.

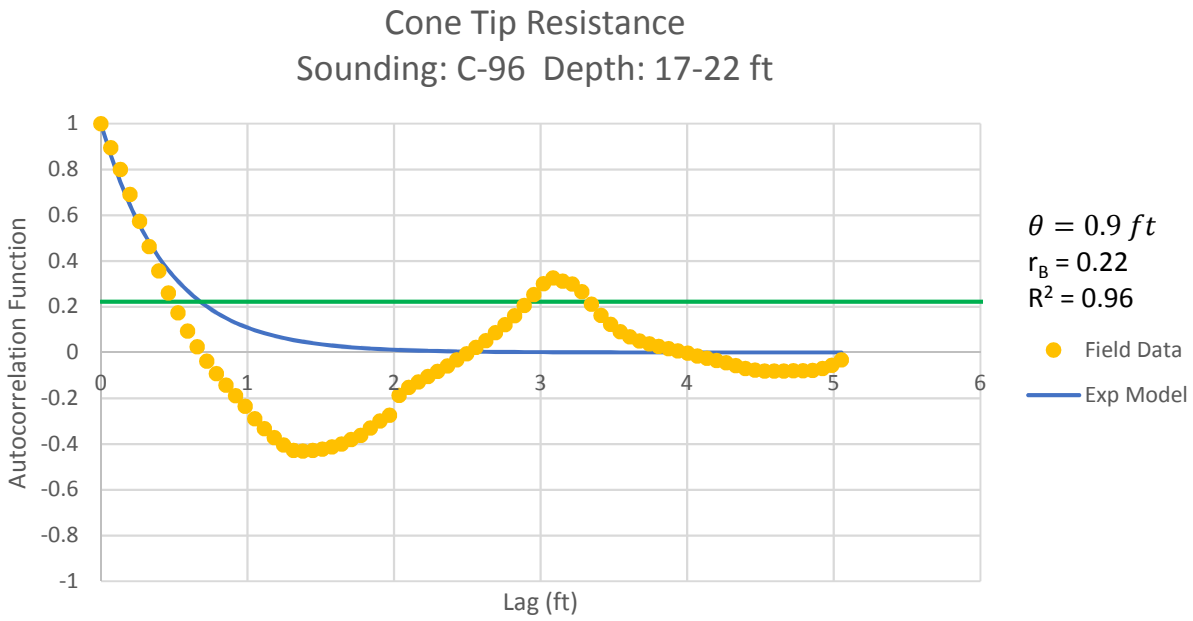

Figure B - 166: Estimation of the Scale of Fluctuation, $\theta = 0.9$ feet, for Cone Tip Resistance Data from Sounding C-96, "Clean sands to silty sands (6)" layer from 17 to 22 feet depth.

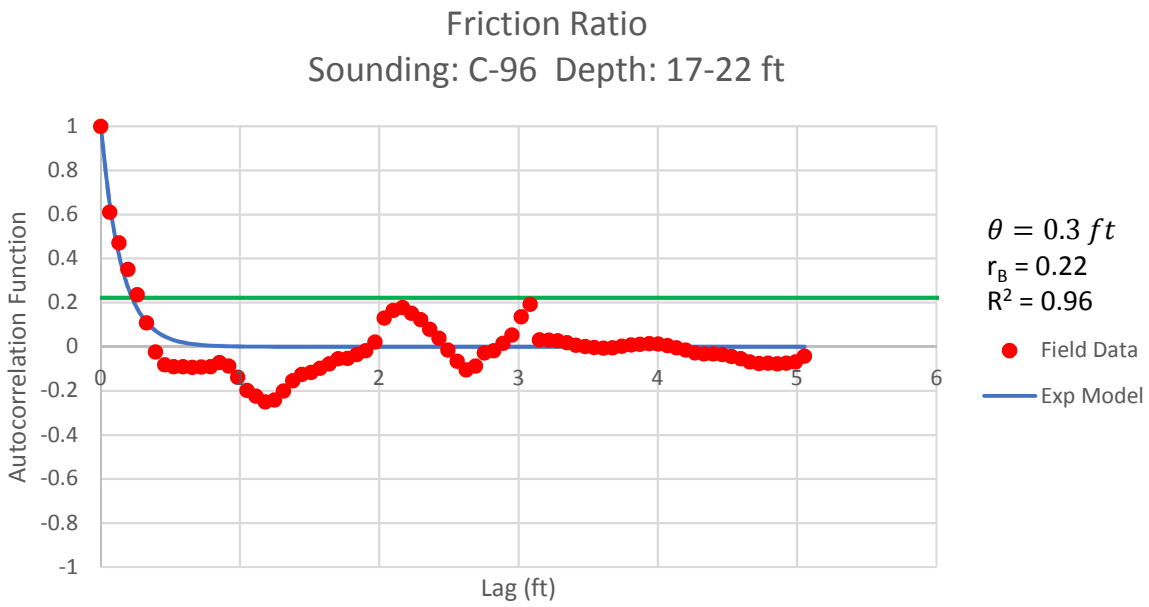

Figure B - 167: Estimation of the Scale of Fluctuation, $\theta = 0.3$ feet, for Friction Ratio Data from Sounding C-96, "Clean sands to silty sands (6)" layer from 17 to 22 feet depth.

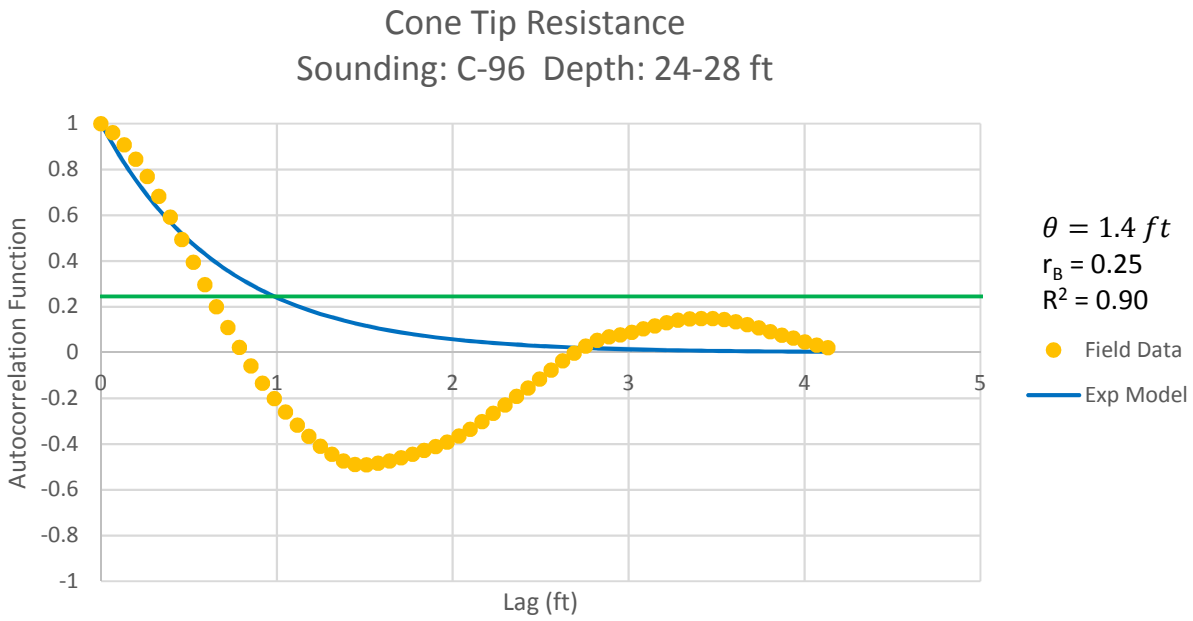

Figure B - 168: Estimation of the Scale of Fluctuation, $\theta = 1.4$ feet, for Cone Tip Resistance Data from Sounding C-96, "Clean sands to silty sands (6)" layer from 24 to 28 feet depth.

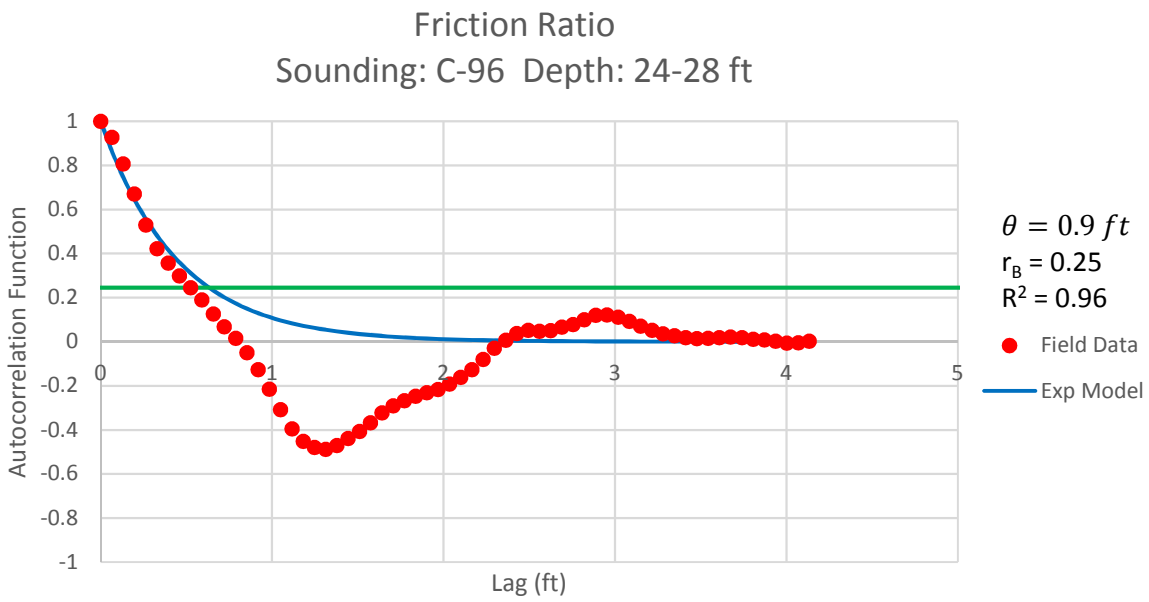

Figure B - 169: Estimation of the Scale of Fluctuation, $\theta = 0.9$ feet, for Friction Ratio Data from Sounding C-96, "Clean sands to silty sands (6)" layer from 24 to 28 feet depth.

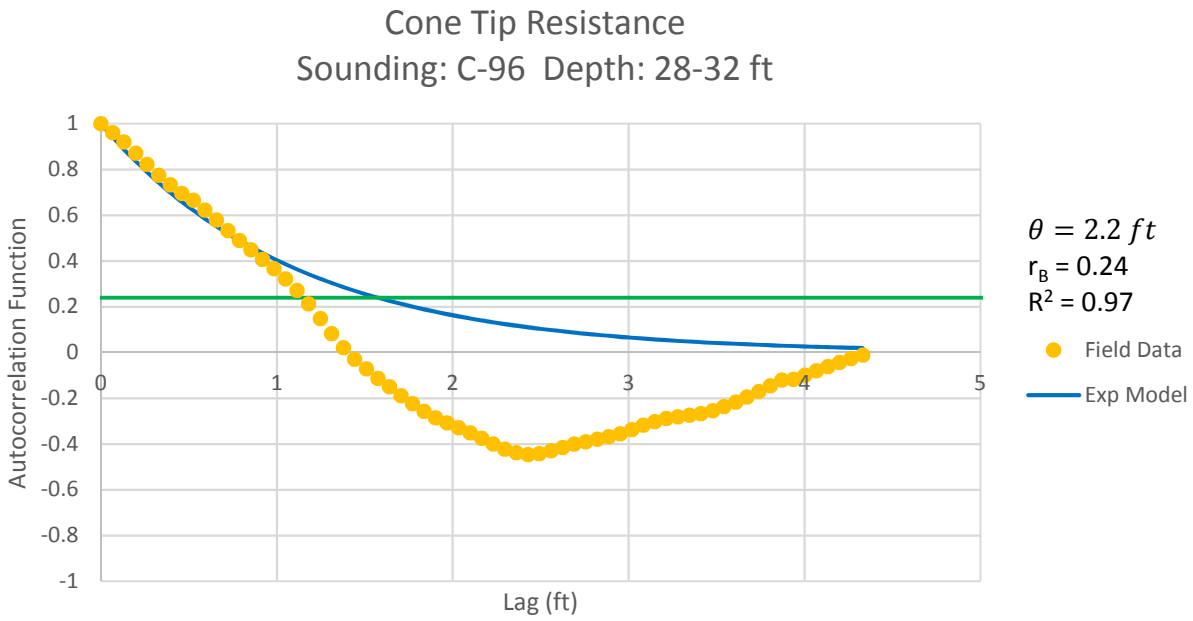

Figure B - 170: Estimation of the Scale of Fluctuation, $\theta = 2.2$ feet, for Cone Tip Resistance Data from Sounding C-96, "Gravelly sand to sand (7)" layer from 28 to 32 feet depth.

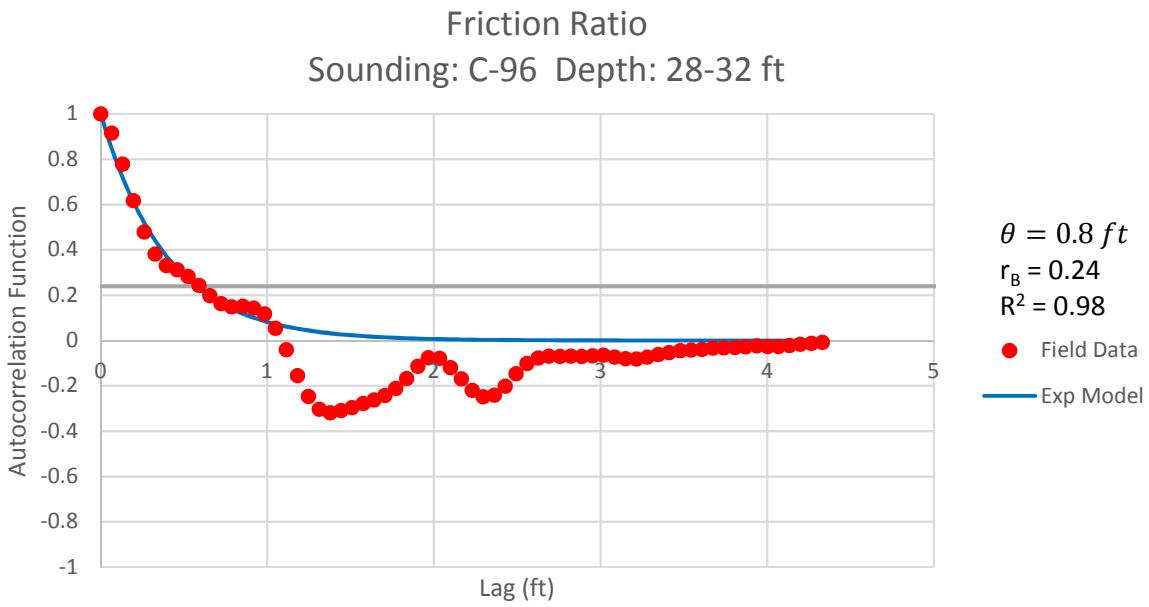

Figure B - 171: Estimation of the Scale of Fluctuation, $\theta = 0.8$ feet, for Friction Ratio Data from Sounding C-96, "Gravelly sand to sand (7)" layer from 28 to 32 feet depth.

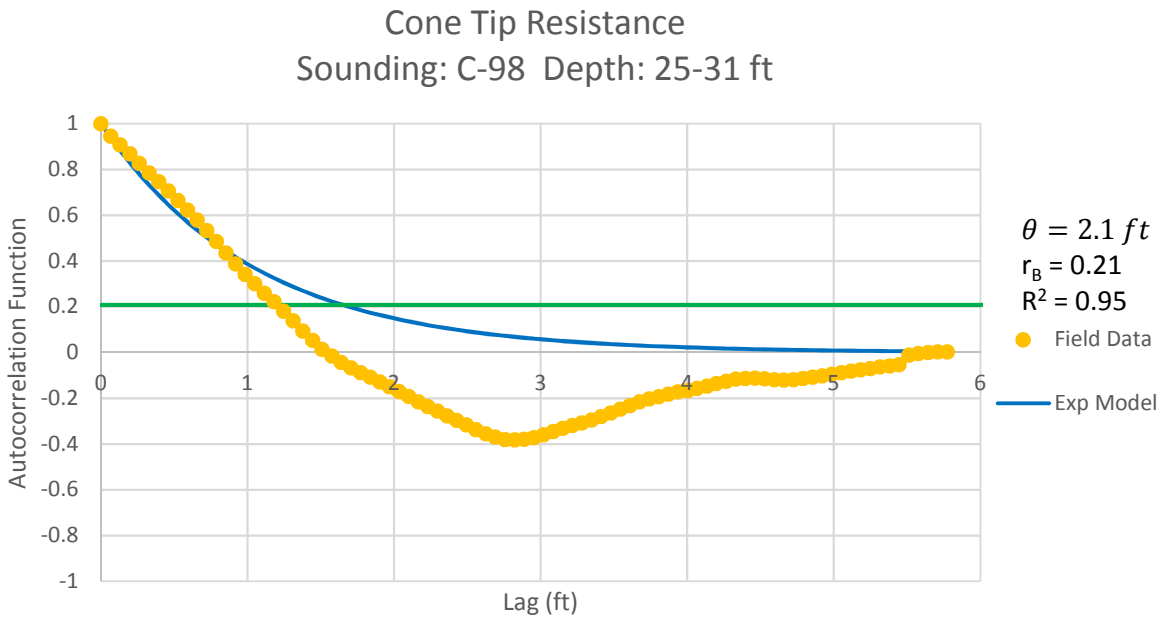

Figure B - 172: Estimation of the Scale of Fluctuation, θ = 2.1 feet, for Cone Tip Resistance Data from Sounding C-98, "Clean sands to silty sands (6)" layer from 25 to 31 feet depth.

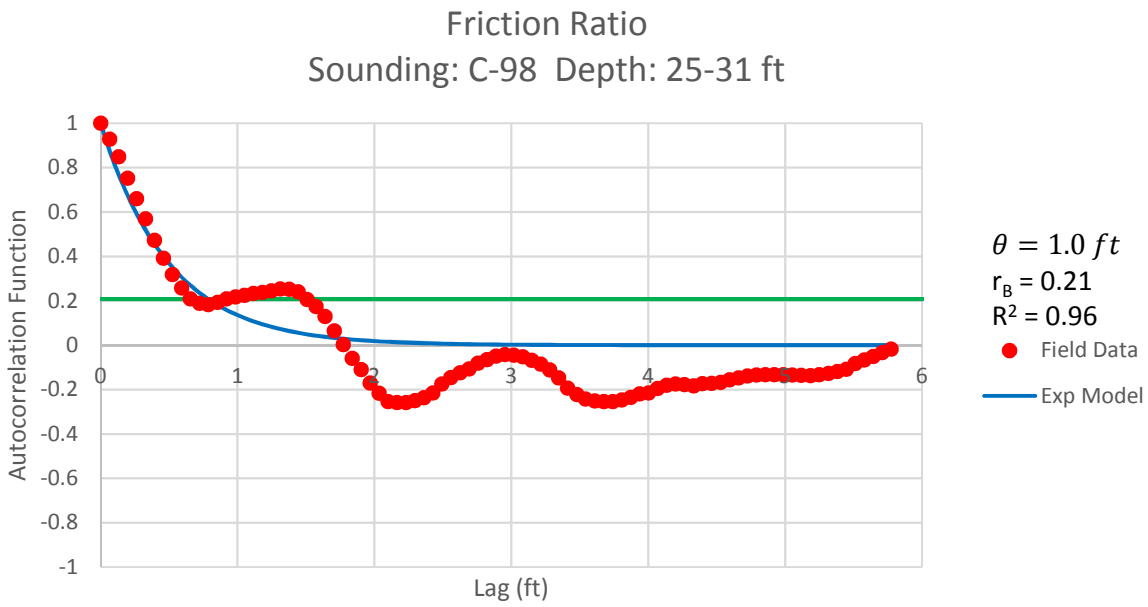

Figure B - 173: Estimation of the Scale of Fluctuation, θ = 1.0 feet, for Friction Ratio Data from Sounding C-98, "Clean sands to silty sands (6)" layer from 25 to 31 feet depth.

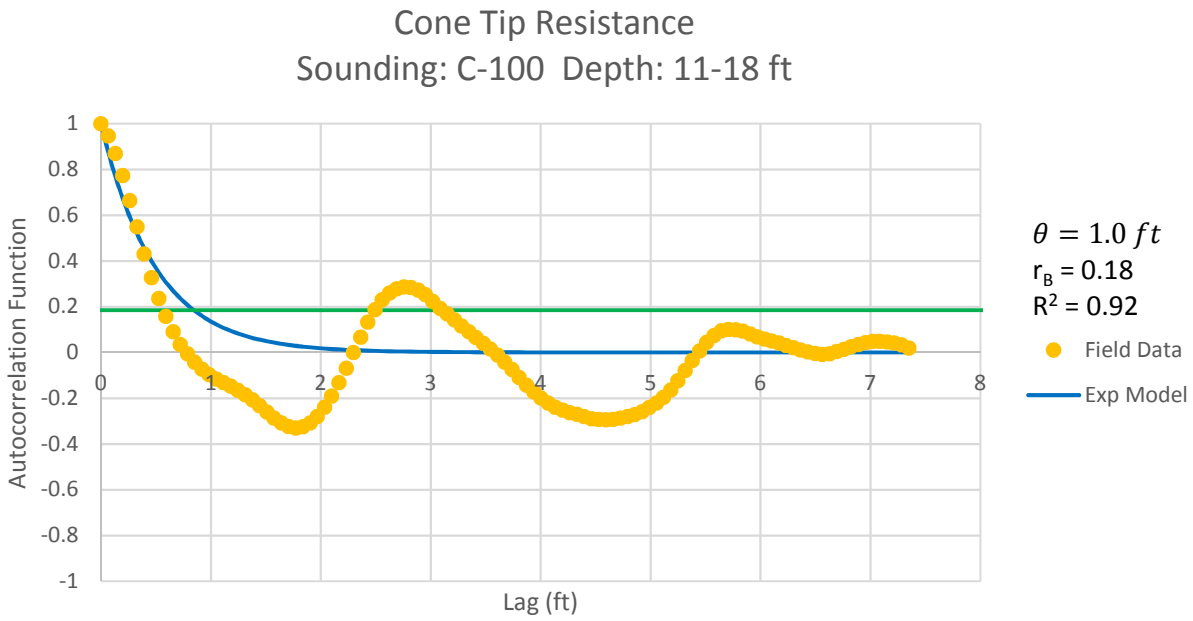

Figure B - 174: Estimation of the Scale of Fluctuation, $\theta = 1.0$ feet, for Cone Tip Resistance Data from Sounding C-100, "Clean sands to silty sands (6)" layer from 11 to 18 feet depth.

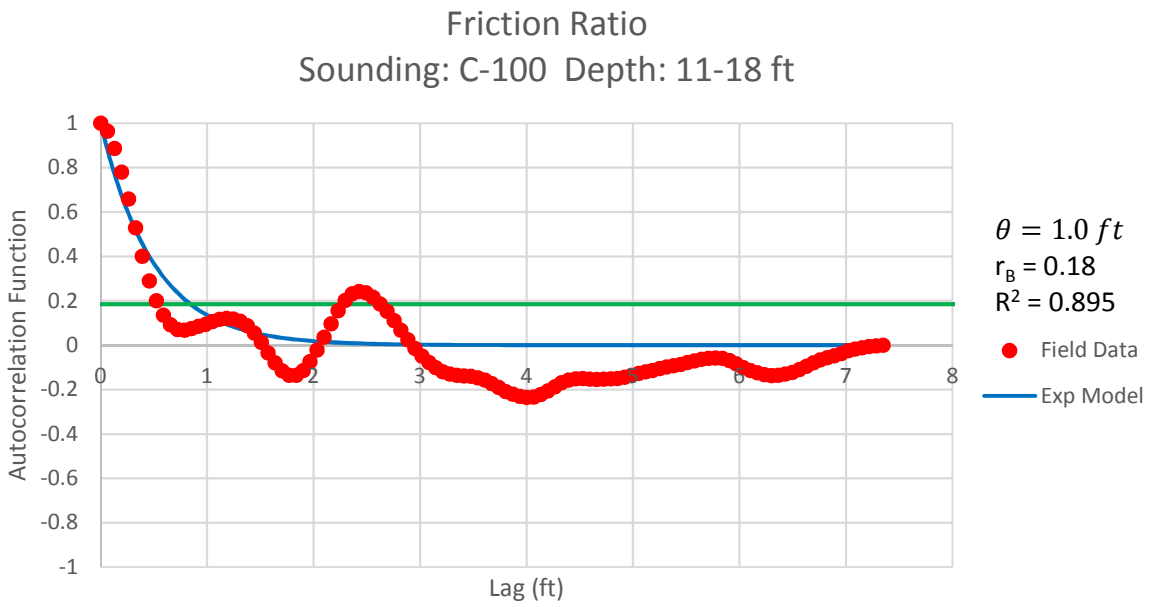

Figure B - 175: Estimation of the Scale of Fluctuation, $\theta = 1.0$ feet, for Friction Ratio Data from Sounding C-100, "Clean sands to silty sands (6)" layer from 11 to 18 feet depth. Data is a poor fit for the points greater than the Bartlett limit of 0.18; coefficient of determination, R^2, value is less 0.9. Therefore, these results were not included in final analysis.

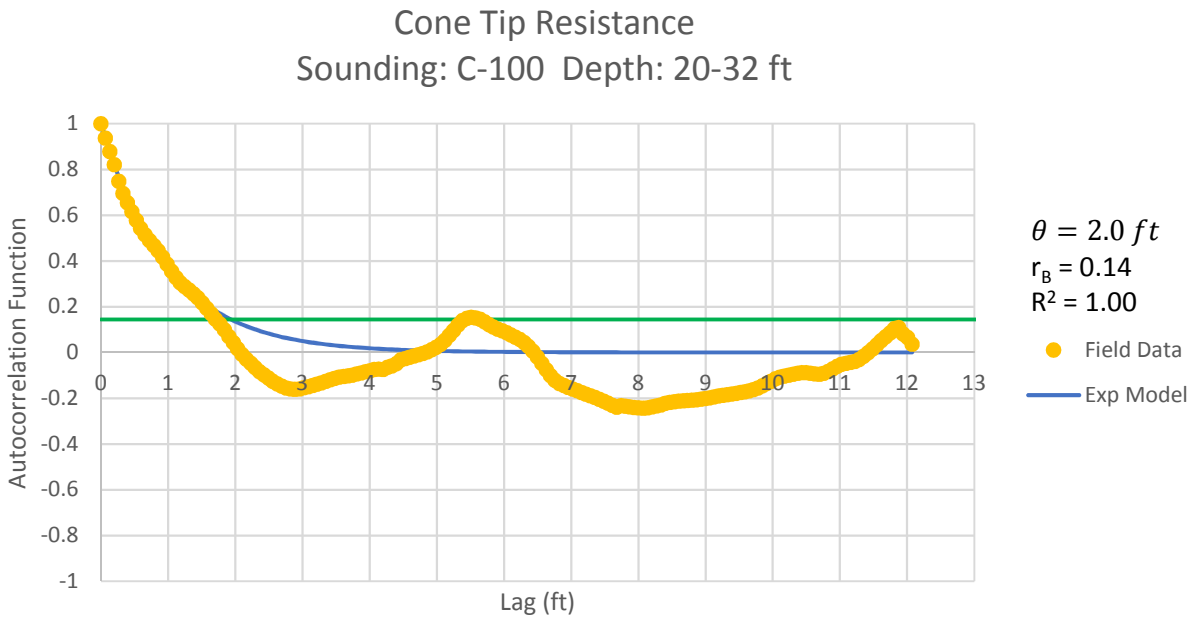

Figure B - 176: Estimation of the Scale of Fluctuation, $\theta = 2.0$ feet, for Cone Tip Resistance Data from Sounding C-100, "Clean sands to silty sands (6)" layer from 20 to 32 feet depth.

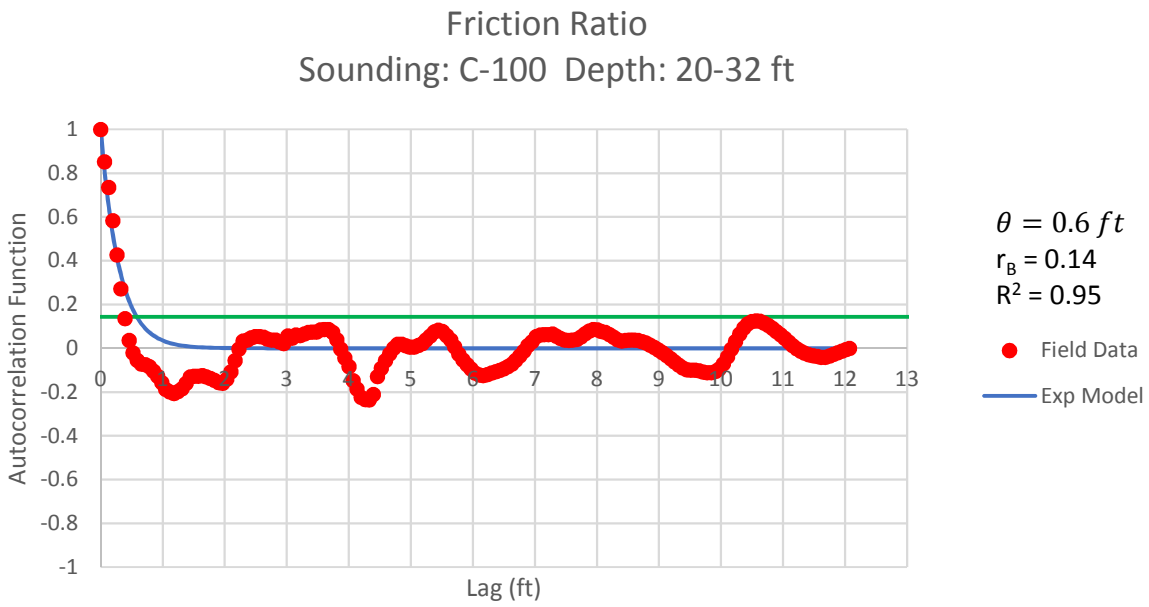

Figure B - 177: Estimation of the Scale of Fluctuation, $\theta = 0.6$ feet, for Friction Ratio Data from Sounding C-100, "Clean sands to silty sands (6)" layer from 20 to 32 feet depth.

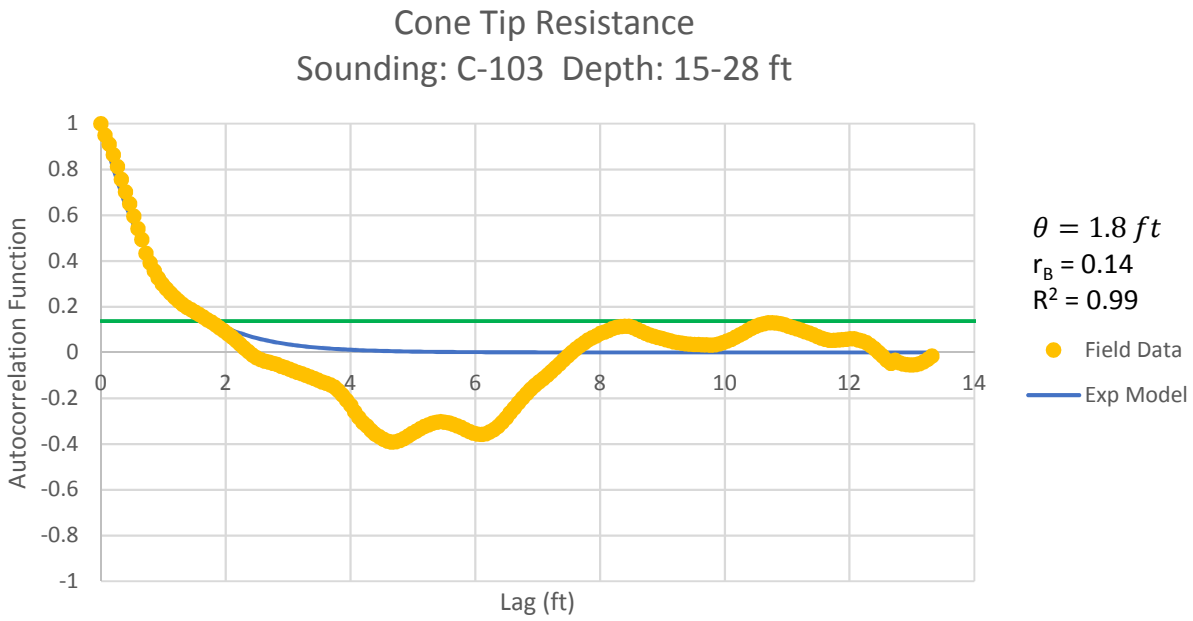

Figure B - 178: Estimation of the Scale of Fluctuation, $\theta = 1.8$ feet, for Cone Tip Resistance Data from Sounding C-103, "Clean sands to silty sands (6)" layer from 15 to 28 feet depth.

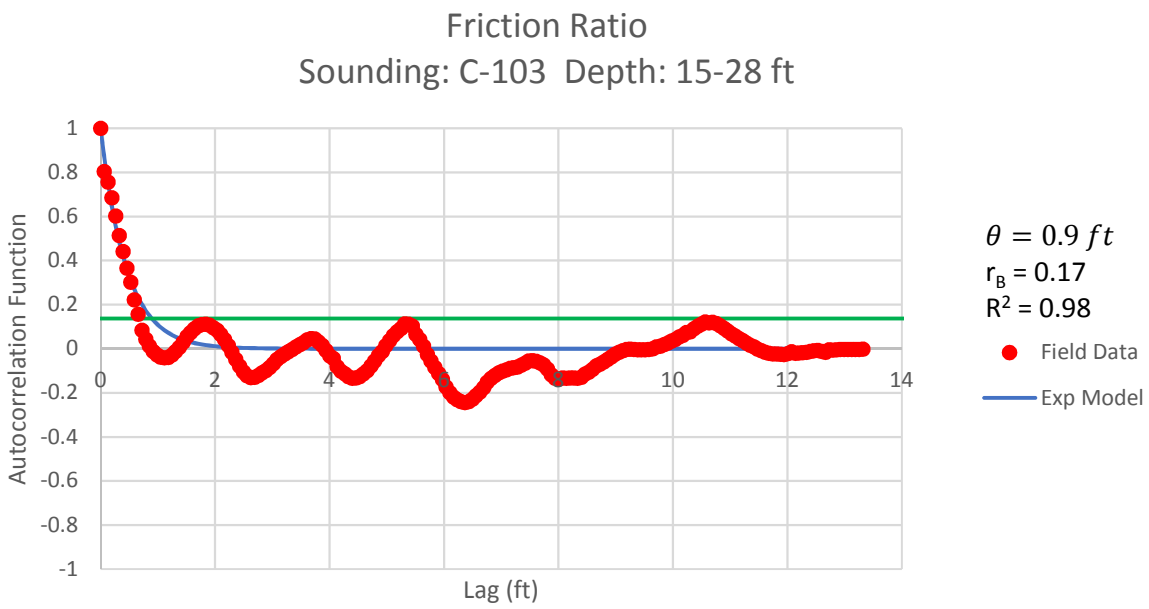

Figure B - 179: Estimation of the Scale of Fluctuation, $\theta = 0.9$ feet, for Friction Ratio Data from Sounding C-103, "Clean sands to silty sands (6)" layer from 15 to 28 feet depth.

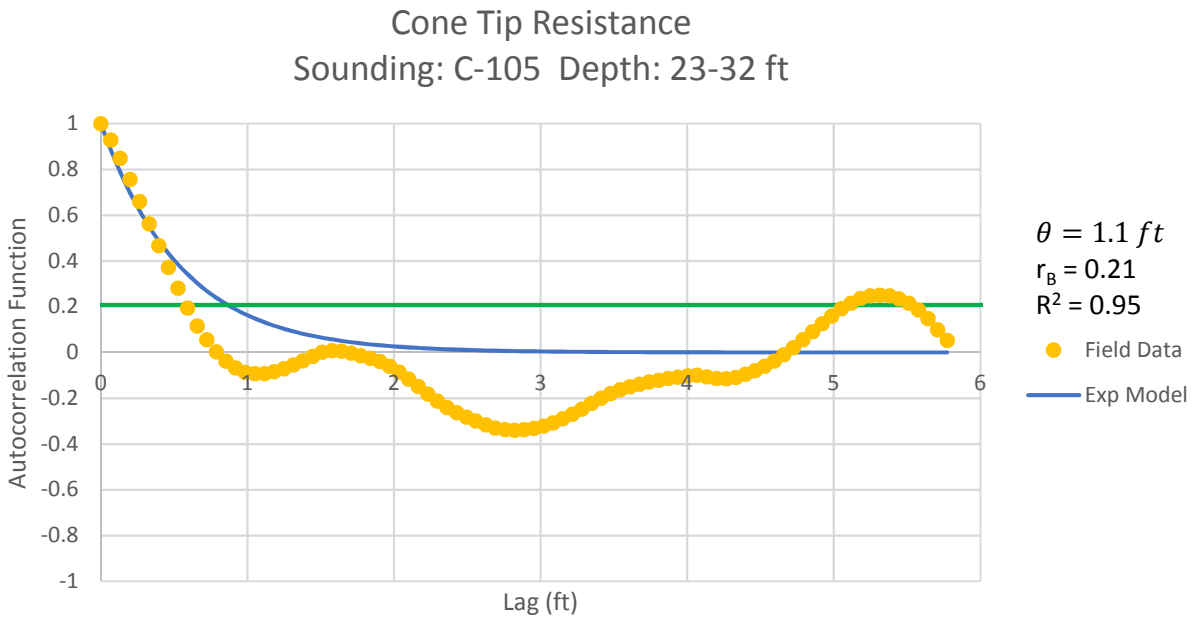

Figure B - 180: Estimation of the Scale of Fluctuation, $\theta = 1.1$ feet, for Cone Tip Resistance Data from Sounding C-105, "Clean sands to silty sands (6)" layer from 23 to 32 feet depth.

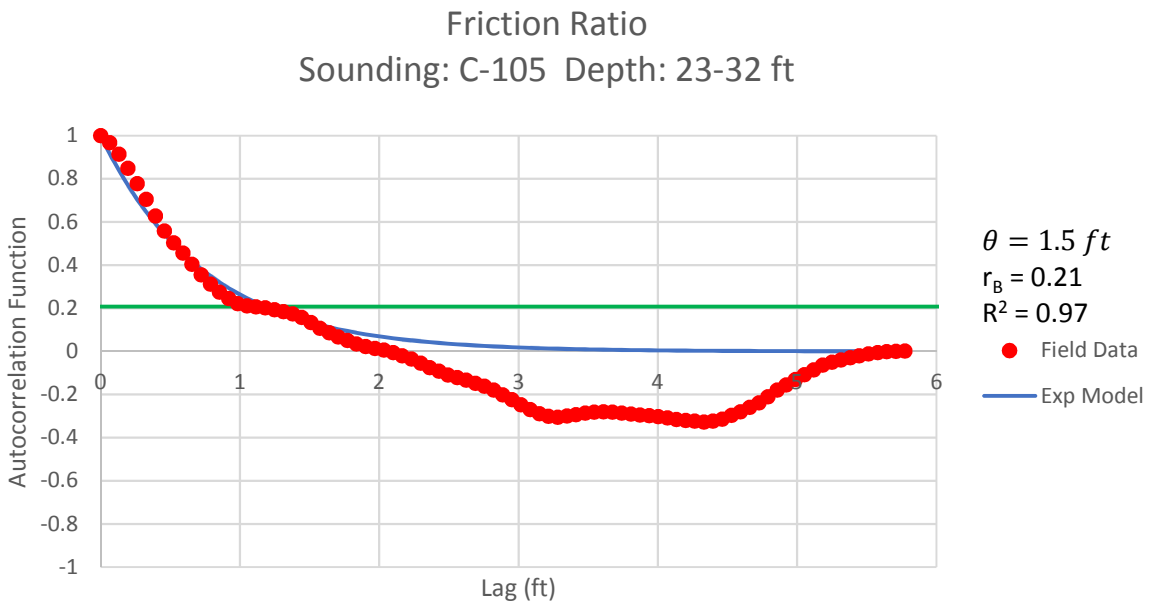

Figure B - 181: Estimation of the Scale of Fluctuation, $\theta = 1.5$ feet, for Friction Ratio Data from Sounding C-105, "Clean sands to silty sands (6)" layer from 23 to 32 feet depth.

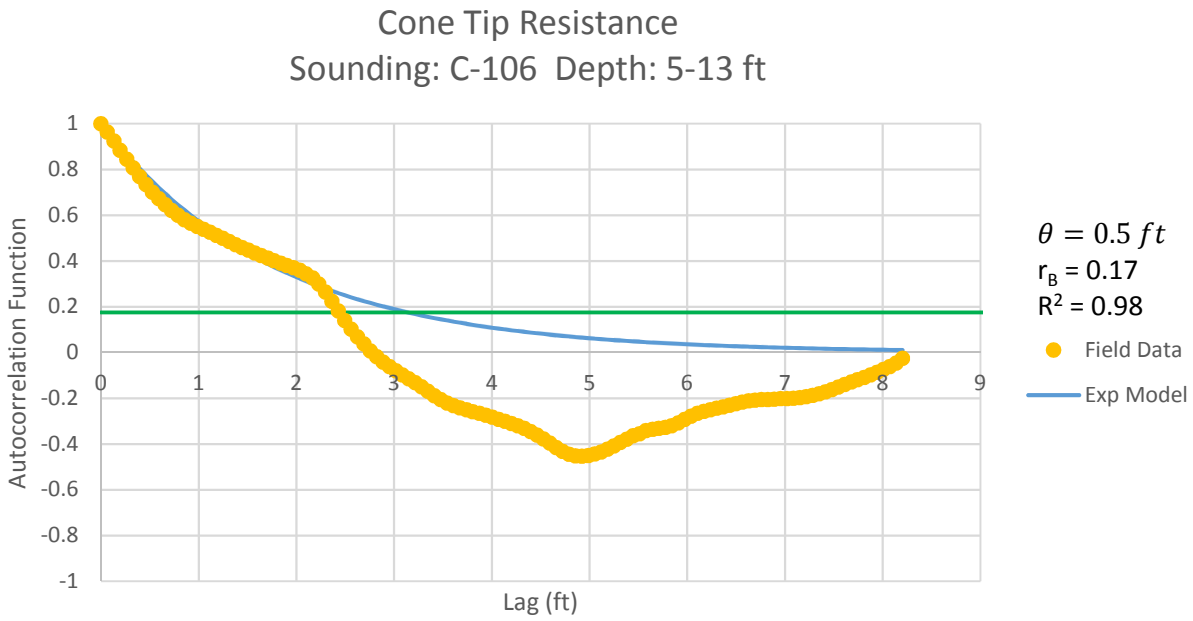

Figure B - 182: Estimation of the Scale of Fluctuation, $\theta = 0.5$ feet, for Cone Tip Resistance Data from Sounding C-106, "Clean sands to silty sands (6)" layer from 5 to 13 feet depth.

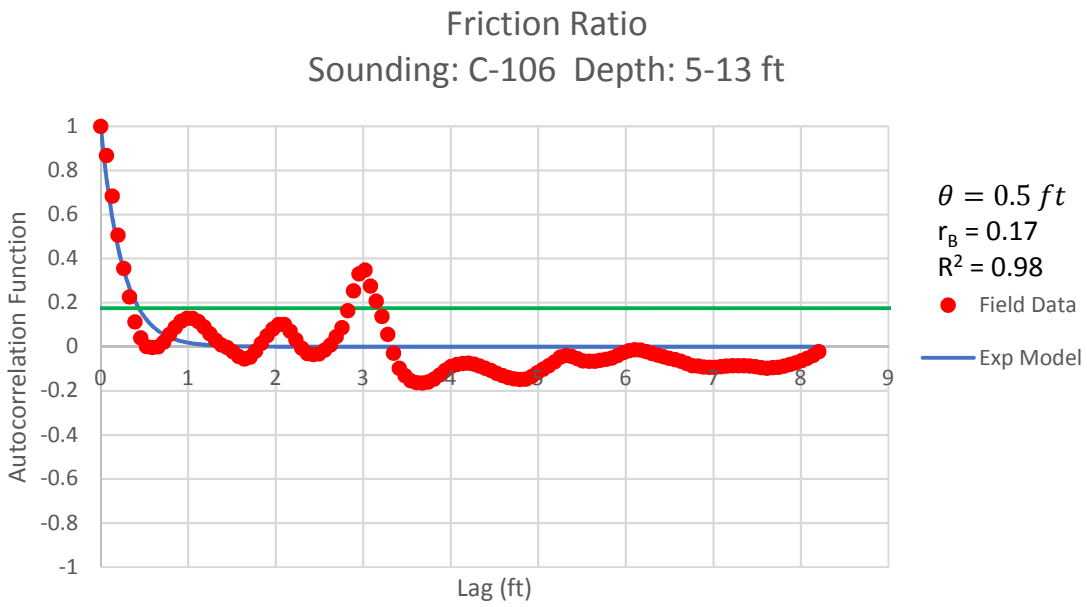

Figure B - 183: Estimation of the Scale of Fluctuation, $\theta = 0.5$ feet, for Friction Ratio Data from Sounding C-106, "Clean sands to silty sands (6)" layer from 5 to 13 feet depth.

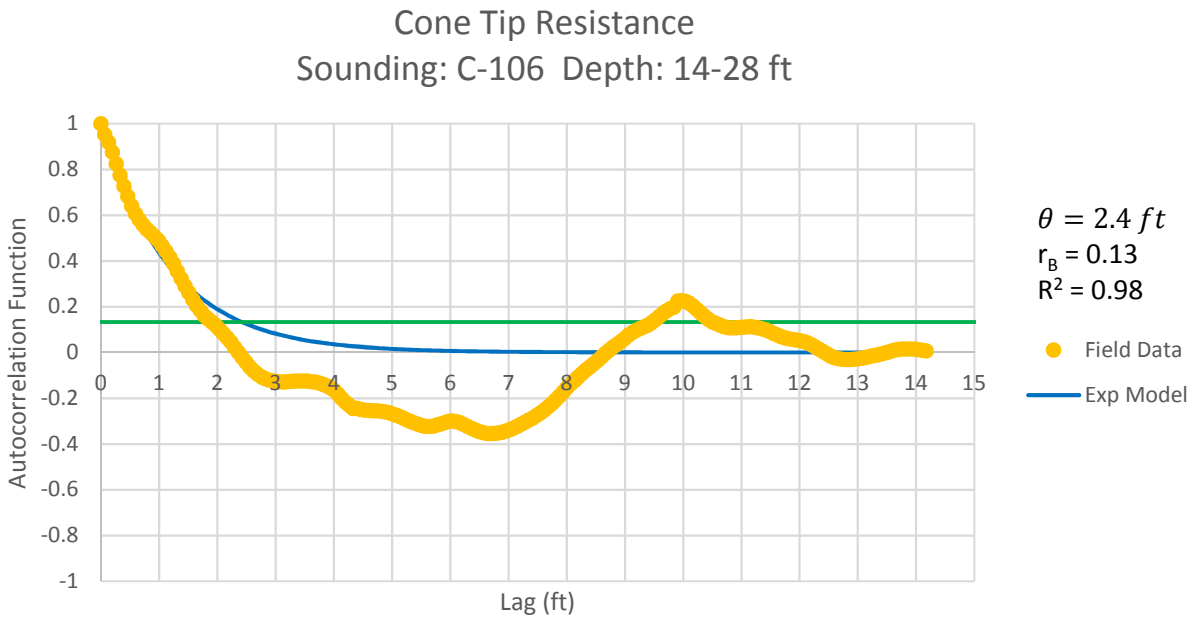

Figure B - 184: Estimation of the Scale of Fluctuation, $\theta = 2.4$ feet, for Cone Tip Resistance Data from Sounding C-106, "Clean sands to silty sands (6)" layer from 14 to 28 feet depth.

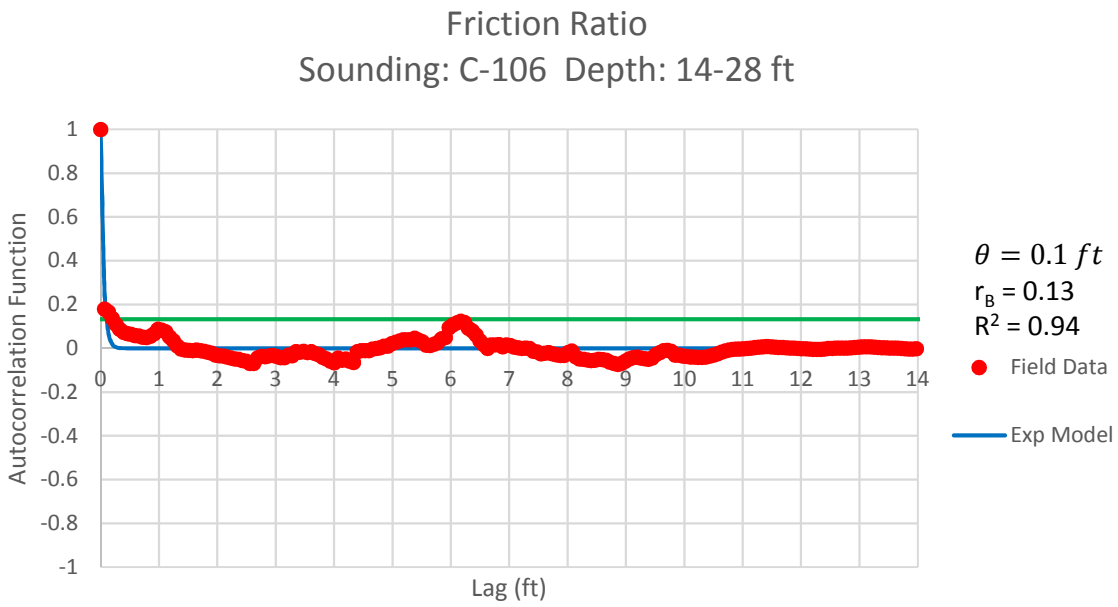

Figure B - 185: Estimation of the Scale of Fluctuation, $\theta = 0.1$ feet, for Friction Ratio Data from Sounding C-106, "Clean sands to silty sands (6)" layer from 14 to 28 feet depth.

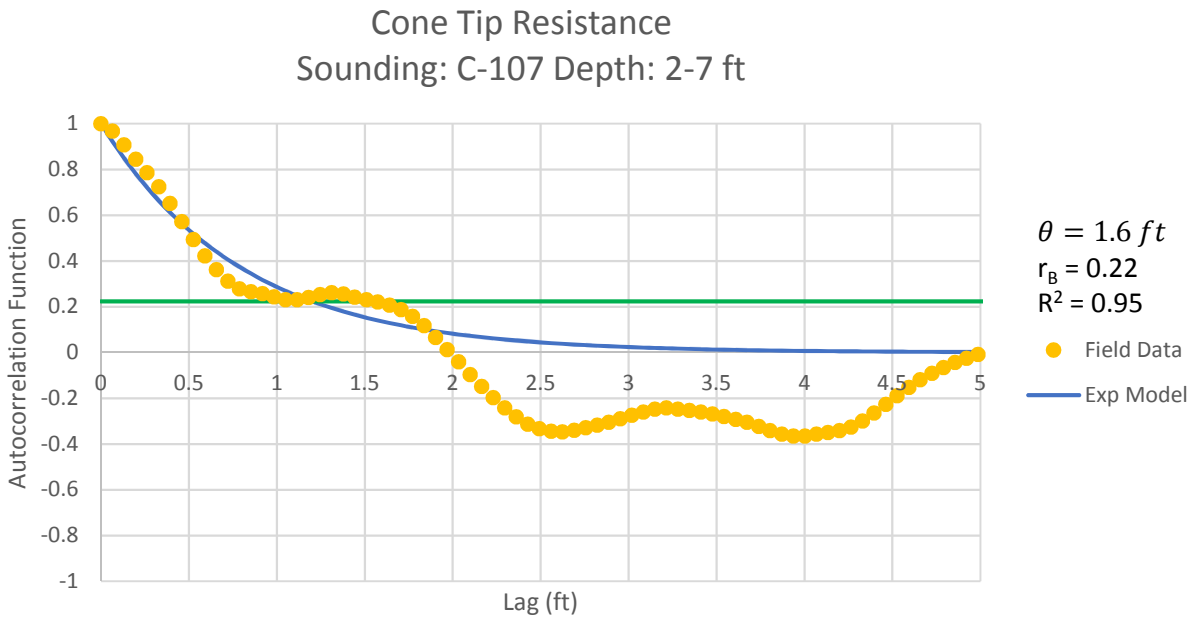

Figure B - 186: Estimation of the Scale of Fluctuation, $\theta = 1.6$ feet, for Cone Tip Resistance Data from Sounding C-107, "Silty sand to sandy silt (5)" layer from 2 to 7 feet depth.

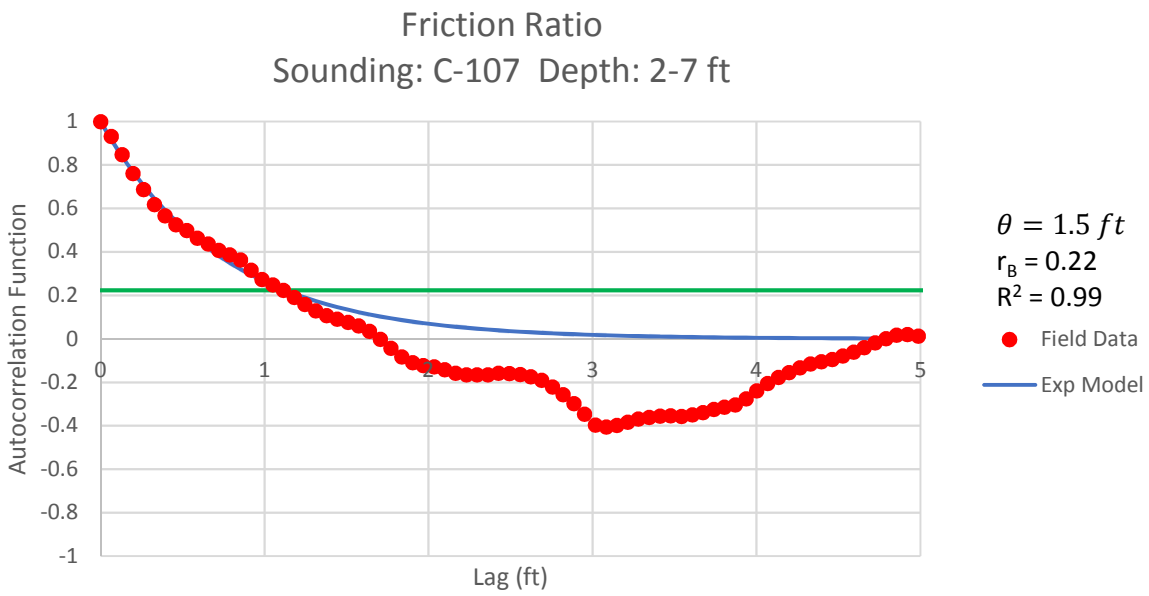

Figure B - 18788: Estimation of the Scale of Fluctuation, $\theta = 1.5$ feet, for Friction Ratio Data from Sounding C-107, "Silty sand to sandy silt (5)" layer from 2 to 7 feet depth.

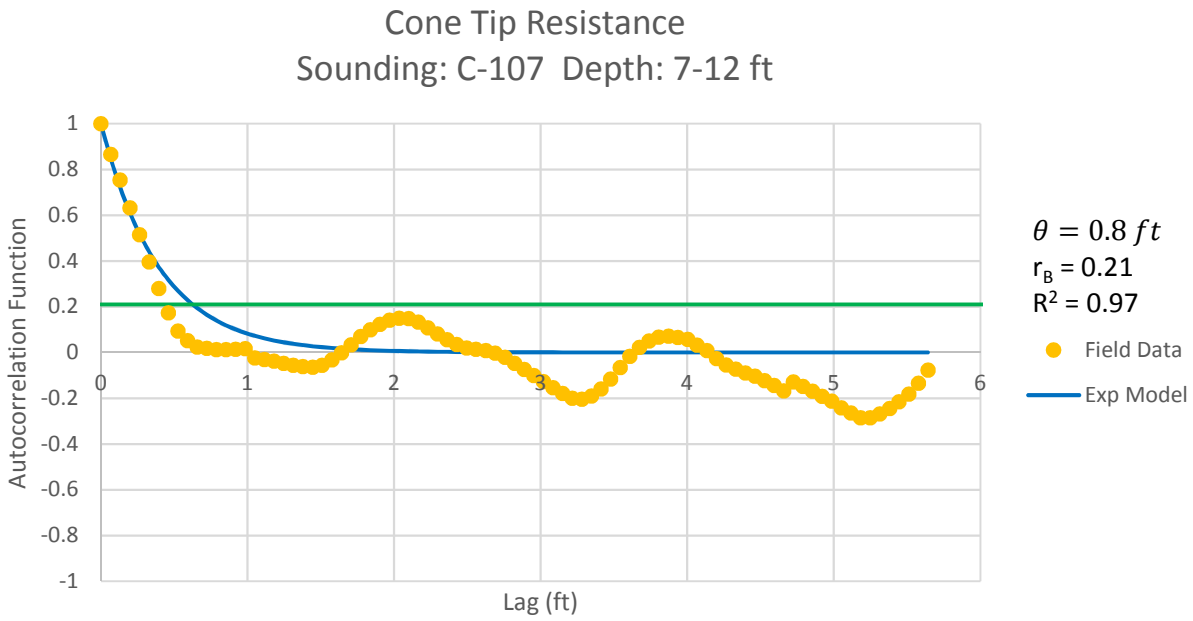

Figure B - 188: Estimation of the Scale of Fluctuation, $\theta = 0.8$ feet, for Cone Tip Resistance Data from Sounding C-107, "Clean sands to silty sands (6)" layer from 7 to 12 feet depth.

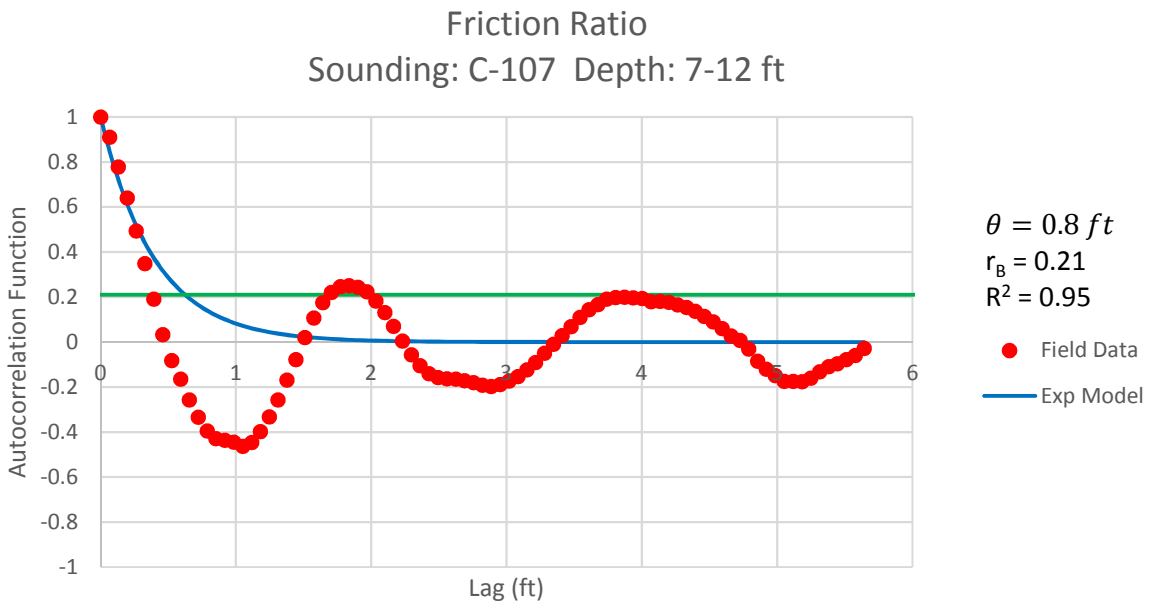

Figure B - 189: Estimation of the Scale of Fluctuation, $\theta = 0.8$ feet, for Friction Ratio Data from Sounding C-107, "Clean sands to silty sands (6)" layer from 7 to 12 feet depth.

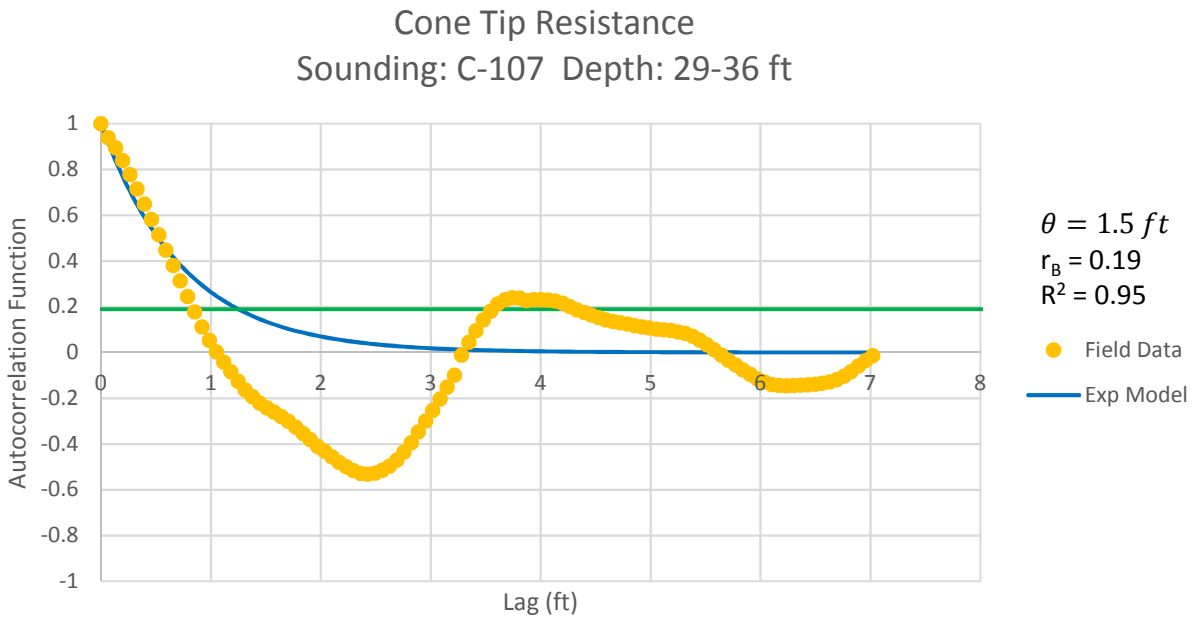

Figure B - 190: Estimation of the Scale of Fluctuation, $\theta = 1.5$ feet, for Cone Tip Resistance Data from Sounding C-107, "Clean sands to silty sands (6)" layer from 29 to 36 feet depth.

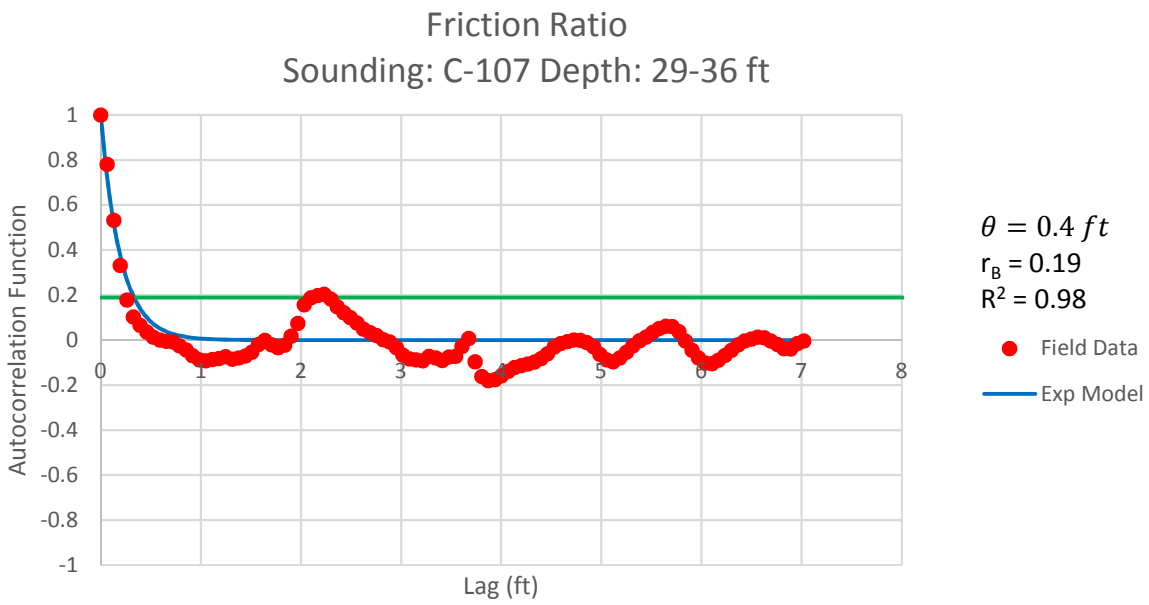

Figure B - 191: Estimation of the Scale of Fluctuation, $\theta = 0.4$ feet, for Friction Ratio Data from Sounding C-107, "Clean sands to silty sands (6)" layer from 29 to 36 feet depth.

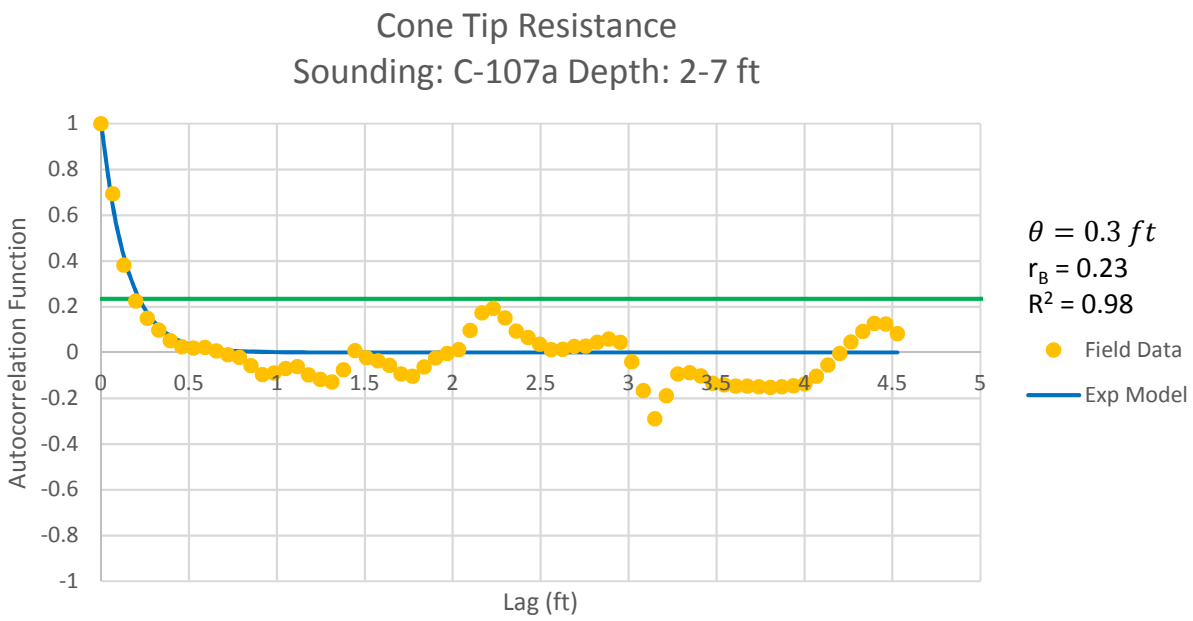

Figure B - 192: Estimation of the Scale of Fluctuation, θ = 0.3 feet, for Cone Tip Resistance Data from Sounding C-107a, "Clays; clay to silty clay (3)" layer from 2 to 7 feet depth.

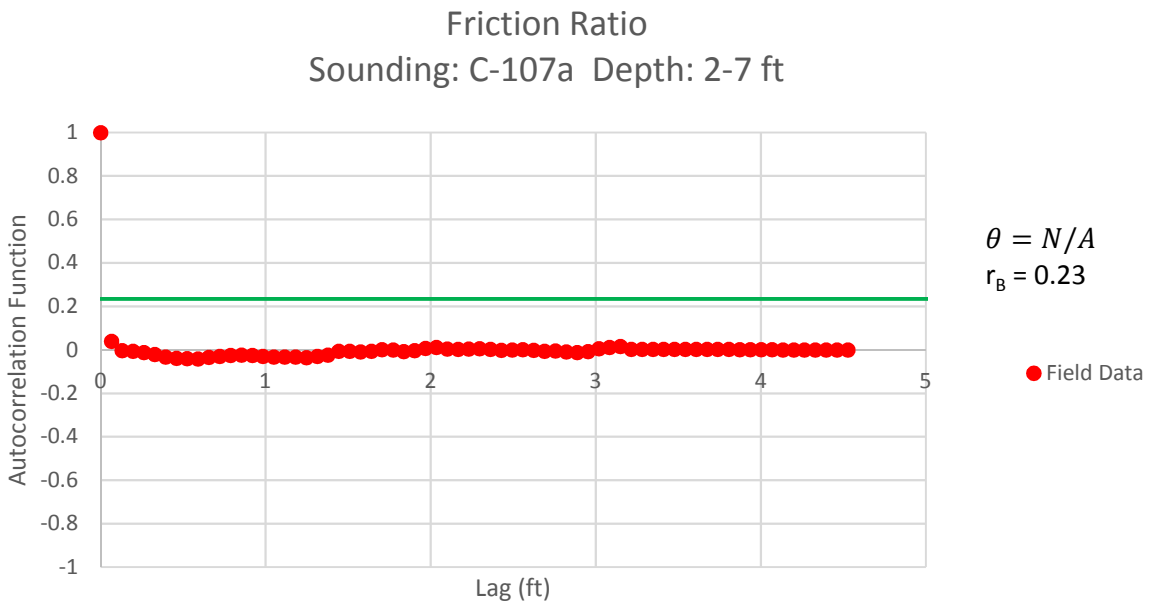

Figure B - 193: Estimation of the Scale of Fluctuation, θ, for Friction Ratio Data from Sounding C-107a, "Clays; clay to silty clay (3)" layer from 2 to 7 feet depth. Data is limited to only 1 point greater than the Bartlett limit of 0.23; therefore, θ could not be estimated, and these results were not included in final analysis.

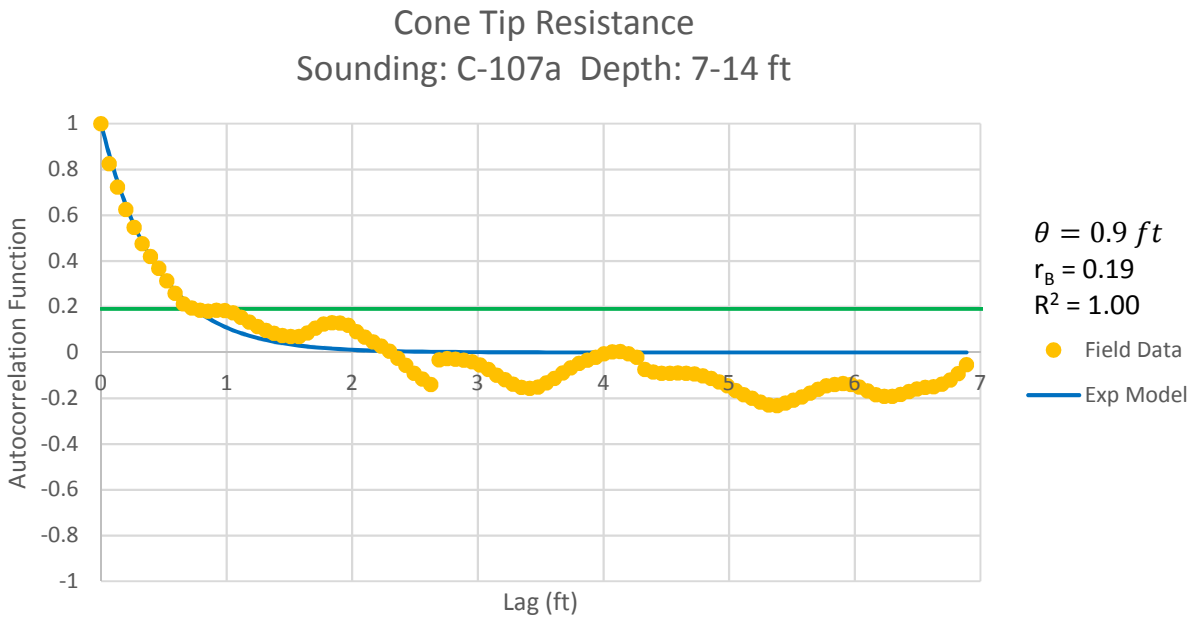

Figure B - 194: Estimation of the Scale of Fluctuation, θ = 0.9 feet, for Cone Tip Resistance Data from Sounding C-107a, "Clean sands to silty sands (6)" layer from 7 to 14 feet depth.

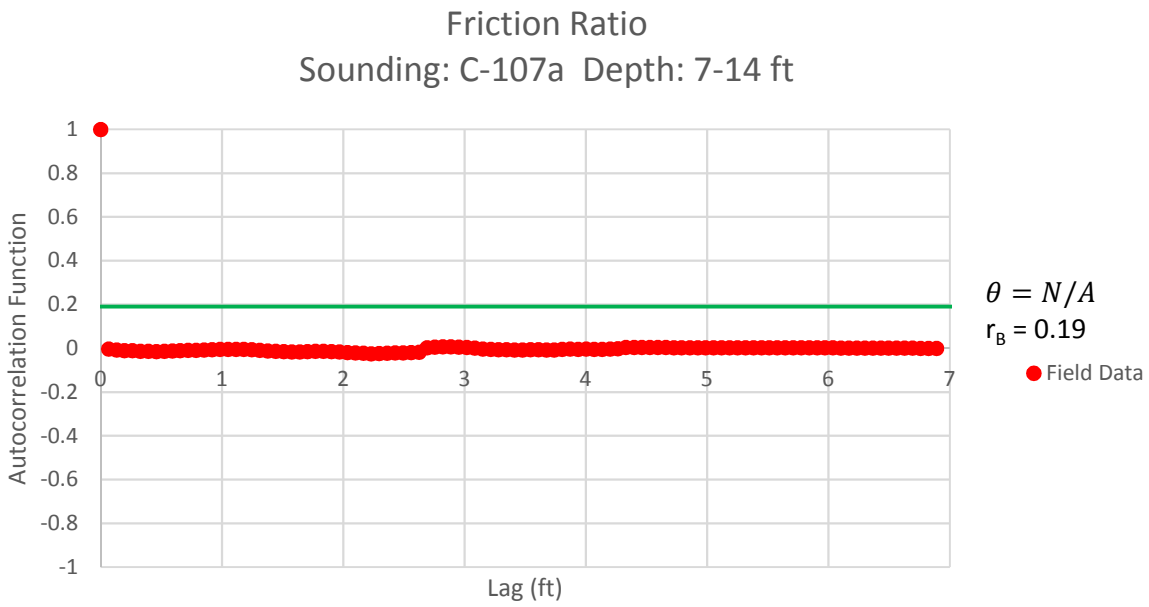

Figure B - 195: Estimation of the Scale of Fluctuation, θ, for Friction Ratio Data from Sounding C-107a, " Clean sands to silty sands (6)" layer from 7 to 14 feet depth. Data is limited to only 1 point greater than the Bartlett limit of 0.19; therefore, θ could not be estimated, and these results were not included in final analysis.

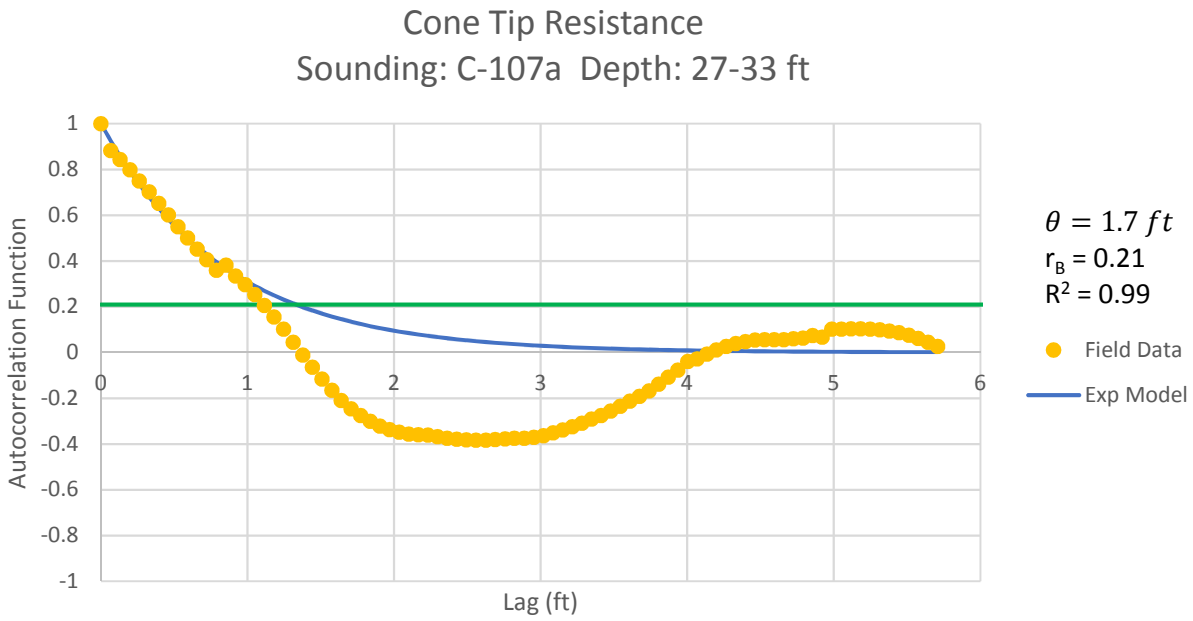

Figure B - 196: Estimation of the Scale of Fluctuation, $\theta = 1.7$ feet, for Cone Tip Resistance Data from Sounding C-107a, "Clean sands to silty sands (6)" layer from 27 to 33 feet depth.

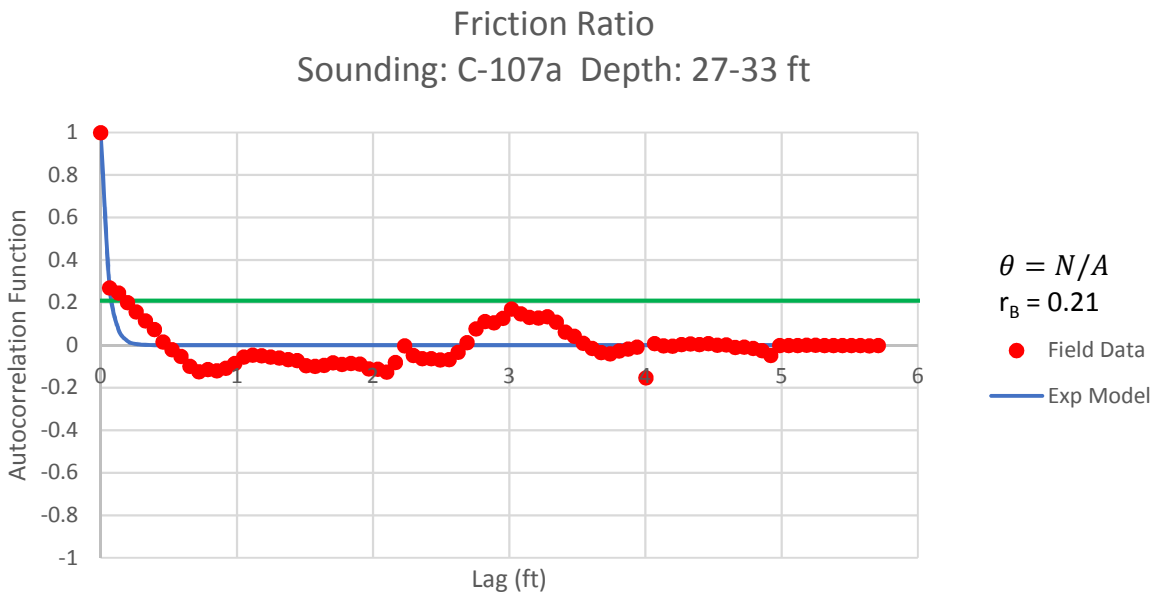

Figure B - 197: Estimation of the Scale of Fluctuation, θ, for Friction Ratio Data from Sounding C-107a, "Clean sands to silty sands (6)" layer from 27 to 33 feet depth. Data is limited to only 3 points greater than the Bartlett limit of 0.21; therefore, θ could not be estimated, and these results were not included in final analysis.

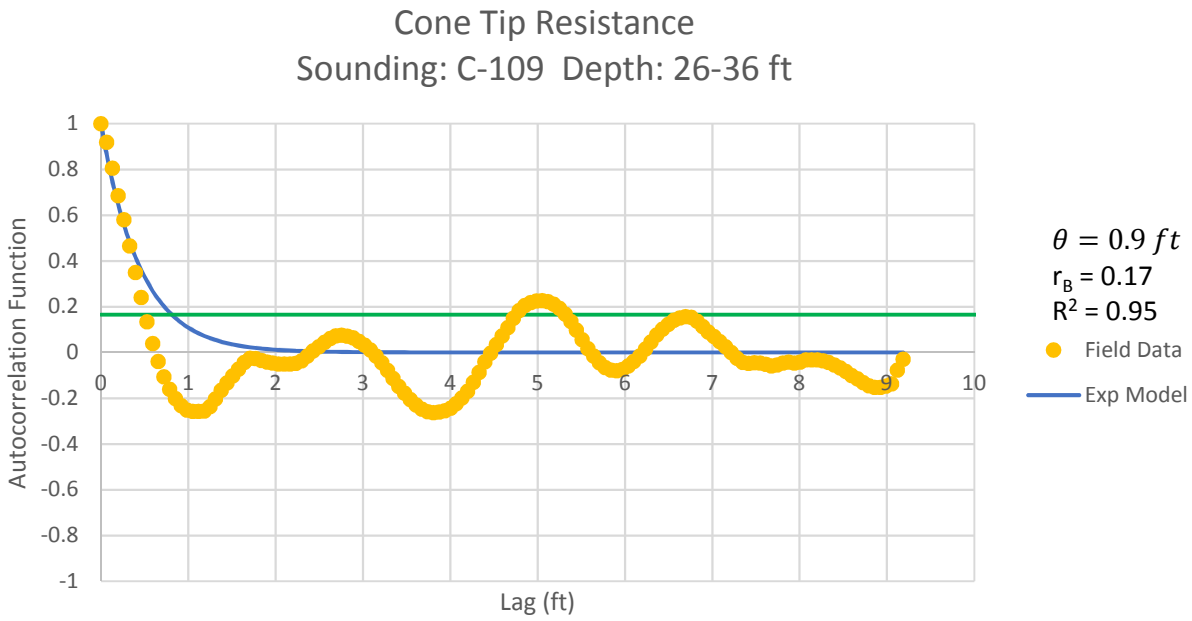

Figure B - 198: Estimation of the Scale of Fluctuation, $\theta = 0.9$ feet, for Cone Tip Resistance Data from Sounding C-109, "Clean sands to silty sands (6)" layer from 26 to 36 feet depth.

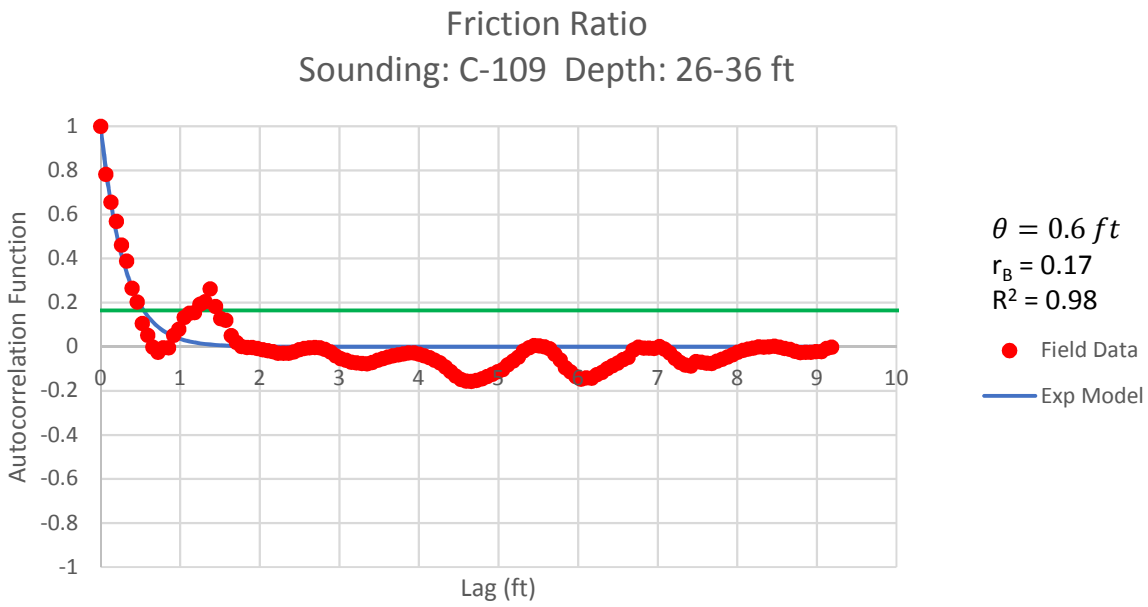

Figure B - 199: Estimation of the Scale of Fluctuation, $\theta = 0.6$ feet, for Friction Ratio Data from Sounding C-109, "Clean sands to silty sands (6)" layer from 26 to 36 feet depth.

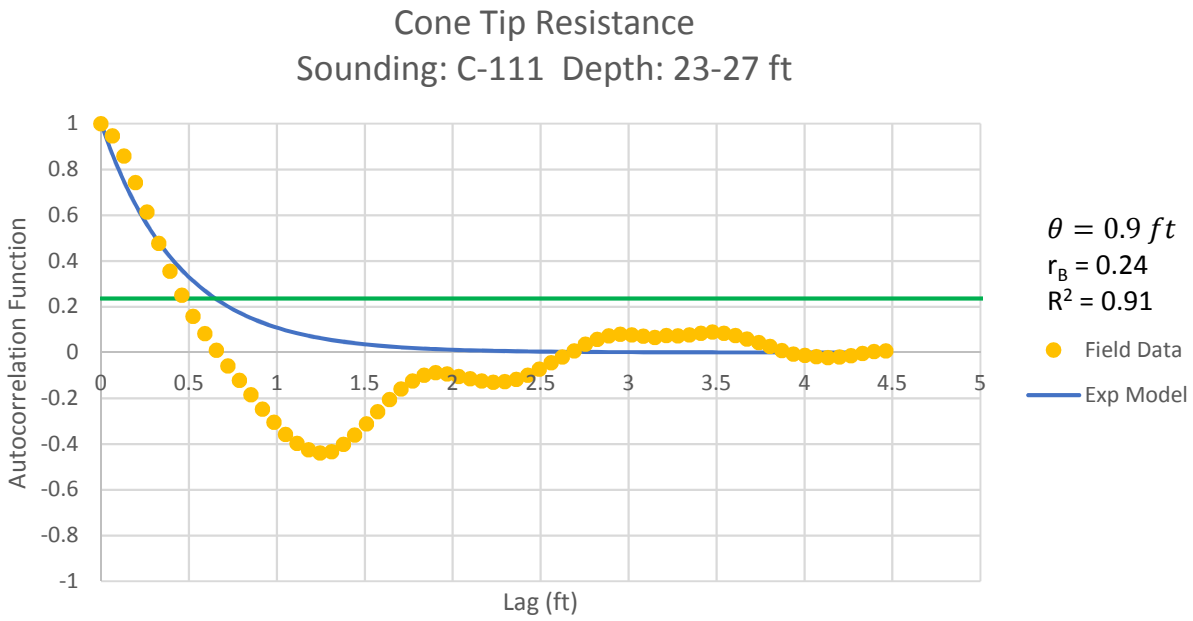

Figure B - 200: Estimation of the Scale of Fluctuation, $\theta = 0.9$ feet, for Cone Tip Resistance Data from Sounding C-111, "Clean sands to silty sands (6)" layer from 23 to 27 feet depth.

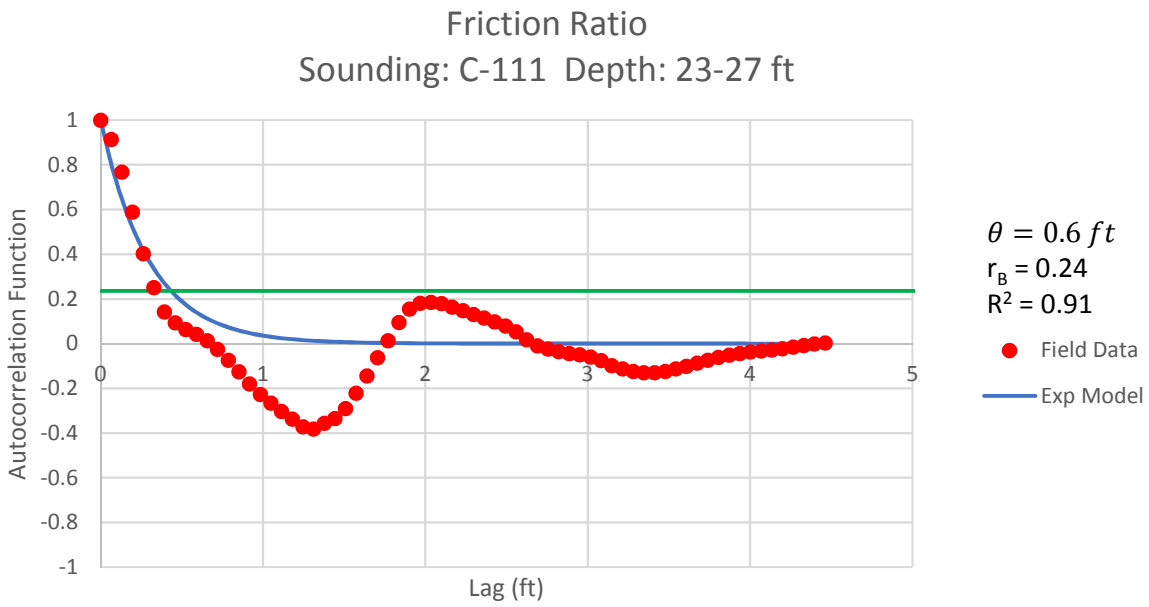

Figure B - 201: Estimation of the Scale of Fluctuation, $\theta = 0.6$ feet, for Friction Ratio Data from Sounding C-111, "Clean sands to silty sands (6)" layer from 23 to 27 feet depth.

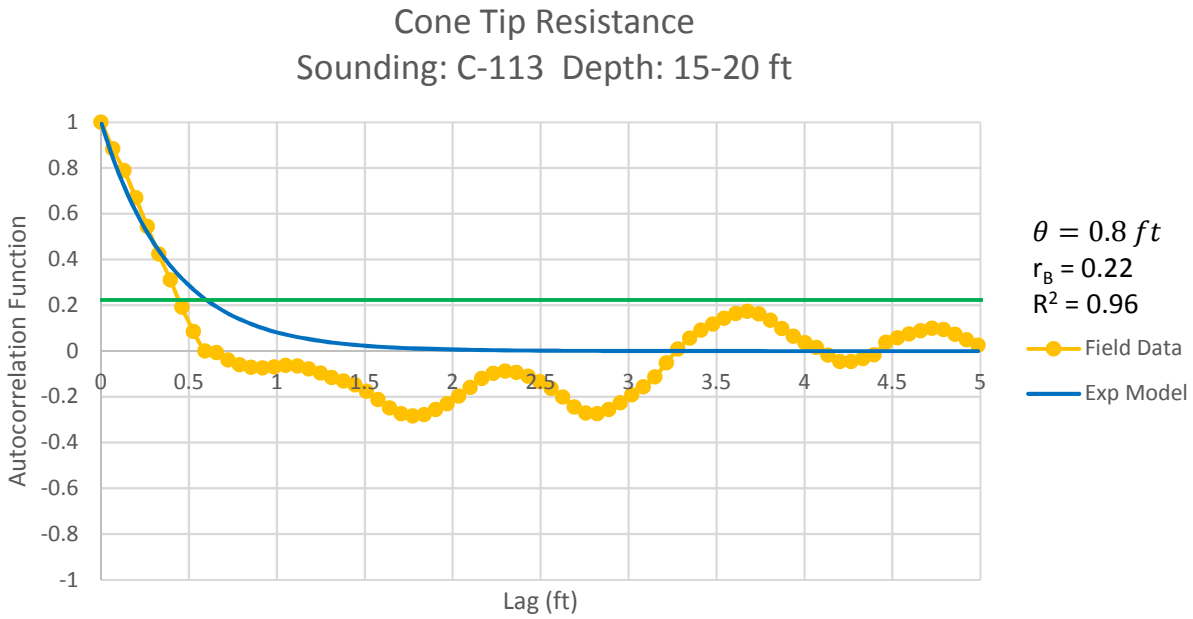

Figure B - 202: Estimation of the Scale of Fluctuation, $\theta = 0.8$ feet, for Cone Tip Resistance Data from Sounding C-113, "Clean sands to silty sands (6)" layer from 15 to 20 feet depth.

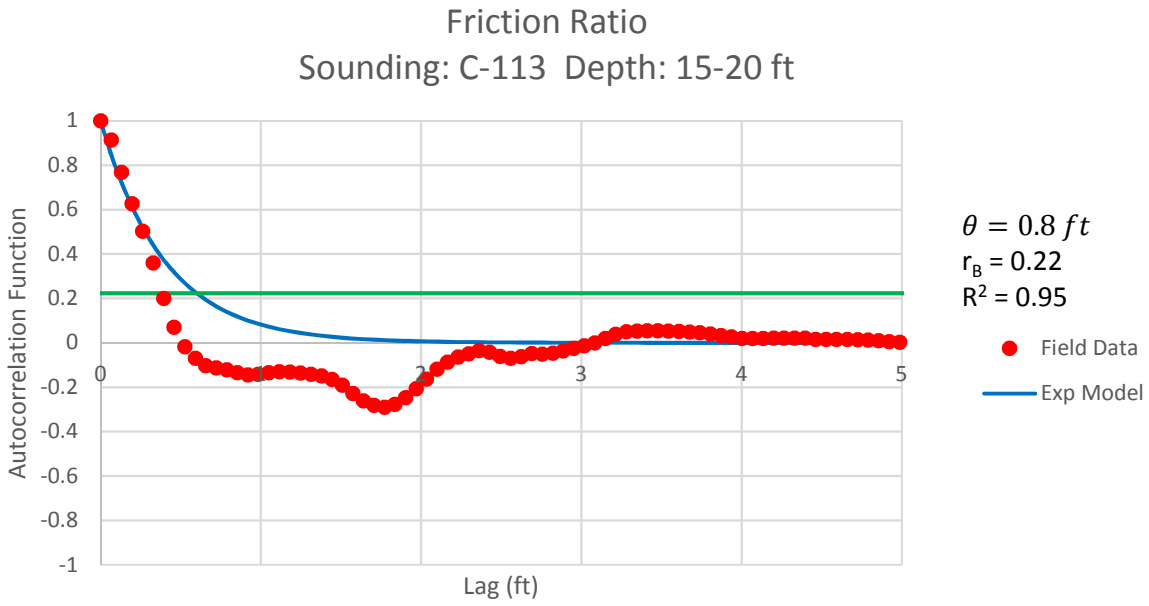

Figure B - 203: Estimation of the Scale of Fluctuation, $\theta = 0.8$ feet, for Friction Ratio Data from Sounding C-113, "Clean sands to silty sands (6)" layer from 15 to 20 feet depth.

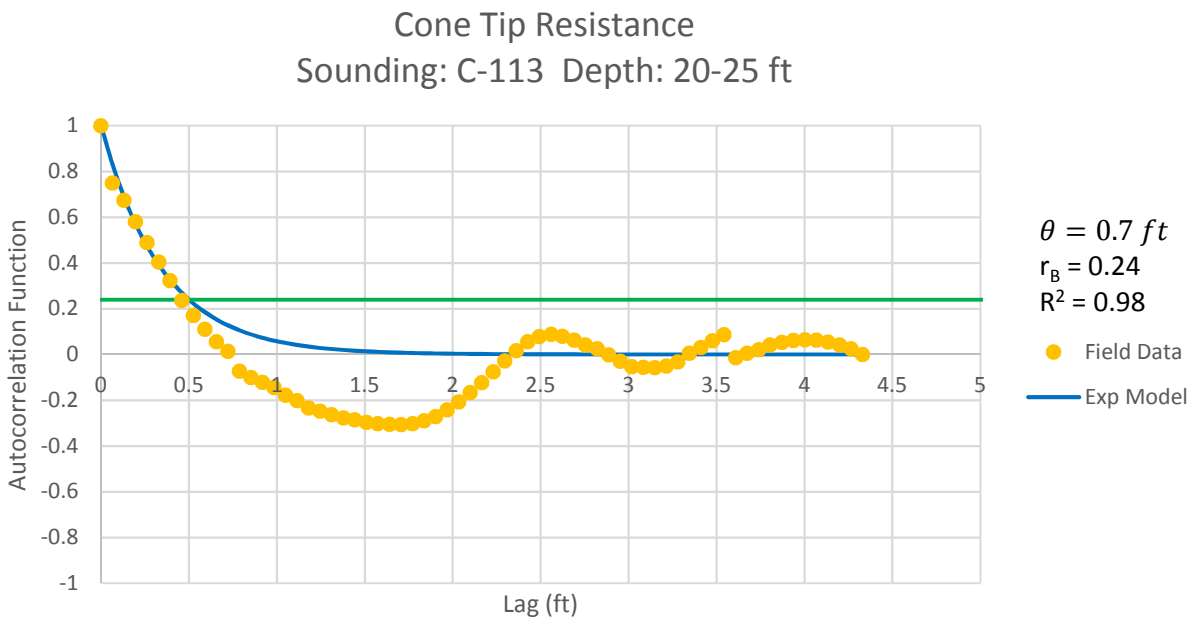

Figure B - 204: Estimation of the Scale of Fluctuation, θ = 0.7 feet, for Cone Tip Resistance Data from Sounding C-113, "Gravelly sand to sand (7)" layer from 20 to 25 feet depth.

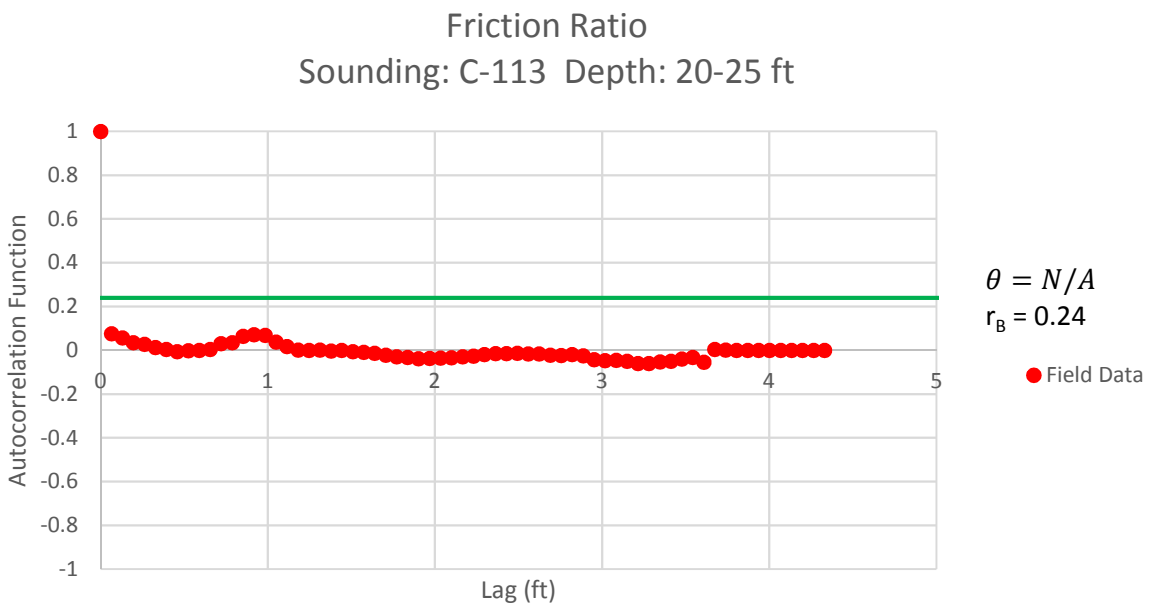

Figure B - 205: Estimation of the Scale of Fluctuation, θ, for Friction Ratio Data from Sounding C-113, "Gravelly sand to sand (7)" layer from 20 to 25 feet depth. Data is limited to only 1 point greater than the Bartlett limit of 0.24; therefore, θ could not be estimated, and these results were not included in final analysis.

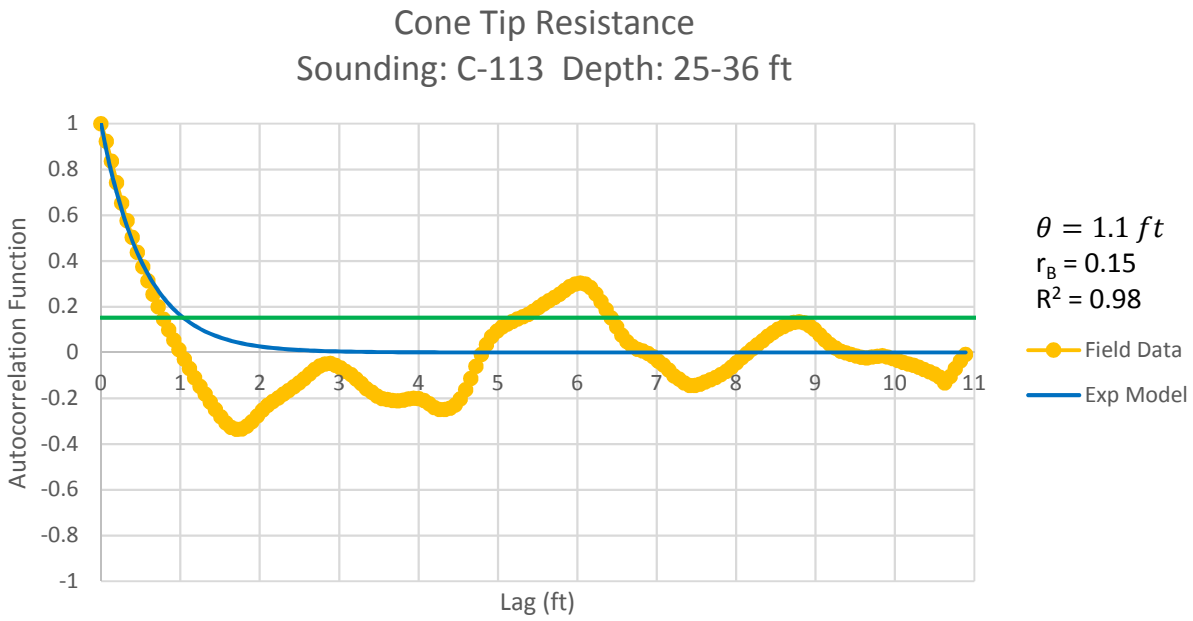

Figure B - 206: Estimation of the Scale of Fluctuation, θ = 1.1 feet, for Cone Tip Resistance Data from Sounding C-113, "Clean sands to silty sands (6)" layer from 25 to 36 feet depth.

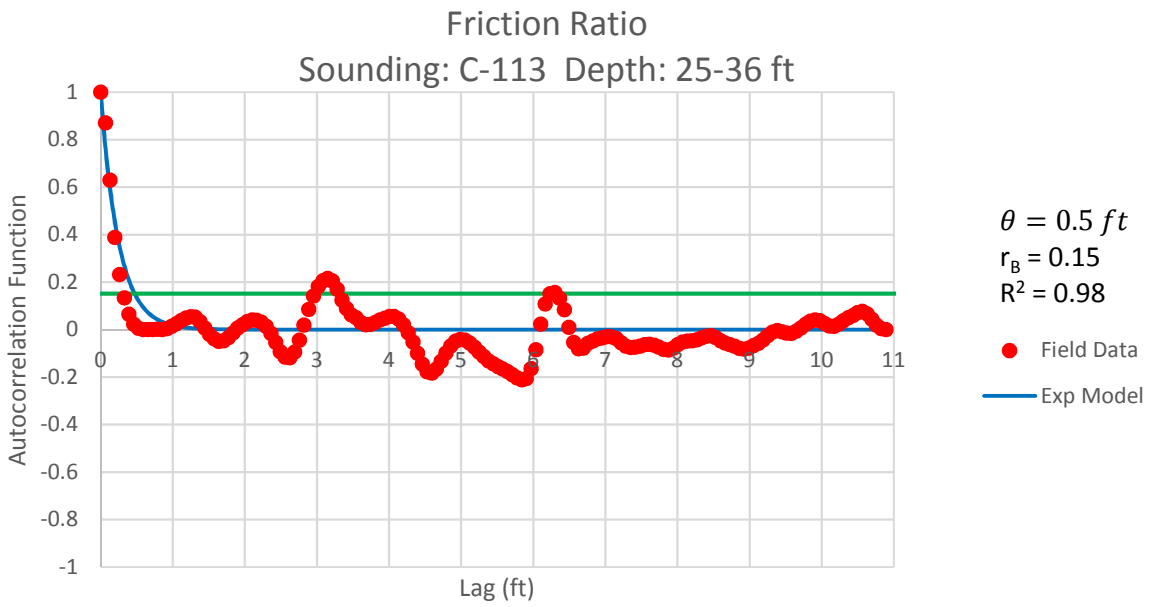

Figure B - 207: Estimation of the Scale of Fluctuation, θ = 0.5 feet, for Friction Ratio Data from Sounding C-113, "Clean sands to silty sands (6)" layer from 25 to 36 feet depth.

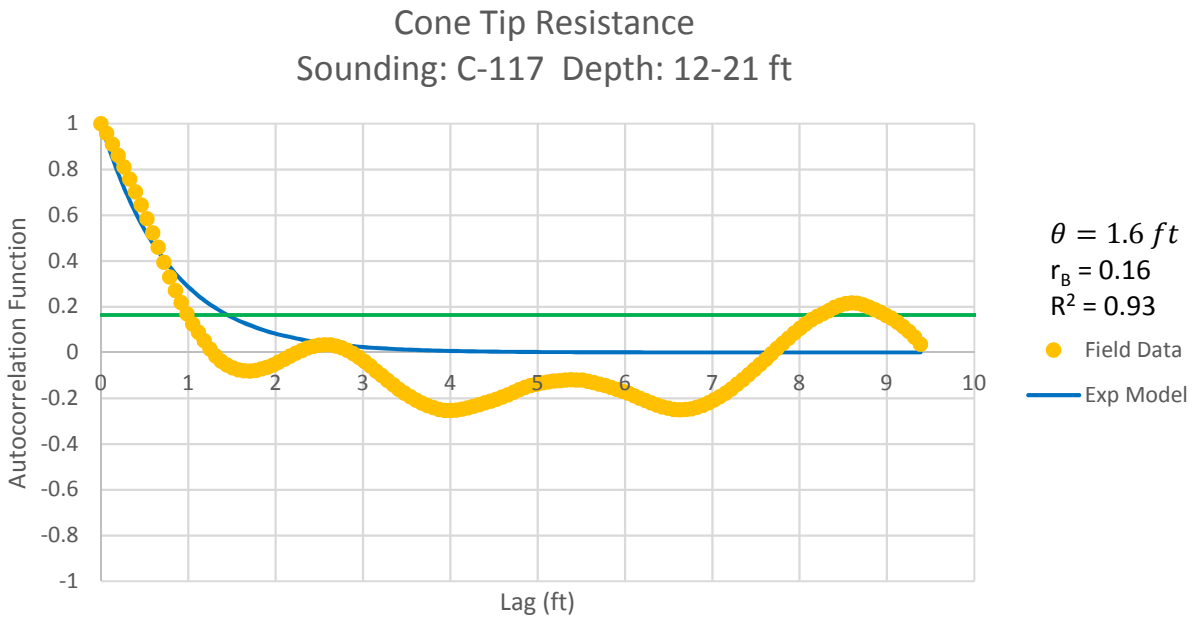

Figure B - 208: Estimation of the Scale of Fluctuation, $\theta = 1.6$ feet, for Cone Tip Resistance Data from Sounding C-117, "Clean sands to silty sands (6)" layer from 12 to 21 feet depth.

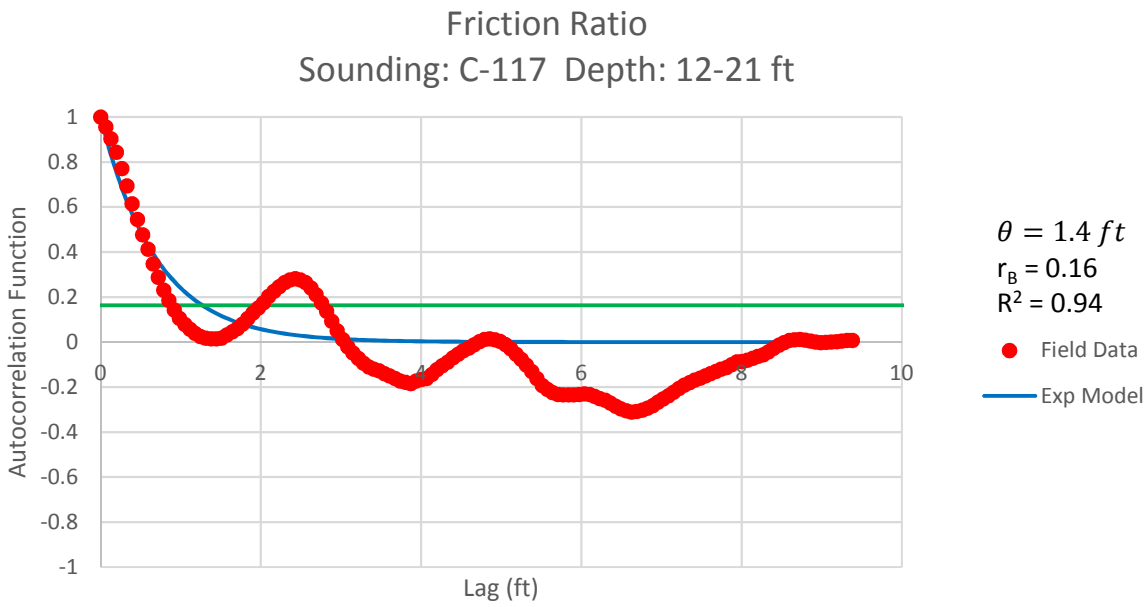

Figure B - 209: Estimation of the Scale of Fluctuation, $\theta = 1.4$ feet, for Friction Ratio Data from Sounding C-117, "Clean sands to silty sands (6)" layer from 12 to 21 feet depth.

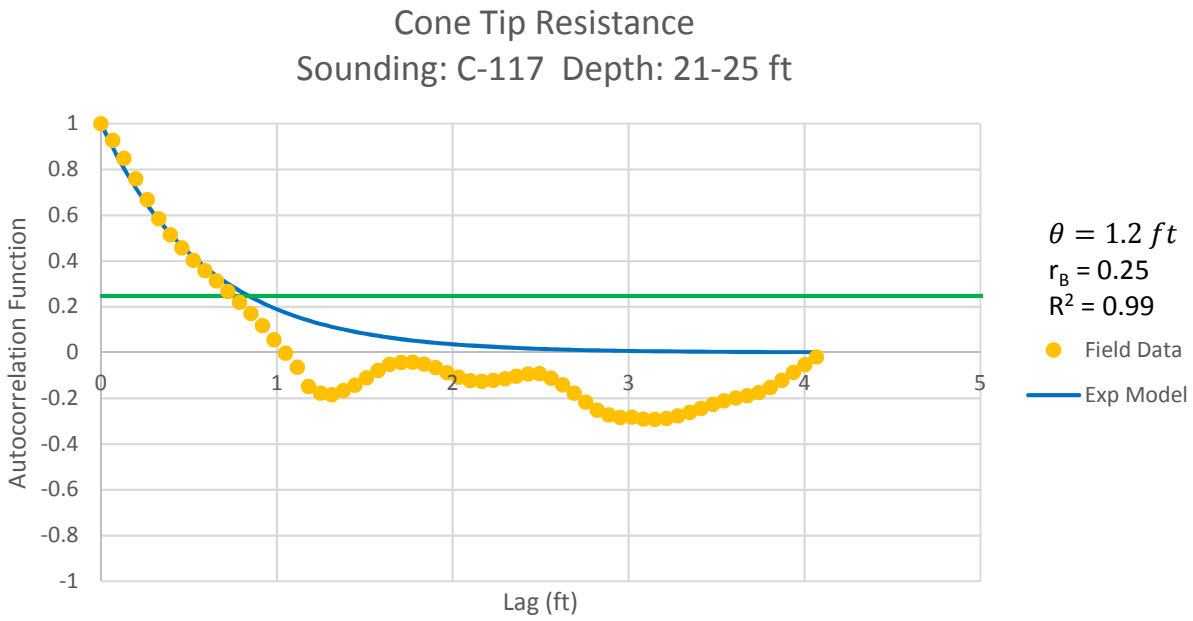

Figure B - 210: Estimation of the Scale of Fluctuation, $\theta = 1.2$ feet, for Cone Tip Resistance Data from Sounding C-117, "Gravelly sand to sand (7)" layer from 21 to 25 feet depth.

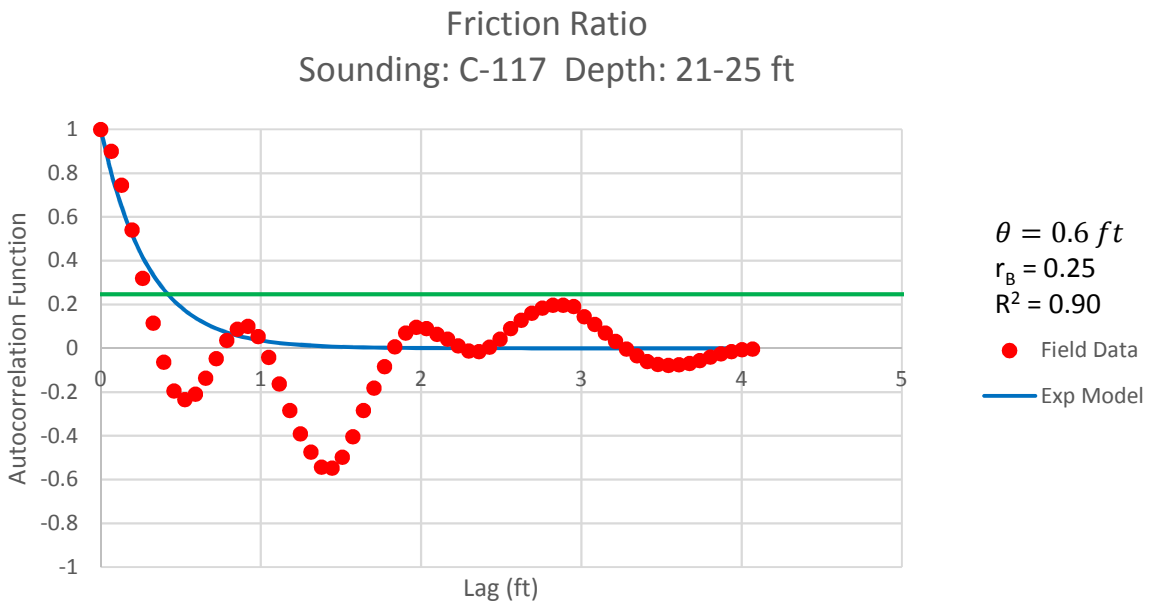

Figure B - 211: Estimation of the Scale of Fluctuation, $\theta = 0.6$ feet, for Friction Ratio Data from Sounding C-117, "Gravelly sand to sand (7)" layer from 21 to 25 feet depth.

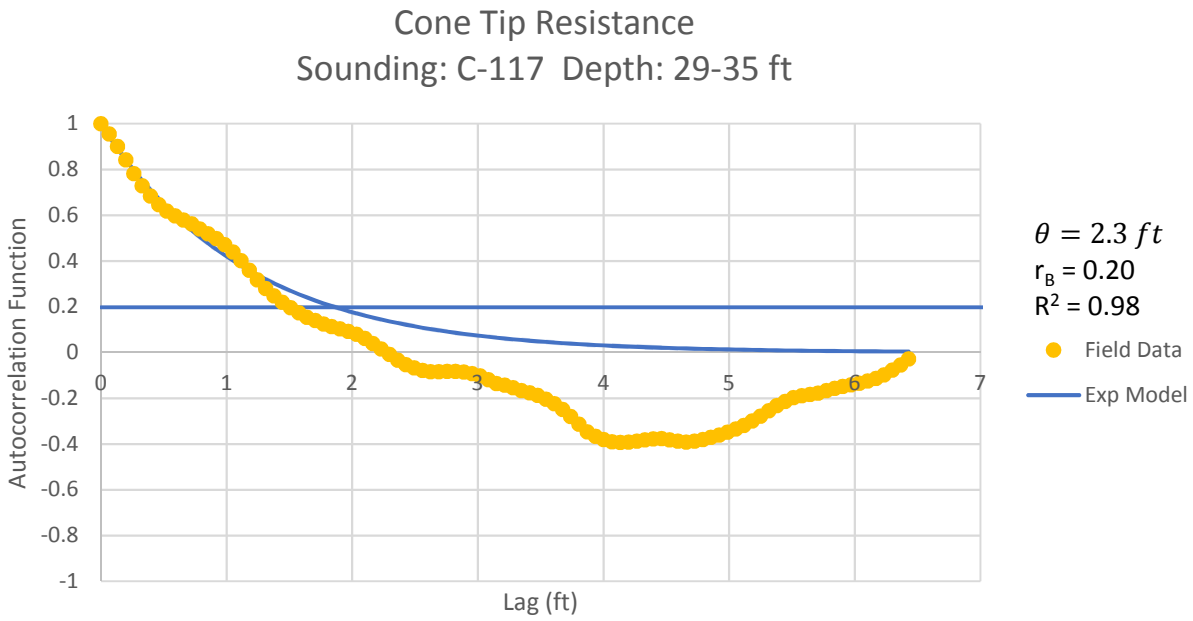

Figure B - 212: Estimation of the Scale of Fluctuation, $\theta = 2.3$ feet, for Cone Tip Resistance Data from Sounding C-117, "Clean sands to silty sands (6)" layer from 29 to 35 feet depth.

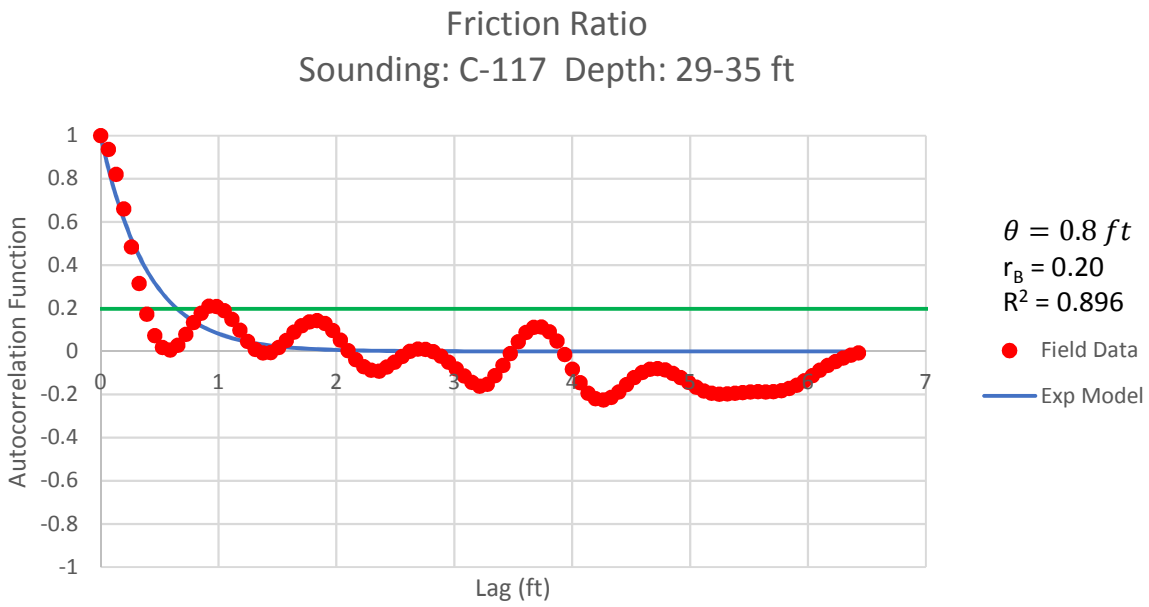

Figure B - 213: Estimation of the Scale of Fluctuation, $\theta = 10.8$ feet, for Friction Ratio Data from Sounding C-117, "Clean sands to silty sands (6)" layer from 29 to 35 feet depth. Data is a poor fit for the points greater than the Bartlett limit of 0.20; coefficient of determination, R^2, value is less 0.9. Therefore, these results were not included in final analysis

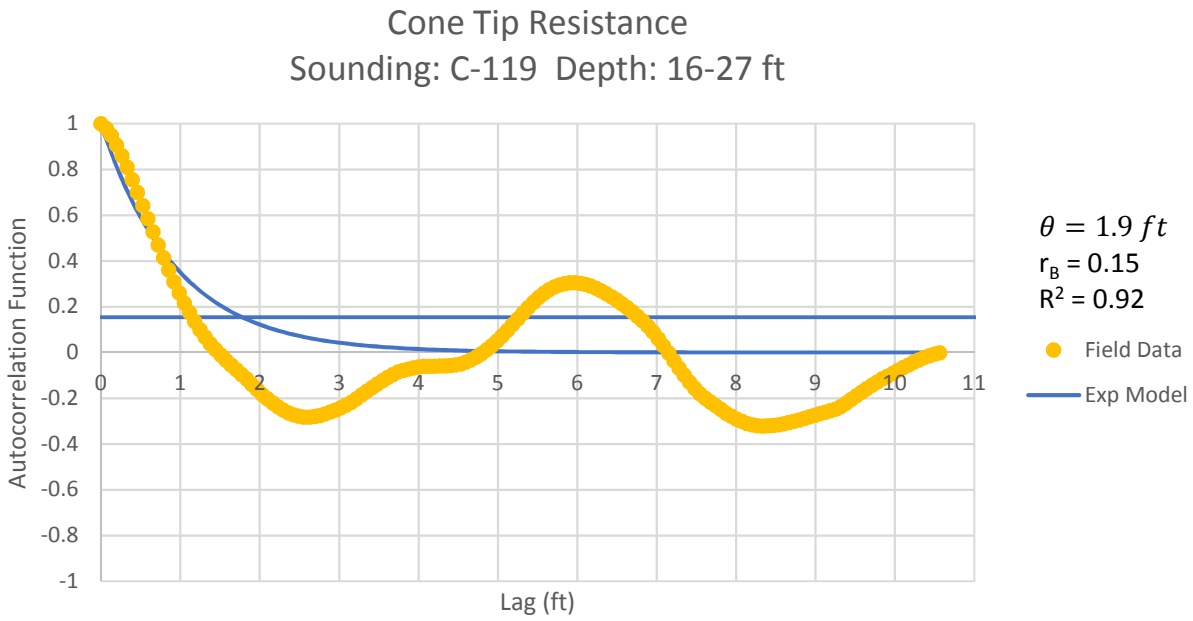

Figure B - 214: Estimation of the Scale of Fluctuation, θ = 1.9 feet, for Cone Tip Resistance Data from Sounding C-119, "Gravelly sand to sand (7)" layer from 16 to 27 feet depth.

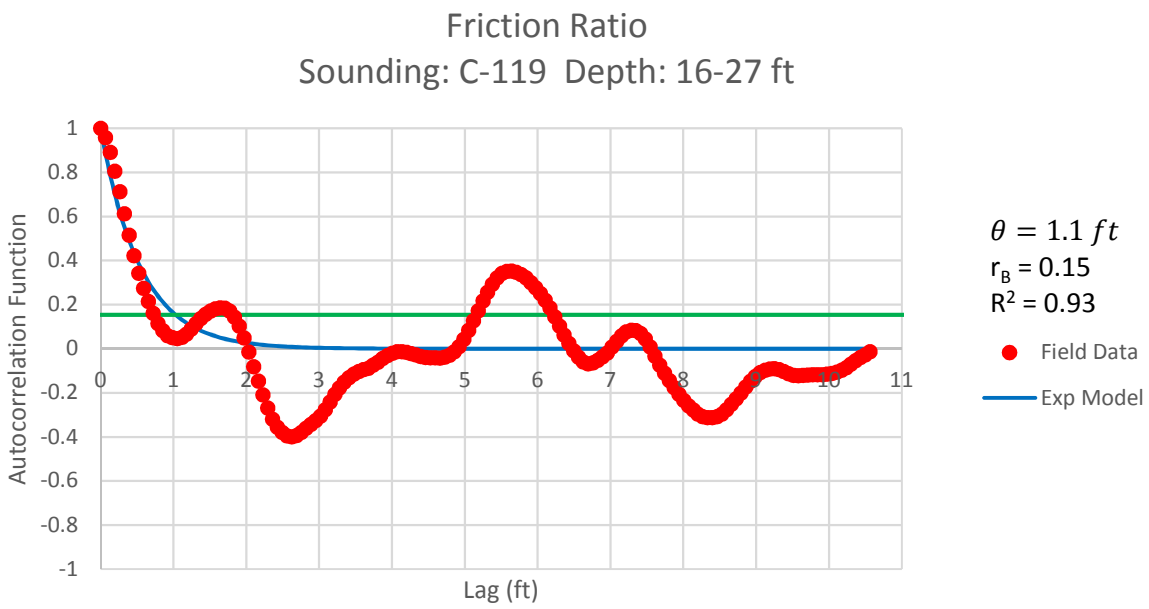

Figure B - 215: Estimation of the Scale of Fluctuation, θ = 1.1 feet, for Friction Ratio Data from Sounding C-119, "Gravelly sand to sand (7)" layer from 16 to 27 feet depth.

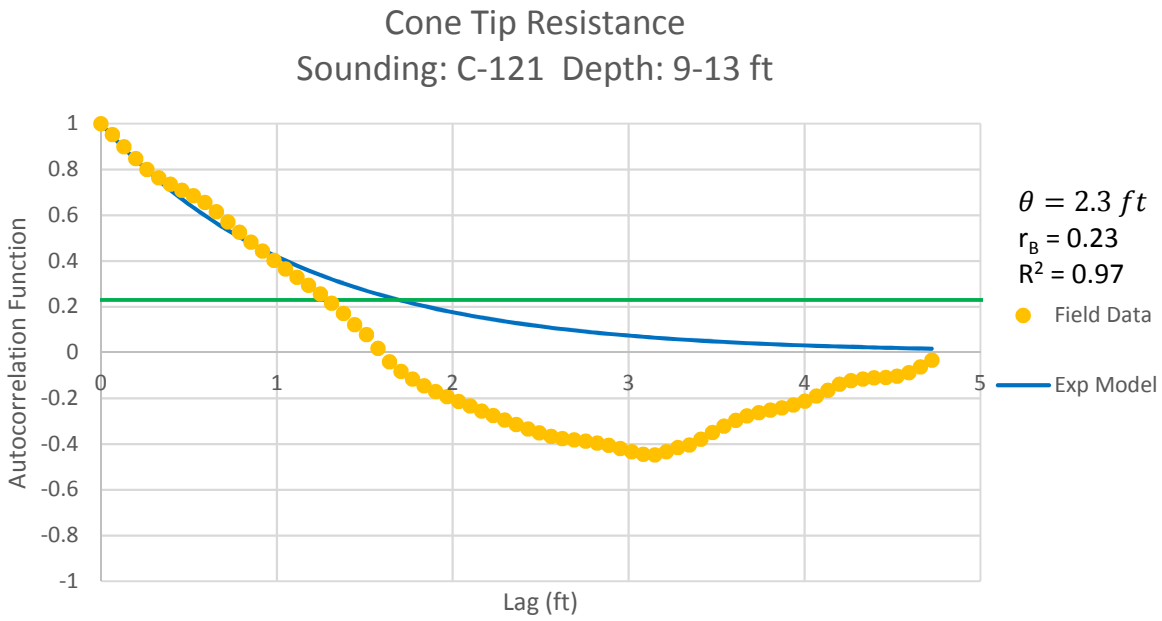

Figure B - 216: Estimation of the Scale of Fluctuation, θ = 2.3 feet, for Cone Tip Resistance Data from Sounding C-121, "Clean sands to silty sands (6)" layer from 9 to 13 feet depth.

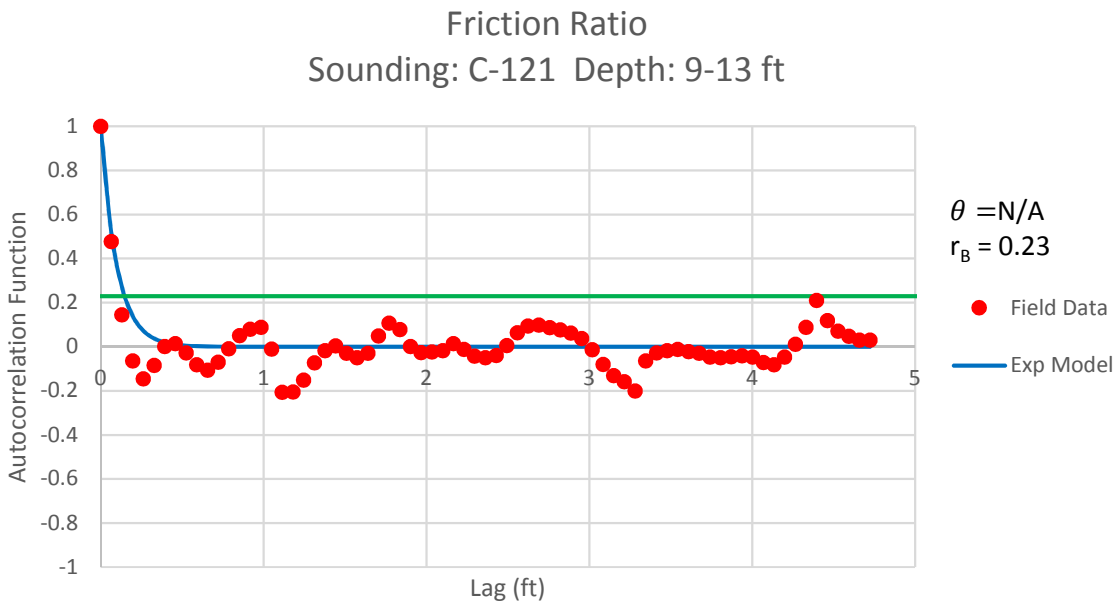

Figure B - 217: Estimation of the Scale of Fluctuation, θ, for Friction Ratio Data from Sounding C-121, "Clean sands to silty sands (6)" layer from 9 to 13 feet depth. Data is limited to only 2 points greater than the Bartlett limit of 0.23; therefore, θ could not be estimated, and these results were not included in final analysis.

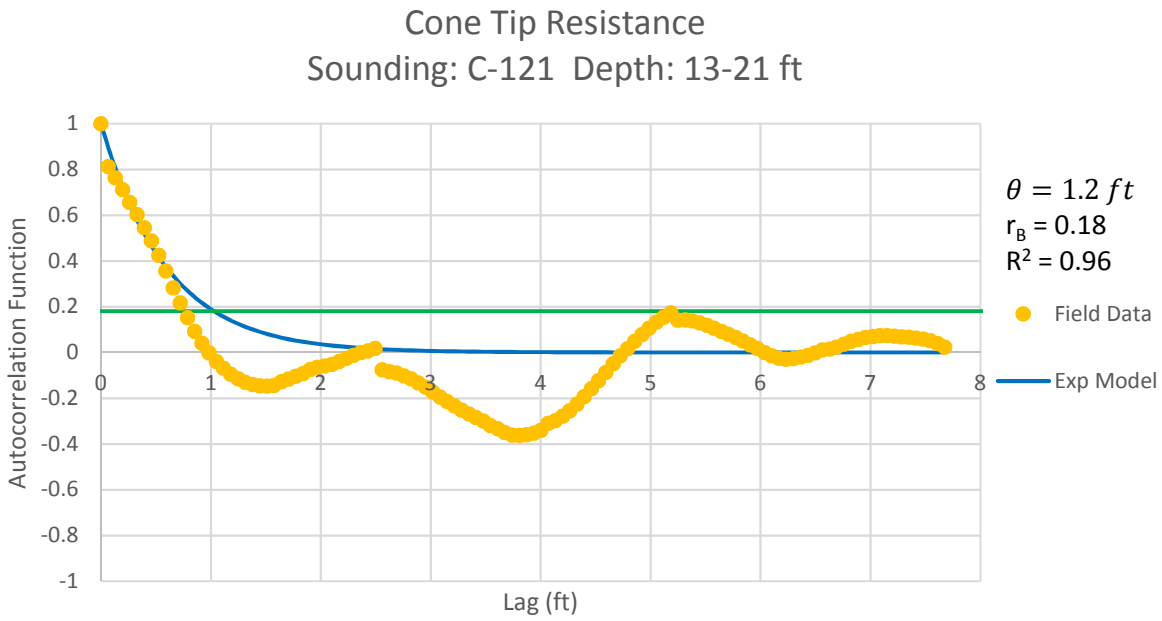

Figure B - 218: Estimation of the Scale of Fluctuation, θ = 1.2 feet, for Cone Tip Resistance Data from Sounding C-121, "Gravelly sand to sand (7)" layer from 13 to 21 feet depth.

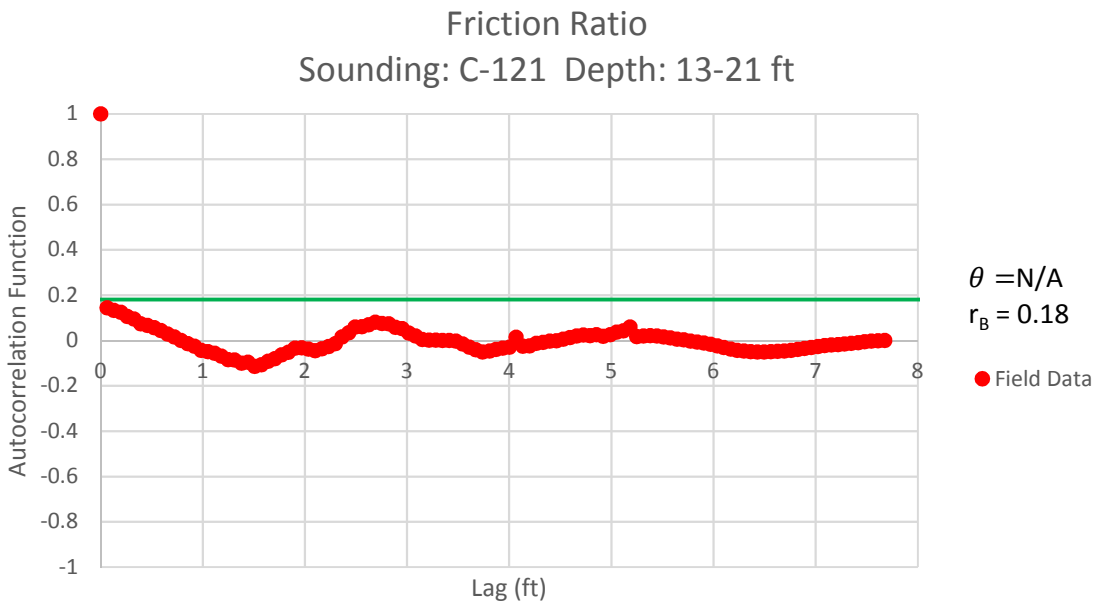

Figure B - 219: Estimation of the Scale of Fluctuation, θ, for Friction Ratio Data from Sounding C-121, "Gravelly sand to sand (7)" layer from 13 to 21 feet depth. Data is limited to only 1 point greater than the Bartlett limit of 0.18; therefore, θ could not be estimated, and these results were not included in final analysis.

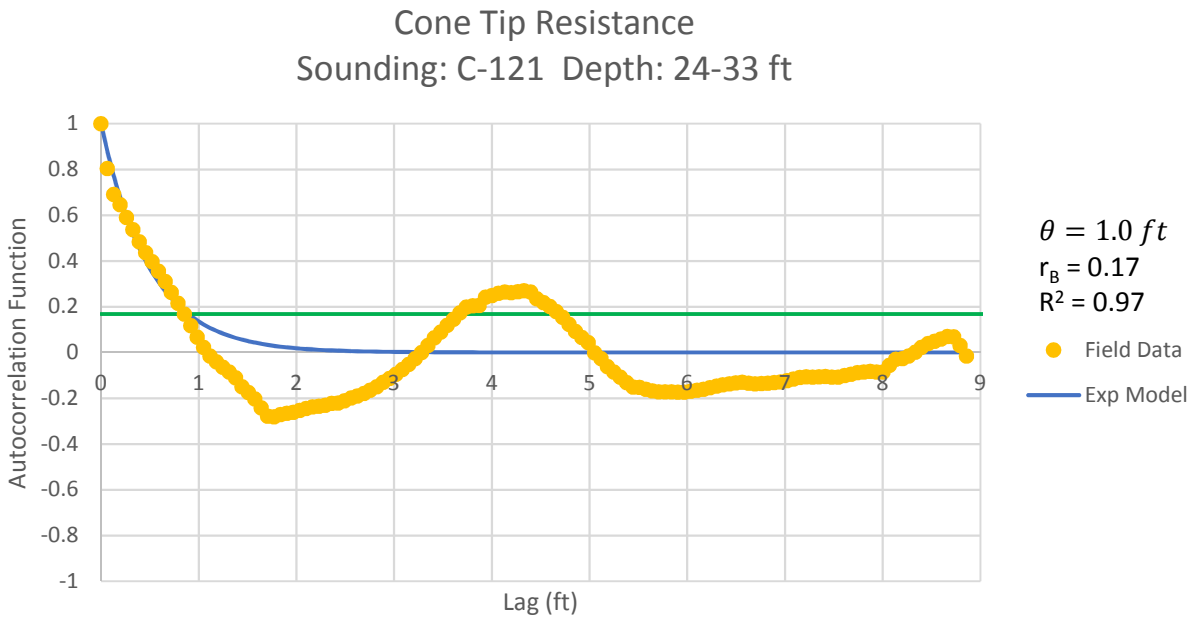

Figure B - 220: Estimation of the Scale of Fluctuation, $\theta = 1.0$ feet, for Cone Tip Resistance Data from Sounding C-121, "Clean sands to silty sands (6)" layer from 24 to 23 feet depth.

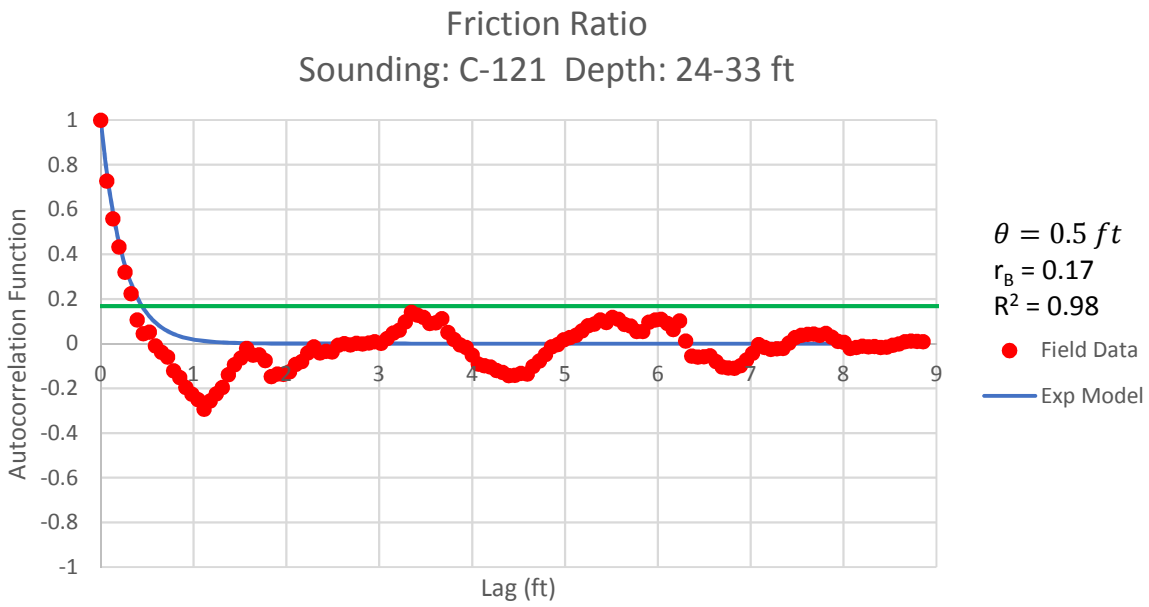

Figure B - 221: Estimation of the Scale of Fluctuation, $\theta = 0.5$ feet, for Friction Ratio Data from Sounding C-121, "Clean sands to silty sands (6)" layer from 24 to 33 feet depth.

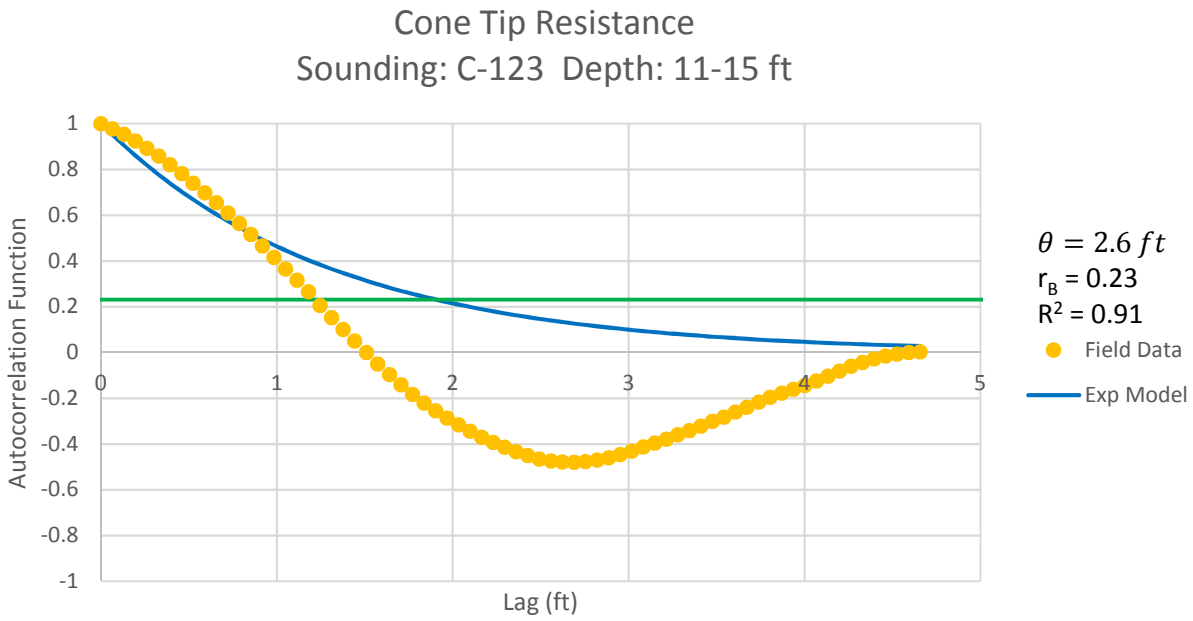

Figure B - 222: Estimation of the Scale of Fluctuation, $\theta = 2.6$ feet, for Cone Tip Resistance Data from Sounding C-123, "Gravelly sand to sand (7)" layer from 11 to 15 feet depth.

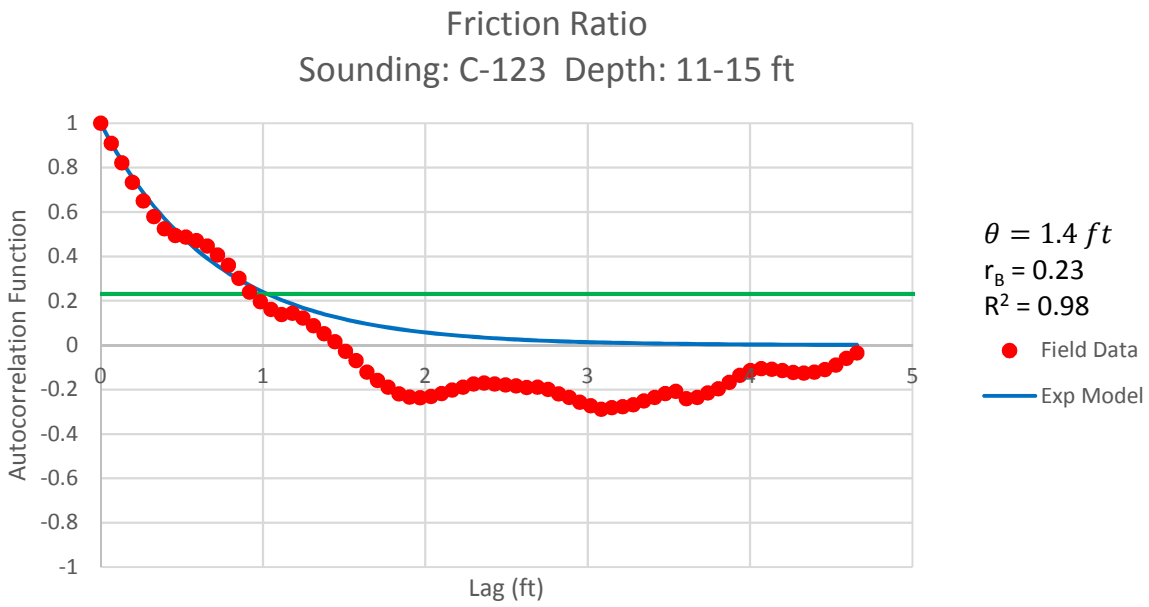

Figure B - 223: Estimation of the Scale of Fluctuation, $\theta = 1.4$ feet, for Friction Ratio Data from Sounding C-123, "Gravelly sand to sand (7)" layer from 11 to 15 feet depth.

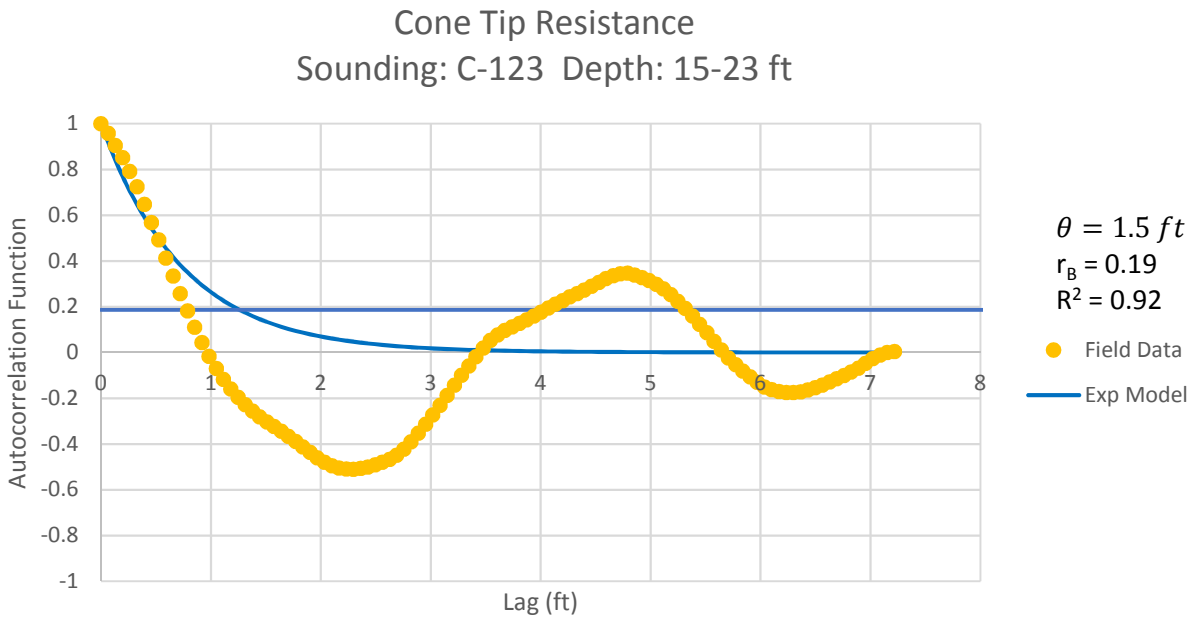

Figure B - 224: Estimation of the Scale of Fluctuation, $\theta = 1.5$ feet, for Cone Tip Resistance Data from Sounding C-123, "Clean sands to silty sands (6)" layer from 15 to 23 feet depth.

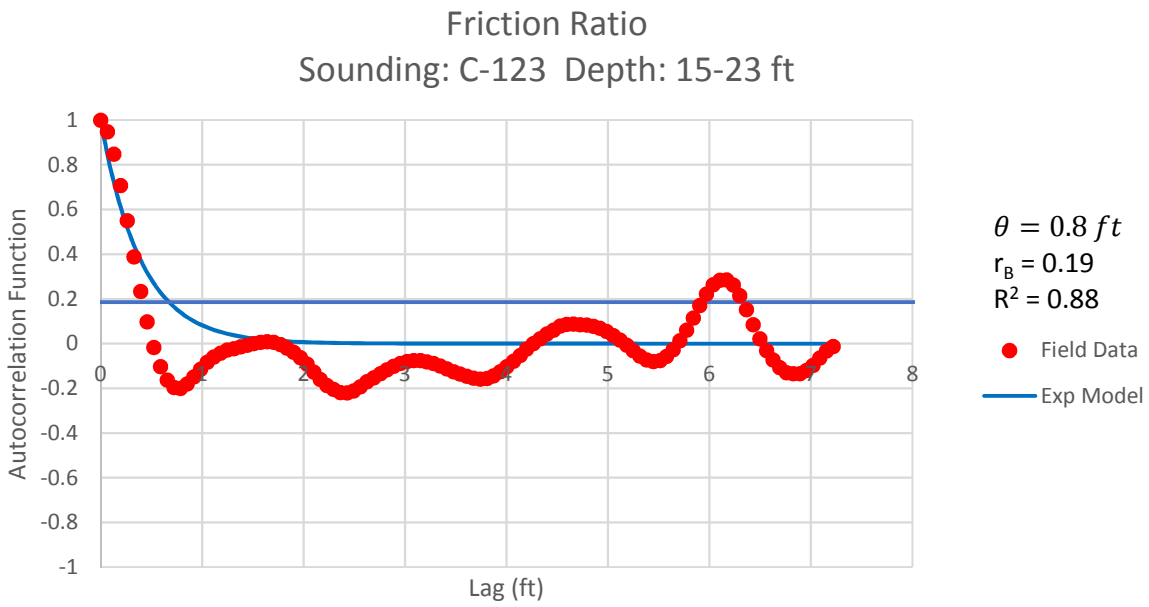

Figure B - 225: Estimation of the Scale of Fluctuation, $\theta = 0.8$ feet, for Friction Ratio Data from Sounding C-123, "Clean sands to silty sands (6)" layer from 15 to 23 feet depth. Data is a poor fit for the points greater than the Bartlett limit of 0.19; coefficient of determination, R^2, value is less 0.9. Therefore, these results were not included in final analysis.

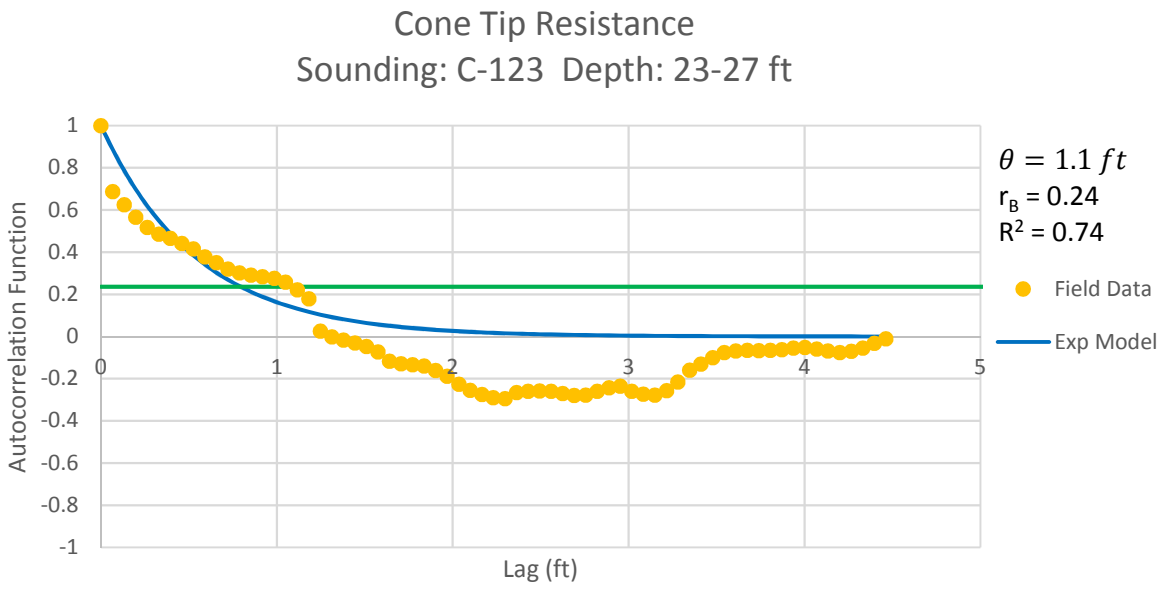

Figure B - 226: Estimation of the Scale of Fluctuation, θ = 1.1 feet, for Cone Tip Resistance Data from Sounding C-123, "Gravelly sand to sand (7)" layer from 23 to 27 feet depth. Data is a poor fit for the points greater than the Bartlett limit of 0.24; coefficient of determination, R^2, value is less 0.9. Therefore, these results were not included in final analysis.

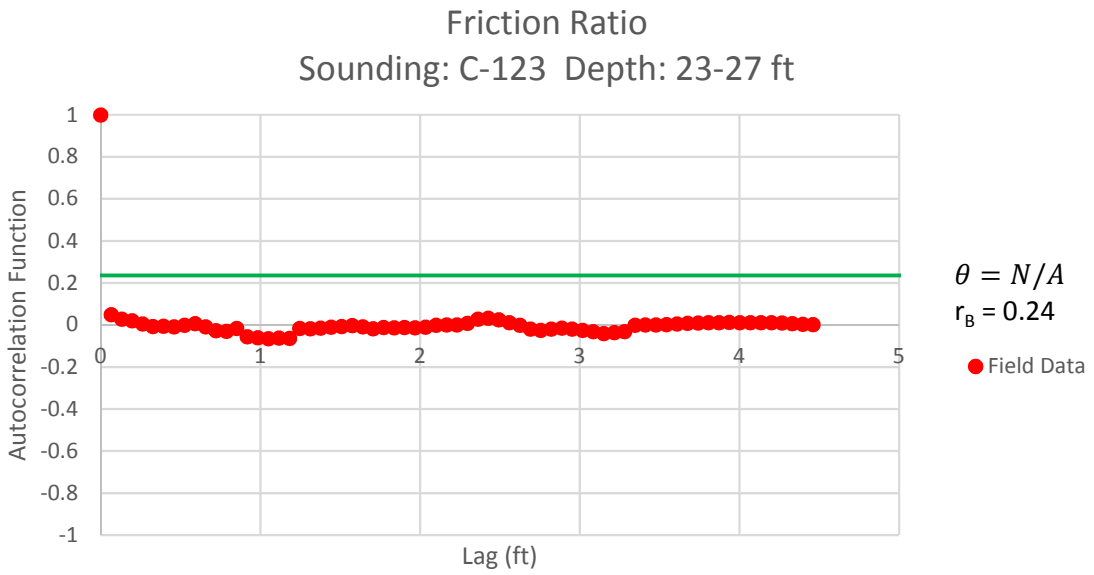

Figure B - 227: Estimation of the Scale of Fluctuation, θ, for Friction Ratio Data from Sounding C-123, "Gravelly sand to sand (7)" layer from 23 to 27 feet depth. Data is limited to only 1 point greater than the Bartlett limit of 0.24; therefore, θ could not be estimated, and these results were not included in final analysis.

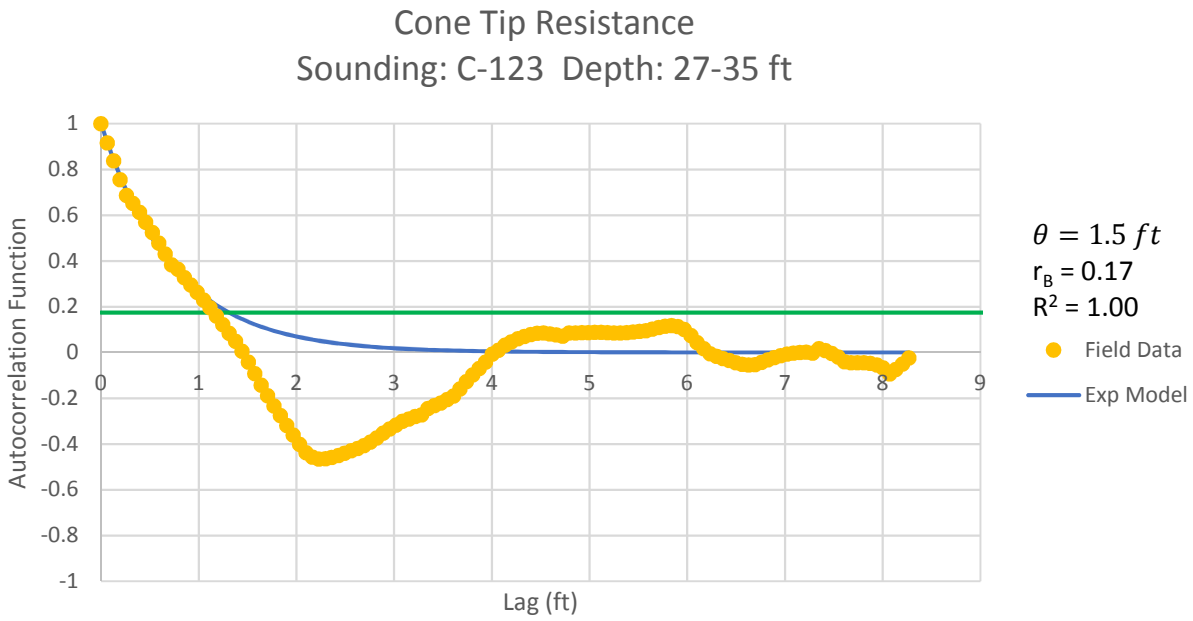

Figure B - 228: Estimation of the Scale of Fluctuation, $\theta = 1.5$ feet, for Cone Tip Resistance Data from Sounding C-123, "Clean sands to silty sands (6)" layer from 27 to 35 feet depth.

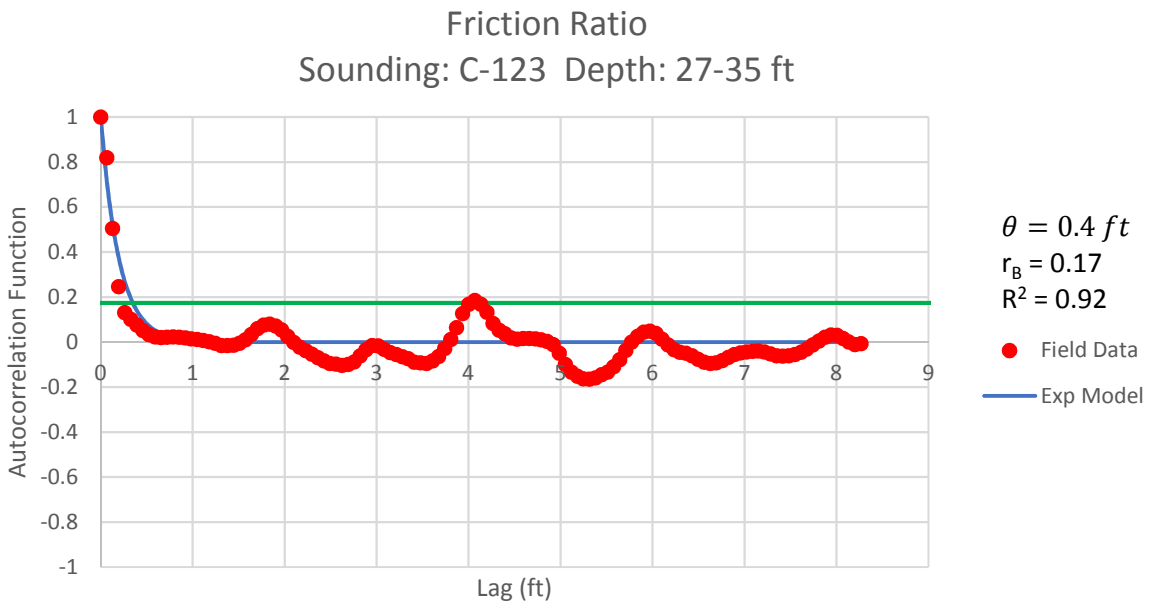

Figure B - 229: Estimation of the Scale of Fluctuation, $\theta = 0.4$ feet, for Friction Ratio Data from Sounding C-123, "Clean sands to silty sands (6)" layer from 27 to 35 feet depth.

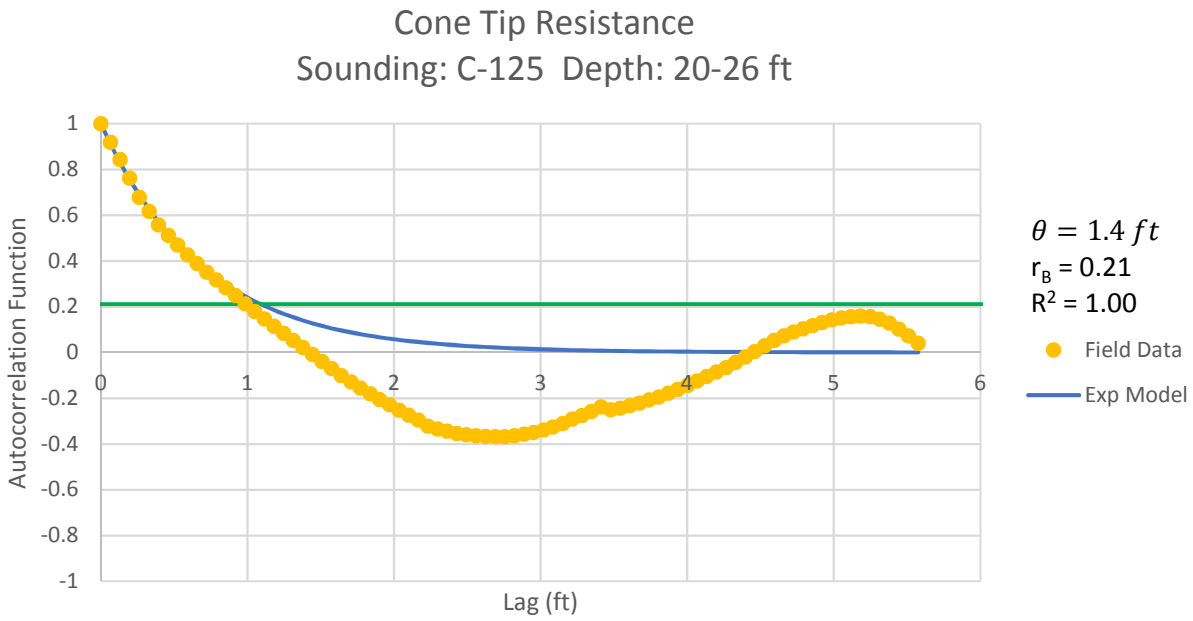

Figure B - 230: Estimation of the Scale of Fluctuation, $\theta = 1.4$ feet, for Cone Tip Resistance Data from Sounding C-125, "Gravelly sand to sand (7)" layer from 20 to 26 feet depth.

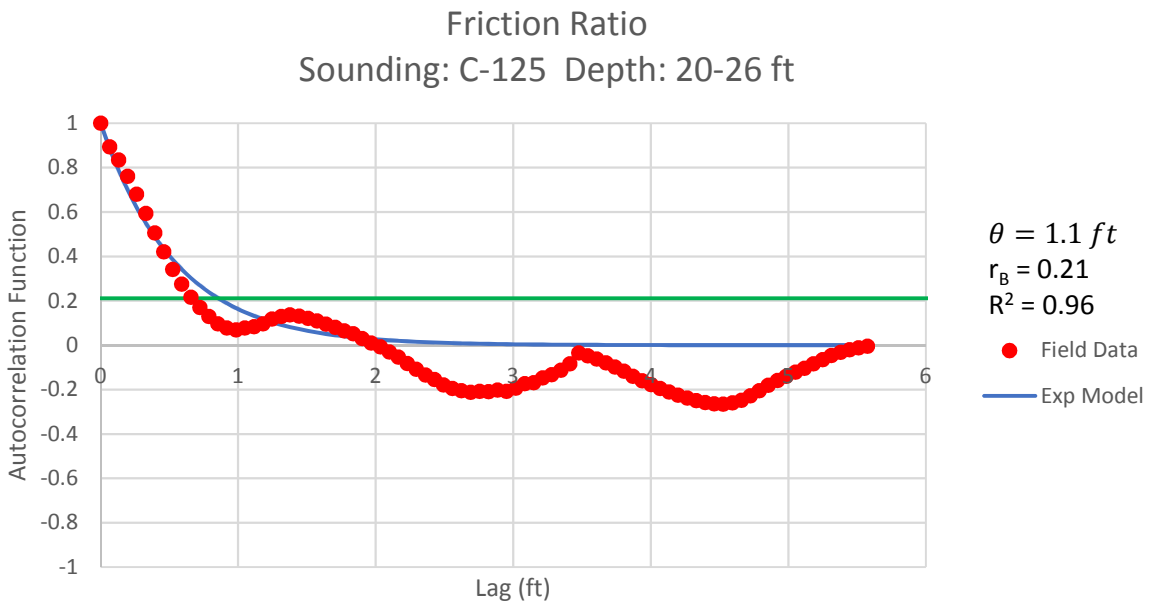

Figure B - 231: Estimation of the Scale of Fluctuation, $\theta = 1.1$ feet, for Friction Ratio Data from Sounding C-125, "Gravelly sand to sand (7)" layer from 20 to 26 feet depth.

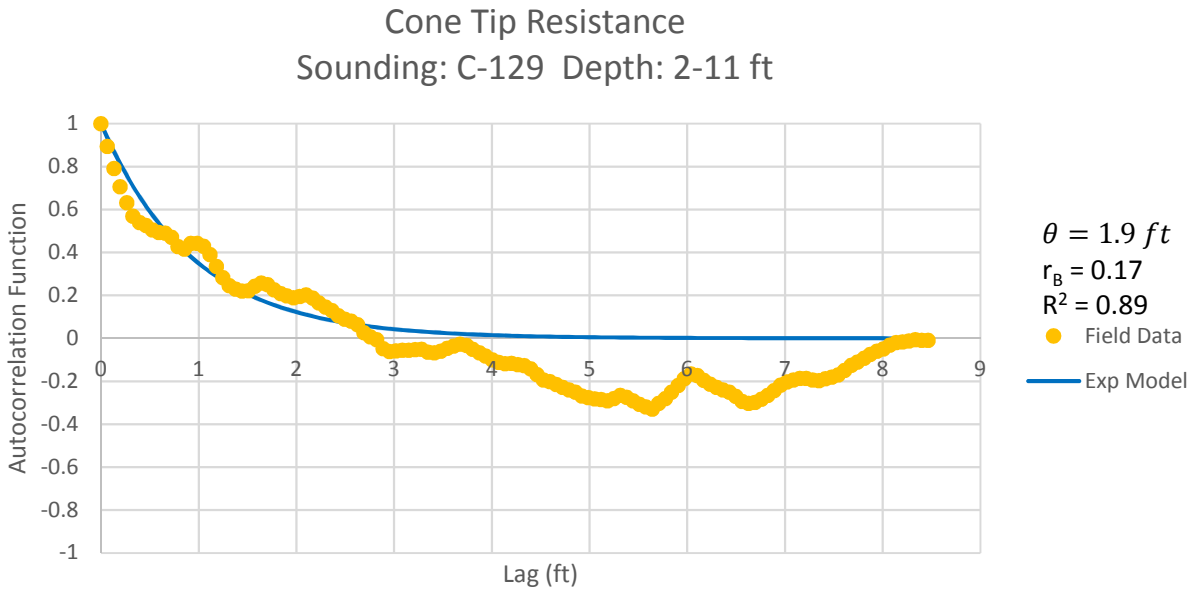

Figure B - 232: Estimation of the Scale of Fluctuation, $\theta = 1.9$ feet, for Cone Tip Resistance Data from Sounding C-129, "Clays; clay to silty clay (3)" layer from 2 to 11 feet depth. Data is a poor fit for the points greater than the Bartlett limit of 0.17; coefficient of determination, R^2, value is less 0.9. Therefore, these results were not included in final analysis.

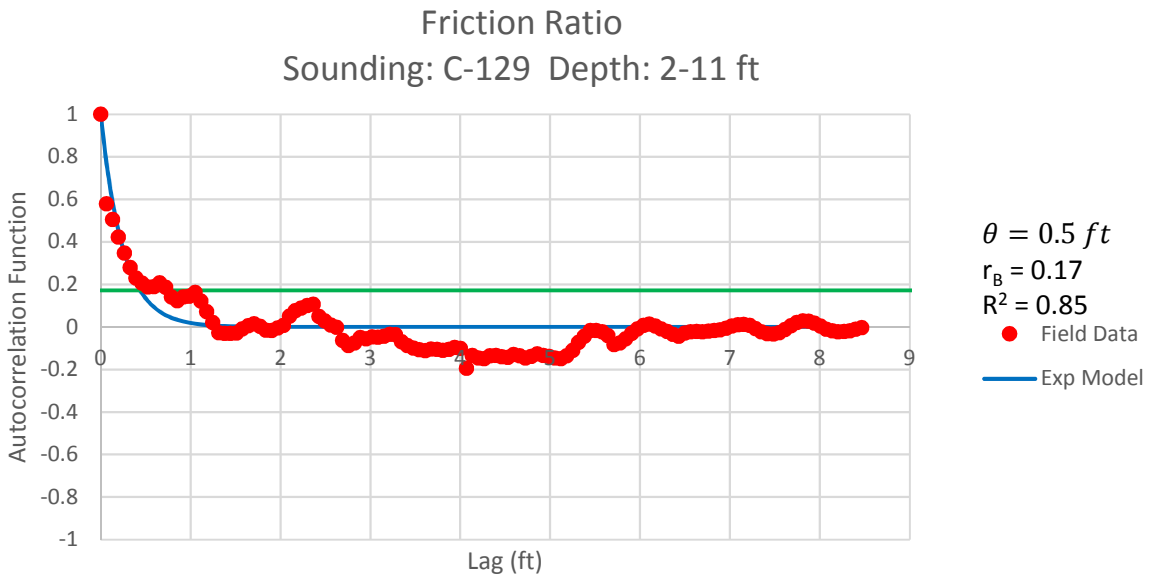

Figure B - 233: Estimation of the Scale of Fluctuation, $\theta = 0.5$ feet, for Friction Ratio Data from Sounding C-129, "Clays; clay to silty clay (3)" layer from 2 to 11 feet depth. Data is a poor fit for the points greater than the Bartlett limit of 0.17; coefficient of determination, R^2, value is less 0.9. Therefore, these results were not included in final analysis.

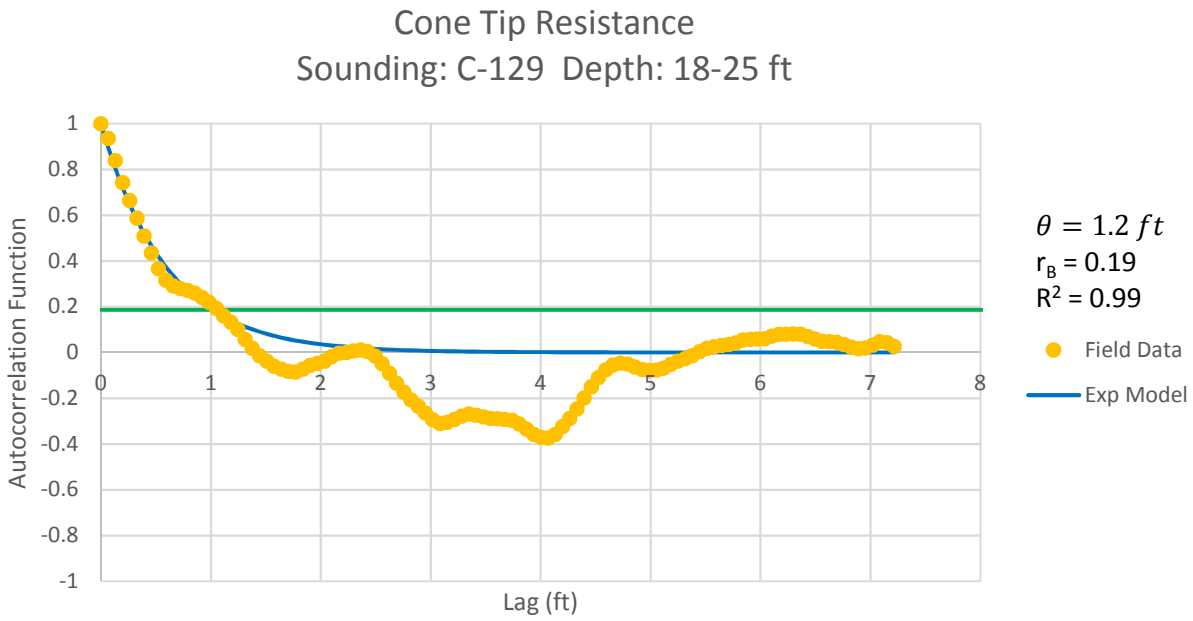

Figure B - 234: Estimation of the Scale of Fluctuation, $\theta = 1.2$ feet, for Cone Tip Resistance Data from Sounding C-129, "Gravelly sand to sand (7)" layer from 18 to 25 feet depth.

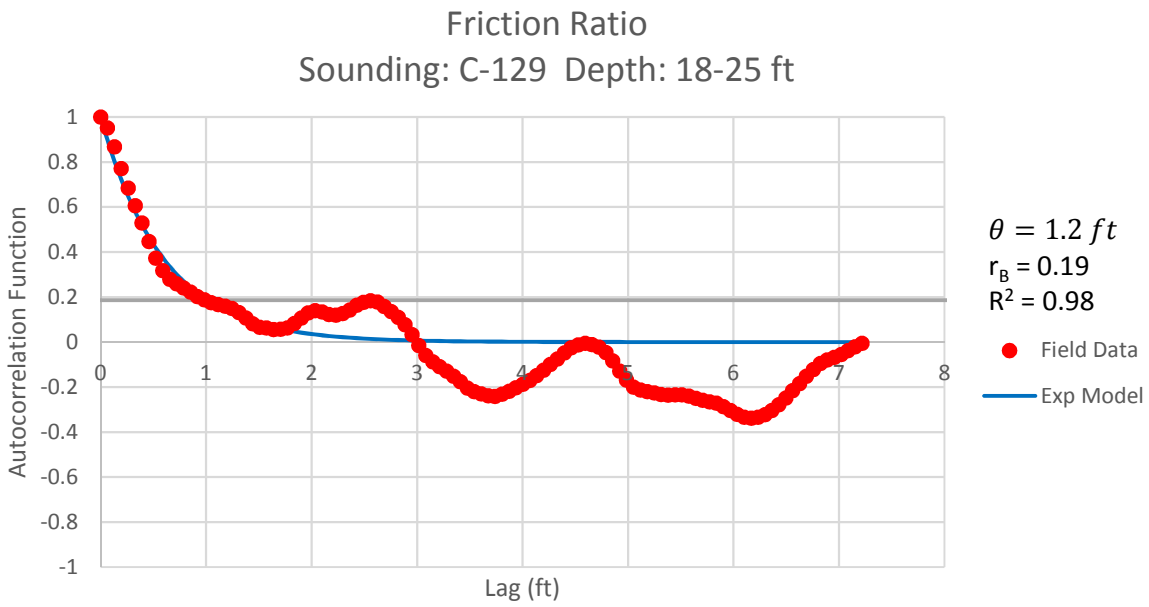

Figure B - 235: Estimation of the Scale of Fluctuation, $\theta = 1.2$ feet, for Friction Ratio Data from Sounding C-129, "Gravelly sand to sand (7)" layer from 18 to 25 feet depth.

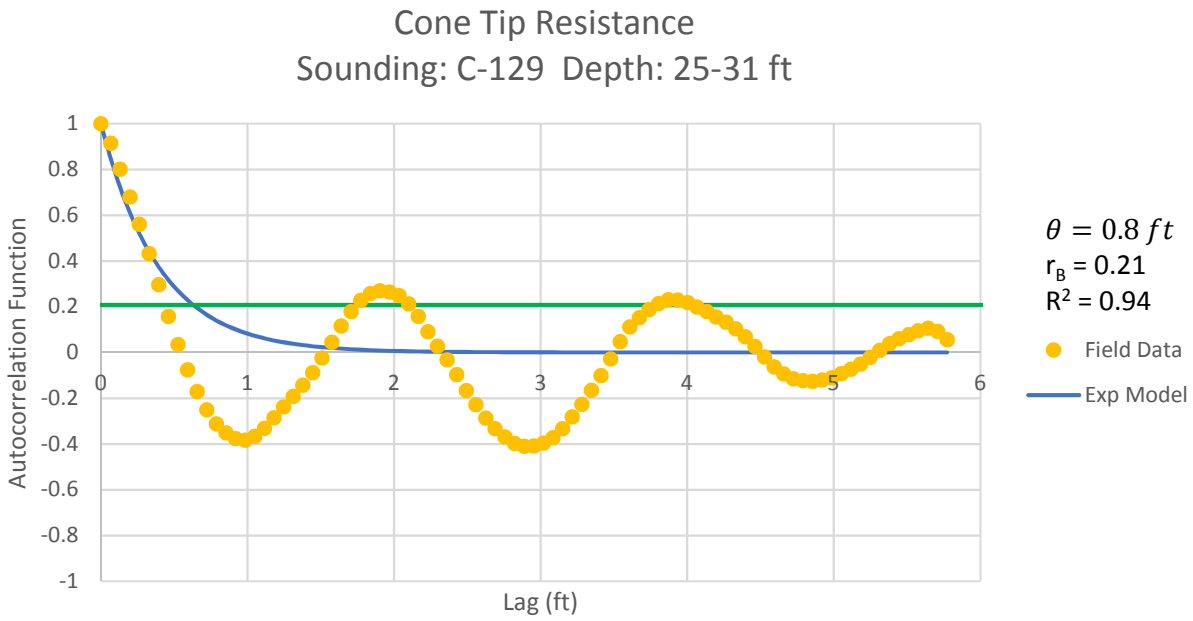

Figure B - 236: Estimation of the Scale of Fluctuation, $\theta = 0.8$ feet, for Cone Tip Resistance Data from Sounding C-129, "Clean sands to silty sands (6)" layer from 25 to 31 feet depth.

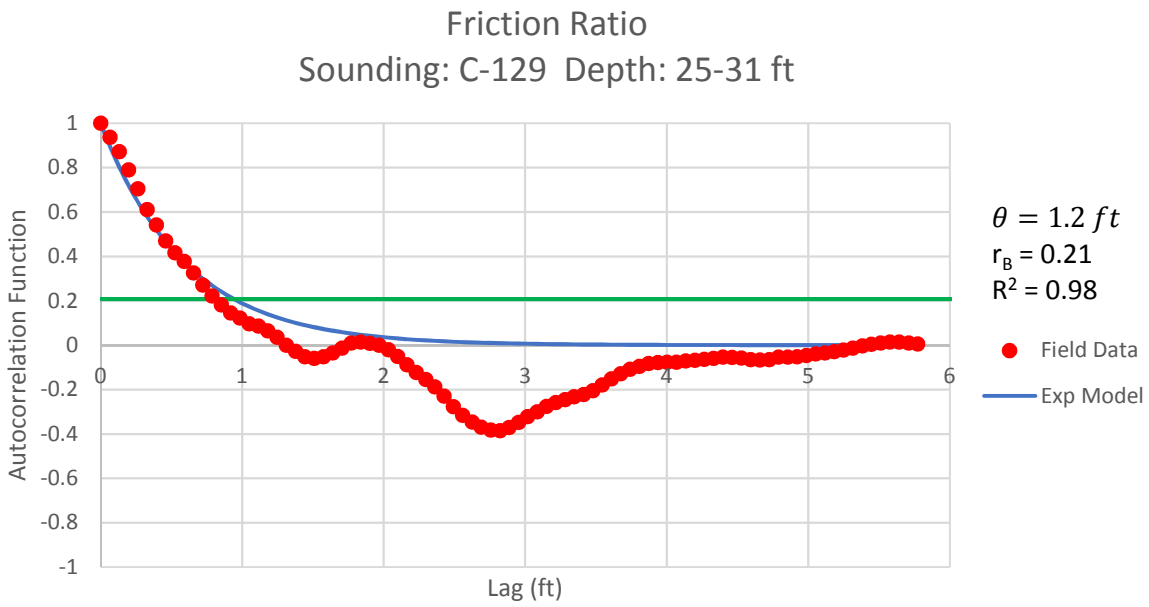

Figure B - 237: Estimation of the Scale of Fluctuation, $\theta = 1.2$ feet, for Friction Ratio Data from Sounding C-129, "Clean sands to silty sands (6)" layer from 25 to 31 feet depth.

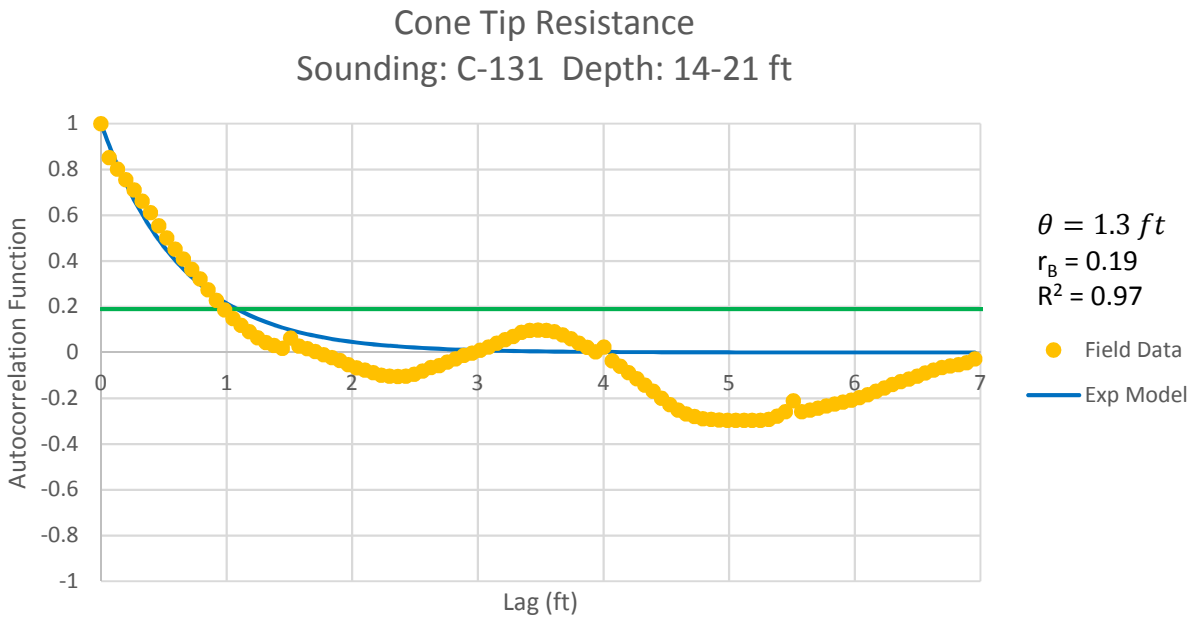

Figure B - 238: Estimation of the Scale of Fluctuation, θ = 1.3 feet, for Cone Tip Resistance Data from Sounding C-131, "Clean sands to silty sands (6)" layer from 14 to 21 feet depth.

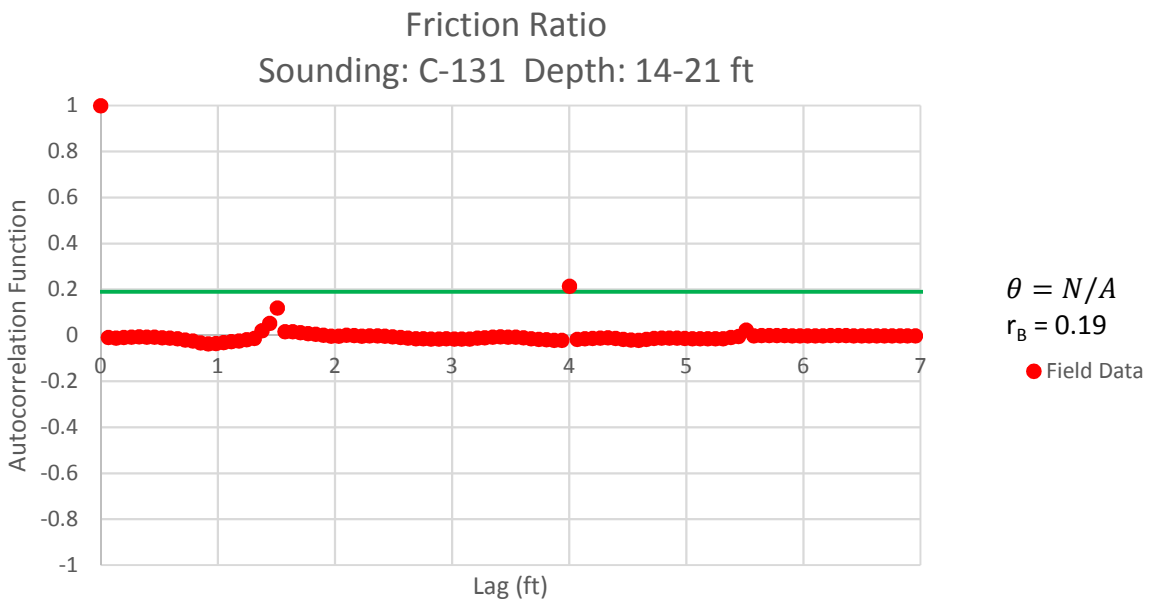

Figure B - 239: Estimation of the Scale of Fluctuation, θ, for Friction Ratio Data from Sounding C-131, " Clean sands to silty sands (6)" layer from 14 to 21 feet depth. Data is limited to only 1 point greater than the Bartlett limit of 0.19; therefore, θ could not be estimated, and these results were not included in final analysis.

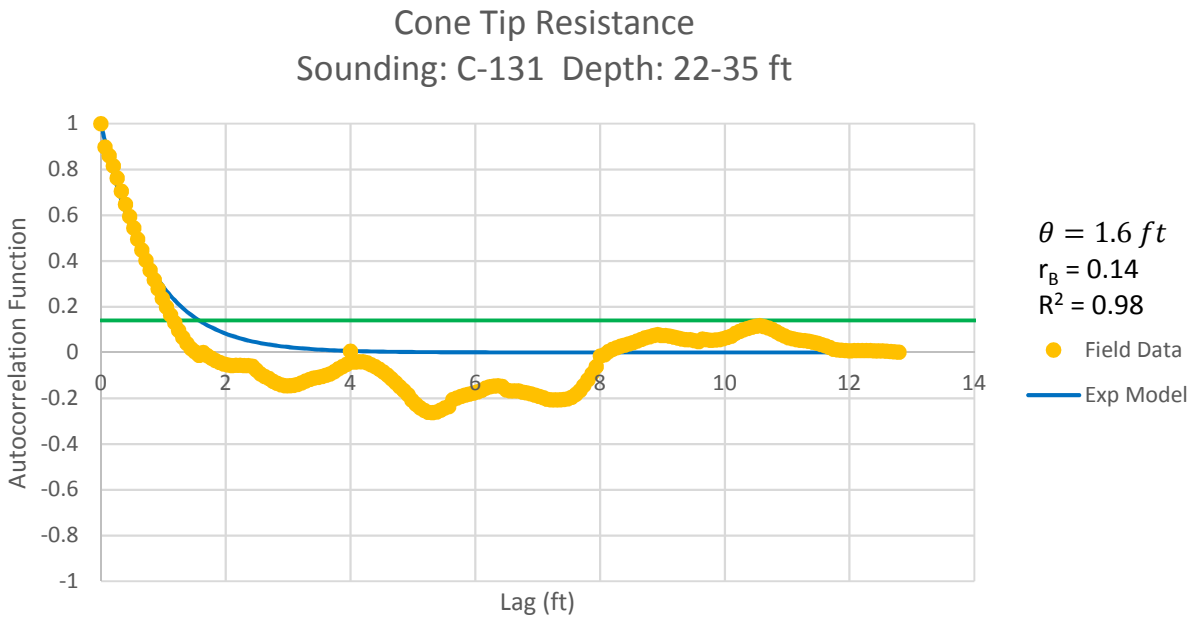

Figure B - 240: Estimation of the Scale of Fluctuation, θ = 1.6 feet, for Cone Tip Resistance Data from Sounding C-131, "Clean sands to silty sands (6)" layer from 22 to 35 feet depth.

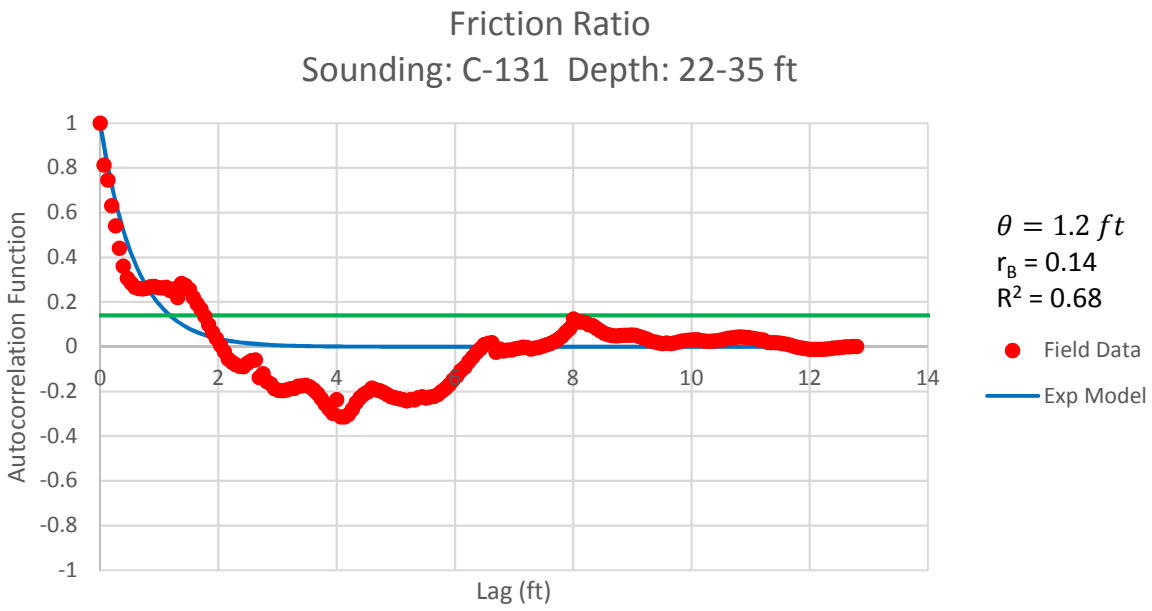

Figure B - 241: Estimation of the Scale of Fluctuation, θ = 1.2 feet, for Friction Ratio Data from Sounding C-131, "Clean sands to silty sands (6)" layer from 22 to 35 feet depth. Data is a poor fit for the points greater than the Bartlett limit of 0.14; coefficient of determination, R^2, value is less 0.9. Therefore, these results were not included in final analysis.

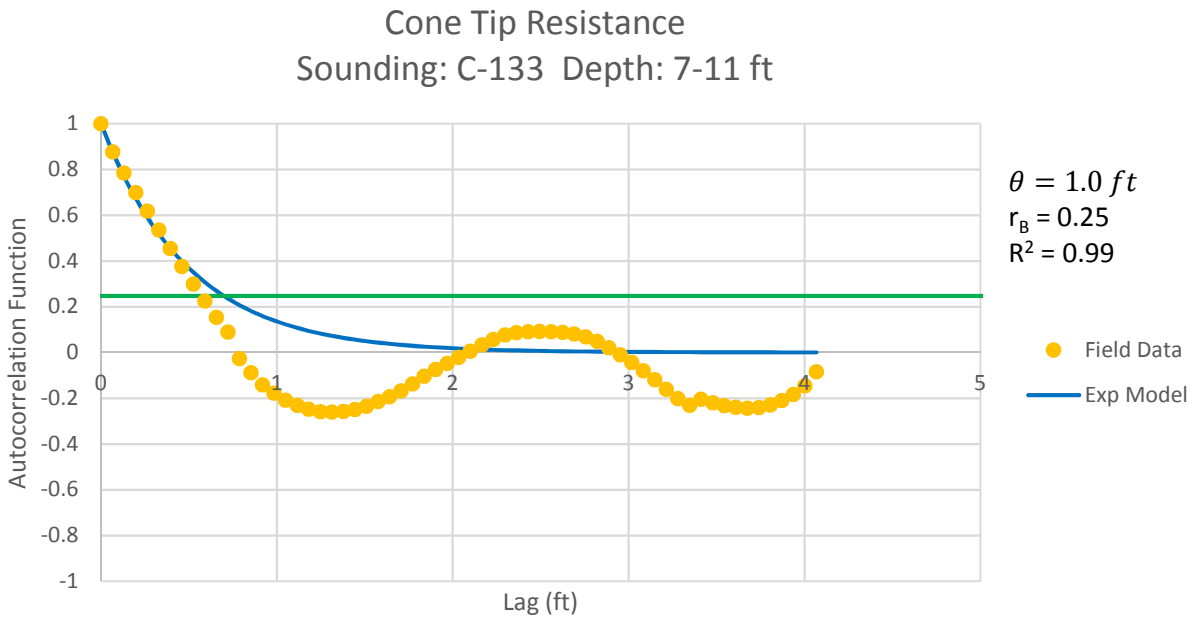

Figure B - 242: Estimation of the Scale of Fluctuation, $\theta = 1.0$ feet, for Friction Ratio Data from Sounding C-133, "Clean sands to silty sands (6)" layer from 7 to 11 feet depth.

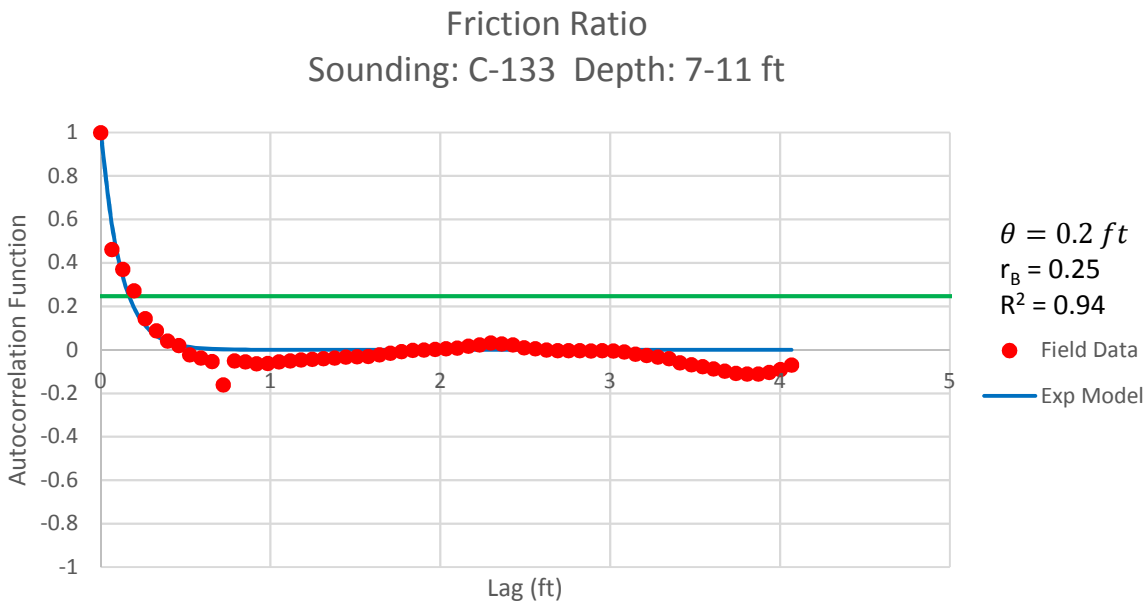

Figure B - 243: Estimation of the Scale of Fluctuation, $\theta = 0.2$ feet, for Friction Ratio Data from Sounding C-133, "Clean sands to silty sands (6)" layer from 7 to 11 feet depth.

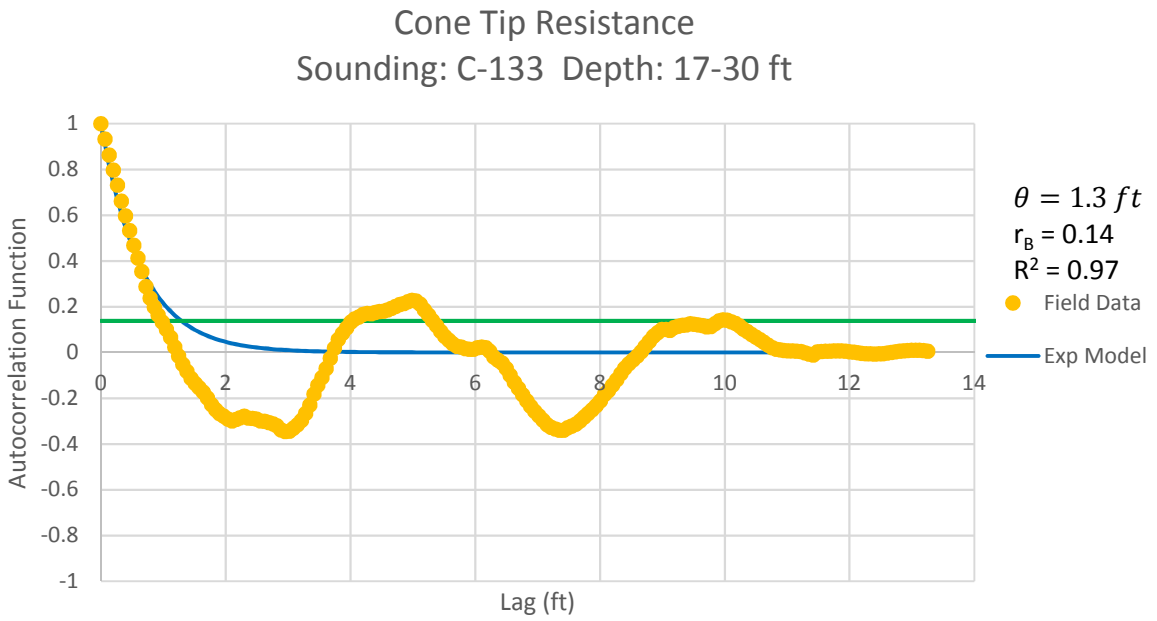

Figure B - 244: Estimation of the Scale of Fluctuation, θ = 1.3 feet, for Cone Tip Resistance Data from Sounding C-133, "Clean sands to silty sands (6)" layer from 17 to 30 feet depth.

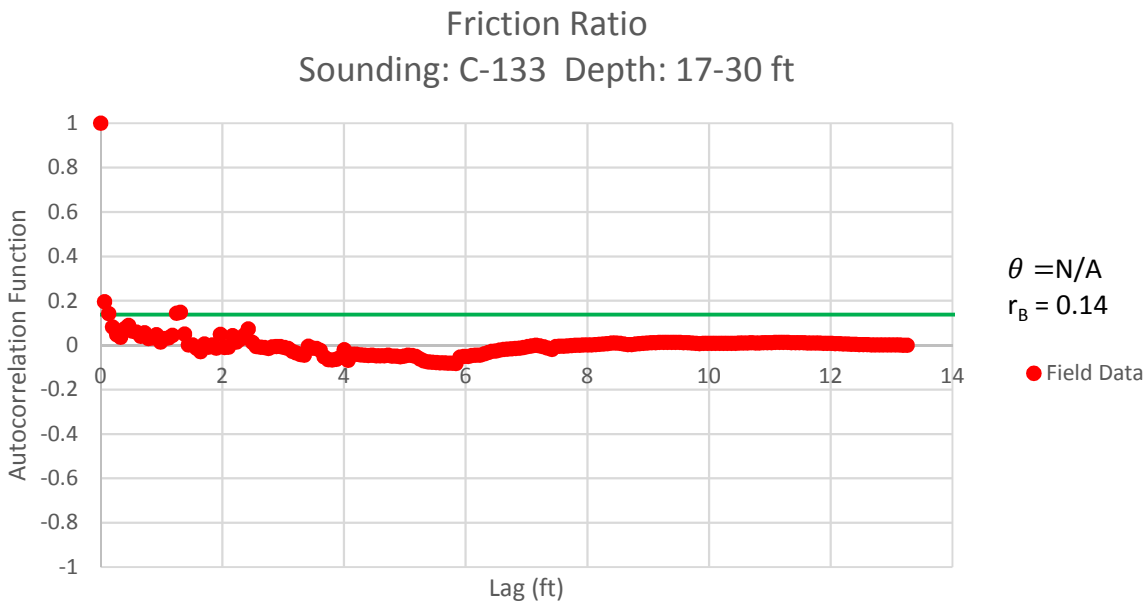

Figure B - 245: Estimation of the Scale of Fluctuation, θ, for Friction Ratio Data from Sounding C-133, " Clean sands to silty sands (6)" layer from 17 to 30 feet depth. Data is limited to only 3 points greater than the Bartlett limit of 0.14; therefore, θ could not be estimated, and these results were not included in final analysis.

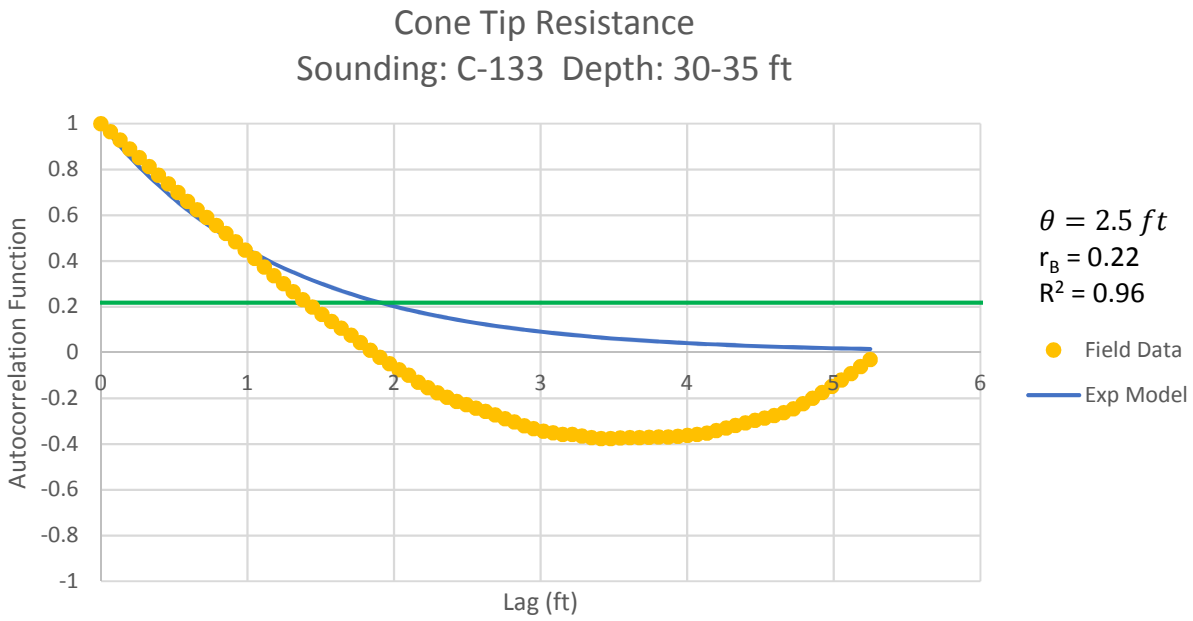

Figure B - 246: Estimation of the Scale of Fluctuation, $\theta = 2.5$ feet, for Cone Tip Resistance Data from Sounding C-133, "Gravelly sand to sand (7)" layer from 30 to 35 feet depth.

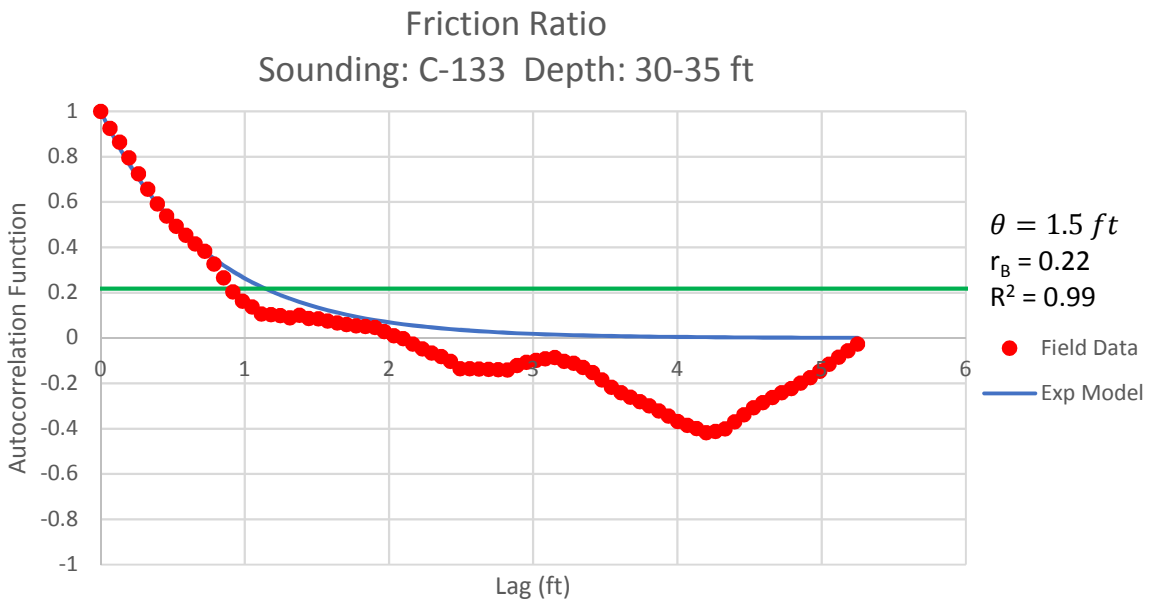

Figure B - 247: Estimation of the Scale of Fluctuation, $\theta = 1.5$ feet, for Friction Ratio Data from Sounding C-133, "Gravelly sand to sand (7)" layer from 30 to 35 feet depth.

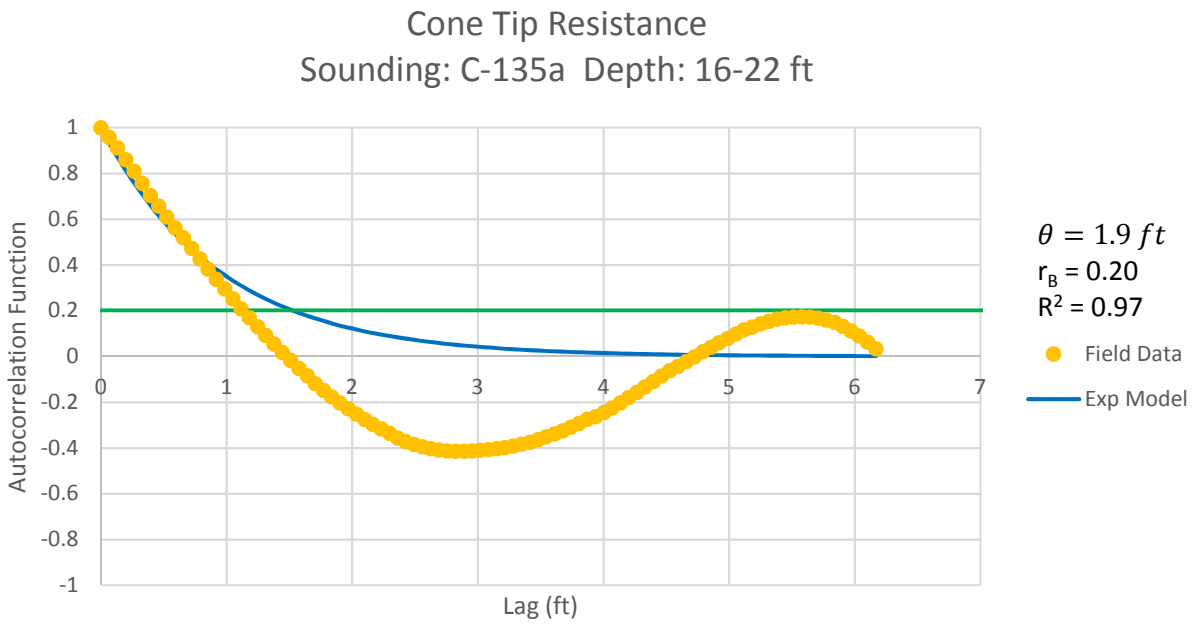

Figure B - 248: Estimation of the Scale of Fluctuation, θ = 1.9 feet, for Cone Tip Resistance Data from Sounding C-135a, "Gravelly sand to sand (7)" layer from 16 to 22 feet depth.

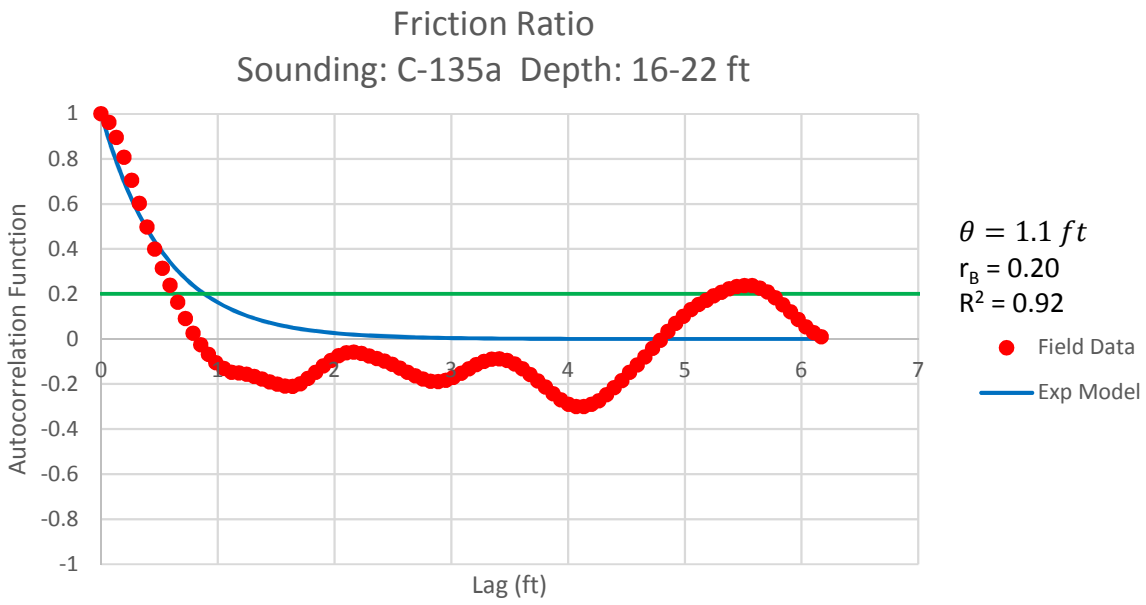

Figure B - 2490: Estimation of the Scale of Fluctuation, θ = 1.1 feet, for Friction Ratio Data from Sounding C-135a, "Gravelly sand to sand (7)" layer from 16 to 22 feet depth.

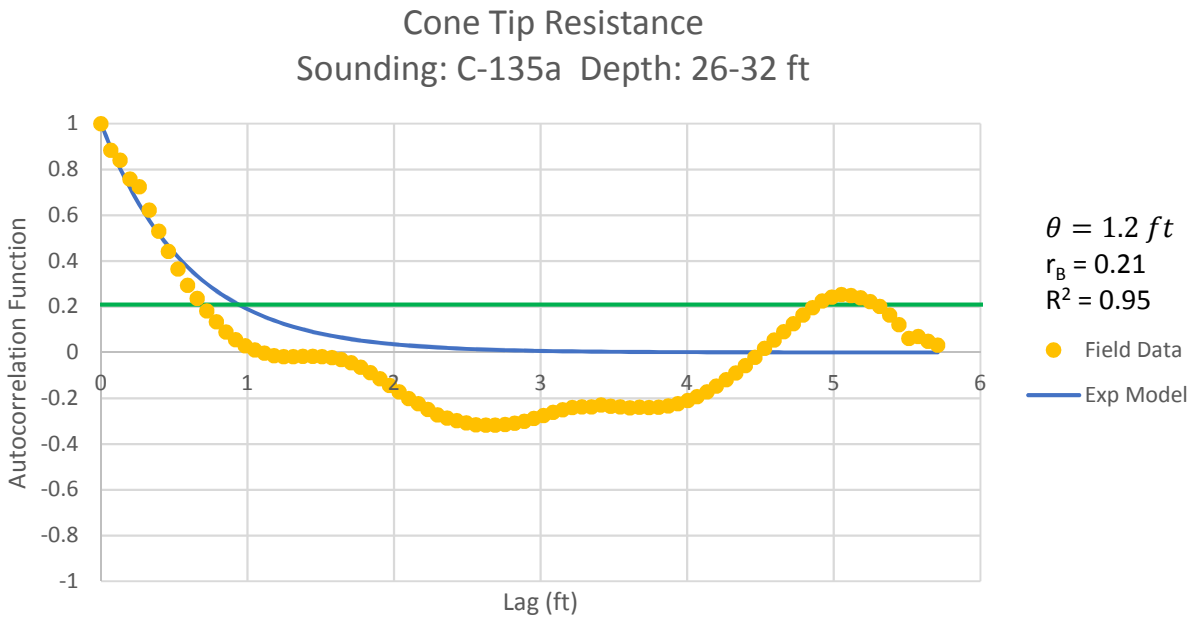

Figure B - 250: Estimation of the Scale of Fluctuation, $\theta = 1.2$ feet, for Cone Tip Resistance Data from Sounding C-135a, "Clean sands to silty sands (6)" layer from 26 to 32 feet depth.

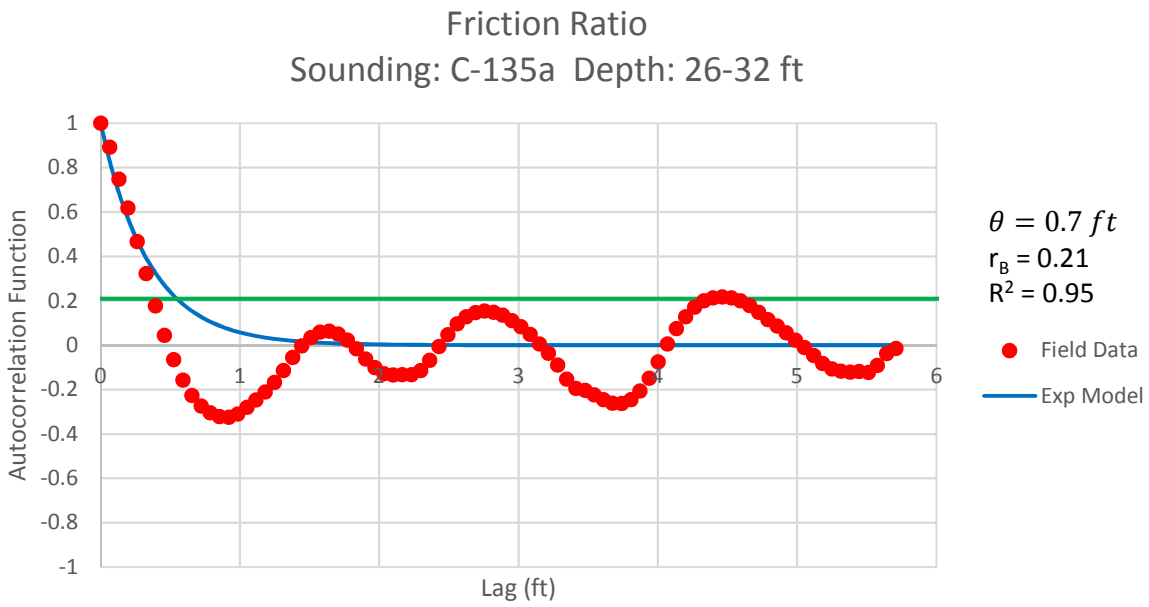

Figure B - 251: Estimation of the Scale of Fluctuation, $\theta = 0.7$ feet, for Friction Ratio Data from Sounding C-135a, "Clean sands to silty sands (6)" layer from 26 to 32 feet depth.

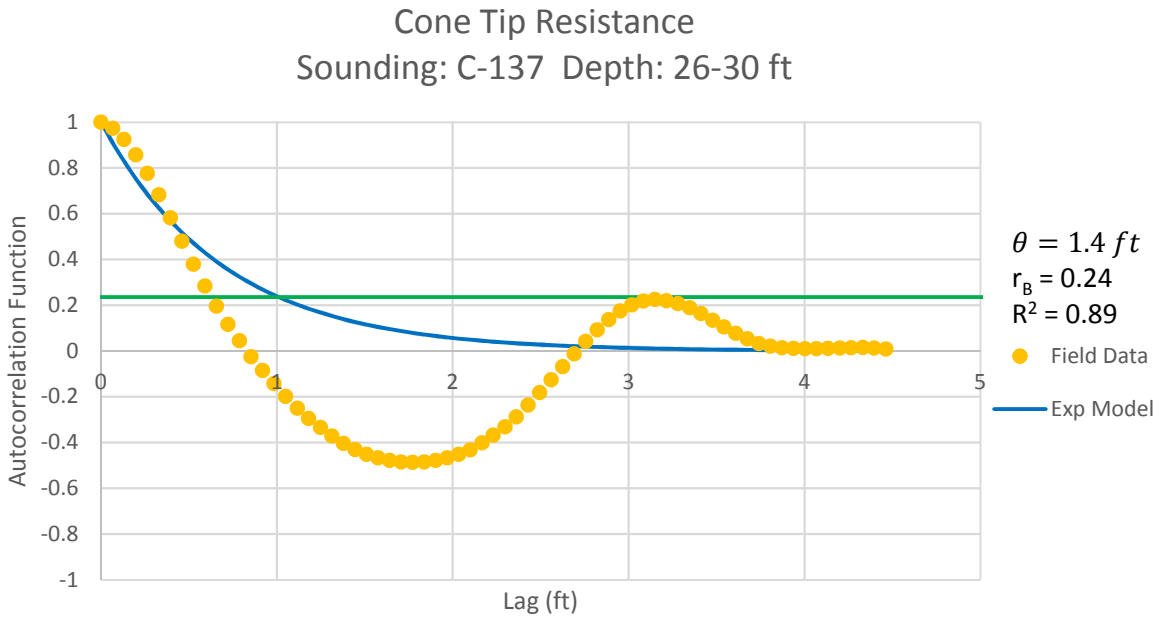

Figure B - 252: Estimation of the Scale of Fluctuation, $\theta = 1.4$ feet, for Cone Tip Resistance Data from Sounding C-137, "Clean sands to silty sands (6)" layer from 26 to 30 feet depth. Data is a poor fit for the points greater than the Bartlett limit of 0.24; coefficient of determination, R^2, value is less 0.9. Therefore, these results were not included in final analysis.

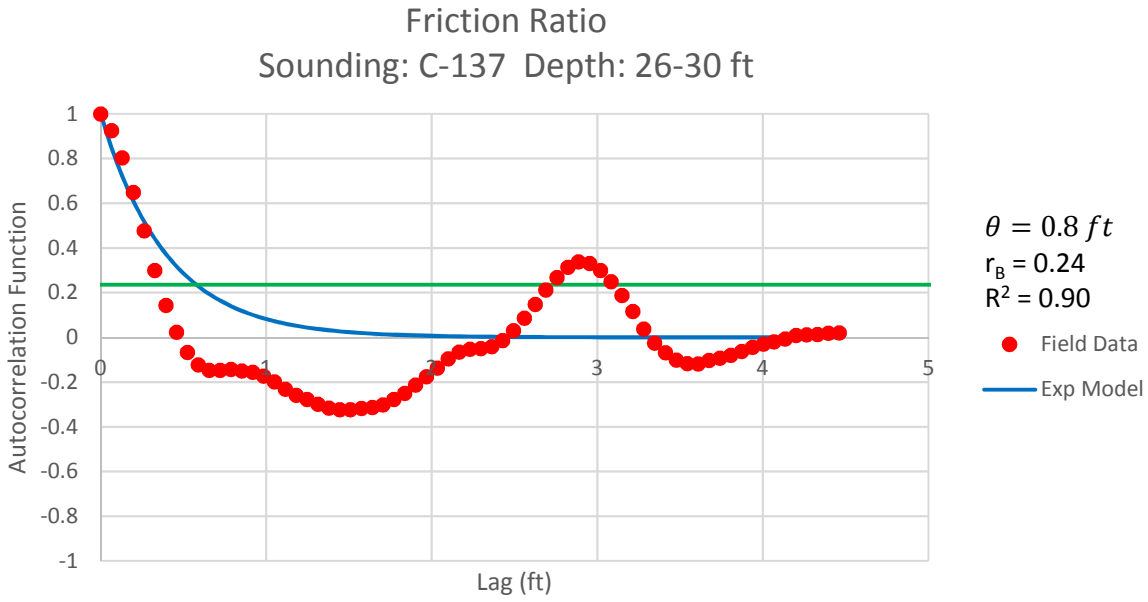

Figure B - 253: Estimation of the Scale of Fluctuation, $\theta = 0.8$ feet, for Friction Ratio Data from Sounding C-137, "Clean sands to silty sands (6)" layer from 26 to 30 feet depth.

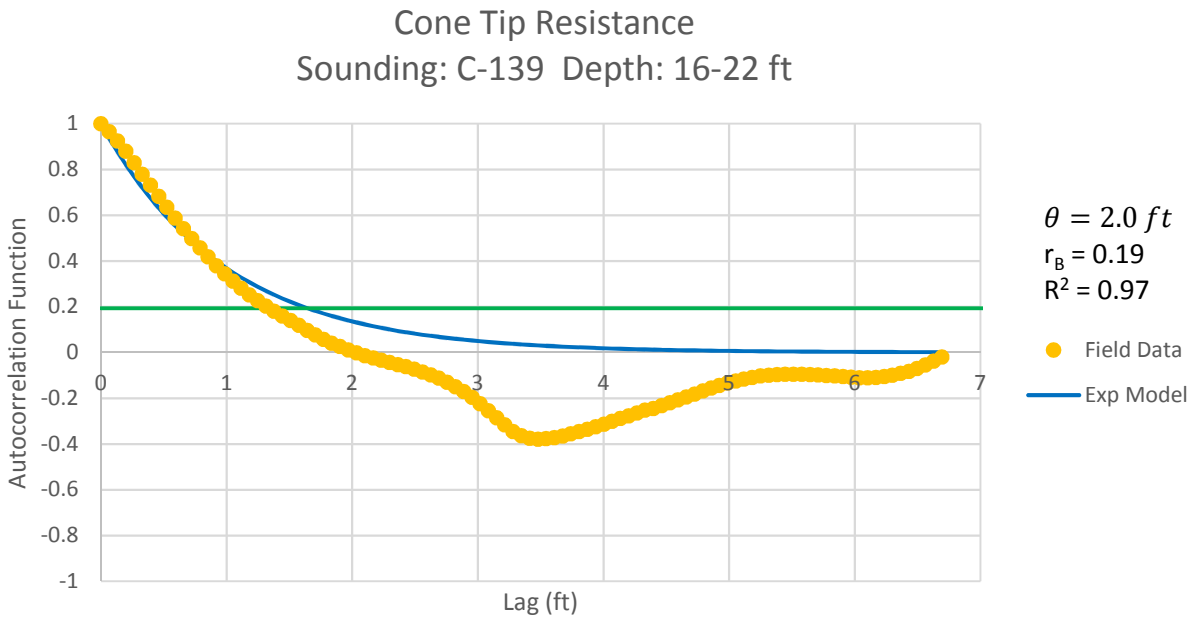

Figure B - 254: Estimation of the Scale of Fluctuation, $\theta = 2.0$ feet, for Cone Tip Resistance Data from Sounding C-139, "Gravelly sand to sand (7)" layer from 16 to 22 feet depth.

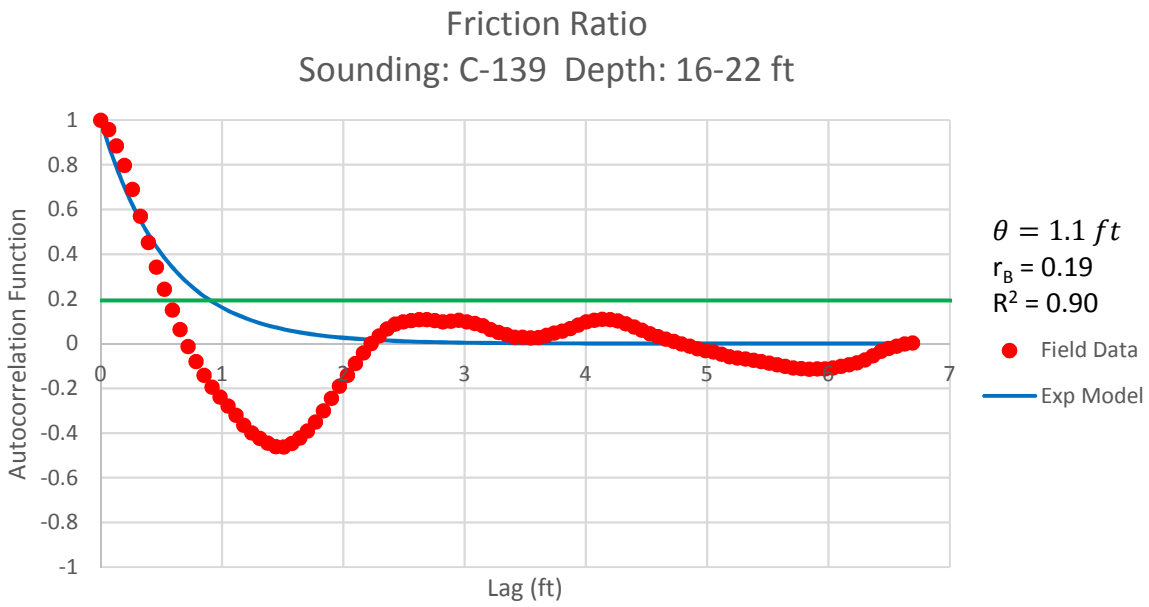

Figure B - 255: Estimation of the Scale of Fluctuation, $\theta = 1.1$ feet, for Cone Tip Resistance Data from Sounding C-139, "Gravelly sand to sand (7)" layer from 16 to 22 feet depth analysis.

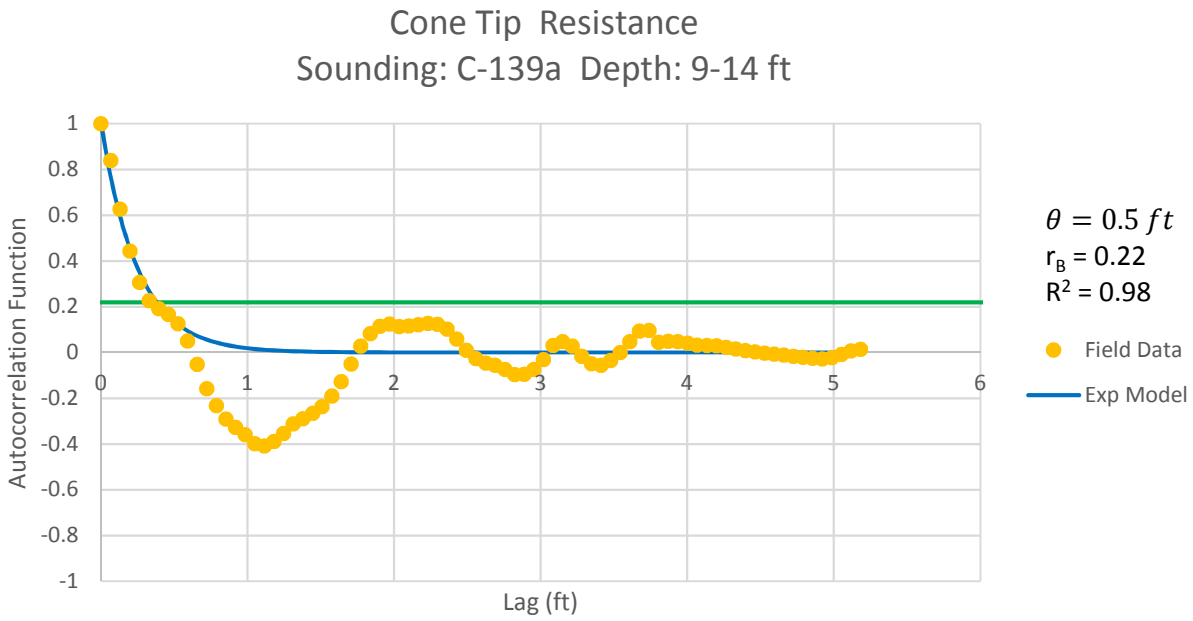

Figure B - 256: Estimation of the Scale of Fluctuation, θ = 0.5 feet, for Cone Tip Resistance Data from Sounding C-139, "Clays; clay to silty clay (3)" layer from 9 to 14 feet depth.

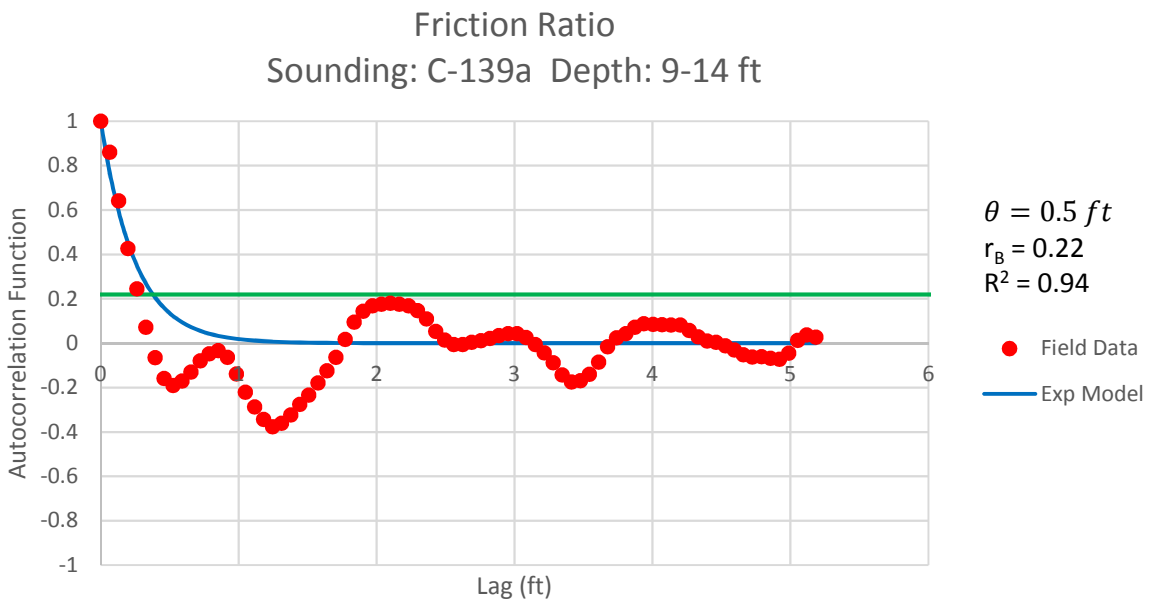

Figure B - 25758: Estimation of the Scale of Fluctuation, θ = 0.5 feet, for Friction Ratio Data from Sounding C-139, "Clays; clay to silty clay (3)" layer from 9 to 14 feet depth.

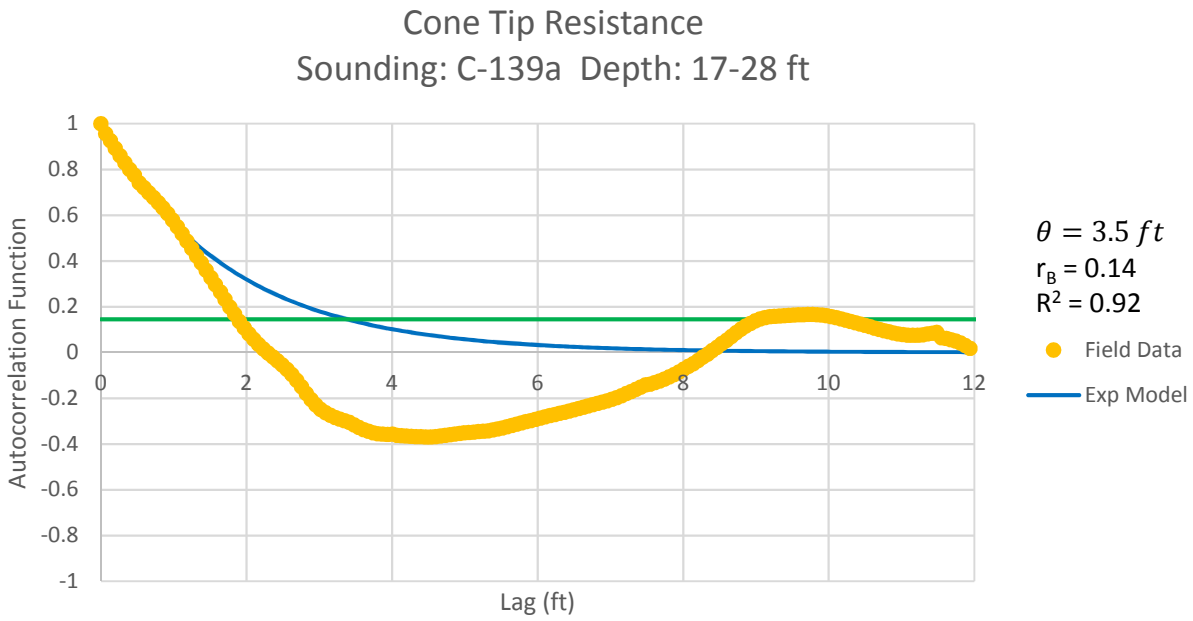

Figure B - 258: Estimation of the Scale of Fluctuation, $\theta = 3.5$ feet, for Cone Tip Resistance Data from Sounding C-139a, "Gravelly sand to sand (7)" layer from 17 to 28 feet depth.

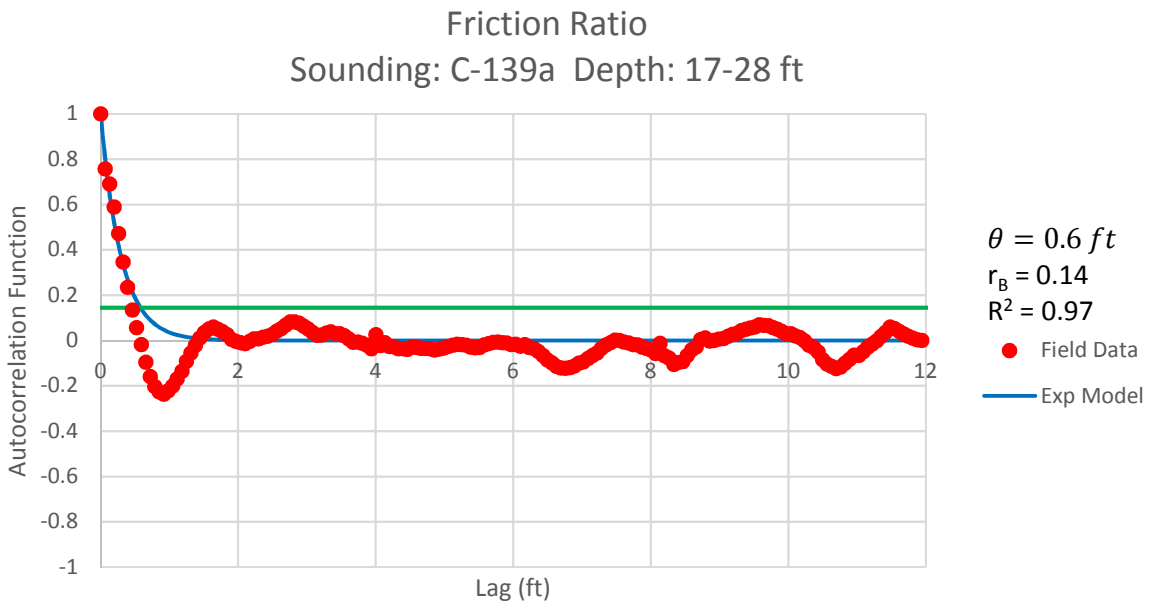

Figure B - 259: Estimation of the Scale of Fluctuation, $\theta = 0.6$ feet, for Friction Ratio Data from Sounding C-139a, "Gravelly sand to sand (7)" layer from 17 to 28 feet depth.

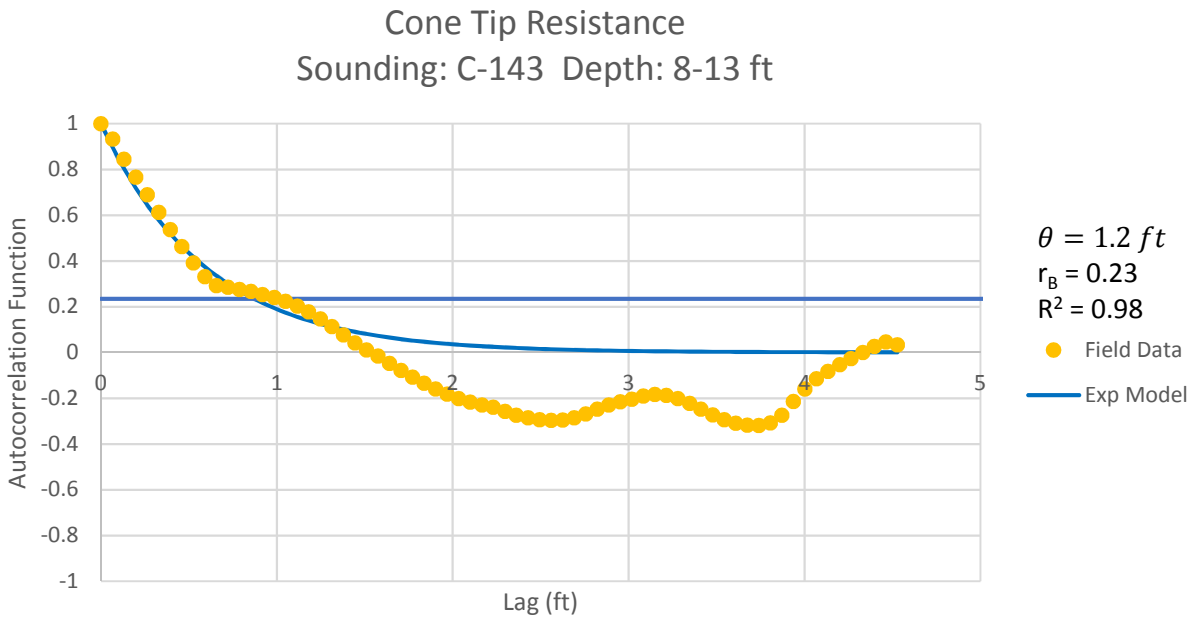

Figure B - 260: Estimation of the Scale of Fluctuation, $\theta = 1.2$ feet, for Cone Tip Resistance Data from Sounding C-143, "Clean sands to silty sands (6)" layer from 8 to 13 feet depth.

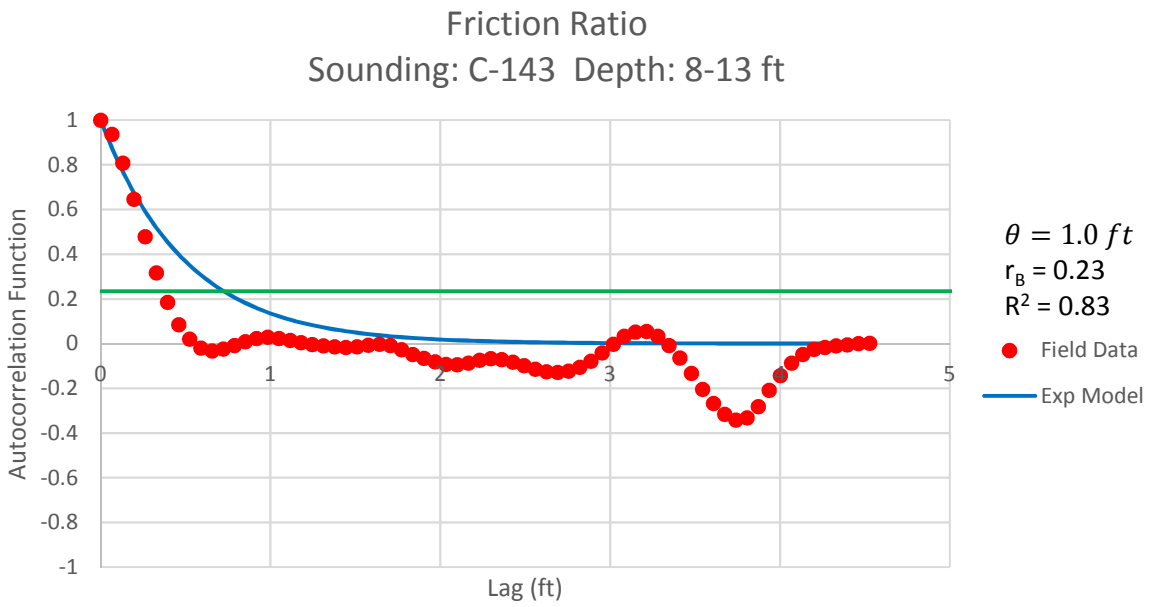

Figure B - 261: Estimation of the Scale of Fluctuation, $\theta = 1.0$ feet, for Friction Ratio Data from Sounding C-143, "Clean sands to silty sands (6)" layer from 8 to 13 feet depth. Data is a poor fit for the points greater than the Bartlett limit of 0.23; coefficient of determination, R^2, value is less 0.9. Therefore, these results were not included in final analysis.

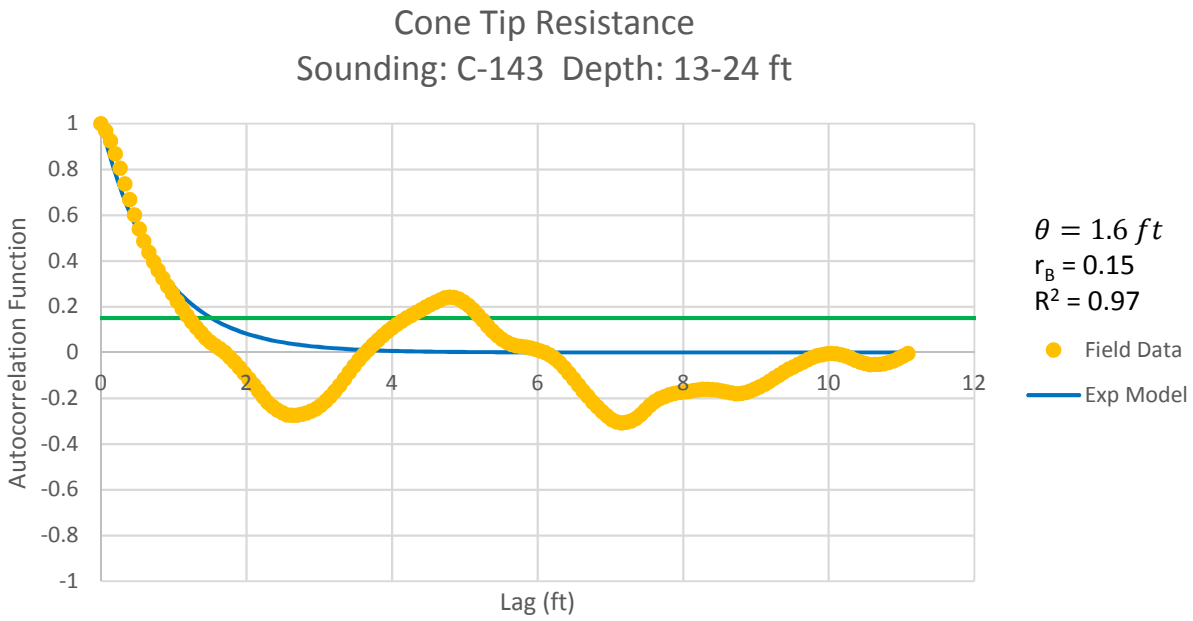

Figure B - 262: Estimation of the Scale of Fluctuation, $\theta = 1.6$ feet, for Cone Tip Resistance Data from Sounding C-143, "Clean sands to silty sands (6)" layer from 13 to 24 feet depth.

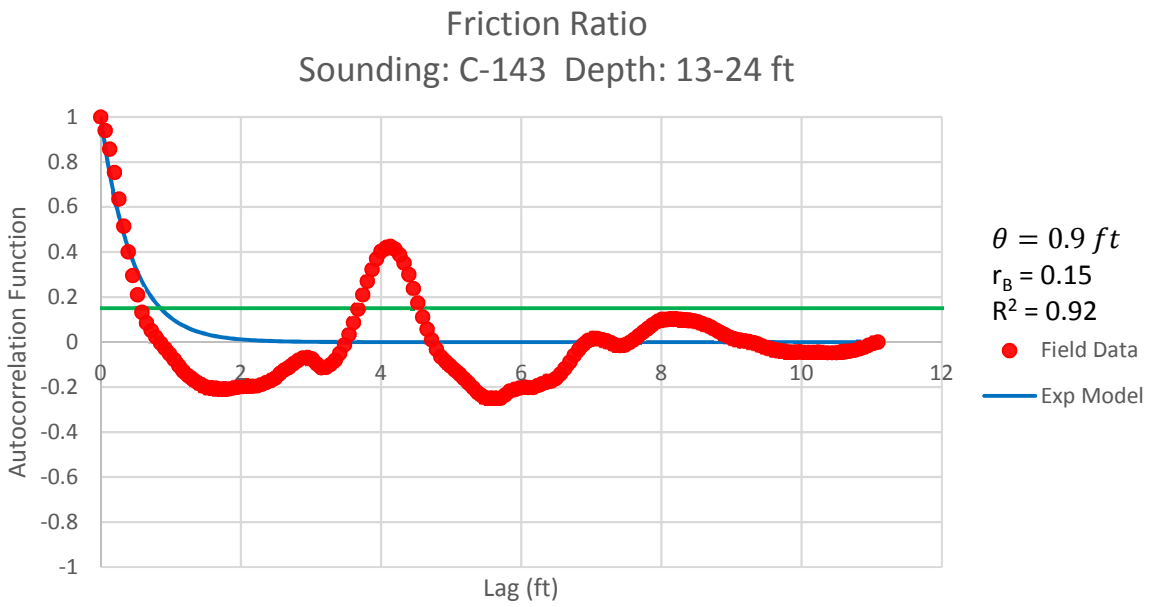

Figure B - 263: Estimation of the Scale of Fluctuation, $\theta = 0.9$ feet, for Friction Ratio Data from Sounding C-143, "Clean sands to silty sands (6)" layer from 13 to 24 feet depth.

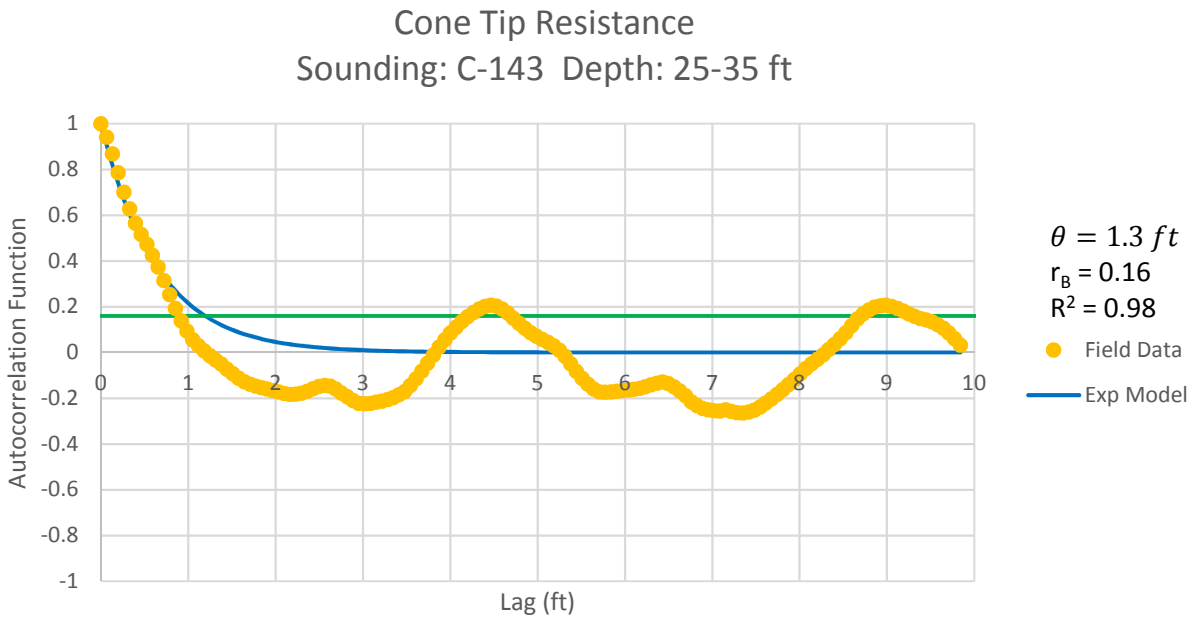

Figure B - 264: Estimation of the Scale of Fluctuation, $\theta = 1.3$ feet, for Cone Tip Resistance Data from Sounding C-143, "Clean sands to silty sands (6)" layer from 25 to 35 feet depth.

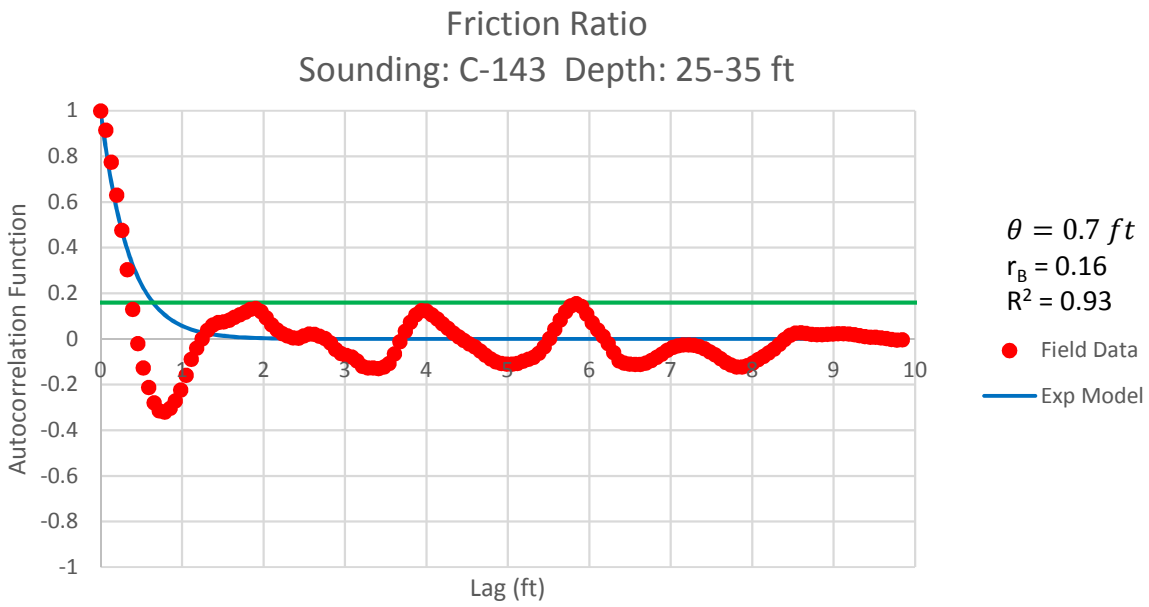

Figure B - 265: Estimation of the Scale of Fluctuation, $\theta = 0.7$ feet, for Friction Ratio Data from Sounding C-143, "Clean sands to silty sands (6)" layer from 25 to 35 feet depth.

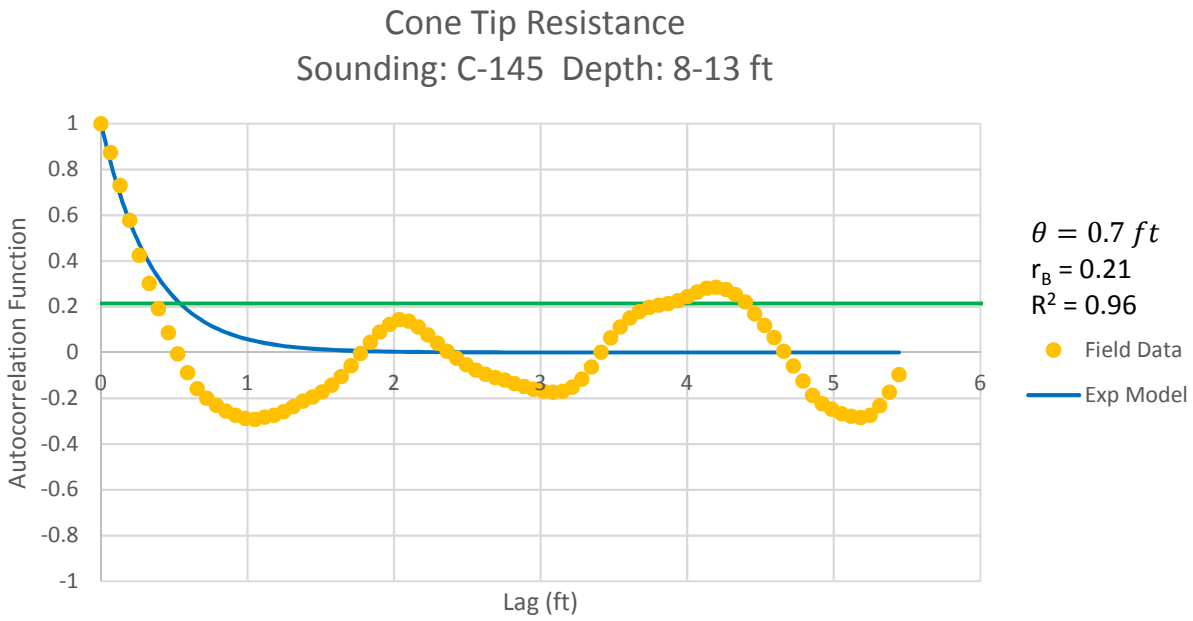

Figure B - 266: Estimation of the Scale of Fluctuation, $\theta = 0.7$ feet, for Cone Tip Resistance Data from Sounding C-145, "Clean sands to silty sands (6)" layer from 8 to 13 feet depth.

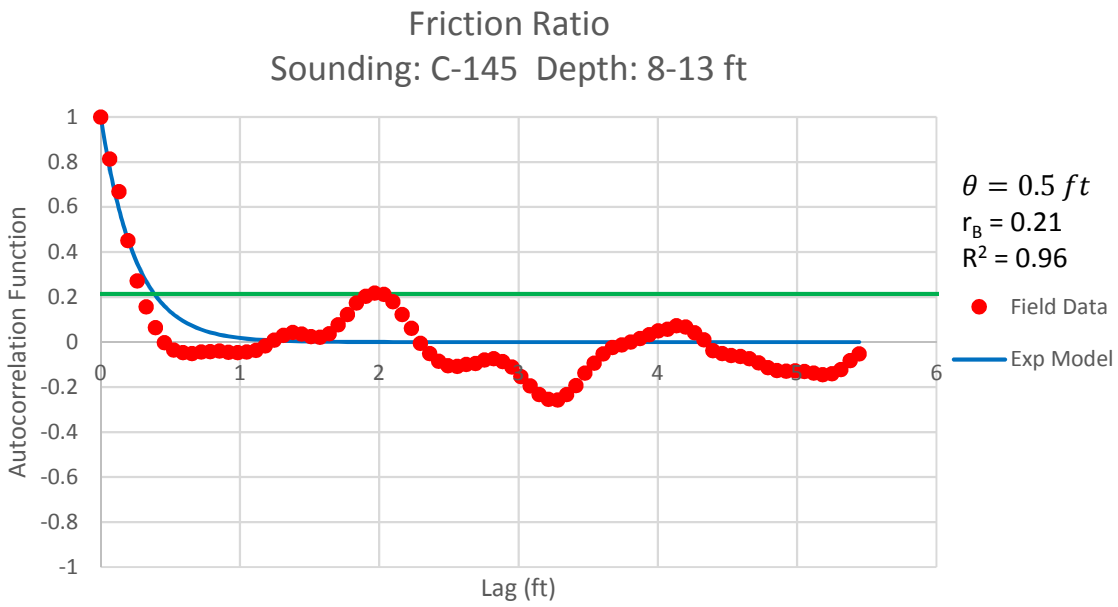

Figure B - 267: Estimation of the Scale of Fluctuation, $\theta = 0.5$ feet, for Friction Ratio Data from Sounding C-145, "Clean sands to silty sands (6)" layer from 8 to 13 feet depth.

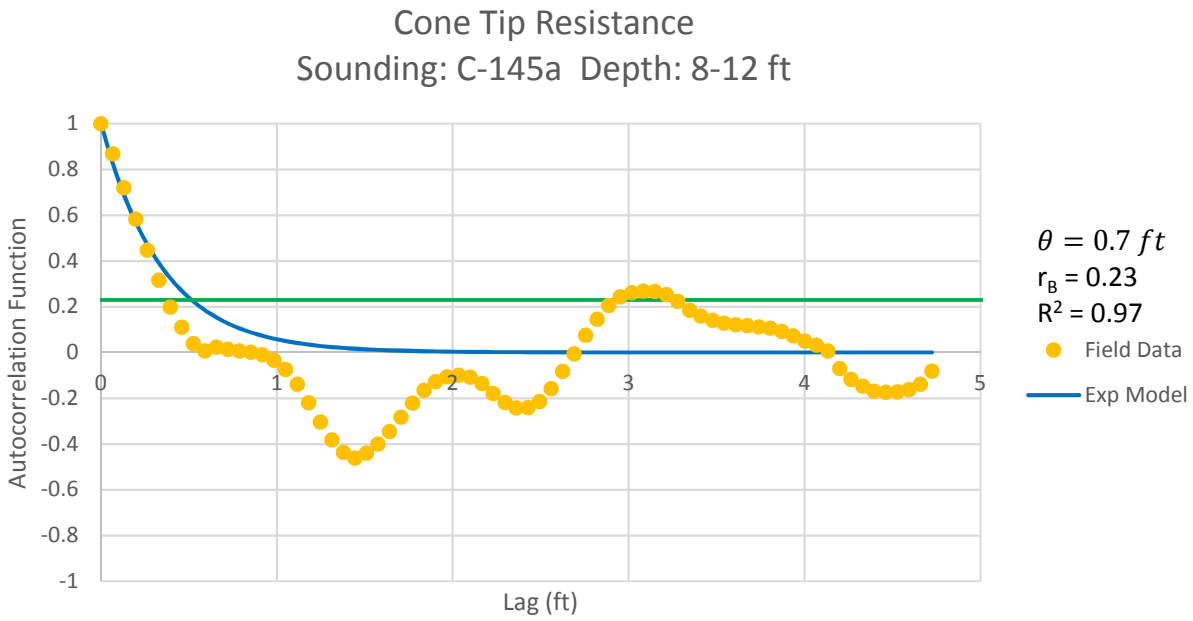

Figure B - 268: Estimation of the Scale of Fluctuation, $\theta = 0.7$ feet, for Cone Tip Resistance Data from Sounding C-145a, "Clean sands to silty sands (6)" layer from 8 to 12 feet depth.

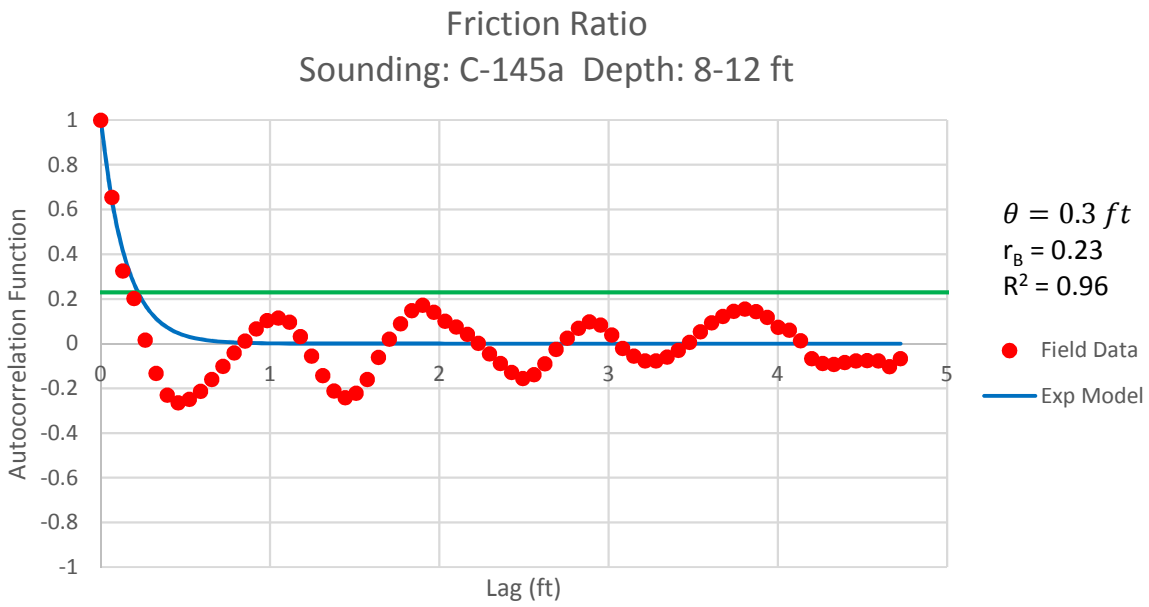

Figure B - 269: Estimation of the Scale of Fluctuation, θ, for Friction Ratio Data from Sounding C-145a, "Clean sands to silty sands (6)" layer from 8 to 12 feet depth. Data is limited to only 3 points greater than the Bartlett limit of 0.23; therefore, θ could not be estimated, and these results were not included in final analysis.

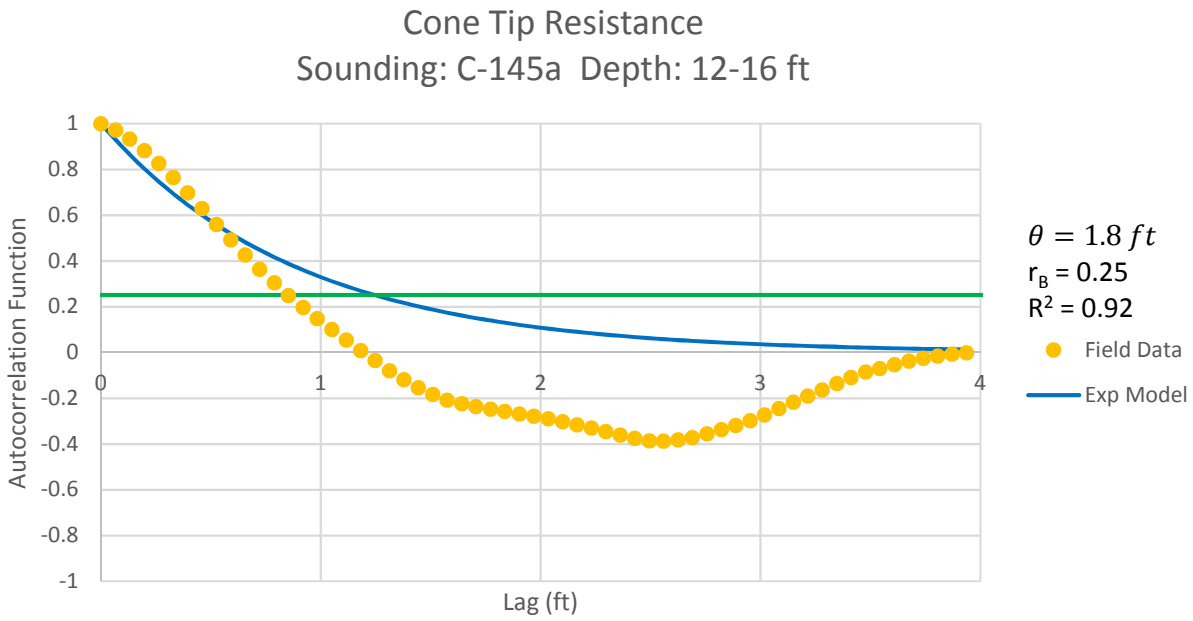

Figure B - 270: Estimation of the Scale of Fluctuation, $\theta = 1.8$ feet, for Cone Tip Resistance Data from Sounding C-145a, "Gravelly sand to sand (7)" layer from 12 to 16 feet depth.

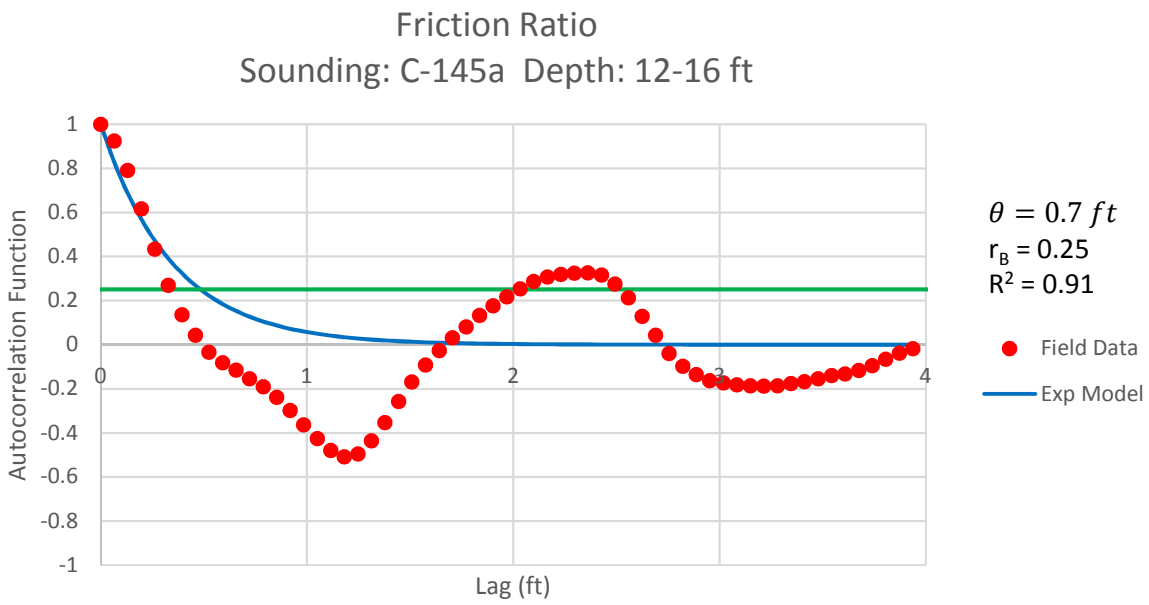

Figure B - 271: Estimation of the Scale of Fluctuation, $\theta = 0.7$ feet, for Friction Ratio Data from Sounding C-145a, "Gravelly sand to sand (7)" layer from 12 to 16 feet depth.

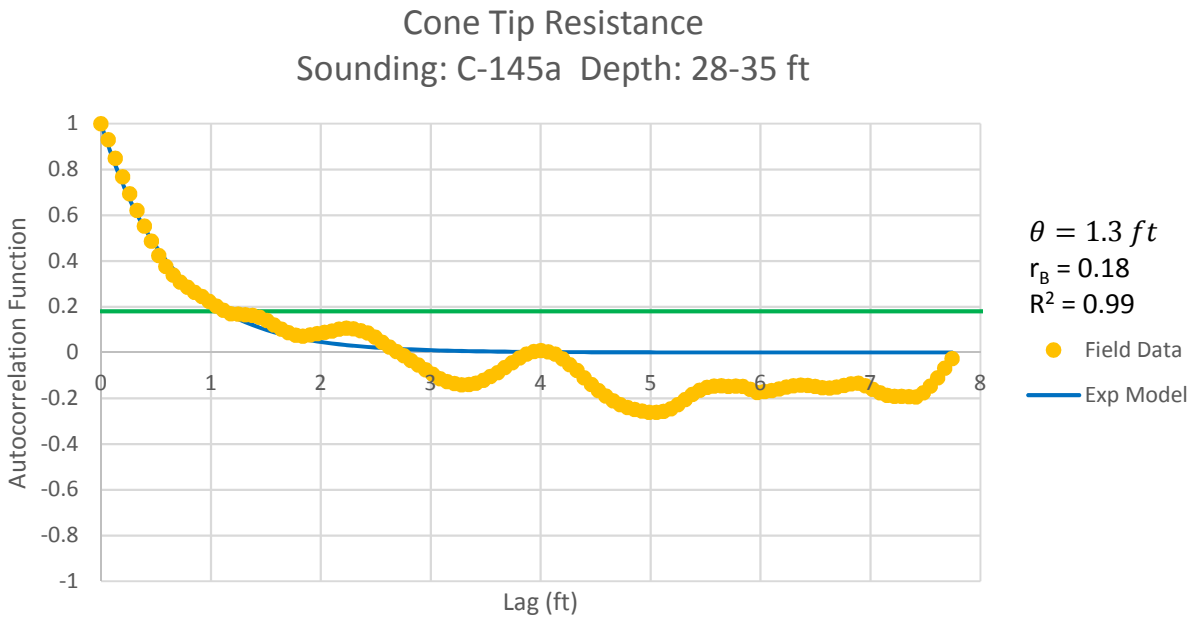

Figure B - 272: Estimation of the Scale of Fluctuation, θ = 1.3 feet, for Cone Tip Resistance Data from Sounding C-145a, "Clean sands to silty sands (6)" layer from 28 to 35 feet depth.

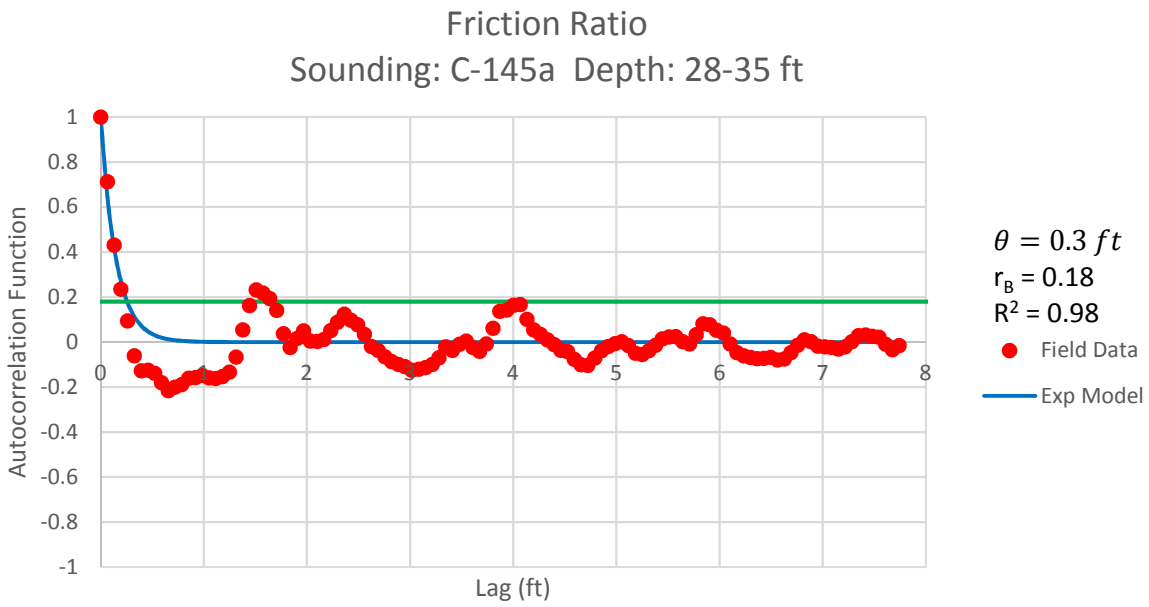

Figure B - 273: Estimation of the Scale of Fluctuation, θ = 0.3 feet, for Friction Ratio Data from Sounding C-145a, "Clean sands to silty sands (6)" layer from 28 to 35 feet depth.

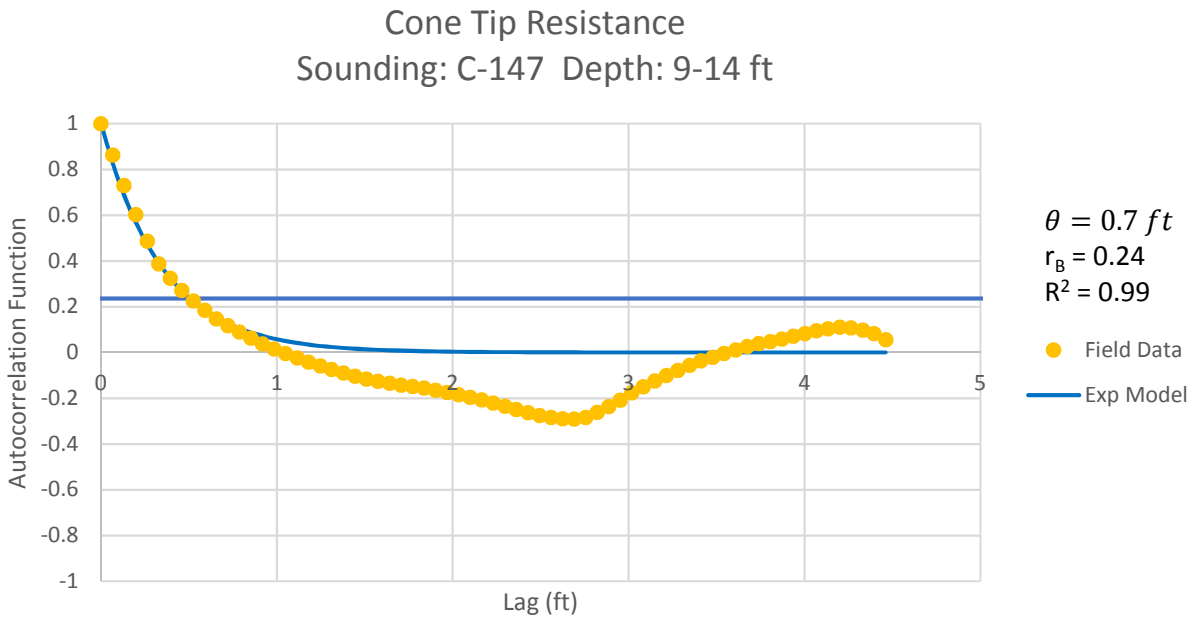

Figure B - 274: Estimation of the Scale of Fluctuation, $\theta = 0.7$ feet, for Cone Tip Resistance Data from Sounding C-147, "Clean sands to silty sands (6)" layer from 9 to 14 feet depth.

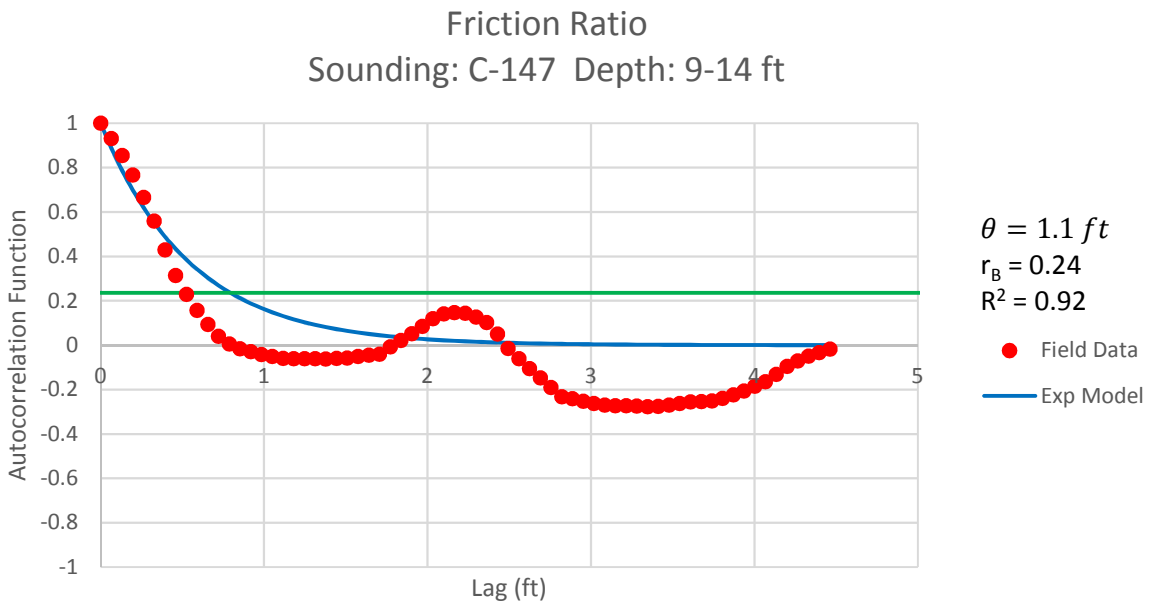

Figure B - 275: Estimation of the Scale of Fluctuation, $\theta = 1.1$ feet, for Friction Ratio Data from Sounding C-147, "Clean sands to silty sands (6)" layer from 9 to 14 feet depth.

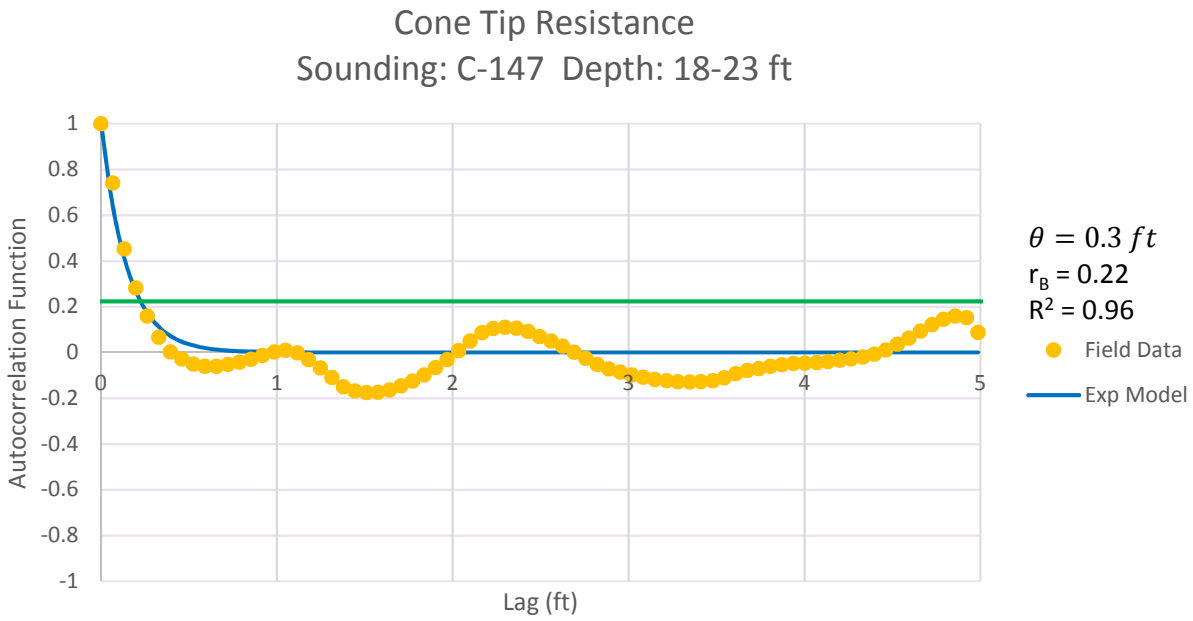

Figure B - 276: Estimation of the Scale of Fluctuation, $\theta = 0.3$ feet, for Cone Tip Resistance Data from Sounding C-147, "Clean sands to silty sands (6)" layer from 18 to 23 feet depth.

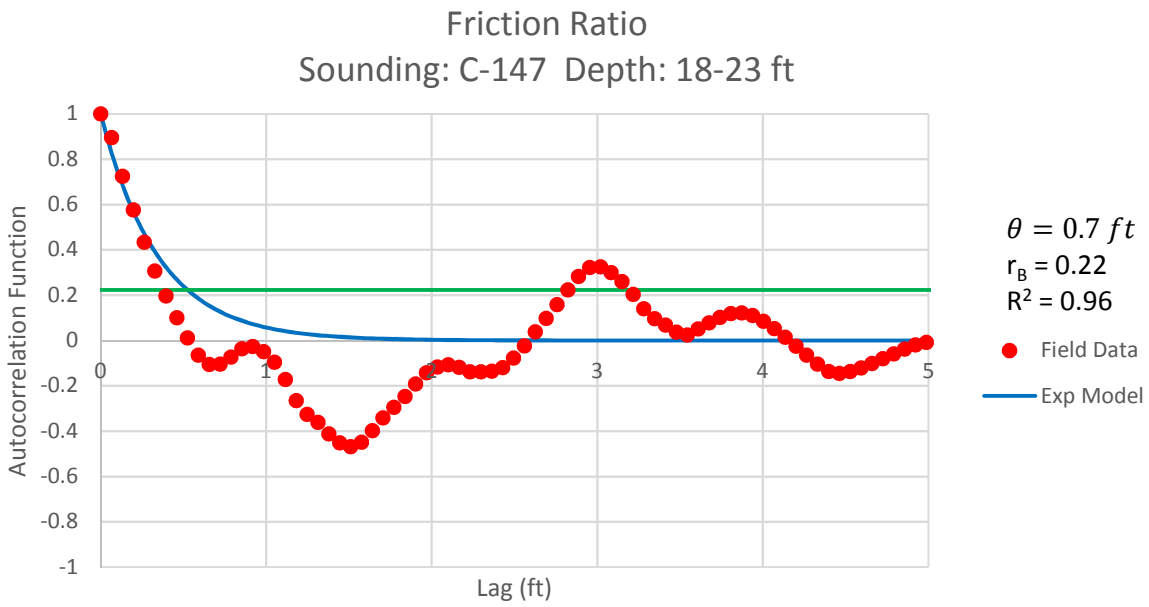

Figure B - 277: Estimation of the Scale of Fluctuation, $\theta = 0.7$ feet, for Friction Ratio Data from Sounding C-147, "Clean sands to silty sands (6)" layer from 18 to 23 feet depth.

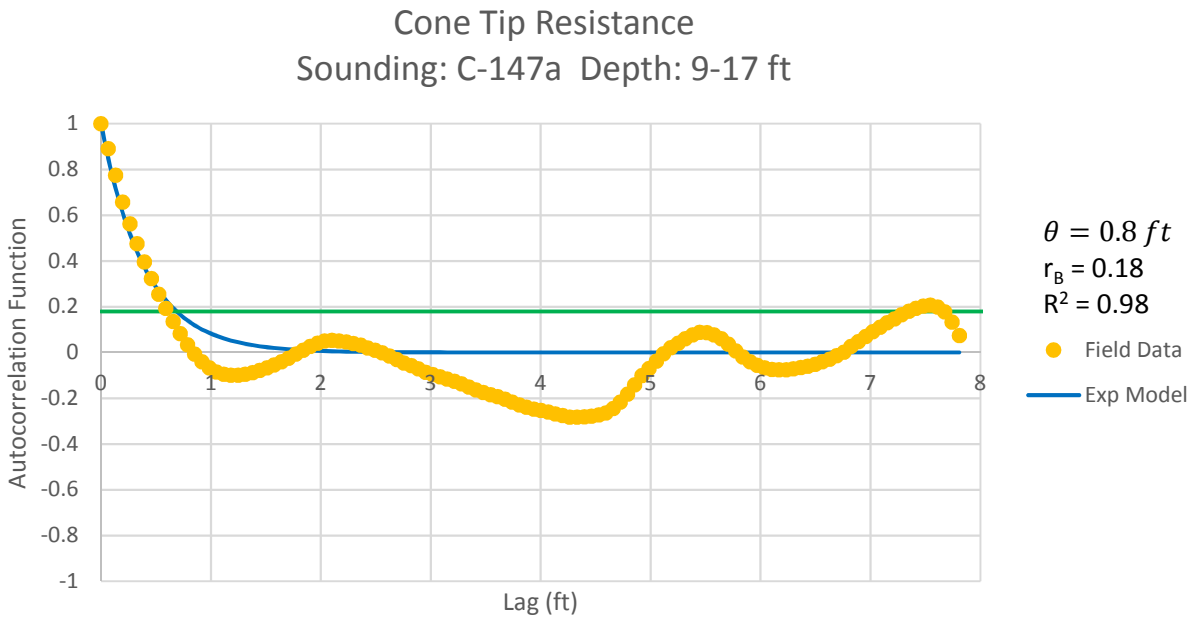

Figure B - 278: Estimation of the Scale of Fluctuation, $\theta = 0.8$ feet, for Cone Tip Resistance Data from Sounding C-147a, "Clean sands to silty sands (6)" layer from 9 to 17 feet depth.

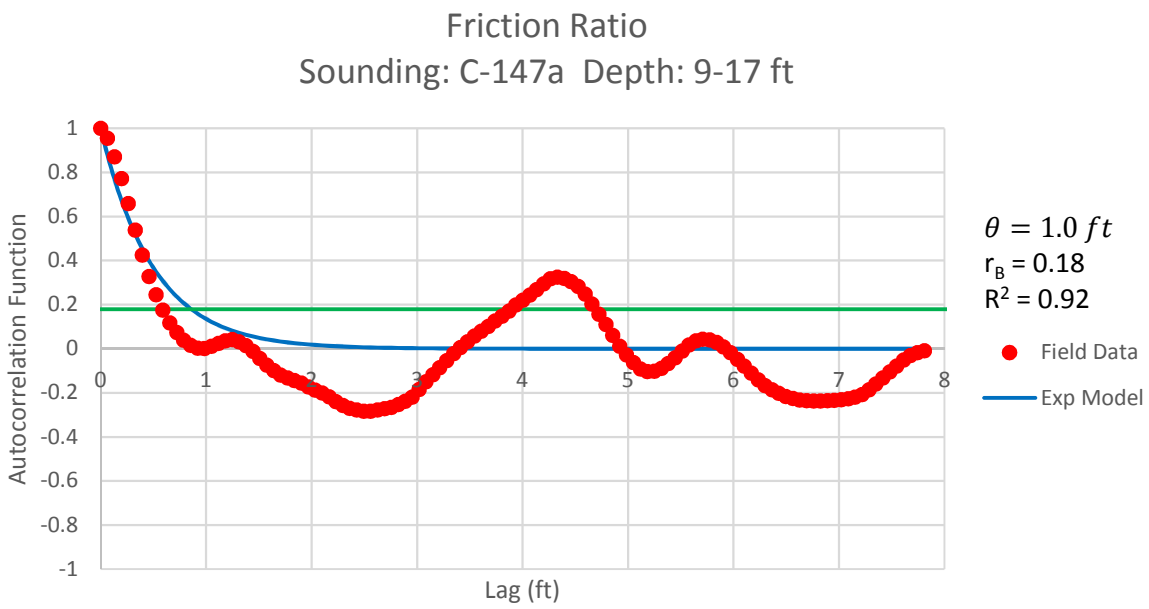

Figure B - 279: Estimation of the Scale of Fluctuation, $\theta = 1.0$ feet, for Friction Ratio Data from Sounding C-147a, "Clean sands to silty sands (6)" layer from 9 to 17 feet depth.

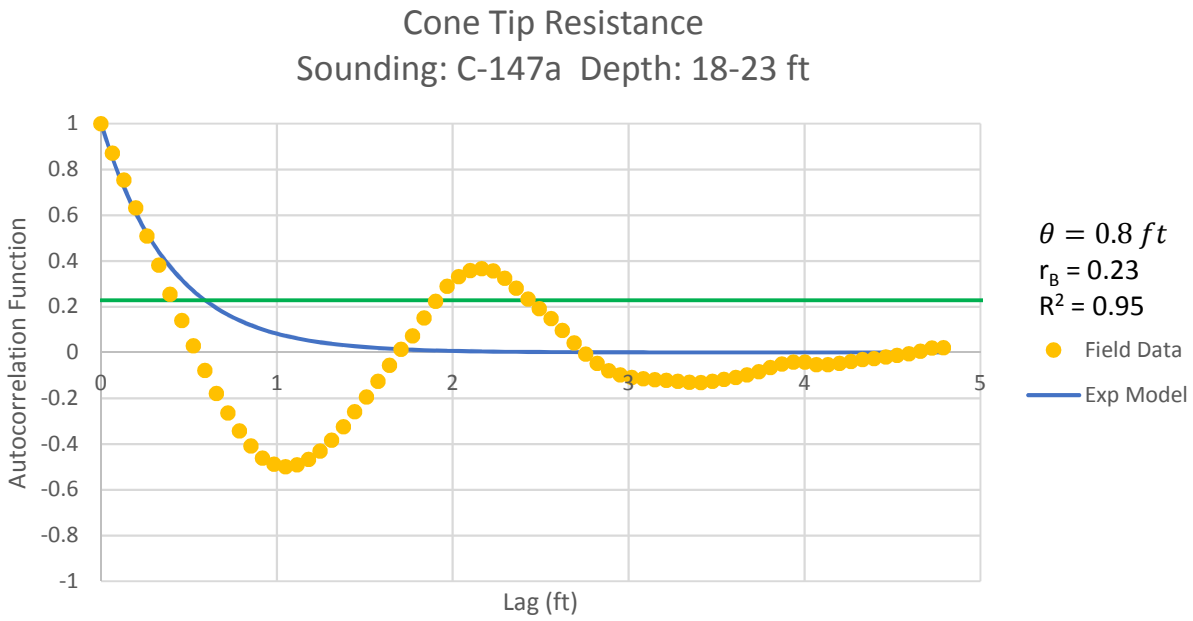

Figure B - 280: Estimation of the Scale of Fluctuation, $\theta = 0.8$ feet, for Cone Tip Resistance Data from Sounding C-147a, "Clean sands to silty sands (6)" layer from 18 to 23 feet depth.

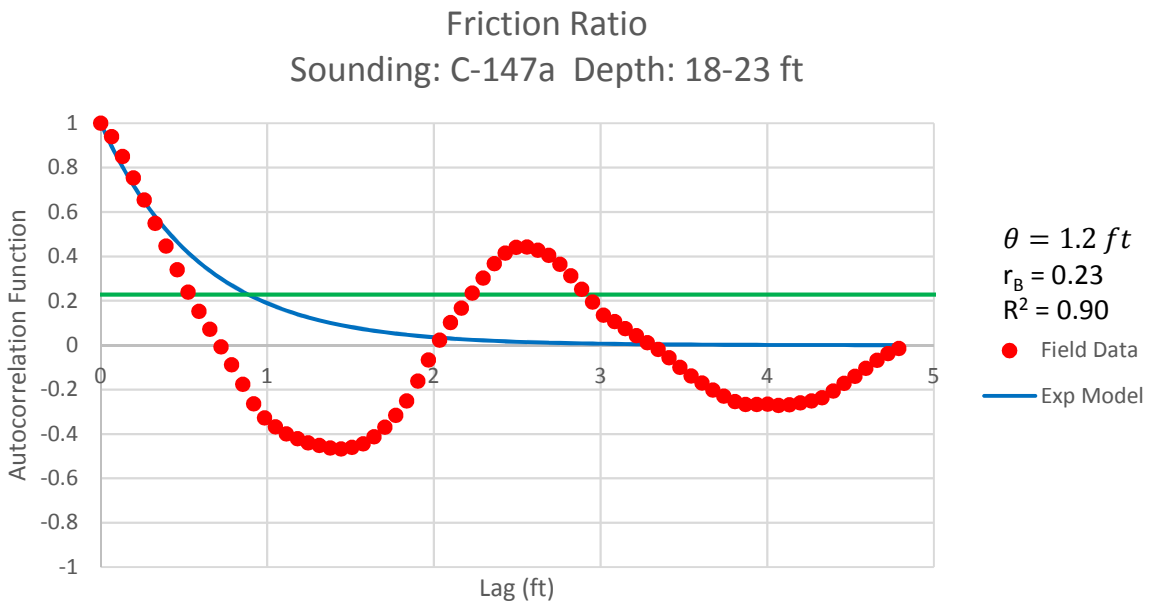

Figure B - 281: Estimation of the Scale of Fluctuation, $\theta = 1.2$ feet, for Friction Ratio Data from Sounding C-147a, "Clean sands to silty sands (6)" layer from 18 to 23 feet depth.

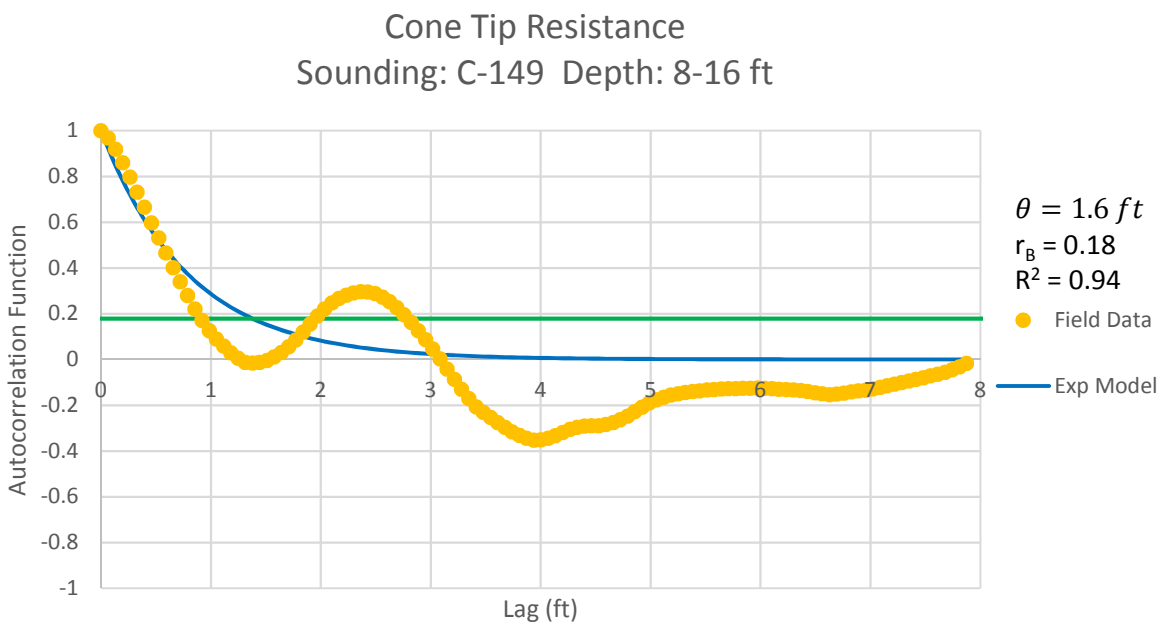

Figure B - 282: Estimation of the Scale of Fluctuation, $\theta = 1.6$ feet, for Cone Tip Resistance Data from Sounding C-149, "Clean sands to silty sands (6)" layer from 8 to 16 feet depth.

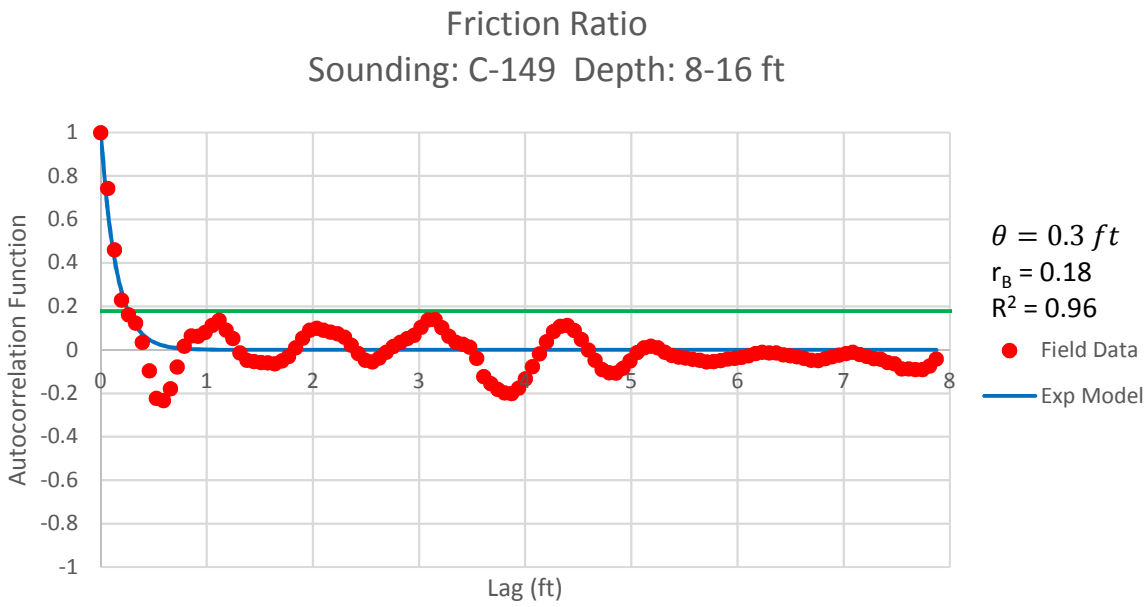

Figure B - 283: Estimation of the Scale of Fluctuation, $\theta = 0.3$ feet, for Friction Ratio Data from Sounding C-149, "Clean sands to silty sands (6)" layer from 8 to 16 feet depth.

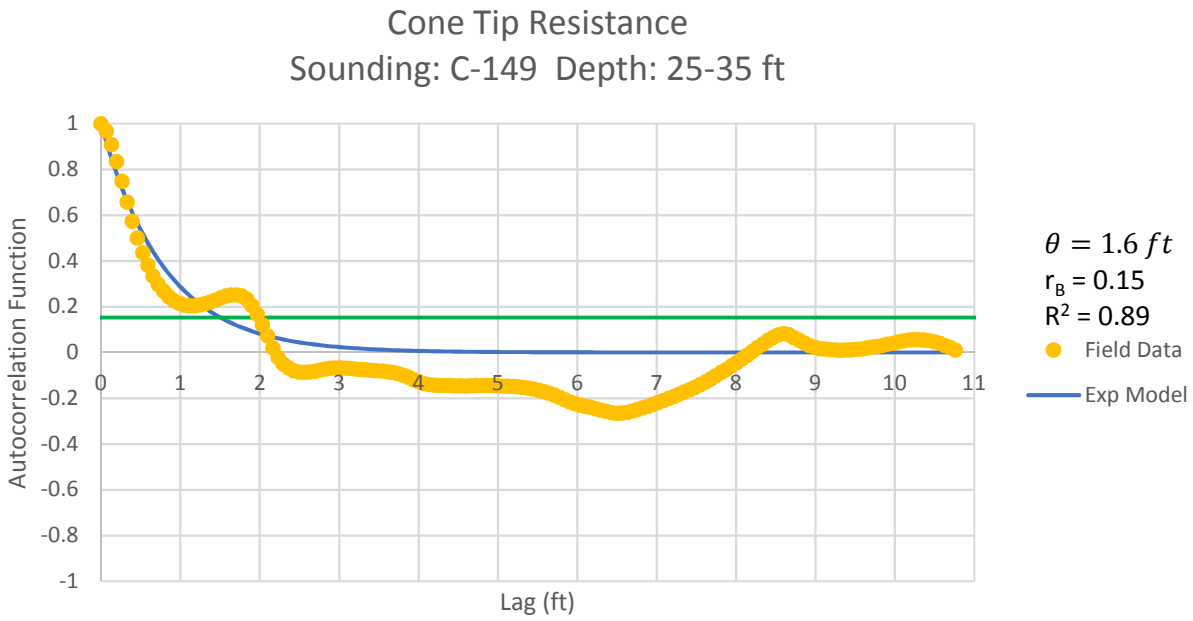

Figure B - 284: Estimation of the Scale of Fluctuation, $\theta = 1.6$ feet, for Cone Tip Resistance Data from Sounding C-149, "Clean sands to silty sands (6)" layer from 25 to 35 feet depth. Data is a poor fit for the points greater than the Bartlett limit of 0.15; coefficient of determination, R^2, value is less 0.9. Therefore, these results were not included in final analysis.

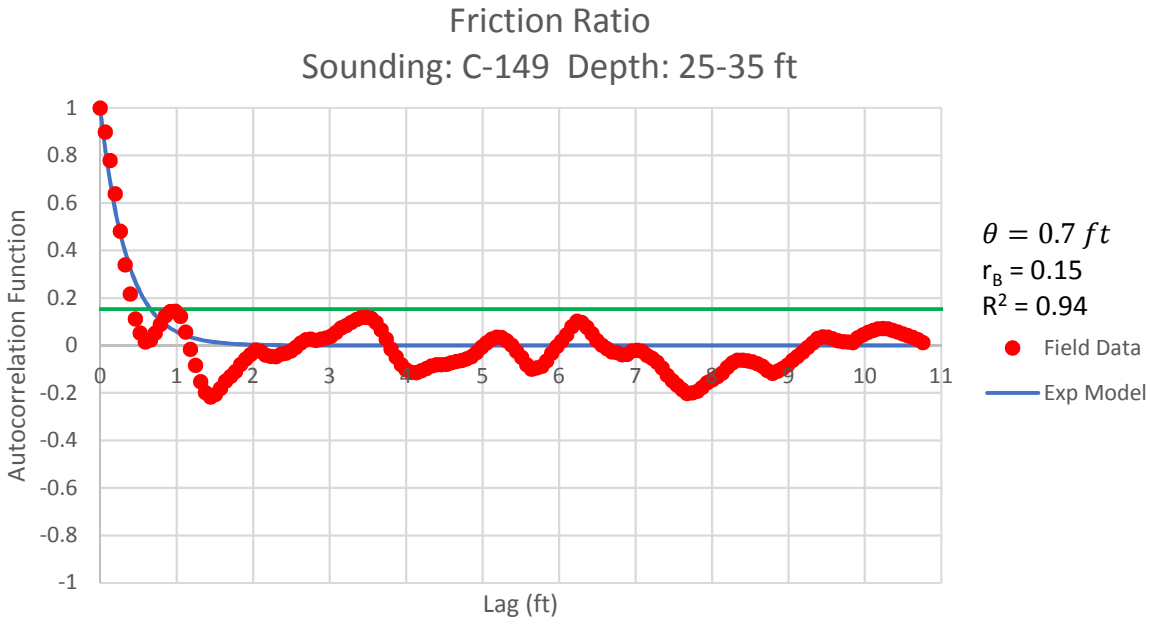

Figure B - 285: Estimation of the Scale of Fluctuation, $\theta = 0.7$ feet, for Friction Ratio Data from Sounding C-146, "Clean sands to silty sands (6)" layer from 25 to 35 feet depth.

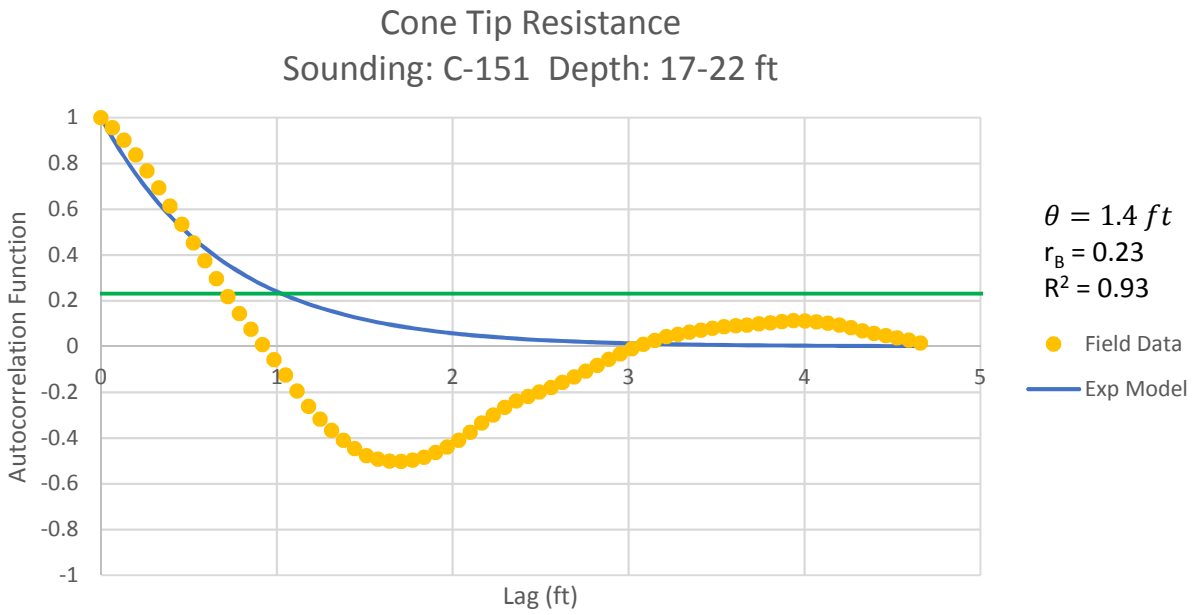

Figure B - 286: Estimation of the Scale of Fluctuation, $\theta = 1.4$ feet, for Cone Tip Resistance Data from Sounding C-151, "Clean sands to silty sands (6)" layer from 17 to 22 feet depth.

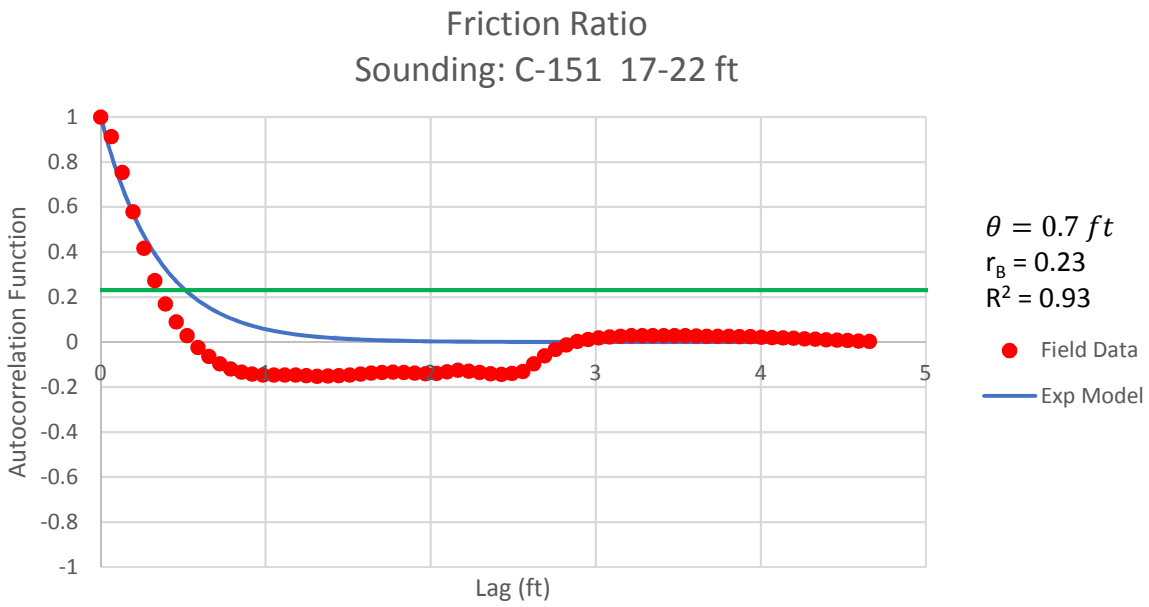

Figure B – 287: Estimation of the Scale of Fluctuation, $\theta = 0.7$ feet, for Friction Ratio Data from Sounding C-151, "Clean sands to silty sands (6)" layer from 17 to 22 feet depth.

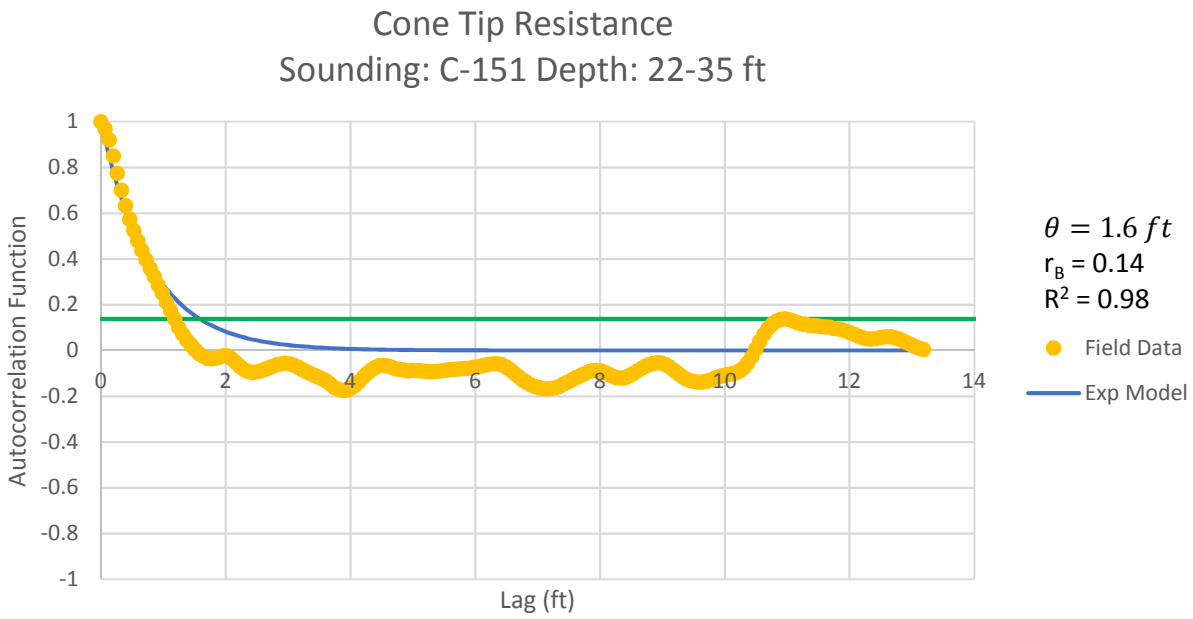

Figure B - 288: Estimation of the Scale of Fluctuation, $\theta = 1.6$ feet, for Cone Tip Resistance Data from Sounding C-151, "Clean sands to silty sands (6)" layer from 22 to 35 feet depth.

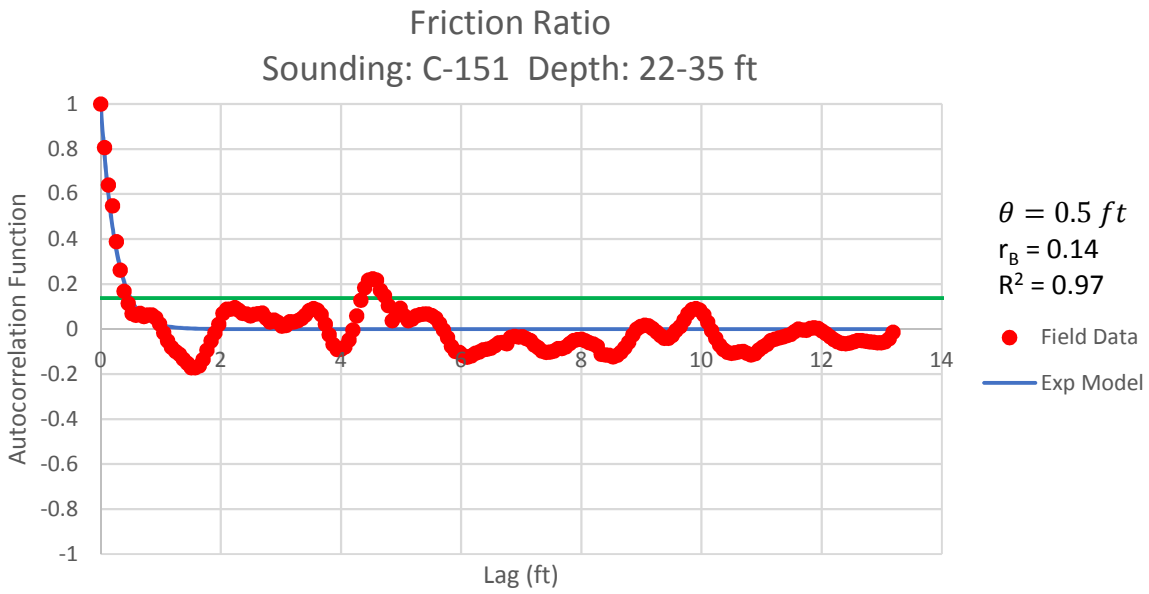

Figure B - 289: Estimation of the Scale of Fluctuation, $\theta = 0.5$ feet, for Friction Ratio Data from Sounding C-151, "Clean sands to silty sands (6)" layer from 22 to 35 feet depth.

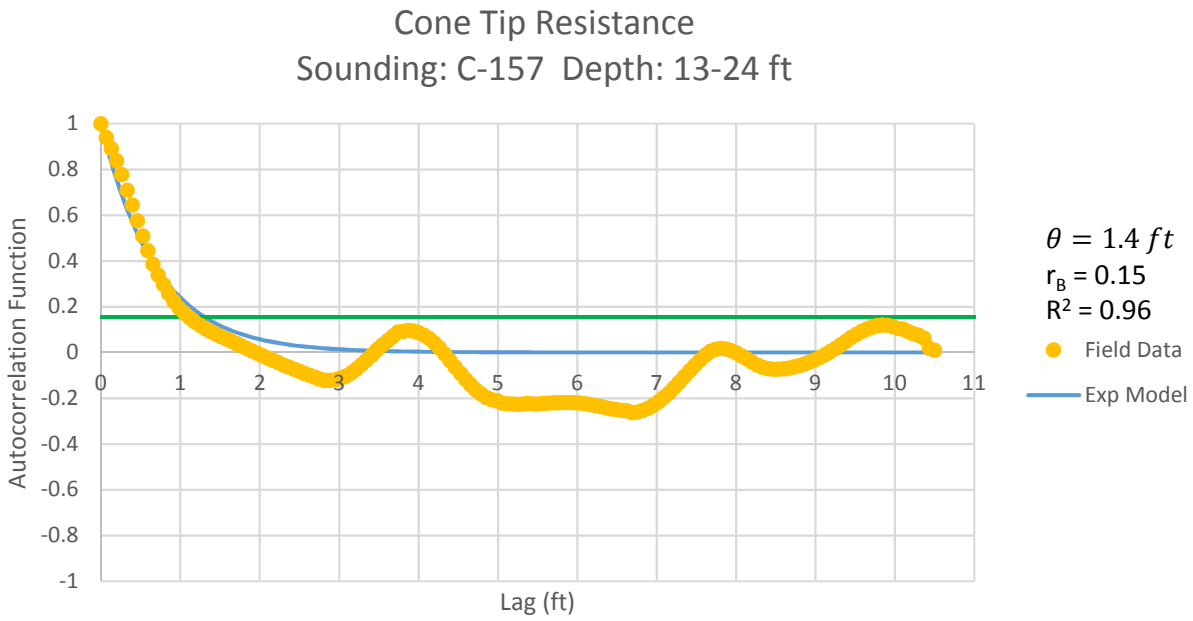

Figure B - 290: Estimation of the Scale of Fluctuation, $\theta = 1.4$ feet, for Cone Tip Resistance Data from Sounding C-157, "Gravelly sand to sand (7)" layer from 13 to 24 feet depth.

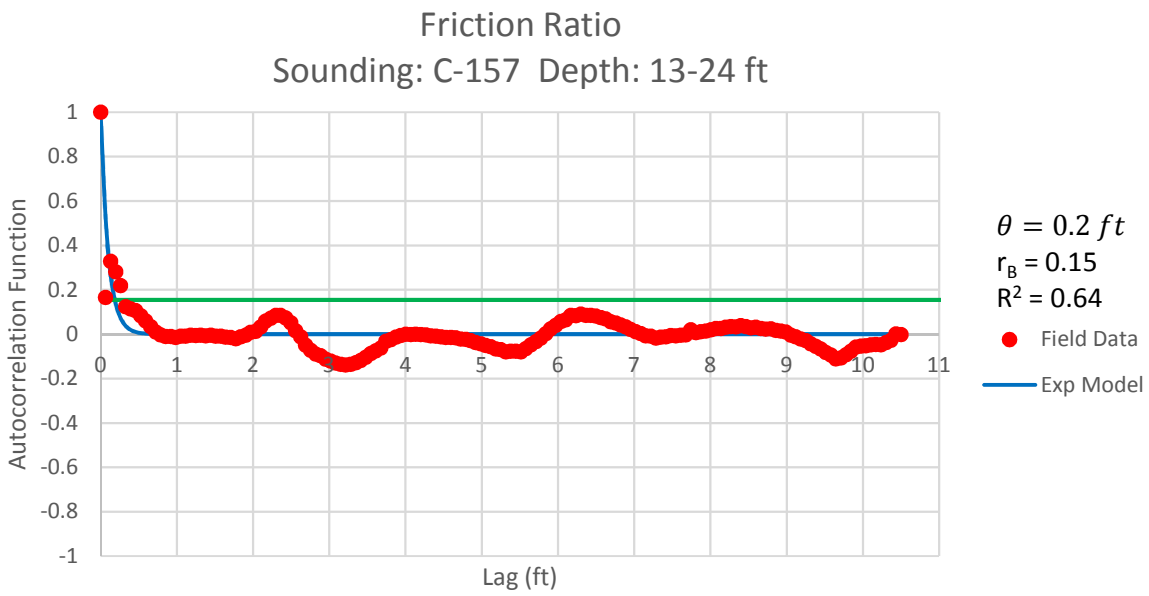

Figure B - 291: Estimation of the Scale of Fluctuation, $\theta = 0.2$ feet, for Friction Ratio Data from Sounding C-157, "Gravelly sand to sand (7)" layer from 13 to 24 feet depth. Data is a poor fit for the points greater than the Bartlett limit of 0.15; coefficient of determination, R^2, value is less 0.9. Therefore, these results were not included in final analysis.

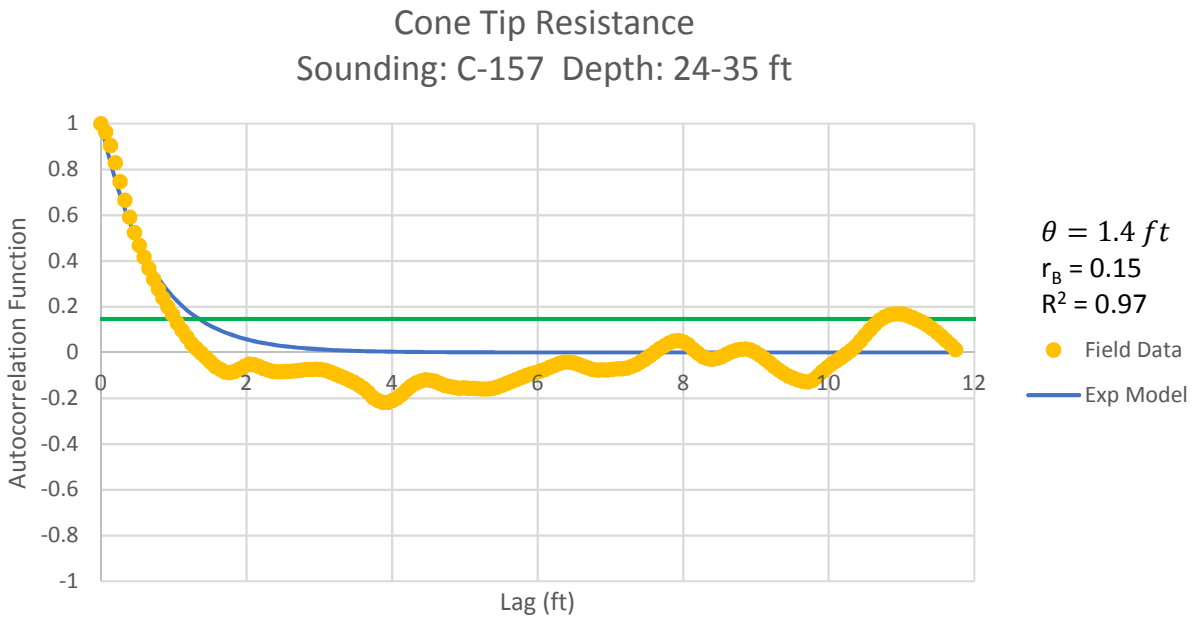

Figure B - 292: Estimation of the Scale of Fluctuation, $\theta = 1.4$ feet, for Cone Tip Resistance Data from Sounding C-157, "Clean sands to silty sands (6)" layer from 24 to 35 feet depth.

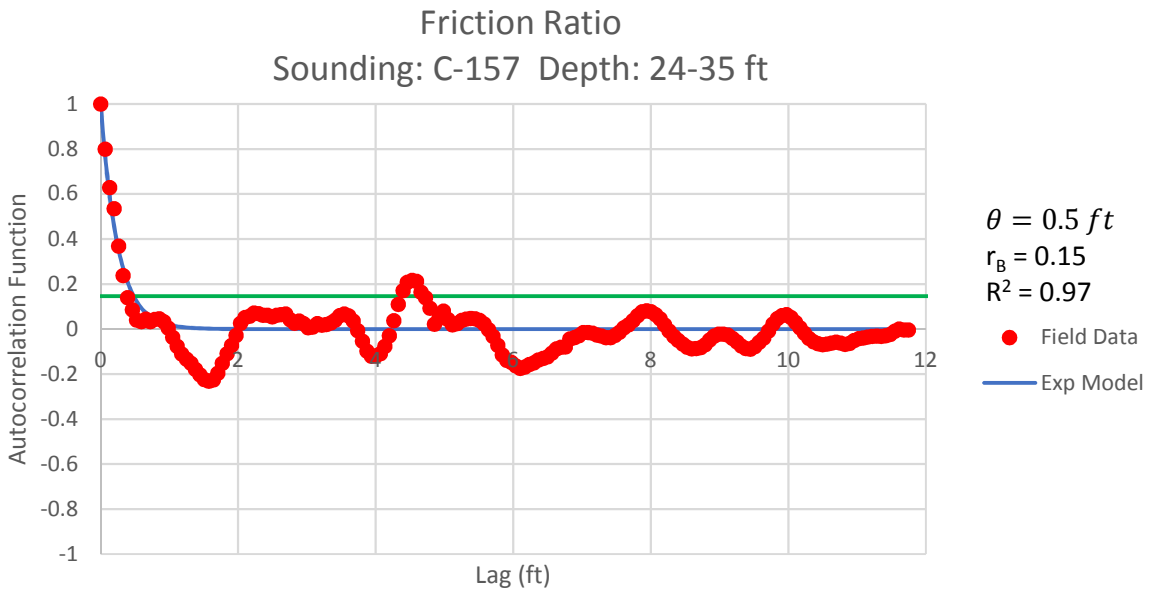

Figure B - 293: Estimation of the Scale of Fluctuation, $\theta = 0.5$ feet, for Friction Ratio Data from Sounding C-157, "Clean sands to silty sands (6)" layer from 24 to 35 feet depth..

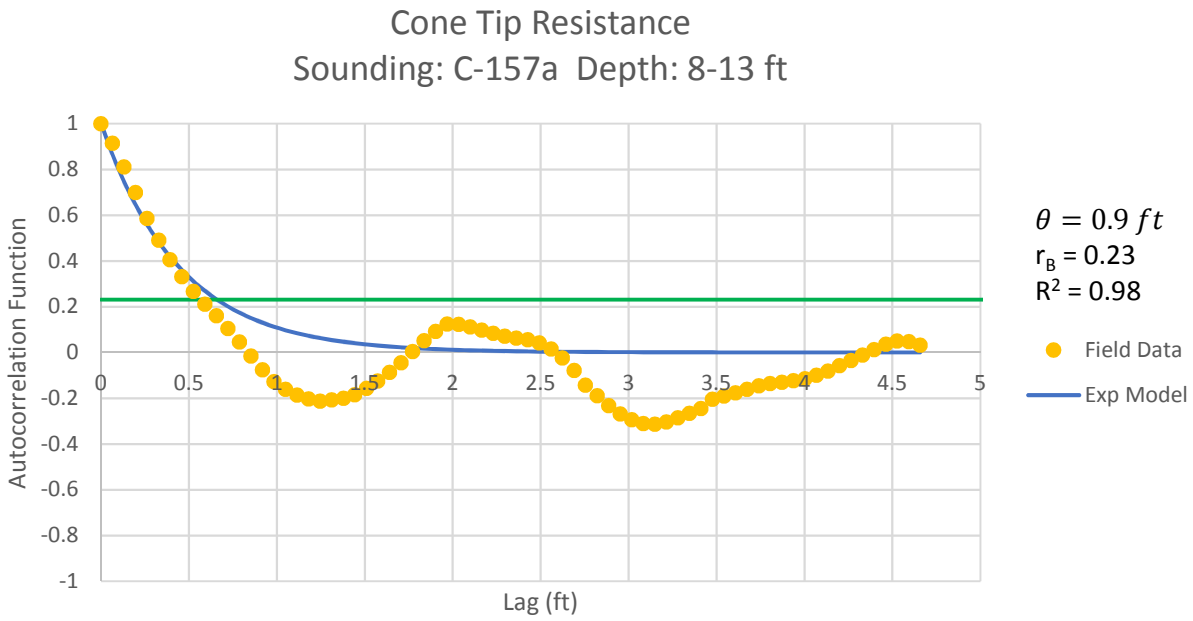

Figure B - 294: Estimation of the Scale of Fluctuation, $\theta = 0.9$ feet, for Cone Tip Resistance Data from Sounding C-157a, "Clean sands to silty sands (6)" layer from 8 to 13 feet depth.

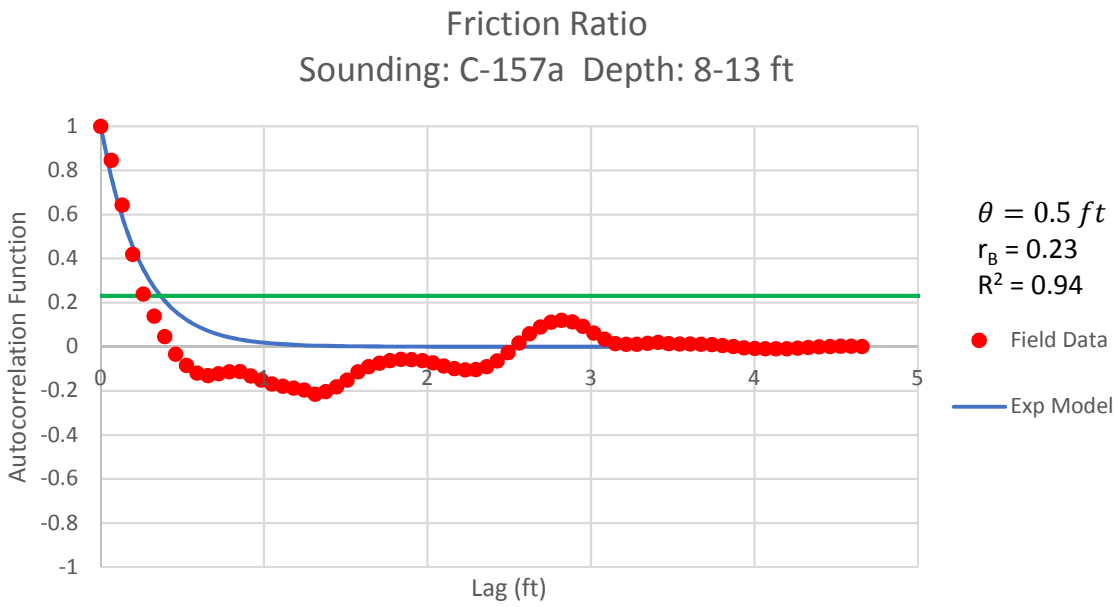

Figure B - 295: Estimation of the Scale of Fluctuation, $\theta = 0.5$ feet, for Friction Ratio Data from Sounding C-157a, "Clean sands to silty sands (6)" layer from 8 to 13 feet depth.

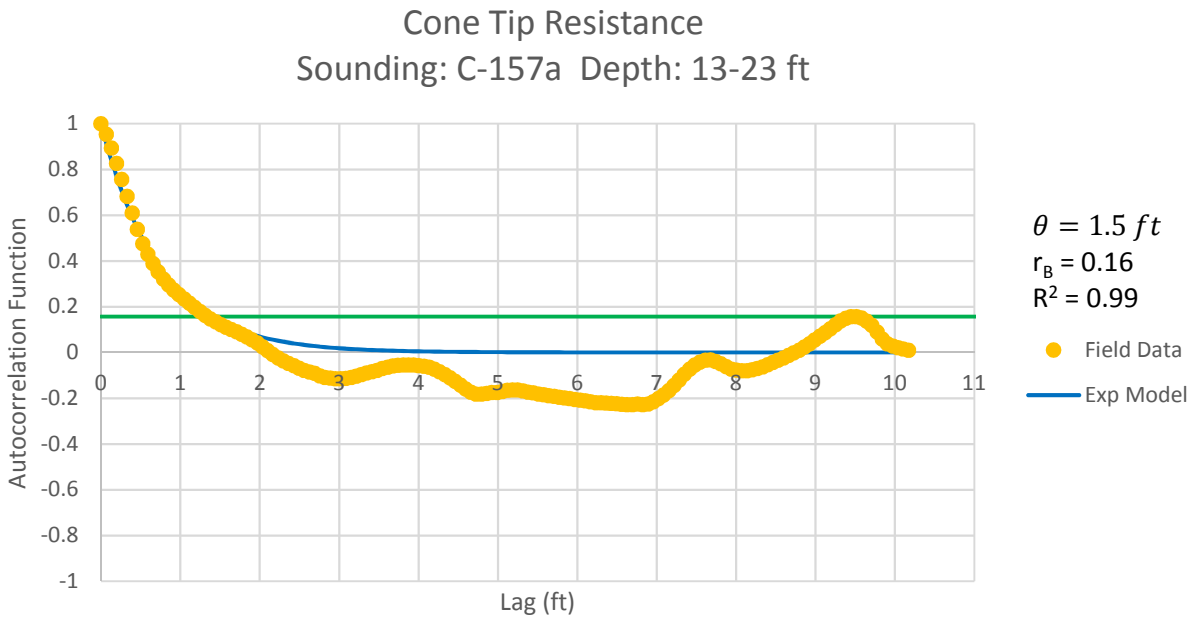

Figure B - 296: Estimation of the Scale of Fluctuation, θ = 1.5 feet, for Cone Tip Resistance Data from Sounding C-157a, "Gravelly sand to sand (7)" layer from 13 to 23 feet depth.

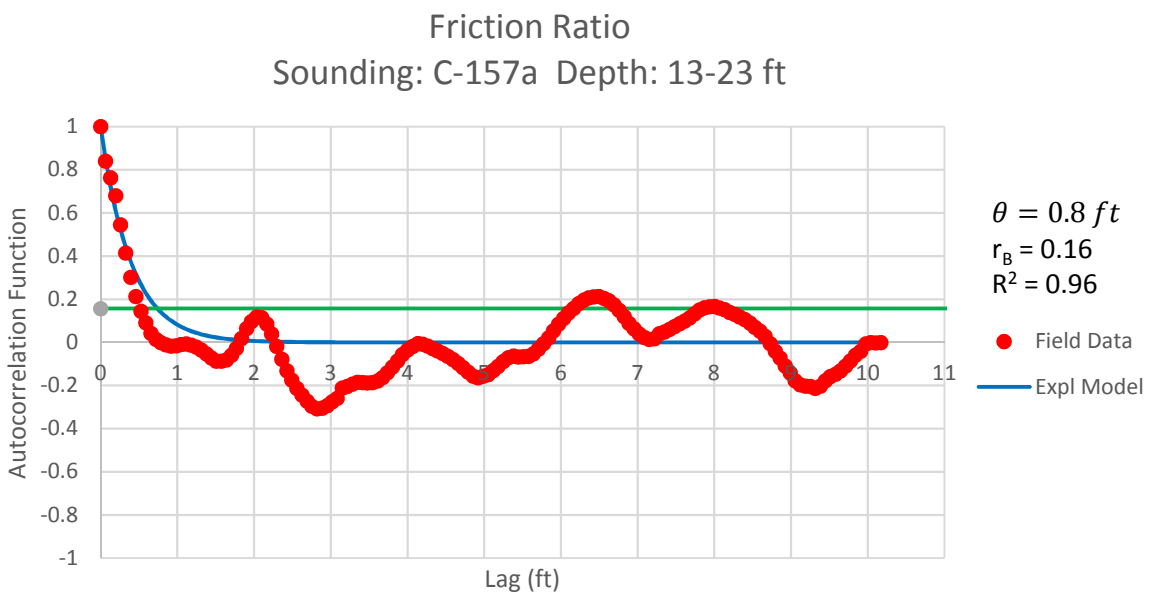

Figure B - 297: Estimation of the Scale of Fluctuation, θ = 0.8 feet, for Friction Ratio Data from Sounding C-157a, "Gravelly sand to sand (7)" layer from 13 to 23 feet depth.

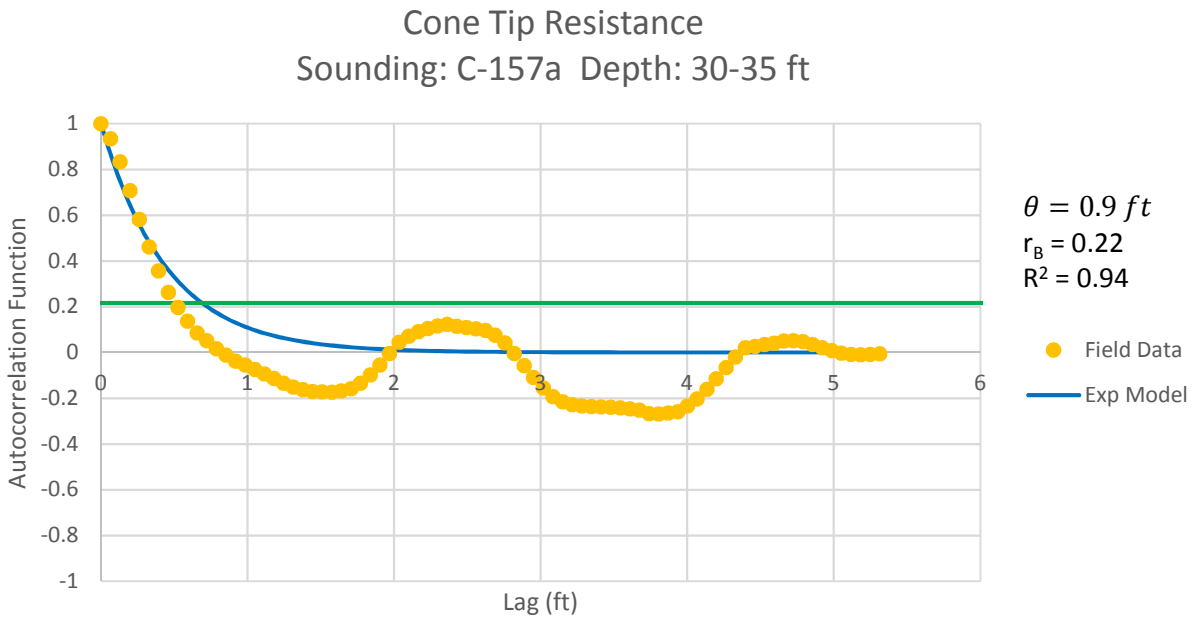

Figure B - 298: Estimation of the Scale of Fluctuation, $\theta = 0.9$ feet, for Cone Tip Resistance Data from Sounding C-157a, "Clean sands to silty sands (6)" layer from 30 to 35 feet depth.

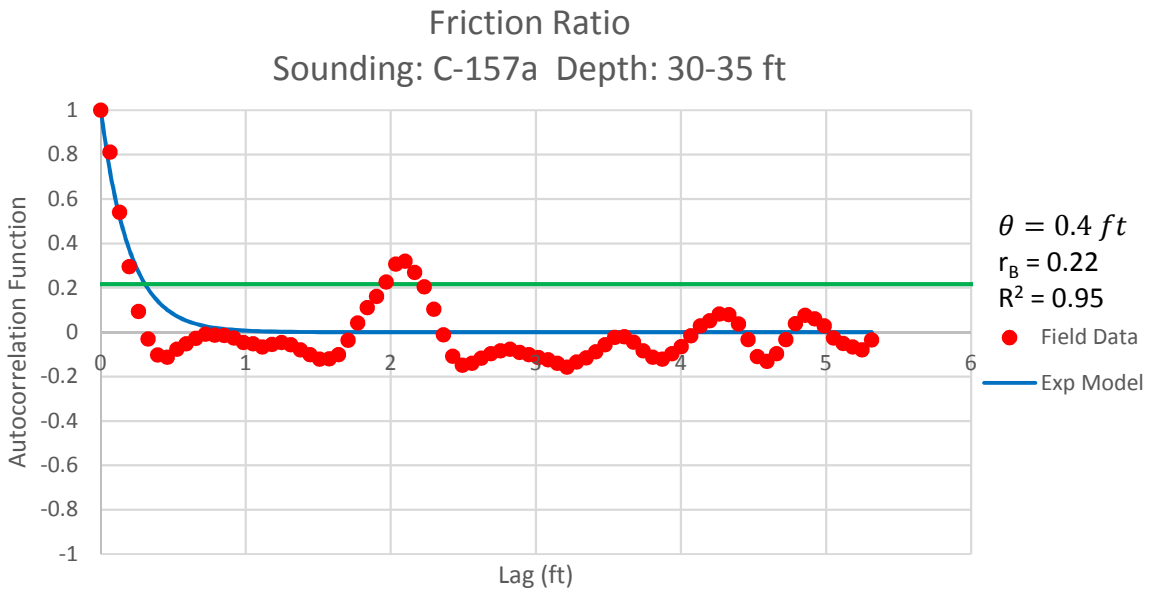

Figure B - 299: Estimation of the Scale of Fluctuation, $\theta = 0.4$ feet, for Friction Ratio Data from Sounding C-157a, "Clean sands to silty sands (6)" layer from 30 to 35 feet depth.

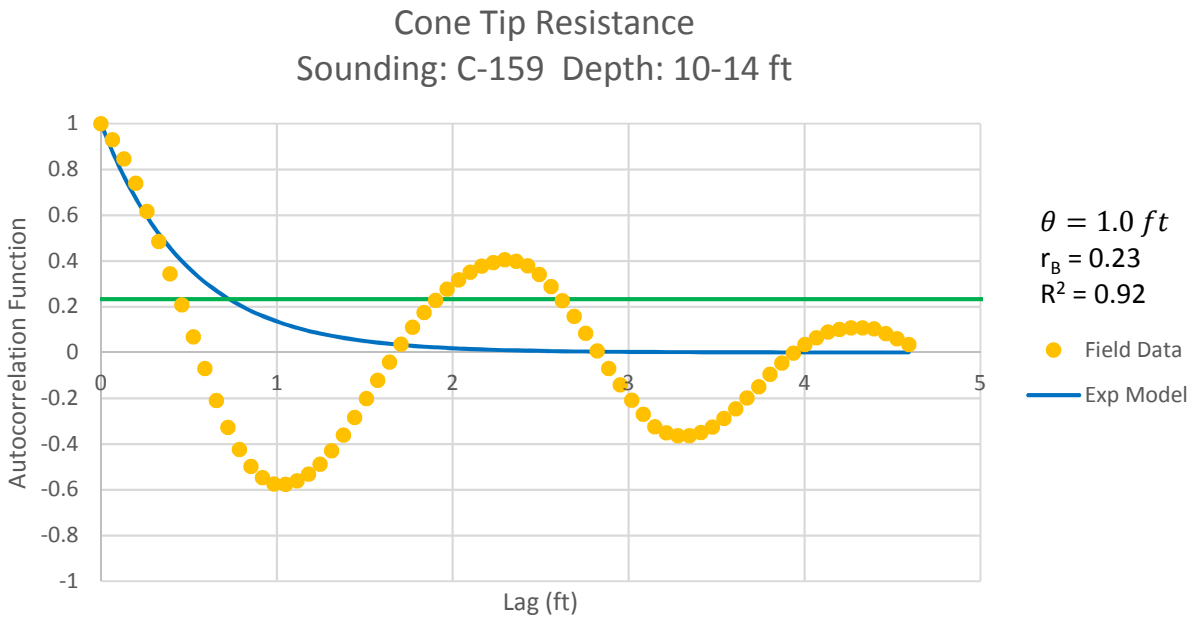

Figure B - 300: Estimation of the Scale of Fluctuation, $\theta = 1.0$ feet, for Cone Tip Resistance Data from Sounding C-159, "Clean sands to silty sands (6)" layer from 10 to 14 feet depth.

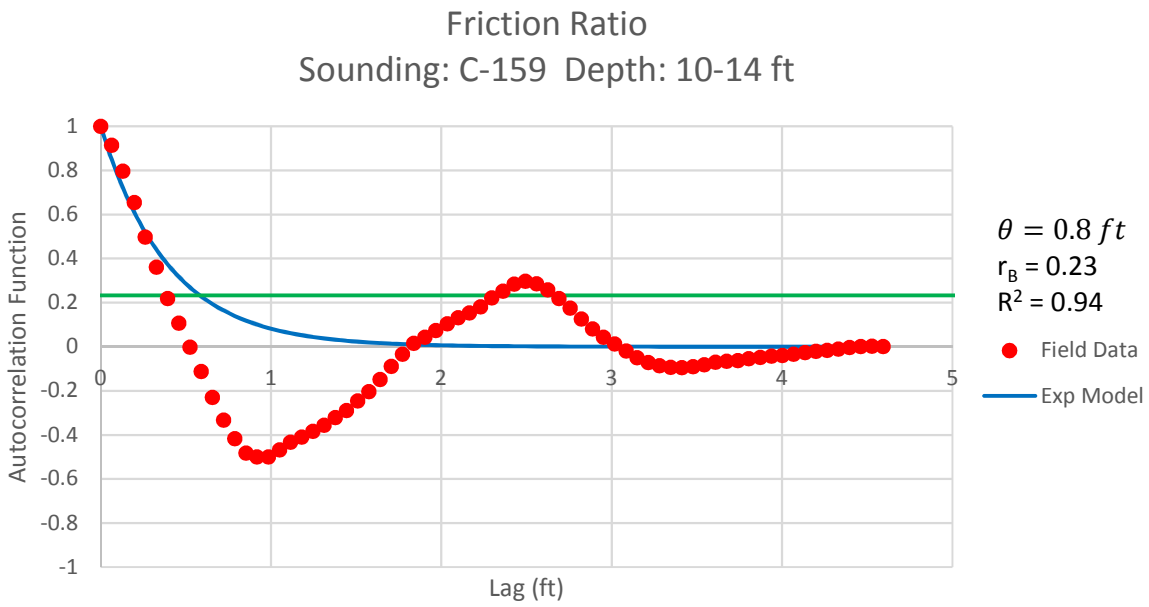

Figure B - 301: Estimation of the Scale of Fluctuation, $\theta = 0.8$ feet, for Friction Ratio Data from Sounding C-159, "Clean sands to silty sands (6)" layer from 10 to 14 feet depth.

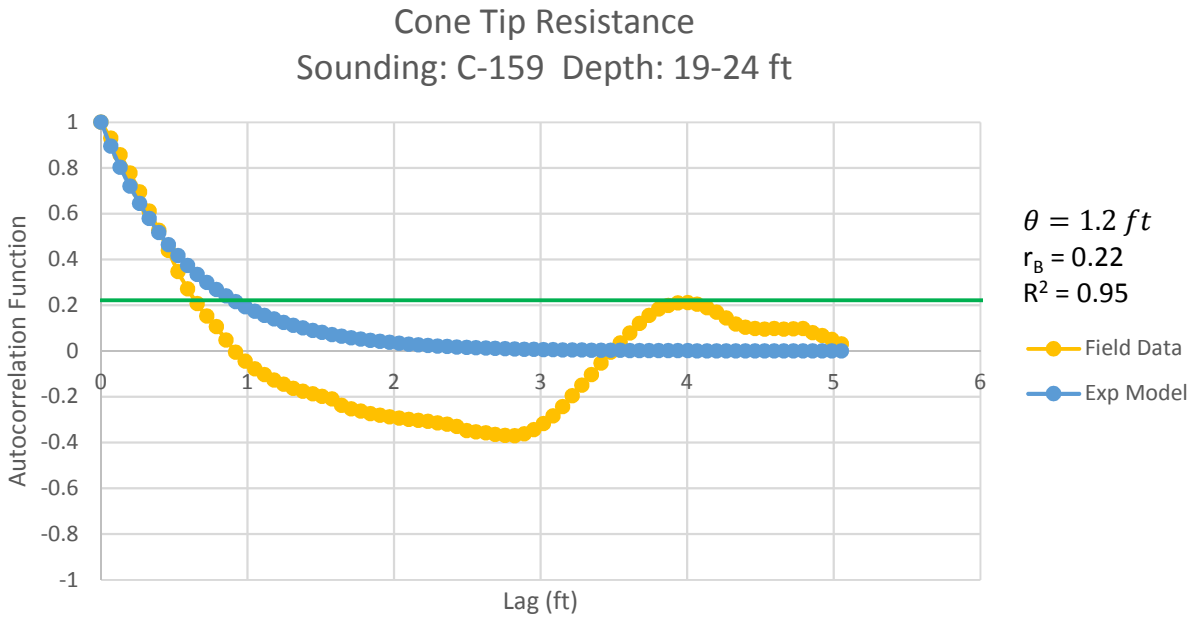

Figure B - 302: Estimation of the Scale of Fluctuation, $\theta = 1.2$ feet, for Cone Tip Resistance Data from Sounding C-159, "Gravelly sand to sand (7)" layer from 19 to 24 feet depth.

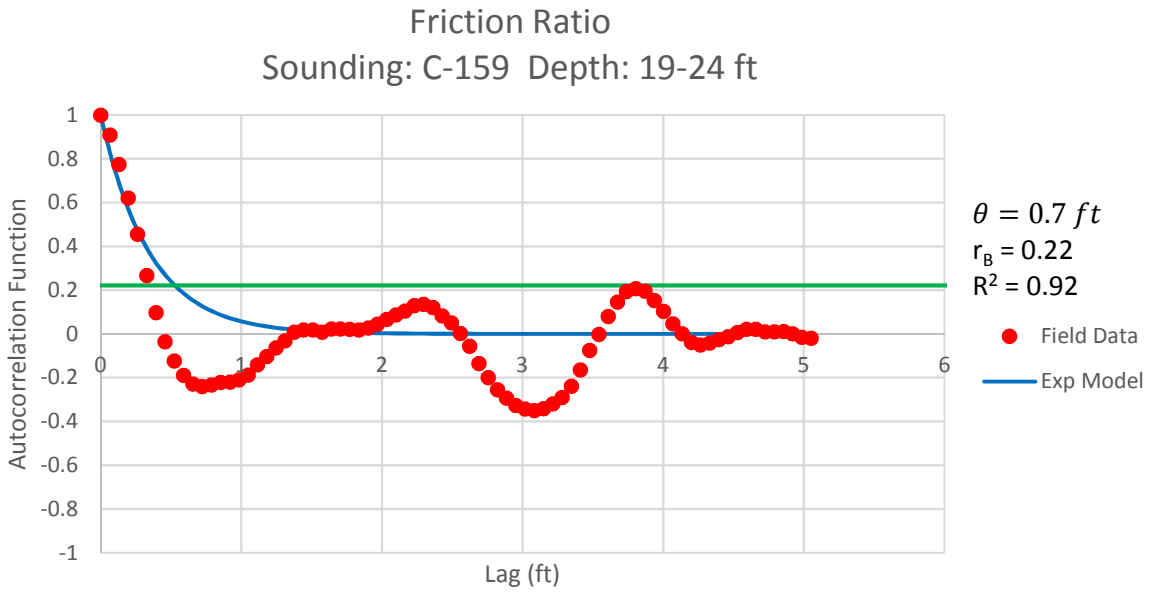

Figure B - 303: Estimation of the Scale of Fluctuation, $\theta = 0.8$ feet, for Friction Ratio Data from Sounding C-159, "Gravelly sand to sand (7)" layer from 19 to 24 feet depth.

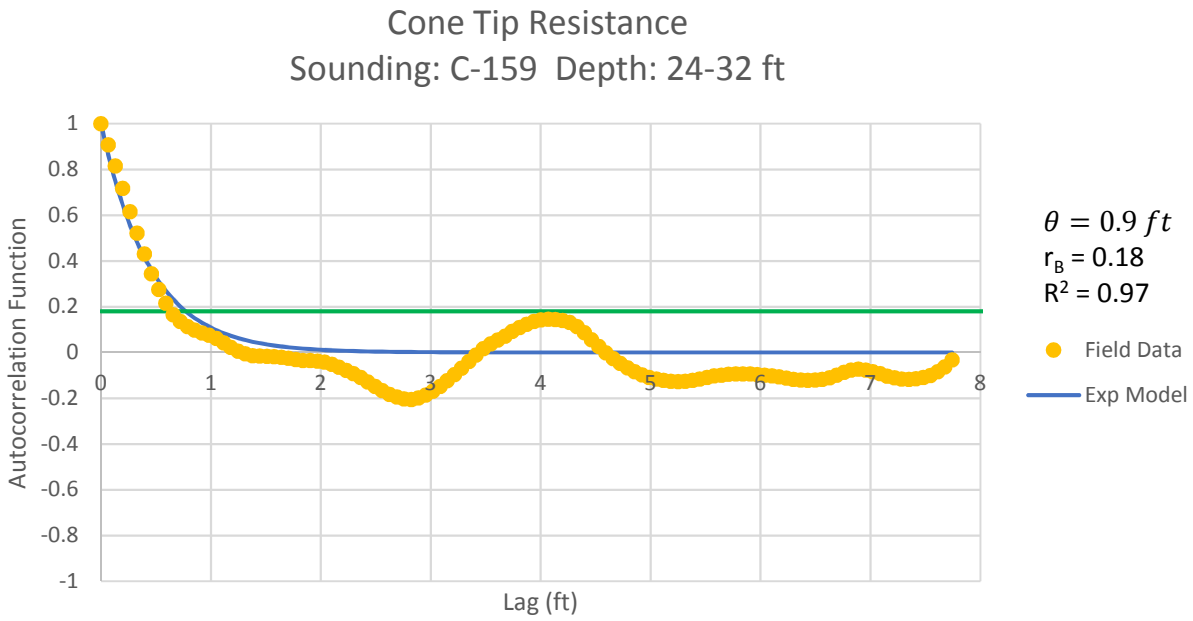

Figure B - 304: Estimation of the Scale of Fluctuation, $\theta = 0.9$ feet, for Cone Tip Resistance Data from Sounding C-159, "Clean sands to silty sands (6)" layer from 24 to 32 feet depth.

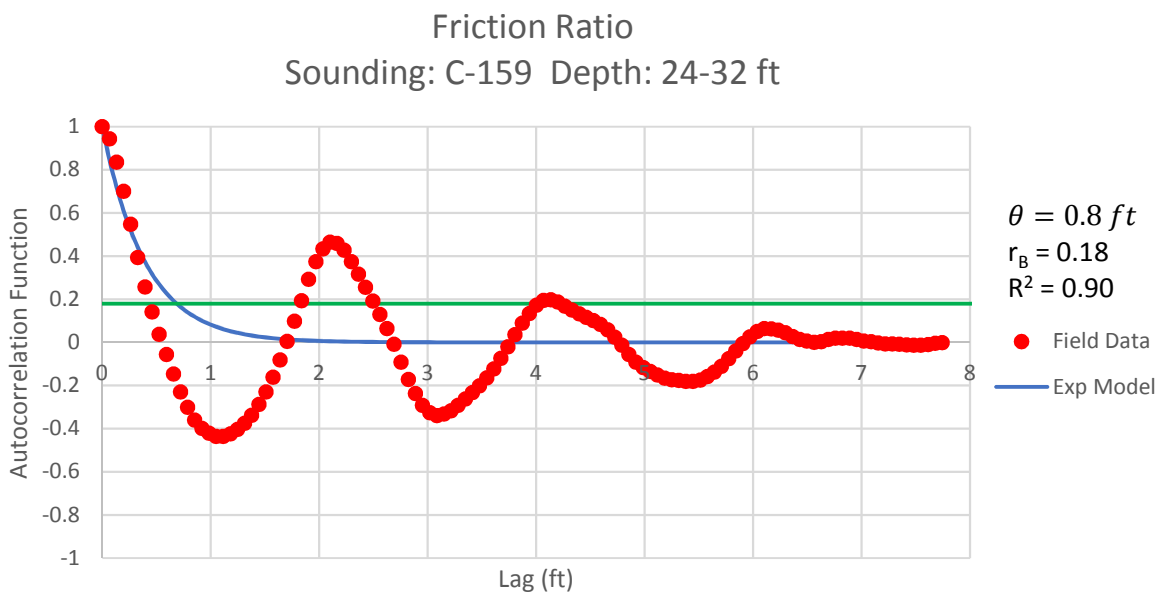

Figure B - 305: Estimation of the Scale of Fluctuation, $\theta = 0.8$ feet, for Friction Ratio Data from Sounding C-159, "Clean sands to silty sands (6)" layer from 24 to 32 feet depth.

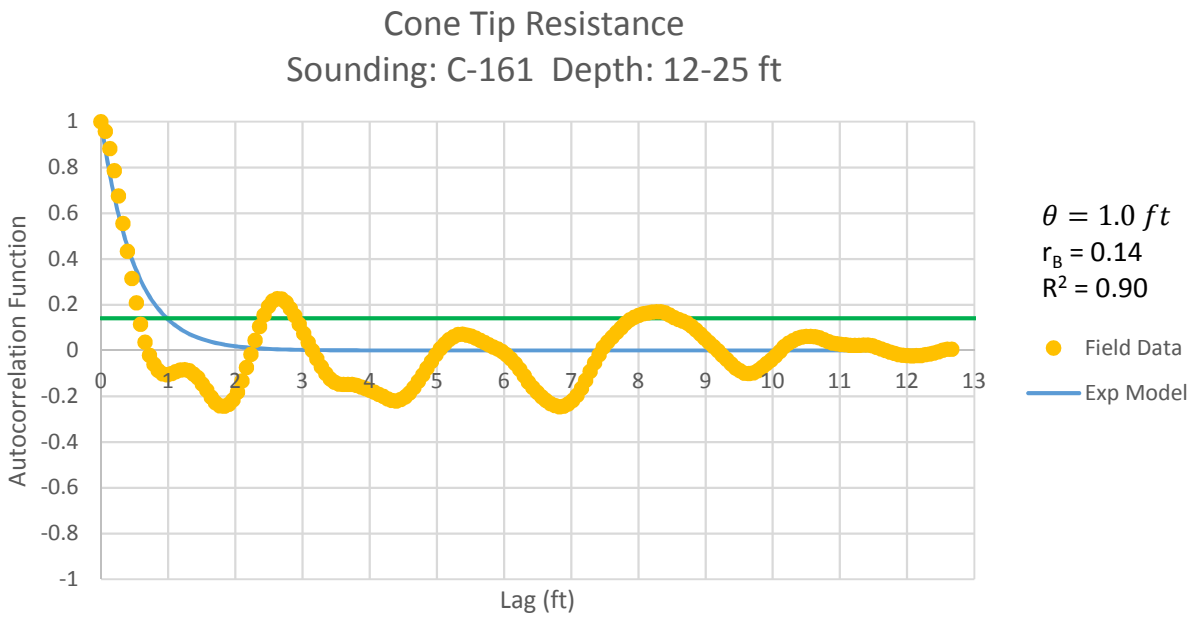

Figure B - 306: Estimation of the Scale of Fluctuation, $\theta = 1.0$ feet, for Cone Tip Resistance Data from Sounding C-161, "Clean sands to silty sands (6)" layer from 12 to 25 feet depth.

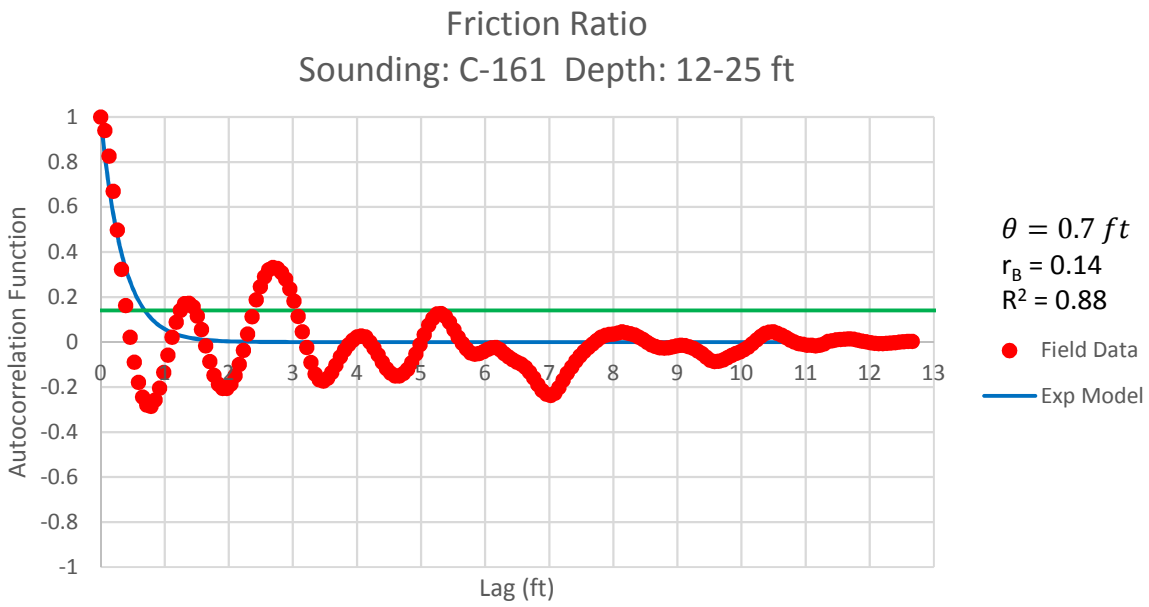

Figure B - 307: Estimation of the Scale of Fluctuation, $\theta = 0.7$ feet, for Friction Ratio Data from Sounding C-161, "Clean sands to silty sands (6)" layer from 12 to 25 feet depth. Data is a poor fit for the points greater than the Bartlett limit of 0.14; coefficient of determination, R^2, value is less 0.9. Therefore, these results were not included in final analysis.

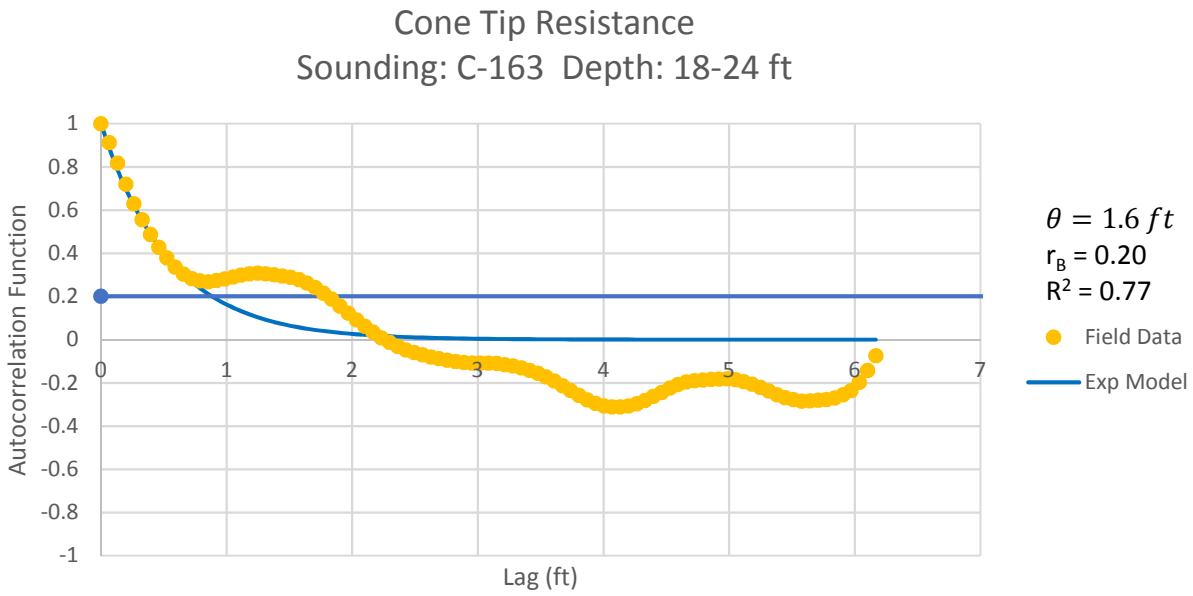

Figure B - 308: Estimation of the Scale of Fluctuation, θ = 1.6 feet, for Cone Tip Resistance Data from Sounding C-163, "Clean sands to silty sands (6)" layer from 18 to 24 feet depth. Data is a poor fit for the points greater than the Bartlett limit of 0.20; coefficient of determination, R^2, value is less 0.9. Therefore, these results were not included in final analysis.

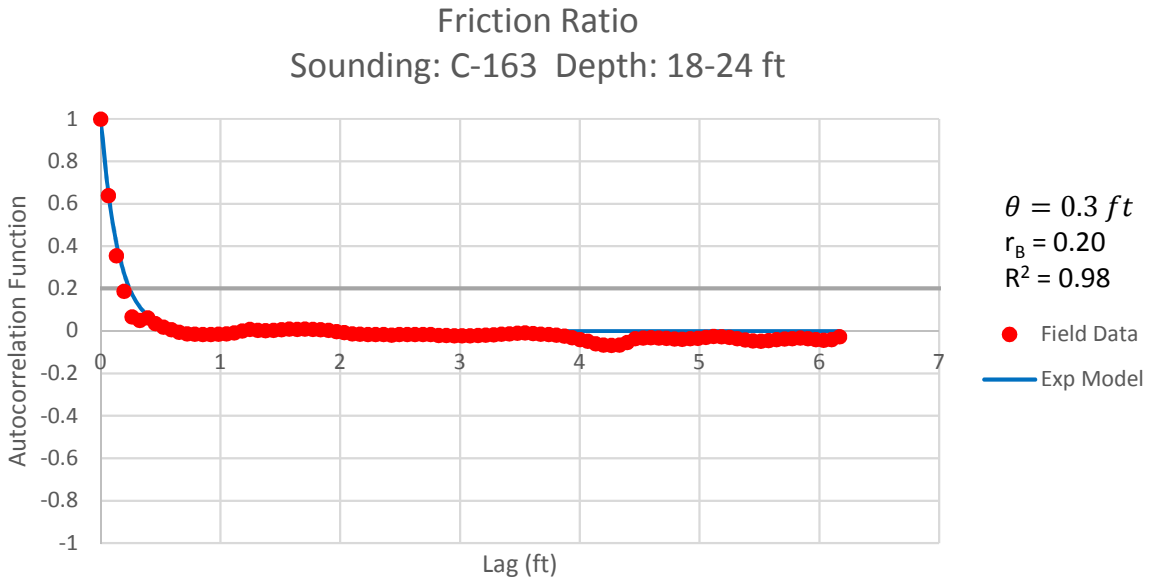

Figure B - 309: Estimation of the Scale of Fluctuation, θ, for Friction Ratio Data from Sounding C-163, "Clean sands to silty sands (6)" layer from 18 to 24 feet depth. Data is limited to only 3 points greater than the Bartlett limit of 0.20; therefore, θ could not be estimated, and these results were not included in final analysis.

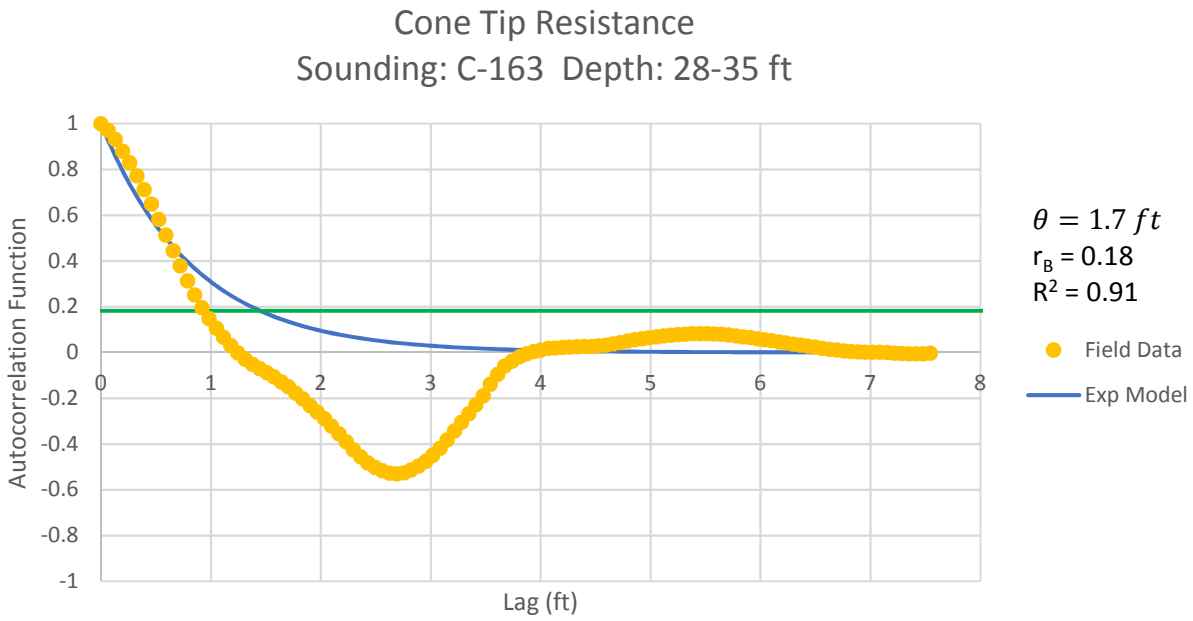

Figure B - 310: Estimation of the Scale of Fluctuation, $\theta = 1.7$ feet, for Cone Tip Resistance Data from Sounding C-163, "Clean sands to silty sands (6)" layer from 28 to 35 feet depth.

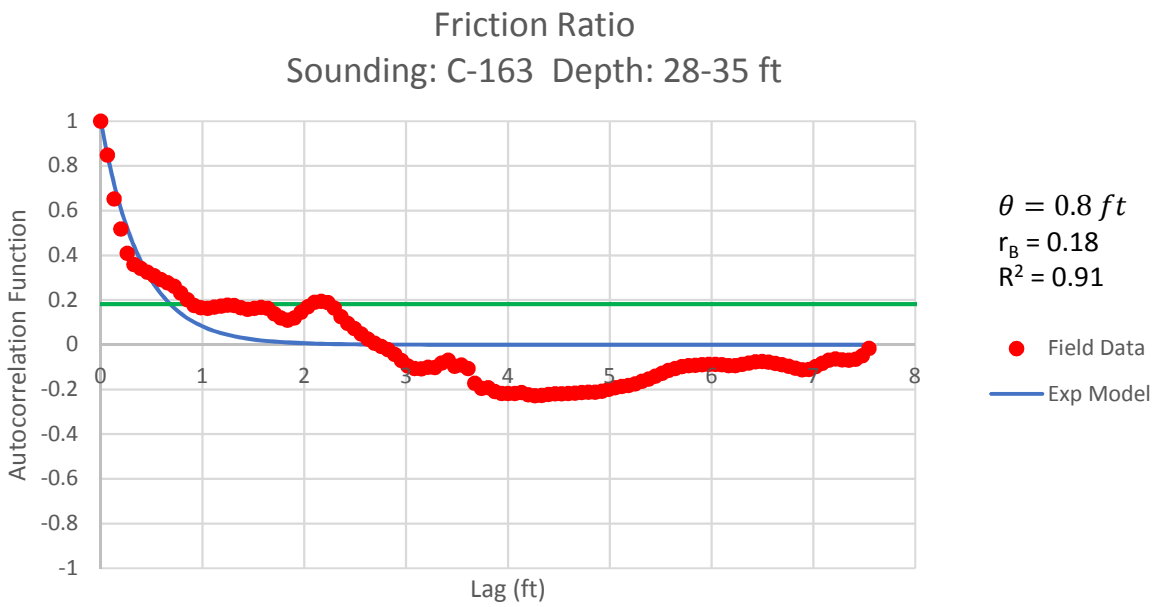

Figure B - 311: Estimation of the Scale of Fluctuation, $\theta = 0.8$ feet, for Friction Ratio Data from Sounding C-163, "Clean sands to silty sands (6)" layer from 28 to 35 feet depth.

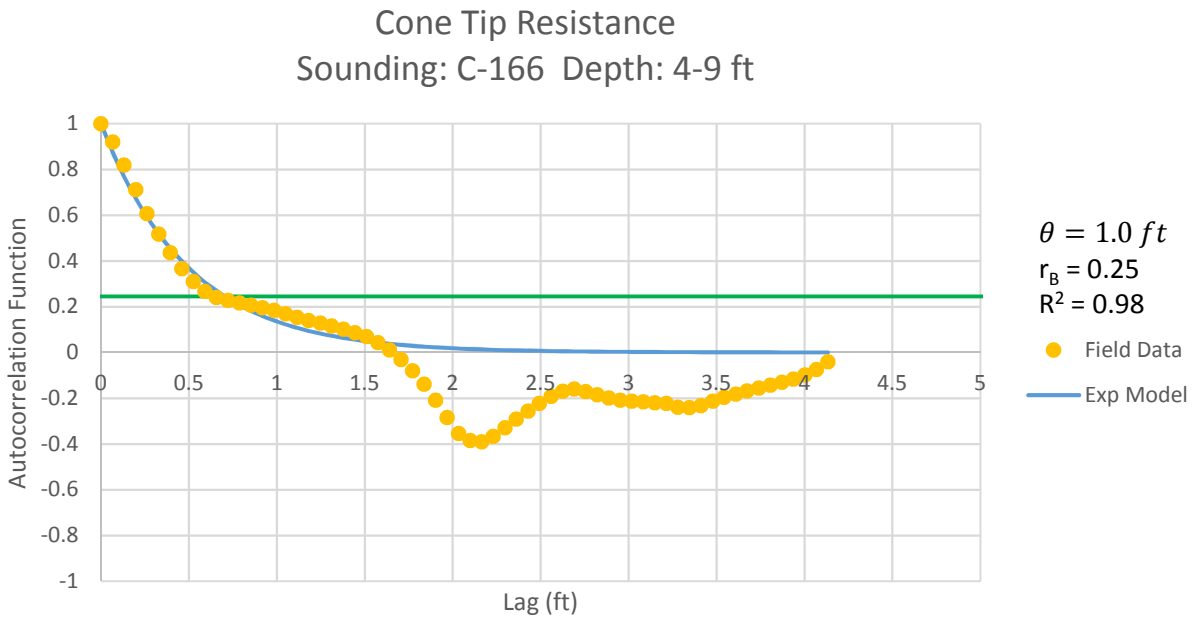

Figure B - 312: Estimation of the Scale of Fluctuation, $\theta = 1.0$ feet, for Cone Tip Resistance Data from Sounding C-166, "Clean sands to silty sands (6)" layer from 4 to 9 feet depth.

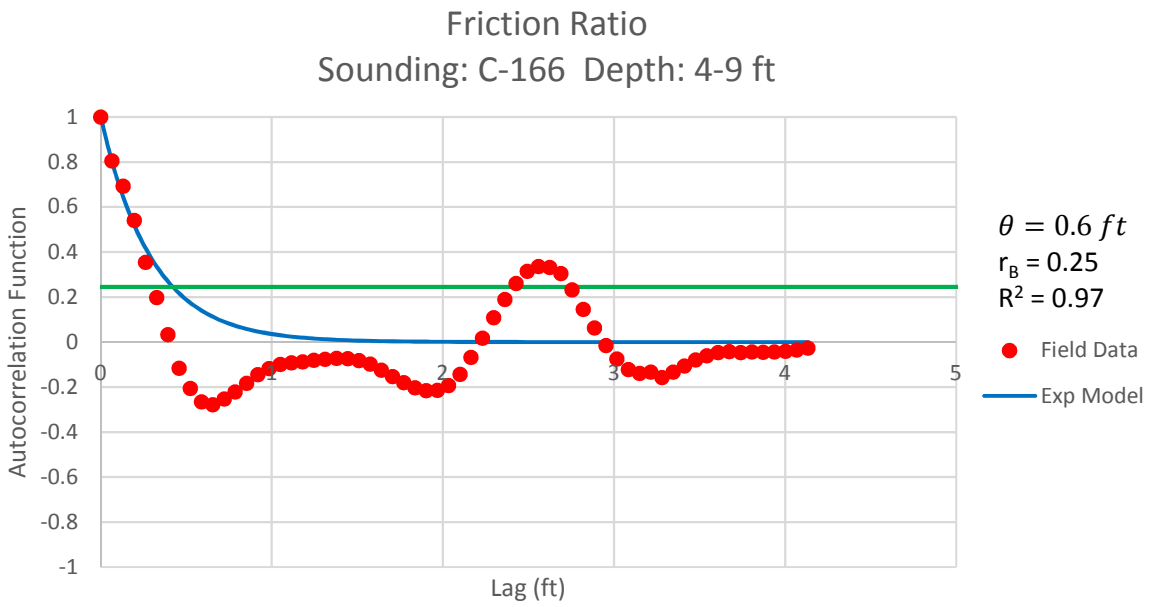

Figure B - 313: Estimation of the Scale of Fluctuation, $\theta = 0.6$ feet, for Friction Ratio Data from Sounding C-166, "Clean sands to silty sands (6)" layer from 4 to 9 feet depth.

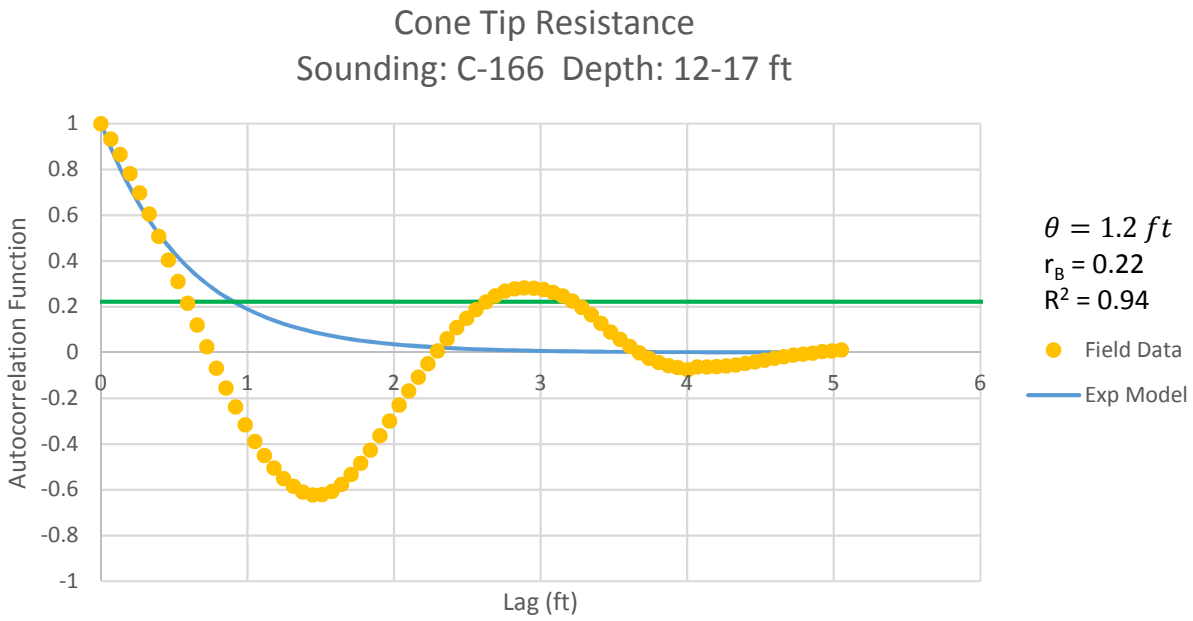

Figure B - 314: Estimation of the Scale of Fluctuation, $\theta = 1.2$ feet, for Cone Tip Resistance Data from Sounding C-166, "Clean sands to silty sands (6)" layer from 12 to 17 feet depth.

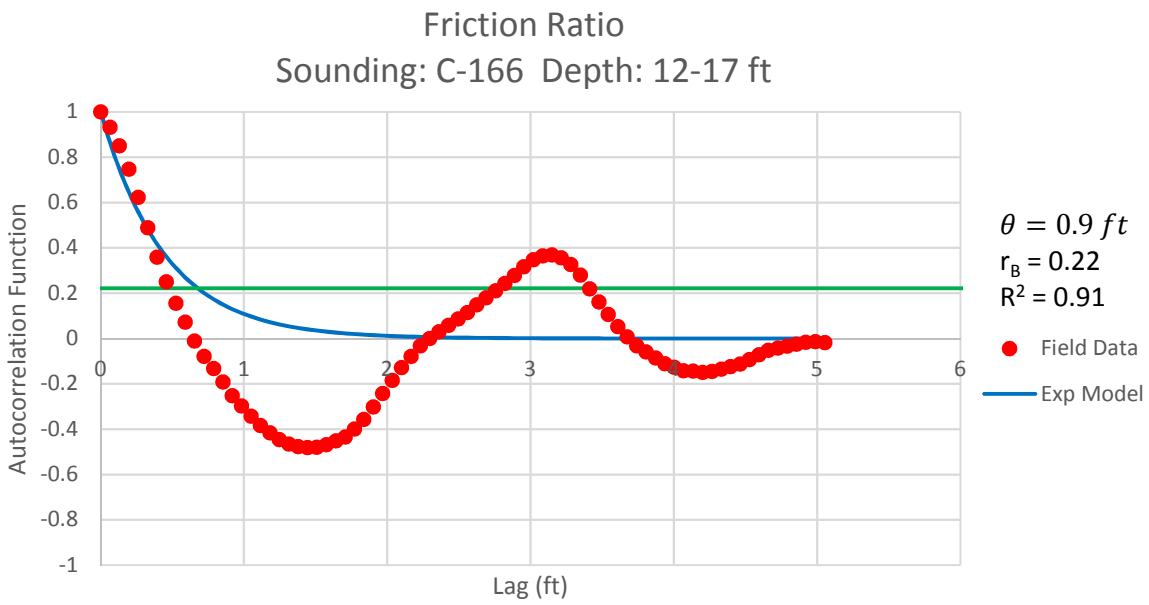

Figure B - 315: Estimation of the Scale of Fluctuation, $\theta = 0.9$ feet, for Friction Ratio Data from Sounding C-166, "Clean sands to silty sands (6)" layer from 12 to 17 feet depth.

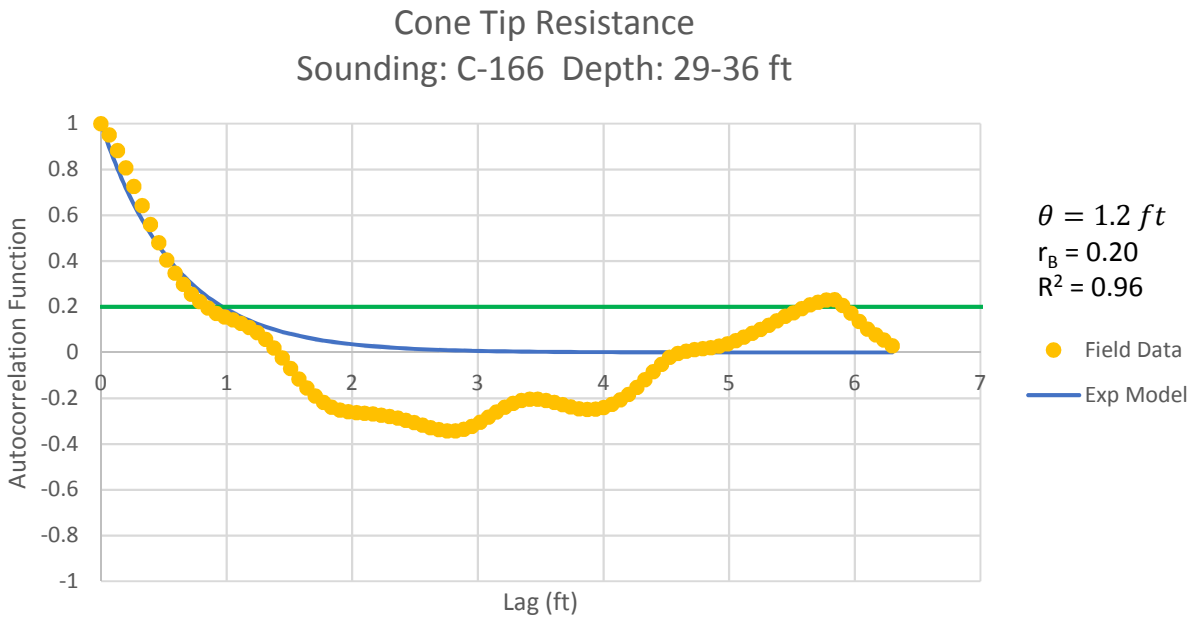

Figure B - 316: Estimation of the Scale of Fluctuation, $\theta = 1.2$ feet, for Cone Tip Resistance Data from Sounding C-166, "Clean sands to silty sands (6)" layer from 29 to 36 feet depth.

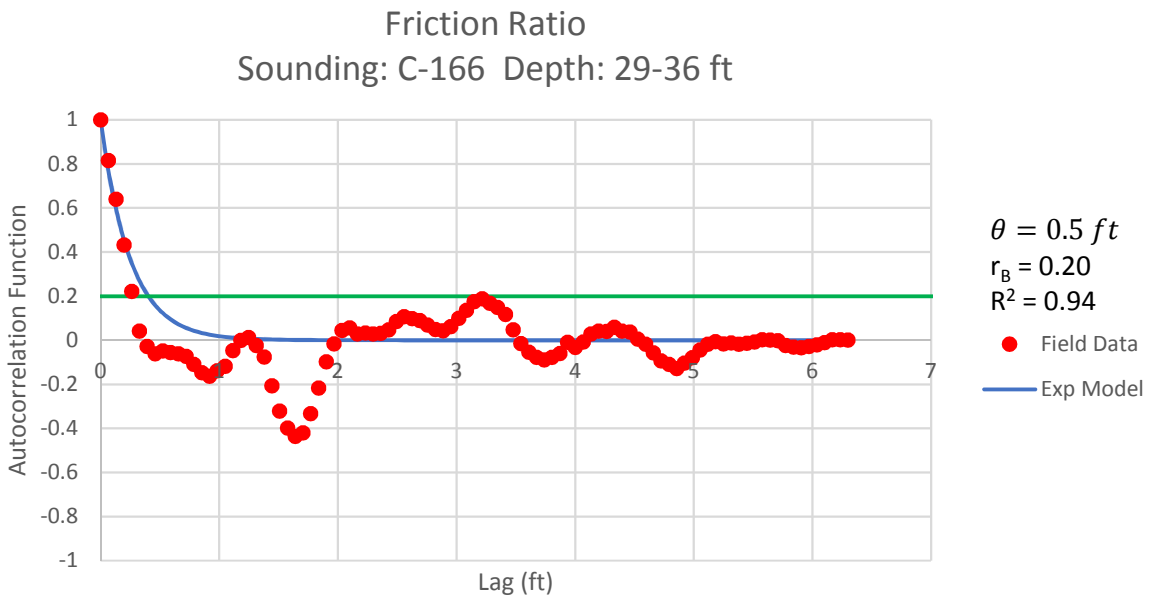

Figure B - 317: Estimation of the Scale of Fluctuation, $\theta = 0.5$ feet, for Friction Ratio Data from Sounding C-166, "Clean sands to silty sands (6)" layer from 29 to 36 feet depth.

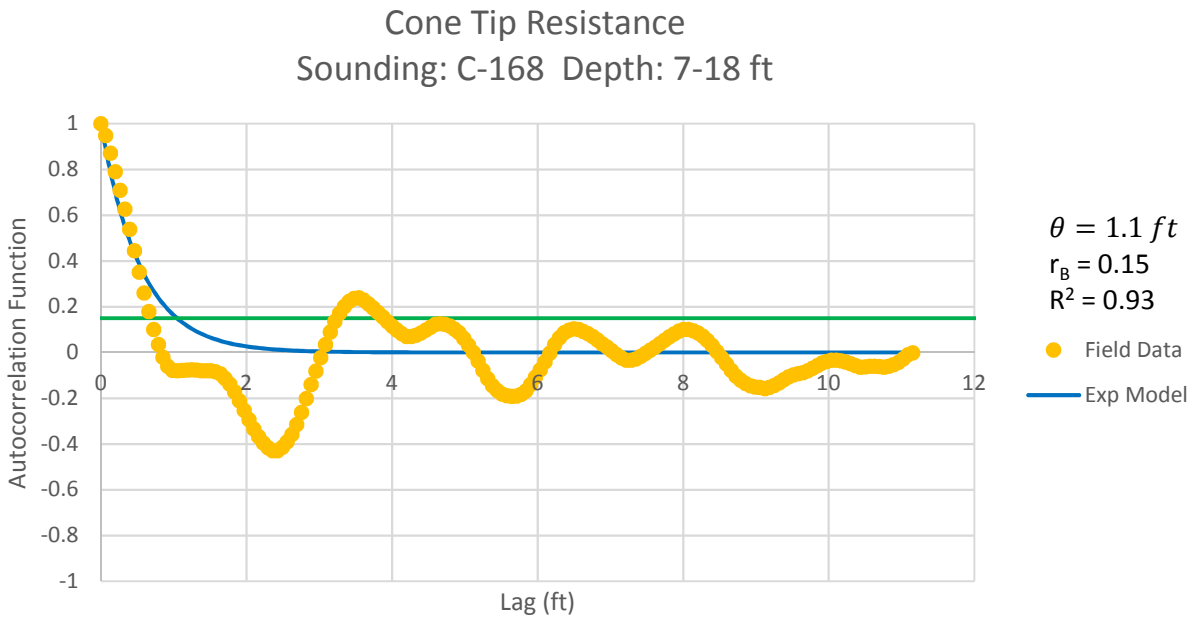

Figure B - 318: Estimation of the Scale of Fluctuation, θ = 1.1 feet, for Cone Tip Resistance Data from Sounding C-168, "Clean sands to silty sands (6)" layer from 7 to 18 feet depth.

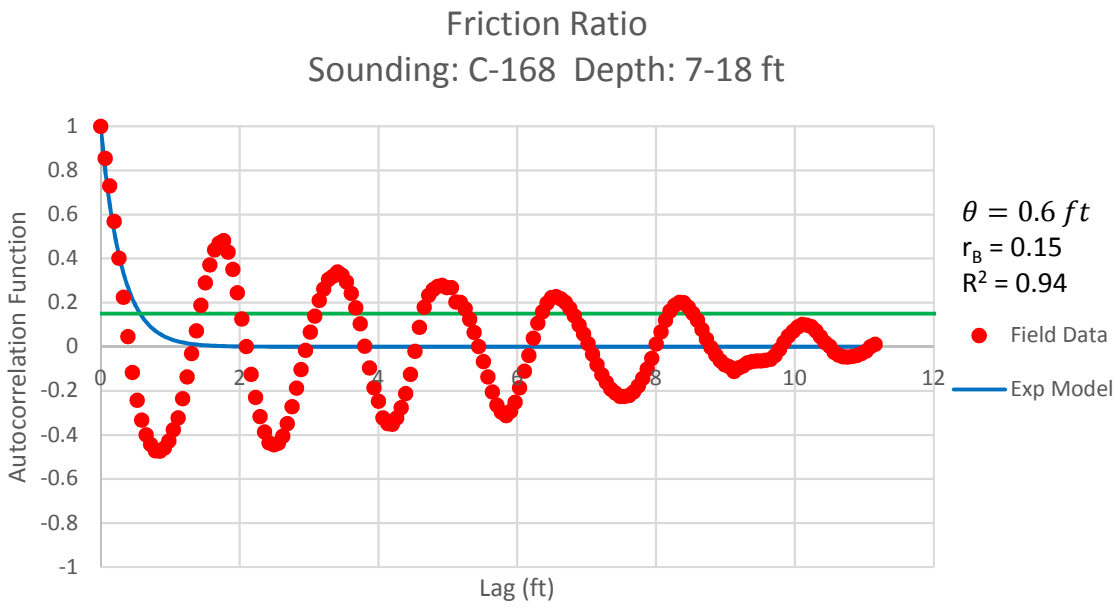

Figure B - 319: Estimation of the Scale of Fluctuation, θ = 0.6 feet, for Friction Ratio Data from Sounding C-168, "Clean sands to silty sands (6)" layer from 7 to 18 feet depth.

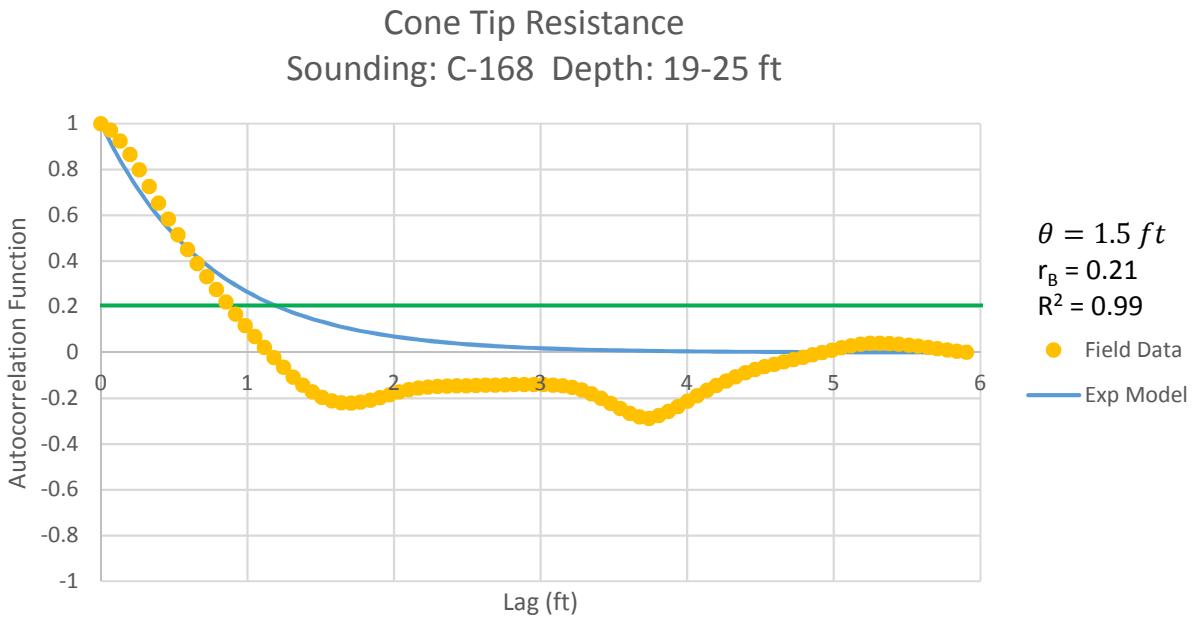

Figure B - 320: Estimation of the Scale of Fluctuation, $\theta = 1.5$ feet, for Cone Tip Resistance Data from Sounding C-168, "Clean sands to silty sands (6)" layer from 19 to 25 feet depth.

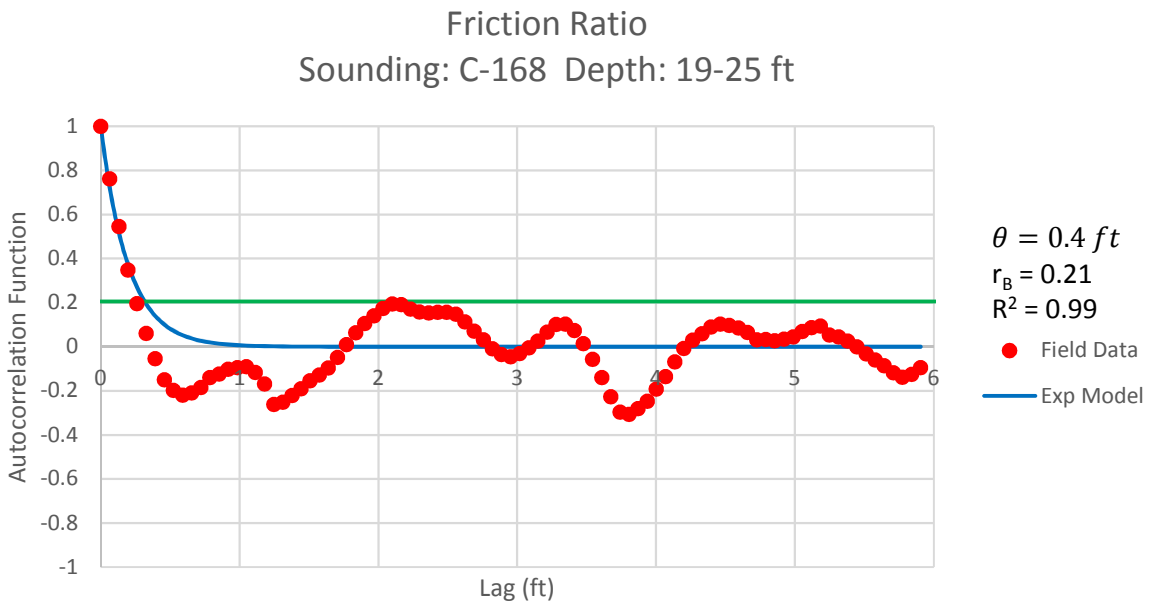

Figure B - 321: Estimation of the Scale of Fluctuation, $\theta = 0.4$ feet, for Friction Ratio Data from Sounding C-168, "Clean sands to silty sands (6)" layer from 19 to 25 feet depth.

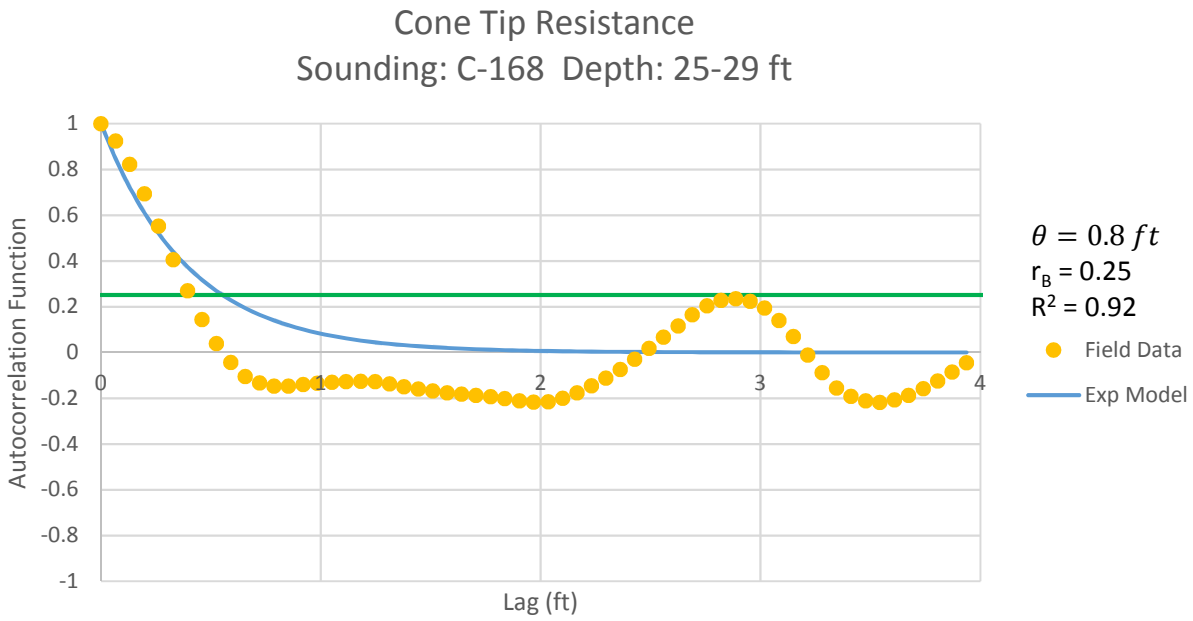

Figure B - 322: Estimation of the Scale of Fluctuation, $\theta = 0.8$ feet, for Cone Tip Resistance Data from Sounding C-168, "Gravelly sand to sand (7)" layer from 25 to 29 feet depth.

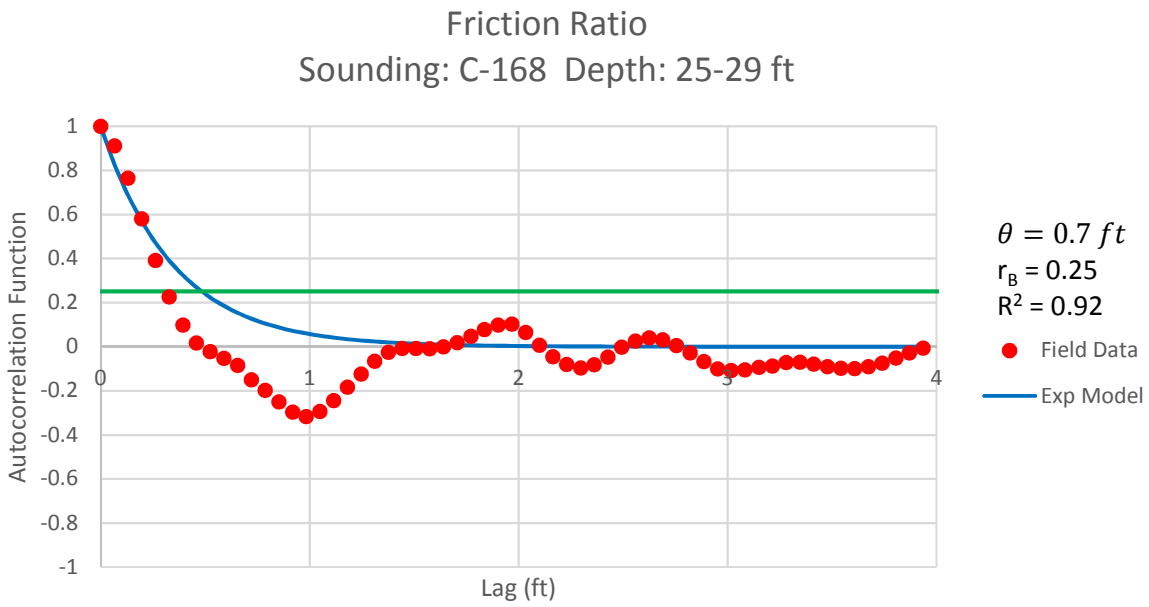

Figure B - 323: Estimation of the Scale of Fluctuation, $\theta = 0.7$ feet, for Friction Ratio Data from Sounding C-168, "Gravelly sand to sand (7)" layer from 25 to 29 feet depth.

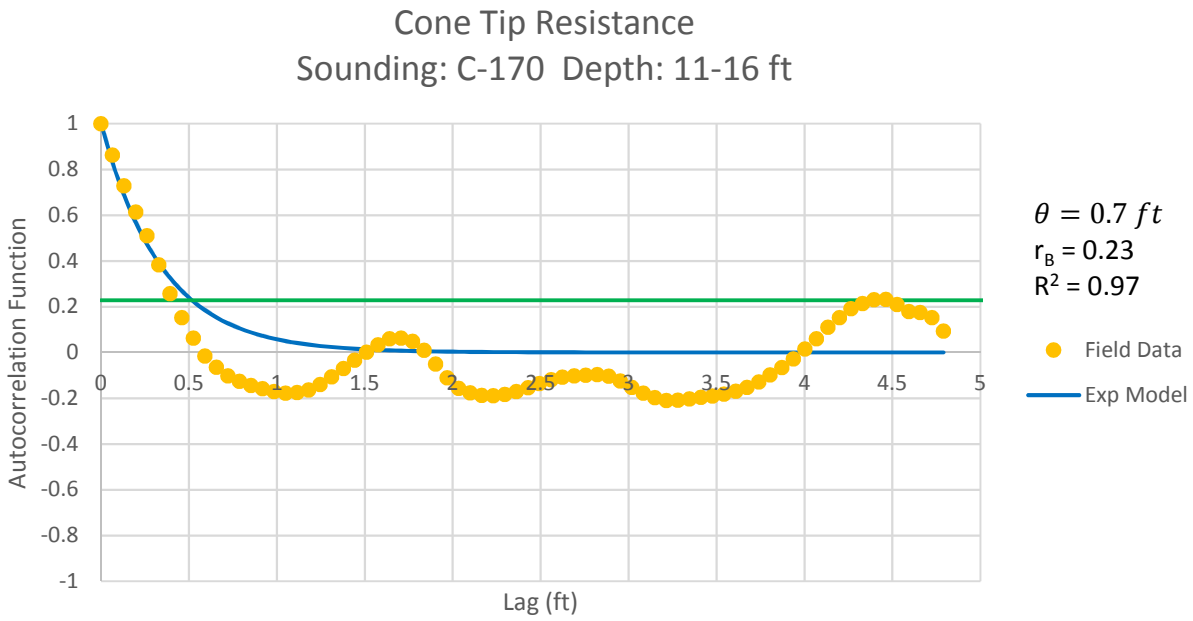

Figure B - 324: Estimation of the Scale of Fluctuation, $\theta = 0.7$ feet, for Cone Tip Resistance Data from Sounding C-170, "Clean sands to silty sands (6)" layer from 11 to 16 feet depth.

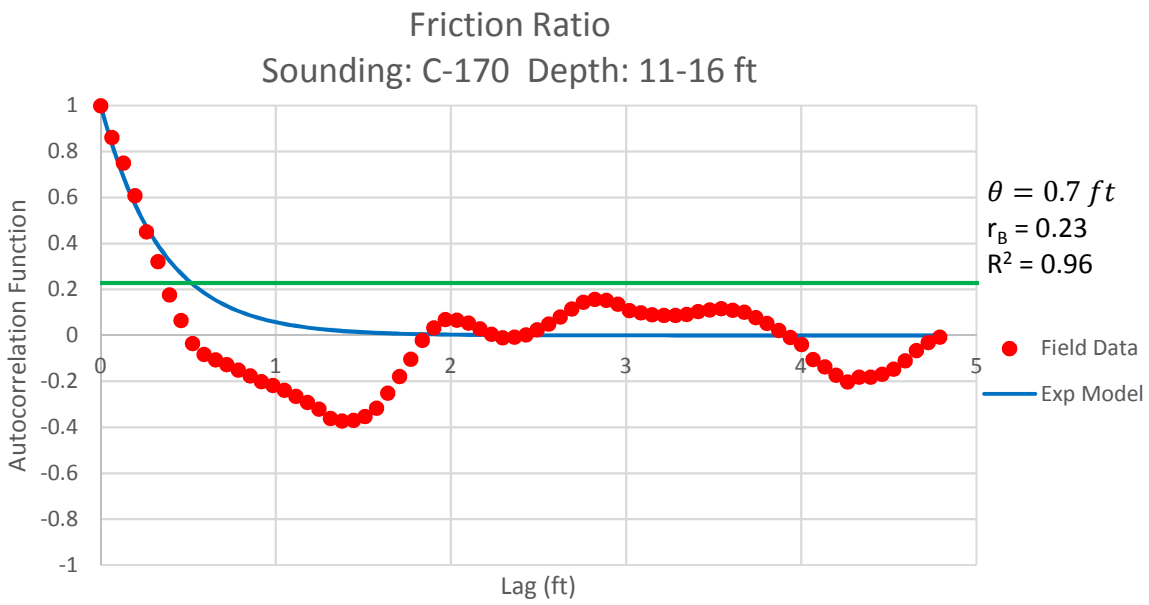

Figure B - 325: Estimation of the Scale of Fluctuation, $\theta = 0.7$ feet, for Friction Ratio Data from Sounding C-170, "Clean sands to silty sands (6)" layer from 11 to 16 feet depth.

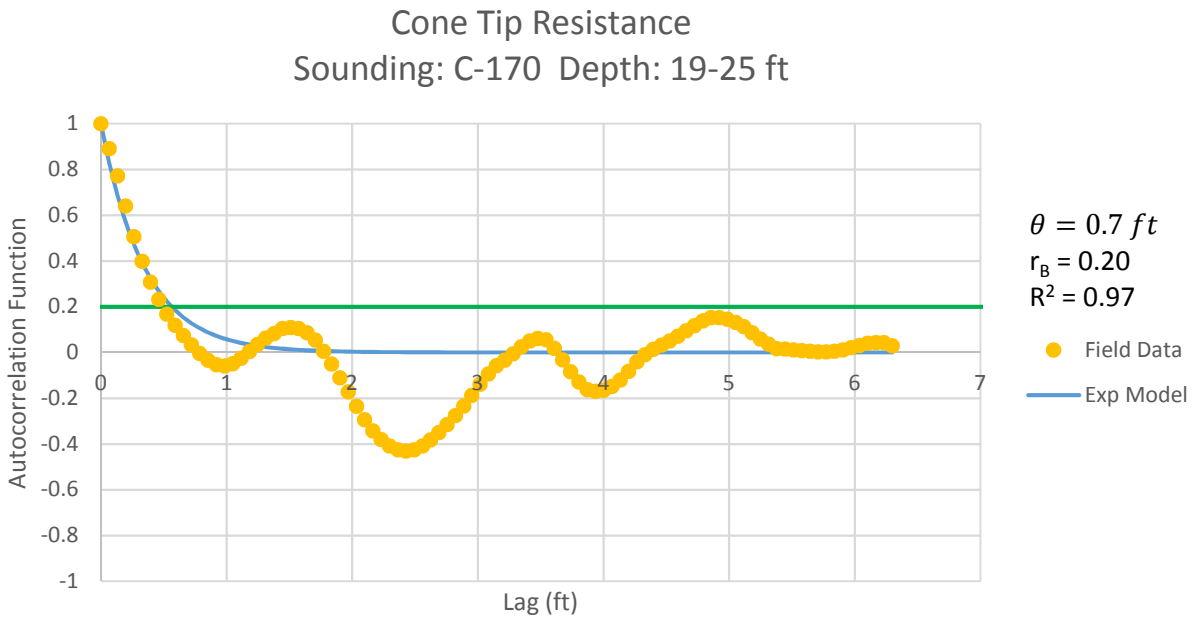

Figure B - 326: Estimation of the Scale of Fluctuation, $\theta = 0.7$ feet, for Cone Tip Resistance Data from Sounding C-170, "Clean sands to silty sands (6)" layer from 19 to 25 feet depth.

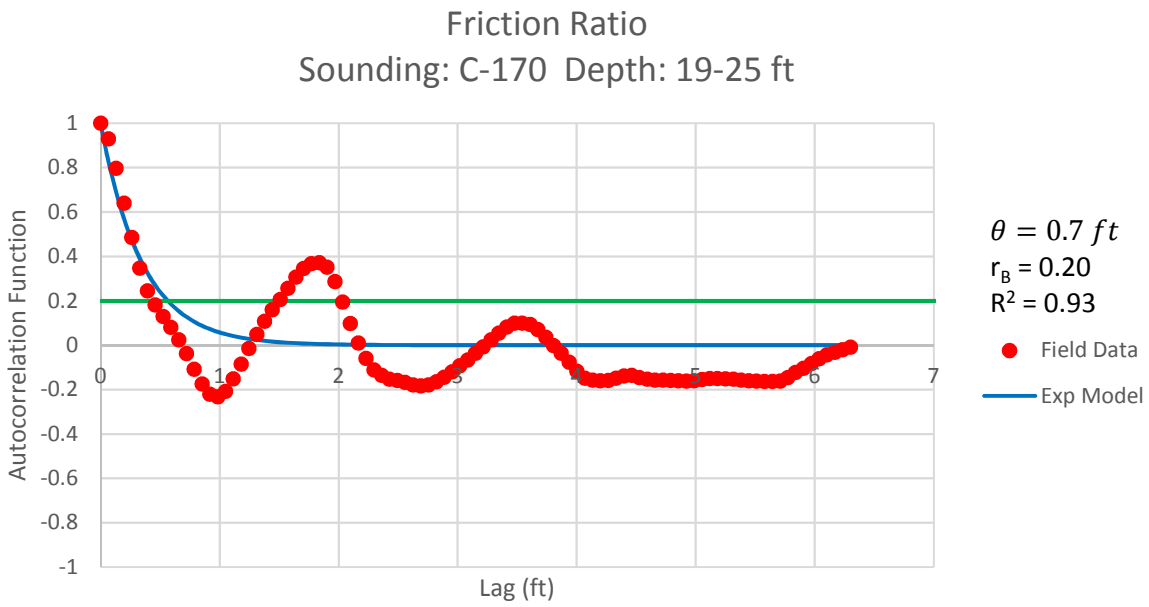

Figure B - 327: Estimation of the Scale of Fluctuation, $\theta = 0.7$ feet, for Friction Ratio Data from Sounding C-170, "Clean sands to silty sands (6)" layer from 19 to 25 feet depth.

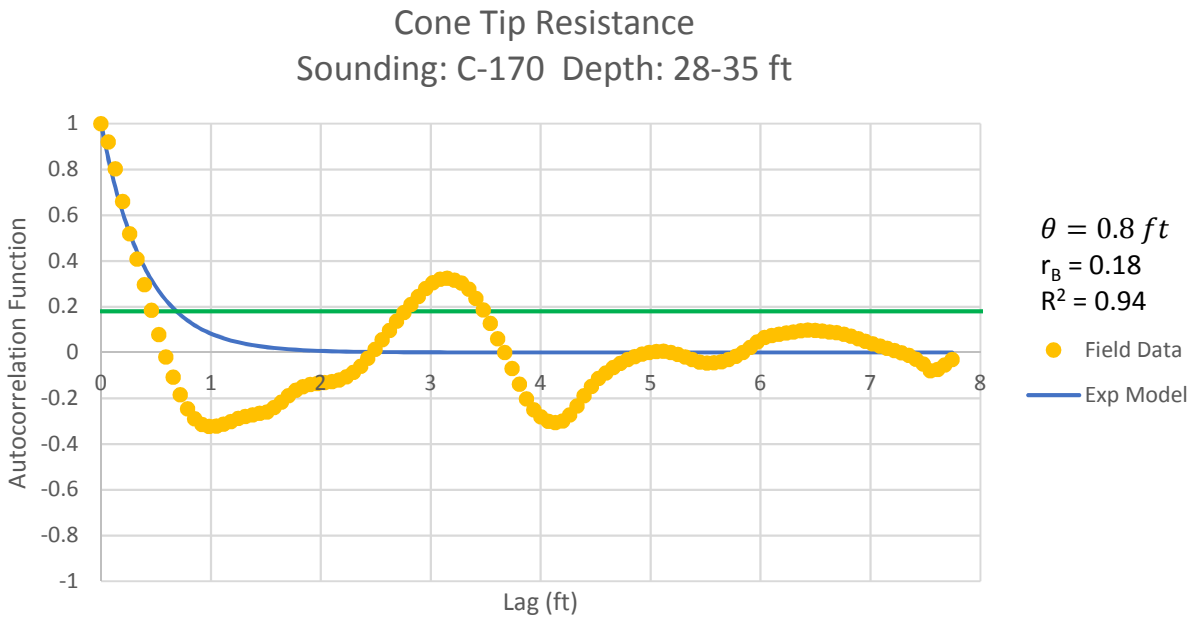

Figure B - 328: Estimation of the Scale of Fluctuation, $\theta = 0.8$ feet, for Cone Tip Resistance Data from Sounding C-170, "Clean sands to silty sands (6)" layer from 28 to 35 feet depth.

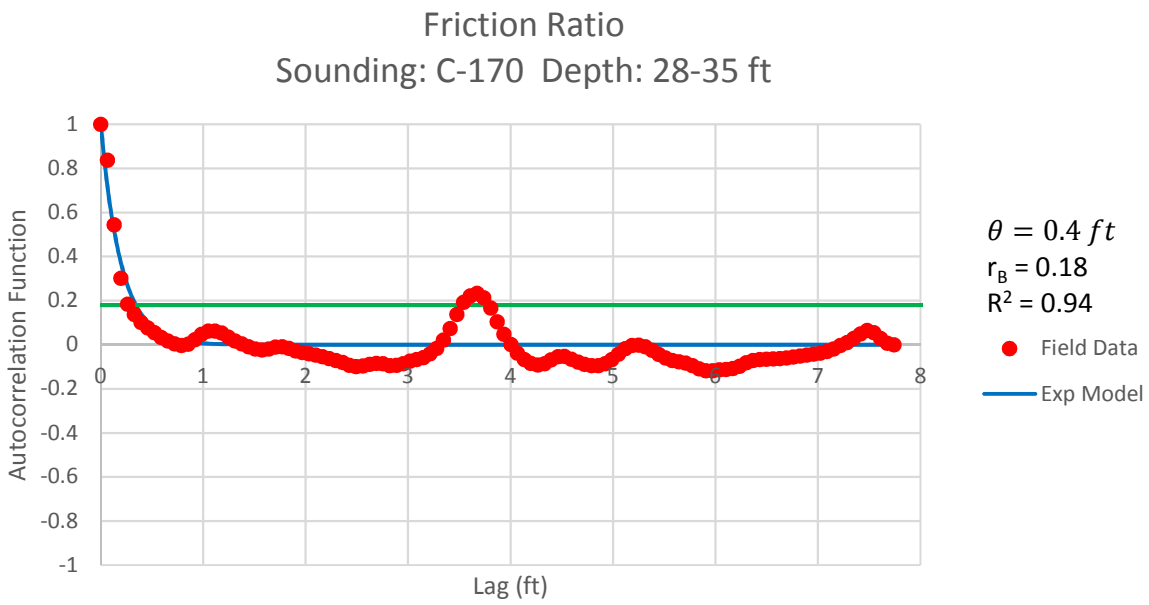

Figure B - 329: Estimation of the Scale of Fluctuation, $\theta = 0.4$ feet, for Friction Ratio Data from Sounding C-170, "Clean sands to silty sands (6)" layer from 28 to 35 feet depth.

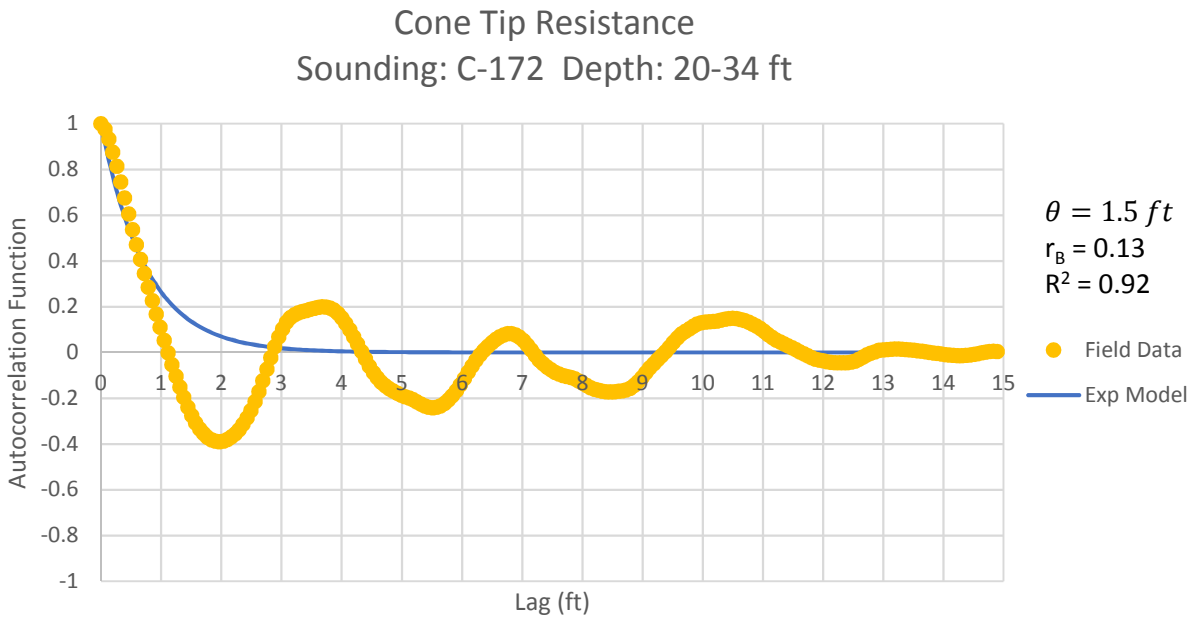

Figure B - 330: Estimation of the Scale of Fluctuation, $\theta = 1.5$ feet, for Cone Tip Resistance Data from Sounding C-172, "Clean sands to silty sands (6)" layer from 20 to 34 feet depth.

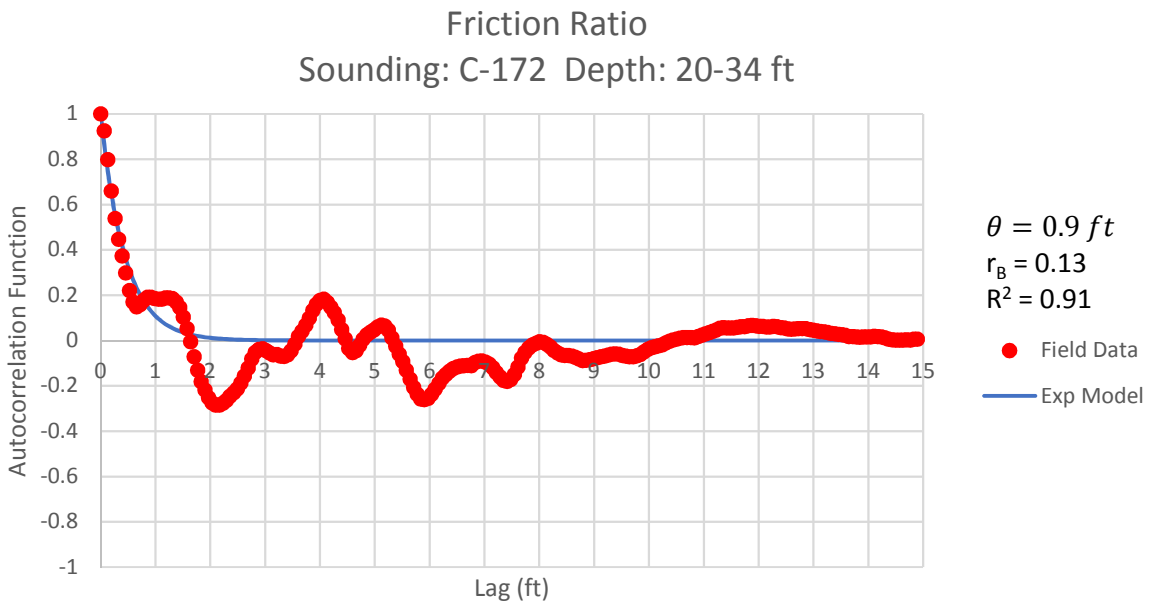

Figure B - 331: Estimation of the Scale of Fluctuation, $\theta = 0.9$ feet, for Friction Ratio Data from Sounding C-172, "Clean sands to silty sands (6)" layer from 20 to 34 feet depth.

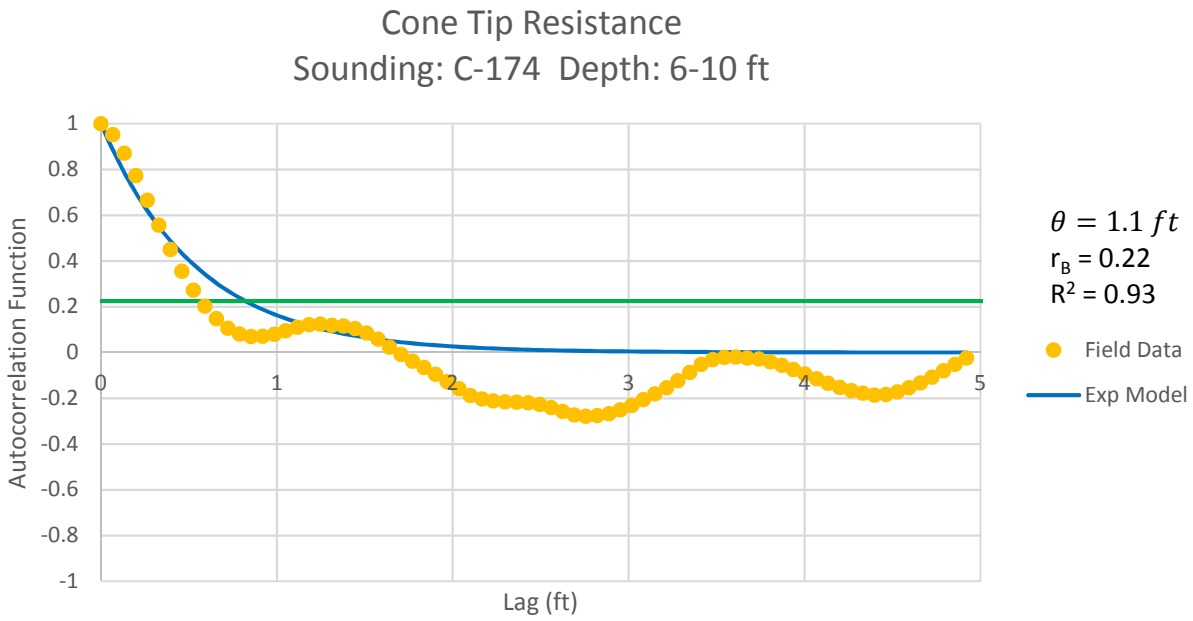

Figure B - 332: Estimation of the Scale of Fluctuation, θ = 1.1 feet, for Cone Tip Resistance Data from Sounding C-174, "Gravelly sand to sand (7)" layer from 6 to 10 feet depth.

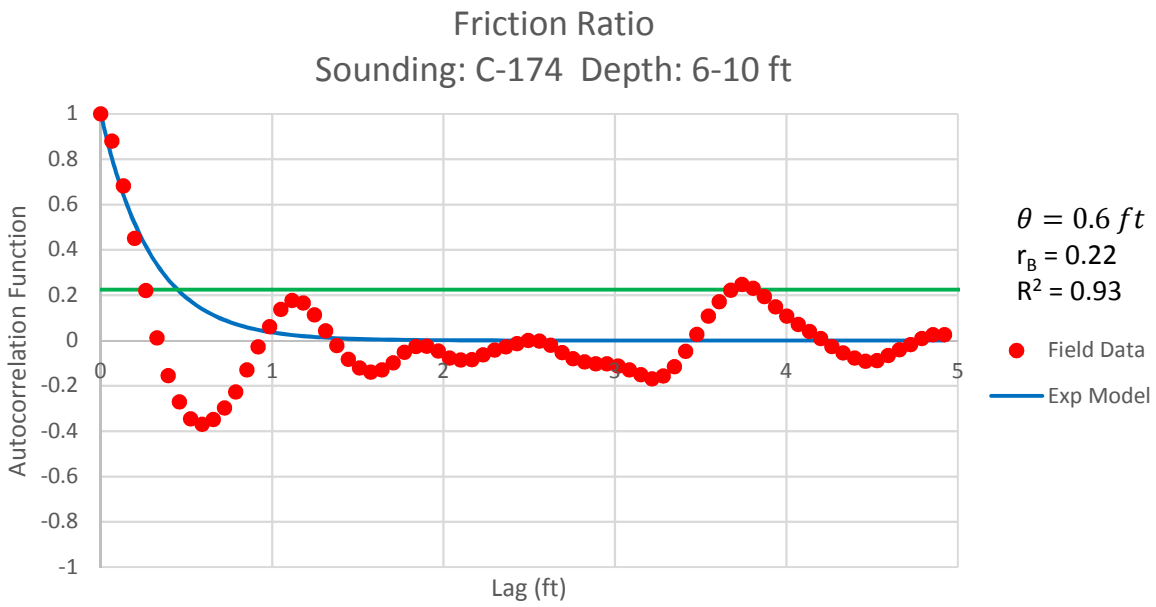

Figure B - 333: Estimation of the Scale of Fluctuation, θ = 0.6 feet, for Friction Ratio Data from Sounding C-174, "Gravelly sand to sand (7)" layer from 6 to 10 feet depth.

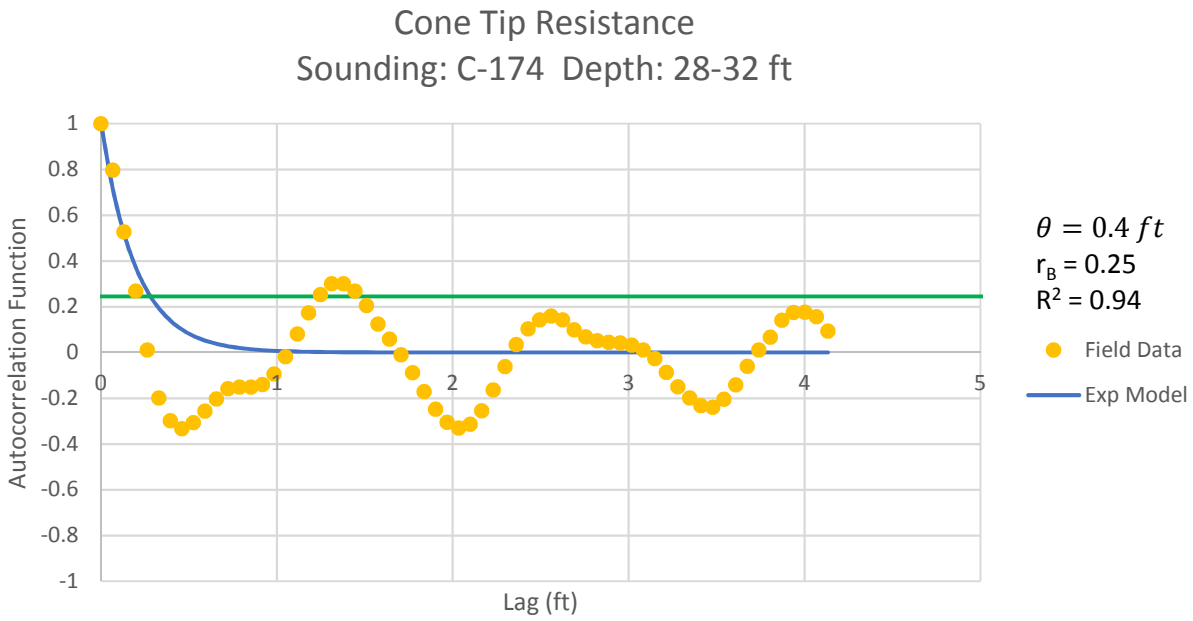

Figure B - 334: Estimation of the Scale of Fluctuation, $\theta = 0.4$ feet, for Cone Tip Resistance Data from Sounding C-174, "Clean sands to silty sands (6)" layer from 28 to 32 feet depth.

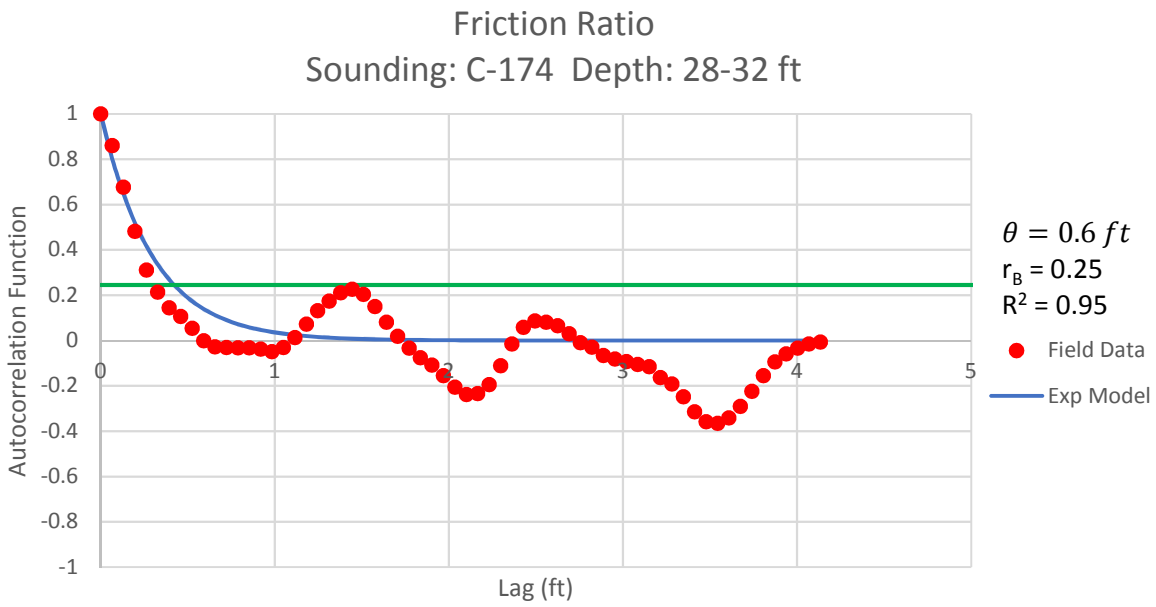

Figure B - 335: Estimation of the Scale of Fluctuation, $\theta = 0.6$ feet, for Friction Ratio Data from Sounding C-174, "Clean sands to silty sands (6)" layer from 28 to 32 feet depth.

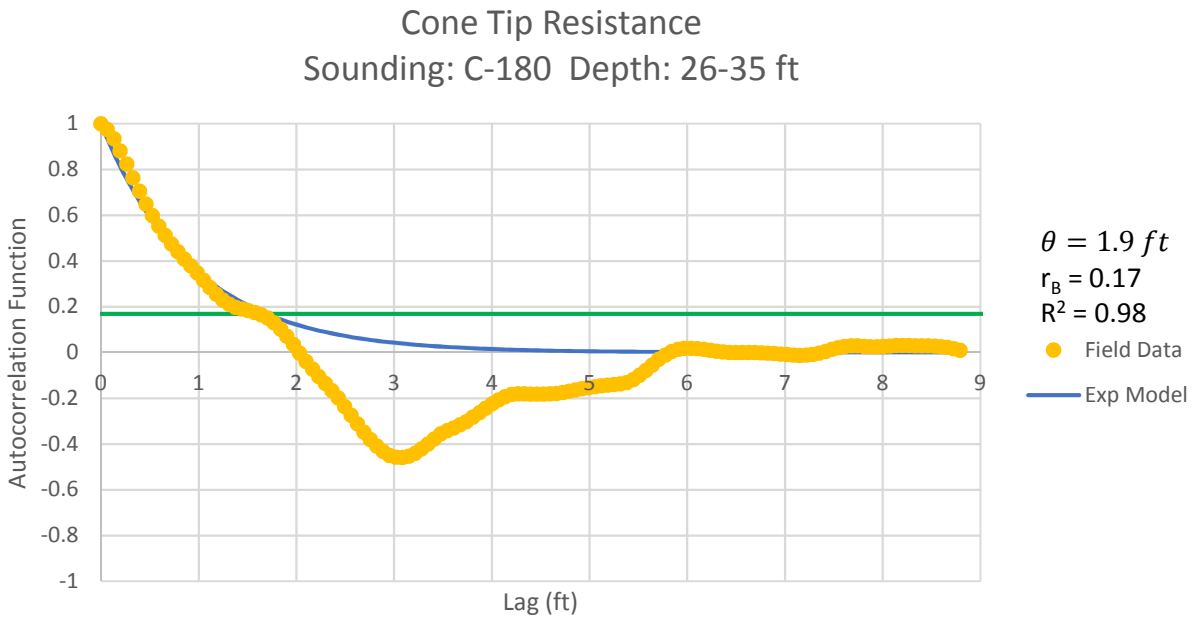

Figure B - 336: Estimation of the Scale of Fluctuation, $\theta = 1.9$ feet, for Cone Tip Resistance Data from Sounding C-180, "Clean sands to silty sands (6)" layer from 26 to 35 feet depth.

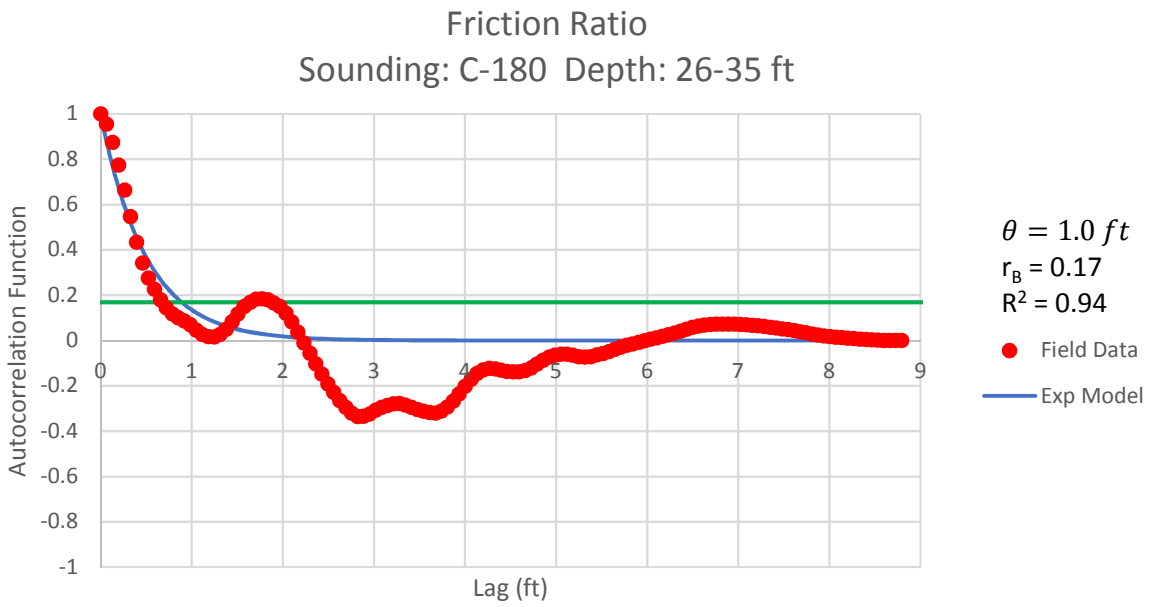

Figure B - 337: Estimation of the Scale of Fluctuation, $\theta = 1.0$ feet, for Friction Ratio Data from Sounding C-180, "Clean sands to silty sands (6)" layer from 26 to 35 feet depth.

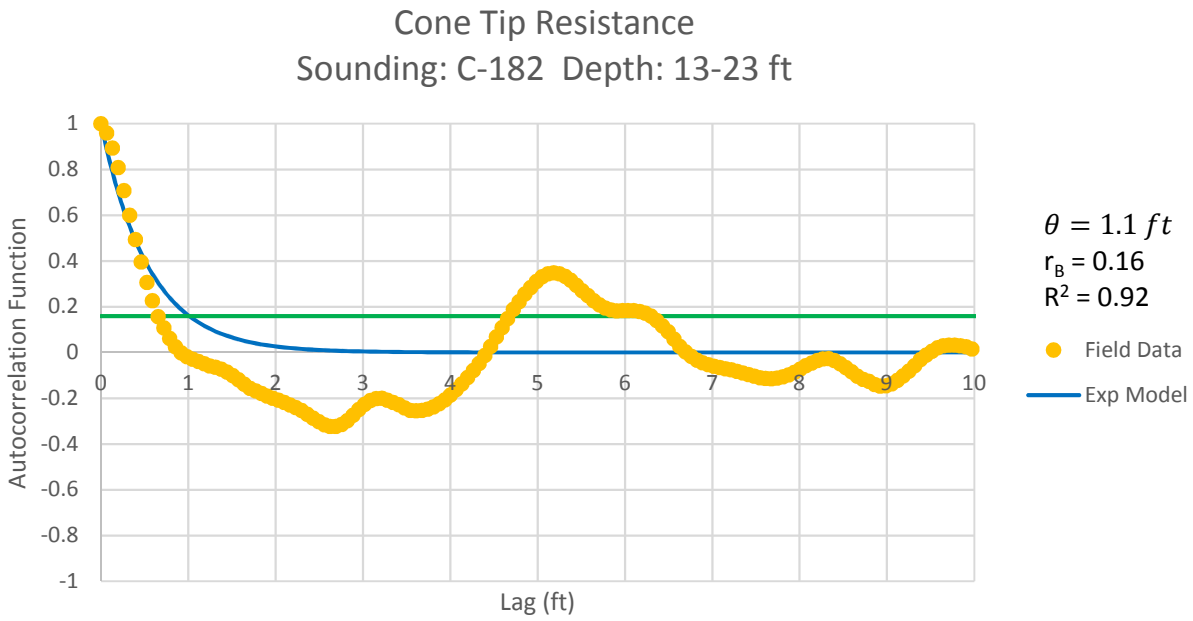

Figure B - 338: Estimation of the Scale of Fluctuation, $\theta = 1.1$ feet, for Cone Tip Resistance Data from Sounding C-182, "Clean sands to silty sands (6)" layer from 13 to 23 feet depth.

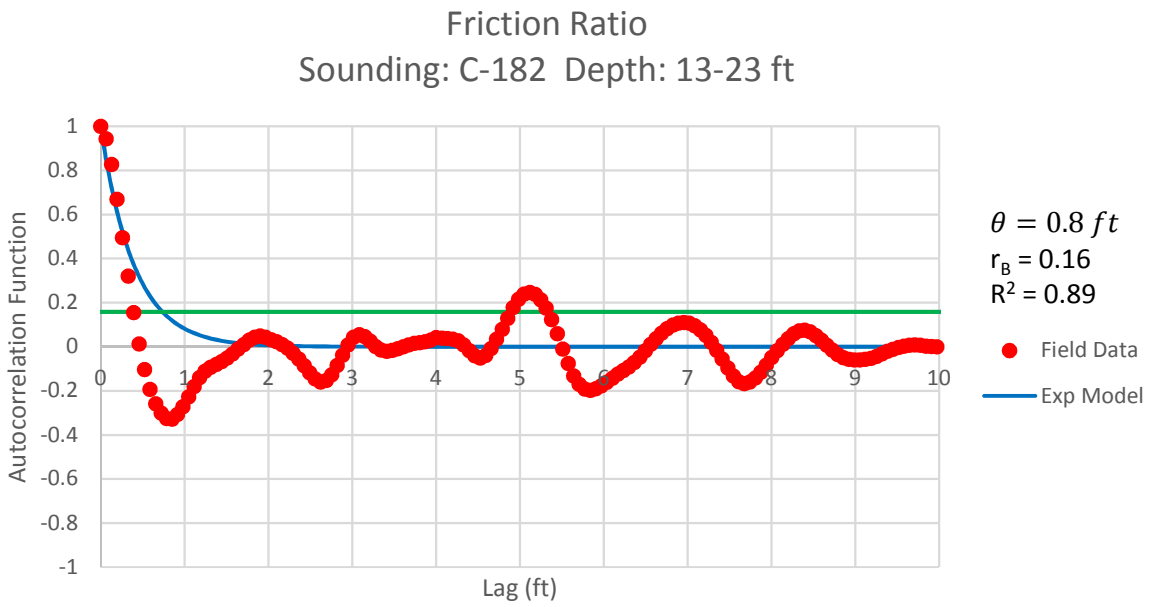

Figure B - 339: Estimation of the Scale of Fluctuation, $\theta = 0.8$ feet, for Friction Ratio Data from Sounding C-182, "Clean sands to silty sands (6)" layer from 13 to 23 feet depth. Data is a poor fit for the points greater than the Bartlett limit of 0.16; coefficient of determination, R^2, value is less 0.9. Therefore, these results were not included in final analysis.

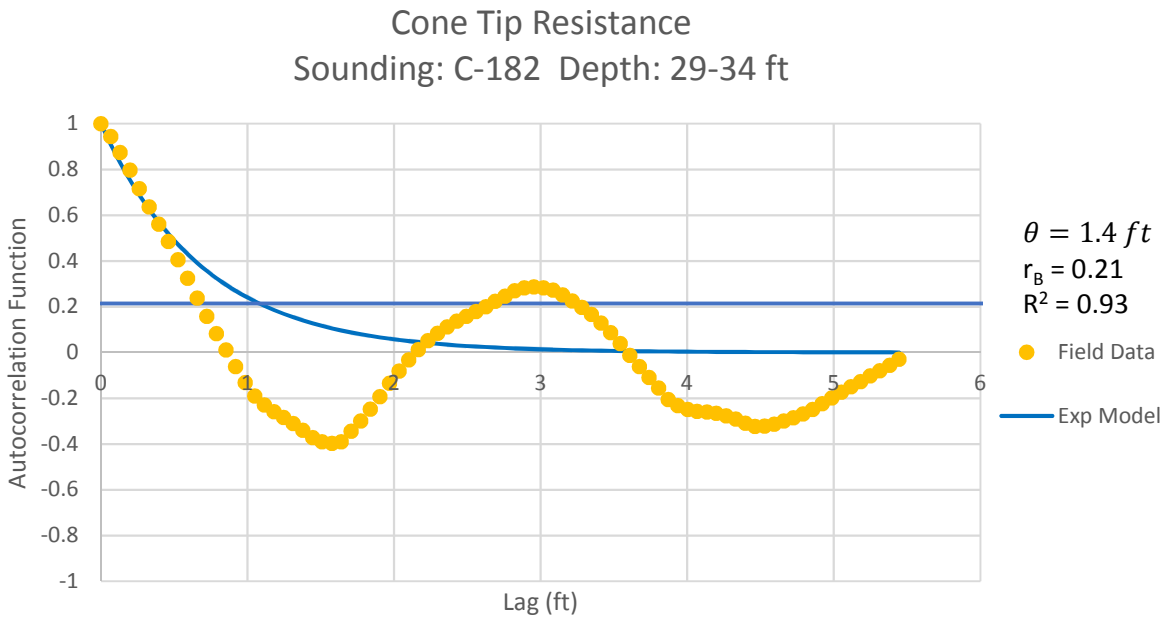

Figure B - 340: Estimation of the Scale of Fluctuation, $\theta = 1.4$ feet, for Cone Tip Resistance Data from Sounding C-182, "Clean sands to silty sands (6)" layer from 29 to 34 feet depth.

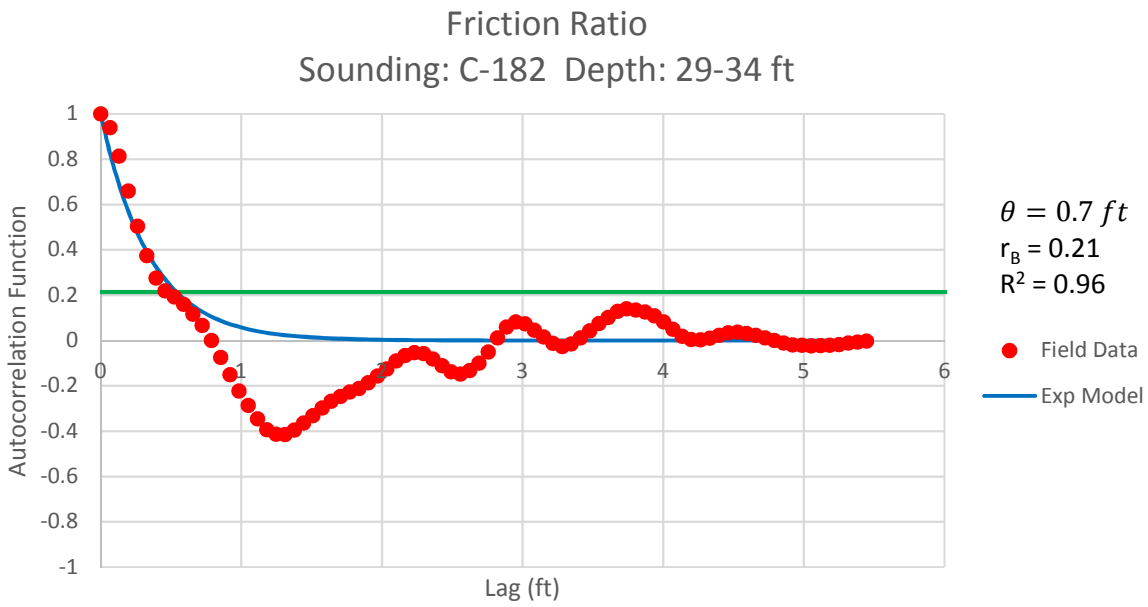

Figure B - 341: Estimation of the Scale of Fluctuation, $\theta = 0.7$ feet, for Friction Ratio Data from Sounding C-182, "Clean sands to silty sands (6)" layer from 29 to 34 feet depth.

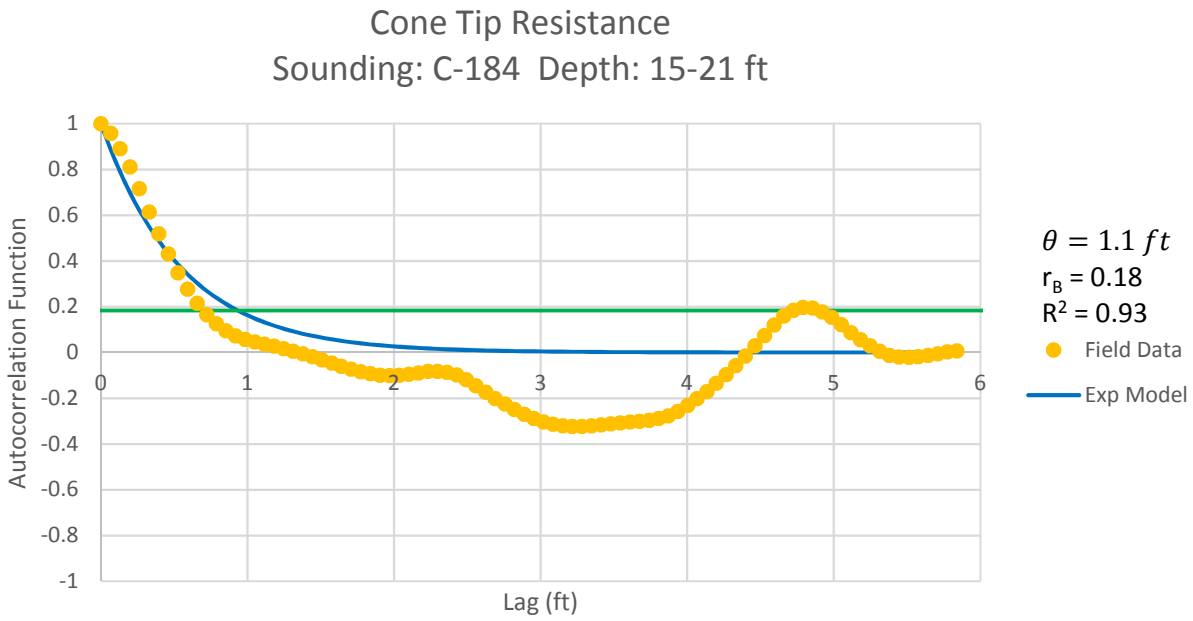

Figure B - 342: Estimation of the Scale of Fluctuation, $\theta = 1.1$ feet, for Cone Tip Resistance Data from Sounding C-184, "Clean sands to silty sands (6)" layer from 15 to 21 feet depth.

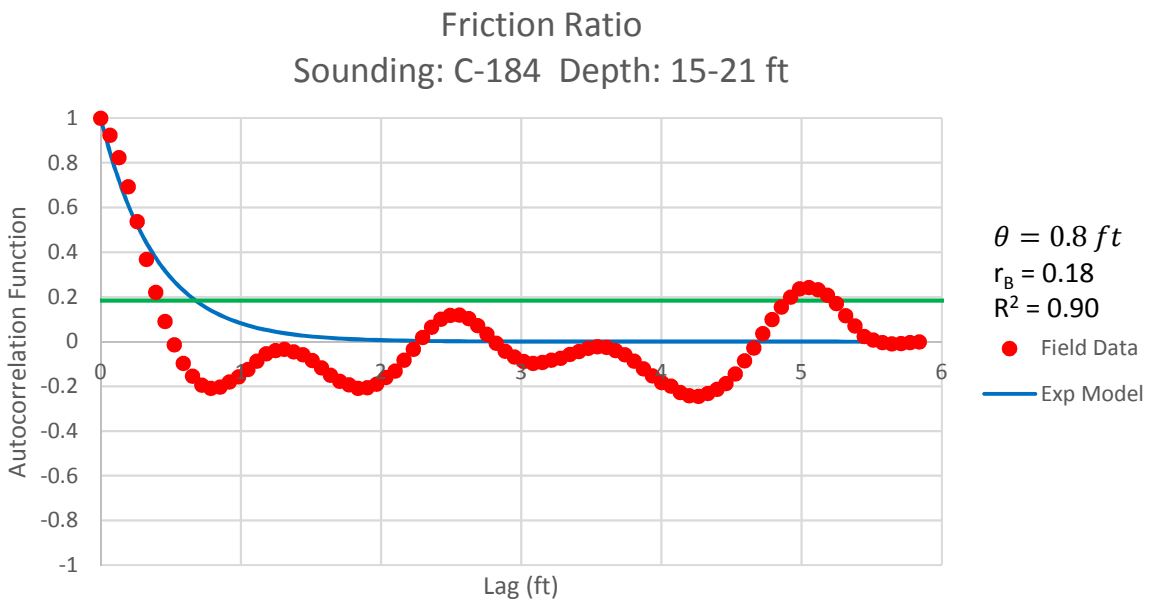

Figure B - 343: Estimation of the Scale of Fluctuation, $\theta = 0.8$ feet, for Friction Ratio Data from Sounding C-184, "Clean sands to silty sands (6)" layer from 15 to 21 feet depth.

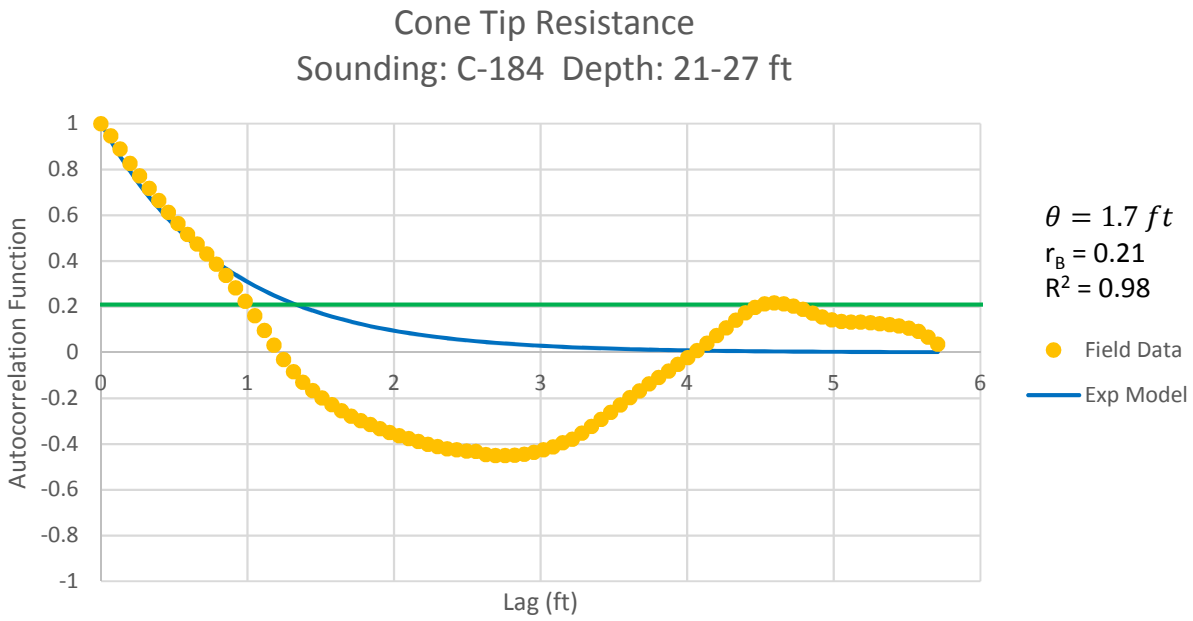

Figure B - 344: Estimation of the Scale of Fluctuation, $\theta = 1.3$ feet, for Cone Tip Resistance Data from Sounding C-184, "Gravelly sand to sand (7)" layer from 21 to 27 feet depth.

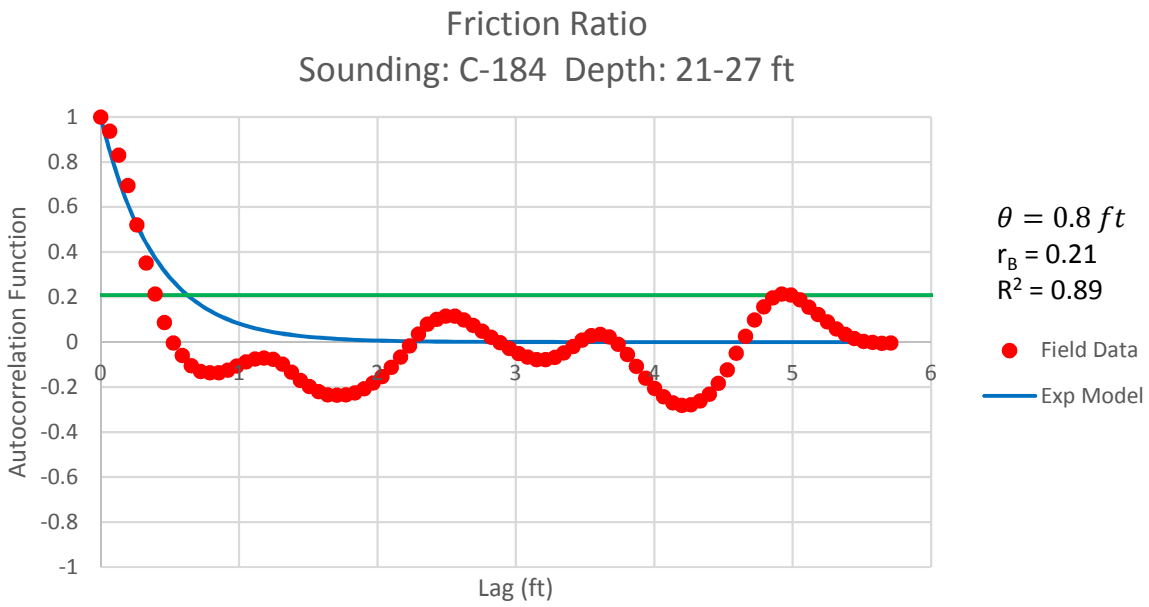

Figure B - 345: Estimation of the Scale of Fluctuation, $\theta = 0.8$ feet, for Friction Ratio Data from Sounding C-184, "Gravelly sand to sand (7)" layer from 21 to 27 feet depth. Data is a poor fit for the points greater than the Bartlett limit of 0.21; coefficient of determination, R^2, value is less 0.9. Therefore, these results were not included in final analysis.

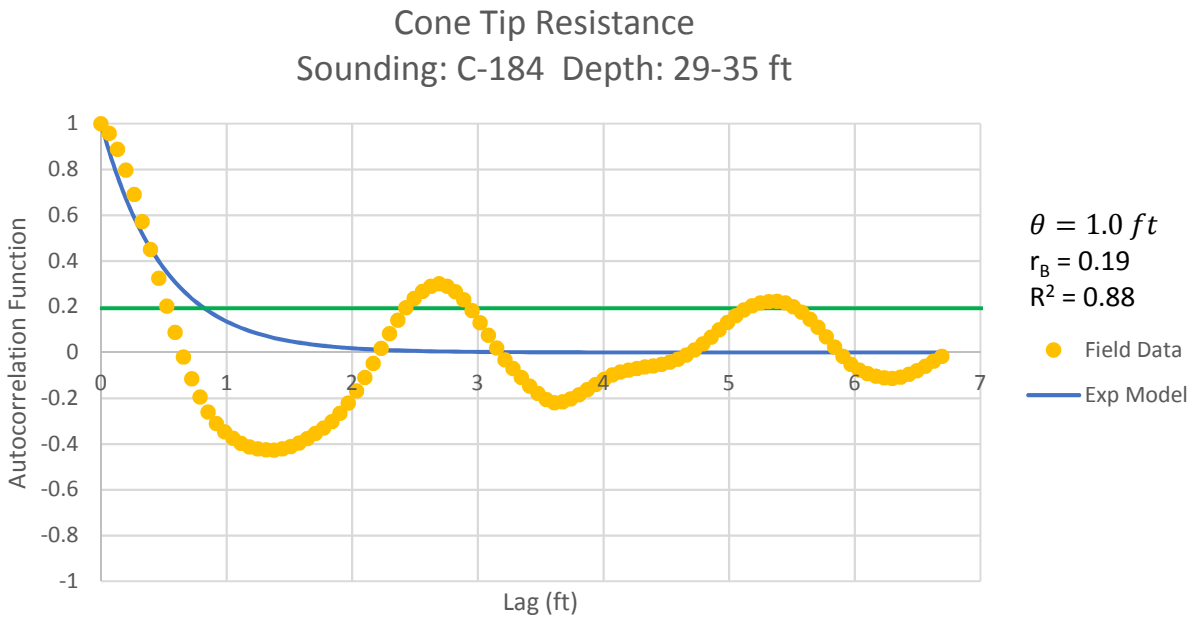

Figure B - 346: Estimation of the Scale of Fluctuation, $\theta = 1.0$ feet, for Cone Tip Resistance Data from Sounding C-184, "Clean sands to silty sands (6)" layer from 29 to 35 feet depth. Data is a poor fit for the points greater than the Bartlett limit of 0.19; coefficient of determination, R^2, value is less 0.9. Therefore, these results were not included in final analysis.

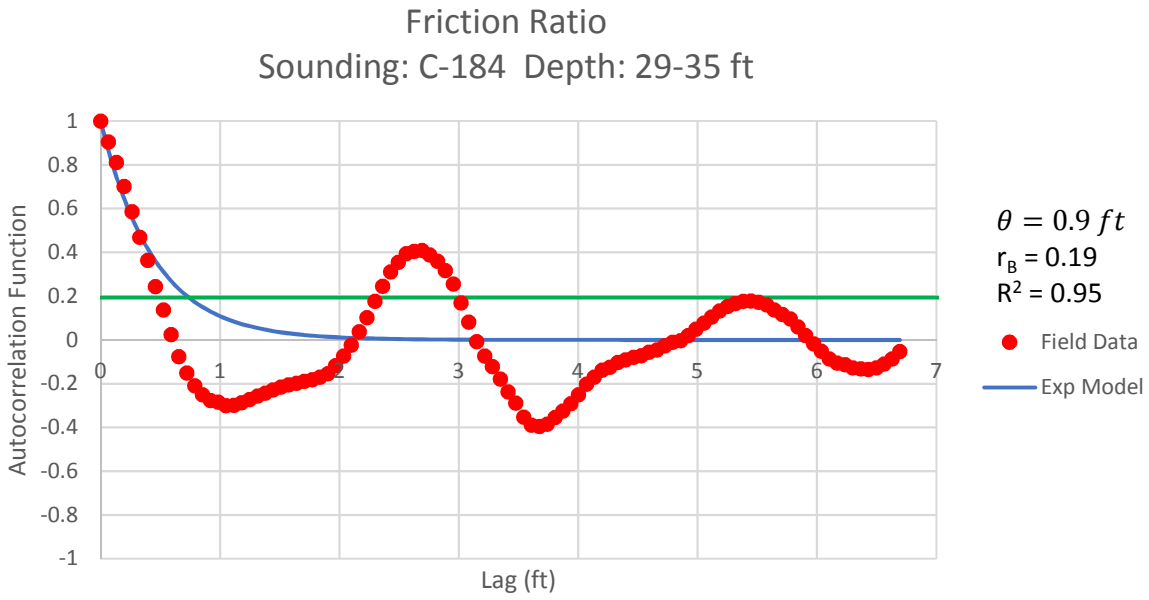

Figure B - 347: Estimation of the Scale of Fluctuation, $\theta = 0.9$ feet, for Friction Ratio Data from Sounding C-184, "Clean sands to silty sands (6)" layer from 29 to 35 feet depth.

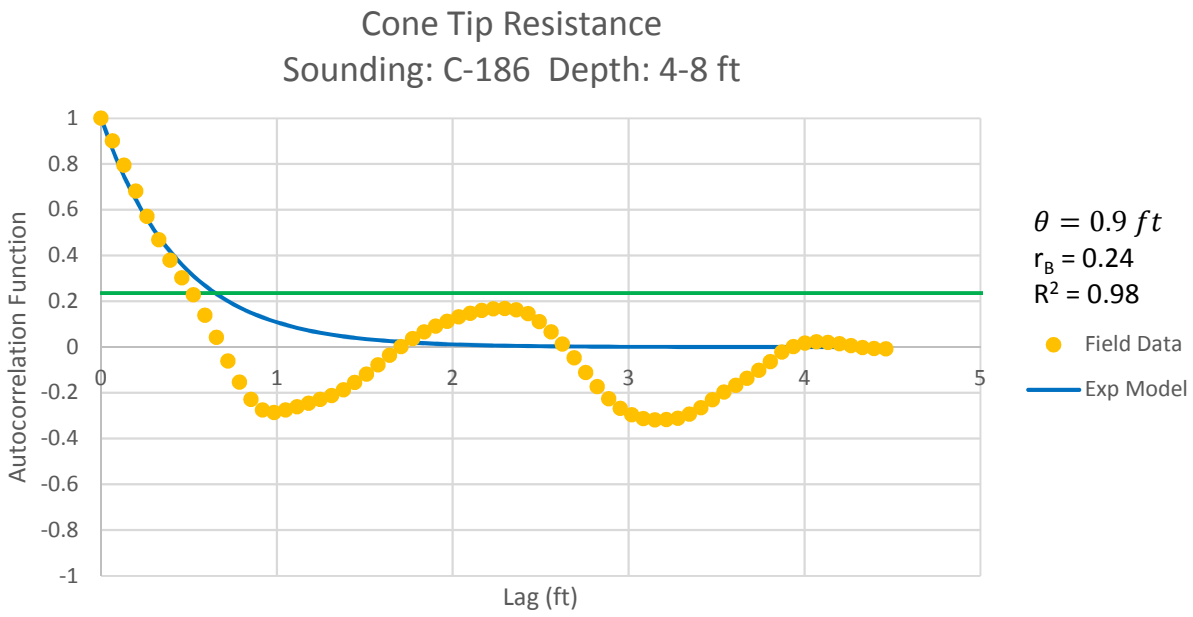

Figure B - 348: Estimation of the Scale of Fluctuation, $\theta = 0.9$ feet, for Cone Tip Resistance Data from Sounding C-186, "Clean sands to silty sands (6)" layer from 4 to 8 feet depth.

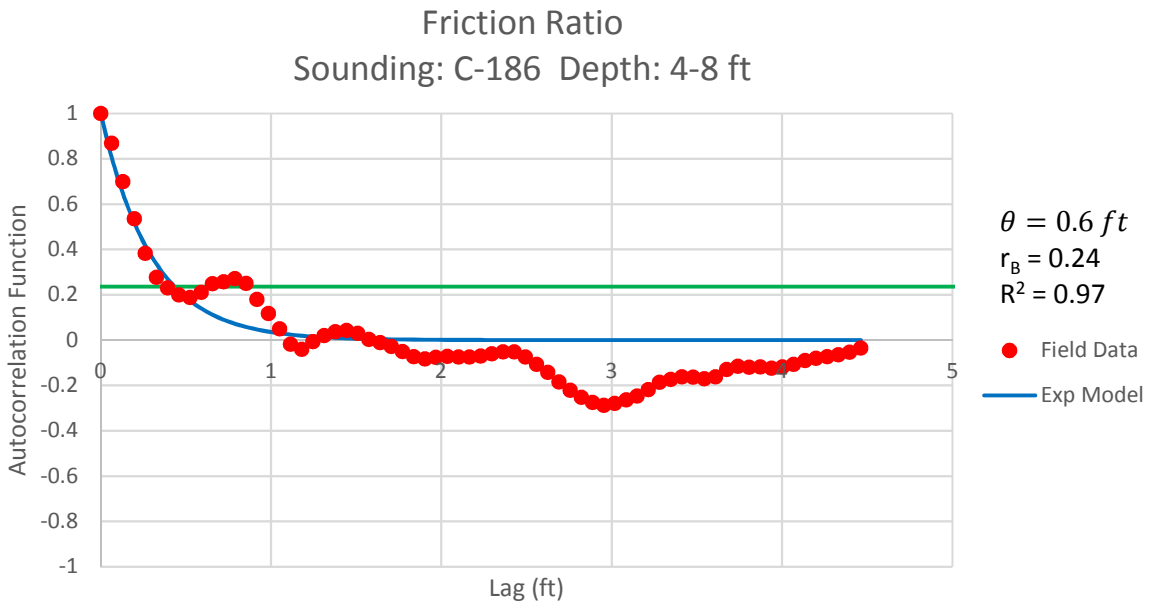

Figure B - 349: Estimation of the Scale of Fluctuation, $\theta = 0.6$ feet, for Friction Ratio Data from Sounding C-186, "Clean sands to silty sands (6)" layer from 4 to 8 feet depth.

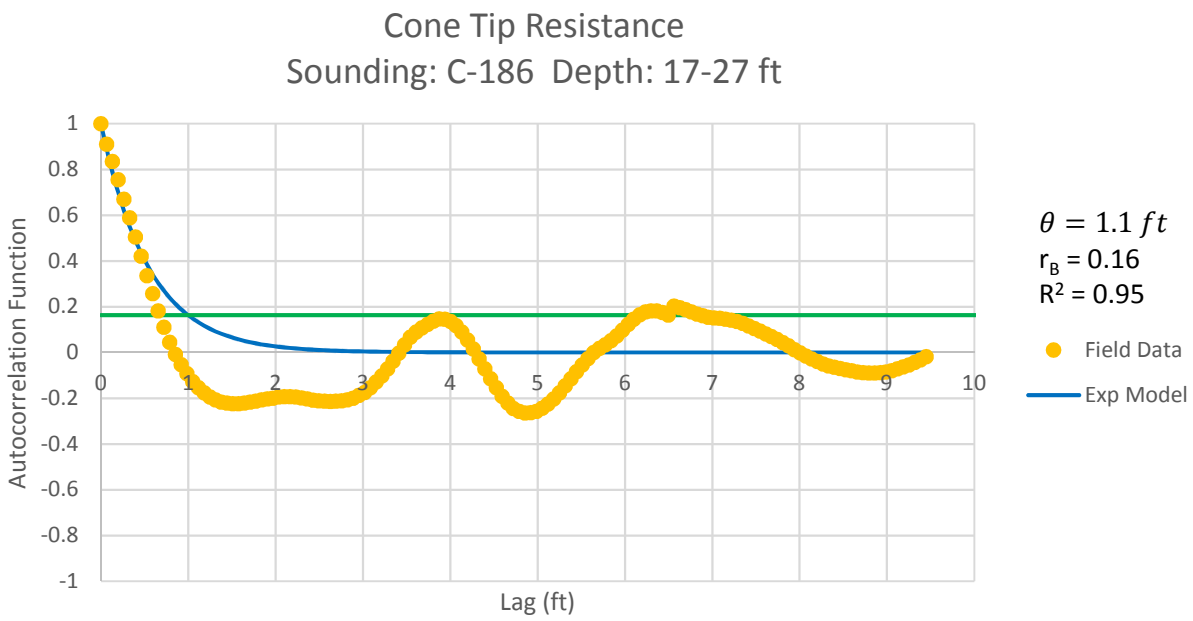

Figure B - 350: Estimation of the Scale of Fluctuation, $\theta = 1.1$ feet, for Cone Tip Resistance Data from Sounding C-186, "Clean sands to silty sands (6)" layer from 17 to 27 feet depth.

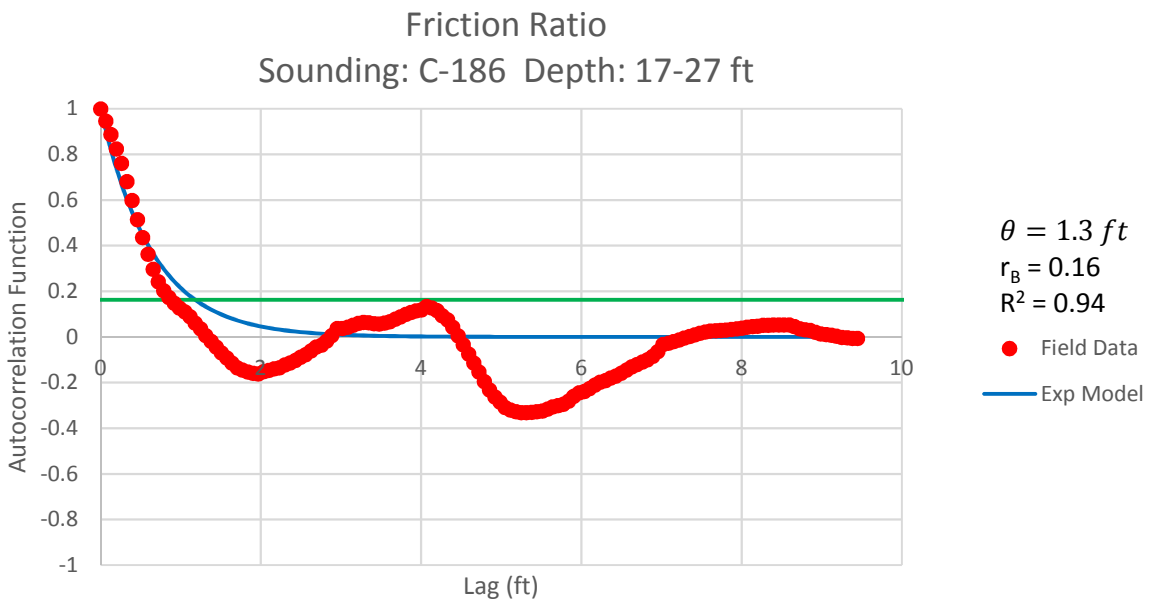

Figure B - 351: Estimation of the Scale of Fluctuation, $\theta = 1.3$ feet, for Friction Ratio Data from Sounding C-186, "Clean sands to silty sands (6)" layer from 17 to 27 feet depth.

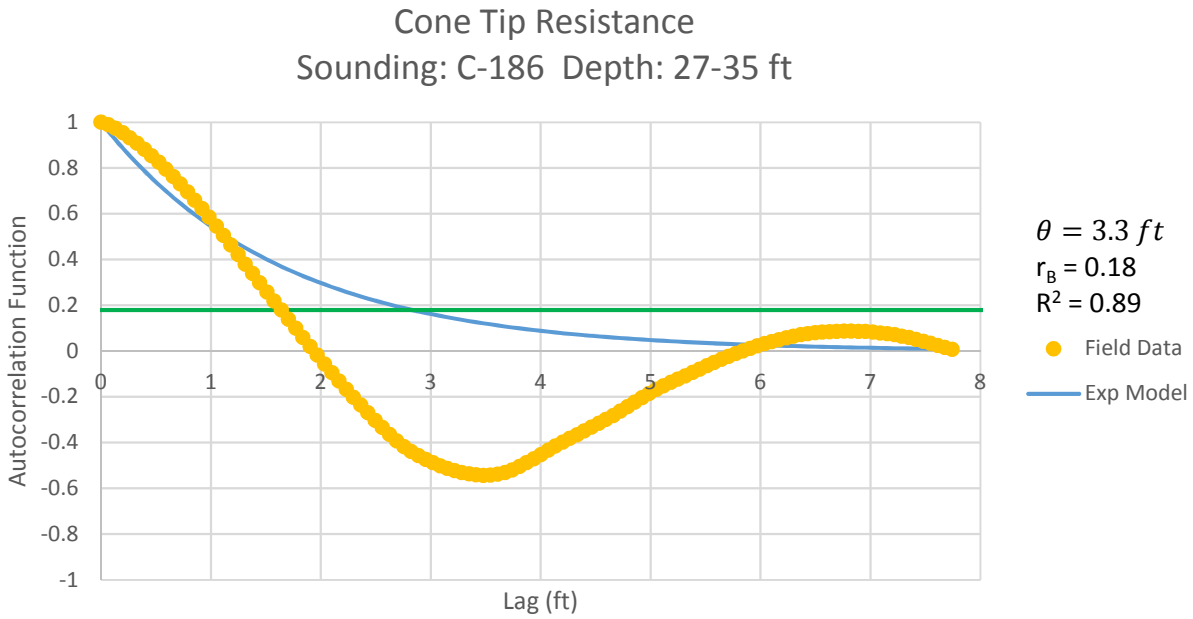

Figure B - 352: Estimation of the Scale of Fluctuation, $\theta = 3.3$ feet, for Cone Tip Resistance Data from Sounding C-186, "Clean sands to silty sands (6)" layer from 27 to 35 feet depth. Data is a poor fit for the points greater than the Bartlett limit of 0.18; coefficient of determination, R^2, value is less 0.9. Therefore, these results were not included in final analysis.

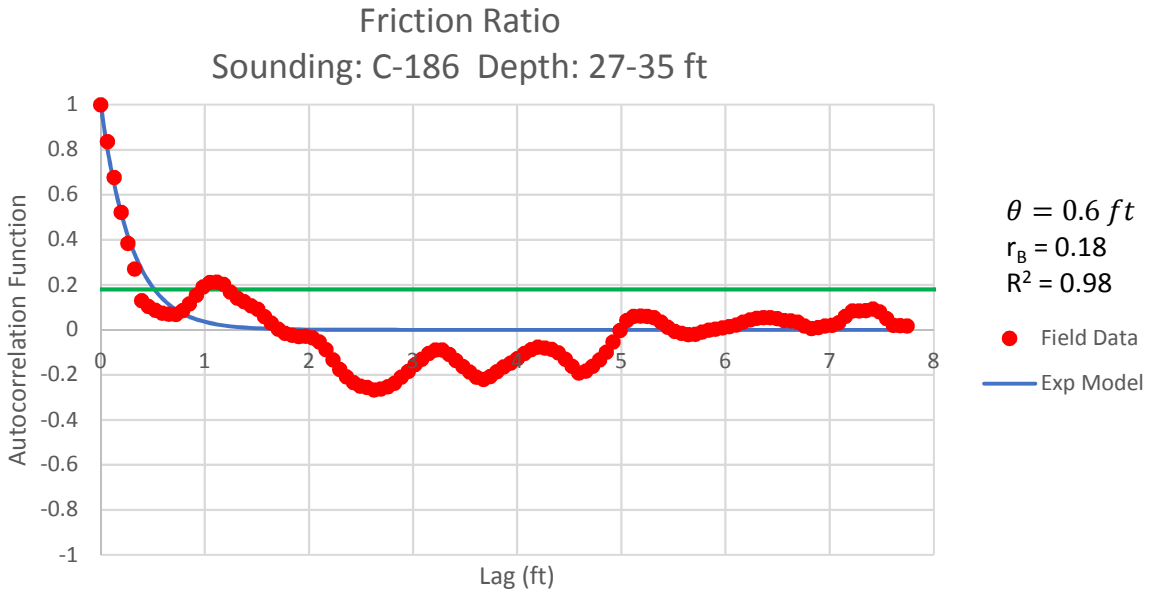

Figure B - 353: Estimation of the Scale of Fluctuation, $\theta = 0.6$ feet, for Friction Ratio Data from Sounding C-186, "Clean sands to silty sands (6)" layer from 27 to 35 feet depth.

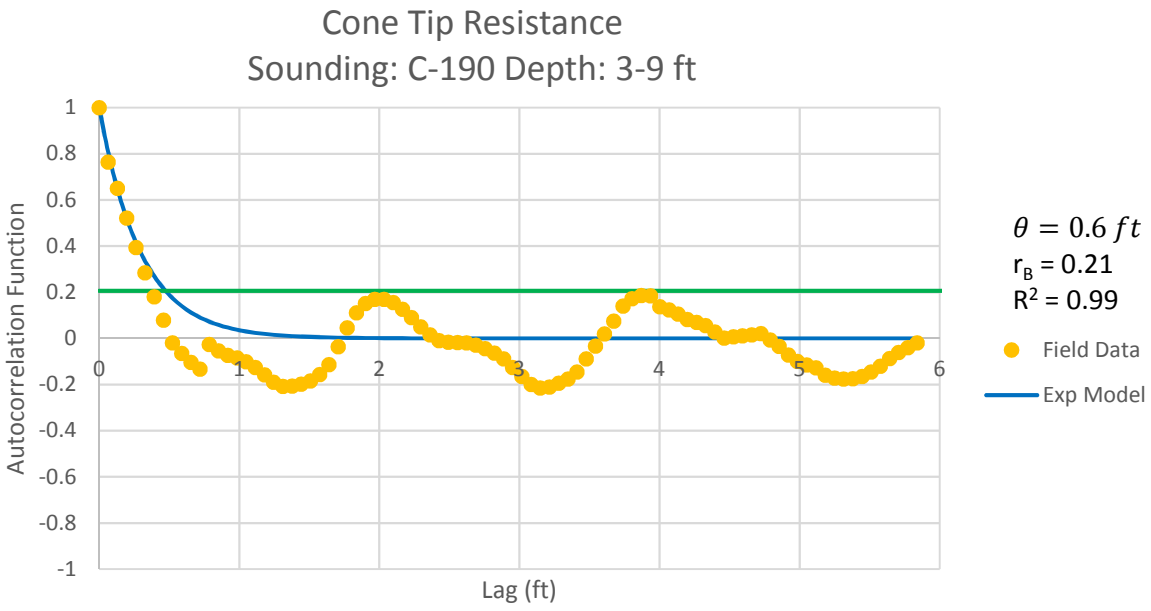

Figure B - 354: Estimation of the Scale of Fluctuation, $\theta = 0.6$ feet, for Cone Tip Resistance Data from Sounding C-190, "Clays; clay to silty clay (3)" layer from 3 to 9 feet depth.

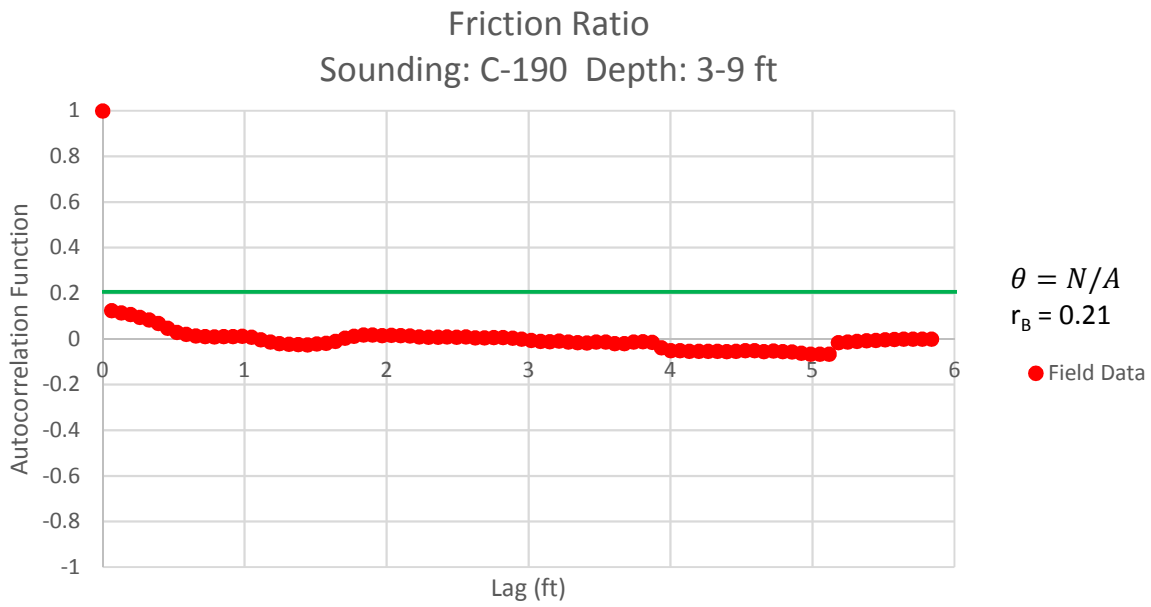

Figure B - 3556: Estimation of the Scale of Fluctuation, θ, for Friction Ratio Data from Sounding C-190, " Clays; clay to silty clay (3)" layer from 3 to 9 feet depth. Data is limited to only 1 point greater than the Bartlett limit of 0.21; therefore, θ could not be estimated, and these results were not included in final analysis.

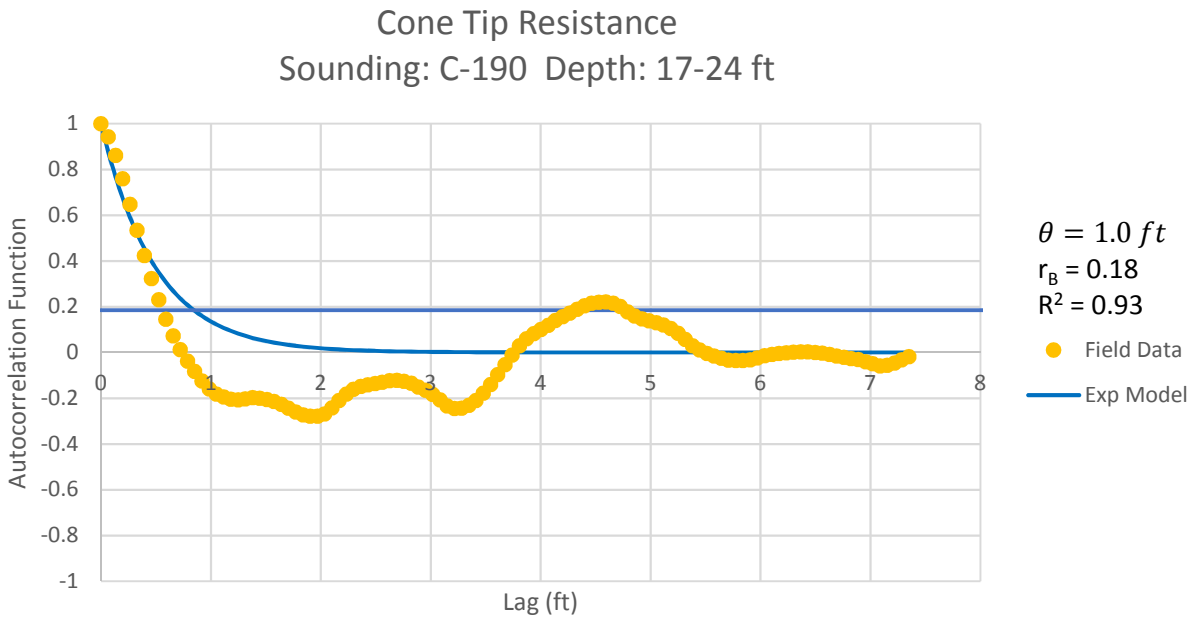

Figure B - 356: Estimation of the Scale of Fluctuation, $\theta = 1.0$ feet, for Cone Tip Resistance Data from Sounding C-190, "Clean sands to silty sands (6)" layer from 17 to 24 feet depth.

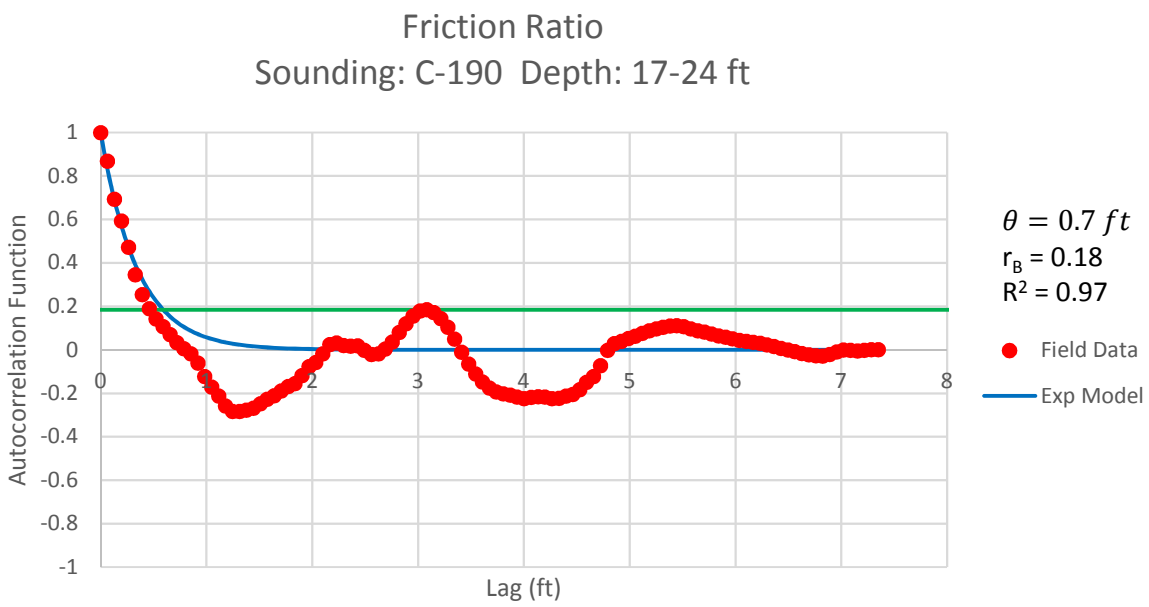

Figure B - 357: Estimation of the Scale of Fluctuation, $\theta = 0.7$ feet, for Friction Ratio Data from Sounding C-190, "Clean sands to silty sands (6)" layer from 17 to 24 feet depth.

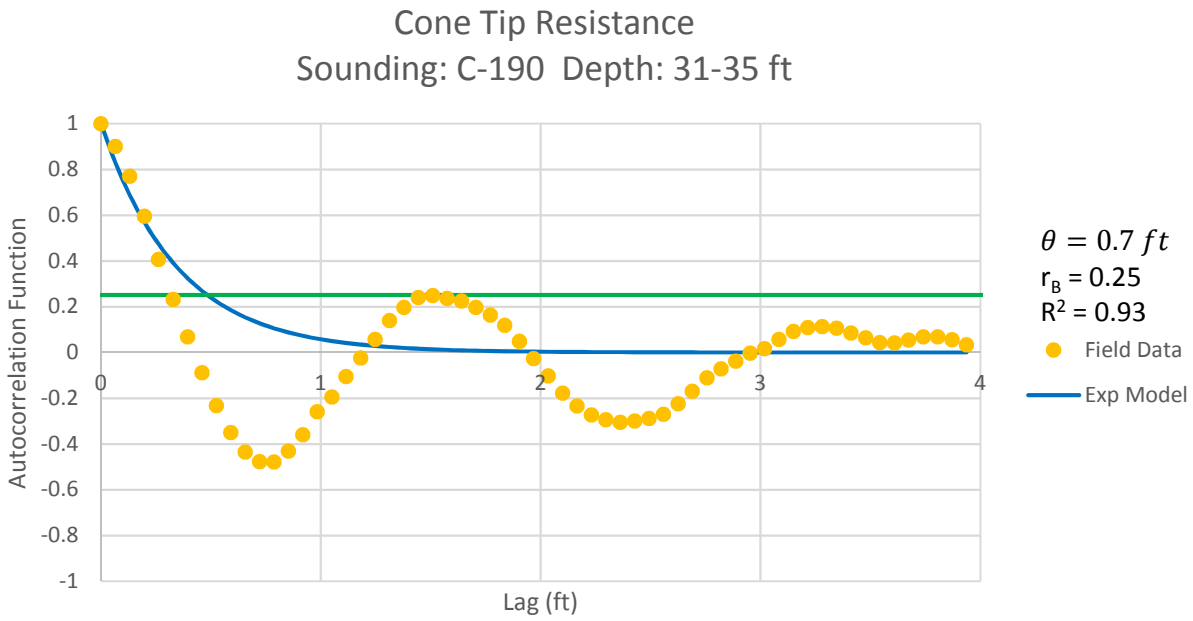

Figure B - 358: Estimation of the Scale of Fluctuation, $\theta = 0.7$ feet, for Cone Tip Resistance Data from Sounding C-190, "Gravelly sand to sand (7)" layer from 31 to 35 feet depth.

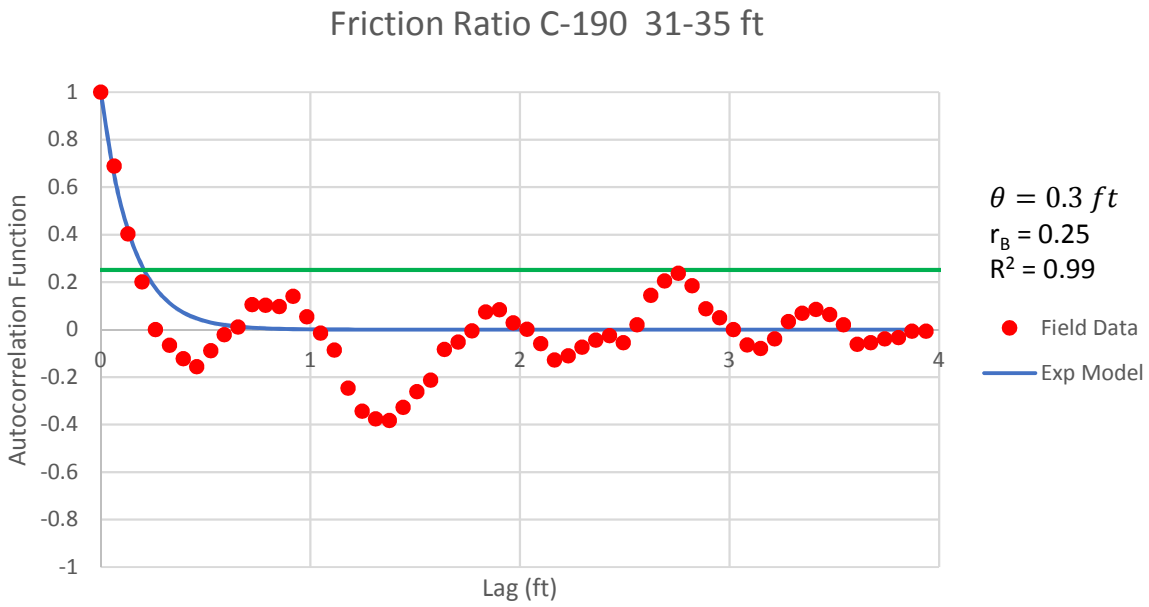

Figure B - 359: Estimation of the Scale of Fluctuation, θ, for Friction Ratio Data from Sounding C-190, "Gravelly sand to sand (7)" layer from 31 to 35 feet depth. Data is limited to only 3 points greater than the Bartlett limit of 0.25; therefore, θ could not be estimated, and these results were not included in final analysis.

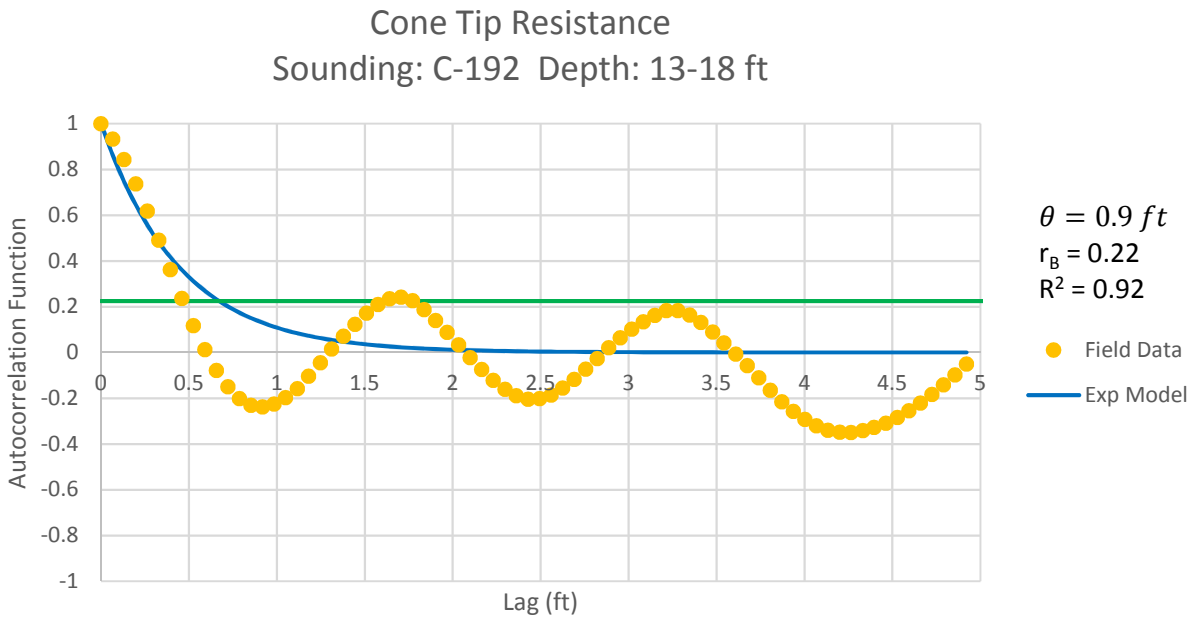

Figure B - 360: Estimation of the Scale of Fluctuation, $\theta = 0.9$ feet, for Cone Tip Resistance Data from Sounding C-192, "Clean sands to silty sands (6)" layer from 13 to 18 feet depth.

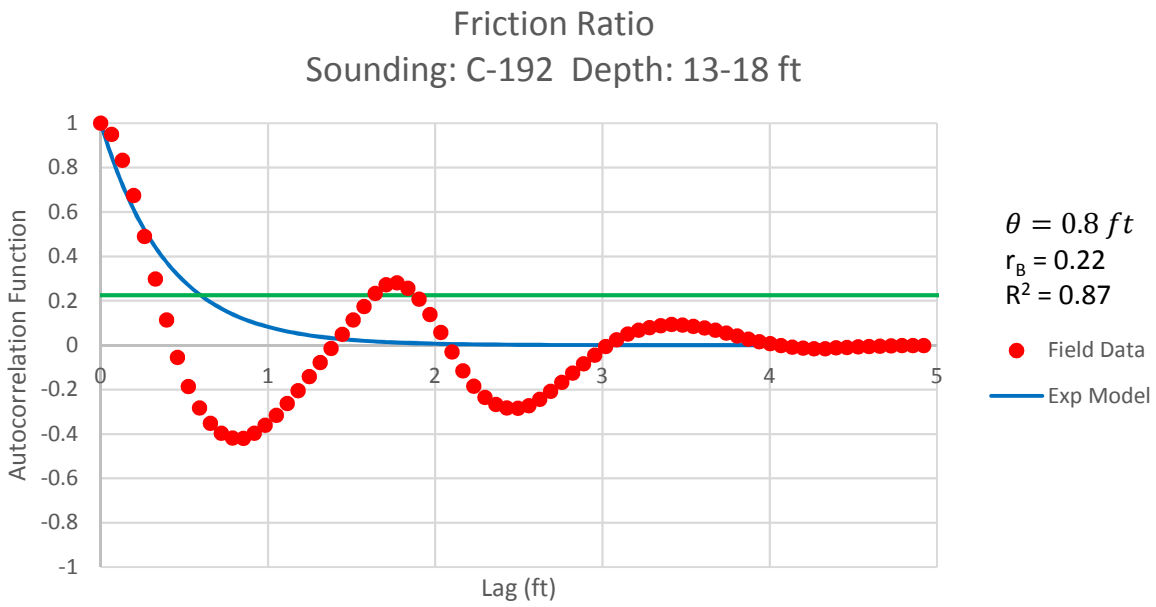

Figure B - 361: Estimation of the Scale of Fluctuation, $\theta = 0.8$ feet, for Friction Ratio Data from Sounding C-192, "Clean sands to silty sands (6)" layer from 13 to 18 feet depth. Data is a poor fit for the points greater than the Bartlett limit of 0.22; coefficient of determination, R^2, value is less 0.9. Therefore, these results were not included in final analysis.

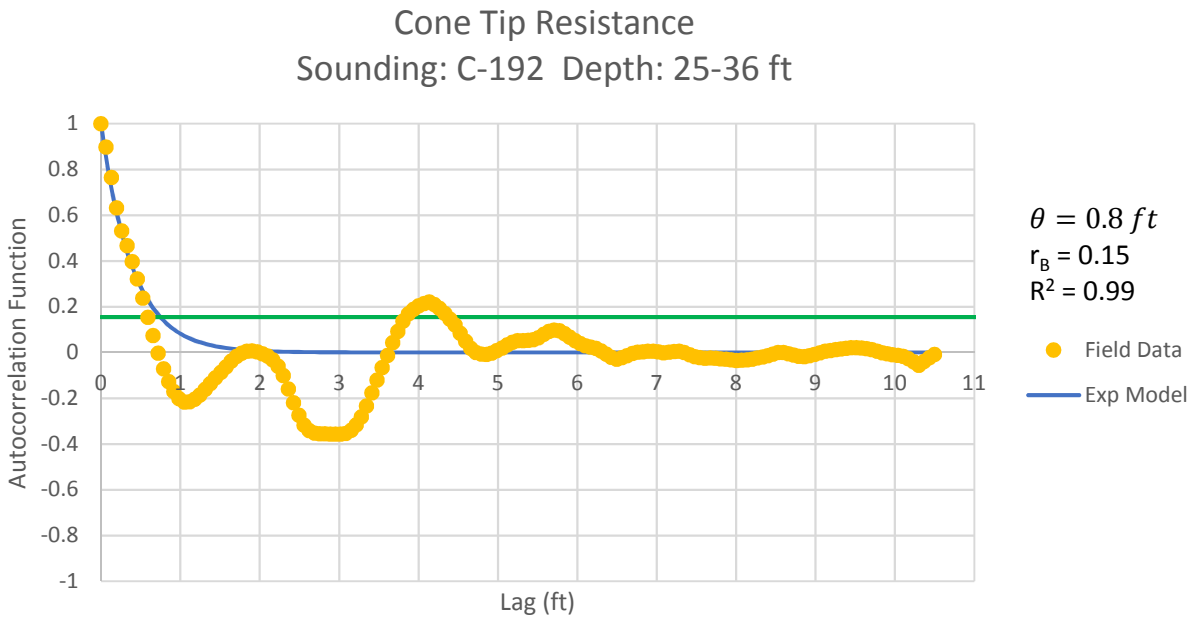

Figure B - 362: Estimation of the Scale of Fluctuation, $\theta = 0.8$ feet, for Cone Tip Resistance Data from Sounding C-192, "Clean sands to silty sands (6)" layer from 25 to 36 feet depth.

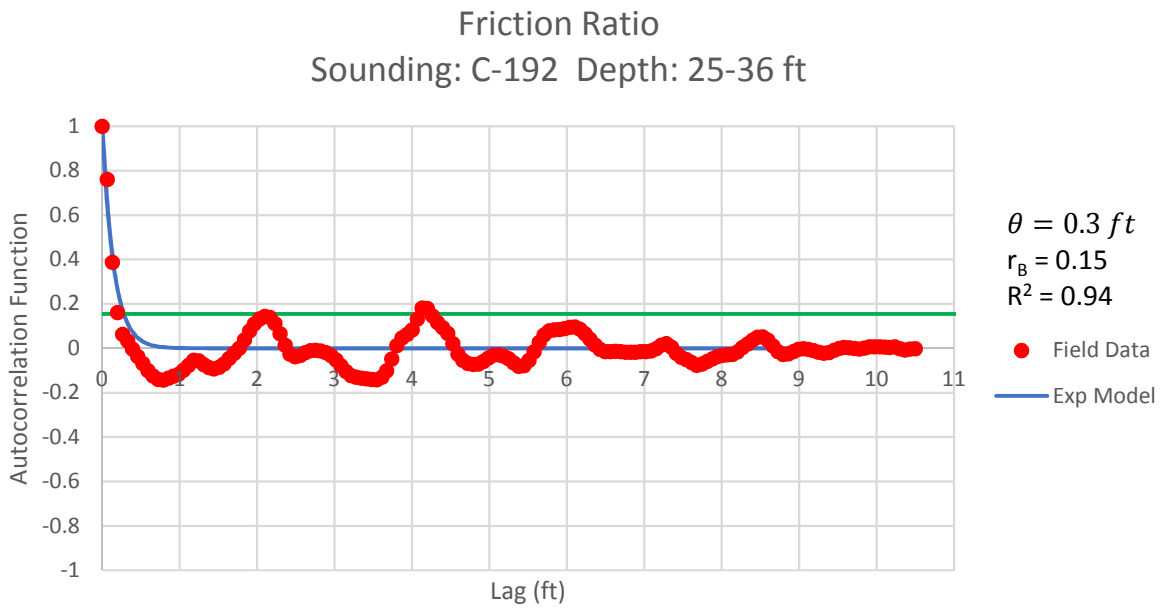

Figure B - 363: Estimation of the Scale of Fluctuation, $\theta = 0.3$ feet, for Friction Ratio Data from Sounding C-192, "Clean sands to silty sands (6)" layer from 25 to 36 feet depth.

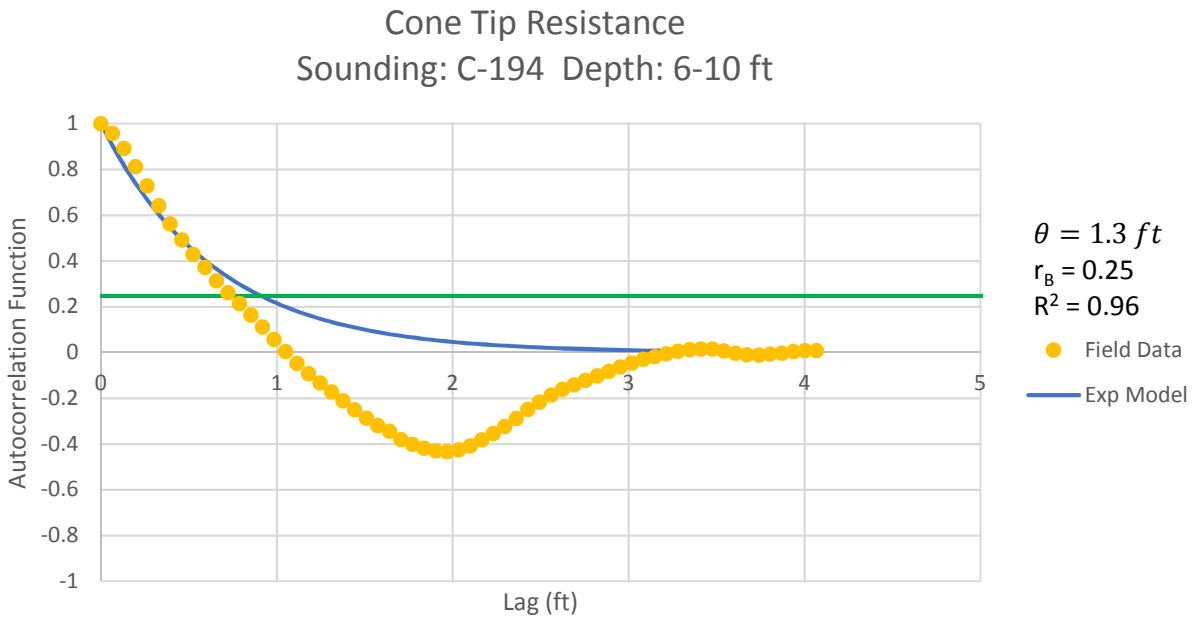

Figure B - 364: Estimation of the Scale of Fluctuation, $\theta = 1.3$ feet, for Cone Tip Resistance Data from Sounding C-194, "Clean sands to silty sands (6)" layer from 6 to 10 feet depth.

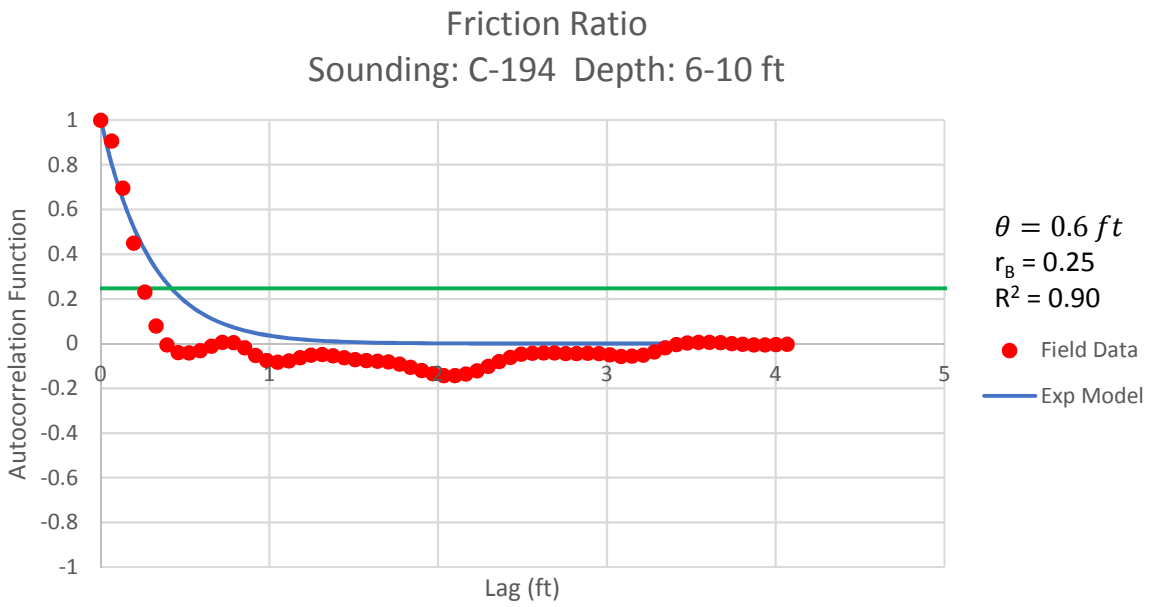

Figure B - 365: Estimation of the Scale of Fluctuation, $\theta = 0.6$ feet, for Friction Ratio Data from Sounding C-194, "Clean sands to silty sands (6)" layer from 6 to 10 feet depth.

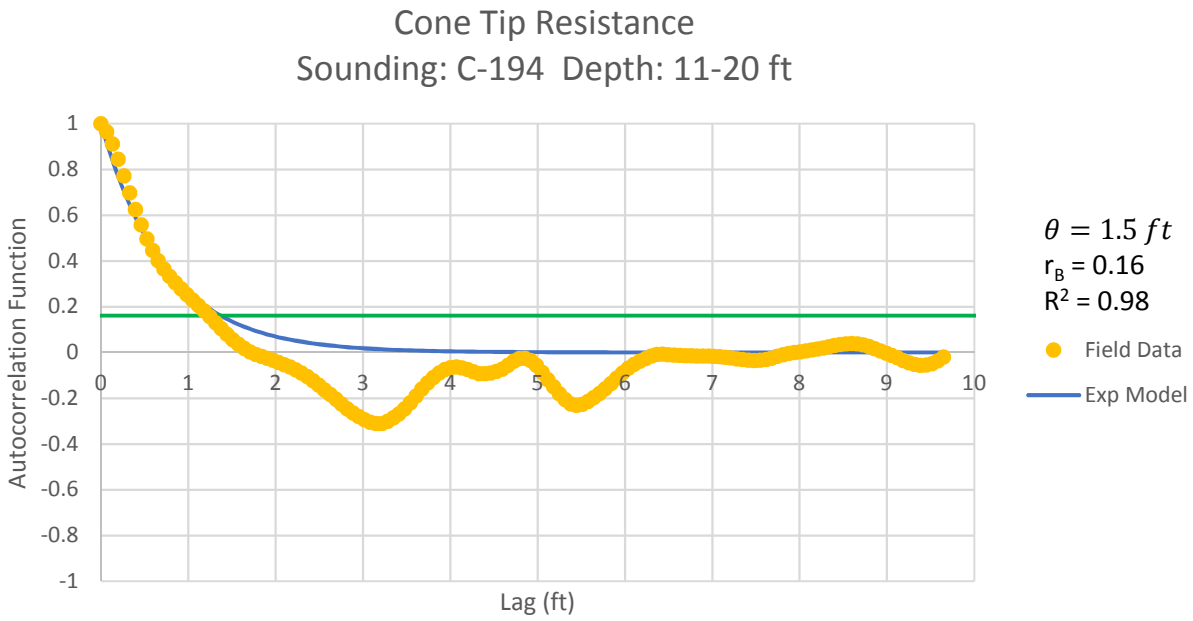

Figure B - 366: Estimation of the Scale of Fluctuation, $\theta = 1.5$ feet, for Cone Tip Resistance Data from Sounding C-194, "Clean sands to silty sands (6)" layer from 11 to 20 feet depth.

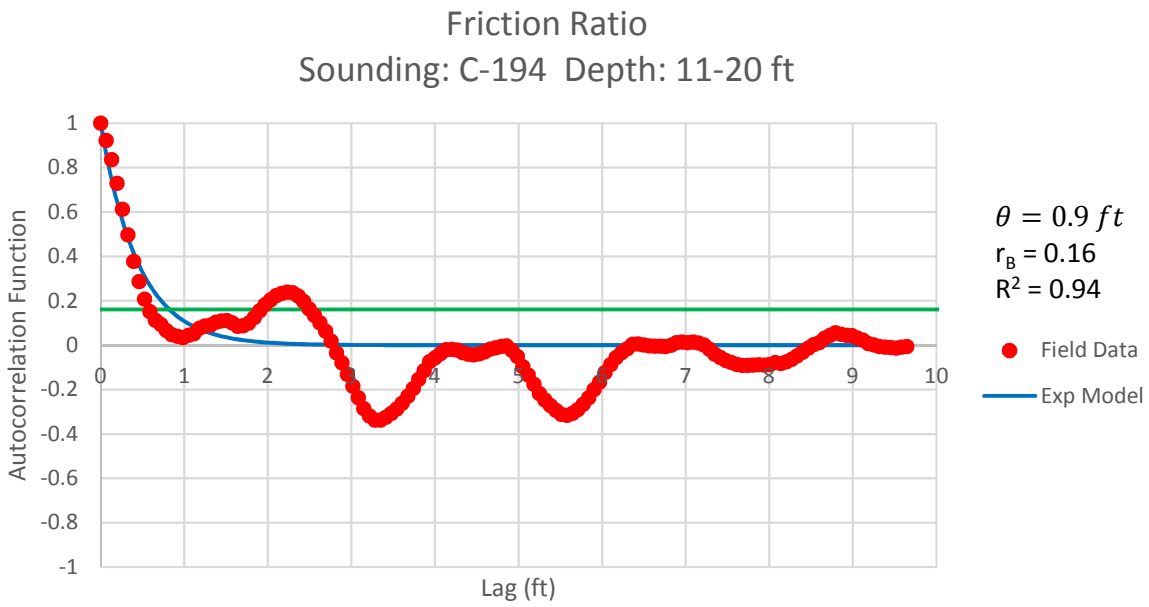

Figure B - 367: Estimation of the Scale of Fluctuation, $\theta = 0.9$ feet, for Friction Ratio Data from Sounding C-194, "Clean sands to silty sands (6)" layer from 11 to 20 feet depth.

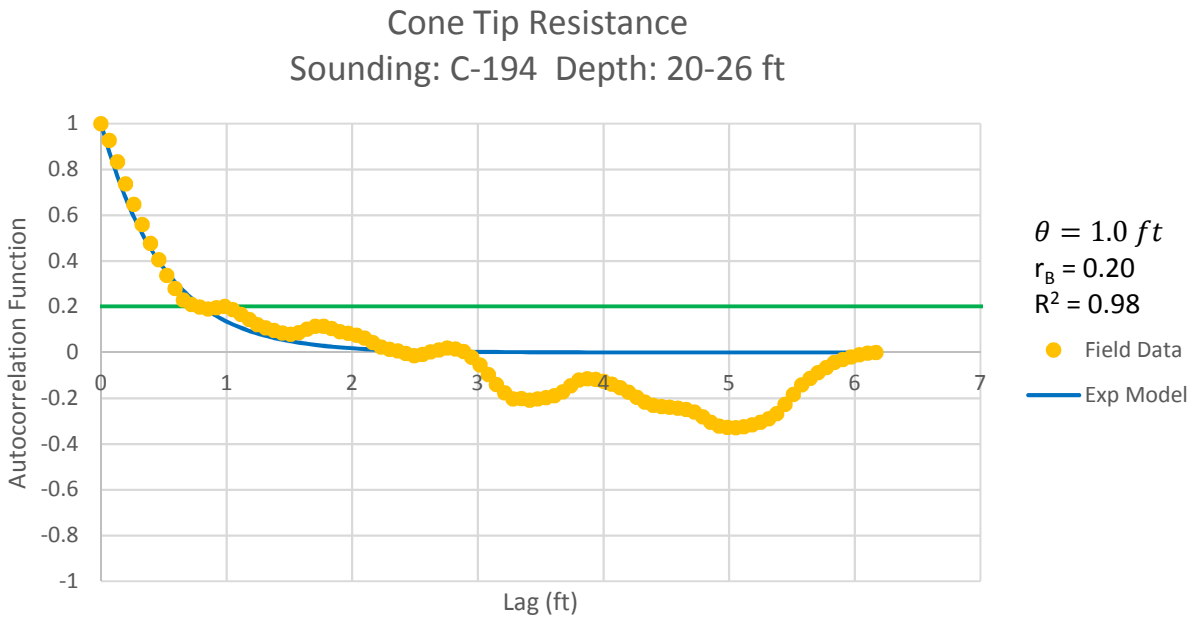

Figure B - 368: Estimation of the Scale of Fluctuation, θ = 1.0 feet, for Cone Tip Resistance Data from Sounding C-194, "Gravelly sand to sand (7)" layer from 20 to 26 feet depth.

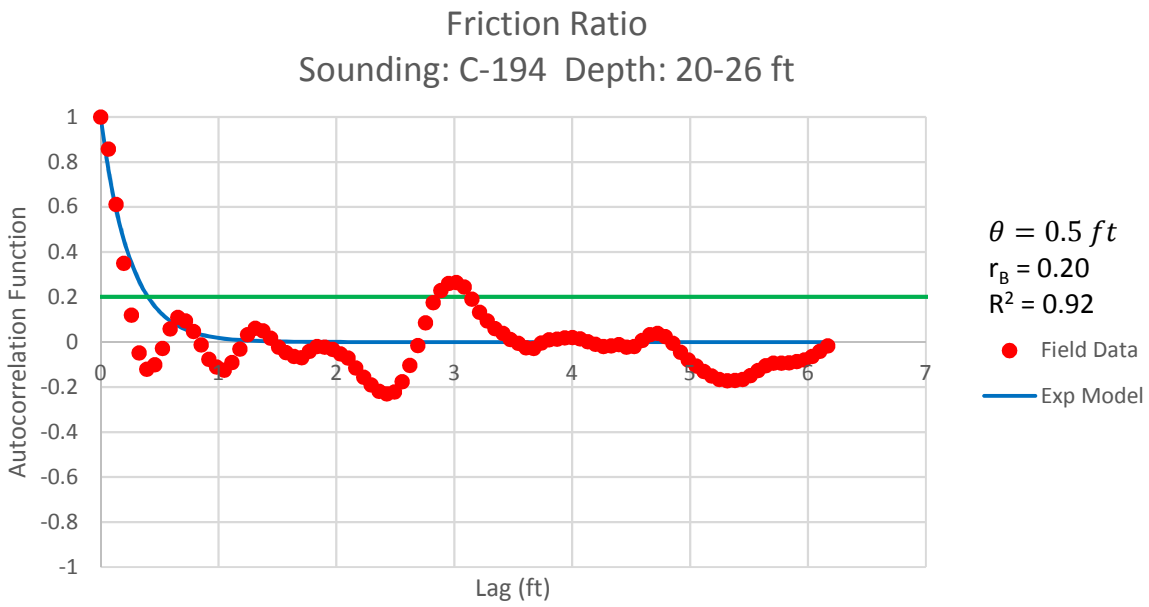

Figure B - 369: Estimation of the Scale of Fluctuation, θ = 0.5 feet, for Friction Ratio Data from Sounding C-194, "Gravelly sand to sand (7)" layer from 20 to 26 feet depth.

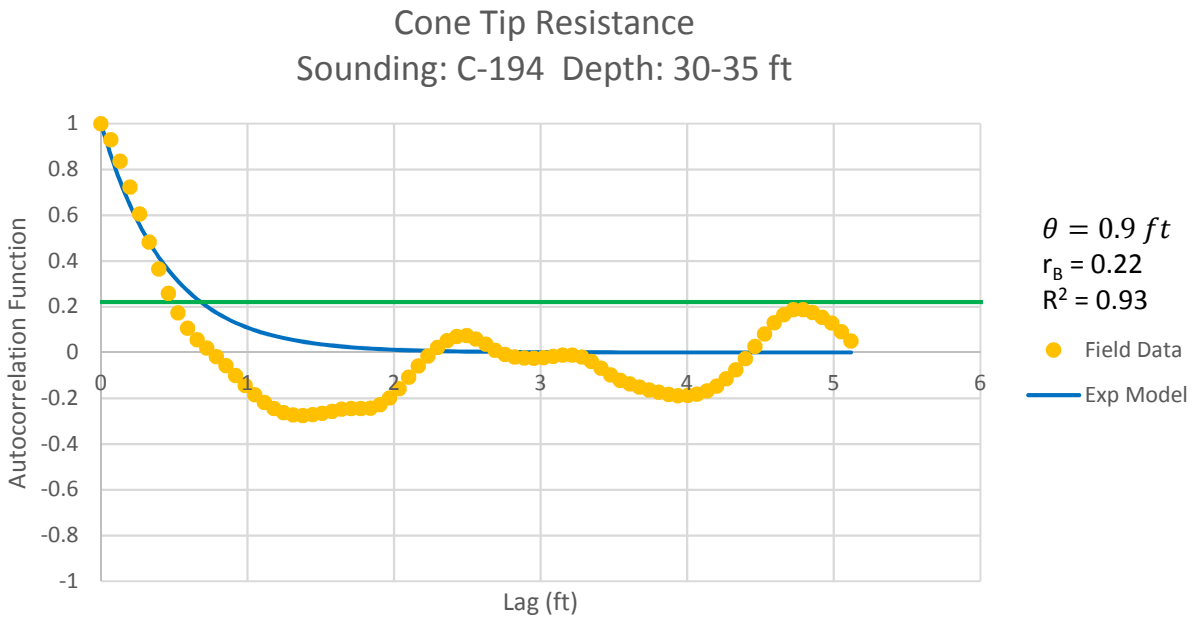

Figure B - 370: Estimation of the Scale of Fluctuation, $\theta = 0.9$ feet, for Cone Tip Resistance Data from Sounding C-194, "Clean sands to silty sands (6)" layer from 30 to 35 feet depth.

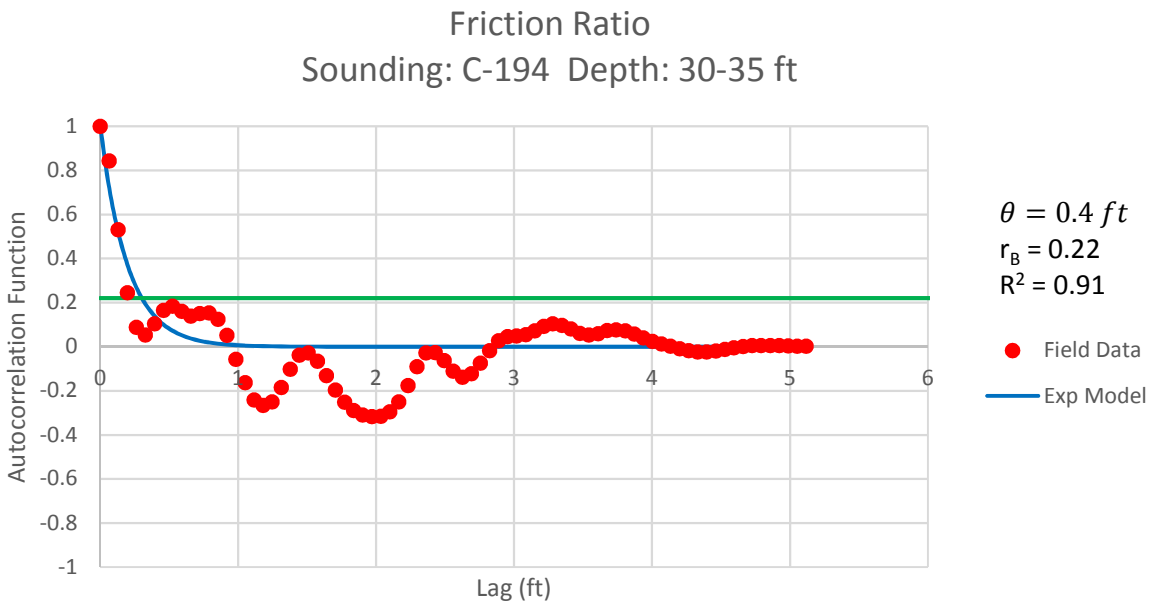

Figure B - 371: Estimation of the Scale of Fluctuation, $\theta = 0.4$ feet, for Friction Ratio Data from Sounding C-194, "Clean sands to silty sands (6)" layer from 30 to 35 feet depth.

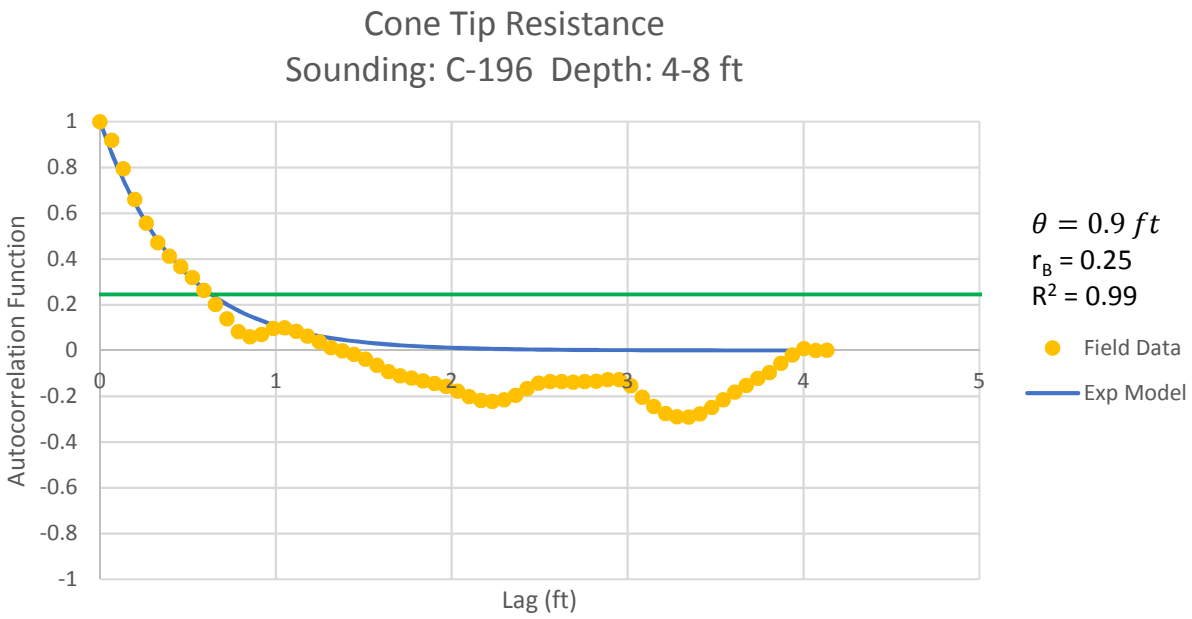

Figure B - 372: Estimation of the Scale of Fluctuation, $\theta = 0.9$ feet, for Cone Tip Resistance Data from Sounding C-196, "Clayey silt to silty clay (4)" layer from 4 to 8 feet depth.

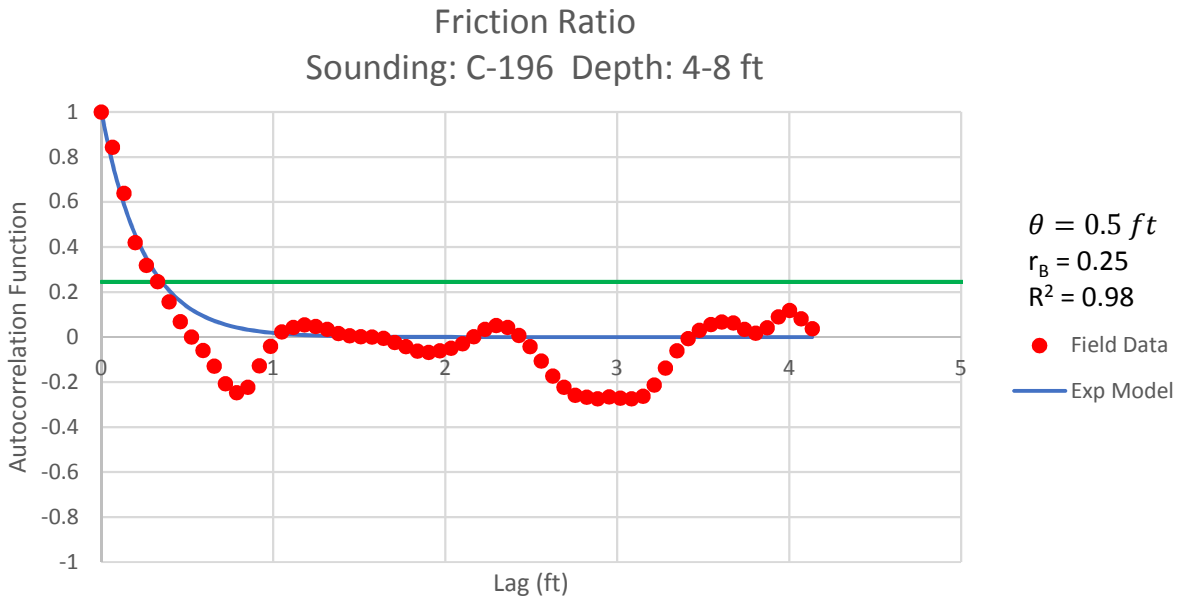

Figure B - 373: Estimation of the Scale of Fluctuation, $\theta = 0.5$ feet, for Friction Ratio Data from Sounding C-196, "Clayey silt to silty clay (4)" layer from 4 to 8 feet depth.

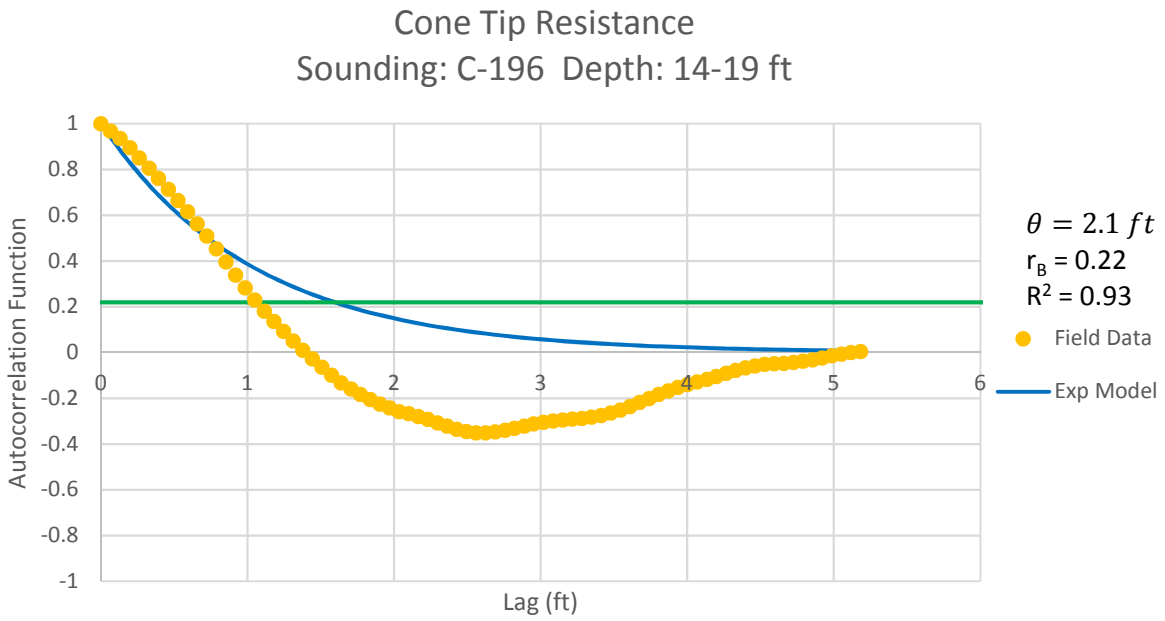

Figure B - 374: Estimation of the Scale of Fluctuation, $\theta = 2.1$ feet, for Cone Tip Resistance Data from Sounding C-196, "Clean sands to silty sands (6)" layer from 14 to 19 feet depth.

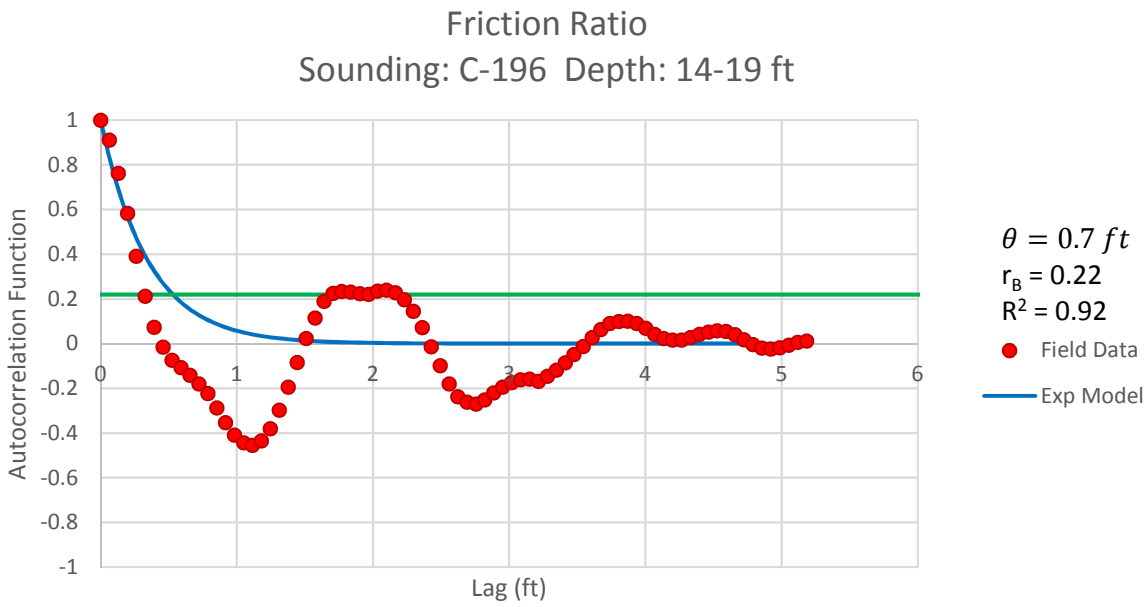

Figure B - 375: Estimation of the Scale of Fluctuation, $\theta = 0.7$ feet, for Friction Ratio Data from Sounding C-196, "Clean sands to silty sands (6)" layer from 14 to 19 feet depth.

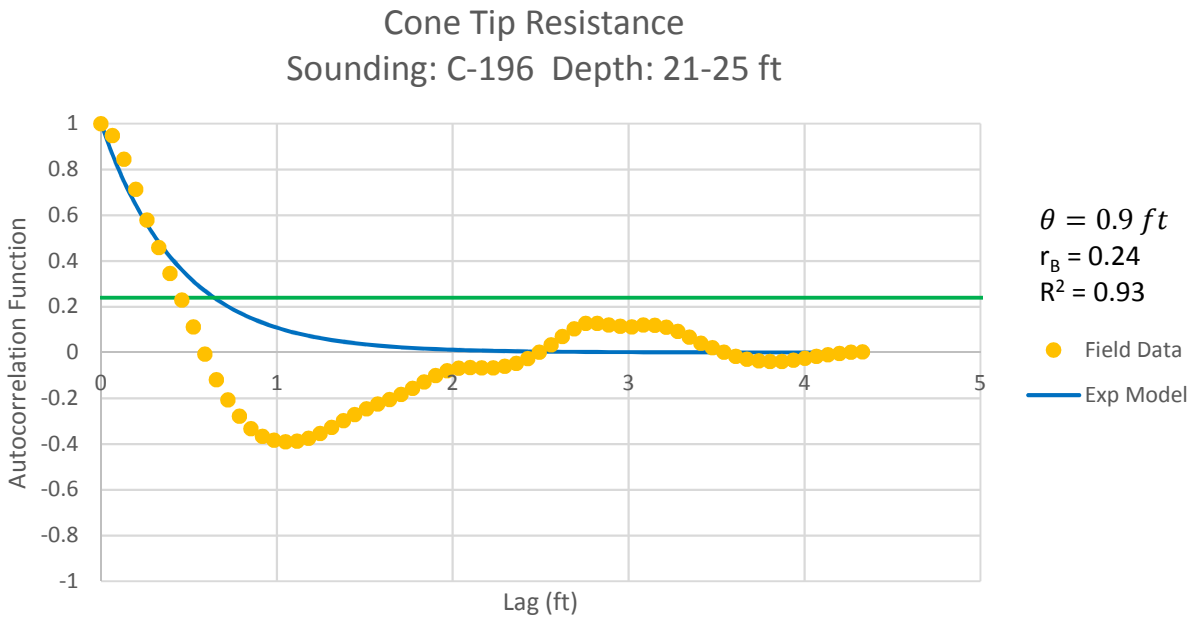

Figure B - 376: Estimation of the Scale of Fluctuation, $\theta = 0.9$ feet, for Cone Tip Resistance Data from Sounding C-196, "Clean sands to silty sands (6)" layer from 21 to 25 feet depth.

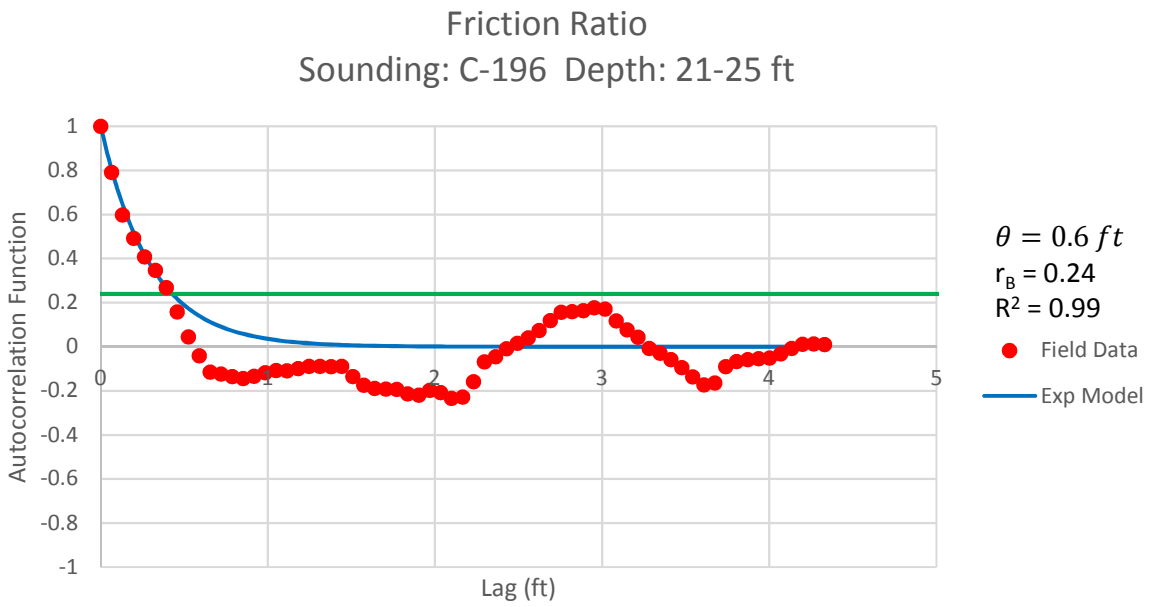

Figure B - 377: Estimation of the Scale of Fluctuation, $\theta = 0.6$ feet, for Friction Ratio Data from Sounding C-196, "Clean sands to silty sands (6)" layer from 21 to 25 feet depth.

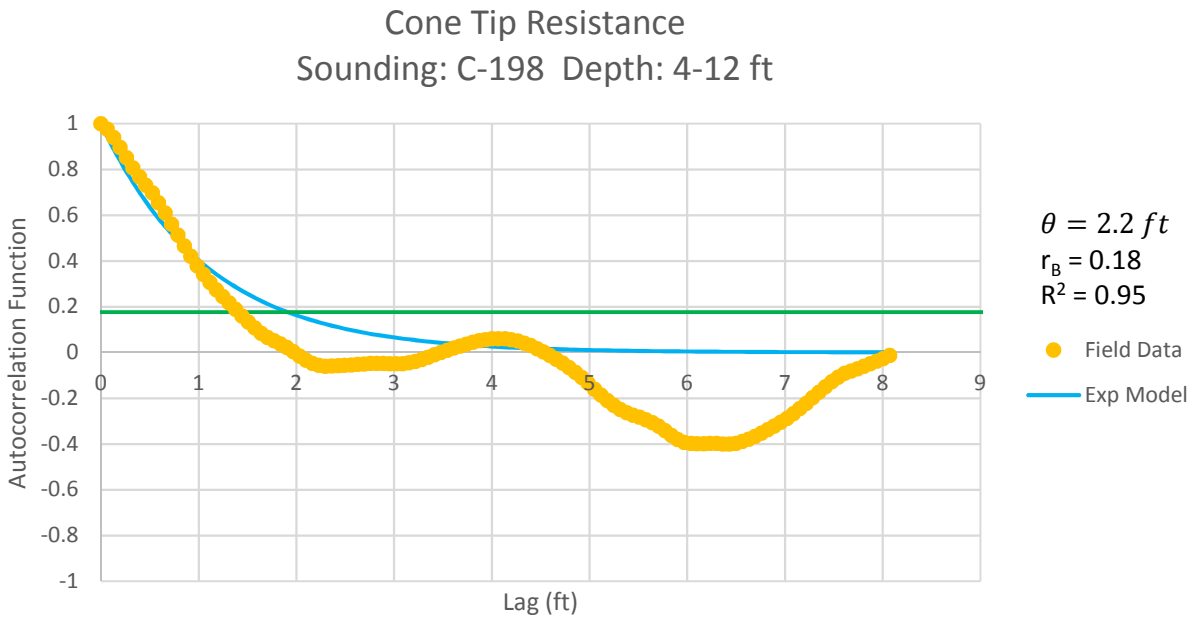

Figure B - 378: Estimation of the Scale of Fluctuation, $\theta = 2.2$ feet, for Cone Tip Resistance Data from Sounding C-198, "Clean sands to silty sands (6)" layer from 4 to 12 feet depth.

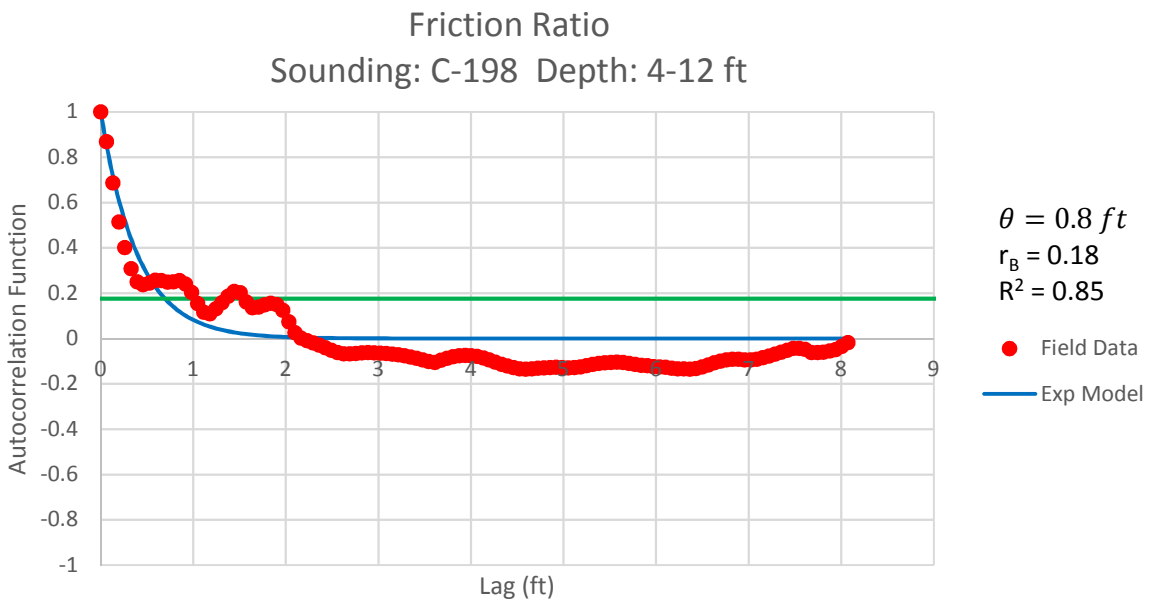

Figure B - 379: Estimation of the Scale of Fluctuation, $\theta = 0.8$ feet, for Friction Ratio Data from Sounding C-198, "Clean sands to silty sands (6)" layer from 4 to 12 feet depth. Data is a poor fit for the points greater than the Bartlett limit of 0.18; coefficient of determination, R^2, value is less 0.9. Therefore, these results were not included in final analysis.

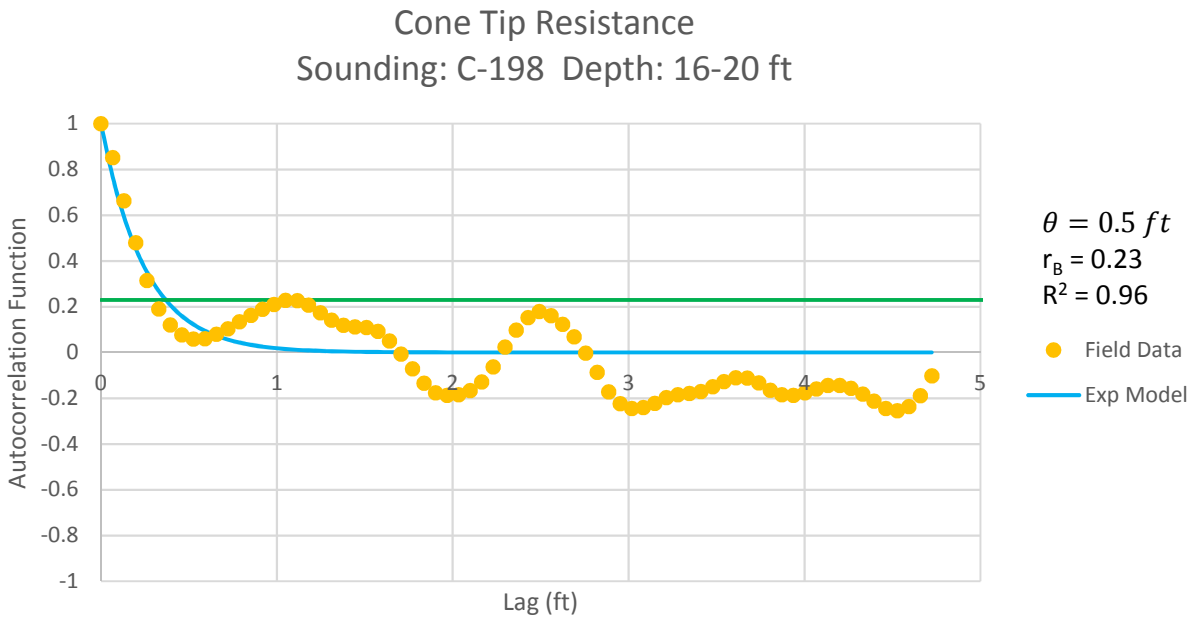

Figure B - 380: Estimation of the Scale of Fluctuation, $\theta = 0.5$ feet, for Cone Tip Resistance Data from Sounding C-198, "Clean sands to silty sands (6)" layer from 16 to 20 feet depth.

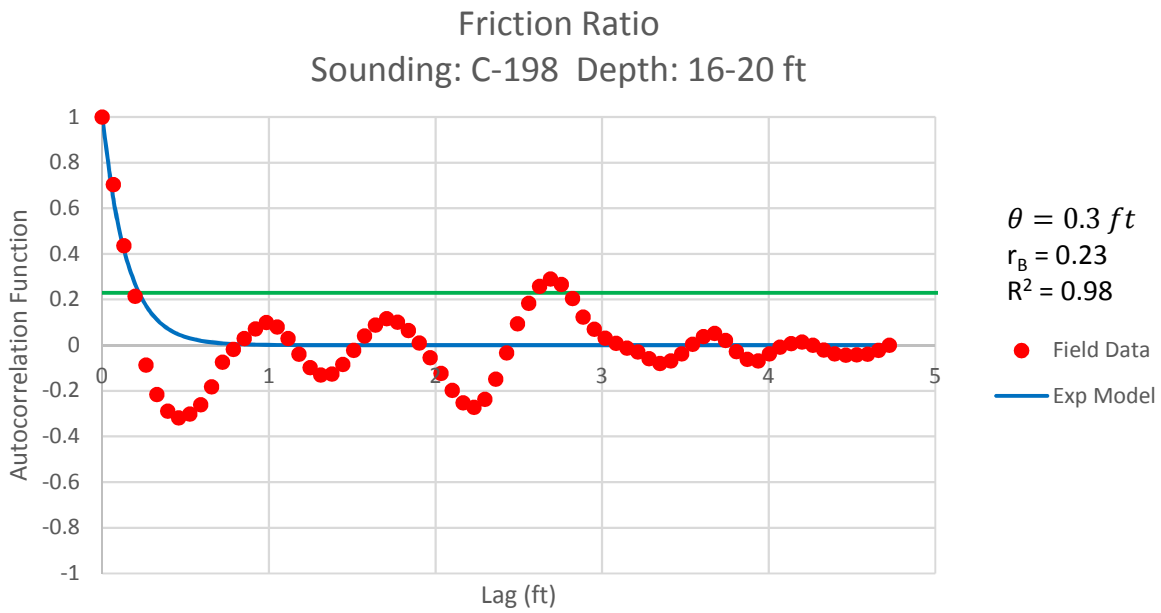

Figure B - 3812: Estimation of the Scale of Fluctuation, $\theta = 0.3$ feet, for Friction Ratio Data from Sounding C-198, "Clean sands to silty sands (6)" layer from 16 to 20 feet depth.

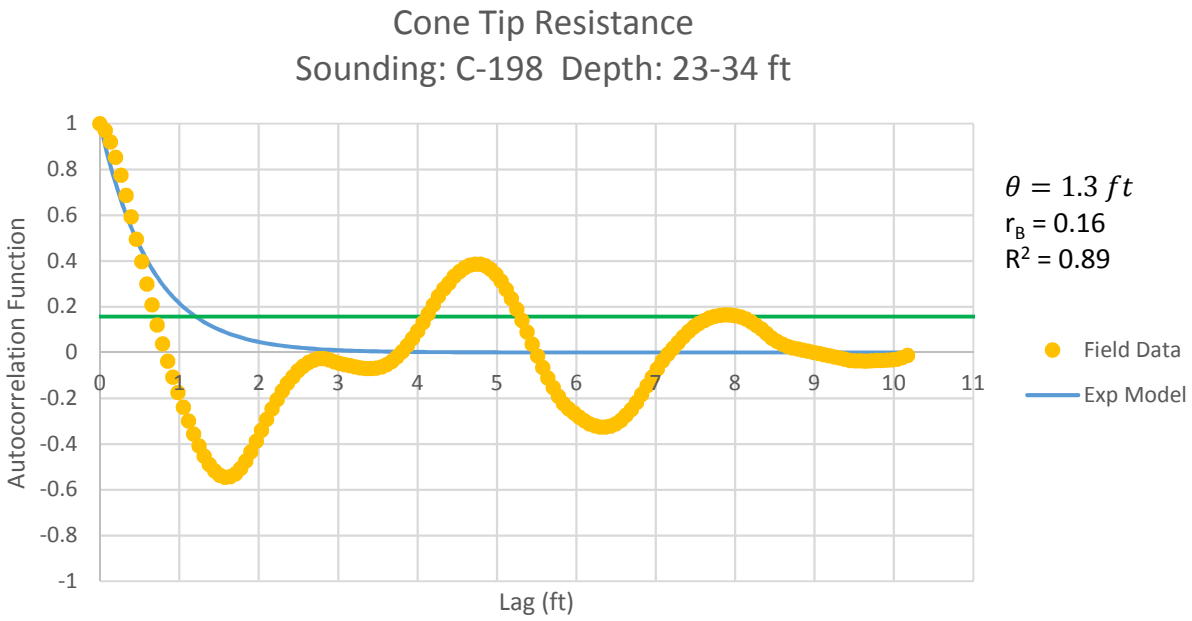

Figure B - 382: Estimation of the Scale of Fluctuation, $\theta = 1.3$ feet, for Cone Tip Resistance Data from Sounding C-198, "Clean sands to silty sands (6)" layer from 23 to 34 feet depth. Data is a poor fit for the points greater than the Bartlett limit of 0.16; coefficient of determination, R^2, value is less 0.9. Therefore, these results were not included in final analysis.

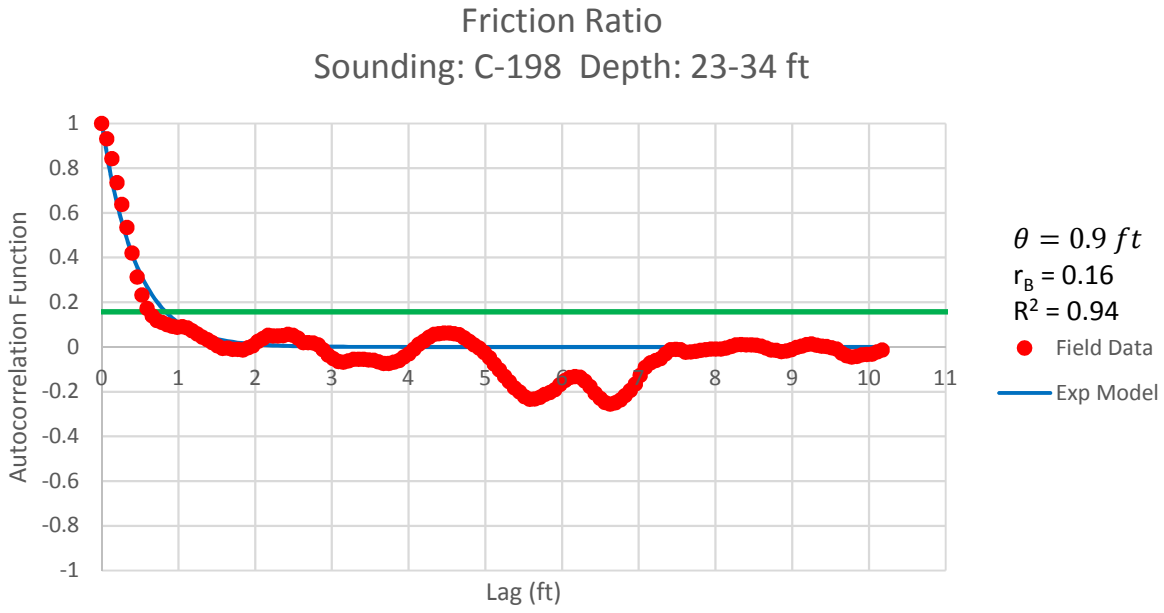

Figure B - 383: Estimation of the Scale of Fluctuation, $\theta = 0.9$ feet, for Friction Ratio Data from Sounding C-198, "Clean sands to silty sands (6)" layer from 23 to 34 feet depth.

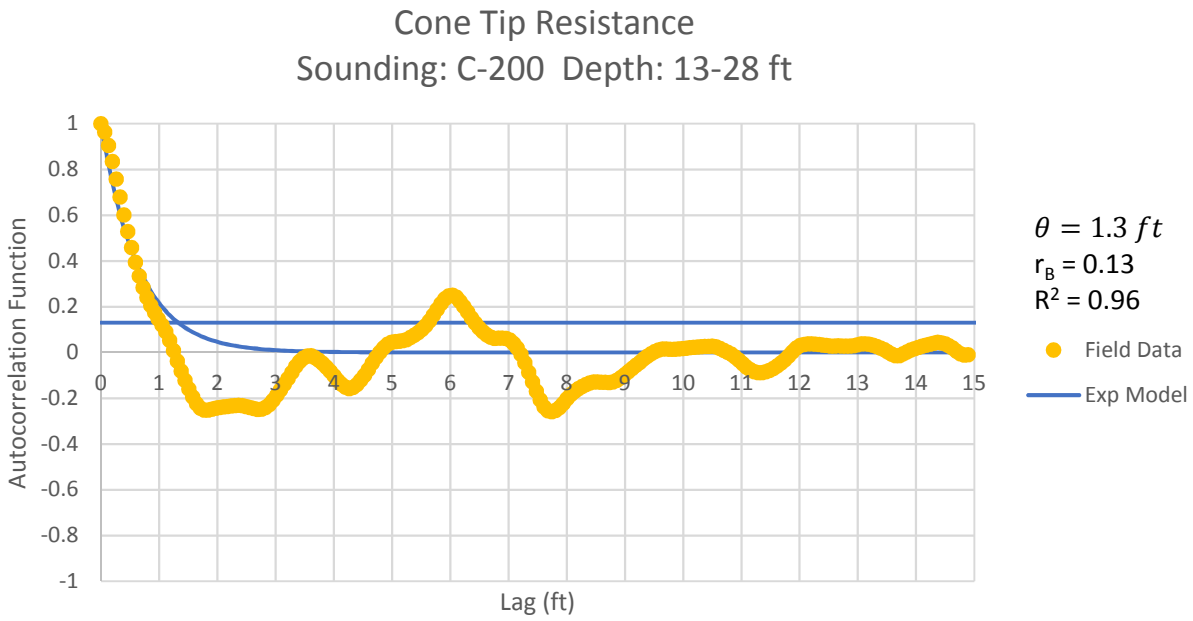

Figure B - 384: Estimation of the Scale of Fluctuation, $\theta = 1.3$ feet, for Cone Tip Resistance Data from Sounding C-200, "Clean sands to silty sands (6)" layer from 13 to 28 feet depth.

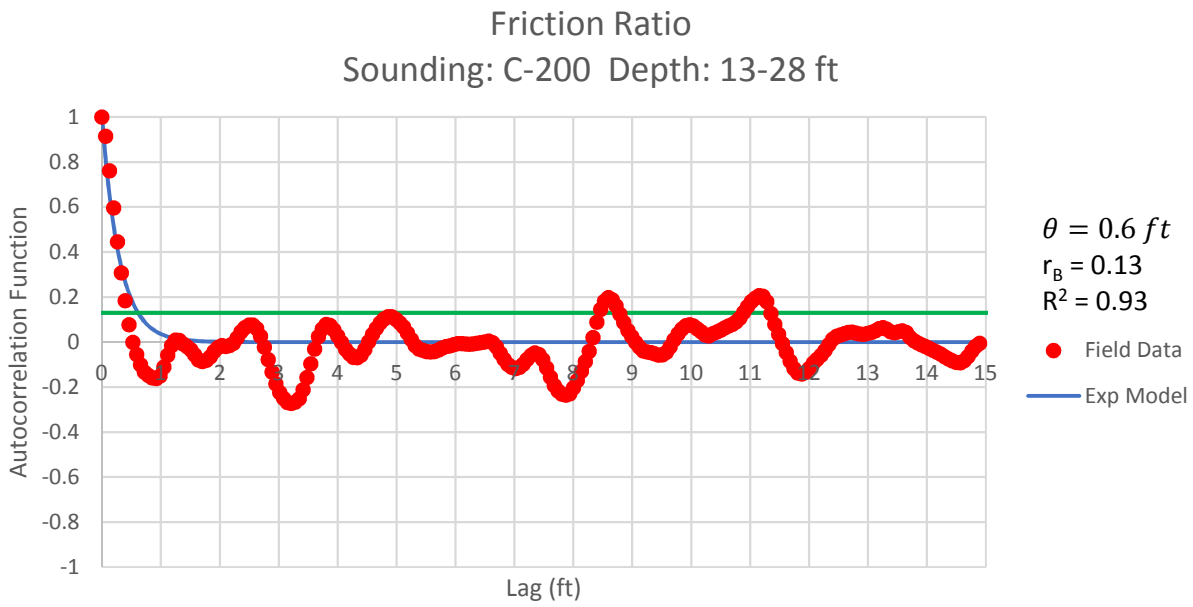

Figure B - 385: Estimation of the Scale of Fluctuation, $\theta = 0.6$ feet, for Friction Ratio Data from Sounding C-200, "Clean sands to silty sands (6)" layer from 13 to 28 feet depth.

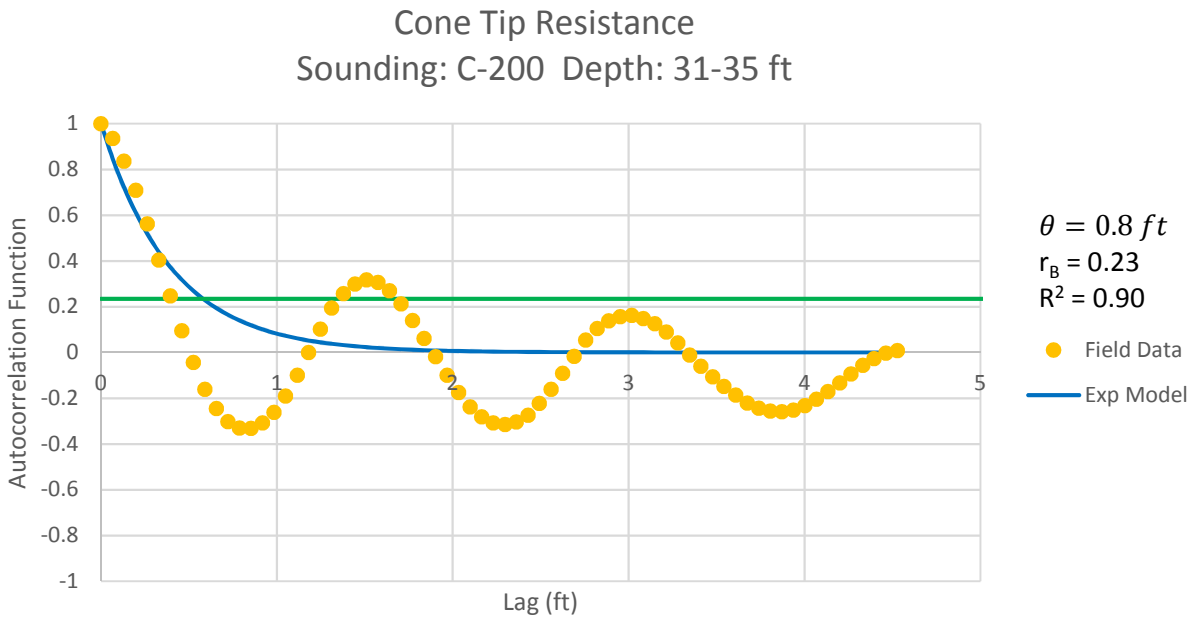

Figure B - 386: Estimation of the Scale of Fluctuation, $\theta = 0.8$ feet, for Cone Tip Resistance Data from Sounding C-200, "Clean sands to silty sands (6)" layer from 31 to 35 feet depth.

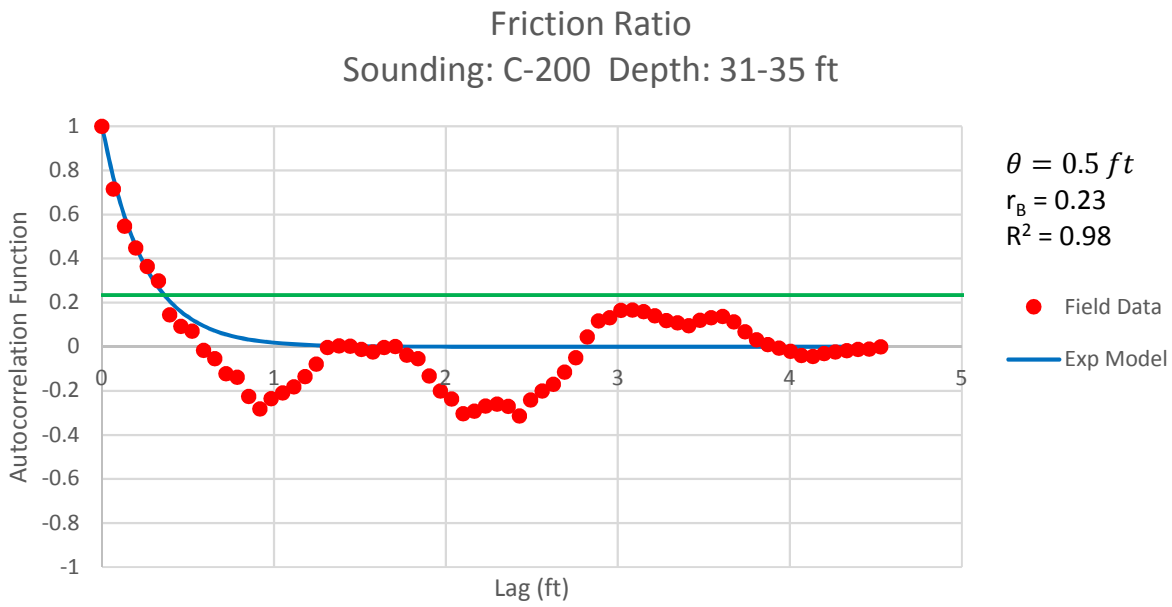

Figure B – 387: Estimation of the Scale of Fluctuation, $\theta = 0.5$ feet, for Friction Ratio Data from Sounding C-200, "Clean sands to silty sands (6)" layer from 31 to 35 feet depth.

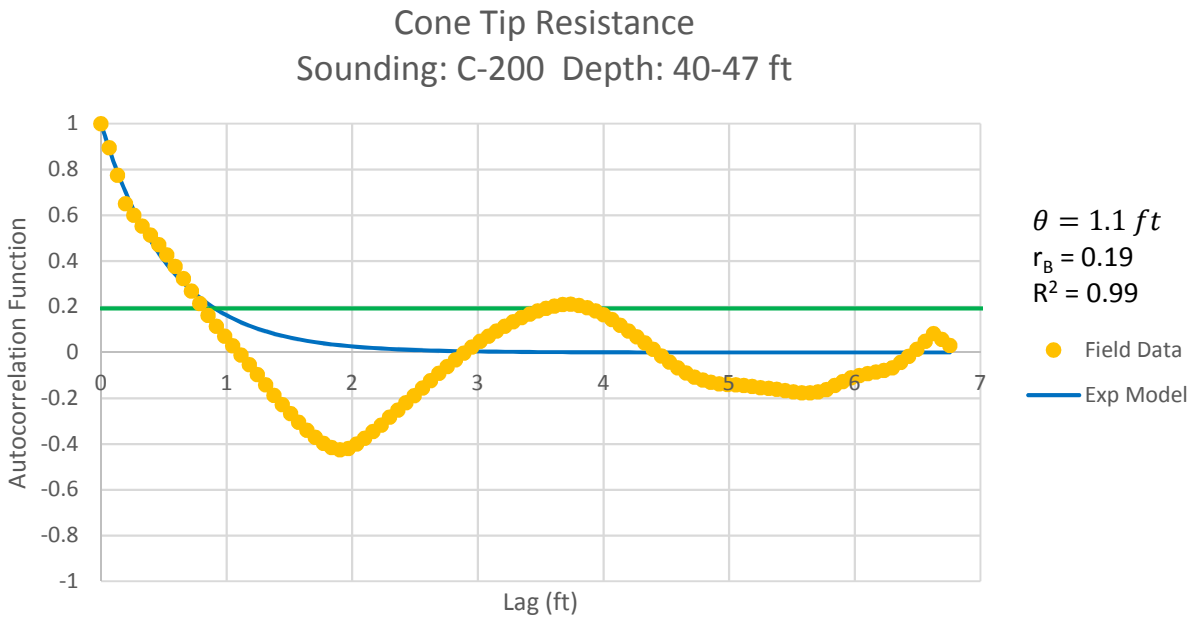

Figure B – 388: Estimation of the Scale of Fluctuation, θ = 1.1 feet, for Cone Tip Resistance Data from Sounding C-200, "Clean sands to silty sands (6)" layer from 40 to 47 feet depth.

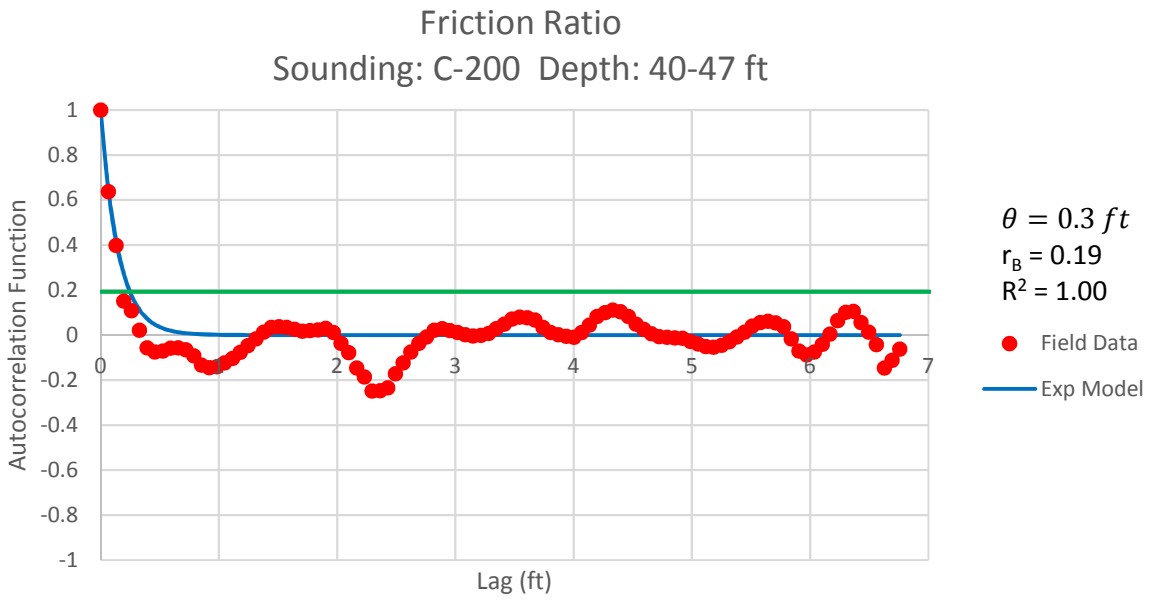

Figure B - 389: Estimation of the Scale of Fluctuation, θ, for Friction Ratio Data from Sounding C-200, "Clean sands to silty sands (6)" layer from 40 to 47 feet depth. Data is limited to only 3 points greater than the Bartlett limit of 0.19; therefore, θ could not be estimated, and these results were not included in final analysis.

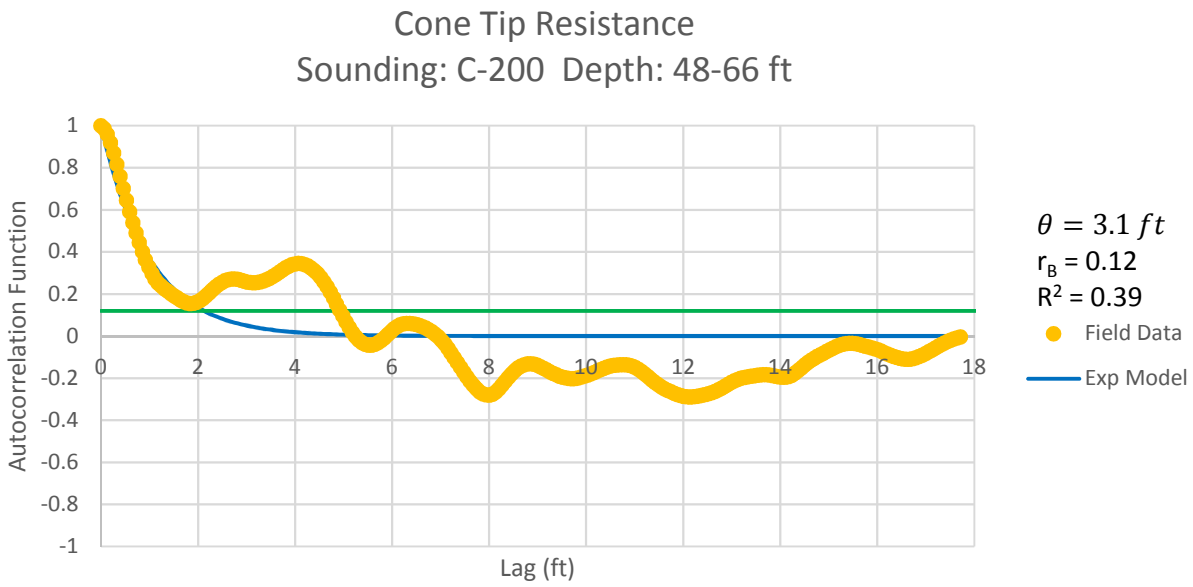

Figure B - 390: Estimation of the Scale of Fluctuation, θ = 3.1 feet, for Cone Tip Resistance Data from Sounding C-200, "Clean sands to silty sands (6)" layer from 48 to 66 feet depth. Data is a poor fit for the points greater than the Bartlett limit of 0.12; coefficient of determination, R^2, value is less 0.9. Therefore, these results were not included in final analysis.

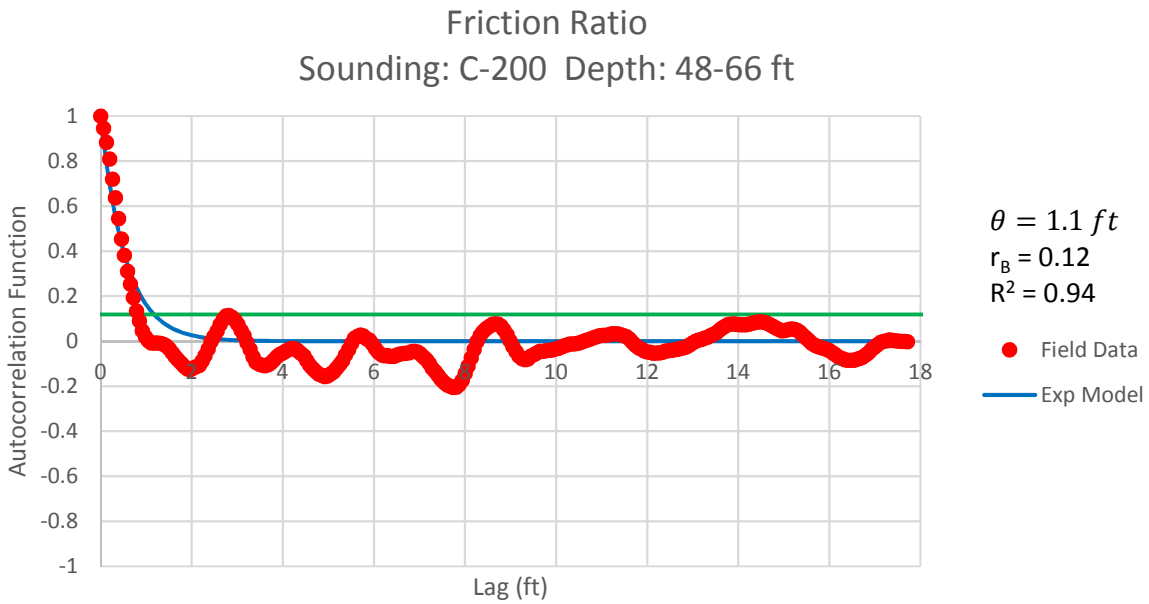

Figure B - 391: Estimation of the Scale of Fluctuation, θ = 1.1 feet, for Friction Ratio Data from Sounding C-200, Clean sands to silty sands (6)" layer from 48 to 66 feet depth.